

THESE TERMS GOVERN YOUR USE OF THIS DOCUMENT

Your use of this Ontario Geological Survey document (the “Content”) is governed by the terms set out on this page (“Terms of Use”). By downloading this Content, you (the “User”) have accepted, and have agreed to be bound by, the Terms of Use.

Content: This Content is offered by the Province of Ontario’s *Ministry of Northern Development and Mines* (MNDM) as a public service, on an “as-is” basis. Recommendations and statements of opinion expressed in the Content are those of the author or authors and are not to be construed as statement of government policy. You are solely responsible for your use of the Content. You should not rely on the Content for legal advice nor as authoritative in your particular circumstances. Users should verify the accuracy and applicability of any Content before acting on it. MNDM does not guarantee, or make any warranty express or implied, that the Content is current, accurate, complete or reliable. MNDM is not responsible for any damage however caused, which results, directly or indirectly, from your use of the Content. MNDM assumes no legal liability or responsibility for the Content whatsoever.

Links to Other Web Sites: This Content may contain links, to Web sites that are not operated by MNDM. Linked Web sites may not be available in French. MNDM neither endorses nor assumes any responsibility for the safety, accuracy or availability of linked Web sites or the information contained on them. The linked Web sites, their operation and content are the responsibility of the person or entity for which they were created or maintained (the “Owner”). Both your use of a linked Web site, and your right to use or reproduce information or materials from a linked Web site, are subject to the terms of use governing that particular Web site. Any comments or inquiries regarding a linked Web site must be directed to its Owner.

Copyright: Canadian and international intellectual property laws protect the Content. Unless otherwise indicated, copyright is held by the Queen’s Printer for Ontario.

It is recommended that reference to the Content be made in the following form: <Author’s last name>, <Initials> <year of publication>. <Content title>; Ontario Geological Survey, <Content publication series and number>, <total number of pages>p.

Use and Reproduction of Content: The Content may be used and reproduced only in accordance with applicable intellectual property laws. *Non-commercial* use of unsubstantial excerpts of the Content is permitted provided that appropriate credit is given and Crown copyright is acknowledged. Any substantial reproduction of the Content or any *commercial* use of all or part of the Content is prohibited without the prior written permission of MNDM. Substantial reproduction includes the reproduction of any illustration or figure, such as, but not limited to graphs, charts and maps. Commercial use includes commercial distribution of the Content, the reproduction of multiple copies of the Content for any purpose whether or not commercial, use of the Content in commercial publications, and the creation of value-added products using the Content.

Contact:

FOR FURTHER INFORMATION ON	PLEASE CONTACT:	BY TELEPHONE:	BY E-MAIL:
The Reproduction of Content	MNDM Publication Services	Local: (705) 670-5691 Toll Free: 1-888-415-9845, ext. 5691 (inside Canada, United States)	Pubsales@ndm.gov.on.ca
The Purchase of MNDM Publications	MNDM Publication Sales	Local: (705) 670-5691 Toll Free: 1-888-415-9845, ext. 5691 (inside Canada, United States)	Pubsales@ndm.gov.on.ca
Crown Copyright	Queen’s Printer	Local: (416) 326-2678 Toll Free: 1-800-668-9938 (inside Canada, United States)	Copyright@gov.on.ca

LES CONDITIONS CI-DESSOUS RÉGISSENT L'UTILISATION DU PRÉSENT DOCUMENT.

Votre utilisation de ce document de la Commission géologique de l'Ontario (le « contenu ») est régie par les conditions décrites sur cette page (« conditions d'utilisation »). En téléchargeant ce contenu, vous (l'« utilisateur ») signifiez que vous avez accepté d'être lié par les présentes conditions d'utilisation.

Contenu : Ce contenu est offert en l'état comme service public par le *ministère du Développement du Nord et des Mines* (MDNM) de la province de l'Ontario. Les recommandations et les opinions exprimées dans le contenu sont celles de l'auteur ou des auteurs et ne doivent pas être interprétées comme des énoncés officiels de politique gouvernementale. Vous êtes entièrement responsable de l'utilisation que vous en faites. Le contenu ne constitue pas une source fiable de conseils juridiques et ne peut en aucun cas faire autorité dans votre situation particulière. Les utilisateurs sont tenus de vérifier l'exactitude et l'applicabilité de tout contenu avant de l'utiliser. Le MDNM n'offre aucune garantie expresse ou implicite relativement à la mise à jour, à l'exactitude, à l'intégralité ou à la fiabilité du contenu. Le MDNM ne peut être tenu responsable de tout dommage, quelle qu'en soit la cause, résultant directement ou indirectement de l'utilisation du contenu. Le MDNM n'assume aucune responsabilité légale de quelque nature que ce soit en ce qui a trait au contenu.

Liens vers d'autres sites Web : Ce contenu peut comporter des liens vers des sites Web qui ne sont pas exploités par le MDNM. Certains de ces sites pourraient ne pas être offerts en français. Le MDNM se dégage de toute responsabilité quant à la sûreté, à l'exactitude ou à la disponibilité des sites Web ainsi reliés ou à l'information qu'ils contiennent. La responsabilité des sites Web ainsi reliés, de leur exploitation et de leur contenu incombe à la personne ou à l'entité pour lesquelles ils ont été créés ou sont entretenus (le « propriétaire »). Votre utilisation de ces sites Web ainsi que votre droit d'utiliser ou de reproduire leur contenu sont assujettis aux conditions d'utilisation propres à chacun de ces sites. Tout commentaire ou toute question concernant l'un de ces sites doivent être adressés au propriétaire du site.

Droits d'auteur : Le contenu est protégé par les lois canadiennes et internationales sur la propriété intellectuelle. Sauf indication contraire, les droits d'auteurs appartiennent à l'Imprimeur de la Reine pour l'Ontario.

Nous recommandons de faire paraître ainsi toute référence au contenu : nom de famille de l'auteur, initiales, année de publication, titre du document, Commission géologique de l'Ontario, série et numéro de publication, nombre de pages.

Utilisation et reproduction du contenu : Le contenu ne peut être utilisé et reproduit qu'en conformité avec les lois sur la propriété intellectuelle applicables. L'utilisation de courts extraits du contenu à des fins *non commerciales* est autorisée, à condition de faire une mention de source appropriée reconnaissant les droits d'auteurs de la Couronne. Toute reproduction importante du contenu ou toute utilisation, en tout ou en partie, du contenu à des fins *commerciales* est interdite sans l'autorisation écrite préalable du MDNM. Une reproduction jugée importante comprend la reproduction de toute illustration ou figure comme les graphiques, les diagrammes, les cartes, etc. L'utilisation commerciale comprend la distribution du contenu à des fins commerciales, la reproduction de copies multiples du contenu à des fins commerciales ou non, l'utilisation du contenu dans des publications commerciales et la création de produits à valeur ajoutée à l'aide du contenu.

Renseignements :

POUR PLUS DE RENSEIGNEMENTS SUR	VEUILLEZ VOUS ADRESSER À :	PAR TÉLÉPHONE :	PAR COURRIEL :
la reproduction du contenu	Services de publication du MDNM	Local : (705) 670-5691 Numéro sans frais : 1 888 415-9845, poste 5691 (au Canada et aux États-Unis)	Pubsales@ndm.gov.on.ca
l'achat des publications du MDNM	Vente de publications du MDNM	Local : (705) 670-5691 Numéro sans frais : 1 888 415-9845, poste 5691 (au Canada et aux États-Unis)	Pubsales@ndm.gov.on.ca
les droits d'auteurs de la Couronne	Imprimeur de la Reine	Local : 416 326-2678 Numéro sans frais : 1 800 668-9938 (au Canada et aux États-Unis)	Copyright@gov.on.ca

**Ontario Geological Survey
Miscellaneous Paper 98**

**Geoscience Research
Grant Program**

**Summary of Research
1980-1981**

**edited by
E.G. Pye**

1981



Ontario

**Ministry of
Natural
Resources**

**Hon. Alan W. Pope
Minister**

**W. T. Foster
Deputy Minister**

Publications of the Ontario Ministry of Natural Resources are available from the following sources. Orders for publications should be accompanied by cheque or money order payable to the *Treasurer of Ontario*.

Reports, maps, and price lists (personal shopping or mail order):

**Public Service Centre, Ministry of Natural Resources
Room 1640, Whitney Block, Queen's Park
Toronto, Ontario M7A 1W3**

Reports only (personal shopping):

**Ontario Government Bookstore
Main Floor, 880 Bay Street
Toronto, Ontario**

Reports and maps (mail order or telephone orders):

**Publications Services Section, Ministry of Government Services
5th Floor, 880 Bay Street
Toronto, Ontario M7A 1N8
Telephone (local calls), 965-6015
Toll-free long distance, 1-800-268-7540
Toll-free from Area Code 807 0-ZENITH-67200**

Every possible effort is made to ensure the accuracy of the information contained in this report, but the Ministry of Natural Resources does not assume any liability for errors that may occur. Source references are included in the report and users may wish to verify critical information.

Parts of this publication may be quoted if credit is given. It is recommended that reference to this report be made in the following form for each individual author:

Bedell, R.L. and Schwerdtner, W.M.

1981: Structural Controls of U-Ore Bodies in the Madawaska Mine Area, Bancroft, Ontario; Grant 82, p. 13-17 in Geoscience Research Grant Program, Summary of Research 1980-1981, edited by E.G. Pye, Ontario Geological Survey, Miscellaneous Paper 98, 340 p.

CONTENTS

Introductory Remarks	iv
1980-1981 Geoscience Research Grant Recipients	vii
Barnes, S.-J., Gorton, M.P., and Naldrett, A.J., Grant 17 Platinum Group Elements in Abitibi Komatiites Associated with Ni-Sulphide Deposits	1
Bedell, R.L. and Schwerdtner, W.M., Grant 82 Structural Controls of U-Ore Bodies in the Madawaska Mine Area, Bancroft, Ontario	13
Bell, K. and Card, J.W., Grant 38 Radon Decay Products and Uranium Exploration	18
Beswick, A.E., Grant 54 Regional Alteration in Archean Greenstones: Applications to Exploration for Massive Sulphide Deposits	25
Brown, J.R., Fyfe, W.S., Murray, F., and Kronberg, B.I., Grant 28 Immobilization of U-Th-Ra in Mine Wastes	38
Campbell, I.H., Coad, P., Franklin, J.M., Gorton, M.P., Hart, T.R., Scott, S.D., Sowa, J., and Thurston, P.C., Grant 80 Rare Earth Elements in Felsic Volcanic Rocks Associated with Cu-Zn Massive Sulphide Mineralization	45
Dixon, J.M. and Summers, J.M., Grant 68 A Centrifuged Model Study of the Tectonic Development of Archean Greenstone Belts	54
Edwards, G.R. and Hodder, R.W., Grant 55 Evolution of an Archean Felsic Volcanic-Plutonic Complex in the Kakagi-Pipestone Lakes Area	67
Fralick, P.W. and Miall, A.D., Grant 84 Sedimentology of the Matinenda Formation	80
Fyon, J.A., Crocket, J.H., Schwarcz, H.P., Kabir, A., and Knyf, M., Grant 49 Trace Element and Stable Isotope Geochemistry of Auriferous Iron Formations in the Timmins Area	90
Gorman, B.E., Kerrich, R., and Fyfe, W.S., Grant 56 Part A Geochemistry and Field Relations of Lode Gold Deposits in Felsic Igneous Intrusions—Porphyries of the Timmins District	108
Guindon, D.L. and Nichol, I., Grant 76 Speciation of Free Gold in Glacial Overburden	125
Hodgson, C.J. and MacGeehan, P.J., Grant 11 Gold Ore Formation at the Campbell and Dickenson Mines, Red Lake Area	132
Kenney, T.C. and Lau, K.C., Grant 7 Field Investigations of Use of Horizontal Deep Drains to Stabilize Clay Slopes	144
Kerrich, R., Robinson, D.J., and Barnett, R.L., Grant 27 Field Relations and Geochemistry of Au, Ni and Cr Deposits in Ultramafic-Mafic Volcanic Rocks	155
MacRae, N.D. Hyatt, M., and Nesbitt, H.W., Grant 75 Asbestos Fibre Degradation in Laboratory Solution	176
Mainwaring, P.R. and Watkinson, D.H., Grant 46 Origin of Chromian Spinel in the Crystal Lake Intrusion, Pardee Township, Ontario	180
Nadon, R.L. and Gale, J.E., Grant 92 Impact of Groundwater on Mining Activities in the Niagara Escarpment Area	187
Otto, J.E. and Dalrymple, R.W., Grant 78 Terrain Characteristics and Physical Processes in Small Lagoon Complexes	202
Richardson, M.L. and Norris, G., Grant 19 Palynostratigraphic Working Standard for Intra-Basinal Correlation of Albian Lignitic Strata, Moose River Basin, Ontario	216
Roberts, R.G. and Reading, D.J., Grant 32 The Volcanic-Tectonic Setting of Gold Deposits in the Timmins District—Carbonate-Bearing Rocks at Dome Mine	222
Roegiers, J.-C. and Mills, R.H., Grant 87 Stability of Compressed Shales in Ontario	229
Rousell, D.H., Grant 96 Mineralization in the Whitewater Group, Sudbury Basin	233
Shegelski, R.J., Grant 88 Metallogeny and Economic Potential of the Western Lake St. Joseph Meta-volcanic-Metasedimentary Belt	243
Strangway, D.W., Geissman, J.W., Bambrick, J., Letros, S., and Tasillo, A., Grant 20 Magnetism and Stratigraphy in Volcanic and Sedimentary Rocks of the Abitibi Belt	251
Studemeister, P.A., Kerrich, R., and Fyfe, W.S., Grant 56 Part B Geochemistry and Field Relations of Lode Gold Deposits in Felsic Igneous Intrusions—The Gutcher Lake Stock	267
Symons, D.T.A., Quick, A.W., and Stupavsky, M., Grant 5 Magnetic and Paleomagnetic Characteristics of the Archean Iron Formation and Host Rocks at the Adams Mine, Ontario	293
West, G.F., Grant 8 Interpretational Support for EM Prospecting	308
Whitehead, R.E.S., Davies, J.F., Cameron, R.A., and Duff, D., Grant 30 Carbonate, Alkali and Arsenic Anomalies Associated with Gold Mineralization, Timmins Area	318
York, D., Masliwec, A., Hall, C.M., Kuybida, P., Kenyon, W.J., Spooner, E.T.C., and Scott, S.D., Grant 62 The Direct Dating of Ore Minerals	334

Introductory Remarks

The Ontario Geoscience Research Grants Program was initiated in early 1978 as a means of supporting mission-oriented research at Ontario universities to complement the work of the Ontario Geological Survey in response to the various issues within its mandate.

"To stimulate exploration for and facilitate sound planning in all matters related to mineral and other earth resources by providing an inventory and analysis of the geology and mineral deposits of Ontario."

The Grants Program is administered by a committee reporting to the Director of the Ontario Geological Survey and is made up of three representatives of the minerals industry, three representatives of the university community, four representatives of the Survey, and a chairman. Appointments of industry and Ontario university representatives are up to three years, renewable once. The members of the present committee are:

Dr. N. Paterson, Chairman	Paterson, Grant & Watson Ltd.
Dr. A. Becker	Questor Surveys Limited
S.N. Charteris	Falconbridge Nickel Mines Ltd.
Dr. J.H. Crocket	McMaster University
Dr. R.N. Farvolden	University of Waterloo
Dr. W.S. Fyfe	University of Western Ontario
Dr. G. Mannard	Texasgulf Inc.
Dr. V.G. Milne	Ontario Geological Survey
J.A. Robertson	Ontario Geological Survey
Dr. P.G. Telford	Ontario Geological Survey
Dr. I. Thomson	Ontario Geological Survey

The role of the committee is to receive, review, and rank proposals from research workers at Ontario universities with respect to scientific merit and relevance to the objectives and activities of the Ontario Geological Survey, and to recommend funding or rejection. A feature of the appraisal process is that each submission is referred by the committee to at least four geoscientists in industry, the university community, and/or government outside the Ontario Geological Survey, and one member of the Survey for critical review and comment to ensure the most thorough and objective appraisal possible. Proposals for projects up to three years duration are acceptable. Original and renewal applications must be submitted by November 15 preceding the fiscal year (April 1 - March 31) for which grants are awarded. Successful applicants are expected to submit a brief report for publication in an annual Summary of Research and to participate in an annual seminar to present the results of his/her research, to the community at large. Publication in scientific journals is encouraged, and a final report is required by the Ontario Geological Survey within six months of the termination of funding.

Six final reports on research projects partially or wholly funded under the Ontario Geoscience Research Grant Program in 1970-1980 have been placed on the Ontario Geological Survey Open File Report 5349, 1981. These reports are as follows:

- Grant 14: A Structural Analysis of the Central Part of the Shebandowan Metavolcanic-Metasedimentary Belt; W.M. Schwerdtner, University of Toronto.
- Grant 37: Engineering Properties of Sedimentary Rocks in Southwestern Ontario and on Manitoulin Island; P.P. Hudec, University of Windsor.
- Grant 42: Ages and Initial ^{87}Sr - ^{86}Sr Ratios from Alkalic Complexes of Ontario; K. Bell, Carleton University.
- Grant 47: Structural Fabric and Uranium Distribution in Shear-Zones Near Cardiff, Ontario; W.V. Fyson, University of Ottawa.
- Grant 48: Geology of the Jogran Disseminated Cu-Mo Deposit, Ryan Township, Ontario; G.A. Armbrust, University of Ottawa.
- Grant 70: Host Rock Alteration at the Silverfields Mine, Cobalt, Ontario; E.C. Appleyard, University of Waterloo.

This publication is the third annual Summary of Research, and presents brief descriptions of the projects funded for the fiscal year ending March 31, 1981. Of the 29 proposals approved for funding in 1980-1981, 19 were renewal projects.

UNIVERSITY	APPROVED		REJECTED	
Brock	(\$5,857)	1 project	(\$12,900)	1 project
Carleton	(\$23,395)	2 projects	(\$24,780)	1 project
Lakehead	(\$8,670)	1 project		0 projects
Laurentian	(\$47,207)	3 projects	(\$20,244)	1 project
McMaster	(\$21,200)	1 project		0 projects
Ottawa		0 projects	(\$65,980)	1 project
Queen's	(\$66,266)	3 projects	(\$12,635)	1 project
Toronto	(\$179,569)	10 projects	(\$95,459)	5 projects
Waterloo	(\$30,490)	2 projects	(\$43,091)	2 projects
Western	(\$93,295)	5 projects	(\$16,448)	1 project
Windsor	(\$23,919)	1 project	(\$32,224)	2 projects
TOTAL	(\$499,668)	29 projects	(\$323,681)	15 projects

New projects, initiated in fiscal 1980-1981 are as follows:

- Grant 75: Asbestos Fibre Degradation in Laboratory Solutions; H.W. Nesbitt, principal applicant, University of Western Ontario.
- Grant 76: Speciation of Free Gold in Glacial Overburden; I. Nichol, principal applicant, Queen's University.
- Grant 78: Terrain Characteristics and Physical Processes in Small Lagoon Complexes; R.W. Dalrymple, principal applicant, Brock University.
- Grant 80: Rare Earth Elements in Acid Volcanic Rocks; I.H. Campbell, principal applicant, University of Toronto.
- Grant 82: Structural Controls of Uranium Deposits, Bancroft-Goderham Area; W.M. Schwerdtner, principal applicant, University of Toronto.
- Grant 84: Sedimentology of the Matinenda Formation; A.D. Miall, principal applicant, University of Toronto.
- Grant 87: Stability of Compressed Shales in Ontario; J.C. Roegiers, principal applicant, University of Toronto.
- Grant 88: Metallogeny & Economic Potential of Western Lake St. Joseph Greenstone Belt; R.J. Shegelski, principal applicant, Lakehead University.
- Grant 92: Impact of Ground Water on Mining Activities in the Niagara Escarpment Area; J.E. Gale, principal applicant, University of Waterloo.
- Grant 96: Mineralization in the Whitewater Group, Sudbury Basin; D.H. Rousell, principal applicant, Laurentian University.

The undersigned would like to thank the chairman and the members of the committee for their hard work and participation in the program during the past year, and to the large number of dedicated scientists who gave freely of their time and expertise to review the proposals and provide objective appraisals to serve as a basis for selecting the projects reported on in this publication. The work of the individual researchers also is gratefully acknowledged, for it is only through their endeavours, and commitment to scientific excellence, that the objectives of the program can be achieved. Finally, special thanks are due to Ms. C. Collins, who served as Grants Administrator and Secretary.

E.G. Pye
 Director
 Ontario Geological Survey

1980-1981 Geoscience Research Grant Recipients

PRINCIPAL APPLICANT	UNIVERSITY	TITLE
Bell, K.	Carleton	Grant 38 Radon Decay Products and Uranium Exploration
Beswick, A.E.	Laurentian	Grant 54 Alteration in Precambrian Volcanic Rocks: Metallic Mineral Deposits
Campbell, I.H.	Toronto	Grant 80 Rare Earth Elements in Acid Volcanics
Crocket, J.H.	McMaster	Grant 49 Stable Isotope Studies, Gold Metallogeny, Timmins
Dalrymple, R.W.	Brock	Grant 78 Terrain Characteristics & Physical Processes in Small Lagoon Complexes
Dixon, J.M.	Queen's	Grant 68 Centrifuge Study of Archean Greenstone-Granite Gneiss Belts
Fyfe, W.S.	Western	Grant 56 Lode Gold Deposits in Felsic Igneous Intrusions
Fyfe, W.S.	Western	Grant 28 Mine Waste: Immobilization of U-Th-Ra by Mineralization
Gale, J.E.	Waterloo	Grant 92 Impact of Ground Water on Mining Activities in Niagara Escarpment Area
Hodder, R.W.	Western	Grant 55 Evolution of an Archean Felsic Volcanic-Plutonic Complex
Hodgson, C.J.	Queen's	Grant 11 Study of Gold Ore Formation at Red Lake
Hutchinson, R.W.	Western	Grant 27 Au, Ni & Cr Deposits in Ultramafic-Mafic Volcanic Rocks
Kenney, T.C.	Toronto	Grant 7 Horizontal Deep Drains to Stabilize Clay Slopes
Miall, A.D.	Toronto	Grant 84 Sedimentology of the Matinenda Formation
Naldrett, A.J.	Toronto	Grant 17 Platinum Group Elements in Magmatic Sulphide Deposits
Nesbitt, H.W.	Western	Grant 75 Asbestos Fibre Degradation
Nichol, I.	Queen's	Grant 76 Speciation of Free Gold in Glacial Overburden
Norris, G.	Toronto	Grant 19 Mesozoic Palynostratigraphy, Moose River Basin
Roberts, R.G.	Waterloo	Grant 32 Hydrothermal Alteration and Gold Vein Environments
Roegiers, J.-C.	Toronto	Grant 87 Stability of Compressed Shales in Ontario
Rousell, D.H.	Laurentian	Grant 96 Mineralization in the White Water Group – Sudbury Basin
Schwerdtner, W.M.	Toronto	Grant 82 Structural Controls of Uranium Deposits, Bancroft-Goderham Area
Shegelski, R.J.	Lakehead	Grant 88 Metallogeny & Economic Potential of Western Lake St. Joseph Greenstone Belt
Strangway, D.W.	Toronto	Grant 20 Magnetism & Stratigraphy in the Blake River Volcanics
Symons, D.T.A.	Windsor	Grant 5 Component Magnetization of Iron Formations and Deposits
Watkinson, D.	Carleton	Grant 46 Potential for Chromite Ore Deposits
West, G.F.	Toronto	Grant 8 Interpretational Support for Electromagnetic Prospecting
Whitehead, R.E.	Laurentian	Grant 30 Gold Exploration Using CO ₂ , H ₂ O and Alkali "Anomalies"
York, D.	Toronto	Grant 62 Direct Dating of Ore Minerals

Grant 17 Platinum Group Elements in Abitibi Komatiites Associated with Nickel Sulphide Deposits

Sarah-Jane Barnes, M.P. Gorton, and A.J. Naldrett

Department of Geology, University of Toronto

ABSTRACT

Platinum group element (PGE), gold, nickel, copper, cobalt and sulphur analyses have been carried out on 65 samples from four nickel-sulphide deposits of the Abitibi Belt. Fifty-one major and trace element analyses have been carried out on rocks (spinifex-textured flows) thought to represent liquids from these deposits in order to study the relationship between melt composition and PGE distribution patterns. Three of the deposits have PGE distributions normal for komatiites while one (Alexo) has a tholeiitic distribution. There appears to be no other difference between the spinifex-textured flows from the four deposits. This suggests that the difference in PGE pattern observed at the Alexo deposit is due to differentiation after the formation of the partial melt rather than different source material or different degrees of partial melting of the mantle.

INTRODUCTION

Recently the platinum group elements (Os, Ir, Ru, Rh, Pt, Pd) have attracted a fair amount of attention (Bird and Basset 1980; Blanders *et al.* 1980; Hetrogen *et al.* 1980; Crockett 1979; Green 1978; Himstra 1979, Hoffmann *et al.* 1979; Naldrett *et al.* 1979; Morgan and Wanderless 1979; Ross and Keays 1979). This interest is a result of (i) the economic importance of these elements—a better understanding of the geochemistry of the platinum group elements could assist in exploration programs, and (ii) the siderophile nature of these elements which means they can be expected to fractionate from the lithophile and chalcophile elements during petrogenesis and hence they may illuminate some aspects of a rock's history that might otherwise remain obscure.

It has been noted (Hetrogen *et al.* 1980; Naldrett *et al.* 1979; Ross and Keays 1979) that rocks of the tholeiitic suite exhibit a fractionation of the PGE's, in order of melting point, from Os to Pd (Figure 1). Naldrett *et al.* (1979) used the $Pt + Pd / Ir + Ru + Os$ ratio to express this and noted that for tholeiites this ratio usually exceeds 12. As this ratio requires a complete PGE analysis it has been reduced here to the Pd/Ir for comparison with other worker's data. In Table 1 it can be seen that there is a gradation in Pd/Ir ratio from ~1 in ultramafic nodules and chondrites to 8-35 in komatiites to 20-220 in layered complexes.

It has been suggested by Naldrett *et al.* (1979) and Ross and Keays (1979) that this difference is a result of Ir being preferentially retained by olivine and that only at the high degrees of partial melting required to produce komatiites is the Ir released from the olivine. However,

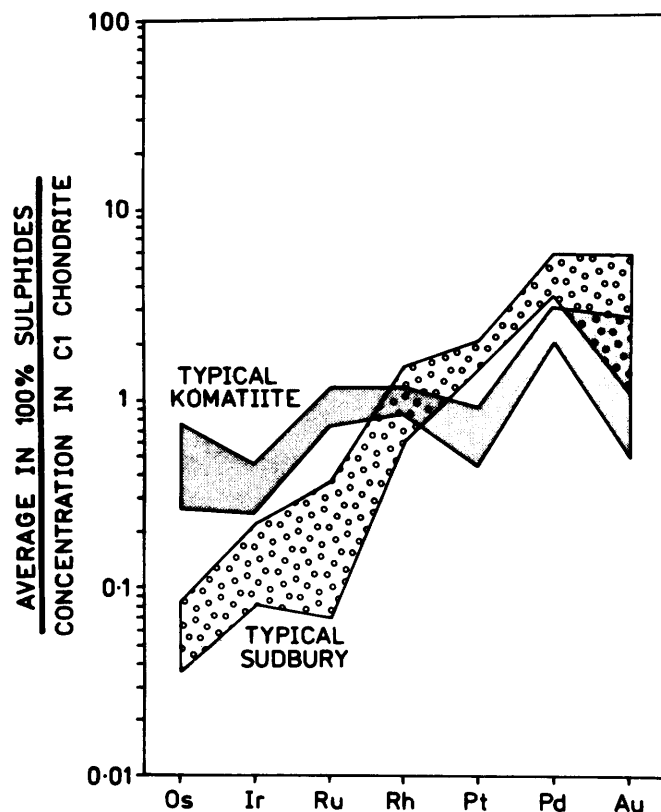


Figure 1—Plot of PGE content, chondrite-normalized, in 100 percent sulphides, against melting point order. This diagram illustrates the difference between the komatiite and tholeiitic (Sudbury) trend (after Naldrett *et al.* 1979).

work by Blanders *et al.* (1980), amongst others, documents the occurrence of Ir, Os and Ru as refractory metal alloys in meteorites. If these elements were present in alloy form in the mantle it is possible that they would remain in the restite (because of the high melting point of the alloys) during moderate partial melting, thus producing fractionated PGE patterns in tholeiites. However, at the high temperatures required to produce komatiites, the alloys melt producing flat patterns. Finally, many authors (Wolf and Agioritis 1978; Gibels *et al.* 1974; Crockett and Chyi 1972; Frominyki and Khvostova 1970) have documented the preferential inclusion of Ir in spinels which led Hetrogen *et al.* (1980) to postulate that chromite fractionation has led to the high Pd/Ir ratio they observed in mid-oceanic ridge basalts. Cousins and Vermaak (1976) pointed out that in the Bushveld Complex there is no correlation between Cr and Ir whereas there is a correlation between Ir and S. On this basis they argued that the platinum group elements found in chromites occur as base metal sulphide inclusions.

In order to test these hypotheses, four nickel-sulphide-bearing komatiites from the Abitibi Belt have been investigated. A suite of sulphide-bearing samples from each of four deposits were collected for PGE analysis, and samples of spinifex-textured flows were taken as close to the ore as possible. The authors believe that the spinifex-textured flows represent primary partial melt, and that the quantitative trace element data can be used to model conditions under which the silicates formed and hence to place restrictions on ore formation.

GEOLOGY

The four deposits under investigation are Alexo, Dundonald, Hart and Texmont. Their locations are shown in Figure 2. All four occur in komatiites which immediately overlie a major unconformity.

Table 1—Pd and Ir contents of mafic and ultramafic rocks.

Rock Type	Pd (ppb)	Ir (ppb)	Pd/Ir	Reference
Mantle nodules	2.8	3.9	0.71	Keays (pers. com.)
C1 Chondrites	545	504	1.1	Naldrett <i>et al.</i> (1980)
Alpine Peridotite	9.5	2.2	4.3	Crockett (1979)
Alaskan Zoned Complexes	28	8.5	3.3	Crockett (1979)
Komatiites				
Kambalda	10	1.2	8.3	Ross and Keays (1979)
Ora Banda	10.8	0.83	13	Ross and Keays (1979)
Munro Peridotites	10	1.1	9.1	Crockett (1979)
Fred's Flow	11	0.37	29.7	Crockett (1979)
Basaltic Komatiites	18	0.48	36.7	Bavington and Keays (1978)
Layered Complexes				
Skaergaard	17.5	0.26	67	Crockett (1979)
Bushveld	1573	21	21	Steele <i>et al.</i> (1975)
Stillwater	55	0.25	220	Crockett (1979)
Tholeiites				
Ocean Islands	10	0.20	50	Keays (pers. com.)
Ocean Ridge Basalt	1.76	0.042	41.2	Hetrogen <i>et al.</i> (1980)
Continental Flood Basalt	12	0.1	120	Keays (pers. com.)

ALEXO DEPOSIT

This section represents a summary of work by Coad (1977), Naldrett (1973), Pyke and Middleton (1970), and Naldrett and Mason (1968). The Alexo deposit occurs at the contact of peridotitic komatiite of the Munro Formation with andesitic pillow lavas possibly of the Hunter Mine Formation (Matheson area, Figure 3). Both are intruded by a differentiated tholeiitic sill (the Dundonald sill). The rocks dip steeply to the northwest. The strata have been folded into a syncline about a northeast-trending axis which plunges 55-75° southwest, and have possibly been refolded along northwest-trending open folds. Because there is little surface outcrop of the Alexo peridotite which hosts the sulphides it is unclear whether it is intrusive or extrusive.

The main ore minerals are pyrrhotite, pentlandite, hazelwoodite, chalcopyrite and violarite. The average analysis of the mixed ore (1914-1917) was Ni 4.69 percent, Co 0.23 percent, Cu 0.69 percent, Fe 40.25 percent, S 24.11 percent, (Pd + Pt) 0.81 ppm (Pullen 1949).

DUNDONALD DEPOSIT

The Dundonald deposit has been described by Naldrett (1964), Naldrett and Mason (1968), Eckstrand (1972, 1973), and Muir and Comba (1979). The following is a summary of these works.

The nickel sulphides occur at the base of peridotitic komatiite flows of the Munro Formation, overlying rhyolitic and andesitic pillowed flows possibly of the Hunter Mine Group. The area has been intruded by a differentiated tholeiitic sill (the Dundonald sill). The komatiitic rocks dip steeply northwest and appear to lie in the nose of an east-trending syncline.

The flows range in thickness from 1 to 30 m. Between flows are bands of volcano-sedimentary material; (tuff, graphitic and pyritiferous metasediments). Where sul-

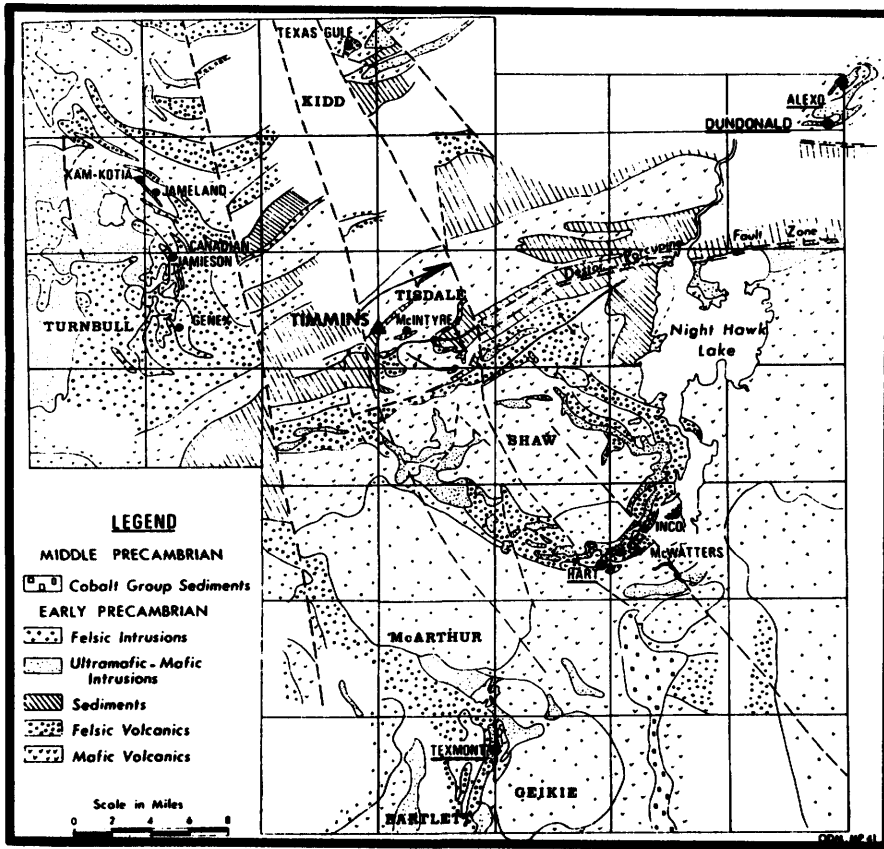


Figure 2—Location of the four nickel-sulphide deposits studied (after Pyke and Middleton 1970).

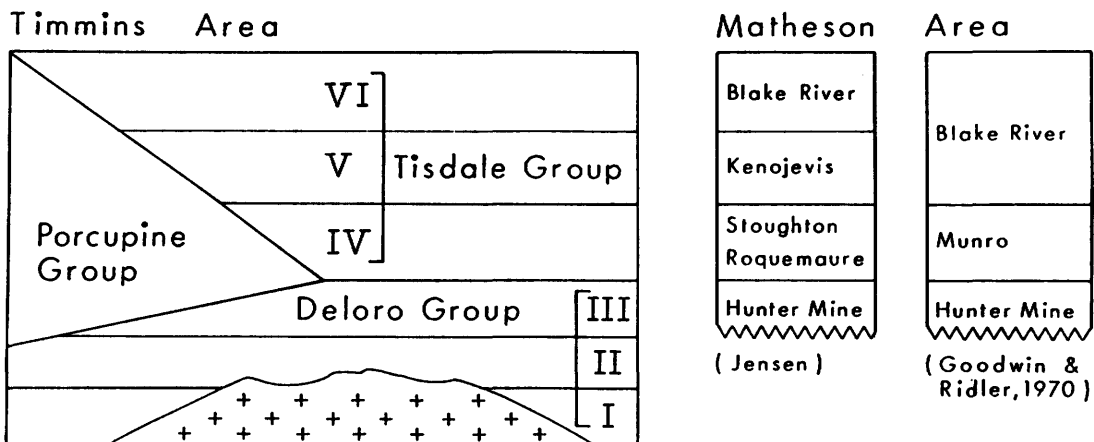


Figure 3—Stratigraphy of the Abitibi Belt (after Pyke 1978a).

phides are present, they occur at the base of flows and occasionally with graphitic material between flows. The sulphide mineralogy consists of pentlandite, hazelwoodite, millerite, godlevskite, maucherite, gersdorffite, sphalerite and chalcopyrite.

HART DEPOSIT

The Hart deposit has been described by Pyke and Middleton (1970), Muir (1975), Pyke (1975), and Coad (1977). Sulphides are located in the komatiites at the contact between the Tisdale Group and iron formation of the Deloro Group (see Figure 3). The iron formation pinches out at 150 m depth and below this the sulphides are located at the contact between komatiite and agglomerate. The deposit is located on the north limb of an easterly plunging syncline which has been refolded by broad open folds with axial planes trending to the northwest.

The komatiites consist of (i) a pyroxene-rich phase in contact with iron formation and agglomerate, (ii) peridotite which overlies the pyroxene-rich phase and contains the nickel sulphides, and (iii) olivine and pyroxene spinifex textured flows overlying the peridotite. The mineralized zone is 200 by 9 m and plunges at 50° southeast, parallel to the axes of the open folds. Massive sulphides occur at the contact and these are overlain by disseminated material. The sulphide minerals are pyrite, pyrrhotite, pentlandite and chalcopyrite.

TEXMONT DEPOSIT

Previous work on the Texmont deposit includes that by Naldrett (1966), Shklanka (1969), Pyke and Middleton (1970), Eckstrand (1972, 1973), Eckstrand and Miller (1973), Pyke (1978b) and Coad (1977).

The deposit is located in peridotite and pyroxene komatiite of the Tisdale Group which are in contact with felsic tuff, volcanic breccia and iron formation of the Deloro Group (see Figure 3). Both sequences have been intruded by gabbro dikes. The rocks form a steeply dipping, east-facing sequence on the western limb of a north trending syncline.

The ore is present in six zones, possibly at the base of flows. The mineralization takes the form of disseminated sulphides in both the cumulate- and spinifex-textured rocks. Sulphides also occur as colliform balls in the interflow carbon-rich sedimentary rocks. The sulphide mineralogy consists of pentlandite, pyrrhotite, millerite, hazelwoodite, pyrite and chalcopyrite.

PLATINUM GROUP ELEMENT ANALYSES

Sixty-five new platinum group element analyses have been completed. The averages for each deposit are presented in Table 2a. These averages have then been recalculated to the concentrations expected if the samples

contained 100 percent sulphide and are presented in Table 2b; Table 2c contains data from other deposits for comparison. The purpose of the calculation is to eliminate the effect of variations in the sulphide content since the sulphides are believed to contain all the PGE's in the rock. The sulphide recalculation does not affect inter-element ratios so that the deposits may be compared with non-sulphide-bearing rocks by means of ratios.

As mentioned in the introduction, PGE's are more fractionated with respect to each other in tholeiites than in komatiites. This is expressed in the high Pd/Ir ratios observed in tholeiites and in the steep chondrite-normalized PGE patterns observed in tholeiites (see Figure 1 and Table 1). The average Pd/Ir for each deposit is shown in Table 2a and Figure 4 presents the chondrite-normalized PGE patterns for each deposit.

At the Dundonald deposit two types of nickel sulphide ore are present: (i) disseminated sulphides within peridotite; and (ii) massive sulphides in graphite-rich layers of interflow material. The PGE patterns indicate that there is no significant difference between the two ore types in level or shape. Pd/Ir ratios are 9.2 and 10 respectively in the two ore types, confirming Muir and Combra's (1979) suggestion that the graphitic ore is of the same origin as the peridotitic type. The shape of the Dundonald PGE curves and Pd/Ir ratio of 9.5 are typically komatiitic although the level is slightly higher.

The Hart and Texmont PGE curves are typically komatiitic in shape and level while the Pd/Ir ratios of 10.5 and 6.07 respectively are close to normal komatiitic ratios.

The Alexo deposits, however, present a different picture. The refractory metals (Os, Ir, Ru) are depleted relative to normal komatiite levels. In fact the Alexo curves fall in the typical Sudbury (tholeiitic) field. At the main pit the Pd/Ir ratio is 63.8 and at the small pit it is 21 which is much higher than in normal komatiite-related deposits. Figure 5 is a plot of Ni/Cu ratios versus Pd/Ir ratio from which it is evident that the Alexo deposit is depleted in Ni relative to the other deposits studied but is not depleted in Ni relative to the Australian komatiites. The Alexo deposits fall off of the komatiite and tholeiite trends on this diagram, having a Ni/Cu ratio appropriate to komatiites and a Pd/Ir ratio of tholeiites. In the komatiite field there is no obvious relationship between the Pd/Ir and Ni/Cu ratios, however in the tholeiitic field there appears to be a negative correlation between Pd/Ir and Ni/Cu ratios. Possibly the Alexo deposits developed as normal komatiites which then underwent the same process of fractionation of Ir from Pd that the tholeiites experienced.

SILICATE GEOCHEMISTRY

As mentioned in the introduction, at each deposit spinifex-textured flows were sampled as close to the ore zone as possible. At Dundonald, Hart and Texmont the spinifex-textured flows actually had sulphides developed at the base. At Alexo the olivine spinifex zone south of the main pit was sampled and, since this zone is not in direct

Table 2—Average abundances of platinum group elements and chalcophile elements in nickel sulphide deposits

A. DEPOSITS STUDIED IN 1980-1981 (this paper)													
Deposit	no. of analyses	Ni (wt. %)	Cu (wt. %)	Co (wt. %)	S (wt. %)	Pt (ppb)	Pd (ppb)	Rh (ppb)	Ru (ppb)	Ir (ppb)	Os (ppb)	Au (ppb)	Pd/Ir
Alexo Main Pit	11	1.48	0.11	0.0314	10.11	180	530	36	54	8.3	3.1	126	63.8
Alexo Small Pit	9	0.29	0.042	0.021	6.7	88	122	11.4	24	5.8	7	14.3	21
Dundonald Peridotitic	10	1.42	0.023	0.03	1.79	200	184	32	73	2.0	29	15	9.2
Dundonald Graphitic	10	1.69	0.03	0.053	1.54	208	251	35	89	25	39	74	10
Hart	8	0.865	0.0275	0.0257	9.56	55	126	30	36	12	17	16	10.5
Texmont	17	1.92	0.017	0.045	2.64	107	158	30.9	91	26	51	67.5	6.07

B. 1980-1981 RESULTS RECALCULATED TO 100% SULPHIDES													
Alexo Main pit	—	4.83	0.359	0.102	—	587	1730	117	176	27	10	411	—
Alexo Small pit	—	1.42	0.21	0.103	—	433	600	56	118	28	34	70	—
Dundonald Peridotitic	—	26.17	0.42	0.55	—	3687	3392	599	1345	368	534	276	—
Dundonald Graphitic	—	36.21	0.64	1.13	—	4457	5378	757	1907	535	836	1585	—
Hart	—	2.98	0.094	0.088	—	189.8	434	103	124	41	58	55	—
Texmont	—	24	0.21	0.56	—	1337	1975	386	1137	325	638	843	—

C. DEPOSITS STUDIED IN 1979-1980 RECALCULATED TO 100% SULPHIDES (Naldrett <i>et al.</i> 1980)													
Strathcona													
Main Zone	18	3.37	1.24	—	0.138	410	380	20	12	7	4	78	—
Hanging Wall	10	3.10	0.37	—	0.208	115	110	60	52	29	20	19	—
Deep Zone	8	4.03	2.28	—	0.130	750	700	16	<4	4	<3	112	—
Cu Ore	1	0.51	32.32	—	0.097	137	40	<3	<5	0.2	<3	13	—
Strathcona Ave.		3.44	1.23	—	0.156	400	380	30	21	12	8	69	—
Falconbridge	23	5.35	1.52	—	0.216	550	380	280	230	140	38	180	—
Great Lakes	29	5.23	9.76	—	0.193	5580	22 440	600	310	74	120	2590	—
Kenbridge	7	8.58	2.32	—	0.210	790	280	30	16	15	17	675	—
Kanichee	13	6.75	8.63	—	0.277	1 3920	4790	430	340	360	300	510	—
Lac Des Iles	25	17.8	12.8	—	0.4	90 200	1 590 000	1100	<300	40	<200	68 000	—
Alexo	15	7.79	0.53	—	0.202	1530	4070	160	240	37	28	290	—
McWatters	5	21.0	0.52	—	0.320	1130	2390	730	1470	560	530	160	—
Werner Lake	4	8.32	1.31	—	0.240	1900	7850	630	700	150	340	320	—
Port Coldwell													
Coubran	8	1.40	14.9	—	0.33	7400	27 060	353	<84	33	<70	3550	—
Middleton	3	0.37	9.11	—	0.14	149	86	32	<42	2	<28	294	—
C1 Chondrites	—	—	—	—	—	1020	545	200	690	514	540	152	—

contact with the ore-bearing peridotite, samples of the latter were also analysed (these samples are designated AXC in Table 3). Table 3 contains the major and trace element analyses of 51 samples from the four deposits. The samples thought to represent liquids resemble undepleted komatiites in composition (Nesbitt *et al.* 1979) in that they are characterized by close to chondritic ratios for $Al_2O_3/TiO_2 \approx 20$, $Ti/Sc \approx 78$, $Hf/Sc \approx 0.0175$, $Zr/Hf \approx 40$, $Sc/Y \approx 3.6$, $Hf/TiO_2 \approx 1.36$, $Hf/Y \approx 0.063$ and a CaO/Al_2O_3 ratio slightly above chondritic at ~ 0.9 . The rocks are all mildly depleted in light rare-earth elements (LREE) with Ce/Yb chondrite normalized ratios of 0.6 ± 0.1 and Sm/Lu chondrite normalized ratios of 0.8 ± 0.1 . If the A_2 zones of ultramafic flow units (Pyke *et al.* 1973) are accepted as representative of the melt composition, estimates of the MgO content of the melts can be made for

the four deposits. At Alexo the melt composition would be ≈ 29 percent MgO. At Dundonald the average melt composition based on three flows would be ≈ 26 percent MgO. At Hart the average melt composition based on three flows is ≈ 23 percent. The average of the three Texmont A_2 zones is 25 percent MgO.

The chondrite-normalized values for the heavy rare earth elements (HREE) from spinifex-textured flows cover a similar range at all four deposits: Alexo (2-6); Dundonald (3-7); Hart (2-7); and Texmont (2-6). As mentioned above, the Ce/Yb (chondrite-normalized) and Sm/Lu (chondrite-normalized) ratios are also similar for all four deposits. The chondritic Ti/Sc ratio and LREE depletion of these rocks suggests that neither garnet nor clinopyroxene was present in the restite of these melts.

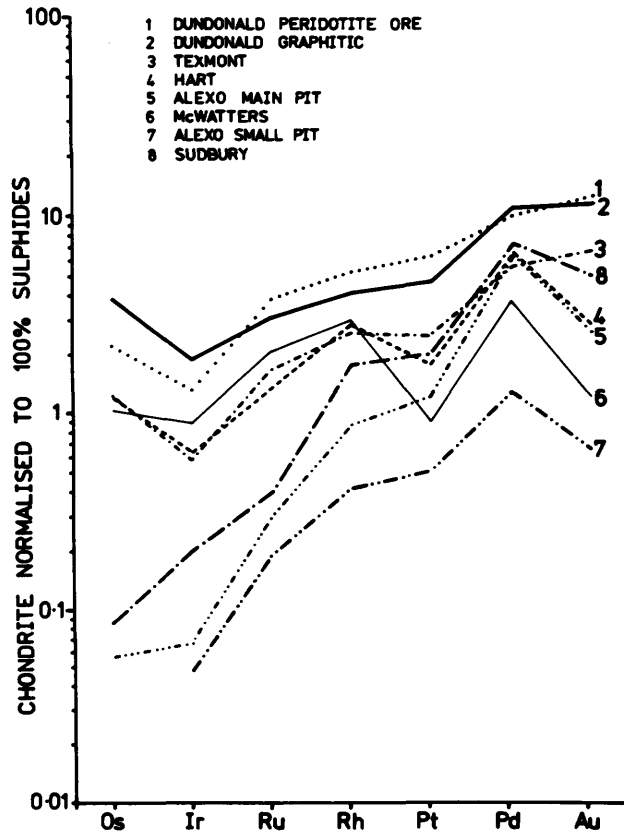


Figure 4—Plot of PGE content, chondrite-normalized, in 100% sulphides, against melting point order for the four deposits studied.

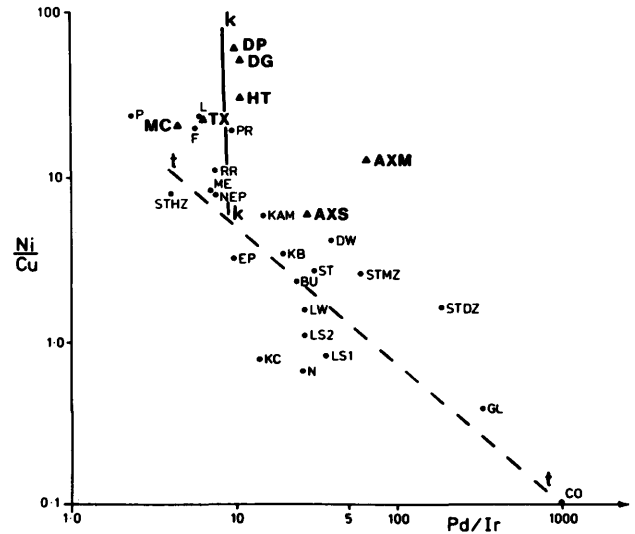


Figure 5—Ni/Cu vs. Pd/Ir for deposits studied and data obtained from the literature illustrating the trend from komatiites to tholeiites. Komatiites include AXM = Alexo main pit, AXS = Alexo small pit, DP = Dundonald peridotitic, DG = Dundonald graphitic, HT = Hart, MC = McWatters, TX = Texmont, L = Langmuir, F = Forrestania, PR = Perververance, RR = Red Ross, ME = Mt. Edward, NEP = Nepean, KAM = Kambalda. Tholeiites include STHZ = Strathcona Hanging wall, STMZ = Strathcona main zone, STDZ = Strathcona deep zone, ST = Ave. Strathcona, GL = Great Lakes, KB = Kenbridge, KC = Kanichee, P = Pipe, CO = Coubran, DW = Dundonald West, BU = Bushveld, LW = Levack West, LS1 = Little Stobie 1, LS2 = Little Stobie 2, N = Noril'ks, EP = Espedalen.

DISCUSSION

The lack of obvious difference between the level and shape of REE patterns from Alexo and the other three deposits suggests that all four have formed from similar degrees of partial melting of a similar mantle source. In fact the four deposits closely resemble each other in terms of their geochemistry except for the difference in PGE patterns at Alexo. This rules out the preferential retention of Ir by olivine in order to explain the PGE patterns at Alexo.

Such a retention is considered unlikely on crystal chemical grounds. Figure 6 shows a plot of experimentally determined partition coefficients for various elements between olivine and liquid against ionic radius and charge. From the curves defined by these experimental values an estimate of D values for the platinum group elements can be made (see Jenson 1973, for a full explanation) on the basis of their ionic radius and charge. The predicted D values for Pd and Ir in olivine are very similar and hence there is no reason to expect that Ir should be preferentially retained by olivine.

Table 3—Major and trace element abundances in komatiites adjacent to nickel sulphide deposits in the Abitibi Belt.

SAMPLE	ABITIBI KOMATIITES									
	AXC 5	AXC 12	AXC 18	AX 19	AX 20	AX 21	AX 22	AX 23	AX 24	AXC 26
SiO ₂	27.46	36.85	39.34	42.79	41.44	41.36	39.80	41.40	41.10	41.20
TiO ₂	0.13	0.23	0.21	0.44	0.30	0.30	0.30	0.32	0.26	0.31
AL ₂ O ₃	2.65	4.56	4.17	8.77	5.86	5.54	6.00	5.89	5.86	6.42
FE ₂ O ₃ *	22.48	14.46	11.17	12.24	10.40	8.94	10.47	10.43	10.98	17.32
MNO	0.17	0.19	0.20	0.20	0.16	0.17	0.18	0.17	0.16	0.13
MCO	22.18	27.85	30.57	20.33	28.58	27.31	26.11	28.10	28.21	20.18
CAO	2.76	3.91	4.14	7.82	5.33	8.04	6.01	5.27	5.51	7.65
NA ₂ O	0.03	0.04	0.04	0.16	0.06	0.26	0.02	0.04	0.26	0.10
K ₂ O	0.02	0.06	0.08	0.10	0.09	0.06	0.04	0.10	0.09	0.04
P ₂ O ₅	0.00	0.00	0.00	0.03	0.00	0.00	0.00	0.04	0.00	0.07
S	11.20	2.30	1.80	0.04	0.08	0.03	0.06	0.03	0.20	5.36
NI	1.42	0.46	0.48	0.06	0.14	0.17	0.12	0.16	0.18	0.28
CU	0.10	0.11	0.11	0.00	0.01	0.01	0.00	0.00	0.01	0.04
CR	0.30	0.04	0.05	0.27	0.25	0.26	0.26	0.24	0.25	0.23
H ₂ O	10.00	9.80	8.50	6.20	8.42	8.26	9.83	7.17	7.26	1.00
TOTAL	100.90	100.86	100.86	99.45	101.12	100.71	99.20	99.36	100.39	100.33
LA	0.49	0.60	0.55	0.89	0.59	0.56	0.48	0.49	0.45	0.66
CE	1.68	1.19	1.19	2.27	1.43	2.13	1.73	2.16	1.76	2.05
SM	0.35	0.41	0.42	0.88	0.62	0.66	0.60	0.62	0.58	0.67
EU	0.12	0.18	0.17	0.35	0.27	0.25	0.21	0.21	0.25	0.25
TB	0.09	0.11	0.11	0.27	0.14	0.18	0.17	0.18	0.19	0.16
HO	.	.	.	0.43	0.25	0.24	0.23	0.18	0.17	0.29
YB	.	0.46	0.42	1.18	0.66	0.80	0.83	0.75	0.82	0.86
LU	0.07	0.08	0.07	0.18	0.09	0.12	0.15	0.11	0.12	0.12
CO	431.00	155.00	170.00	88.00	102.00	108.00	100.00	96.00	105.00	241.00
SC	12.70	15.00	15.00	31.00	23.00	23.00	21.00	21.00	23.00	21.00
HF	0.33	0.35	0.36	0.71	0.37	0.44	0.38	0.48	0.41	0.47
SB	0.37	0.33	0.23	0.61	0.66	0.58	0.58	0.51	0.59	0.62
ZR	.	.	.	20.75	.	.	17.30	19.36	.	20.58
Y	5.50	5.50	5.59	9.83	6.85	6.62	6.64	5.56	6.20	6.29
SR	.	.	.	20.00	5.00	25.00	24.00	.	23.00	.
RB	.	.	.	3.00	3.81	4.50	3.80	1.50	1.00	.
TH
U
AL ₂ O ₃ /TiO ₂	20.3846	19.8261	19.8571	19.9318	19.5333	18.4667	20.0000	18.4063	21.0000	20.7097
CAO/AL ₂ O ₃	1.0415	0.8575	0.9928	0.8917	0.9096	1.4513	1.0017	0.8947	0.9371	1.1916
MG NO.	0.6612	0.7921	0.8441	0.7667	0.8446	0.8580	0.8315	0.8420	0.8356	0.6974
LA/LUN	0.7175	0.7688	0.8054	0.5068	0.6719	0.4783	0.3280	0.4566	0.3844	0.5637
CE/YBN	.	0.6667	.	0.4957	0.5583	0.6861	0.5371	0.7422	0.5531	0.6143
SM/LUN	0.8505	0.8718	1.0206	0.8316	1.1718	0.9355	0.6804	0.9587	0.8221	0.9497
HF/SC	0.0260	0.0233	0.0240	0.0229	0.0161	0.0191	0.0181	0.0229	0.0178	0.0224
ZR/HF	.	.	.	29.2254	.	.	45.5263	40.3333	.	43.7872
SC/Y	2.3091	2.7273	2.6834	3.1536	3.3577	3.4743	3.1627	3.7770	3.7097	3.3386
HF/TiO ₂	2.5385	1.5217	1.7143	1.6136	1.2333	1.4667	1.2667	1.5000	1.4643	1.5161
TI/SC	61.3559	91.9080	83.9160	85.0761	78.1826	78.1826	85.6286	91.3371	72.9704	68.4829
CO/SC	33.9370	10.3333	11.3333	2.8387	4.4348	4.6957	4.7619	4.5714	4.5652	11.4762
HF/Y	0.0600	0.0636	0.0644	0.0722	0.0540	0.0665	0.0572	0.0863	0.0661	0.0747
CR/TiO ₂	2.3077	0.1739	0.2381	0.6136	0.8333	0.8667	0.8667	0.7500	0.8929	0.7419
SAMPLE	AX 29	AX 45	AXC 58	AXC 56	AXC 57	AXC 55	AX 59	DU 6	DU 16	DU 20
SiO ₂	38.02	38.33	40.02	40.81	41.08	38.24	38.72	39.86	38.86	40.41
TiO ₂	0.32	0.15	0.33	0.28	0.38	0.21	0.19	0.24	0.24	0.23
AL ₂ O ₃	6.26	2.88	7.31	5.48	7.28	4.01	3.71	4.59	4.59	4.51
FE ₂ O ₃ *	21.96	7.74	14.41	13.07	11.95	11.98	8.23	10.41	10.41	9.37
MNO	0.15	0.10	0.21	0.17	0.17	0.15	0.14	0.22	0.22	0.17
MCO	18.43	36.80	21.01	27.36	23.54	31.04	34.43	30.94	31.52	31.41
CAO	7.68	0.49	8.05	5.03	6.88	3.15	2.40	2.86	2.87	3.15
NA ₂ O	0.03	0.05	0.03	0.03	0.04	0.04	0.04	0.05	0.09	0.05
K ₂ O	0.04	0.01	0.05	0.03	0.04	0.04	0.06	0.06	0.06	0.10
P ₂ O ₅	0.06	0.00	0.03	0.01	0.03	0.02	0.02	0.01	0.01	0.02
S	4.48	0.56	0.56	.
NI	0.25	0.60	0.60	0.22
CU	0.04	0.01	0.01	.
CR	0.36	0.18	0.28	0.25	0.27	0.32	0.16	0.51	0.16	0.26
H ₂ O	1.62	14.42	7.37	7.44	9.43	9.20	12.40	11.62	12.18	11.50
TOTAL	99.70	101.15	99.10	99.96	101.09	98.40	100.50	102.54	102.38	101.44
LA	1.23	0.45	0.74	0.48	1.01	0.60	0.43	0.50	0.72	0.53
CE	2.90	1.23	1.98	1.18	2.20	1.51	1.08	.	1.74	1.34
SM	0.94	0.29	0.61	0.51	0.72	0.36	0.37	0.57	0.59	0.50
EU	0.33	0.11	0.22	0.23	0.23	0.14	0.11	0.20	0.20	0.23
TB	0.26	0.09	0.14	0.15	0.20	0.10	0.09	.	0.13	0.15
HO	0.31	0.24	.
YB	1.12	0.34	0.79	0.69	0.88	0.49	0.42	0.66	0.64	0.71
LU	0.17	0.06	0.13	0.11	0.15	0.08	0.07	0.11	0.10	0.11
CO	141.00	103.00	164.00	126.00	103.00	122.00	96.00	200.00	202.00	106.00
SC	22.00	12.00	27.00	22.00	29.00	17.50	14.24	9.20	9.19	22.00
HF	0.47	0.13	0.42	0.26	0.44	0.28	0.23	0.26	0.38	0.37
SB	0.45	0.46	0.45	0.42	0.43	0.45	0.44	0.26	0.67	0.64
ZR	19.54	11.54	5.01	.
Y	5.61	4.94	2.91	4.76
SR	2.38	7.80	1.00
RB	6.19	.	7.00
TH
U
AL ₂ O ₃ /TiO ₂	19.5625	19.2000	22.1515	19.5714	19.1579	19.0952	19.5263	19.1250	19.1250	19.6087
CAO/AL ₂ O ₃	1.2268	0.1701	1.1012	0.9179	0.9451	0.7855	0.6469	0.6231	0.6253	0.7073
MG NO.	0.6241	0.9039	0.7426	0.8055	0.7958	0.8368	0.8922	0.8547	0.8565	0.8690
LA/LUN	0.7416	0.7687	0.5835	0.4473	0.6902	0.7688	0.6296	0.4659	0.7380	0.4939
CE/YBN	0.6673	0.9323	0.6459	0.4407	0.6442	0.7941	0.6627	.	0.7006	0.4864
SM/LUN	0.9406	0.8221	0.7982	0.7886	0.8165	0.7655	0.8991	0.8814	1.0036	0.7732
HF/SC	0.0214	0.0108	0.0156	0.0118	0.0152	0.0160	0.0162	0.0283	0.0413	0.0168
ZR/HF	41.5745	44.3846	13.1842	.
SC/Y	3.9216	1.8623	3.1581	4.6216
HF/TiO ₂	1.4687	0.8667	1.2727	0.9286	1.1579	1.3333	1.2105	1.0833	1.5833	1.6087
TI/SC	87.1855	74.9250	73.2600	76.2873	78.5421	71.9280	79.9761	156.3652	156.5354	62.6645
CO/SC	6.4091	8.5833	6.0741	5.7273	3.5517	6.9714	6.7416	21.7391	21.9804	4.6182
HF/Y	0.0838	0.0526	0.1306	0.0777
CR/TiO ₂	1.1250	1.2000	0.8485	0.8929	0.7105	1.5238	0.8421	2.1250	0.6667	1.1304

Table 3—continued.

SAMPLE	DU 21	DU 22	DU 23	DU 28	DU 29	DU 30	DU 40	DU 41	HT 16	HT 10
S102	39.46	42.13	41.10	40.25	41.28	39.91	41.29	42.21	38.48	37.46
T102	0.24	0.32	0.27	0.26	0.39	0.35	0.40	0.34	0.14	0.13
AL203	5.11	6.47	5.57	4.91	8.19	7.10	7.84	6.79	2.54	2.50
FE203*	10.11	11.07	10.51	9.89	11.47	10.87	11.26	10.43	9.10	10.30
MNO	0.21	0.18	0.22	0.23	0.22	0.18	0.15	0.08	0.12	0.13
MCO	29.59	26.69	28.43	31.23	22.32	24.42	23.70	27.52	32.06	32.58
CAO	3.32	6.38	4.79	2.92	10.33	8.58	7.50	3.72	2.96	2.60
MA20	0.10	0.04	0.10	0.04	0.05	0.05	0.03	0.05	0.02	0.02
K20	0.05	0.04	0.07	0.07	0.05	0.07	0.05	0.05	0.06	0.04
P205	0.00	0.03	0.02	0.02	0.03	0.00	0.04	0.04	0.02	0.02
S	1.16	0.95	1.14	1.10
NI	0.21	0.10	0.23	0.22	.
CU	0.01	0.01	0.01	.
CR	0.13	0.21	0.21	0.22	0.24	0.30	0.25	0.24	0.17	0.39
H2O	10.46	8.84	8.85	11.35	6.60	8.07	7.08	8.36	13.60	13.17
TOTAL	98.99	102.40	100.14	101.39	101.17	99.90	100.86	101.02	100.64	100.84
LA	1.18	1.31	0.66	0.74	0.92	1.22	0.85	1.11	0.47	0.63
CE	1.54	2.09	2.00	1.95	2.40	2.40	2.70	2.10	1.09	0.50
SM	0.55	0.72	0.55	0.48	0.85	0.76	0.96	0.72	0.29	0.21
EU	0.21	0.24	0.20	.	0.31	0.31	0.44	0.28	0.11	.
TB	0.12	0.17	0.17	.	.	0.22	0.26	0.21	0.08	.
HO	0.28
YB	0.68	0.79	0.71	0.70	1.04	0.99	1.14	0.82	0.41	0.26
LU	0.10	0.15	0.12	0.12	0.18	0.17	0.21	0.14	0.06	0.03
CO	117.00	71.00	68.00	67.00	56.00	72.00	65.00	84.00	104.00	62.00
SC	20.20	23.50	21.00	19.00	26.00	26.00	32.00	26.00	11.00	10.00
HF	0.37	.	0.52	.	0.43	0.44	0.45	0.44	.	.
SB	0.74	0.49	0.59	0.57	0.66	0.49	0.55	0.49	0.67	0.75
ZR	.	.	15.00	.	20.00
Y	5.09	7.03	5.10	4.60	8.50	8.40	9.20	7.30	2.50	2.70
SR	3.20	.	5.80	2.20	1.00	.	5.70	2.50	70.00	35.00
RB	8.50	5.50	8.40	8.80	5.80	2.20	2.70	3.70	1.40	1.00
TH
U
AL203/T102	21.2917	20.2188	20.6296	18.8846	21.0000	20.2857	19.6000	19.9706	18.1429	19.2308
CAO/AL203	0.6497	0.9861	0.8600	0.5947	1.2613	1.2085	0.9566	0.5479	1.1654	1.0400
MG NO.	0.8527	0.8267	0.8426	0.8620	0.7938	0.8163	0.8064	0.8392	0.8745	0.8637
LA/LUN	1.2095	0.8952	0.5637	0.6321	0.5239	0.7356	0.4149	0.8127	0.8029	2.1525
CE/YBN	0.5836	0.6818	0.7259	0.7179	0.5947	0.6247	0.6103	0.6600	0.6851	0.4956
SM/LUN	0.9355	0.8165	0.7796	0.6804	0.8032	0.7604	0.7776	0.8748	0.8221	1.1907
HF/SC	0.0183	.	0.0248	.	0.0165	0.0169	0.0141	0.0169	.	.
ZR/HF	.	.	28.8462	.	46.5116
SC/Y	3.9686	3.3428	4.1176	4.1304	3.0588	3.0952	3.4783	3.5616	4.4000	3.7037
HF/T102	1.5417	.	1.9259	.	1.1026	1.2571	1.1250	1.2941	.	.
TI/SC	71.2158	81.6204	77.0657	82.0232	89.9100	80.6885	74.9250	78.3831	76.2873	77.9220
CO/SC	5.7921	3.0213	3.2381	3.5263	2.1538	2.7692	2.0313	3.2308	9.4545	6.2000
HF/Y	0.0727	.	0.1020	.	0.0506	0.0524	0.0489	0.0603	.	.
CR/T102	0.5417	0.6562	0.7778	0.8462	0.6154	0.8571	0.6250	0.7059	1.2144	3.0000
SAMPLE	HT 17	HT 18	HT 21	HT 22	HT 27	HT 28	HT 29	TX 21	TX 22	TX 23
S102	43.65	41.07	41.07	42.17	40.72	43.15	43.96	38.75	43.53	41.87
T102	0.32	0.42	0.42	0.41	0.52	0.33	0.39	0.11	0.38	0.38
AL203	6.13	7.43	7.79	7.36	8.84	5.93	7.55	2.30	7.83	8.02
FE203*	10.36	11.70	10.72	11.29	12.65	10.60	11.61	9.33	12.63	11.96
MNO	0.15	0.15	0.14	0.17	0.20	0.17	0.16	0.11	0.23	0.16
MCO	23.47	21.68	19.53	22.72	20.30	21.94	22.57	34.92	20.73	21.59
CAO	6.31	7.02	7.32	7.41	8.47	8.62	6.85	0.37	8.23	7.50
MA20	0.07	0.15	0.03	0.04	0.10	0.09	0.22	0.02	0.05	0.03
K20	0.04	0.05	1.00	0.04	0.08	0.04	0.14	0.01	0.06	0.04
P205	0.00	0.03	0.02	0.04	0.03	0.04	0.06	0.00	0.04	0.06
S	0.43	0.02	0.08
NI	0.40	0.14	0.12
CU	0.04	.	0.01
CR	0.23	0.26	0.19	0.32	0.26	0.22	0.29	0.15	0.42	0.27
H2O	8.67	8.17	11.52	7.86	7.26	7.84	7.93	14.50	5.66	5.93
TOTAL	99.40	98.13	99.75	99.83	99.43	98.97	101.73	101.44	99.97	100.12
LA	0.85	0.90	1.54	0.88	0.72	0.70	0.80	0.32	0.74	0.96
CE	1.71	2.73	3.34	2.58	2.09	2.39	2.19	2.25	2.25	2.80
SM	0.56	0.81	1.12	0.82	1.01	0.85	0.89	0.24	0.77	0.78
EU	0.22	0.31	0.45	0.29	0.37	0.30	0.33	0.10	0.34	0.30
TB	0.15	0.26	.	.	0.28	0.27	.	0.06	0.24	0.23
HO
YB	0.80	1.13	1.16	1.02	1.38	1.11	1.13	0.29	1.06	0.96
LU	0.12	0.19	0.18	0.17	0.21	0.18	0.17	0.04	0.16	0.16
CO	55.00	71.00	63.00	91.00	66.00	70.00	101.00	192.00	67.00	82.00
SC	20.00	30.00	25.00	27.00	34.00	29.00	29.00	10.00	30.00	28.00
HF	.	0.48	0.73	0.65	0.84	0.55	0.52	0.12	0.46	0.43
SB	0.48	0.65	0.64	0.66	0.47	0.67	0.57	.	0.65	0.51
ZR	17.00	20.00	26.00	21.00	22.00	20.00	25.00	2.80	20.00	16.00
Y	6.20	10.00	9.80	8.80	8.80	8.80	11.00	.	8.80	8.90
SR	48.00	39.00	56.00	27.00	16.00	21.00	22.00	.	4.50	6.20
RB	1.30	2.00	30.00	6.00	2.50	1.25	3.20	2.00	.	2.00
TH	0.11	.	.
U	1.00	.	.
AL203/T102	19.1563	17.6905	18.5476	17.9512	17.0000	17.9697	19.3590	20.9091	20.6053	21.1053
CAO/AL203	1.0294	0.9448	0.9397	1.0068	0.9581	1.4536	0.9073	0.1609	1.0511	0.9451
MG NO.	0.8176	0.7857	0.7828	0.7993	0.7605	0.8037	0.7936	0.8610	0.7646	0.7812
LA/LUN	0.7260	0.4855	0.8765	0.5306	0.3514	0.3986	0.4824	0.8200	0.4214	0.5467
CE/YBN	0.5508	0.6226	0.7420	0.6518	0.3903	0.5549	0.4994	.	0.5470	0.7516
SM/LUN	0.7938	0.7252	1.0584	0.8205	0.8181	0.8032	0.8905	1.0206	0.7276	0.7371
HF/SC	.	0.0180	0.0292	0.0241	0.0247	0.0190	0.0179	0.0120	0.0153	0.0154
ZR/HF	.	41.6667	35.6164	32.3077	26.1905	36.3636	48.0769	23.3333	43.4763	41.6605
SC/Y	3.2258	3.0000	2.5510	3.0682	3.8636	3.2955	2.6364	.	3.4091	3.1461
HF/T102	.	1.1429	1.7381	1.5854	1.6154	1.6667	1.3333	1.0909	1.2105	1.1316
TI/SC	95.9040	83.9160	100.6992	91.0200	91.6729	68.2076	80.6090	65.9340	75.9240	81.3471
CO/SC	2.7500	2.3667	2.5200	3.3704	1.9412	2.4138	3.4828	19.2000	2.2333	2.9286
HF/Y	.	0.0480	0.0745	0.0739	0.0955	0.0625	0.0473	.	0.0523	0.0483
CR/T102	0.7188	0.6190	0.4524	0.7895	0.5000	0.6667	0.7436	1.3636	1.1053	0.7105

Table 3—continued.

SAMPLE	TX 25	TX 26	TX 27	TX 28	TX 29	TX 30	TX 31	TX 36	TX 43	TX 44
SI02	46.39	42.64	37.22	39.34	39.33	37.17	36.43	42.47	44.28	43.76
TI02	0.30	0.40	0.19	0.14	0.17	0.13	0.13	0.33	0.42	0.16
AL2O3	6.06	8.66	4.24	2.86	3.09	2.45	2.62	7.06	8.75	3.85
FE2O3*	11.11	13.46	11.15	7.80	8.69	7.03	7.93	10.64	12.33	8.32
MNO	0.15	0.16	0.09	0.08	0.12	0.22	0.11	0.16	0.21	0.08
MCO	24.33	22.79	35.85	35.40	37.28	36.49	36.74	22.71	18.79	24.54
CAO	3.63	5.65	0.11	0.91	1.27	0.17	0.81	6.02	8.47	6.55
NA2O	0.02	0.03	0.04	0.03	0.13	0.80	0.02	0.02	0.44	0.04
K2O	0.02	0.05	0.02	0.02	0.02	0.05	0.01	0.05	0.18	0.00
P2O5	0.01	0.03	0.08	0.00	0.00	0.00	0.00	0.02	0.02	0.00
S	0.01	0.01	0.14	0.17	0.18	0.10	0.17	.	.	.
NI	0.13	0.13	0.18	0.11	0.19	0.20	0.20	0.13	0.11	0.03
CU	0.02	.	.	.
CR	0.14	0.16	0.21	0.27	0.21	0.15	0.18	0.26	0.21	0.34
H2O	9.00	8.62	12.81	12.26	8.41	14.27	13.29	9.28	5.73	11.29
TOTAL	101.30	102.79	102.33	99.39	99.09	101.23	98.66	95.17	99.94	96.96
LA	0.85	0.68	0.68	0.36	0.36	.	.	0.44	.	0.81
CE	2.41	2.76	1.32	1.45	1.11	.	.	1.28	2.17	0.31
SM	0.68	0.76	0.36	0.39	0.28	0.62	.	0.55	0.86	0.36
EU	0.23	0.27	0.18	0.14	0.92	.	.	0.23	0.37	0.18
TB	0.20	.	0.10	.	0.11	.	.	0.19	0.25	0.08
HO
YB	0.74	0.95	0.42	0.42	0.36	0.19	.	0.81	1.15	0.31
LU	0.13	0.18	0.08	0.06	0.06	0.05	.	0.13	0.17	0.05
CO	82.00	106.00	108.00	112.00	116.00	99.00	91.00	108.00	97.00	110.00
SC	25.00	51.00	22.00	11.00	20.00	15.00	18.00	27.00	33.00	13.00
HF	0.48	0.57	0.43	0.49	0.12
SB	0.51	0.51	0.61	0.70	0.57	0.55	0.55	0.43	.	0.41
ZR	.	18.00	.	12.00	10.00	5.00	5.30	.	.	.
Y	7.00	8.00	3.80	5.00	3.90	2.50	2.90	.	.	.
SR	2.00	52.00	5.00	.	4.00	.	3.10	.	.	.
RB	.	0.30	2.00	.	.	4.00
TH	0.12	0.13	.
U	0.89	1.25	1.74
AL2O3/TI02	20.2000	21.6500	22.3158	20.4286	18.1765	18.8462	20.1538	21.3935	20.8333	24.0625
CAO/AL2O3	0.5990	0.6524	0.0259	0.3182	0.4110	0.0694	0.3092	0.8527	0.9680	1.7013
MG NO.	0.8125	0.7701	0.8642	0.8998	0.8946	0.9155	0.9016	0.8085	0.7509	0.8537
LA/LUN	0.6702	.	0.8712	.	0.6150	.	.	0.3469	.	1.6605
CE/YBN	0.8393	0.7487	0.8099	0.8897	0.7946	.	.	0.4072	0.4863	0.2577
SM/LUN	0.8898	0.7182	0.7655	0.8292	0.7938	2.1092	.	0.7197	0.8605	1.2247
HF/SC	0.0192	0.0112	0.0159	0.0148	0.0092
ZR/HF	.	31.5789
SC/Y	3.5714	6.3750	5.7895	2.2000	5.1282	6.0000	6.2069	.	.	.
HF/TI02	1.6000	1.4250	1.3030	1.1667	0.7500
TI/SC	71.9280	47.0118	51.7664	76.2873	50.9490	51.9480	43.2900	73.2600	76.2873	73.7723
CO/SC	3.2800	2.0784	4.9091	10.1818	5.8000	6.6000	5.0556	4.6000	2.9394	8.4615
HF/Y	0.0686	0.0712
CR/TI02	0.4667	0.4000	1.1053	1.9246	1.2353	1.1538	1.3846	0.7879	0.5000	2.1250

SAMPLE	TX 47
SI02	37.47
TI02	0.19
AL2O3	4.12
FE2O3*	10.00
MNO	0.16
MCO	31.58
CAO	2.21
NA2O	0.03
K2O	0.00
P2O5	0.01
S	.
NI	0.28
CU	.
CR	0.24
H2O	13.25
TOTAL	99.54
LA	0.39
CE	1.01
SM	0.37
EU	0.09
TB	0.14
HO	0.36
LU	0.05
CO	116.00
SC	16.00
HF	0.15
SB	.
ZR	.
Y	.
SR	.
RB	0.09
TH	1.57
U	1.57
AL2O3/TI02	21.6842
CAO/AL2O3	0.5364
MG NO.	0.8620
LA/LUN	0.7995
CE/YBN	0.7230
SM/LUN	1.2587
HF/SC	0.0094
ZR/HF	.
SC/Y	0.7895
HF/TI02	71.1787
TI/SC	7.2500
CO/SC	7.2500
HF/Y	1.2632
CR/TI02	1.2632

Fe₂O₃* = all iron as Fe₂O₃
 . = no analysis available
 AXC = Alexo pit samples
 AX = alexo spinifex flow samples
 DU = Dundonald samples
 HT = Hart samples
 TX = Texmont samples
 Analyst S-J Barnes.

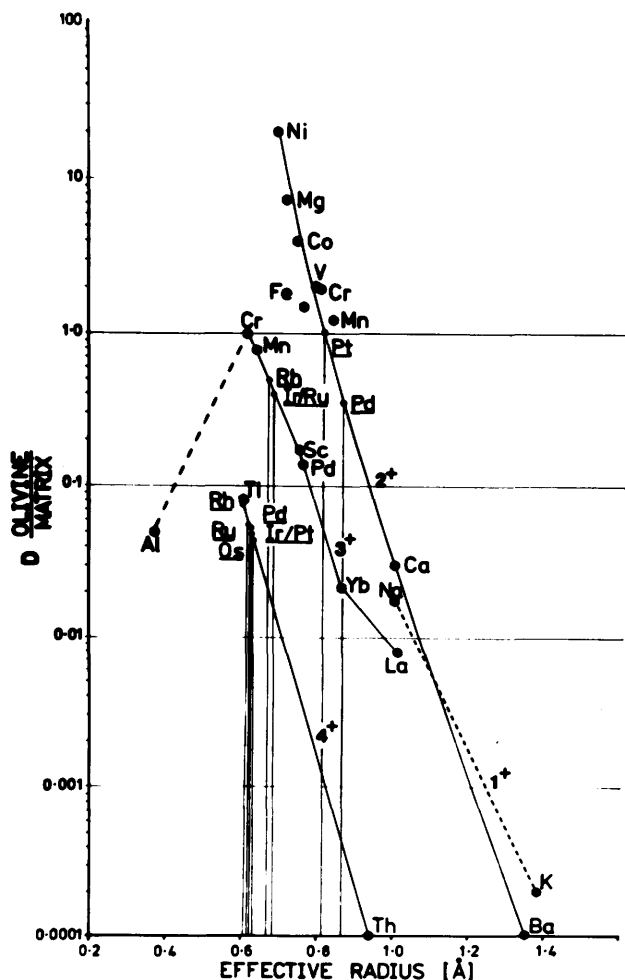


Figure 6—Plot of experimentally determined *D* values for olivine liquid against ionic radius and charge to estimate *D* values for the PGE's. After Naldrett et al. 1980.

The refractory metal theory would be consistent with the data only if the particular portion of the mantle which underwent melting to produce the Alexo deposits did not contain any refractory metals. There is no obvious justification for such an assumption.

The fact that Fred's Flow has a high Pd/Ir ratio (see Table 1) and that it is a differentiated komatiite suggests that possibly crystal fractionation is important in changing the ratio. In order to investigate the effects of crystal fractionation, regression lines for MgO and Al₂O₃, TiO₂, Sc, Yb, CaO were calculated. (The analyses were first recalculated on a water- and sulphur-free basis; these elements all exhibited a significant correlation with MgO at the 95 percent confidence level.) The rationale behind this approach is that for trends dominated by olivine fractionation it would be expected that elements not contained in olivine should cross the X-axis at the composition of the olivine crystallizing from the melt. Since the observed forsterite content of olivines from spinifex zones is 88-95, it would be expected that regression lines of elements not contained in olivine should cross the X-axis between MgO 47.3 percent and 53.3 percent reflecting these limits.

The intercepts obtained from Al₂O₃, TiO₂, Sc and Yb are similar for any one deposit although there is a difference between deposits. Table 4 lists the average for each deposit with error estimates. The intercepts are within the range quoted and hence are consistent with olivine fractionation. However CaO yields markedly lower intercepts (Table 4). The difference in the behaviour of Al₂O₃ and CaO is expressed by the CaO/Al₂O₃ ratio which decreases from ≈1 in the A zones (upper part) of flow units to ≈0.5 in the B zones (lower part) of the flow units (cumulate textures) (Table 3). This difference in behaviour rules out the crystallization of clinopyroxene as the source of the lower intercept for CaO. It is possible that during serpentinization of the B zone CaO is lost while in the A zones which typically experience less serpentinization CaO is retained.

There appears to be no significant correlation between Cr and MgO.

Table 4—Regression analysis of Al₂O₃, TiO₂, Sc, Yb, and CaO vs. MgO in komatiites.

Deposit	Intercept on MgO (wt. %) axis	
	Ave. Al ₂ O ₃ , TiO ₂ , Sc, Yb	CaO
Alexo Spinifex	53.95 ± 4	44.09 ± 2.3
Pits	46.21 ± 3	43.44 ± 1.3
Dundonald	51.08 ± 2	39.41 ± 0.91
Hart	45.13 ± 2	47.06 ± 2.1
Texmont	49.68 ± 4	42.91 ± 1.0

CONCLUSIONS

Of the four deposits investigated, three have normal komatiitic PGE distribution patterns while one (Alexo) has a tholeiitic PGE pattern. In terms of the major and trace element patterns of the spinifex-textured flows the Alexo deposit exhibits no obvious difference from the other three deposits. It is possible that the differences in PGE patterns is due to crystal fractionation of chromite. This hypothesis is presently under investigation.

REFERENCES

- Agiortitis, G., and Wolf, R.
1978: Aspects of osmium, ruthenium and iridium contents in some Greek chromites; *Chem. Geol.*, Vol. 23, p.267-272.
- Bavington, O.A., and Keays, R.R.
1978: Precious metal values from interflow sedimentary rocks from the Komatiite sequence at Kambalda, Western Australia; *Geochim. Cosmochim. Acta*, Vol. 42, p.1151-1163.
- Bird, J.M., and Basset, W.A.
1980: Terrestrial osmium-iridium-ruthenium alloys (Evidence for a deep mantle history); *Jour. Geophys. Res.*, Vol. 85, B10, p.5461-5470.
- Blanders, M., Fuchs, L.H., Horowitz, C., and Land, R.
1980: Primordial refractory metal particles in the Allende meteorite; *Geochim. Cosmochim. Acta*, Vol. 44, p.217-224.
- Coad, P.R.
1977: Nickel sulphide deposits associated with ultramafic rocks of the Abitibi Belt and economic potential of mafic-ultramafic intrusions; Ontario Geol. Survey Open File Report 5332.
- Cousins, C.A., and Vermaak, C.T.
1976: The contribution of South African ore deposits to the geochemistry of the platinum group metals; *Econ. Geol.* Vol. 71, p.287-305.
- Crockett, J.H.
1979: Platinum group elements in mafic and ultramafic rocks, a survey; *Canadian Miner.*, Vol. 17, p.391-402.
- Crockett, J.H., and Chyi, L.L.
1972: Abundances of Pd, Ir, Os and Au in an alpine ultramafic pluton; 24th Inter. Geol. Cong. Vol. 10, p.202-209.
- Eckstrand, R.
1972: Ultramafic flows and nickel sulphide deposits in the Abitibi Orogenic Belt, p. 75-81 *in* *Geol. Surv. Canada Paper 72-1*.
1973: Spinifex, ultramafic flows and nickel deposits in the Abitibi Orogenic Belt, p.111-128 *in* *Volcanism and Volcanic Rocks*, *Geol. Surv. Canada, Open File Report 164*.
- Eckstrand, R., and Miller, A.R.
1973: A study of sulphide and spinifex distribution of the Textmont nickel deposits; *Geol. Surv. Canada, Paper 73-1*, p.125-126.
- Frominyki, V.G., and Khvostova, V.P.
1970: Distribution of platinum metals in rock forming minerals of the Gusevogorskoye deposit; *Dok. Akad. Nauk. SSSR*, Vol. 200, p.443-445.
- Gibels, R.H., Millard, H.J., Desborough, G.A., and Bartel, A.J.
1974: Osmium, ruthenium, iridium and uranium in silicates and chromites from the eastern Bushveld Complex, South Africa; *Geochim. Cosmochim. Acta*, Vol. 38, p.319-337.
- Green A.H.
1978: Evolution of Fe-Ni sulphide ores associated with Archean ultramafic komatiites, Langmuir Township, Ontario; Unpublished Ph.D. thesis, Univ. Toronto.
- Hetrogen J., Janssen, M.J., and Palme, H.
1980: Trace elements in ocean ridge basalt glasses: implications for fractionation during mantle evolution and petrogenesis; *Geochim. Cosmochim. Acta.*, Vol. 44, p.2125-2143.
- Hemstra, S.A.
1979: The role of collectors in the formation of platinum deposits in the Bushveld Complex; *Canadian Mineral.* Vol. 17, p.469-482.
- Hoffman, E.L. Naldrett, A.J., Alcock, R.A., and Hancock, R.G.V.
1979: The noble-metal content of ore in the Levack West and Little Stobie Mines, Ontario; *Canadian Mineral.* Vol. 17, p.437-451.
- Jenson, B.
1973: Patterns of trace element partitioning; *Geochim. Cosmochim. Acta*, Vol. 37, p.2227-2242.
- Morgan, J.W., and Wanderless, G.A.
1979: Terrestrial upper mantle: siderophile and volatile trace element abundances; *Lunar Planet. Sci., Conf. X*, p.855-857.
- Muir, J.E., and Comba, D.A.
1979: The Dundonald deposit: an example of volcanic-type nickel-sulphide mineralization; *Canadian Mineral* Vol. 17, p.351-359.
- Muir, J.L.
1975: A petrological study of the ultramafic and related rocks of the Shaw Dome, S.E. of Timmins, Ontario; Unpub. M.Sc. thesis, Queen's University.
- Naldrett, A.J.
1964: Ultrabasic rocks of the Porcupine and related nickel deposits; Unpubl. Ph.D. thesis, Queen's University.
1966: The role of sulphurization in the genesis of iron-nickel sulphide deposits of the Porcupine District, Ontario; *Canadian Inst. Min. Metal. Trans.* Vol. 69, p.147-155.
1973: Nickel sulphide deposits, their classification and genesis, with special emphasis on deposits of volcanic association; *Canadian Inst. Min. Metal. Trans.* Vol. 76, p.183-201.
- Naldrett, A.J., and Mason, G.D.
1968: Contrasting Archean ultramafic igneous bodies in Dundonald and Clergue Townships, Ontario; *Canadian Jour. Earth Sci.*, Vol. 5, p.111-143.
- Naldrett, A.J., Hoffman, E.L., Green, A.H., Chen-Lin Chou, and Naldrett, S.R.
1979: The composition of Ni-sulphide ore, with particular reference to their content of PGE and Au; *Canadian Mineral.* Vol. 17, p.403-415.
- Naldrett, A.J., Innes, D.G., and Sowa, J.M.
1980: Platinum group element concentration in some magmatic ores in Ontario; Ontario Geol. Surv. Miscellaneous Paper 93, p.171-178.
- Nesbitt, R.W., Sun, S.S., and Purvis, A.C.
1979: Komatiites: geochemistry and genesis; *Canadian Mineral.* Vol. 17, p.165-186.
- Pullen, E.F.
1949: Notes on Alexo Nickel Mine, Porquis Junction, Ontario; Unpublished report for Alexo Mining Co.

GRANT 17 PLATINUM GROUP ELEMENTS IN ABITIBI KOMATIITES

- Pyke, D.R.
1975: Geology of Adams and Eldorado Townships, District of Cochrane; Ontario Div. Mines Geol. Rept. 121.
1978a: The geology of the Timmins area; Mineral. Assoc. Canada, Field Conference on nickel sulphide deposits, unpublished.
1978b: Geology of the Redstone River Area, District of Temiskaming; Ontario Div. Mines Geosci. Rept. 161.
Pyke, D.R., and Middleton, R.S.
1970: Distribution and Characteristics of the Sulphide Ores of the Timmins Area; Ontario Dept. Mines, Miscellaneous Paper 41, 24 p.
Pyke, D.R., Naldrett, A.J., and Eckstrand, O.R.
1973: Archean Ultramafic flows in Munro Township, Ontario; Geological Society of America Bulletin, Vol. 84, p.955-978.
- Ross, J.R., and Keays, R.R.
1979: Precious metals in volcanic type nickel sulphide deposits in Western Australia, 1. Relationship with the composition of the ores and their host rocks; Canadian Mineral. Vol. 17, p.417-435.
- Shklanka, R.
1969: Copper, nickel, lead and zinc deposits of Ontario; Ontario Dept. Mines, MRC 12.
- Steele, J.W., Levin, J., and Copelowetz, J.
1975: The preparation and certification of a reference sample of a precious metal ore; Nat. Inst. Met. Ref. 1696.
- Wolf, R., and Agioritis, G.
1978: On the unusual platinum element enrichment in chromites from Skyros Islands, Greece; Neus. Jb. Miner Monat, p.39-41.

Grant 82 Structural Controls of U-Ore Bodies in the Madawaska Mine Area, Bancroft, Ontario

R.L. Bedell and W.M. Schwerdtner

Department of Geology, University of Toronto

ABSTRACT

Ore-grade pegmatites in the Madawaska Mine area are confined to a deformed anorthositic gabbro complex, the Faraday Metagabbro Complex (FMC). The pegmatite bodies are largely undeformed. Locally the mineral fabric of the FMC is parallel to the pegmatite bodies. This evidence suggests that the pegmatite fluids intruded the FMC following a major deformation event, the Grenville Orogeny.

Prior to the Grenville Orogeny, the FMC intruded an ENE-trending metasedimentary sequence. Strained mafic minerals define a foliation that is broadly concordant to the outer arcuate contact of the FMC. It remains to be determined whether the arcuate geometry of the outer contact is due to the shape of the original intrusion or to subsequent deformation.

The majority of pegmatites at the Madawaska Mine are broadly concordant to the mineral fabric and therefore the outer arcuate contact of the FMC. It is apparent that the deformation of the FMC created structures that became paths of least resistance for the subsequent intrusion of pegmatites.

INTRODUCTION

Of the numerous uranium deposits in the Grenville Province of Ontario, the Madawaska Mine deposits are the only ones currently being mined. The Madawaska Mine originally started production in 1957 as the Faraday Mine and closed in 1964. It did not resume production until 1976 when it was reactivated by Madawaska Mines Limited. The ore minerals are predominantly uraninite-uranothorite plus accessories, and ore grade averages 0.07-1 percent U_3O_8 . The mill has a 1500 ton per day capacity and from 1976 to 1979 produced 1,717,048 pounds U_3O_8 . The concentrate is eventually shipped to Italy for use in reactors (R. Alexander, Chief Geologist, Madawaska Mines Limited, personal communication, 1980).

ORE-BEARING PEGMATITES

The ore is confined to pegmatite bodies and their immediate vicinity. These pegmatite bodies are relatively undeformed and are therefore considered to be later than

the peak of metamorphism during the Grenville Orogeny. They are mostly syenitic in composition and for the most part medium to coarse grained. Rarely do crystals reach the size of those in typical granitic pegmatites which have abundant quartz and contain crystals many centimetres in length. However, the compositions and textures of these rocks are still within the confines of the definition of pegmatite by Jahns (1955) as "holocrystalline rocks that are at least in part very coarse grained, whose major constituents include minerals typically found in ordinary igneous rocks, and in which extreme textural variations, especially in grain size, are characteristic."

The basic pegmatite mineralogy is microcline, albite, peristerite, alkalic pyroxene, and amphibole with sporadic occurrences of biotite, magnetite, and quartz. Accessories are apatite, titanite, tourmaline, and sulphides, including chalcopyrite, pyrite, pyrrotite, marcasite, and molybdenite. Calcite and anhydrite form well segregated masses both within and outside the pegmatite bodies. The anhydrite has been interpreted as being of magmatic origin (Little 1969).

The ore minerals are mainly uraninite-uranothorite with a U/Th ratio of approximately 2. Other radioactive species are thorite, kainosite, tritomite-(Y), allanite, and zircon. Back-scattered electron imaging studies (Rimsaite 1980) have found additional phases of fluorite, tin oxide, galena, and Fe-Si-U-Ca alteration compounds associated with the ore.

The pegmatites are relatively anhydrous, having little mica or significant zoning. In most areas, a detectable strain was imposed on the host rock during intrusion by the pegmatites which created a local foliation parallel to their lengths. These features suggest a tectonic style of intrusion by a relatively anhydrous and therefore viscous silicate melt.

All ore grade pegmatites contain deep red hematite staining, and there appears to be a correlation between grade and depth of colour (Alexander, personal communication, 1980). This appears to be a common feature of uranium-bearing pegmatites, but it has seldom been determined whether this is a pervasive ferruginous staining or an internal feature of the feldspar (Adams *et al.* 1980). At the Madawaska Mine the staining occurs as discrete particles of ferruginous material most commonly along twin planes in plagioclase.

The pegmatites have commonly been quenched against the mafic country rock, creating a sharp contact which contains higher grades of uranium ore. The effect

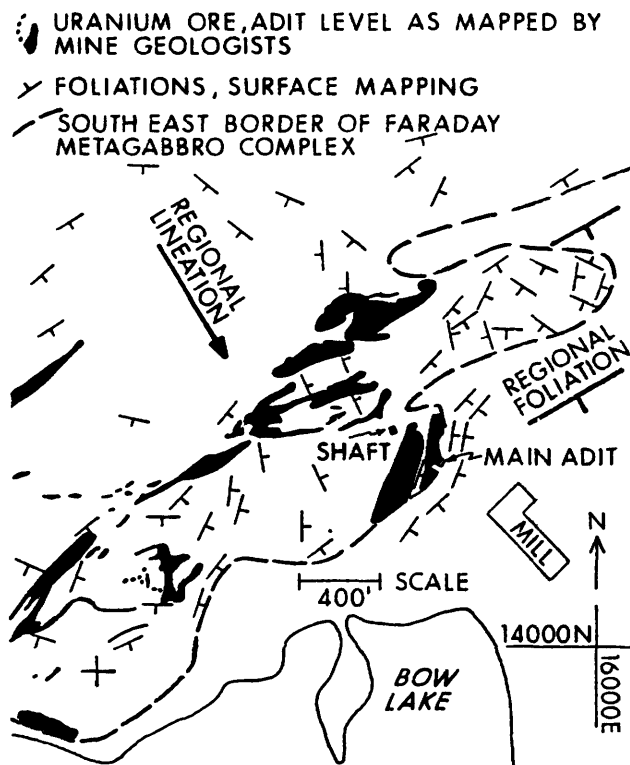


Figure 1—Southeast margin of the Faraday Metagabbro Complex showing surface foliations and adit level pegmatites.

is most pronounced where the dikes intrude the most mafic phases of the complex (gabbro).

STRUCTURAL GEOLOGY

The Madawaska Mine is bounded by two fault zones. The McArthur Mills fault zone extends approximately NE parallel to Highway 28. The Derry Lake fault zone strikes roughly east parallel to Monck Road just north of the FMC (Masson, in prep.).

Figure 1 represents surface mapping done in the 1980 field season (Bedell and Schwerdtner 1980). The pegmatites are those mapped at adit level by the mine geologists. The southeast boundary of the Faraday Metagabbro Complex (FMC) is shown and the ore is well confined within it. This relationship expresses the importance of the FMC to the formation of the ore. The FMC intrudes the dominantly ENE-trending metasediments which locally consist of marble and minor metasandstones. These metasediments occur as xenolithic sheets within the border of the FMC. Immediately outside the FMC, a zone of mylonitized marble and an adjacent unit of disharmonically folded metasandstone represent the severe

deformation suffered by the metasediments when the gabbro body intruded them. Also intruding the metasediments are conformable fine-grained gabbroic sills. Diopside-rich skarn assemblages have formed where the gabbroic sills are in contact with the marble.

Faulting occurs along lithologic contacts and the strain increases toward the McArthur Mills fault, as shown by an increase in foliations and slickensided surfaces. Also, the regional ENE fabric becomes gradually concordant toward the northeast-trending fault zone.

A regional lineation is present throughout all the local rocks and extends northward into the Algonquin Batholith (Schwerdtner and Lumbers 1980); in all of these rocks the level of strain and the attitudes of the lineation are similar. This could be due to diapirism of the batholith during the Grenville Orogeny (Schwerdtner and Lumbers 1980). The lineation dies out to the south and east of the McArthur Mills fault zone (S.B. Lumbers, Curator of Geology, Royal Ontario Museum, personal communication, 1980). Within the ENE-trending metasediments it occurs as a down dip lineation. Within the FMC it occurs as stretched ferromagnesian minerals. The lineations in the mine area strike dominantly $S 40 E \pm 10^\circ$ with plunges averaging 40° and ranging from 20° to 70° . The implications of this lineation are not fully understood at present, but it does exhibit important structural controls. To date, any folds delineated within the FMC are coaxial with the lineation. In addition, the prominent set of joints within the FMC are parallel to the strike of lineation (Figure 2).

Foliations within the FMC are also defined by strained ferromagnesian minerals. The boundary of the

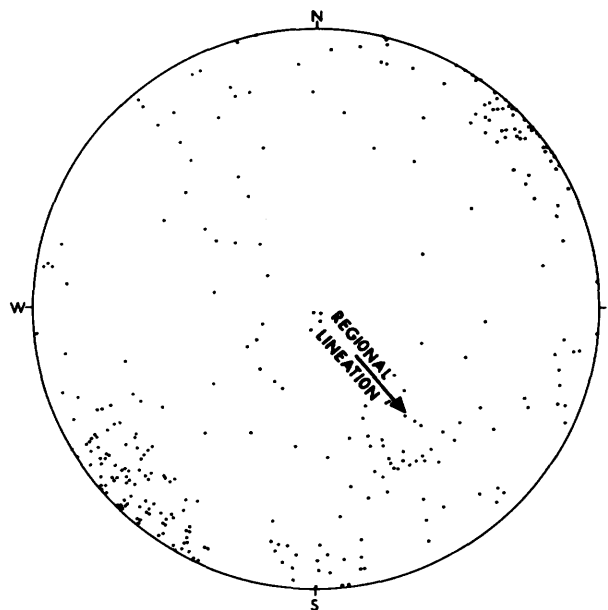


Figure 2—Stereonet showing how the major joint population of the FMC defines the same plane as the regional lineation.

FMC shows excellent foliation (see Figure 1), but this becomes less pronounced toward the center of the complex where lineation is the dominant strain feature. Foliation is also well developed parallel to the pegmatites. When these bodies intruded the complex, they produced a local foliation superimposed on the original fabric of the FMC. The foliations shown in Figure 1 were all measured during surface mapping; the FMC is a topographic high and therefore the fabric observed is above the adit-level pegmatites.

The textures and proportions of minerals within the FMC are variable and may be related to variations in strain. The least strained and metamorphosed portions of the complex consist of alkalic anorthositic gabbro. The plagioclase is andesine, the pyroxene is alkalic, and nepheline is present. With increase in strain, there is an increase in the reactions pyroxene→amphibole, and andesine→peristerite, and a general increase in amphibole and biotite. The increase in ferromagnesian minerals is similar to that found in the Algonquin Batholith by Lumbers, who also correlated strain with an increased bulk density of the rocks (Schwerdtner and Lumbers 1980).

The arcuate southeast border zone of the FMC features concordant foliations that are parallel to the pegmatite bodies. This relationship holds for all levels of the mine in the southeast border zone. This region of high strain presumably was created during intrusion of the FMC and became a preferred zone for pegmatite emplacement during late Grenville metamorphism. An alternative hypothesis is that these pegmatite bodies were emplaced prior to Grenville metamorphism and remained relatively undeformed because they acted as competent bodies while the gabbro around them deformed. This is at variance with regional geology and detailed structural observations (Figure 3).

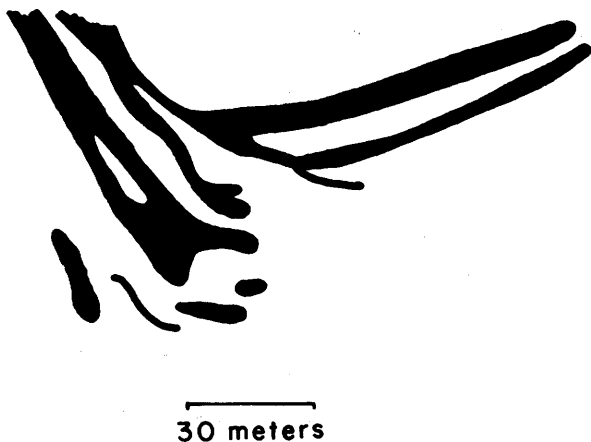


Figure 3—Plan view of pegmatite bodies as mapped by Madawaska Mine geologists on the 750-foot level. The curved and bifurcated portions of these bodies would be the most susceptible to deformation, but are undeformed.

Pegmatites within the central parts of the complex are not easily correlated with other structures. However, the general alignment of these pegmatites with the regional foliation is notable. We will be testing the hypothesis that a pre-existing regional ENE fabric influenced the synplutonic strain pattern of the gabbro. The alignment of the pegmatites may be related to that strain pattern.

CRYSTAL DEFORMATION MECHANISMS

Field observations suggest that the strain pattern of the FMC imposed a structural control on the subsequent emplacement of the pegmatite bodies. This macroscopic strain pattern and local strain intensity depend, in turn, on the crystal deformation mechanisms that operated during the structural evolution of the FMC.

In the past winter a petrographic study of the rock types was undertaken and particular attention was paid to deformation features of the various minerals. The least deformed portions of the FMC are composed of anorthositic gabbro. As the strain increases, andesine feldspar becomes more albitic in composition and alkalic pyroxene changes to alkalic amphibole and biotite.

Deformation microstructures have recently been examined in experimentally deformed Maryland diabase (Kronenberg and Shelton 1980) that closely resembles deformed rocks having similar composition and metamorphosed to upper greenschist to almandine-amphibolite facies. With an experimental strain rate of 3×10^{-6} /sec and a confining pressure of 15 kb, plagioclase was found to become weaker than pyroxene at temperatures greater than roughly 700°C. At much lower strain rates (geologically applicable) this transition occurs at somewhat lower temperatures. Therefore, under crustal conditions in which gabbro is ductile, plagioclase is relatively weaker than pyroxene. Heard and Raleigh (1972) have shown experimentally that less heat is needed at lower strain rates to produce a given amount of strain in ductile rocks.

Thin section examination of the Faraday metagabbro suggests that plagioclase was always weaker than pyroxene or amphibole. The petrographic criteria established in deformation experiments with diabase and used for the Faraday metagabbro are (i) fewer twins and (ii) a lower dislocation density in the pyroxenes. The ferromagnesian minerals of the FMC have little twinning and slight undulatory extinction in comparison to plagioclase. Therefore plagioclase is the rate controlling mineral and examination of its deformation mechanisms is most important.

Plagioclase shows a wide variety of plastic deformation features. At the beginning of plastic deformation (Figure 4) grains become undulatory due to the build up of dislocations. The start of subgrain formation is distinguished by domains of relatively straight extinction within an otherwise undulatory grain. Primary growth twins may have their lamellae bent into a broad arc. As deformation increases, grains become polygonized or more undulatory, subgrains become more evident and mechanical

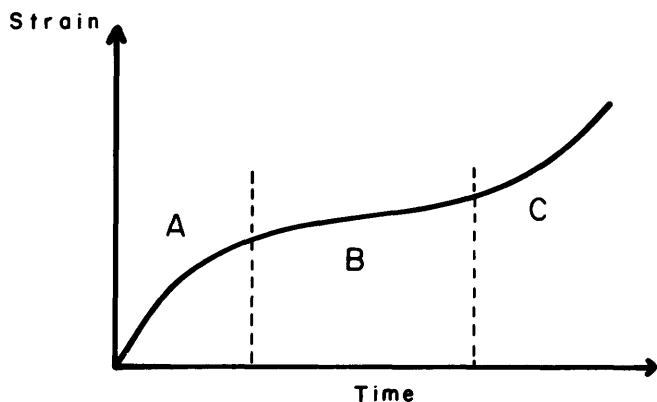


Figure 4—Stages of creep behavior. Zone A, transient creep; Zone B, steady-creep, recognized by subgrain formation and the onset of mechanical twinning; Zone C, accelerating (tertiary) creep, recognized by fracturing or recrystallization.

twins develop. Mechanical twins may be distinguished from earlier growth twins because they tend to form with a taper in order to minimize strain associated with the terminations at twin and grain boundaries (Hall 1954). As deformation increases further, more growth twins develop and several generations may be seen in the same grain. Often, intersecting periclinal and albite twins are found with later lamellae offsetting earlier ones.

The highly strained rocks of the FMC, with which many ore-grade pegmatite bodies are associated, were deformed under conditions near the upper boundary of steady-state creep or plastic deformation and within the field of accelerating (tertiary) creep (see Figure 4). This high level of crystal deformation is indicated by dynamic recrystallization. Subgrain formation reaches a point where further deformation is taken by a gradual disorientation of the subgrains. There is a certain degree of disorientation (10-15°) whereby subgrains are considered as new dislocation free grains (Nicolas and Poirier 1976, p.170). This is a domain in which recovery is less rapid than the strain rates, increasing the deformation energy to a point where recrystallization takes over. The recrystallized grains rapidly harden and the process starts again. Therefore, work expended hardening the grains alternates with dynamic recrystallization, observed experimentally as stress and strain oscillations (Nicolas and Poirier 1976, p.135-136).

Using these petrographic criteria we can distinguish rocks with different strain levels and understand the crustal deformation mechanisms. This summer (1981), we will be doing a routine statistical fabric and modal analysis to accompany the petrographic descriptions.

A problem in the analysis of strain is that varying amounts of strain observed in rocks may be due to either different conditions of stress, or simply to availability of water. As the rock becomes more strained there is an increase in hydrous ferromagnesian minerals. If more water

is readily available, that portion of the complex will undergo greater deformation (Griggs 1967).

CONCLUSIONS

Prior to the Grenville Orogeny, an alkalic anorthositic gabbro, the Faraday gabbro, intruded a regional ENE-trending sedimentary rock sequence. The Faraday gabbro complex was then subjected to high rank regional metamorphism (Grenville Orogeny) of upper amphibolite grade. During the later stages of metamorphism, pegmatite fluids intruded along paths of least resistance in the strained metagabbro complex.

Detailed knowledge of the structure and lithology of the Faraday Metagabbro Complex is vital to our understanding of the pegmatite emplacement distribution in the Madawaska Mine area. Structure and lithology also play an important geochemical role (Bedell, in prep.) Uraninite was preferentially precipitated at contacts with the most mafic phases of country rock (gabbro) or around xenoliths within the pegmatite (Alexander, personal communication, 1980).

The ore at the Madawaska Mine is associated with at least two periods of alteration (Alexander, personal communication, 1980). Given the susceptibility of uranium to remobilization in hydrothermal environments, the nonporous nature of the FMC must certainly have assisted in restricting the flow of pegmatite fluids during their intrusion, and also in retaining uranium throughout subsequent alteration events. These two features, i.e. (i) the steep geochemical gradient between pegmatitic dikes and mafic metagabbro, and (ii) the relatively low porosity, make the FMC a favorable host rock for uranium deposits.

REFERENCES

- Adams, J.W., Arengi, J.T., and Parrish, I.S.
1980: Uranium- and Thorium-Bearing Pegmatites of the United States; prepared for the United States Department of Energy, Grand Junction Colorado, 81501.
- Bedell, R.L.
in prep: Influence of a Metamorphosed Gabbro in the control of Uranium-Bearing Syenite—Pegmatite Dykes, Madawaska Mines, Bancroft, Ontario; Uranium in Granites, Special Paper, Geological Association of Canada.
- Bedell, R.L. and Schwerdtner, W.M.
1980: Structural Controls of U-Ore Bodies in the Madawaska Mines Area, Bancroft Ontario; Ontario Geological Survey, Geoscience Research Abstracts.
- Griggs, D.T.
1967: Hydrolitic Weakening of Quartz and Other Silicates; *Geophysical Journal of the Royal Astronomical Society*, vol. 14, p. 19-31.
- Hall, E.O.
1954: *Twinning and Diffusionless Transformation in Metals*; Butterworth, London.
- Heard, H.C. and Raleigh, C.B.
1972: Steady-State Flow in Marble at 500°C to 800°C; *Geological Society of America, Bulletin* Vol. 83, p. 935-956.

Jahns, R.H.

1955: The Study of Pegmatites; Economic Geology, 50th Anniversary Vol., Part II, p. 1025-1130.

Kronenberg, A.K. and Shelton, G.L.

1980: Deformation Microstructures in Experimentally Deformed Maryland Diabase; Journal of Structural Geology, Vol. 2, p. 341-353.

Little, H.W.

1969: Anhydrite-Pegmatite Uranium Ore at Bancroft Ontario; Economic Geology, Vol. 64, p. 691-693.

Masson, S.

in prep: Geology and Uranium-Thorium Mineralization in the Bancroft Area; Ontario Geological Survey, Preliminary Map.

Nicolas, A. and Poirier, J.P.

1976: Crystalline Plasticity and Solid State Flow in Metamorphic Rocks; John Wiley and Sons.

Rimsaite, J.

1980: Mineralogy of Radioactive Occurrences in the Grenville Structural Province, Bancroft Area, Ontario: A Progress Report; Geological Survey of Canada, Paper 80-1A, p. 253-264.

Schwerdtner, W.M. and Lumbers, S.B.

1980: Major Diapiric Structures in the Superior and Grenville Provinces of the Canadian Shield; Geological Association of Canada, Special Paper 20, p. 149-179.

Grant 38 Radon Decay Products and Uranium Exploration

Keith Bell and J. W. Card

Department of Geology, Carleton University

ABSTRACT

The collector method of uranium exploration has delineated anomalies at a new test site in Palmerston Township, Ontario, in the Grenville Province. Both the in-situ and soil-sample techniques effectively outlined the known uranium-bearing pegmatites.

Collector measurements can be corrected for any thoron (^{220}Rn) decay-product activity by counting the activity from the collector for a second time several hours after the initial reading. The formula for the thoron correction depends on both the length of the time interval during which the collector was exposed and the length of the waiting period between the end of the exposure and the beginning of the second counting interval. Thoron correction factors calculated from the Palmerston Township test site data were negligible.

The Alphacard system, a new commercially available instrument based on the collector method has now been field tested and shown to be effective at both the Palmerston Township and South March test sites.

New laboratory investigations into the behaviour of radon (^{222}Rn) decay products have shown that (i) although the sensitivity of the method is enhanced by placing a negative charge on the collector, activity significantly above background can be measured if the collectors are positively charged, (ii) decay products, although firmly fixed to the collectors, can be removed from copper plates by cleaning with metal polish, whereas other methods such as rinsing with water and reversing the polarity of the charge on the plates failed to remove the decay products, and (iii) decay products are not readily collected in water. These results corroborate earlier conclusions by other workers, in atmospheric physics, that the transportation of radon decay products in air is probably by more than one mode.

INTRODUCTION

Recent studies of the spontaneous deposition of the short-lived decay products of ^{222}Rn (^{218}Po , ^{214}Pb , ^{214}Bi , and ^{214}Po) onto "collectors" have resulted in the development of a new uranium exploration technique (Card 1978; Bell and Card 1979, 1980; Card and Bell 1979). The previous work involved field tests in both unmetamorphosed Palaeozoic and metamorphosed Precambrian terrains, and the evaluation in the laboratory of different collector

materials, geometries, exposure intervals, and methods of counting. The results of several comparative studies at the South March uranium-copper occurrence have shown that the collector method compares favourably with conventional methods of in-situ radon detection and soil analysis.

During 1980-1981, additional field tests were completed at the previous test site near South March and measurements made at a new test site, a pegmatite occurrence in Palmerston Township, Ontario. In addition, theoretical studies and laboratory and field experiments have shown that corrections can be made to the data for the thoron (^{220}Rn) decay products.

On the basis of our earlier work a new instrument package, the "Alphacard system," was developed and marketed by Alpha Nuclear Company of Mississauga. This has now been thoroughly field tested and shown to be comparable with other commercially available methods, and comparable with our approach to the collector method.

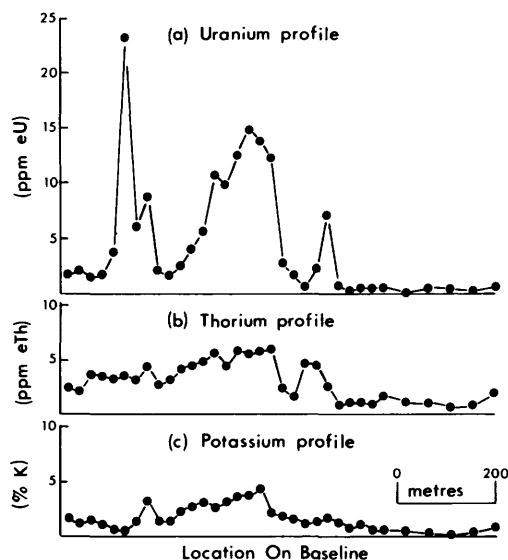


Figure 1—Gamma-ray profiles along the base line at the South March uranium-copper occurrence.

FIELD TESTS

During the last three years the test site near South March, Ontario, has been studied by a variety of methods. Radon was measured by the soil-gas suction technique (Christie 1980) and by the alphameter technique (Gratton 1980). Radium in soils was measured by an immersion technique (Bradley 1979) and by alpha-particle counting following total sample digestion (Wilson 1979). To complete the studies, a GAD-6 gamma-ray survey has recently been completed at all of the grid stations used for the collector studies. Previously we had relied for comparison on a gamma-ray survey of the area documented by Ford (1975), but because this survey covered a much broader area, relatively few stations occurred on our grid and these were at different locations from ours. The uranium channel of the new gamma-ray profile (Figure 1) outlines two peaks that correspond to the two mineralized zones in the underlying Palaeozoic rocks. These results substantiate, in greater detail, the work of Ford (1975) and

provide yet another good comparison between the collector method and an alternative well-established exploration technique.

A zone of uranium-bearing pegmatites in Palmerston Township (Longitude 76°44'45''W, Latitude 44°54'15''N) was chosen as the test site for additional field studies of the collector method. The tabular pegmatite bodies strike nearly north, and are concordant with the enclosing gneisses and marbles. Uranium occurrences in the Grenville rocks of the area have already been investigated by geophysical and geochemical surveys (Barlow and Ware 1977; Closs and Coker 1977; Ford and Charbonneau 1979), and some drilling programs have been initiated by private industry. A geological cross-section of the test site is shown in Figure 2a.

Copper collectors were exposed in inverted plastic containers (flower pots, 14 cm deep and 15 cm wide at the open end) in holes up to 45 cm deep; the holes were back-filled after covering each container with a large plastic sheet. Following an overnight exposure, the alpha activity from each collector was counted for a five-minute interval. Five or six hours after the end of the initial counting interval, a second count was taken; these data were then used to correct the original counts for the thoron (^{220}Rn) contribution. Results from one survey line, with stations at 5 m spacings delineated the anomalies associated with two pegmatite outcrops (Figure 2b). A profile (not shown) from a second survey line 180 m north of the first, showed a similar pattern to that illustrated in Figure 2b. The calculated contribution to the total activity from the thoron decay products from data obtained along both lines was shown to be negligible.

At previous test sites (Bell and Card 1979, 1980), collectors had been exposed in cylindrical holes, which were then covered by a plywood sheet. Because plywood is bulky, deployment in remote areas can be difficult; in an attempt to alleviate this problem, aluminum plates were used as hole covers. A few tests at the Palmerston Township site showed that the anomaly could be delineated in this way, but unfortunately the plates were not rigid enough to support the weight of the backfill used to hold them in place. As an alternative, inverted plastic flower pots were used during the tests. The flower pots ensured that identical exposure geometries could be achieved at all locations, a feature often difficult to achieve in boulder-rich overburden. The flower pots also have the additional feature of being lightweight.

The highest anomalies from total-count gamma-ray readings (Figure 2c) occurred immediately above the pegmatite outcrops and lower readings were obtained at the soil-covered sites. It is interesting to note that the signal-to-background ratio for the highest gamma-ray readings was about 6-to-1, while that for the collectors was much more favourable at about 45-to-1.

An additional profile was obtained by using 50 g aliquots of soil from each site (Figure 2d). This profile is consistent with that from the in-situ study. Each soil sample was placed in a container and a collector suspended above it for a period of seven days. Radon produced from the soil-sample radium provides decay products to the collector. Although this method generally yields less

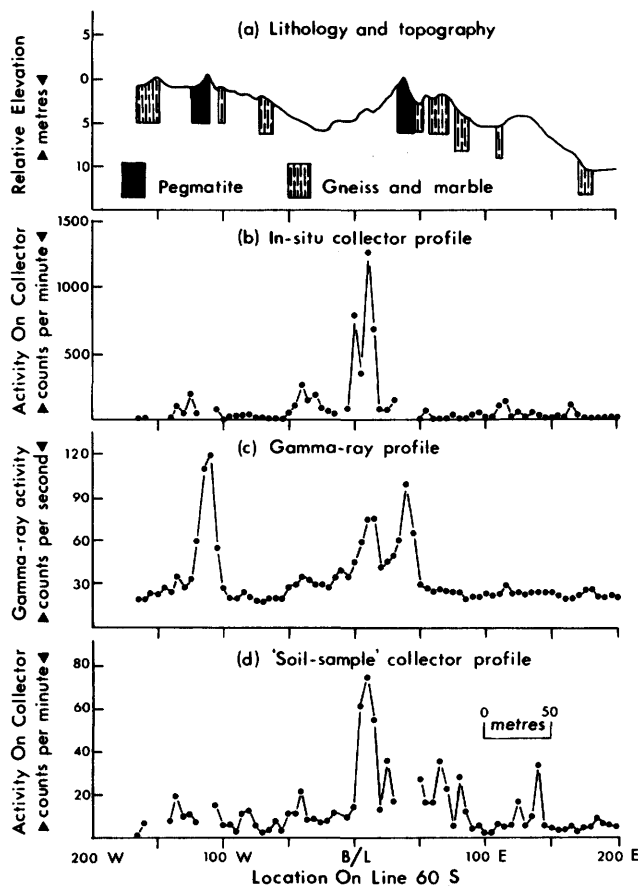


Figure 2—Comparative profiles from a pegmatite uranium occurrence in Palmerston Township, Ontario.

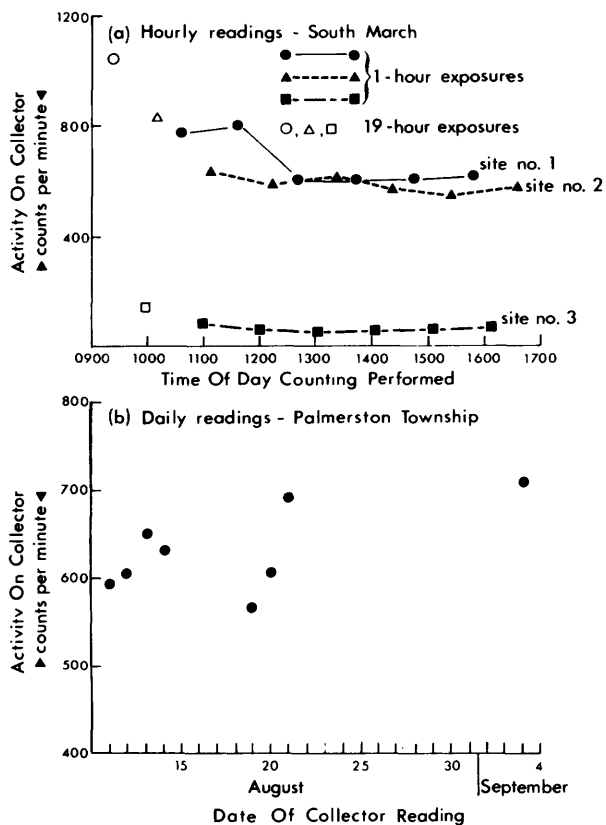


Figure 3—In-situ replicate collector measurements.

counts than the in-situ approach (no doubt due to the small sample mass), it may be useful in exploration by providing an indication of whether an anomaly measured in an in-situ survey has been generated proximally, from radium in the soil, or distally, from radon which migrated from below. In the Palmerston Township area, it is clear that a significant number of the decay products detected during the in-situ study were derived from radium in the soils. All thoron readings from the soil samples were negligible.

An interesting aspect of the current research is the extremely favourable reproducibility achieved in the field by the collector method. Hourly readings from collectors at three locations on the South March grid were remarkably similar (Figure 3a), and in one case agreed to within 10 percent of the mean values. In addition, when daily readings were carried out at various times during a period of 25 days at a base station at the Palmerston Township test site, none varied by more than 15 percent from the mean (Figure 3b). These reproducibility studies suggest that the diurnal variations in soil-gas radon concentrations proposed by many workers may not always be significant, and that long integration times are not essential in exploration.

THORON DISCRIMINATION

In our 1979-1980 report (Bell and Card 1980), we summarized experiments evaluating the collection of thoron (^{220}Rn) decay products (^{216}Po , ^{212}Pb , ^{212}Bi , and ^{212}Po) and concluded that these can be collected in a similar way to the radon decay products. It was also noted that a steady-state exposure resulted in a decay curve consistent in shape with that predicted from the equations for successive transformations (Rutherford 1913). Such thoron decay product curves can be used to apply a thoron correction factor to collector readings. Further analysis has now shown that the decay curves following short exposure intervals can also be predicted mathematically, using the equation shown in Appendix 1. When applying this equation the assumption is made that the thoron decay products are collected at a constant rate during the exposure of the collector to the thoron-bearing atmosphere. A number of different decay curves for theoretical exposures, from 10 minutes up to 9 days, were calculated. Observed data for various exposure durations show good agreement with the theoretical results.

The activity from the collected radon decay products drops to negligible levels about 3 hours after the end of an exposure, but much of the thoron decay product activity remains. A second reading from the collector, perhaps 5 or 6 hours after the end of an exposure, can thus be used with the theoretical decay curves to estimate the contribution of the thoron decay products during the initial counting interval. Correction factors for different exposure times and waiting periods are shown graphically in Figure 4. (The values from the curves are divided into the second collector reading to yield the thoron correction, which is subtracted from the initial reading.) Calculations using the data obtained in situ at Palmerston Township showed that the thoron correction was negligible.

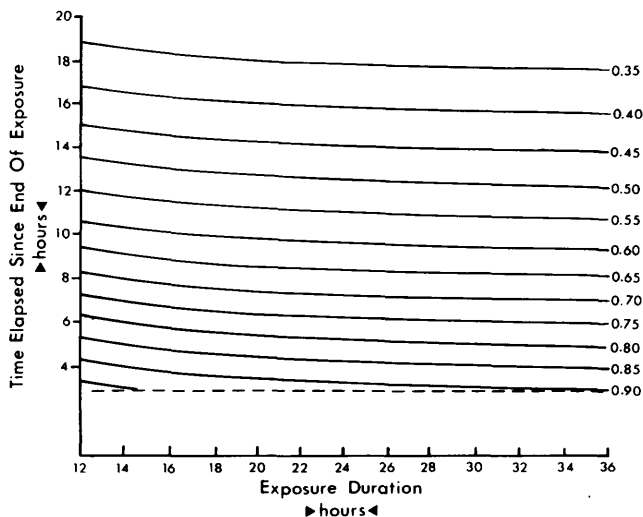


Figure 4—Correction factors for discrimination against thoron decay products.

ALPHACARD SYSTEM

An instrument package, the "Alphacard system", based on the collector principle has been designed by Alpha Nuclear Company of Mississauga. The collector, or "Alphacard", is a 4.6 cm by 4.9 cm plastic card which supports a thin 2.5 cm diameter aluminized mylar disc in the centre. The Alphacard is deployed in the normal manner, either in situ or in containers with soil samples, and is subsequently removed and inserted into a "card reader" for counting. The alpha particles from decay products collected on the aluminized mylar are detected by two parallel solid-state silicon detectors; the mylar is sufficiently thin that the alpha particles can penetrate it, thus increasing the number of counts by a factor of two. Being insensitive to excitation from light, the instrument is considerably easier to use than the original scintillation-chamber detector. The card reader counts the alpha particles from the card for a 5-minute interval; at the end of this time, an audio signal is given and the total number of counts, normalized to counts per minute, is displayed. As each new Alphacard is inserted into the reader, the previous Alphacard is mechanically fed into a storage magazine; in this way, all of the cards are retained in the order originally counted, for possible re-reading for thoron decay product activity.

The readings from each card can be manually recorded or, alternatively, can be stored along with the card serial number and a grid location code in a memory module which interfaces with the cardreader. The time of day that each reading is taken is also stored. Using this data-manipulation mode the day's readings can be recalled at the end of the day for plotting.

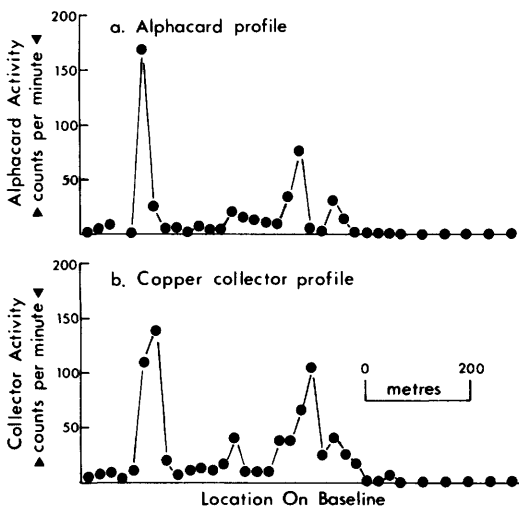


Figure 5—Comparison of an Alphacard profile with copper collector results at the South March uranium-copper occurrence.

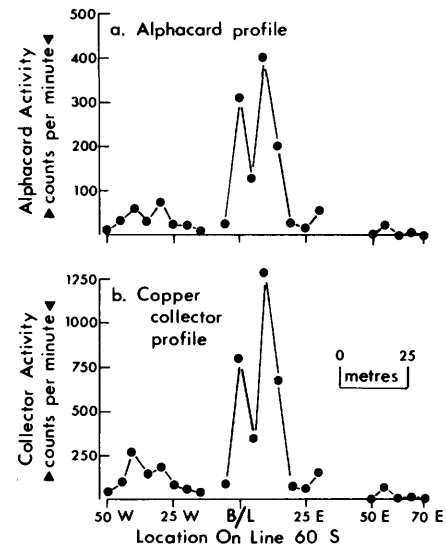


Figure 6—Comparison of an Alphacard profile with copper collector results at a pegmatite occurrence in Palmerston Township, Ontario.

Field tests at both the South March and Palmerston Township tests sites have confirmed the effectiveness of the Alphacard system (see comparative profiles in Figures 5 and 6). The anomalies are readily delineated by both the in-situ and the soil-sample methods. Both field and laboratory tests have indicated that, under identical exposure conditions, the Alphacard system provides about one-third of the total number of counts as the original scintillation-counting method; this appears to relate mainly to differences in the counting geometries. The Alphacard system has, however, yielded a sufficient number of counts under all test conditions to readily delineate the radon and radium anomalies.

Exposures of Alphacards to 2 g of a $\text{Th}(\text{CO}_3)_2$ source have shown that the thoron decay product curves are consistent in shape with those from copper collectors and can be predicted from the equations for successive transformations.

LABORATORY TESTS

The processes by which decay products are transported through air and become attached to collectors are still not fully understood and a great deal of work has to be done in the future in these areas. Although the main emphasis for the current year's work was on field studies, some laboratory investigations have yielded results which may provide some insight into these problems. Summarized below are some of the important findings.

1) **Positively-charged collectors.** We have previously shown that the activity on a collector can be enhanced by

Table 1—Collection of radon decay products on copper plates at both positive and negative potentials. All trials involved 7-day exposures of the collectors; potentials were applied for the 3 hours immediately preceding the end of the exposure.

	Sources:	
	Soil From South March *Activity On Collector (counts per minute)	CANMET Standard BL-3 *Activity On Collector (counts per minute)
Collectors negatively-charged	80.0 ± 3.8	267.3 ± 10.2
Collectors positively-charged	6.0 ± 0.9	19.7 ± 6.6
Collectors uncharged	29.9 ± 5.0	84.9 ± 3.9

*Note: Uncertainty is expressed as one standard deviation from the mean of five independent trials.

applying a negative charge. However, a related feature is that a small, but nonetheless significant, amount of activity can still be counted even after a positive charge has been applied to copper plates during collection (Table 1). This observation is confirmed by tests using the $\text{Th}(\text{CO}_3)_2$ source (Table 2). It is interesting to note that the activity tends to be lower for higher potentials.

Some recent literature indicates that decay products

Table 2—Collection of thoron (^{220}Rn) decay products on copper plates at various positive potentials. Collectors were exposed for 30 minutes with 2.0 g of thorium carbonate, and the activity counted for 30 minutes.

Potential (V ⁺)	Activity On Collector (counts per minute)
0	66.0
10	69.7
20	74.1
40	46.9
60	40.0
80	38.5
100	22.3
200	15.7
300	13.1
400	9.0
500	12.0

can occur as free positively charged atoms and neutral ions, or can be attached to various sites on solid particles (Smith *et al.* 1976; Nakatani 1978; Porstendörfer and Mercer 1978). The availability and size distribution of the solid particles appear to be affected by atmospheric nucleation, rainout, washout, settling, and coagulation (Vohra 1978; Moore *et al.* 1978). Our observations that decay products can be collected both spontaneously and under charged conditions (either positively or negatively) are consistent with the theory that the decay products may be transported in more than one mode in the air.

2) Removal of decay products with metal polish. Most of the radon and thoron decay products, whether collected spontaneously or under charged conditions cannot be easily removed by physical abrasion or by immersion in water (Bell and Card 1980). However they can be removed from copper collectors simply by cleaning the plates with metal polish. This suggests that the decay products are restricted to a relatively thin surface layer on the collector.

3) Failure to remove decay products with a positive charge. Although the collection of radon decay products can be significantly enhanced by charging the collectors negatively for a few hours preceding the end of the exposure, the obverse process, i.e., applying a positive charge after the end of the exposure, fails to remove the decay products. Positive charges of up to 2500 V applied for as long as 30 minutes failed to reduce the total number of counts.

4) Collection from aqueous solution. Attempts to collect radon decay products from aqueous solution were unsuccessful. To minimize possible effects from sus-

Table 3—Test of the collectibility of radon decay products from water. Copper collectors were exposed for 7 days in 226 ml containers with 50.0 g aliquots of soil from South March; the trials with the water involved complete immersion of the collector.

<u>Exposure Condition</u>	<u>*Activity On Collector (counts per minute)</u>
Soil, unwrapped, without water	30.3 ± 6.4
Soil, wrapped in polyethylene (type 1), without water	29.0 ± 4.1
Soil, wrapped in polyethylene (type 1), with water	2.0 ± 0.7
Soil, wrapped in polyethylene (type 2), without water	17.9 ± 3.1
Soil, wrapped in polyethylene (type 2), with water	0.2 ± 0.2

*Note: Uncertainty is expressed as one standard deviation from the mean of five independent trials.

pendent matter such as clay minerals and organic colloids originating in the sample, the source material (50 g soil aliquots from South March) was wrapped in a thin layer of polyethylene during the exposures. Although Table 3 suggests that the radon can readily migrate through the polyethylene into air, the activity from the immersed collectors was clearly negligible.

Although a great deal of careful work will be required before the fundamental physical and chemical factors influencing the migration and attachment of decay products can be fully understood, the results from these simple experiments may help set some useful boundary conditions.

CONCLUSIONS

Field tests from the Palmerston Township site, coupled with our previous results (Bell and Card 1979; Card and Bell 1979; Bell and Card 1980) show that the collector method is effective in detecting radon associated with uranium occurrences in several different types of environment. The thoron (^{220}Rn) decay products, collected along with those of radon (^{222}Rn) are not troublesome since their fairly long half-lives enable corrections to be made to the original activity counted from the collectors. Counting the

collectors a second time 5 or 6 hours after the original counts have been recorded provides data that can be used to calculate a "thoron contribution" to the total measured activity.

During the three years (1978-1981) of funding by the Ontario Geoscience Research Grants Program the collector method has been developed and evaluated both in the field and in the laboratory, and has provided the basis for a successful commercial detection system designed and marketed by Alpha Nuclear Company of Mississauga, Ontario. It is hoped that the utilization of this simple method in the future will make a significant contribution to the search for new uranium ore resources.

ACKNOWLEDGEMENTS

The authors are grateful to Mr. K. L. Ford of the Geological Survey of Canada for pointing out the features of the geology of the Palmerston Township site, and to AJM Explorations for permitting access to the property. Thanks are also extended to the Geological Survey of Canada for the loan of the GAD-6 gamma-ray spectrometer for the South March measurements, and to Mr. G. M. Cameron of the Resource Geophysics and Geochemistry Division for the computer compilation of the data from the gamma-ray survey.

APPENDIX 1. Formula to predict the shapes of the thoron decay product curves.

Following an exposure of duration T , during which thoron decay products are collected at a constant rate, n_0 , the total number of counts, ΣN , from a collector during any counting interval which starts at t_1 after the end of the exposure and ends at t_2 (where λ_1 is the decay constant for ^{212}Pb , λ_2 is the decay constant for ^{212}Bi , and D is the detection efficiency of the counter) is as follows:

$$\Sigma N = \frac{\left(\frac{e^{-\lambda_2 t_2} - e^{-\lambda_2 t_1}}{-\lambda_2} \times f_1 \right) + \left(\frac{e^{-\lambda_1 t_2} - e^{-\lambda_1 t_1}}{-\lambda_1} \times f_2 \right)}{D}$$

$$\text{where } f_1 = \left\{ n_0 \times \left(1 - \frac{[\lambda_1 e^{-\lambda_2 T} - \lambda_2 e^{-\lambda_1 T}]}{\lambda_1 - \lambda_2} \right) \right\}$$

$$- \left\{ \frac{\lambda_2 \times n_0 \times [1 - e^{-\lambda_1 T}]}{\lambda_2 - \lambda_1} \right\}, \text{ and}$$

$$f_2 = \left\{ \frac{\lambda_2 \times n_0 \times [1 - e^{-\lambda_1 T}]}{\lambda_2 - \lambda_1} \right\}$$

By assigning arbitrary values to n_0 and D and successive values to t_1 and t_2 , representing a series of short counting intervals, the shapes of the decay curves can be established.

REFERENCES

- Barlow, R. B., and Ware, C.
1977: Geophysical, Geochemical and Geological Investigations of some Uranium Occurrences, Sharbot Lake Area, Southeastern Ontario; p. 174-177 in Summary of Field Work, 1977, by the Geological Branch, edited by V. G. Milne, O. L. White, R. B. Barlow, and J. A. Robertson, Ontario Geological Survey MP75, 208 p.
- Bell, K., and Card, J. W.
1979: Radon Decay Products and Uranium Exploration; Grant 38, p. 117-124 in Geoscience Research Grant Program, Summary of Research, 1978-1979, edited by E. G. Pye, Ontario Geological Survey MP87, 152 p.
- 1980: Further Investigations of the Radon Decay Product Collector Method of Uranium Exploration; Grant 38, p. 24-38 in Geoscience Research Grant Program, Summary of Research, 1979-1980, edited by E. G. Pye, Ontario Geological Survey MP93, 263 p.
- Bradley, C. J.
1979: Delineation of a Soil Radium Anomaly: An Evaluation of a Soil-Immersion Technique; unpubl. B.Sc. thesis, Carleton University, Ottawa, Ontario, 43 p.
- Card, J. W.
1978: Spontaneous Deposition of Radon Decay Products from Air; unpubl. M.Sc. thesis, Carleton University, Ottawa, Ontario, 108 p.
- Card, J. W., and Bell K.
1979: Radon Decay Products and their Application to Uranium Exploration; Canadian Inst. Min. and Met. Bull., vol. 72, No. 812, p. 81-87.
- Christie, D. S.
1980: Radon-Thoron Survey of a Known Uranium-Copper Occurrence; An Evaluation of a Soil-Gas Suction Emanometry Technique; unpubl. B.Sc. thesis, Carleton University, Ottawa, Ontario, 37 p.
- Closs, L. G., and Coker, W. B.
1977: Joint Federal-Provincial Lake Sediment Geochemistry Follow-Up Program, Southeastern Ontario; p. 178-180 in Summary of Field Work, 1977, by the Geological Branch, edited by V. G. Milne, O. L. White, R. B. Barlow, and J. A. Robertson, Ontario Geological Survey MP75, 208 p.
- Ford, K. L.
1975: Petrography, Geochemistry and Geophysics of a Uranium-Copper Occurrence, South March, Ontario; unpubl. B.Sc. thesis, Carleton University, Ottawa Ontario, 62 p.
- Ford, K. L., and Charbonneau, B. W.
1979: Investigation and Regional Significance of Airborne Gamma Ray Spectrometry Patterns in the Sharbot Lake Area, Eastern Ontario; p. 207-222 in Current Research, Part B, Geological Survey of Canada, Paper 79-1B, 420 p.
- Gratton, F. J.
1980: Radon Variations in Soil Gas at the South March Uranium-Copper Occurrence; unpubl. B.Sc. thesis, Carleton University, Ottawa, Ontario, 45 p.
- Moore, H. E., Poet, S. E., and Martell, E. A.
1978: Size Distribution of Rn-222 Daughters on Tropospheric Aerosol Particles; p. 71-73 in The Natural Radiation Environment III Book of Summaries.
- Nakatani, S.
1978: The Mean Size among the Particles of Short-Lived Radon Daughter Products in the Atmosphere; p. 49 in The Natural Radiation Environment III Book of Summaries.
- Porstendörfer, J., and Mercer, T. T.
1978: The Diffusion Coefficient of Radon Decay Products and their Attachment Rate to the Atmospheric Aerosol; p. 47-48 in The Natural Radiation Environment III Book of Summaries.
- Rutherford, E.
1913: Radioactive Substances and their Radiations; Cambridge University Press, 699 p.
- Smith, A. Y., Barretto, P. M. C., and Pournis, S.
1976: Radon Methods in Uranium Exploration; p. 185-211 in International Atomic Energy Agency, Exploration for Uranium Ore Deposits, Proceedings of Symposium.
- Vohra, K. G.
1978: Role of Natural Radiation Environment in Earth Sciences; p. 29-31 in The Natural Radiation Environment III Book of Summaries.
- Wilson, J. S.
1979: Soil-Radium Geochemistry of a Uranium-Copper Occurrence, South March, Ontario; unpubl. B.Sc. thesis, Carleton University, Ottawa Ontario, 26 p.

Grant 54 Regional Alteration in Archean Greenstones: Applications to Exploration for Massive Sulphide Deposits

A.E. Beswick

Department of Geology, Laurentian University

ABSTRACT

Comparative studies of chemical alteration in two mineralized (massive sulphide bearing) and two unmineralized Archean "greenstone" belt segments indicate differences in the nature of their alterations. The four areas chosen for study were Kakagi Lake and Halliday Dome (unmineralized) and Uchi-Confederation and Sturgeon Lakes (mineralized). Each area covers several hundred square kilometres. Major oxide additions and depletions (alteration parameters) were calculated for some 4000 samples from these areas using a new computer technique based on procedures outlined by Beswick and Soucie. Discriminant function analysis of the alteration parameters for all samples from these areas correctly identified between 47 percent and 82 percent of samples from any one area. Restricting the discriminant analysis to samples of felsic composition improved correct identifications to between 63 percent and 90 percent. When probability levels are associated with these discriminant scores, samples identified as being from a mineralized area with greater than 80 percent probability are found to cluster in relatively small areas around known massive sulphide deposits. Two small clusters in the northwest and northeast parts of the Sturgeon Lake area suggest the possibility of massive sulphide mineralization to the north of Sturgeon Lake.

INTRODUCTION

Based on comparisons of chemical variation trends displayed by fresh, post-Mesozoic, volcanic rocks and Archean "greenstones", Beswick and Soucie (1978) outlined a graphical procedure to identify altered rocks and to estimate additions and depletions of major oxides due to chemical alteration.

In the first year of the present project, computer programs (Fortran IV) were developed to calculate major oxide additions and depletions in altered volcanic rocks following the procedures outlined by Beswick and Soucie (1978). These programs were tested on Archean greenstone data from various areas within the Abitibi, Birch-Uchi and Wabigoon greenstone belts, compiled by Lavin (1976), McConnell (1976) and Sopuck (1977). Results of this testing suggested that significant differences exist between the nature of the chemical alteration in mineral-

ized (massive sulphide bearing) and unmineralized segments of these greenstone belts.

A description of the analytical data base, the computer programs and the preliminary results of their testing was given by Beswick and Nichol (1980). It was noted that CaO additions and Na₂O depletions were more intense in the Uchi-Confederation Lakes area (757 samples over a 470 km² area), particularly in a small section around Selco Mining Corporation Limited's South Bay Mine (191 samples over a 3 km² area), than in the unmineralized Kakagi Lake region (859 samples over a 330 km² area). It was therefore concluded that the alteration intensities in the Uchi-Confederation Lakes region might be a reflection of alteration associated with the Cu-Zn massive sulphide mineralization at South Bay. In order to test the general validity of this conclusion alteration in several other areas has been examined in the past year.

RESULTS

COMPARISONS OF SINGLE ALTERATION PARAMETERS

In addition to the Uchi-Confederation and Kakagi Lakes areas, alteration parameters (major oxide additions and depletions) have been calculated for the 'unmineralized' Halliday Dome area (646 samples covering 638 km²) and the 'mineralized', Sturgeon Lake area (900 samples covering 513 km²).

Comparison of individual oxide alteration parameters between each of the two mineralized and each of the two unmineralized sample data sets did not support the conclusion that the intensity of CaO additions and Na₂O depletions could be used in general to distinguish mineralized from unmineralized areas. It therefore became necessary to determine whether some combination of alteration parameters might be a better and more generally applicable tool for distinguishing between sample populations from mineralized and unmineralized areas. From that point to date, efforts were therefore concentrated on discriminant function analysis: a standard statistical procedure for distinguishing between members of two populations which are described by many variables rather than one (see for example Klován and Billings 1967; Sopuck *et al.* 1980).

DISCRIMINANT ANALYSIS OF ALTERATION PARAMETERS

Using the SPSS (Statistical Package for the Social Sciences) discriminant analysis procedure (Nie *et al.* 1970) on the Laurentian University DEC 2020 computer, comparisons of the calculated oxide alterations between each of the two mineralized and each of the two unmineralized areas referred to above, were made i.e. Kakagi Lake vs. Uchi-Confederation Lakes; Halliday Dome vs. Uchi-Confederation Lakes; Kakagi Lake vs. Sturgeon Lake; and Halliday Dome vs. Sturgeon Lake. These comparisons resulted in four different discriminant functions, each a linear combination of eight oxide alteration parameters (for SiO₂, TiO₂, Fe₂O₃, MgO, CaO, Na₂O, P₂O₅). However, it was noted that P₂O₅, Fe₂O₃ and SiO₂ alterations were always ranked within the top five most significant variables in each function. This suggested that a single function based only on these three variables might be capable of identifying whether any individual sample belonged to a mineralized or unmineralized regional data set. To test this hypothesis the four comparisons were repeated restricting consideration to these three variables. In each of the four comparisons approximately 70 percent of samples from unmineralized areas (Kakagi Lake and Halliday Dome) were correctly identified whereas correct identification of samples from mineralized areas (Uchi-Confederation and Sturgeon Lakes) ranged from

47 percent to 82 percent. Overall these results were extremely encouraging. However, it was necessary to consider whether the results were a function of differences not directly related to mineralization. In particular, if one population is dominated by basaltic rocks whereas another is dominantly made up of felsic rocks, is the function merely distinguishing between mafic and felsic rock types?

In an attempt to answer this question the computations were again repeated using the same three variables to establish the discriminant function but restricting comparisons only to felsic rocks with greater than 60 percent SiO₂. The comparative results, summarized in Table 1, indicate that in almost every case there is a significant increase in the percentage of samples correctly identified, the lowest score now being 63 percent rather than 47 percent for correct identification of samples from mineralized areas.

This is a particularly satisfying result since it clearly indicates that alteration differences are more readily identified in the felsic rather than mafic volcanic rocks and it is well known that massive sulphide mineralization is characteristically associated with Archean felsic volcanism. In other words the differences observed in the alteration of mineralized and non-mineralized regions are not only real — they make geologic sense!

It was next decided to determine how the correctly identified and misidentified samples in each area were

Table 1—Summary of the percentage of samples correctly identified in form discriminant function comparisons. Note that the percentage correctly identified in most cases increase significantly when comparisons are restricted to samples with greater than 60 percent SiO₂.

	All SiO ₂		SiO ₂ > 60%	
	Mineralized	Unmineralized	Mineralized	Unmineralized
UCHI	82.3%		78.7%	
KAKAGI		74.2%		89.6%
UCHI	78.1%		76.9%	
HALLIDAY		67.8%		86.4%
STURGEON	72.0%		63.9%	
KAKAGI		71.4%		89.1%
STURGEON	47.0%		63.0%	
HALLIDAY		72.5%		83.2%

spatially distributed, particularly with respect to the location of known deposits within the mineralized regions. At the same time it was decided to determine the probability of the correctness of such identifications so that plots for various probability levels would be possible.

COMPUTER MAPPING AND DISCRIMINANT SCORE PROBABILITIES

Using the SPSS package, probabilities (from 0 to 100

percent) that any particular sample was from a mineralized area were determined for all samples from all four regions. Each regional data set was then divided into six subsets according to probability levels. (Subset boundary levels used were 20, 40, 60, 80 and 95 percent). For each region the distribution of samples in each subset were plotted using a Tektronix, two-pen, flat-bed plotter. Figures 1, 2, 3, and 4 show the areal distribution of all samples from each area: Kakagi Lake, Halliday Dome, Sturgeon Lake and Uchi Lake respectively. Figures 1a, 2a, 3a and 4a show the distribution of those samples in

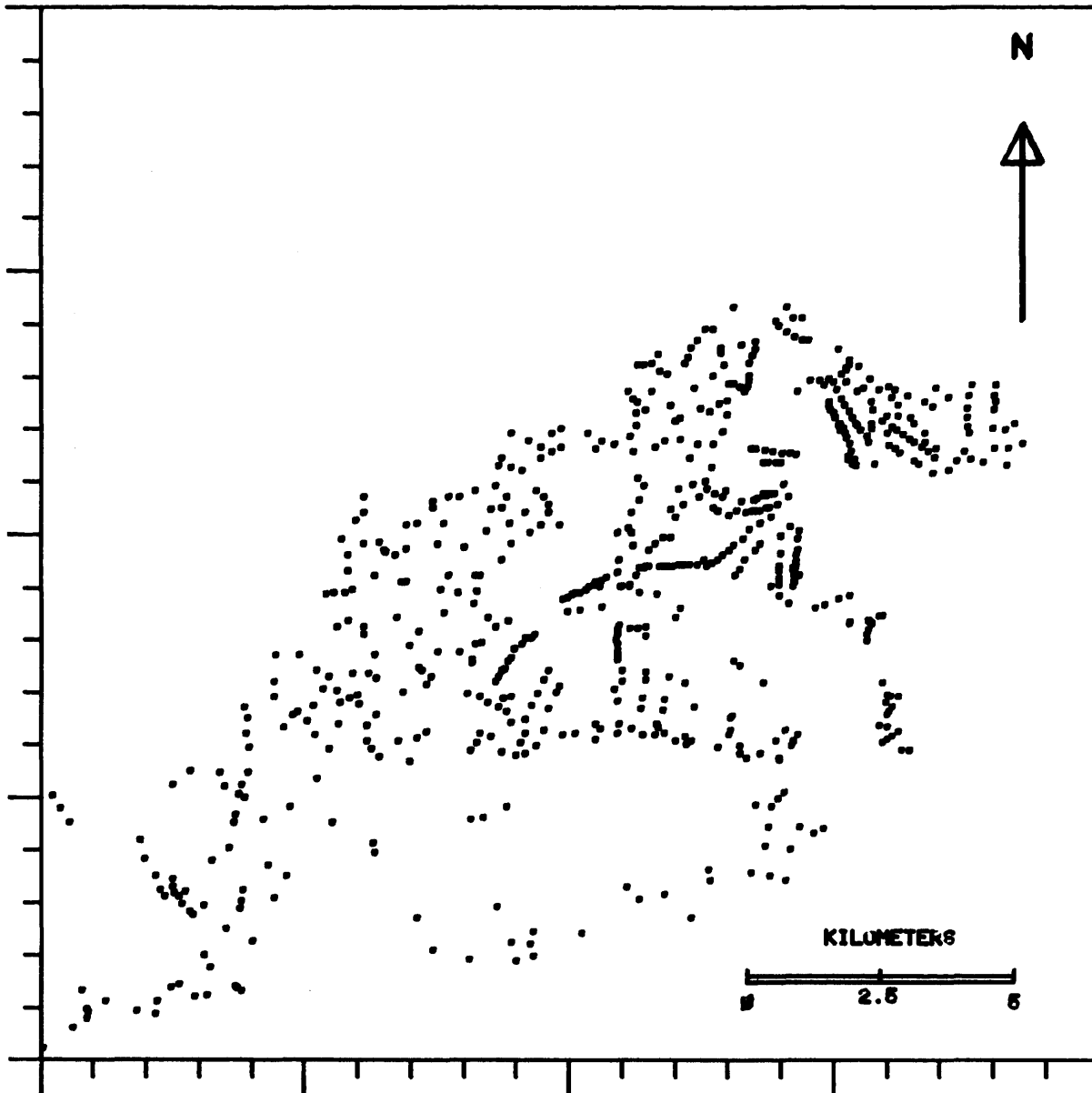


Figure 1—Locations of 842 samples from the Kakagi Lake area (N-S and E-W coordinates are arbitrary).

each area identified as being from a mineralized region (i.e. misidentified samples in the case of Kakagi Lake and Halliday Dome area) at the greater than 60 percent probability level.

Plots for Kakagi Lake (Figure 1a) and Halliday Dome (Figure 2a) show no major clusters of misidentified samples. The plot for Sturgeon Lake (Figure 3a), on the other hand, shows significant clustering of correctly identified samples in a southerly east-trending band and in two

smaller areas in the northeast and northwest parts of the area. The Mattabi, Sturgeon Lake and Lyon Lake properties and several 'showings' in this region all fall within the southern area (indicated by stars on Figure 3). The plot for the Uchi Lake area (Figure 4a) shows correctly identified samples throughout most of the area with a major density in the south around South Bay Mine (star).

A plot of the greater than 80 percent probability levels for the Sturgeon Lake region is shown in Figure 3b.

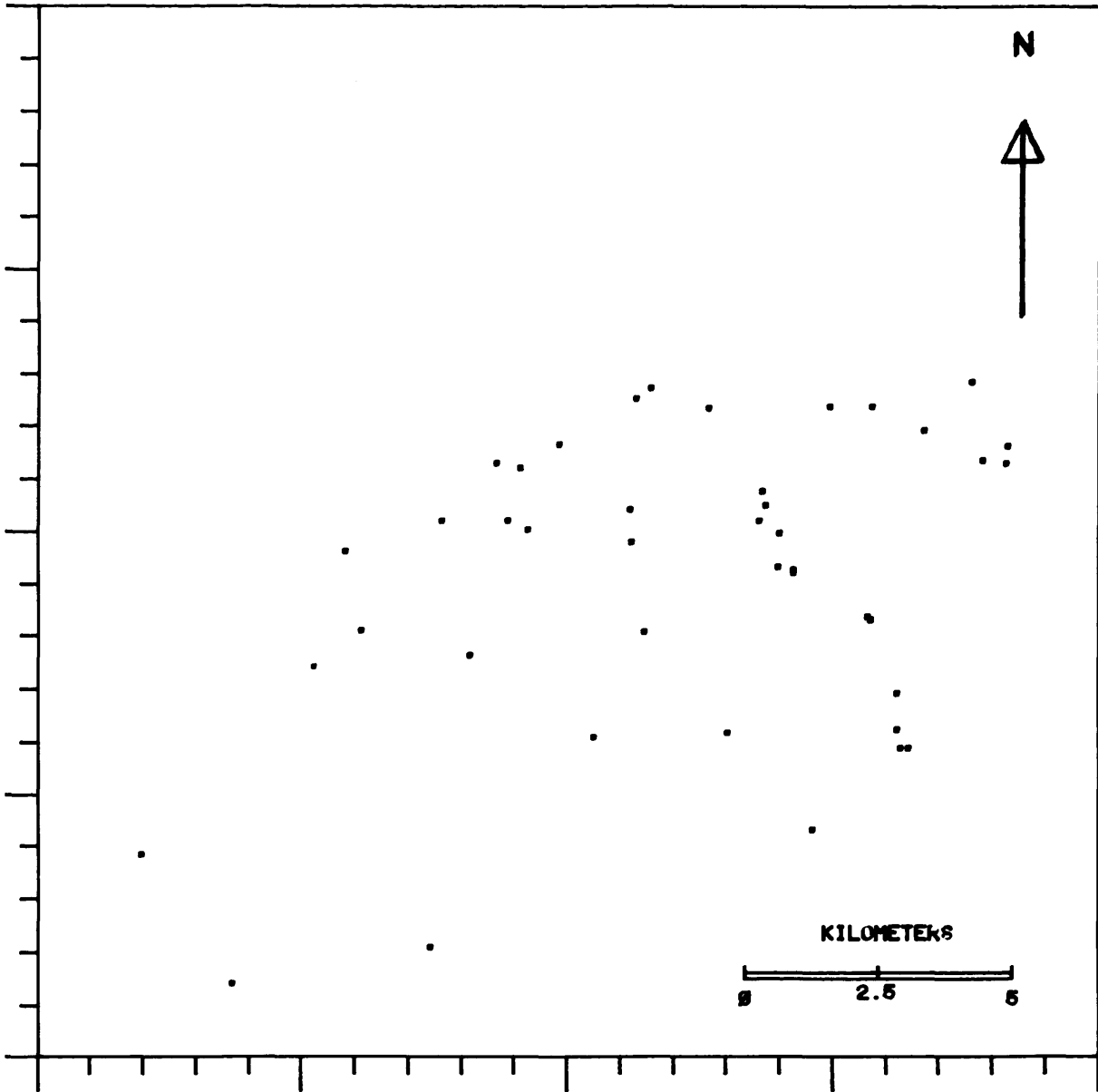


Figure 1a—Locations of 48 samples classified at the greater than 60 percent probability level as being from a mineralized area by discriminant analysis for the Kakagi Lake area.

This plot precisely locates the Mattabi Mine in the southwest part of the area and also suggests a high probability that massive sulphide deposits are present in the northwest and northeast parts of the area to the north of Sturgeon Lake. A similar plot for the Uchi Lake area indicates that samples with high probability are largely restricted

to a small area around South Bay Mine. This can be seen on Figure 4b, which shows the distribution of samples with greater than 80 percent probabilities of being from a mineralized region. Only two or three samples in the Kakagi Lake and Halliday Dome areas show high probabilities of being from a mineralized region.

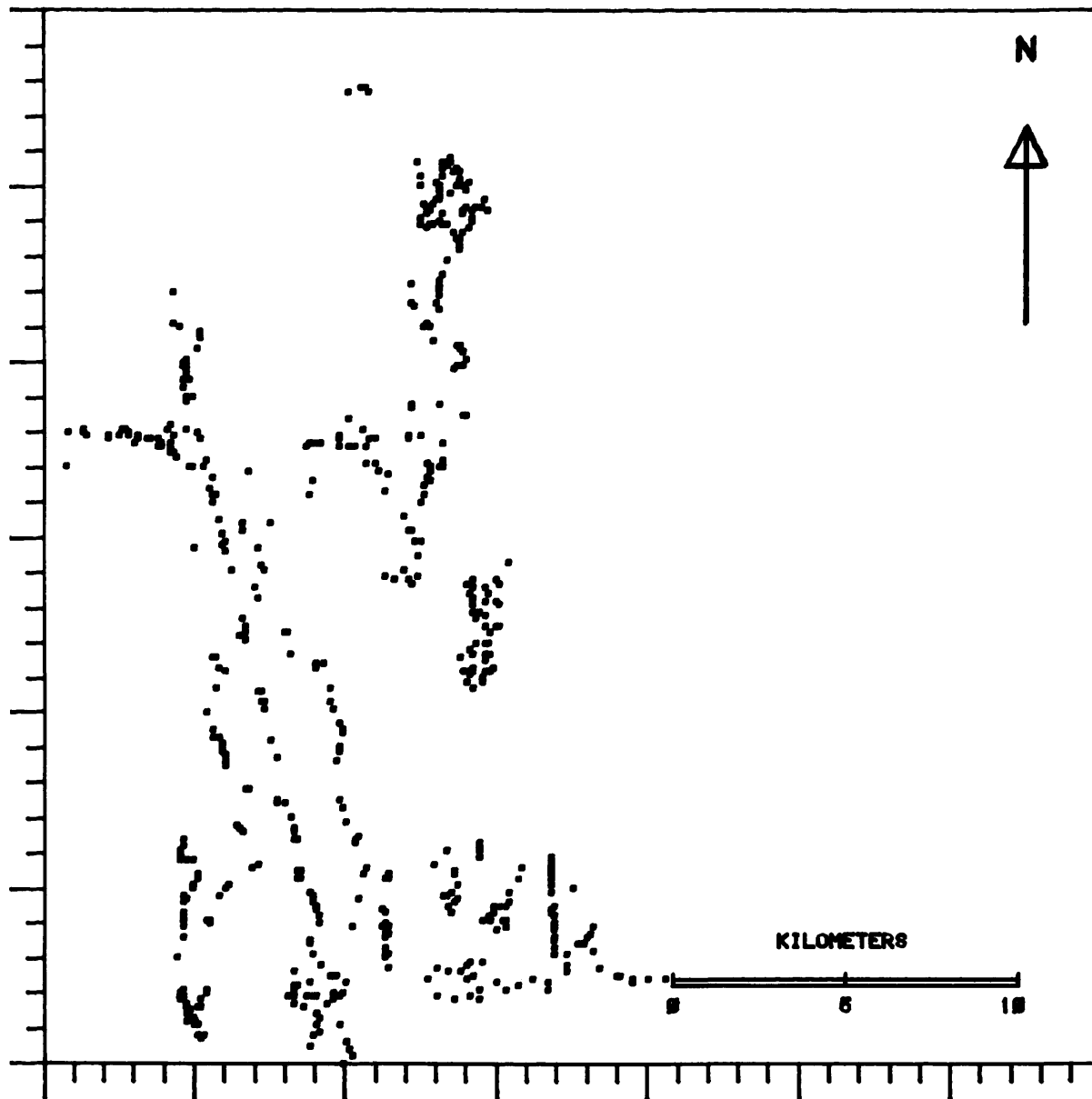


Figure 2—Locations of 636 samples from the Halliday Dome area (N-S and E-W coordinates are arbitrary).

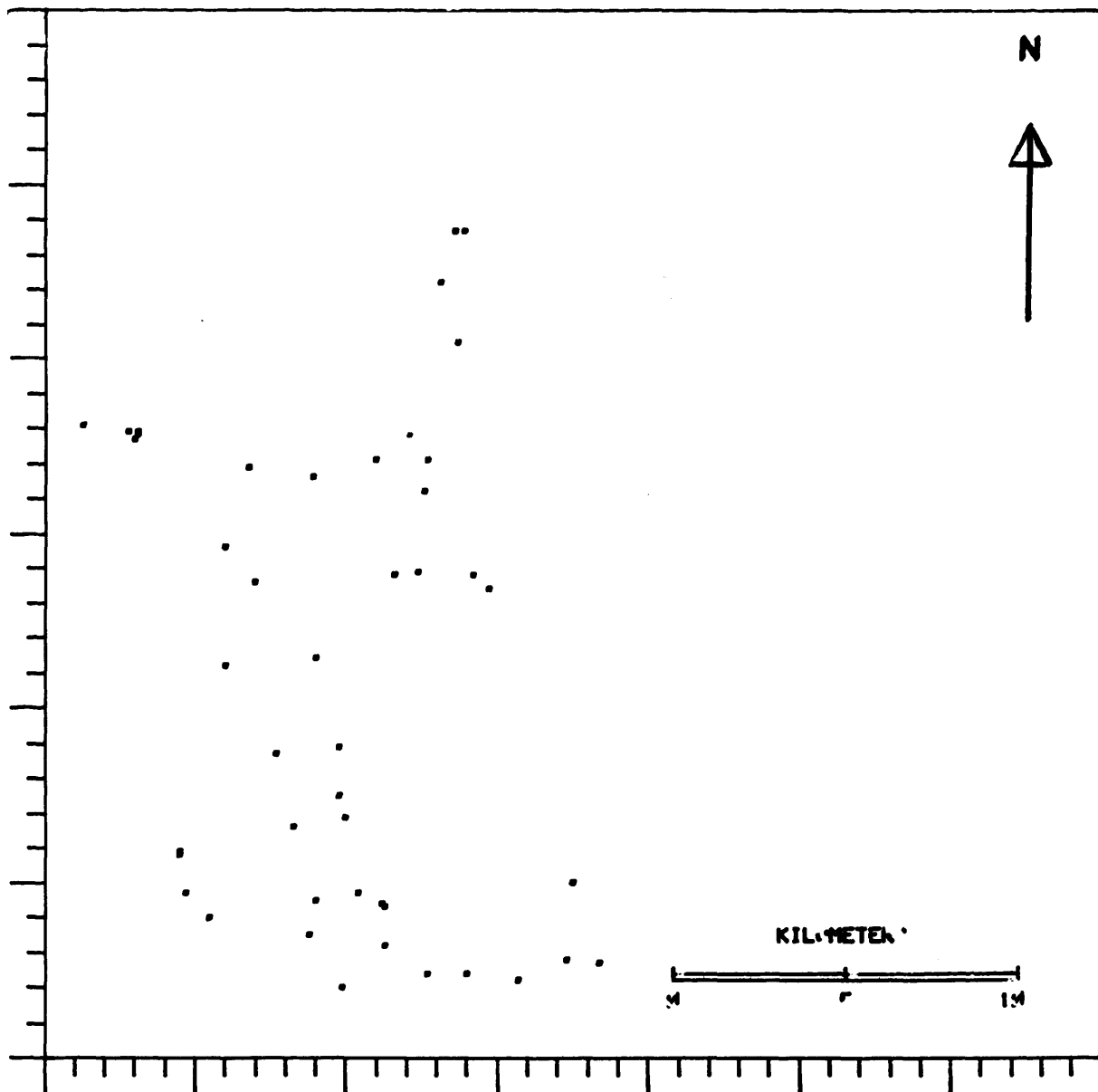


Figure 2a—Locations of 53 samples classified at the greater than 60 percent probability level as being from a mineralized area for the Halliday Dome area.

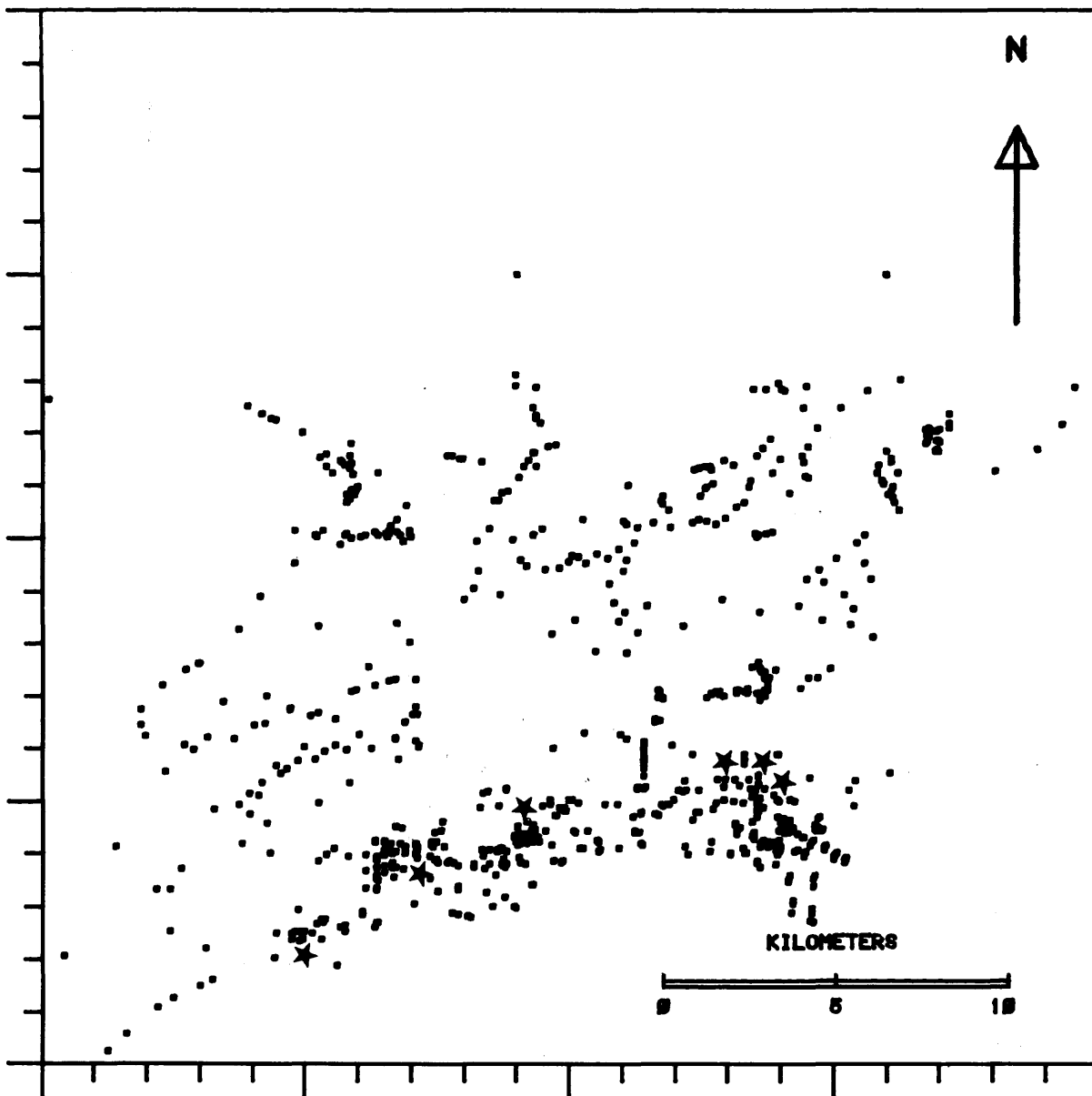


Figure 3—Locations of 820 samples from the Sturgeon Lake area (N-S and E-W coordinates are arbitrary).

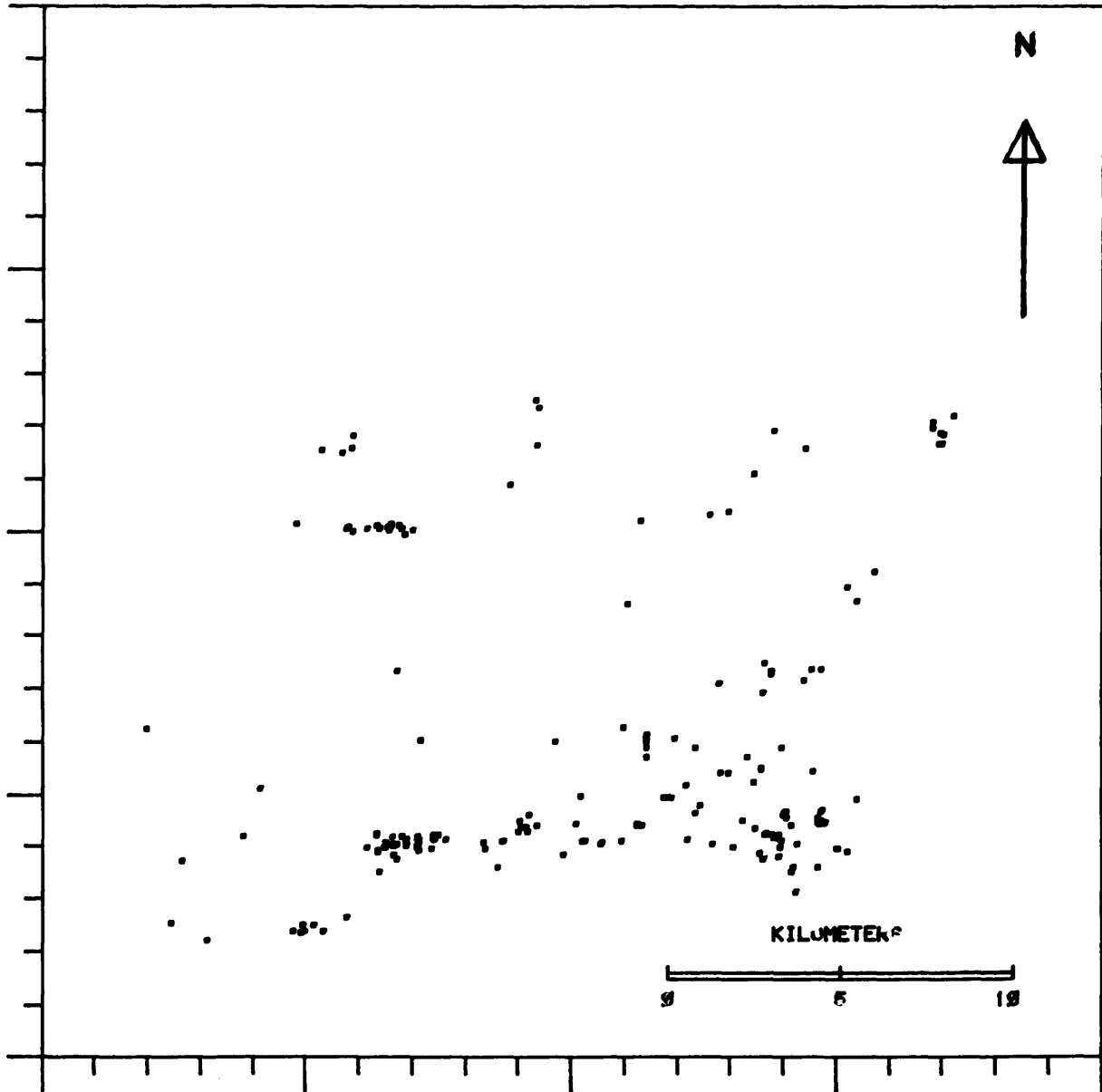


Figure 3a—Locations of 213 samples classified at the greater than 60 percent probability level as being from a mineralized area for the Sturgeon Lake area.

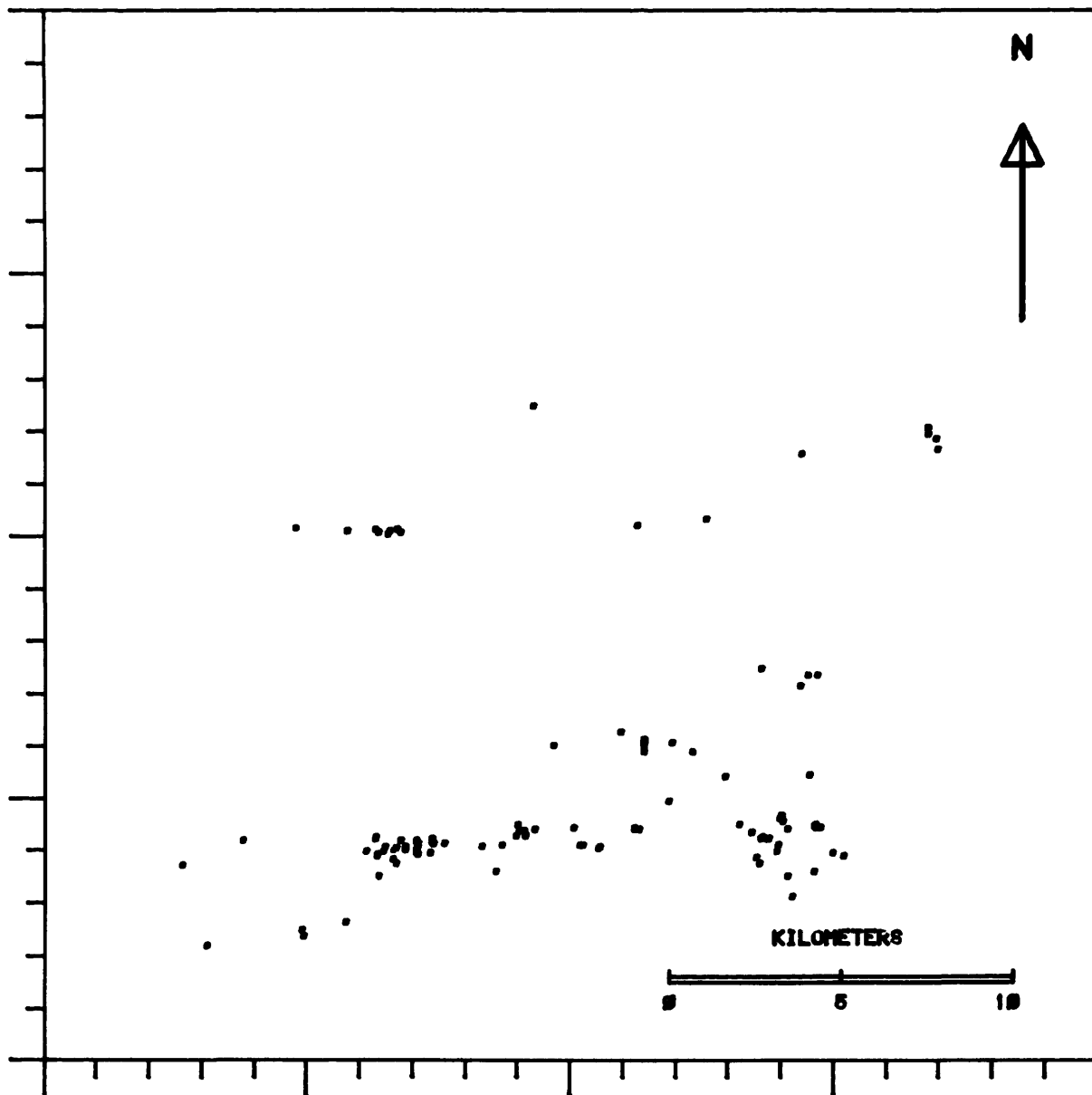


Figure 3b—Locations of 123 samples classified at the greater than 80 percent probability level as being from a mineralized area for the Sturgeon Lake area.

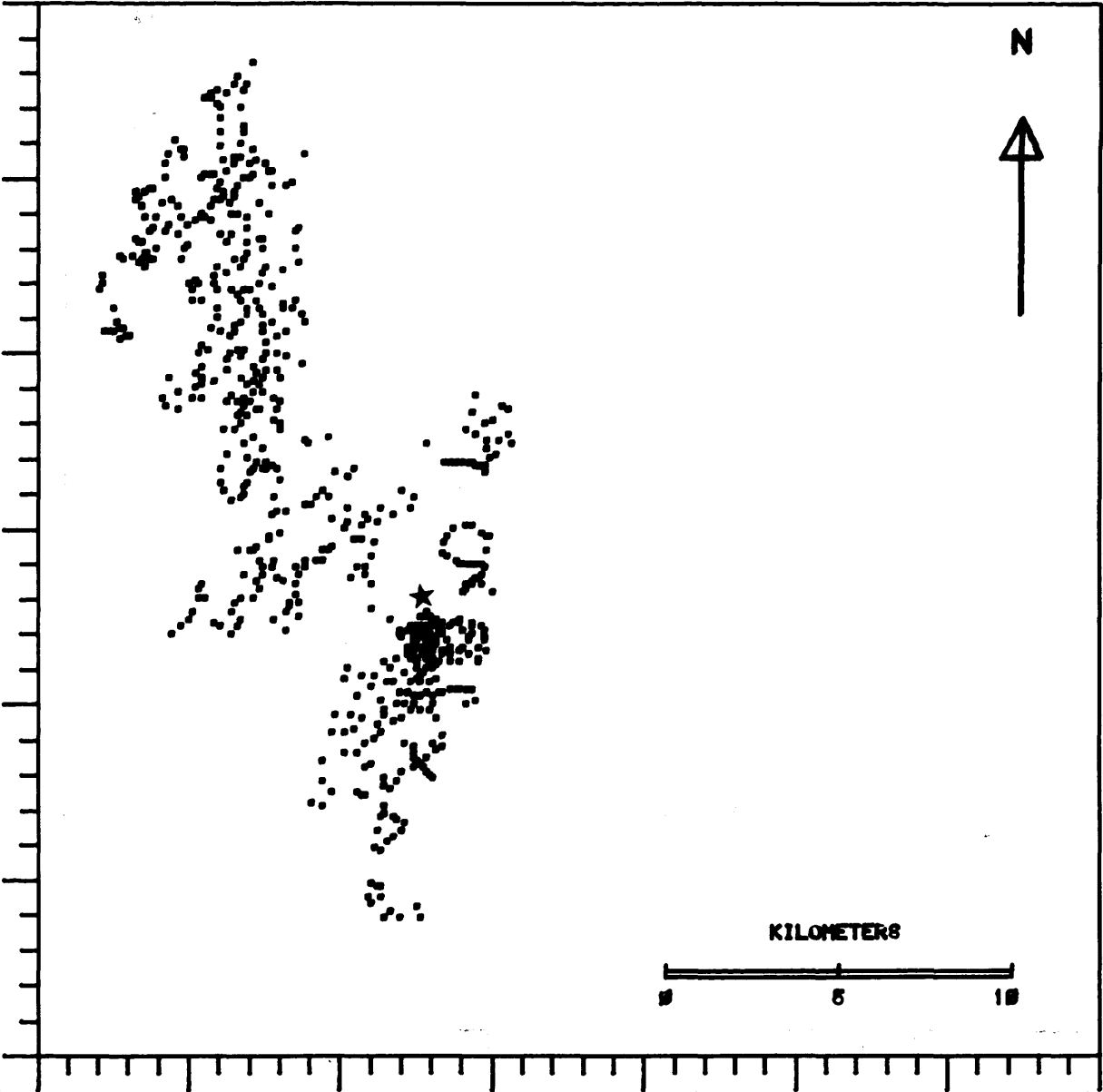


Figure 4—Locations of 761 samples from the Uchi Lake area (N-S and E-W coordinates are arbitrary).

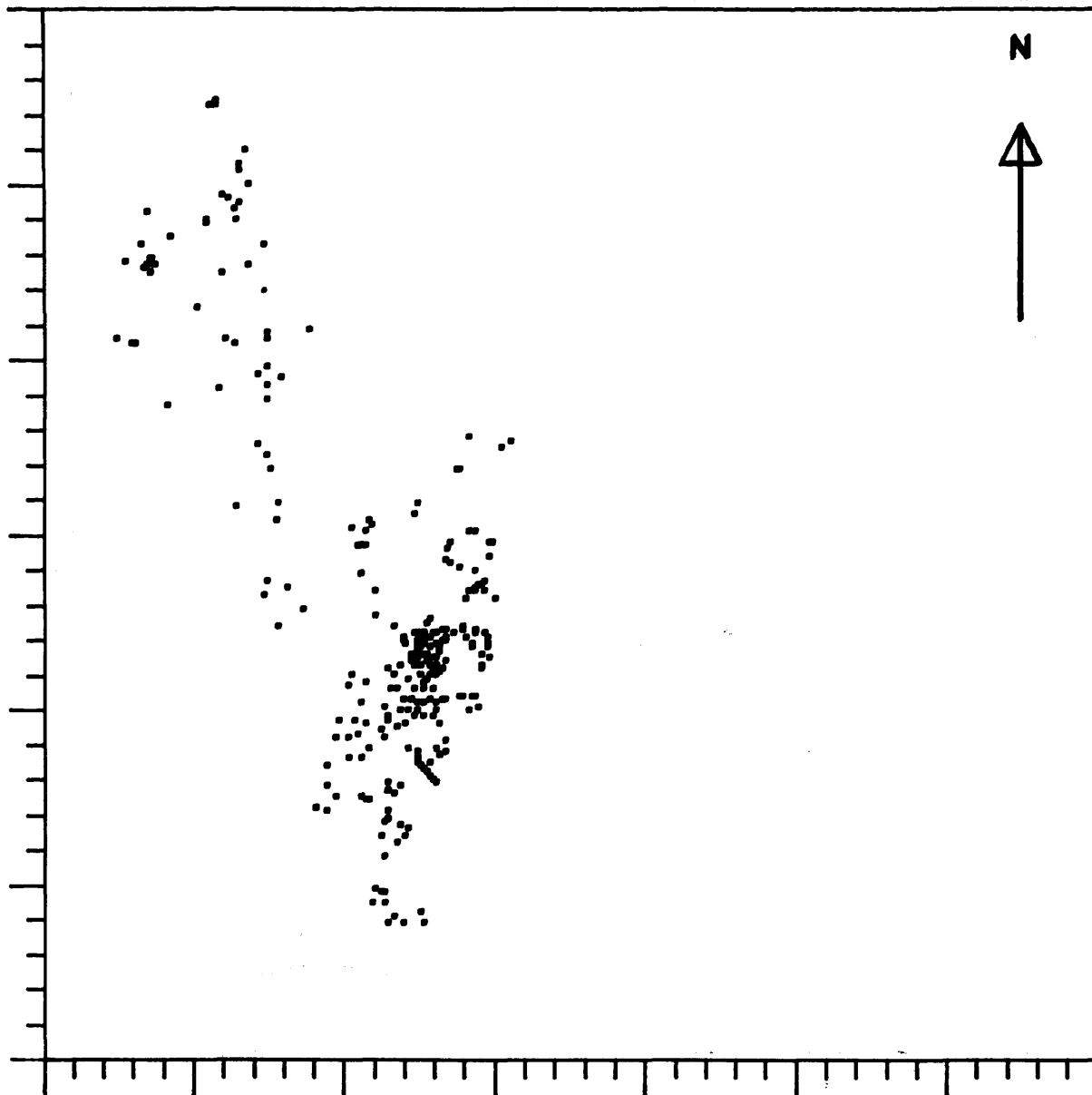


Figure 4a—Locations of 323 samples classified at the greater than 60 percent probability level as being from a mineralized area for the Uchi Lake area.

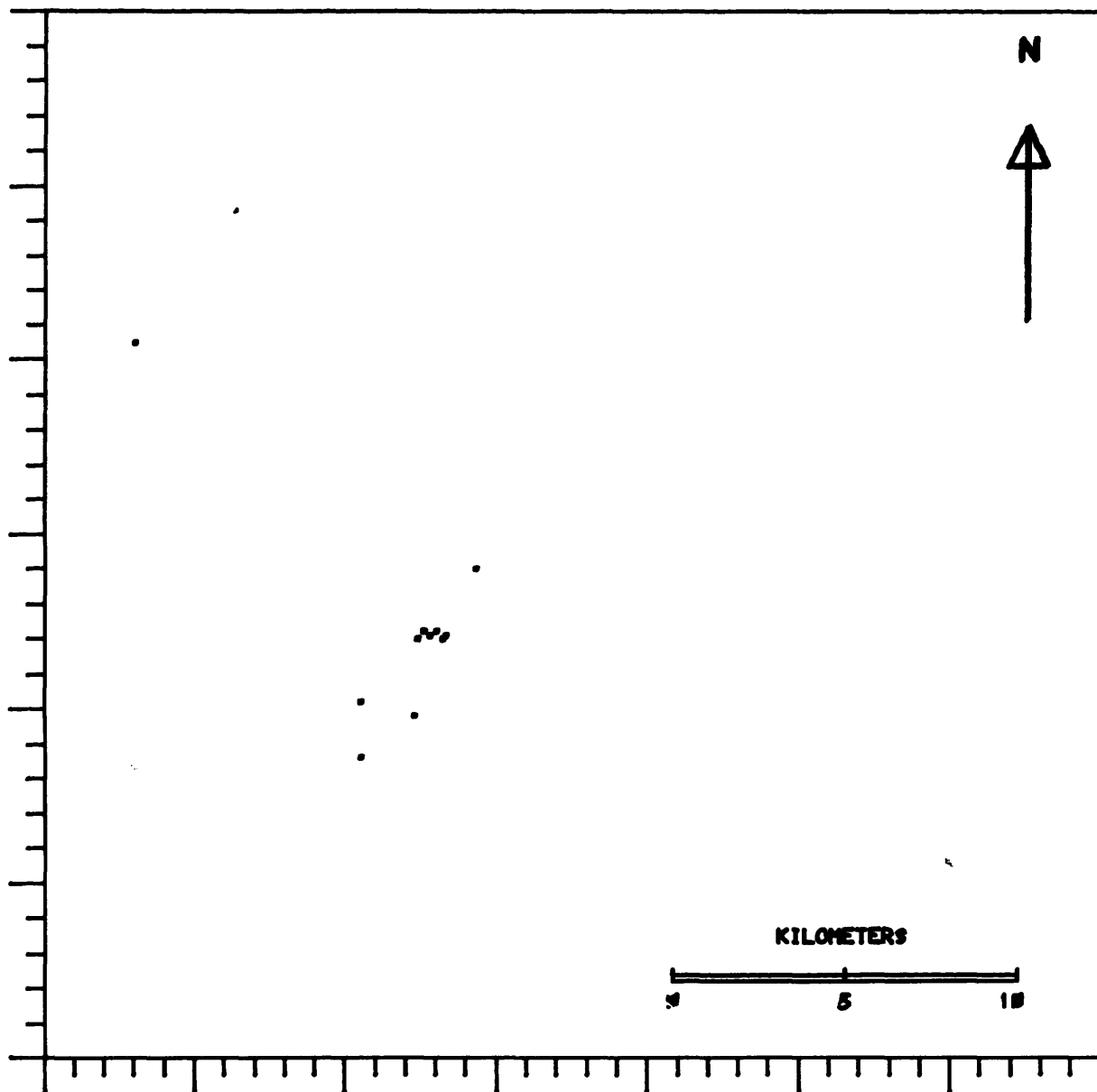


Figure 4b—Locations of 20 samples classified at the greater than 80 percent probability level as being from a mineralized area for the Uchi Lake area.

CONCLUSIONS

1) Mineralized (massive sulphide bearing) and unmineralized areas of Archean greenstone belts, on the scale of several hundred square kilometres, have distinct differences in individual oxide alteration gains and losses as calculated by this new procedure.

2) Discriminant functions, based on a linear combination of several major oxide alteration parameters, give a more reliable and more generally applicable indication of whether or not an area hosts massive sulphide deposits than does the alteration parameter of any individual oxide.

3) When comparisons between mineralized and unmineralized areas are restricted to considering only those samples with greater than 60 percent SiO₂ the percentage of samples correctly identified by the discriminant functions is significantly improved.

4) Within mineralized areas, probability data, used in conjunction with discriminant function scores, are capable of identifying relatively small (1 km²), high probability, target areas which might be suitable for supportive geological, geophysical and detailed geochemical investigations.

ACKNOWLEDGEMENTS

The writer would like to thank Dr. Ian Nichol of Queen's University for supplying the analytical data which forms the basis of this study. Thanks are also due to Mr. Walter Megown whose assistance with computer programming was invaluable. The computer graphics facilities used for this project were purchased with NSERC Canada Equipment Grants. I would also like to thank Miss Susan Cunningham for typing the manuscript.

REFERENCES

- Beswick, A.E. and Nichol, I.
1980: Alteration in mineralized and unmineralized greenstones; p.39-47 in Geoscience Research Grant Program, Summary of Research 1979-80, ed. E.G. Pye, Ontario Geol. Surv. Miscellaneous Paper 93.
- Beswick, A.E. and Soucie, G.
1978: A correction procedure for metasomatism in an Archean greenstone belt; *Precamb. Res.* Vol. 6, p.235-248
- Klovan, J.E. and Billings, G.K.
1967: Classification of Geological Samples by Discriminant Function Analysis; *Bull. Can. Pet. Geol.* vol. 15, no. 3, p.313-330.
- Lavin, O.P.
1976: Lithochemical Discrimination between Mineralized and Unmineralized Cycles of Volcanism in the Sturgeon Lake and Ben Nevis Areas of the Canadian Shield; unpublished M.Sc. thesis, Queen's University, 249p.
- McConnell, J.W.
1976: Geochemical Dispersion in Wallrocks of Archean Massive Sulphide Deposits; unpublished M.Sc. thesis, Queen's University, 230p.
- Nie, N.H., Bent, D.H., and Hull, C.H.
1970: Statistical Package for Social Sciences, Users Manual; McGraw Hill Inc., 343p.
- Sopuck, V.J.
1977: A Lithochemical Approach in the Search for Areas of Felsic Volcanic Rocks Associated with Mineralization in the Canadian Shield; unpublished Ph.D. thesis, Queen's University, 295p.
- Sopuck, V.J., O.P. Lavin, and Nichol, I.
1980: Lithochemistry as a guide to identifying favourable areas for the discovery of volcanogenic massive sulphide deposits; *CIM Bulletin*, November 1980, p.152-166.

Grant 28 Immobilization of U-Th-Ra in Mine Wastes

J. R. Brown, W. S. Fyfe, F. Murray and B. I. Kronberg

Department of Geology, University of Western Ontario

ABSTRACT

By treating typical Elliot Lake uranium mine effluents with calcite, potassium phosphate solutions (300 ppm), with or without glacial tills, radium leach levels have been reduced to below 0.1 pCi/l. Such radium values are in the range of ocean waters and high quality fresh waters. Mine tailing permeabilities can be reduced to low levels by use of appropriate clay additives and in particular by the use of thin bentonite layers before closure.

INTRODUCTION

In previous reports (Fyfe 1979; Brown *et al.* 1980) the general concept of using phosphate mineralization as a method of fixing U-Th-Ra was outlined. Perhaps the most convincing natural evidence for this concept is the great stability of uranium-bearing apatite minerals observed during the tropical weathering of phosphate-rich carbonates in Brazil where the laterite profiles over carbonates are used as a source of phosphate and are being investigated as possible sources of uranium. Russian work (Gaushin *et al.* 1973) has shown that uranium decay products are effectively retained by the apatite structure.

Recently Phillips and Poon (1980) have reviewed the present technology for uranium extraction from ores and have discussed new possibilities for improving the radium problem by solvent extraction techniques. They state "although the existing techniques of ore processing are adequate for the purpose of obtaining uranium from a wide range of ores, they were not developed to deal with the closely-related problem of radium in solid and liquid effluents (tailings). The present method of disposal of radium—coprecipitation with barium sulphate—has a negative impact on profit and is of limited efficiency." We would add that all sulphates in the surface environment are subject to bacterial decomposition with potential release of the trapped radium. Bloch (1980) has shown that uranium in the marine environment is closely coupled to phosphate while Kanel and Morse (1978) showed that calcium carbonate surfaces may be excellent phosphate absorbers and provide nucleation sites for growth of phosphate minerals.

EXPERIMENTAL VERIFICATION

Data in our previous reports have shown the following.

- (a) Calcium carbonate and calcium sulphate minerals can be replaced by calcium phosphate minerals at room temperature in periods of weeks or months by treatment with alkali phosphate solutions in the concentration range 1-0.01 molar (P 31,000-310 ppm).
- (b) It was possible to measure growth rates of 10^{-5} g/cm²/day at room temperature on single crystals of apatite.
- (c) Surface adsorption studies using electron spectroscopy for chemical analysis (ESCA) showed that U is strongly adsorbed on apatite surfaces and that in two weeks solutions at the 1 ppm level were reduced to the 1 ppb range by adsorption on fine-grained apatite. Barium (comparable to Ra) behaved in a similar manner.
- (d) Highly concentrated mine by-products very rich in U-Th-Ra were diluted in sodium borate-calcium phosphate glasses. Leaching of these glasses by Beak Consultants of Mississauga showed below background release rates of U-Ra.

D. Moffett of Rio Algom Limited supplied us with two large samples of mine effluent from their Elliot Lake operation. The first type (A) consisted of older dried tailings from an active waste pile, and the second type (B) consisted of fresh wet tailings taken directly from the mill discharge in slurry form. We have studied radium fixation in these tailings by treatment with calcium carbonate and potassium phosphate solutions in the concentration range 1-0.01 molar (note there is no special reason for the use of K rather than Na phosphate but we had used K-phosphate in the apatite growth experiments).

In other experiments Port Hope glacial till which had been treated with phosphate for three months was added to the tailings. These tills are impermeable, and in laboratory studies of loosely packed till permeabilities of 10^{-4} darcy were easily obtained. The tills have a large component of calcite and the pretreatment with phosphate must induce apatite growth before addition to the tailings. Obviously, the purpose of till addition is to leave the tailings with a very low permeability after phosphate fixation. In other permeability experiments we have been able to show that addition of thin (1 inch) layers of bentonite can further reduce the permeabilities by orders of magnitude, the thin bentonite layers having effective permeabilities less than 10^{-8} darcy when confined by a few metres of overburden. We would stress that permeability control is of

great importance in producing a final stable state in the tailings after mining operations cease.

After appropriate treatment, samples of effluent water were removed and analysed for radium by Beak Consultants of Mississauga. Samples were either of 100 or 1000 ml volume. With 100 ml samples the sensitivity limit for radium determination was 1 pCi/l while with the 1000 ml samples 0.1 pCi/l could be determined.

Our main data are summarized in Table 1. Unless otherwise specified, 125 g of tailings were treated with 2.5 litres of solution for times ranging from 11-227 days before sampling. All solutions were filtered through micropore filters in the range 1.2-0.05 μm , 0.45 μm being the most commonly used.

It is clear from the data in Table 1, that extremely low radium values can be obtained. Values for litre samples

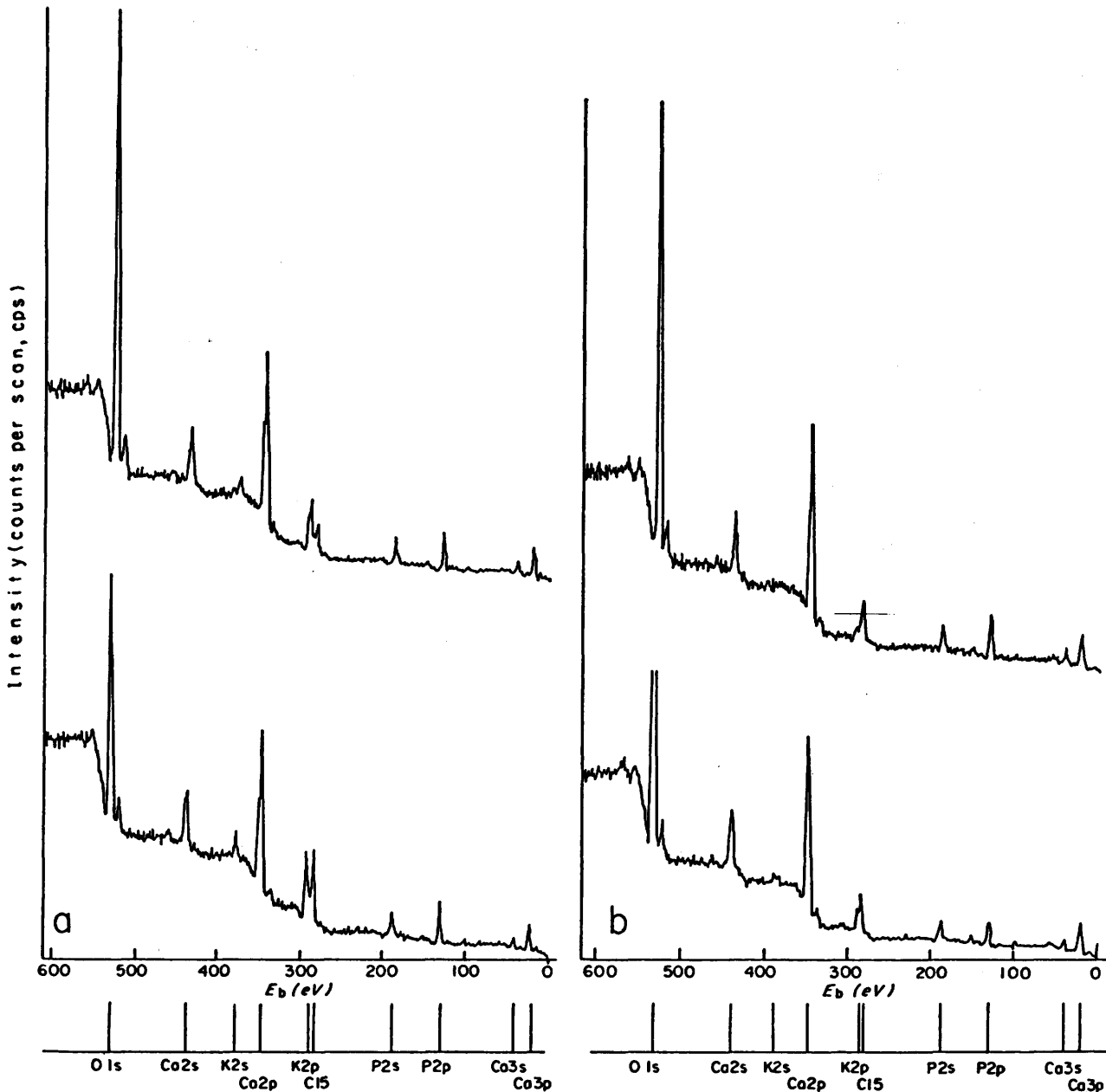


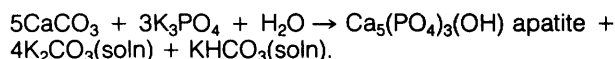
Figure 1—ESCA scan of calcite-rich regions of tailings samples treated for more than 200 days. **a.** Sample C-6, top, C-5, bottom. **b.** Sample C-3, top, C-1, bottom.

GRANT 28 IMMOBILIZATION OF U-TH-RA IN MINE WASTES

Table 1—Radium activity in treated samples of tailings from uranium mines. See text for explanation.

Sample No.	Tailing Type	Till	[PO ₄ ³⁻]	Time	Filter size in μm	Mass of CaCO ₃	Ra pCi/l	Notes
A-1	B	nil	0.01 M	11 days	0.45	25 g	< 1	
A-3	B	nil	1.0 M	11 days	0.45	25 g	15	
A-3	B	nil	1.0 M	11 days	0.45	25 g	11	
A-4	A	nil	0.01 M	11 days	0.45	25 g	3	
A-4	A	nil	0.01 M	11 days	0.45	25 g	3	
A-6	A	nil	1.0 M	11 days	0.45	25 g	57	
A-12	B	nil	nil		0.05	nil	170	filtrate from tailings
A-12	B	nil	nil		0.05	nil	170	filtrate
A-13	B	nil	nil		1.2	nil	240	filtrate
A-14	A	nil	nil	48 days	0.45	nil	200	Blank - tailings in D.I.W.
A-14	A	nil	nil	48 days	0.45	nil	200	Blank - tailings in D.I.W.
A-16	B	nil	nil	41 days	0.45	nil	260	Blank - tailings in D.I.W.
A-17	A (85g)	213g	0.1 M	11 days	0.45	nil	< 1	
A-19	B (85g)	213g	0.1 M	11 days	0.45	nil	< 1	
A-20	A	nil	nil			nil	140	solid sample
A-20	A	nil	nil			nil	130	solid sample
A-20	A	nil	nil			nil	130	solid sample
A-21		nil	nil		0.45	nil	1	acidified deionized water
B-2	A (85g)	213g	0.1 M	84 days	0.45	nil	0.2	
B-2	A (85g)	213g	0.1 M	84 days	0.45	nil	0.3	
B-3	B	nil	1.0 M	69 days	0.45	25 g	7.8	
B-4	A	nil	0.01 M	87 days	0.45	25 g	14	Samples B-2, B-3, B-5,
B-5	B (85g)	213g	0.1 M	84 days	0.45	nil	0.1	B-6 and B-7 were 1 litre samples
B-5	B (85g)	213g	0.1 M	84 days	0.45	nil	0.1	
B-6	A	nil	1.0 M	69 days	0.45	25 g	17	
B-7	B	nil	0.01 M	87 days	0.45	25 g	1.6	
B-7	B	nil	0.01 M	87 days	0.45	25 g	1.2	
B-12	B	nil	1.0 M	87 days	0.45	525 g	2.4	The first 69 days were with
B-13	A	nil	1.0 M	87 days	0.45	525 g	13	25g of CaCO ₃ in 2.5 l. The last 18 days were with 525g in 1.5 l.
B-14	A	nil	nil	124 days	0.45	nil	24	Blank - tailings in D.I.W.
B-14	A	nil	nil	124 days	0.45	nil	21	Blank - tailings in D.I.W.
B-16	B	nil	nil	117 days	0.45	nil	91	Blank - tailings in D.I.W.
B-16	B	nil	nil	117 days	0.45	nil	98	Blank - tailings in D.I.W.
B-21		nil	nil		0.45	nil	4.0	Tap water, acidified
C-1	A	nil	0.01 M	227 days	0.45	25 g	< 0.1	
C-2	B	nil	0.01 M	227 days	0.45	25 g	< 0.1	
C-3	A	nil	0.1 M	227 days	0.45	25 g	0.1	All C series were
C-4	B	nil	0.1 M	227 days	0.45	25 g	< 0.1	1 litre samples
C-5	A	nil	1.0 M	227 days	0.45	525 g		158 days with 525g CaCO ₃ in 1.5 l and 69 days with 25g of CaCO ₃ in 2.5 l.
C-7	A	nil	nil	264 days	0.45	nil		Blank - tailings in D.I.W.
C-9	A (85g)	213g	0.1 M	224 days	0.45	nil	0.3	
C-10	B (85g)	213g	0.1 M	224 days	0.45	nil	0.3	

are commonly below the detection limit of 0.1 pCi/l or in the range of common ocean water values (0.02-0.17) and high quality fresh waters (0.04-0.20). In fact, many of our leach waters are superior to the tap water sampled in the geology department! The data also show that the more dilute phosphate treatment (0.01 molar, 300 ppm) is at least as good or even better than treatment with more concentrated phosphate. This is possibly due to pH effect induced by the replacement reaction:



Four samples of the products treated for over 200 days (C series) were studied by ESCA and analytical SEM (scanning electron microscope) using facilities at the CANMET laboratories of the Department of Energy, Mines and Resources in Ottawa. Standard X-ray diffractometer patterns revealed mainly quartz and calcite in the materials as would be expected for samples with no added tills. The quantities of phosphates formed would be too small for production of significant signals on a diffractometer pattern.

Surface ESCA studies of the calcite-rich regions of powdered products (the sample area observed is of the order of 0.5 cm²) showed high concentrations of fixed phosphates (Figure 1). The major element concentrations which could be detected included Ca, P, C, O, K, Si, Fe and in one case minor U. Typical ESCA scans are shown

in Figure 1. Reasonably strong potassium signals appeared in two samples. Quantitative studies of the ESCA scans show Ca/P values close to those expected for apatite formation and apatite and calcite account for much of the data as would be expected. Table 2 shows the chemical analysis related to the ESCA scan for sample C-3.

Samples which showed a significant quantity of potassium fixed in the surface materials (C-2 and C-1) were examined by a scanning electron microscope with analytical capability. In these samples calcite was clearly observed along with very common plate-like crystals which contained significant Ca-K-P (Figures 2a, b). Other samples contained granular and prismatic materials more typical of apatite (see Fyfe 1979). We have not positively identified the platy material. The samples appear to have powdery surfaces so that contamination by evaporated solution is possible. In various samples the peak heights of K-Ca signals are highly variable supporting this possibility. But Ca-K phosphates do occur in nature (dehrnite, lewistonite). We would note that Avimelech (1980) has reported the formation of a complex carbonate phosphate, $\text{Ca}_3(\text{HCO}_3)_3\text{PO}_4$, as a surface compound on calcite and aragonite. This may well be intermediate in the apatite-forming process. A comparison of ESCA and SEM data indicate that many of the apparently clear calcite crystals do have a phosphate surface coating.

Table 2—Surface chemistry analysis for sample C-3, based on ESCA for carbonate-rich portions of sample.

	<u>Atomic %</u>	<u>Wt. %</u>
O	53.7	40.2
C	17.0	9.5
P	8.2	12.6
Ca	15.7	29.4
Fe	0.9	2.4
Si	2.2	2.9
K	1.3	2.4

Ca/P = 1.70 (experimental), carbonate—free basis

Ca/P = 1.67 (theoretical, from $\text{Ca}_5(\text{PO}_4)_3\text{OH}$)

Note: carbon measured is 90% hydrocarbon surface contamination from ultra-high vacuum system.

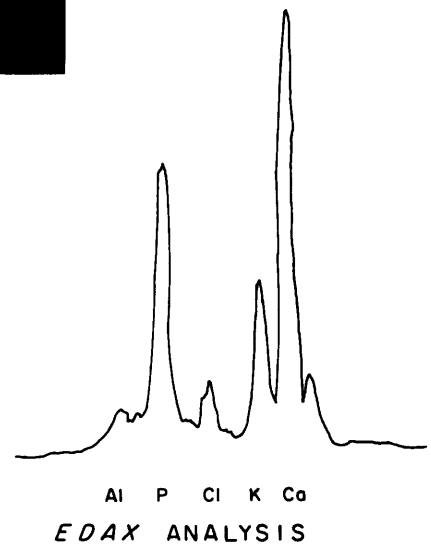
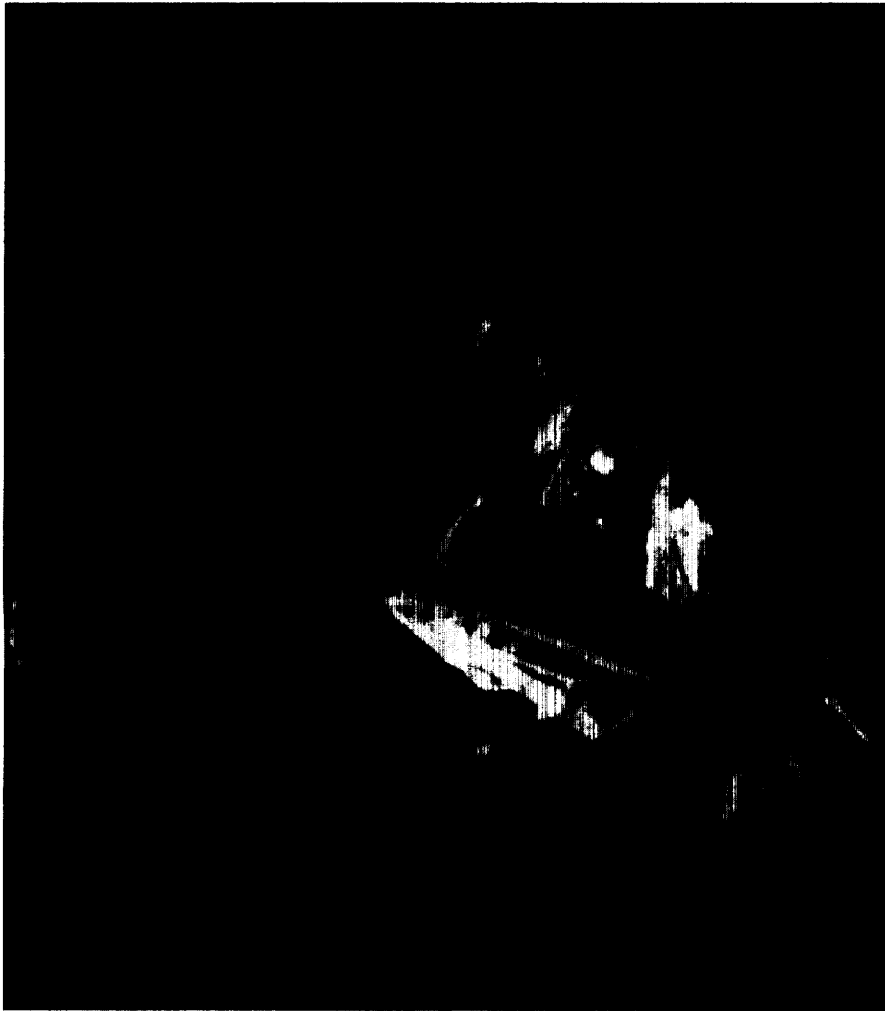


Figure 2a—Scanning electron photomicrograph (3000X) of K-rich areas of tailings sample C6, and Energy Dispersive X-ray analysis of circled areas on photo.

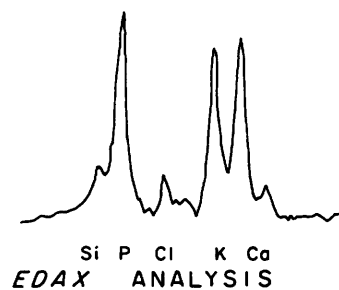


Figure 2b—Same as Figure 2a, for sample C5.

CONCLUSION

It has been shown that by treating uranium mine effluents with calcium carbonate and dilute phosphate solutions, radium can be fixed and leach solutions carry this element at levels reduced to values below 0.1 pCi/l, i.e., ocean water values. The permeability of tailings can be reduced by addition of appropriate clays and in particular by the use of bentonite layers which could be added in the basal and upper layers of tailings deposits before closure of an operation. Phosphate treatment should be considered by industry as a potentially superior method of treatment to the barium sulphate method commonly used.

REFERENCES

- Avimelech, Y.
1980: Calcium-Carbonate-Phosphate Surface Complex in Calcareous Systems; *Nature*, vol. 288, p.255-257.
- Bloch, S.
1980: Some Features Controlling the Concentration of Uranium in the World Ocean; *Geochim. Cosmochim. Acta.*, vol. 44, p.373-377.
- Brown, J. R., Fyfe, W. S., Murray, F., and Kronberg, B.I.
1980: Immobilization of U-Th-Ra in Mine Wastes; p. 48-57 in *Geoscience Research Grant Program, Summary of Research, 1979-80*, edited by E.G. Pye, Ontario Geological Survey, MP 93, 263 p.
- Fyfe, W.S.
1979: Immobilization of U-Th-Ra in Mine Wastes by Mineralization; p. 79-83 in *Geoscience Research Grant Program, Summary of Research, 1978-1979*, edited by E.G. Pye, Ontario Geological Survey, MP 87, 152 p.
- Gaushin, U. M., Bubrov, U. A., Pyalling, A. O., and Reznikov, N. V.
1973: The Two Types of Uranium Accumulation in Rocks by Sorption; *Geochemistry International*, vol. 10, p.687-690.
- Kanel, J. De., and Morse, J. W.
1978: The Chemistry of Orthophosphate Uptake from Seawater on to Calcite and Aragonite; *Geochim. Cosmochim. Acta.*, vol. 42, p.1335-1340.
- Phillips, C. R., and Poon, Y. C.
1980: Status and Future Possibilities for the Recovery of Uranium, Thorium and Rare Earths from Canadian Ores, with Emphasis on the Problem of Radium; *Minerals Sci. Engineering*, vol. 12, p.53-72.

Grant 80 Rare Earth Elements in Felsic Volcanic Rocks Associated with Cu-Zn Massive Sulphide Mineralization

I.H. Campbell¹, P. Coad², J.M. Franklin³, M.P. Gorton¹, T.R. Hart¹, S.D. Scott¹, J. Sowa¹ and P.C. Thurston⁴

¹Department of Geology, University of Toronto

²Texasgulf Canada Ltd.

³Economic Geology Division, Geological Survey of Canada

⁴Ontario Geological Survey

ABSTRACT

Massive sulphide deposits are closely associated with felsic volcanism. This association is believed to be genetic and forms the cornerstone for most exploration programs, but unfortunately not all felsic volcanic rocks contain ore. It seems likely that ore-bearing felsic volcanic rocks have a different genetic history from barren felsic volcanic rocks and, if this is so, these differences should be reflected in their rare earth element (REE) geochemistry.

A preliminary study of REE in Archean felsic volcanic rocks has shown that those associated with ore have flat REE patterns with well developed Eu anomalies whereas those from barren volcanic rocks have steep REE patterns with weak or absent Eu anomalies. The felsic volcanic rocks associated with ore can be subdivided into two types: tholeiitic and calc-alkaline. Those at the Kam-Kotia, Matagami and South Bay mines are tholeiitic whereas those at the Sturgeon Lake and Golden Grove deposits are calc-alkaline.

The well-developed Eu anomalies in the ore-related felsic volcanic rocks indicate that the melt has undergone a high degree of fractional crystallization en route to the surface, suggesting the existence of a subvolcanic magma chamber below the ore body. We believe that these subvolcanic sills are an integral part of the ore-forming process and are therefore required for the formation of massive sulphide deposits.

The characteristic REE patterns of the ore-associated felsic volcanic rocks should help mining companies in selection of areas for massive sulphide exploration.

INTRODUCTION

An important characteristic of Archean Cu-Zn massive sulphide deposits is their close association with felsic volcanic rocks. This association is believed to be genetic and forms the cornerstone for most exploration programmes. The presence of felsic volcanic rocks on an exploration property does not guarantee success, however, as most are barren. If some way can be found to distinguish

between barren and ore-bearing felsic volcanic rocks, or if certain types can be eliminated as potential target areas, exploration companies will be able to direct their efforts where they are most likely to succeed.

Where Cu-Zn deposits are found in areas of cyclic volcanism, they occur in specific units. For example, at Sturgeon Lake they are found at the top of cycles 1a and 1b (Franklin 1978) and at Uchi Lake in the uppermost of three felsic horizons (Thurston, in press). The implication is that certain felsic volcanic rocks, by virtue of their genetic history, are associated with massive Cu-Zn mineralization. Although the genetic significance of REE patterns is not always clear, we can be confident that they are governed by fundamental partial melting and fractionation processes (Gast 1968; Shaw 1970). There should therefore be a distinct difference between the REE geochemistry of barren and ore-bearing rocks.

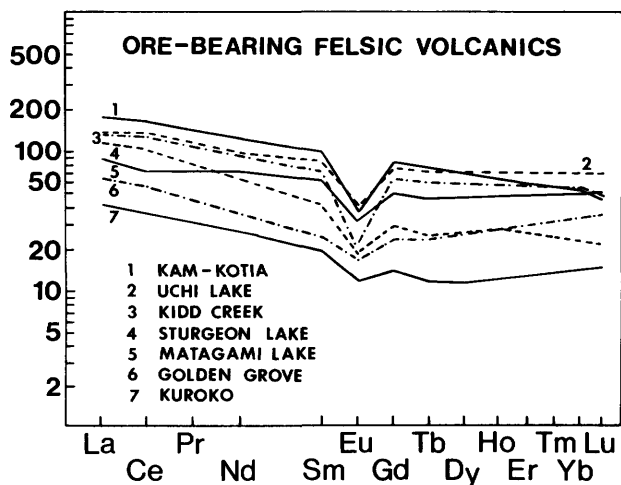


Figure 1—Chondrite-normalized REE patterns for seven ore-bearing felsic volcanic units. Data for Matagami Lake unit from MacGeehan and MacLean (1980).

To test this hypothesis we have commenced a study of the trace element geochemistry of ore-bearing felsic volcanic rocks, paying special attention to immobile trace elements such as Y, Ti, Zr and the REE. In this report we present preliminary data from four ore-bearing units. The results are encouraging and should be of interest to mining companies.

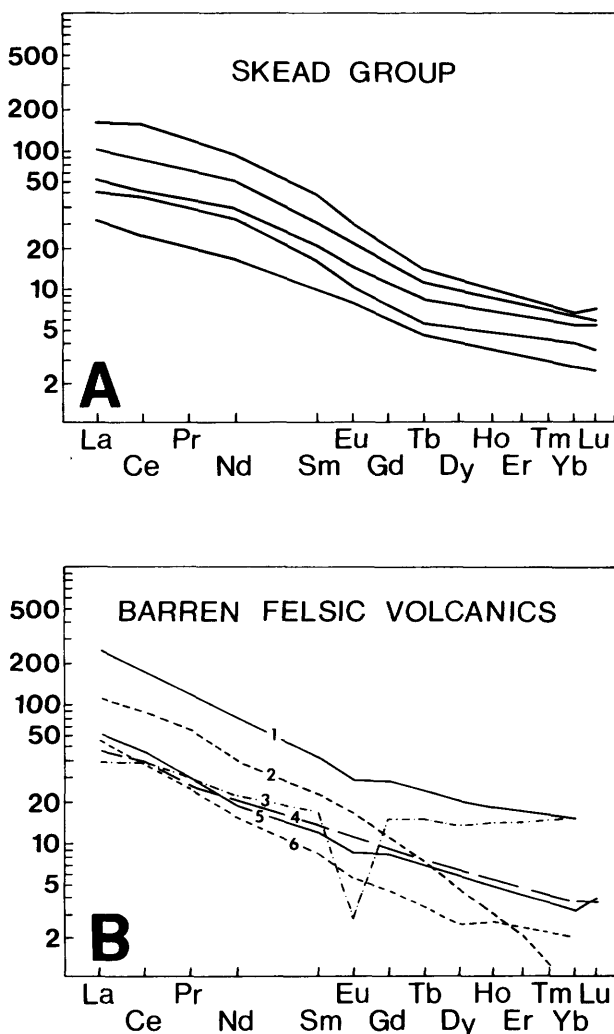


Figure 2—A. Chondrite-normalized REE patterns for six barren felsic volcanic units from the Skead area, Abitibi "greenstone" belt. (From unpublished data, Goodwin and Gorton). **B.** REE patterns for six barren felsic volcanic units. 1 = Marda dacite (Taylor and Hallberg 1977), 2 = Middle Marker porphyry (Glikson 1976), 3 = Marda rhyolite (Taylor and Hallberg 1977), 4 = Rhyolite, cycle 4, Sturgeon Lake, 5 = Hanging wall quartz-eye ash flow, Golden Grove, 6 = Onverwacht porphyry (Glikson 1976).

Prior to the commencement of this study Thurston (in press) demonstrated that the REE patterns of samples from the ore-bearing horizon of the South Bay Mine were distinctly and consistently different from those of the other horizons. He found that the patterns from ore-bearing horizons were only slightly enriched in light rare earth elements (LREE) and had a pronounced Eu anomaly whereas those from barren felsic volcanic rocks showed strong LREE enrichment and Eu anomalies were weak or absent. Thurston has also presented REE patterns of a reconnaissance nature for ore-bearing volcanic rocks from the Kam-Kotia area near Timmins, Ontario. These patterns appear to be similar to those of the South Bay ore-bearing rhyolite.

RESULTS

The data from our study, together with one pattern obtained from the literature, are presented in Figure 1. The patterns from the ore-bearing felsic volcanic rocks are characteristically flat (low La/Lu ratios) and have well developed Eu anomalies. REE patterns for barren felsic volcanic rocks from the Abitibi "greenstone" belt are presented in Figure 2a and for other "greenstone" belts in Figure 2b. With one exception, they show strong LREE enrichment and Eu anomalies are weak or absent. The exception is a rhyolite from the Marda area in Western Australia. It has a flat REE pattern similar to those in Figure 1 and a well developed Eu anomaly. Significantly, several showings of Cu-Zn mineralization have been found in the Marda area, but none has been shown to be economic.

EFFECTS OF ALTERATION

The volcanic rocks which host massive Cu-Zn sulphide deposits are invariably altered. MacGeehan and MacLean (1980) have suggested that the alteration associated with massive sulphide deposits can result in mobilization of so-called "immobile" trace elements such as Y, Zr, Ti and REE. Before REE can be used as a guide to area selection in massive sulphide exploration, some assessment must be made of their mobility. We have begun such a study in the Sturgeon Lake area. Here Franklin *et al.* (1975) recognised two types of alteration: pervasive, low intensity alteration extending up to 4 km from the ore deposits, and more localized high-intensity alteration which forms the alteration pipes below the ore bodies. We have collected samples from both alteration zones and from the unaltered rhyolite. REE patterns from the low intensity alteration zone, which is characterized by alkali depletion, are identical to those from unaltered samples. Samples from the mine rhyolite, collected from the alteration pipe below the ore body, have variable REE patterns and do show evidence of REE mobility. They have a lower REE content than unaltered rhyolites and most samples show evidence of heavy rare earth element (HREE) enrichment (Figure 3d). Chloritized samples from Golden Grove and Kidd Creek also show HREE enrichment.

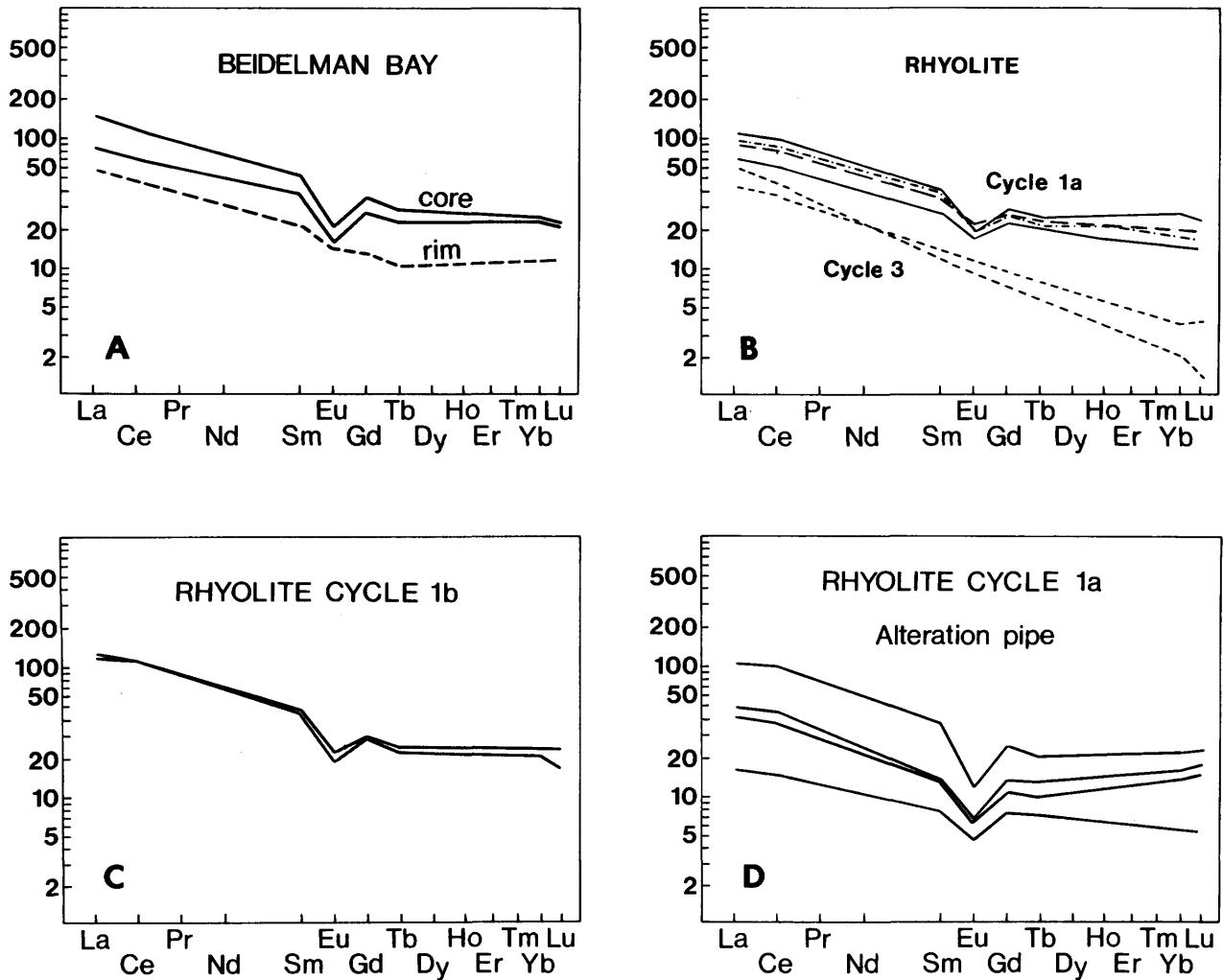


Figure 3—Chondrite-normalized REE patterns for rhyolites from Sturgeon Lake. **A.** Beidelman Bay Complex; **B.** volcanic cycles 1a and 3; **C.** volcanic cycle 1b; **D.** samples from the alteration pipe below the Mattabi Mine.

SUBVOLCANIC MAGMA CHAMBERS

The flat REE patterns of ore-bearing horizons with their characteristic Eu anomalies indicate that the parent magmas have undergone extensive fractional crystallization, implying the existence of magma chambers beneath the ore deposits. This hypothesis is in agreement with current theories for the origin of the Kuroko massive sulphides. These deposits, like Archean massive sulphides, are typically accompanied by extensive alteration zones. Calculations by Cathles (1978) and Urabe and Sato (1978) indicate that the heat released by the rhyolite dome during volcanism can produce only a small fraction of the heat necessary to drive the required hydrothermal system. They predict the existence beneath the ore deposits of a shallow-level magma chamber which they argue would act as a heat engine.

Archean massive sulphide deposits, unlike the Kuroko deposits, are turned on their side, exposing their "plumbing" for inspection and sampling. Significantly, most Archean massive sulphide deposits have subvolcanic sills (high-level magma chambers) in their footwalls. Examples are found at Uchi Lake, Snow Lake, Sturgeon Lake, Noranda, Kam-Kotia and Matagami. Two examples are illustrated in Figures 4 and 5.

We have tested this hypothesis by comparing the trace and major element abundances of the ore-bearing felsic volcanic rocks with those of the subvolcanic magma chamber. Typical results from Sturgeon Lake and Kam-Kotia are given in Figures 3 and 6 (REE) and in Tables 1 and 2 (major elements). It is clear from these results that these subvolcanic sills were the magma chambers which fed the overlying volcanic sequence. We

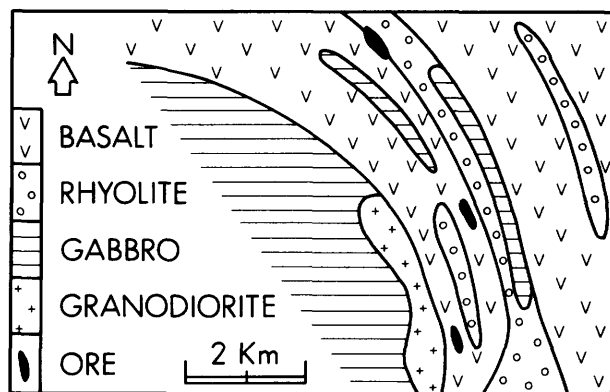


Figure 4—Simplified plan of the Kam-Kotia area showing the relationship between the volcanic rocks and the subvolcanic magma chamber. Dips in the area are steep and stratigraphic tops face northeast.

believe this link is important and that the subvolcanic sills form an essential part of the ore-forming system.

RESULTS FOR INDIVIDUAL AREAS

1. STURGEON LAKE AREA

The geology of the Sturgeon Lake area is described by Franklin *et al.* (1975; Franklin 1978). Three cycles of volcanism are recognized, a typical cycle having basaltic andesite at its base and felsic pyroclastic rocks at the top. The ore deposits are found at the top of cycles 1a and 1b (see Figure 5). The base of the sequence is intruded by a subvolcanic sill, the Beidelman Bay Complex, which geochemical evidence suggests is the magma chamber which fed cycles 1a, 1b and 2. The barren felsic volcanic rocks of cycle 3, however, had a different source. Their REE patterns are steeper than those of the Beidelman Bay Complex and they have no Eu anomalies (Figure 3b).

Franklin (1978) has divided the Beidelman Bay Complex into two zones: an outer quartz diorite margin or rim and an inner trondhjemitic core. The outer dioritic margin has a calc-alkaline REE pattern, no Eu anomaly and an SiO₂ content of 65 percent, whereas the inner core has SiO₂ contents in the range of 74-78 percent, higher REE contents and strong Eu anomalies (Figure 3a). The inner liquid has clearly developed from fractional crystallization of a parent liquid represented by the outer dioritic margin. This has two effects on the REE pattern, firstly it raises the level of REE in the melt, producing a pattern parallel to that in the original melt but at a higher level and, secondly, it results in the development of a Eu anomaly. Fractional crystallization cannot be the result of crystal settling as the rate of separation of crystals from melt in a viscous felsic magma is too slow to produce efficient fractiona-

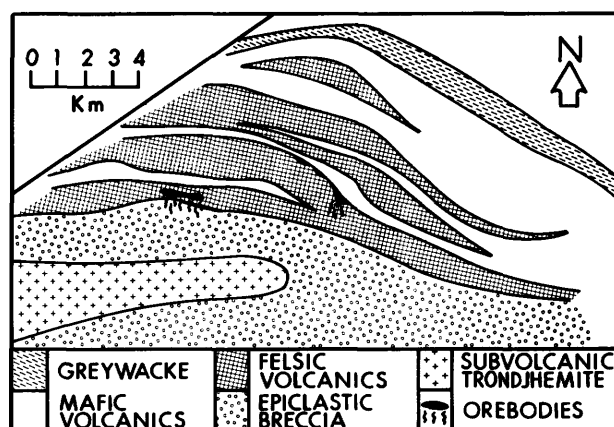


Figure 5—Simplified plan of the Sturgeon Lake area showing the relationship between the Beidelman Bay Complex (subvolcanic trondhjemite) and the ore deposits. Dips in the area are steep and stratigraphic tops face north.

tion. It is more likely that the intrusion has crystallized from the outside in, the liquid being separated from the growing crystals by a combination of diffusion and convection. Most petrologists studying layered intrusions now accept that fractional crystallization results from in situ growth of the cumulus minerals at the sides and floor of the magma chamber (Campbell 1973, 1978; McBirney and Noyes 1979; Irvine 1980) and this would seem the most viable mechanism to explain fractional crystallization in granitoid magmas.

2. KAM-KOTIA AREA

The massive sulphides of the Kam-Kotia area are associ-

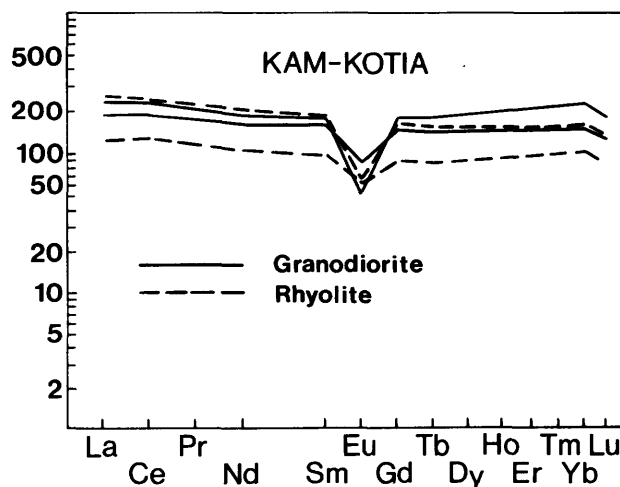


Figure 6—REE patterns for the Kam-Kotia subvolcanic magma chamber and the ore-associated rhyolites.

Table 1—Major element abundances in rocks from Kam-Kotia Mine area.

Sample No.	1	2	3	4	5	6	7	8	9
SiO ₂	49.77	47.20	51.73	50.94	73.17	71.20	72.32	73.12	77.58
TiO ₂	1.07	0.76	1.37	1.13	0.32	0.35	0.53	0.28	0.27
Al ₂ O ₃	14.40	15.05	13.67	12.40	10.71	10.36	11.77	11.62	11.15
FeO*	10.93	9.14	12.95	13.37	4.50	5.10	5.59	3.45	1.41
MnO	0.19	0.10	0.23	0.38	0.02	0.08	0.11	0.01	0.01
MgO	6.43	8.25	5.87	7.70	0.04	0.45	0.22	0.99	0.18
CaO	10.17	8.45	7.79	3.73	1.33	1.55	4.17	0.47	0.16
Na ₂ O	1.53	2.76	3.89	1.31	5.51	5.21	0.63	2.50	0.67
K ₂ O	0.63	0.22	0.50	0.26	0.89	1.57	2.15	4.89	8.16
P ₂ O ₅	0.20	0.03	0.11	0.14	0.03	0.03	0.10	0.04	0.03
Loss	2.75	6.77	2.86	7.01	3.58	4.62	2.19	2.89	0.95
TOTAL	98.07	98.73	100.97	98.37	100.10	100.52	99.78	100.26	100.57

Sample Description: No. 1-2 gabbro, 2-3 basalt, 5-6 granodiorite, 7-9 rhyolite.

*Total Fe as FeO

ated with a bimodal sequence of rhyolite and tholeiitic basalt. This sequence is underlain by a large layered tholeiitic sill which has fractionated with a strong Fe-enrichment trend (Middleton 1974). At the top of the sill is a layer of granodiorite which is geochemically similar to the overlying felsic volcanic rocks (Figure 6). Although the granodiorite is clearly related to the underlying gabbro it is unlikely to be the product of simple fractional crystallization since Fe-enrichment in a tholeiite is typically accompanied by SiO₂ depletion (Wager and Brown 1968). One possible explanation for the granodiorite is that it separated as an immiscible liquid during the final stages of fractionation of the sill. Immiscible liquids are a common feature in Fe-rich tholeiites (McBirney and Nakamura 1974; Gélinas *et al.* 1976) and it is possible that, during

the final stages of crystallization, the magma may have split into two immiscible fractions; a felsic liquid and an Fe-rich tholeiite. Studies of the partitioning of REE between immiscible felsic and mafic melts have shown that the REE preferentially enter the mafic liquid but that the La/Lu ratio in the two liquids is the same (Hess 1980). La/Lu ratios in the granodiorite are similar to those in the felsic volcanic rocks and the underlying gabbros, but we have not yet found Fe-rich tholeiites with a REE content greater than that of the granodiorite.

An alternative explanation is that the granodiorite represents the SiO₂-rich top of the type of zoned magma chamber envisaged by Hildreth (1979). We suggest that the felsic volcanic rocks of the Kam-Kotia area are the eruptive equivalent of the granodiorite and that both derive their flat REE patterns from their tholeiitic parent.

Table 2—Major element abundances in rocks from Sturgeon Lake area.

Sample No.	1	2	3	4	5	6	7	8
SiO ₂	61.47	73.88	73.95	73.60	74.30	73.62	70.16	77.36
TiO ₂	0.75	0.51	0.30	0.68	0.39	0.50	0.35	0.19
Al ₂ O ₃	15.05	13.54	11.93	12.88	11.23	13.29	11.92	10.95
FeO*	5.74	2.17	3.14	6.32	5.12	2.17	5.41	1.40
MnO	0.05	0.03	0.06	0.16	0.09	0.03	0.10	0.03
MgO	2.26	1.04	0.72	1.54	3.31	1.24	1.25	0.74
CaO	4.07	2.39	1.46	0.24	0.49	2.36	2.16	1.53
Na ₂ O	4.09	4.43	4.93	0.16	0.15	2.35	1.09	0.43
K ₂ O	1.28	1.19	0.85	0.46	1.58	1.18	1.84	3.17
P ₂ O ₅	0.14	0.06	0.03	0.14	0.04	0.05	0.03	0.00
Loss	4.07	1.20	1.79	2.27	2.66	2.59	4.14	3.67
TOTAL	98.97	100.44	99.16	98.45	99.36	99.38	98.45	99.47

1 Beidelman Bay Complex, rim; 2-3 Beidelman Bay Complex, core;
4-7 cycle 1a; 8 cycle 1b.

3. KIDD CREEK MINE AREA

We have analysed eleven rhyolite samples from the mine area and three massive sulphide samples. All of the rhyolites have flat REE patterns similar to the Uchi Lake rhyolites but have much stronger Eu anomalies (Figure 7a). The patterns show significant variations in La/Lu and La/Sm ratios which could be due to fractionation of an accessory phase in the magma chamber or mobility of the REE during alteration of the rhyolite. Two patterns (Figure 7b) are HREE-enriched suggesting the introduction of some HREE by the mineralizing solutions. Analyses of two massive sulphide samples gave LREE-enriched patterns (Figure 8) and hence failed to support this hypothesis (see also Graf 1977).

4. UCHI LAKE

The ore at the South Bay Mine in the Uchi Lake area is associated with rhyolite flows and a high-level quartz-

feldspar porphyry intrusion. Both the porphyry and the rhyolites have the same flat REE patterns with well-developed Eu anomalies (Figure 9) and are clearly cogenetic. The porphyries are believed to be the feeder connecting the rhyolites to an underlying subvolcanic magma chamber. The existence of a subvolcanic chamber is consistent with gravity studies (Thurston, personal communication).

We have studied the effects of alteration on REE patterns by comparing analyses of unaltered rhyolites with rhyolites from the alteration pipe below the ore body. Differences between altered and unaltered rhyolites are negligible.

DISCUSSION

MacGeehan and MacLean (1980) have argued that "calc-alkaline" rocks associated with massive sulphides at Matagami, Quebec, are actually an altered tholeiitic

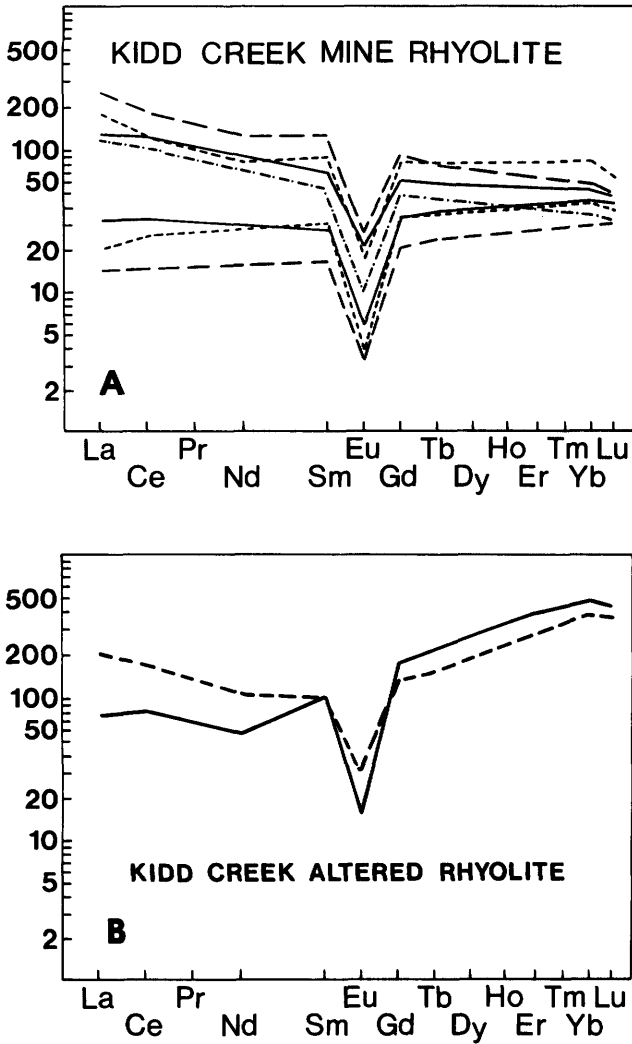


Figure 7—REE patterns for rhyolites from Kidd Creek. **A.** moderately altered rhyolites from the mine area; **B.** highly altered rhyolites collected within a few feet of massive ore.

sequence which, as a consequence of the alteration process, have developed the chemical signature of andesites. The Kam-Kotia sequence is similar to that described by MacGeehan and MacLean. Both consist of bimodal sequences of rhyolite and tholeiitic basalt underlain by large gabbroic sills and are clearly tholeiitic in character. This conclusion, however, does not apply to Sturgeon Lake. Both the Beidelman Bay Complex and the overlying volcanic rocks are calc-alkaline in both their major and minor element geochemistry. Thus Cu-Zn massive sulphide mineralization can be associated with calc-

alkaline or tholeiitic felsic volcanic rocks. Preliminary studies of other massive sulphides suggest that the felsic volcanic rocks associated with the South Bay, Matagami and possibly the Kidd Creek deposits are tholeiitic in character whereas those associated with the Golden Grove (Western Australia) and Kuroko deposits are calc-alkaline (Campbell *et al.* in press).

Thurston (in press) has suggested that the high HREE content of the ore-associated felsic volcanic rocks may be due to the introduction of HREE by the ore-bear-

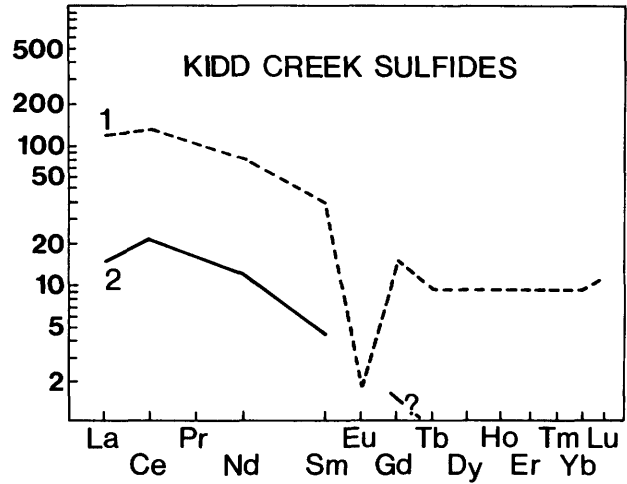


Figure 8—REE patterns for two samples of massive sulphide from the Kidd Creek Mine area.

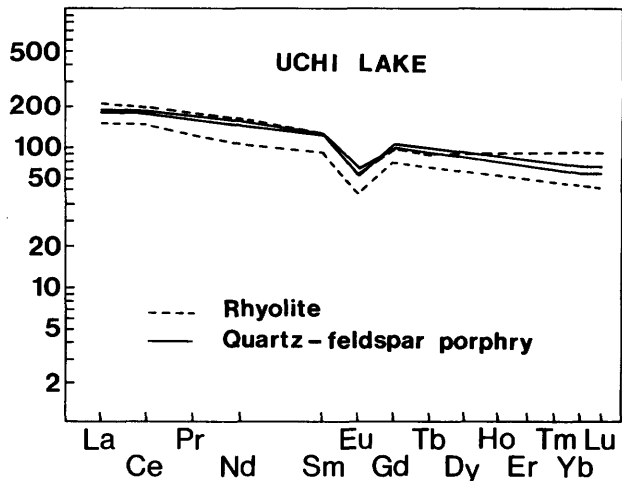


Figure 9—REE analyses for a quartz-feldspar porphyry intrusion and rhyolite flows from the Uchi Lake area.

ing solutions. Our study has shown that the distinctive REE patterns of the ore-bearing felsic volcanic rocks are not confined to the volcanic rocks adjacent to ores, but persist over the entire length of the ore-bearing stratigraphic unit. It seems unlikely that the ore-forming solutions could have enriched such an extensive volume of rock in the HREE. We believe that the REE geochemistry of the ore-bearing felsic volcanic rocks is a primary feature which results from a partial melting process in the crust or upper mantle and subsequent fractional crystallization.

The geochemical link between subvolcanic sills and ore-bearing felsic volcanic rocks demonstrated in this study suggests that subvolcanic sills are an integral part of the ore-forming process. The simplest explanation is that subvolcanic sills play a passive role in ore formation, acting purely as the heat engine which drives the hydrothermal system. In this model, sea water convects through the volcanic pile, producing extensive alteration of the mineral assemblage and leaching out the base metals which are subsequently re-deposited at the sea floor by submarine hot spring activity. If this model is correct, the link between ore deposits and fractionated REE patterns may be connected with the role of volatiles. Volatiles concentrate during the final stages of fractionation of a magma and, if the vapour pressure exceeds the confining pressure, explosive volcanism will result. Massive sulphides are invariably associated with pyroclastic rocks, suggesting that the role of explosive volcanism, in breaking up the volcanic pile and increasing its porosity, may be an essential requirement for ore formation.

There are two other possibilities which should also be considered, both of which require the magma chamber to play a more active role in ore formation. The first is that hydrothermal fluids derive much of their base metal content from the sill by passing through the top of the cooling magma chamber immediately following solidification of the pluton but while its temperature is still well in excess of 300°C.

The second possibility is that the ore-forming solutions are derived directly from a subvolcanic magma chamber. Volatiles and certain base metals (including Cu, Zn and Pb) behave as incompatible elements during silicate fractionation and concentrate in the residual liquid. Eventually, during the final stages of fractional crystallization, a hydrothermal fluid, rich in alkalis and certain base metals (Cu, Pb and Zn) and precious metals (Au and Ag), will separate from the silicate liquid. If the magma chamber leaks, this fluid may escape to the sea floor and form an ore-deposit. Recent isotopic studies of the Kuroko deposits in Japan (Ohmoto and Rye 1974; Pisuha-Arnond and Ohmoto 1980) suggest that the solutions which formed these ore-bodies may have contained up to 20 percent magmatic water, the remainder being sea water. Thus, if subvolcanic sills play an active role in ore genesis, most of the water involved must still be sea water which has either diffused into the magma chamber or mixed with the magmatic fluids en route to the surface. It should be noted that REE geochemistry cannot be used to distinguish between the possible roles of subvolcanic sills.

CONCLUSIONS

It must be stressed that the results presented in this report are preliminary. Although all of the ore-bearing felsic volcanic rocks studied to date show similar distinctive flat REE patterns, it does not follow that all ore-bearing felsic volcanic rocks will have this type of REE geochemistry. Further testing is needed to clarify this point. Nevertheless it does appear that felsic volcanic rocks with flat REE patterns and pronounced Eu anomalies are prime exploration targets and we hope this information will assist mining companies in their search for massive sulphide deposits.

REFERENCES

- Campbell, I.H.
1973: Aspects of the Petrology of the Jimberlana Layered Intrusion of Western Australia; Unpublished Ph.D. Thesis, London University.
1978: Some Problems with the Cumulus Theory; *Lithos*, vol. 11, p.311-323.
- Campbell, I.H., Coad, P., Franklin, J.M., Gorton, M.P., Scott, S.D., Sowa, J.M., and Thurston, P.C.
in press: Rare Earth Elements in Acid Volcanics Associated with Cu-Zn Massive Sulfide Mineralization: A Preliminary Report; *Canadian Journal of Earth Sciences*.
- Cathles, L.M.
1978: Hydrodynamic Constraints on the Formation of Kuroko Deposits; *Mining Geology*, vol. 28, p.257-265.
- Franklin, J.M.
1978: Petrochemistry of the South Sturgeon Lake Volcanic Belt; p.161-180 in *Proceedings of the 1978 Archean Geochemistry Conference*, Editors Smith, I.E.M., and William, J.G.
- Franklin, J.M., Kasarda, J., and Poulsen, K.H.
1975: Petrology and Chemistry of the Alteration Zone of the Mat-tabi Massive Sulfide Deposit; *Economic Geology*, Vol. 70, p.63-79.
- Gast, P.W.
1968: Trace Element Fractionation and the Origin of Tholeiitic and Alkaline Magma Types; *Geochimica et Cosmochimica Acta*, Vol. 32, p.1057-1086.
- Gélinas, L., Brooks, C., and Trzcinski, W.E.
1976: Archean Variolites—Quenched Immiscible Liquids; *Canadian Journal of Earth Sciences*, Vol. 13, p.210-230.
- Glikson, A.Y.
1976: Barberton Mountain Land, Transvaal; *Geochimica et Cosmochimica Acta*, Vol. 40, p.1261-1280.
- Graf, J.L.
1977: Rare Earth Elements as Hydrothermal Traces During the Formation of Massive Sulfide Deposits in Volcanic Rocks; *Economic Geology*, Vol. 72, p.572-590.
- Hess, P.C.
1980: Polymerization Model for Silicate Melts; p.3-48 in *Physics of Magmatic Processes*, Editor Hargraves, R.B., Princeton University Press.
- Hildreth, W.
1979: The Bishop Tuff: Evidence for the Origin of Compositional Zonation in Silica Magma Chambers; *Geological Society of America, Special Paper 180*, p.43-75.

- Irvine, T.N.
1980: Infiltration Metasomatism, Adcumulus Growth, and Double-diffusive Fractional Crystallization in the Muskox Intrusion and Other Layered Intrusions; in *Physics of Magmatic Processes*, Editor Hargraves, R.B., Princeton University Press.
- MacGeehan, P.J.
1978: The Geochemistry of Altered Volcanic Rocks at Matagami, Quebec: a Geothermal Model for Massive Sulfide Genesis; *Canadian Journal of Earth Sciences*, Vol. 15, p.551-570.
- MacGeehan, P.J., and MacLean, W.H.
1980: Tholeiitic Basalt-Rhyolite Magnetism and Massive Sulfide Deposits at Matagami, Quebec; *Nature*, Vol. 286, p.767-771.
- McBirney, A.R., and Nakamura, Y.
1974: Immiscibility in Late-Stage Magmas of the Skaergaard Intrusion; *Carnegie Institute Washington Yearbook*, Vol. 73, p.348-351.
- McBirney, A.R., and Noyes, R.M.
1979: Crystallisation and Layering of the Skaergaard Intrusion; *Journal of Petrology*, Vol. 20, p.487-554.
- Middleton, R.S.
1974: Godfrey Township District of Cochrane; Ontario Division of Mines, Preliminary Map P.967.
- Ohmoto, H., and Rye, R.O.
1974: Hydrogen and Oxygen Isotopic Composition of Fluid Inclusions in the Kuroko Deposits, Japan; *Economic Geology*, Vol. 69, p.947-953.
- Pisutha-Arnond, V., and Ohmoto, H.
1980: Chemical and Isotopic Compositions of the Kuroko Ore-forming Fluids; *Geological Society of America, Abstracts with Program*, Vol. 12, No. 7, p.500-501.
- Shaw, D.M.
1970: Trace Element Fractionation During Anatexis; *Geochimica et Cosmochimica Acta*, Vol. 34, p.237-243.
- Taylor, S.R., and Hallberg, J.A.
1977: Rare-earth Elements in the Marda Calc-Alkaline suit: An Archean Geochemical Analogue of Andean-type Volcanism; *Geochimica et Cosmochimica Acta*, Vol. 41, p.1125-1129.
- Thurston, P.C.
in press: Economic Evaluation of Archean felsic volcanic rocks using REE geochemistry; *Geological Society of Australia*.
- Urabe, T., and Sato, T.
1978: Kuroko Deposits of the Kosaka Mine, Northeast Honshu, Japan-products of Submarine Hot Springs on Miocene Sea Floor; *Economic Geology*, Vol. 73, p.161-179.
- Wager, R.L., and Brown, G.M.
1968: *Layered Igneous Rocks*; Oliver and Boyd Limited, Edinburgh.

Grant 68 A Centrifuged Model Study of the Tectonic Development of Archean Greenstone Belts

John M. Dixon and John M. Summers

Department of Geological Sciences, Queen's University

ABSTRACT

An increased understanding of the tectonic evolution and structure of Archean "greenstone" belts can be gained using the technique of centrifuged model experiments. Experiments included in this report have been designed to investigate deformation patterns produced by vertical gravity tectonics — one possible model for the structural evolution of Archean greenstone belts. The experiments involve simple models with an unstable inverse density stratification: a thin, relatively dense surface layer (representing a greenstone supracrustal sequence), and a lighter, buoyant substrate (representing the source layer for diapiric gneiss domes). Gravitational subsidence of the simulated greenstones occurs within narrow troughs, resembling inverted diapirs, that are separated by broader basement domes. Passive grids have been used to monitor the development of incremental and finite strains within the models. In some models, the simulated greenstone supracrustal sequence has been constructed with initially horizontal, active laminations in order to reproduce patterns of fold and fault structures resulting from vertical gravity tectonics.

INTRODUCTION

A large part of northern Ontario is underlain by the Archean Superior Province, a province characterized by linear and branching "greenstone" belts, surrounded by granitoid gneisses and intruded by granitic plutons. The objective of the research reported in this paper is to increase understanding of the origin, evolution, and internal structure of the greenstone belts by using the particular technique of experimental centrifuge modelling.

A wide range of hypotheses have been proposed in the literature for the crustal framework in which Archean greenstone belts initially accumulated and were subsequently deformed. Many of these models differ fundamentally in their assumptions concerning the configuration of the crust during greenstone belt evolution and the tectonic processes which were responsible for the deformation of the belts. Deformation has been attributed, for example, both to vertical gravity-driven tectonics (e.g., Glikson 1971, 1972; Anhaeusser 1973; Schwerdtner *et al.* 1979; Mareschal and West 1980) and to predominantly

horizontal tectonics associated with Archean plate interactions (e.g., Burke *et al.* 1976; Windley 1977).

The experimental modelling carried out by the authors has been concentrated on a study of vertical gravity tectonics as a mechanism for greenstone belt deformation. The basic theme of published hypotheses which involve vertical tectonics is that deformation involved the subsidence of supracrustal greenstone sequences, due to their relatively high average density and the synchronous diapiric rise of adjacent granitoid batholiths or domes to produce the current pattern of ovoid tonalitic gneiss domes and intervening pinched-in synclines of greenstone. Fundamental problems concern the nature and location of the source layer for the tonalitic gneiss domes and the mechanism of emplacement of the domes. Glikson (1972) has argued that the ultramafic-mafic rocks at the base of the greenstones represent a "primitive" or "once extensive" simatic crust. In this model, the tonalitic domes are assumed to result from partial melting at the base of this crust and subsequent intrusion of the melt as batholiths into the overlying greenstones. In contrast, B.E. Gorman *et al.* (1978) and J-C. Mareschal and G.F. West (1980) among others have proposed that the greenstone sequences accumulated on a widespread sialic crust which was later reactivated, possible by elevation of crustal temperature, into diapiric domes.

W.M. Schwerdtner *et al.* (1979) have pointed out an apparent paradox concerning the contact relationship between basal greenstones and tonalitic gneisses in the Superior Province. In their view this contact is intrusive, implying the intrusion of tonalitic magma. However, tectonic fabrics produced within the tonalites during the main phase of diapirism indicate that diapirism occurred when the tonalites were in the solid state and that there was a "negligible" ductility contrast between tonalite and adjacent greenstone during this event. Schwerdtner *et al.* attempt to resolve this paradox by assuming a two-stage process involving the initial intrusion and consolidation of extensive tabular batholiths of tonalite beneath a pre-existing greenstone cover and the subsequent reactivation and solid state diapirism of the tonalite.

The approach adopted by the authors has been to keep the design of models as simple as possible in order to establish basic patterns of deformation which would result from gravity tectonics imposed on geometrically simple systems which incorporate an unstable, inverse density stratification. The models are made up from a relatively thin, relatively dense upper layer representing a

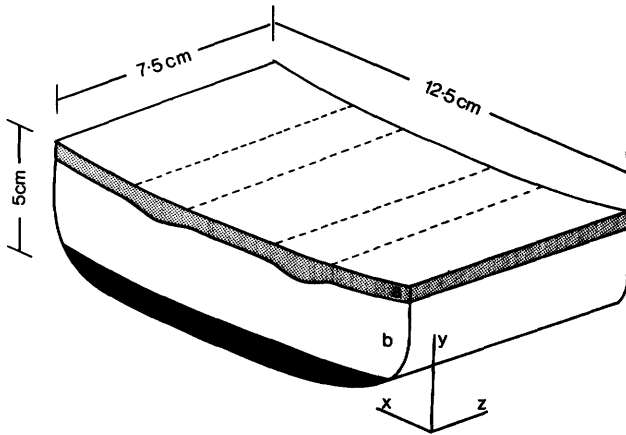


Figure 1—Initial geometry of models containing cylindrical trough initiators (e.g. models A5, A17). There is no contrast in ductility between layers *a* and *b*. The density contrast of *a/b* is 1.07. Layer *c* is constructed from 'plasticene' and acts as an effectively rigid base to the models.

uniform, extensive greenstone blanket and a thicker, lighter substrate which acts as a source layer for buoyant domes. This substrate played the role either of a sialic basement to the greenstones or the sub-greenstone tonalitic batholiths that have been proposed in the model of Schwerdtner *et al.* The configuration of these models is shown schematically in Figure 1.

EXPERIMENTS

The theory of scale models, particularly as applied to centrifuged models of large-scale tectonic processes, has been described in detail by H. Ramberg (1967). A centrifuge is essential to the simulation of most types of large-scale tectonic process in order that controlled experiments constructed from relatively 'stiff' model materials can be run. The experimental tectonics laboratory at Queen's University is equipped with a large centrifuge which is capable of subjecting models measuring 12.5 by 7.5 by 5 cm to accelerations as high as 20,000 g^* .

The principal modelling material chosen for greenstone belt study is silicone putty, as a visco-elastic material which has an approximately linear relationship between stress and strain rate during steady state creep. The material is available in three grades SP1, SP2, and SP3, with approximate viscosities of 8×10^5 poise† (SP1), 2×10^6 poise (SP2), and 4×10^6 poise (SP3).

The first experiments carried out in this program involved simple two-layer models constructed using uni-

form isotropic sheets of silicone putty. Two types of experiments were run.

1) The upper dense layer was locally thickened to form parallel cylindrical troughs as illustrated in Figure 1. These troughs were designed to act as controlled initiators for the subsidence of the simulated greenstones represented by this layer and to ensure that deformation was approximately planar strain in the *xy* profile plane of Figure 1.

2) No attempt was made to localise doming or subsidence and structures evolve naturally from an initially planar interface.

Following Schwerdtner's observations on natural structures no ductility contrast between simulated greenstone and basement was built into these models. In all experiments both upper layer and substrate were constructed from the same grade of silicone putty and a geologically realistic density contrast of 1.07/1 (greenstone/basement) was achieved by addition of finely powdered barium sulphate to the surface layer. The thickness ratio between surface and base layers is 1/5.

These simple two-layer models were designed to study, in detail, the progressive evolution of strain patterns resulting from the gravitational subsidence of relatively dense sheet into a buoyant basement. Progressive strain development on the upper, free surface of the models was monitored by the use of a 1 mm orthogonal grid printed on this surface. Strain within the structural profile plane of models incorporating trough initiators (*xy* plane, Figure 1) was analyzed using a technique developed by J.M. Dixon (1974; 1975).

In a later series of experiments the simulated greenstones were constructed, in whole or in part, as a multi-layer unit built up from regular horizontal alterations and relatively competent and incompetent laminae. These laminations were introduced into the experiments in order to simulate the presence and effect of a mechanically active stratification within a natural volcano-sedimentary pile. The models demonstrate the geometry and vergence* of fold structures that might be expected to be developed during the gravitational subsidence of such a stratified sequence.

DEFORMATION PATTERNS WITHIN MODELS CONTAINING CYLINDRICAL TROUGH INITIATORS

Four stages in the progressive evolution of surface deformation of a model seeded with trough initiators are shown in Figure 2. The deformation of the surface grid clearly illustrates the control of the two, parallel initiators on the subsidence of the dense upper layer. A series of profile sections, normal to the axis of the belt labelled **1** in Figure 2c, have been constructed to illustrate the approximate evolution of this belt in profile (Figure 3).

* g (in italic) signifies standard gravity.

† 1 poise = 0.1 Pa.s

*The direction of overturning or of inclination of a fold.

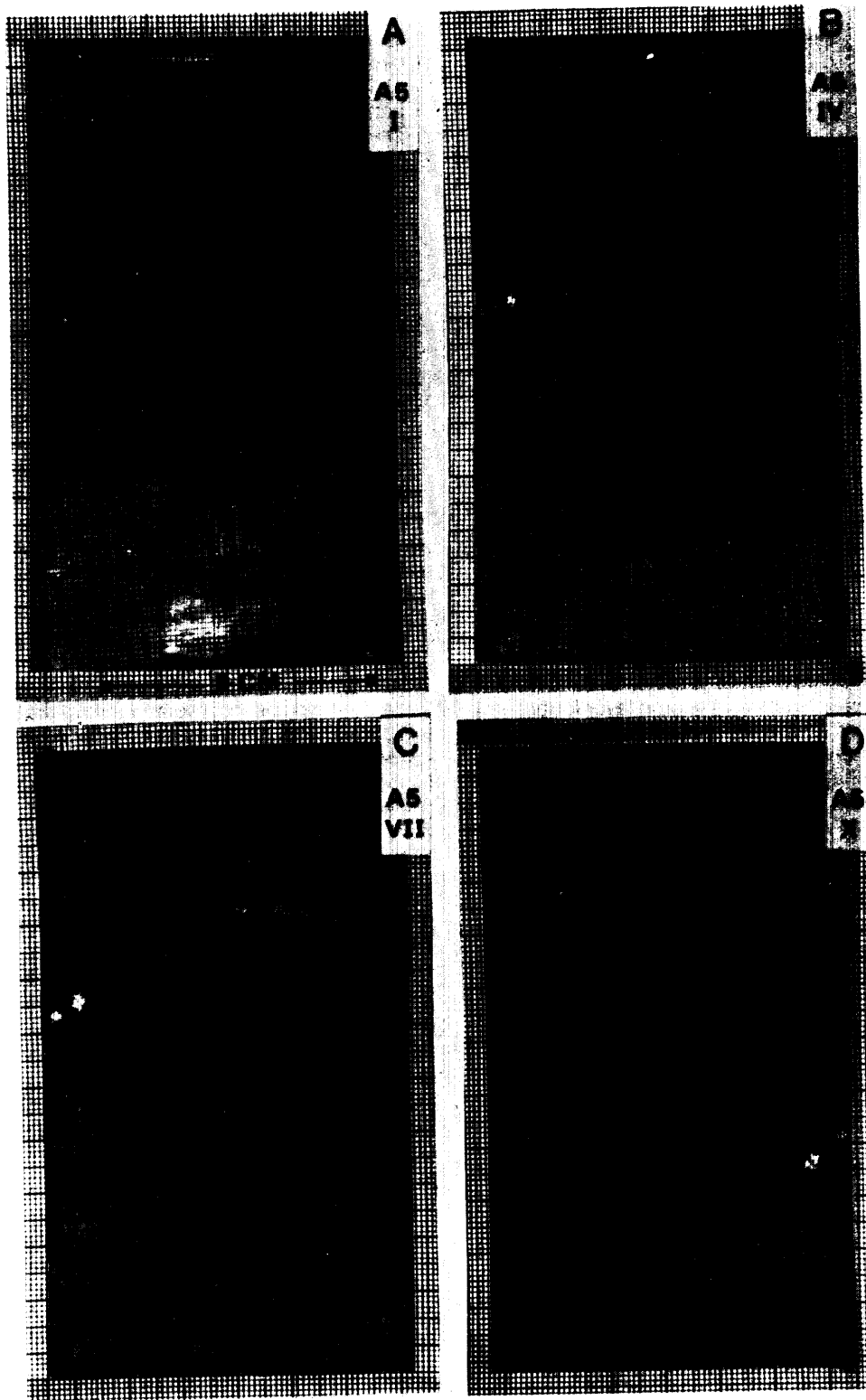


Figure 2—Four representative stages showing the development of surface deformation in model A5. The model was subjected to ten successive centrifuge cycles giving a total run-time of 50 minutes at 2000 g. The initial configuration of this model was as shown in Figure 1. Figure 2A shows the undeformed model and surface grid.

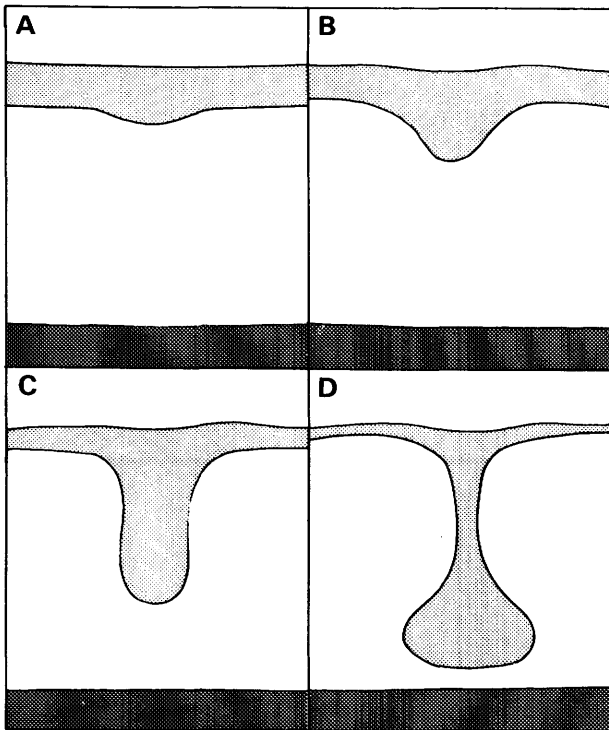


Figure 3—Approximate evolution in the profile geometry of the trough numbered 1 in Figure 2c. These stages correspond to the sequence of surface deformation shown in Figure 2.

The simulated greenstone belts evolved progressively into an inverted "mushroom" shape in profile and can be likened to inverted diapirs. Deformation of the passive surface grid shows that large horizontal displacements occur within the dense surface layer as material migrates towards the subsiding troughs from regions overlying the adjacent broad basement domes. Computer analysis of digitized information from surface grids has been used to obtain a large amount of data detailing surface strain evolution of this and other models. Figure 4 has been included to show one method of representing this data. This figure is a contoured plot of the variation in vertical strain, normal to the model surface, at the stage of trough subsidence illustrated in Figure 2c. Surface deformation can be divided into two belts of vertical extension ($1 + e_v > 1$), lying over the subsiding troughs, and intervening regions of vertical contraction ($1 + e_v < 1$) indicating areas where the simulated greenstone sheet has thinned above the basement domes.

Displacement of surface material occurs principally in a direction normal to the trough axes and results in the accumulation of significant horizontal shortening within the surface core of the subsiding troughs. At the stage of deformation represented in Figure 2c, for example, horizontal shortening in excess of 95 percent is developed

along the trough axis. Analysis of surface deformation also reveals locally complex histories of progressive strain affecting material elements which initially undergo horizontal contraction as the elements migrate into regions overlying the subsiding troughs (Dixon and Summers 1980).

A number of experiments have been carried out to study the progressive evolution of strain with profile sections, normal to the axes of subsiding troughs. Figure 5 illustrates the results of a strain analysis applied to the material within a single, cylindrical trough at a relatively mature stage of trough subsidence.

A significant feature of this mature deformation pattern is the concentration of very high magnitudes of vertical extension within a narrow, deep wedge straddling the axial plane of the trough. The pattern of deformation seen in Figure 5 clearly does not represent a simple, uniform vertical extension imposed upon a body of material drawn down to depth. More accurately, the dense surface layer behaved almost like an extendable conveyor belt, rolling into the subsiding trough from the flanking basement domes and producing strong vertical extension within a narrow band of material trapped within the pinched core of the resulting downfold.

DEFORMATION PATTERNS WITHIN MODELS WITH NO INITIATORS

Model A7 (Figure 6a) provides an example of a deformation pattern developed within a simple, two-layer model in which no attempt was made to control subsidence or doming. Apart from the critical absence of trough initiators, the initial geometry and physical properties of this model were essentially the same as those of models A5 and A17, described previously.

Figure 6a shows the final state of deformation of model A7 as expressed by the passive surface grid. Subsidence of the dense, uniform upper layer occurred initially within a broadly canoe-shaped trough aligned along the centre of the model. At a later stage in the experiment, however, two sites of preferential subsidence developed at either end of this trough. These can be recognized in a series of parallel, vertical sections cut normal to the trough axis (Figure 6b). The depth of the trough has a distinct maximum towards the right end (section 5) with a secondary maximum towards the left (section 12). These maxima can be considered as inverse equivalents to the culminations on diapiric ridges, produced experimentally by L.L. Nettleton (1943) and H. Ramberg (1967).

The development of this non-cylindrical geometry of the trough at depth is clearly reflected by variation in the flow pattern of surface material as expressed by the deformation of the surface grid. Figure 7a shows the pattern of vertical strain, normal to the model surface, calculated from the grid. The location of the trough is represented on the model surface by an enclosed region of vertical extension ($1 + e_v > 1$). Within this area, vertical extension reaches a maximum in two zones which overlie the sites of greatest trough subsidence. Movement of surface material both off the basement highs and along the trough

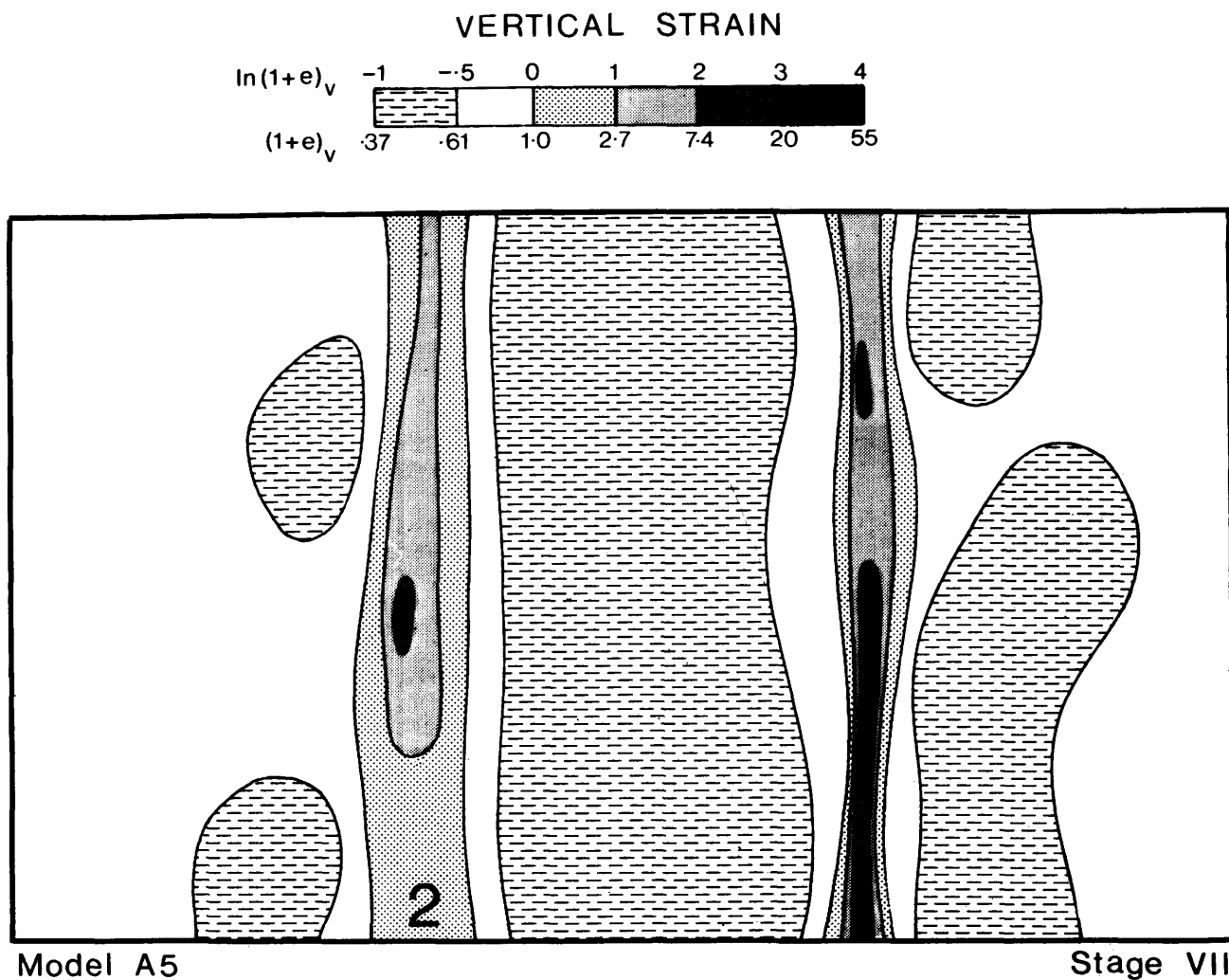


Figure 4—Variation in vertical strain across the surface of model A5 at the run stage illustrated in Figure 2c.

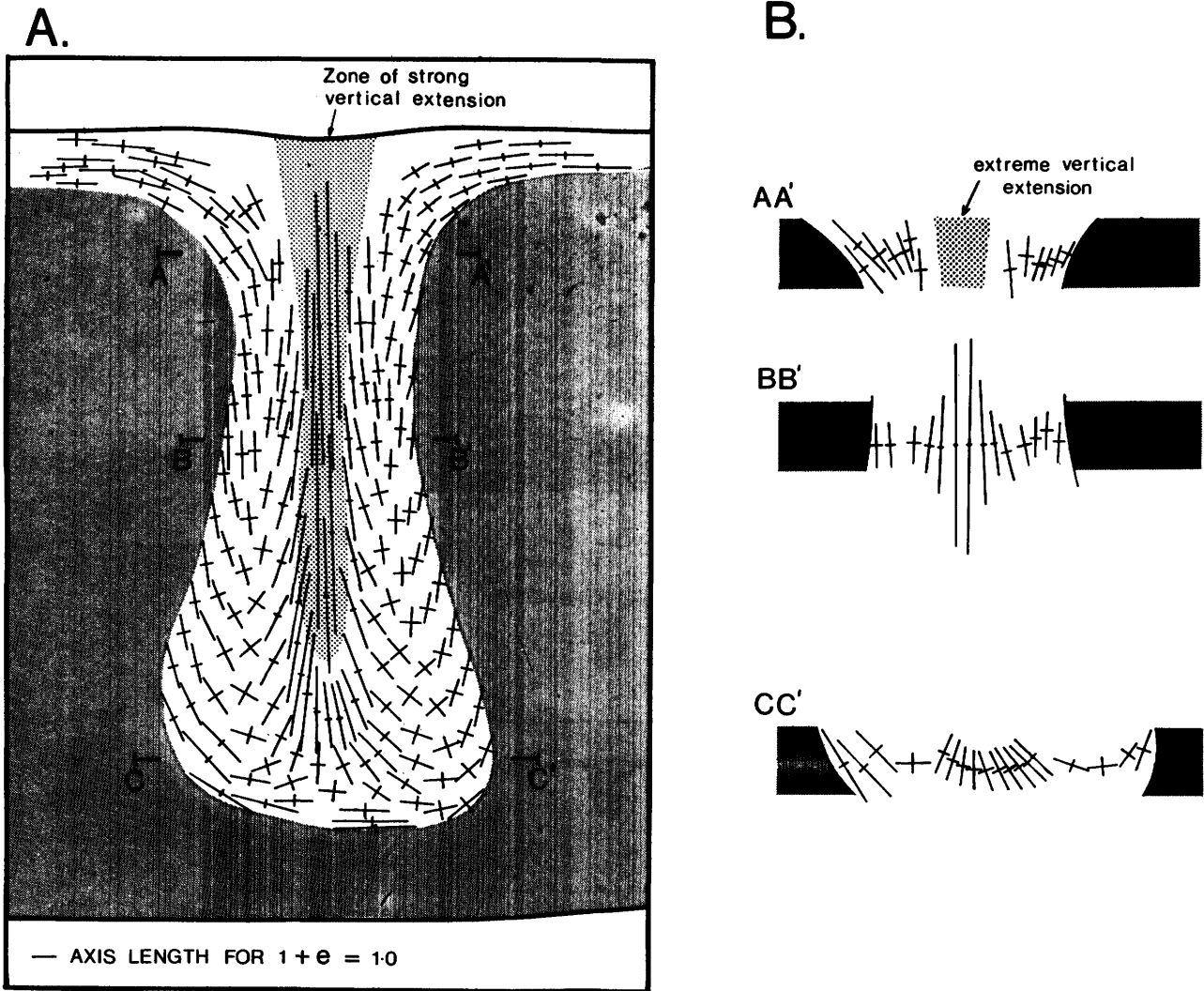


Figure 5—**A.** Variation in magnitude and orientation of principal strains within a mature trough. Profile section, model A17. **B.** Detailed strain variation across levels of the trough shown in Figure 5a.

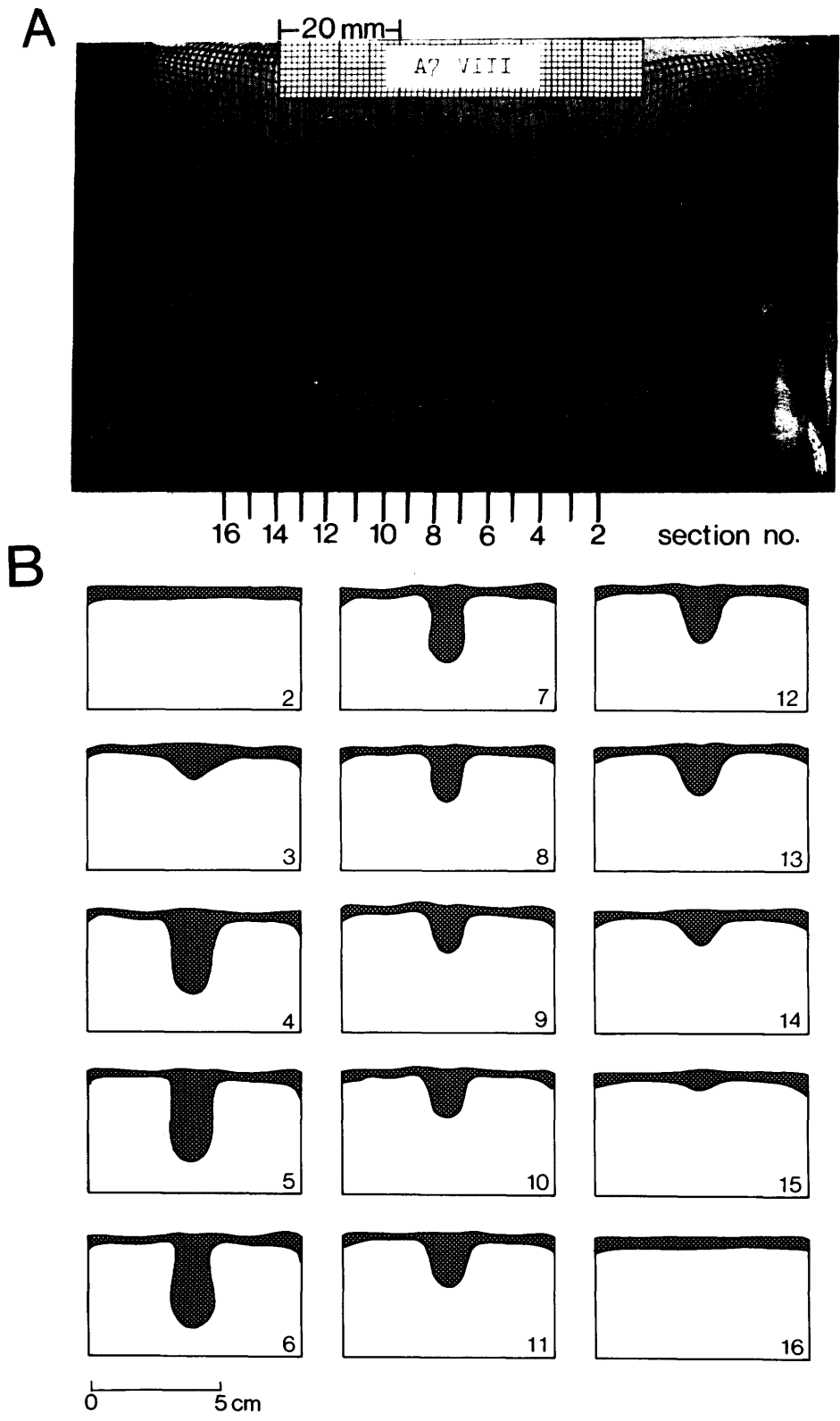


Figure 6—**A.** Final state of deformation of surface grid in model A7. **B.** Series of vertical sections, normal to the trough axis of model A7. The location of these serial sections on the surface of the model is shown in Figure 6a.

Model A7

Stage VII

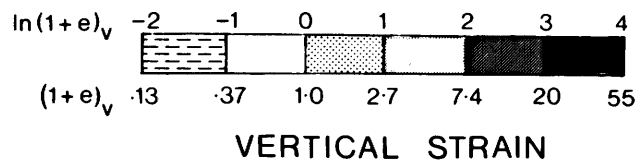
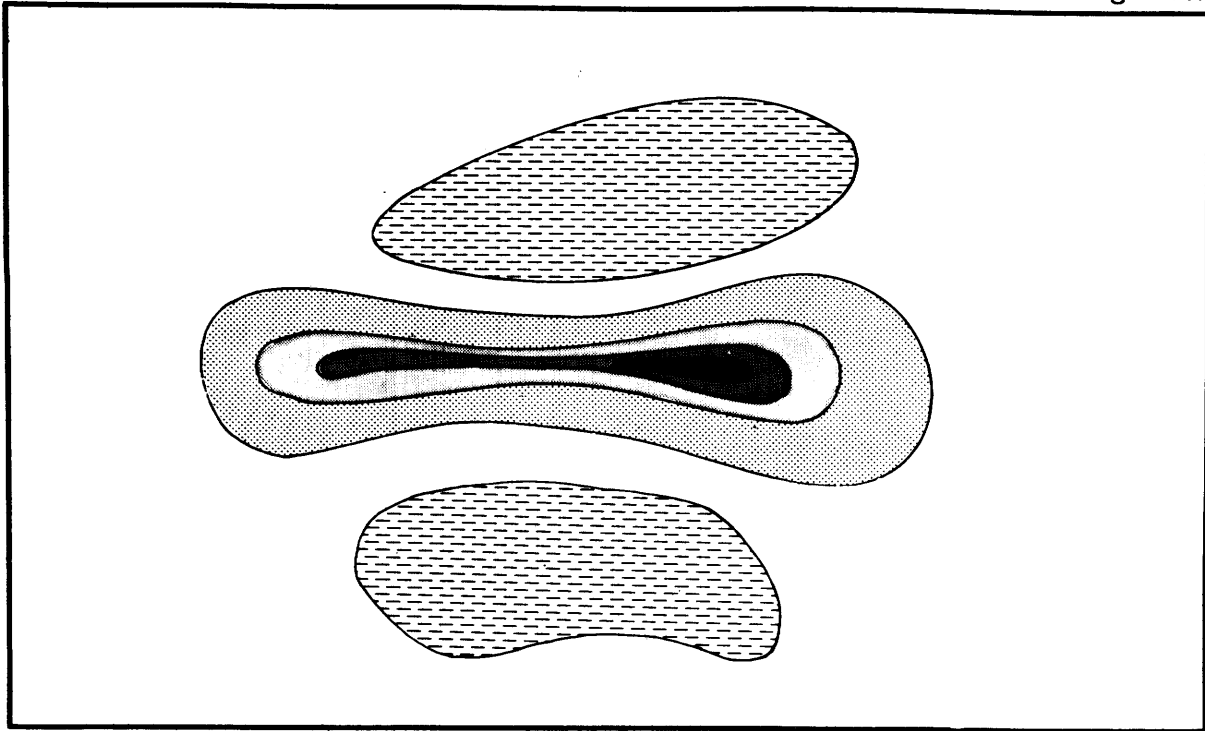


Figure 7A—Variation in vertical strain across the surface of model A7 at the run stage illustrated in Figure 6a.

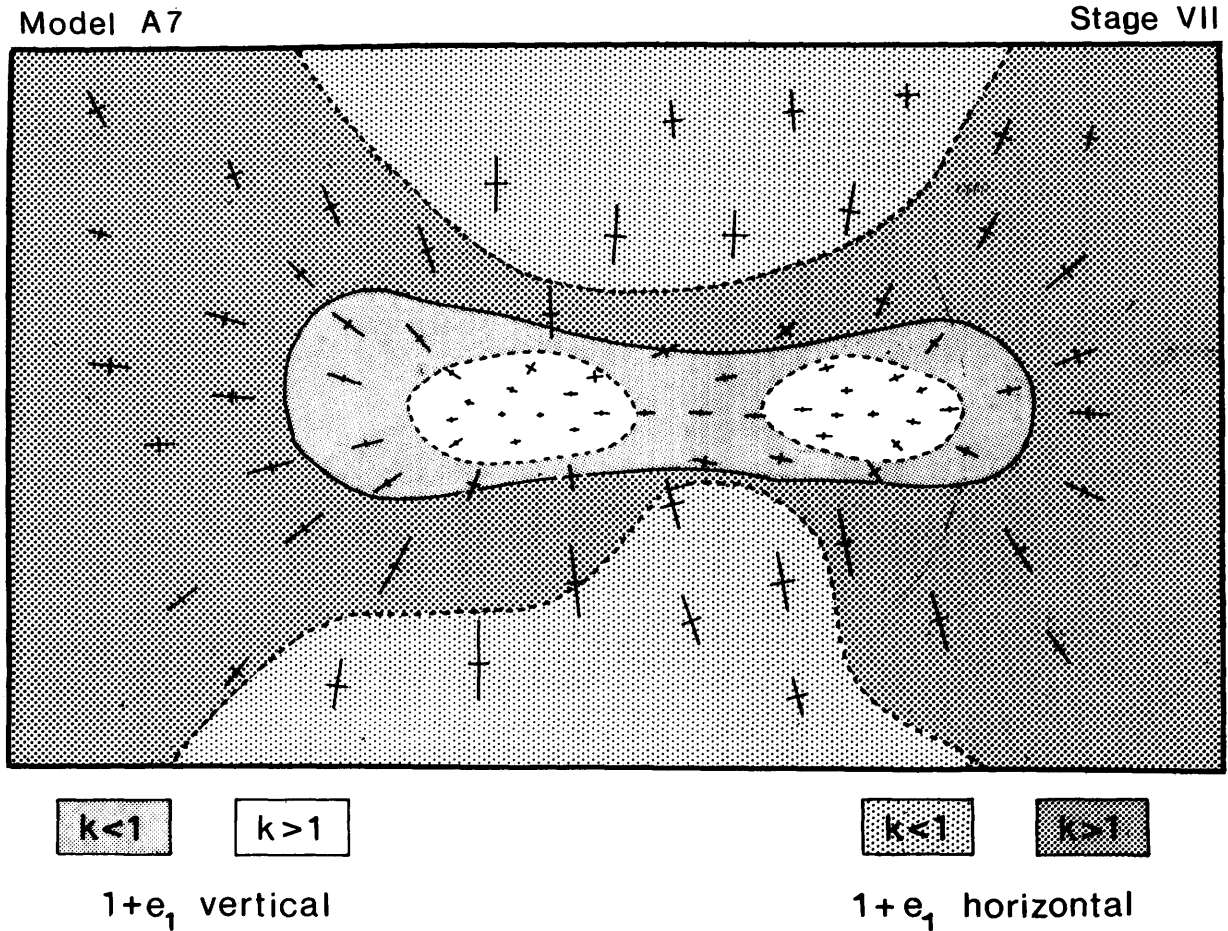


Figure 7B—Variation in the 'k' value of surface deformation of model A7, as determined from the deformed grid shown in Figure 6a. The 'k' value is a measure of the relative prolateness or oblateness of the local strain ellipsoid and is defined as $k = (a/b - 1)/(b/c - 1)$ where a, b and c are the lengths of the maximum, intermediate and minimum strain axes, respectively, of the strain ellipsoid.

axis itself has converged towards these points of maximum subsidence.

The variation in the shape of the surface strain ellipsoid also reflects control of the trough geometry at depth by the surface deformation pattern. This can be demonstrated by a plot of the variation in 'k' value of surface strain (Figure 7b). The 'k' value (Flinn 1965) is an index of the relative prolateness or oblateness of the strain ellipsoid. Strain above the points of maximum subsidence is prolate ($k > 1$; "cigar" shaped ellipsoid) and results from a convergent flow along all directions in the model surface with a corresponding strong vertical extension normal to this surface.

In the area lying above the trough, these two zones of prolate strain are surrounded by a region of oblate de-

formation ($k < 1$; "pancake" shaped ellipsoid) in which surface deformation involves extension in all directions in a vertical plane and a maximum contraction normal to this plane. Regions of prolate deformation in naturally deformed tectonites would be recognized by the presence of a mineral lineation; oblate deformations would tend to produce a planar foliation with no preferred direction of mineral alignment.

STRUCTURES DEVELOPED IN MODELS WITH A STRATIFIED SURFACE LAYER

Models run during the first phase of the research were constructed with similar flow strengths but contrasting densities. In a later series of experiments, represented in

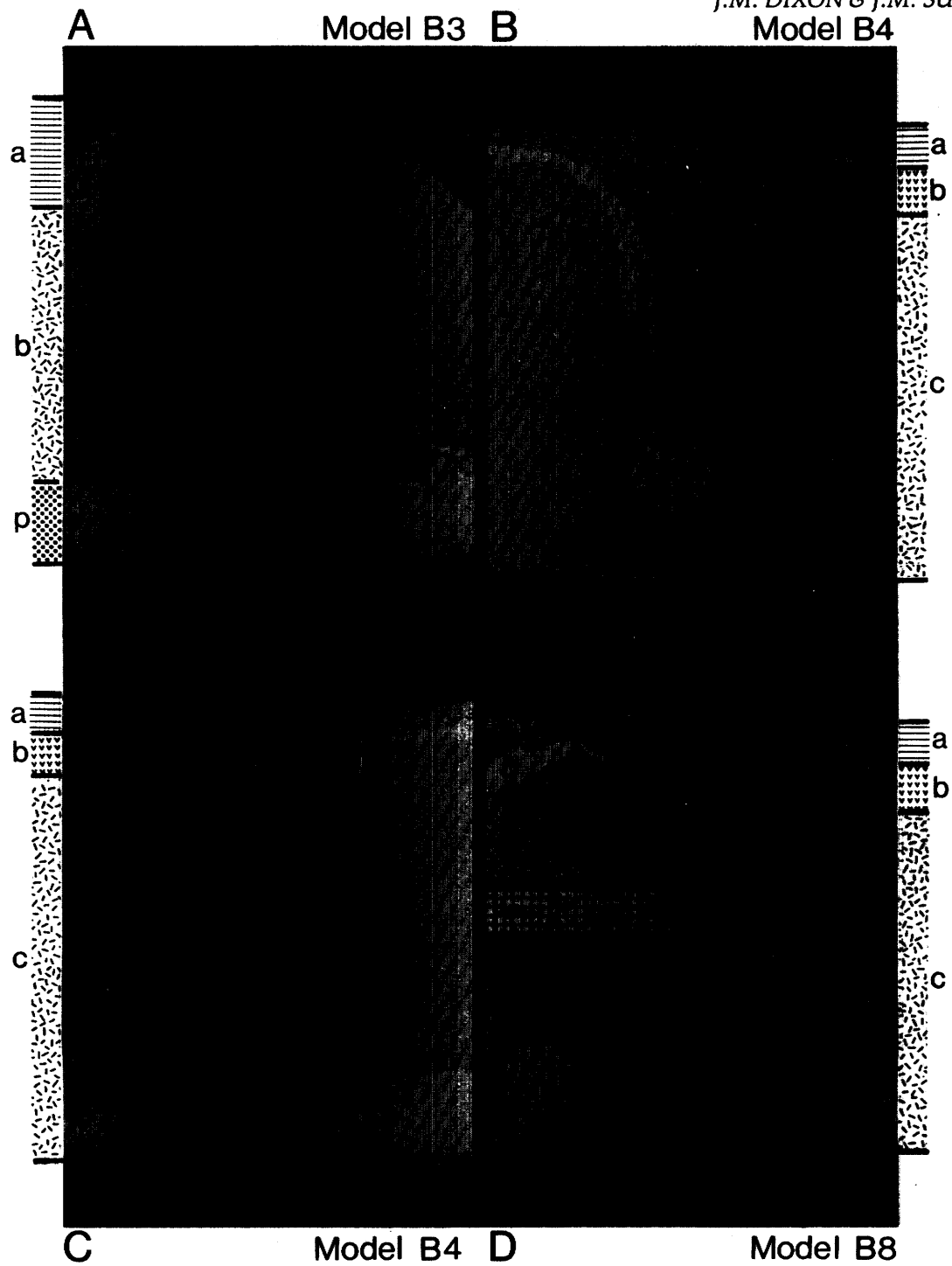


Figure 8—Profile sections showing structures developed in models incorporating a fine, mechanically active layering within the simulated 'greenstone' cover sequence. Differences between structures developed in the models reflect differences in the initial layer configuration and density stratification built into the models. Initial layer thicknesses are shown in column form next to the corresponding model. Details of initial layer thicknesses (t) and specific gravities (SG) are as follows: A. Model B3, $t_a = 10$ mm, $SG_a = 1.51$; $t_b = 25$ mm, $SG_b = 1.41$; p = 'plasticene' base. B, C. Model B4, $t_a = 5$ mm, $SG_a = 1.40$; $t_b = 5$ mm, $SG_b = 1.54$; $t_c = 40$ mm, $SG_c = 1.39$; B is section at end of trough, C is section at centre of trough. D. Model B8, $t_a = 5$ mm, $SG_a = 1.36$; $t_b = 5$ mm, $SG_b = 1.54$; $t_c = 40$ mm, $SG_c = 1.41$.



Figure 9—Four representative stages showing the progressive evolution of structures in model B7, as expressed on the free upper surface of the model (oblique lighting). Model was constructed with a relatively high density surface multilayer (total thickness, 5 mm; total number of laminae, 32; individual layer thickness, 0.16 mm; mean specific gravity, 1.47) and thicker, buoyant base layer (thickness, 40 mm; specific gravity, 1.40). See text for discussion.

Figures 8 and 9, a mechanically active layering was introduced into the simulated greenstone supracrustal sheet in order to study patterns of fold development which might be produced within a stratified volcano-sedimentary pile through gravitational subsidence. In these models, horizontal stratification is represented by fine, regular alterations of competent ("plasticene") and incompetent ("plasticene"/silicone putty mix) laminae. Necessarily this regular layering is a gross oversimplification of the vertical and horizontal lithological variations which would likely be present in a natural supracrustal sequence.

Figure 8 illustrates four examples of structures produced in these experiments, shown in profile section normal to the axes of the descending troughs. In each case, subsidence was localized by the use of trough initiators of the type illustrated in Figure 1 and fold structures seen in profile are developed on axes normal to the plane of the figure. Details of the densities and initial thicknesses of the main units incorporated into the models are given in the figure caption. Densities assigned to the multilayered units represent mean densities measured for each unit as a whole.

Differences between the trough geometries and internal structures developed in these models reflect differences in initial density stratification. In experiment B3 (Figure 8a) the simulated supracrustal sequence was laminated throughout (unit a) and had a higher mean density ($SG = 1.51$) than the underlying, isotropic basement (unit b, $SG = 1.41$). Thus the laminated unit was in a gravitationally unstable position with respect to the basement and was actively involved in subsidence. Fold structures developed within the core of the trough reflect the horizontal contraction and strong vertical extension noted in the strain patterns developed in isotropic materials. Folds are angular, tight to isoclinal, with vertical axial surfaces and horizontal fold axes. The supracrustal-basement interface is characterized by extension along the plane of this contact at all levels within the main structure, as seen in contact-parallel disruption or boudinage of competent laminae. Horizontal extension of competent laminae in regions flanking the subsiding trough had the effect of weakening the surface multilayer. As a result, forceful emplacement of buoyant basement material became localized along these weakened zones.

In contrast to model B3, the simulated supracrustal sequence in model B8 (Figure 8d) was formed from two layers; a relatively light, multilayered upper sheet (unit a, $SG = 1.36$) and a relatively dense and isotropic lower sheet (unit b, $SG = 1.54$). This sequence was, in turn, underlain by a thick isotropic basement with a density (unit c, $SG 1.41$) which was intermediate between the densities of the two units making up the supracrustals. This initial configuration could be taken as a crude approximation for a natural situation involving a supracrustal sequence dominated at a high level by relatively light, stratified sedimentary material and at lower levels by relatively dense volcanic rocks.

Structures developed within the multilayered surface sheet resulted from the progressive draw-down of the dense intermediate layer into the subsiding trough. The main body of the multilayer remained at a high structural

level because of its low mean density. Folds range from upright structures along the trough axis to overturned structures near the margins of the trough and axial planes fan symmetrically away from the core of the trough. With the exception of structures on the trough axis, folds verge consistently away from the axis. Locally, fracturing of the tightly folded hinge zones of competent laminae has occurred. In some places it is possible to recognize small thrust displacements along these dislocations with a sense of upper plate movement away from the trough. It should be noted that the sense of fold vergence developed in each of the models illustrated in Figure 8 is opposite to that suggested in a conceptual model of gravity driven greenstone belt deformation by Gorman *et al.* (1978). The limited evidence for thrust displacement in B8 is also opposite in sense to that suggested by these authors.

Fyson (1981) has recently described patterns of 'divergent fold overturning' developed across the widths of individual Archean metasedimentary belts of the Slave Province. These patterns are similar, in their geometric relationship to adjacent diapiric domes, to the pattern of fold vergence and axial plane fanning seen in Figure 8d. Fyson interprets these structural fans as representing the combined effects of a regional compression and local diapirism on the margins of individual belts rather than having been produced solely by diapirism as is the case with model B8.

Figure 9 illustrates four stages in the progressive deformation of model B7, showing the expression of fold and fault structures on the upper, free surface of a relatively dense surface multilayer. The initial internal configuration and density stratification of the model are listed in the figure caption. The base of the surface multilayer was locally thickened in constructing this model to produce the type of trough geometry developed in model A7 (Figures 6 and 7), i.e. a single trough along the long axis of the model with maximum subsidence at either end of the trough. This attempt was partly successful in that maximum subsidence occurred below point X and the pattern of fold and fault structures developed in the area surrounding X reflect the type of movement pattern illustrated in Figure 7 (isotropic surface sheet). Oblate ("pancake shaped") bulk deformation at points A and B, for example, is indicated by the presence of upright fold structures with hinge-normal fractures. These features demonstrate axis-parallel extension associated with the convergence of surface material on point X. Broad fractures and fracture complexes surrounding the main trough are the surface expression of stacked low angle normal faults and multilayer disruption within zones which become favourable to the local rise of buoyant basement material.

CONCLUSIONS

The experiments consistently demonstrate a number of features which would be likely to find expression during the gravitational subsidence of a complex Archean vol-

cano-sedimentary supracrustal sequence. For example:

1) Strain within the main body of the subsiding belts is dominated by strong vertical extension and horizontal contraction. In a natural situation such strains would act to produce strong vertical foliations and a tendency for mineral lineations to plunge steeply within the foliation. Pre-deformation layering tends to become rotated into a vertical orientation, sub-parallel to foliation.

2) Flattening within the simulated greenstones near the margins of a trough generally trends parallel with or at a low angle to the greenstone-basement interface at all levels within the trough. This experimental observation is consistent with the tendency for foliation within natural belts to follow or 'wrap around' the contact between supracrustal rocks and adjacent gneisses.

3) Patterns of strain within the models, at least as expressed in surface deformation, reflect the geometry of the greenstone-gneiss interface at depth (e.g. model A7). Flow within the supracrustal units, for example, converges towards points of maximum subsidence to produce strong local vertical extension and prolate strains. Deformation above saddles or highs within a trough is characterised by oblate or flattening strains reflecting combined vertical extension and horizontal extension associated with movement of material towards adjacent trough depressions.

4) Horizontal shortening within a subsiding, stratified cover sequence produces first generation folds developed on horizontal axes, with vertical or steeply inclined axial surfaces. Where the stratified sequence forms a relatively low density unit within the cover sequence, folds verge consistently away from the axis of the trough. Evidence from small thrust displacements indicates that the sense of overthrusting is compatible with fold asymmetry and vergence, and is directed away from the trough axis. In the relatively cold, mechanically anisotropic upper levels of a natural greenstone sequence, it is possible that horizontal shortening would be expressed by the development of outward directed, stacked low angle thrusts. Such thrusts would produce a tectonic thickening of the greenstones and would tend later to become rotated into a steeply dipping attitude by continued contraction and subsidence.

REFERENCES

- Anhaeusser, C.R.
1973: The Evolution of the Early Precambrian Crust of Southern Africa; *Phil. Trans. R. Soc. London*, Vol. A273, p.359-388.
- Burke, K., Dewey, J.F., and Kidd, W.S.F.
1976: Dominance of Horizontal Movements, Arc and Microcontinental Collisions During the Later Permian Regime; p.113-129 *in* The Early History of the Earth, ed. B.F. Windley, Wiley Interscience, London.
- Dixon, J.M.
1974: A New Method for the Determination of Finite Strain in Models; *Tectonophysics*, Vol.24, p.99-114.
1975: Finite Strain and Progressive Deformation in Models of Diapiric Structures; *Tectonophysics*, Vol.28, p.80-124.
- Dixon, J.M. and Summers, J.M.
1980: A Centrifuge Model Study of the Tectonic Development of Archean Greenstone Belts; Grant 68, p.58-71 *in* Geoscience Research Grant Program, Summary of Research, 1979-80, ed. E.G. Pye, Ontario Geological Survey, MP 93, p.262.
- Flinn, D.
1965: On the Symmetry Principle and the Deformation Ellipsoid; *Geol. Mag.*, Vol.102, p.36-45.
- Fyson, W.K.
1981: Divergent Fold Overturning and Regional Tectonics, Southern Slave Province, Northwest Territories; *Precambrian Res.*, Vol.14, p.107-118.
- Glikson, A.Y.
1971: Structure and Metamorphism of the Kalgoorlie System; *Geol. Soc. Australia*, Sp. Publ., p.443-459.
1972: Early Precambrian Evidence of a Primitive Ocean Crust and Island Nuclei of Sodic Granite; *Bull. Geol. Soc. America*, p.3323-3344.
- Gorman, B.E., Pearce, T.H., and Birkett, T.C.
1978: On the Structure of the Archean Crust; *Precambrian Res.*, Vol.6, p.23-41.
- Mareschal, J.-C. and West, G.F.
1980: A Model for Archean Tectonism, Pt.2 Numerical Models of Vertical Tectonism in Greenstone Belts; *Canadian Jour. Earth Sci.*, Vol.17, p.60-71.
- Nettleton, L.L.
1943: Recent Experimental and Geophysical Evidence of Mechanics of Slat Dome Formation; *Bull. American Assoc. Petrol. Geologists*, Vol.18, p.1175-1185.
- Ramberg, H.
1967: Gravity, Deformation and the Earth's Crust; Academic Press, New York, 214p.
- Schwerdtner, W.M., Stone, D., Osadetz, K., Morgan, J., and Stott, G.M.
1979: Granitoid Complexes and the Archean Tectonic Record in the Southern Part of Northwestern Ontario; *Canadian Jour. Earth Sci.*, Vol.16, p.1965-1977.
- Windley, B.F.
1977: The Evolving Continents; Wiley, New York, 385p.

Grant 55 Evolution of an Archean Felsic Volcanic-Plutonic Complex in the Kakagi-Pipestone Lakes Area

G.R. Edwards and R.W. Hodder

Department of Geology, University of Western Ontario

ABSTRACT

In the Kakagi-Pipestone Lakes area of northwestern Ontario, a sequence of steeply dipping submarine tholeiitic basalt, 5 to 10 km thick, is folded in an anticline around a tonalitic intrusion of the Sabaskong Batholith. At the hinge of the fold the basalt is intruded by satellitic, subvolcanic tonalitic stocks and is overlain by dacitic to rhyolitic volcanic rocks and attendant chemical and clastic sedimentary rocks. Near the hinge of the fold the tonalite-basalt contact is concordant and the grade of metamorphism is low. Twenty kilometres west of the fold, the tonalite is gneissose, the basalt is gneissic amphibolite and their mutual contact is occupied by amphibolite-inclusion-rich diorite, quartz diorite and gabbro. Similar diorite and gabbro intrude an enclave of metamorphosed mafic to ultramafic rocks at Caliper Lake.

Melting of the plagioclase component of basalt at P_{H_2O} of 5 kbar yields an aluminous, low temperature trondhjemitic melt and an amphibole-rich residuum which may become segregated in the liquid allowing amphibole to be transported by convection. Major element and rare earth element data and compositions of amphibole in the diorite and tonalite support a model for the origin of the diorite (and gabbro) by accumulation of xenocrystic amphibole in the tonalitic magma. The tonalite breached the basalt to form the dacitic to rhyolitic volcanic rocks at the hinge of the fold. Because the tonalitic melt had a low temperature and did not crystallize amphibole it may not have supported an extensive hydrothermal system or explosive volcanism.

INTRODUCTION

The genesis of calc-alkaline magmas and their subsequent role in the formation of ore deposits has long been a subject of controversy. Bowen (1928) proposed that calc-alkaline magmas were derived by simple fractional crystallization of a basaltic magma. The precipitation of minerals such as olivine and pyroxene however, would require a large volume of basalt to yield a moderate volume of calc-alkaline magma. Osborne (1959, 1962) suggested that calc-alkaline magma may form from a fractionating basaltic magma kept at constant oxygen partial pressure. This allows magnetite to crystallize as an early liquidus phase depleting the liquid in iron and vanadium while enriching it in silica. Conditions of magnetite precipitation were obtained during the crystallization of the

cumulate-olivine-free Middle Zone of the Skaergaard intrusion due to a change in the oxygen-silica activity ratio (Morse *et al.* 1980). The apparent residual liquid trend however did not follow a calc-alkaline line but proceeded to further iron enrichment.

Green and Ringwood (1968) experimentally melted synthetic basalt at moderate pressures. They concluded that basalt, partially melted under crustal conditions would yield calc-alkaline liquids. This conclusion was supported by Helz (1973, 1976) who observed that basalt, partially melted at P_{H_2O} of 5 kb, yielded aluminous trondhjemite-like liquid.

The genesis of Archean bimodal trondhjemite-basalt suites by the partial melting of basalt was modelled by Barker and Arth (1976) and in a companion paper, Arth and Barker (1976) discussed the role of rare earth element partitioning between hornblende and dacitic liquid during trondhjemite-tonalite genesis.

The Phinney-Dash Lakes Complex and allied intrusive rock of the Sabaskong Batholith are essentially a section through an Archean, bimodal basalt-dacite volcanic-plutonic system. This section provides an opportunity 1) to study the petrogenesis of diorite, tonalite and trondhjemite and dacite by field relationship as well as by chemical comparison and modelling, 2) to study physical volcanic processes, and 3) to compare a volcanic system hitherto unproductive in terms of ore genesis to those in more productive areas.

The area studied is between Kenora and Fort Frances in the vicinity of Nestor Falls, Kakagi and Pipestone Lakes in the Wabigoon Subprovince (Figure 1). Mapping at a scale of 1:15 840 by G.R. Edwards (1976, 1978) while under contract with the Ontario Geological Survey revealed the Phinney-Dash Lakes Complex. Additional mapping and sampling was done in 1979 and 1980 during the tenure of the present Ontario Geoscience Research Grant. Computer modelling of the petrogenesis of these rocks using the major and trace element data is currently in progress.

GENERAL GEOLOGY

In the Kakagi-Pipestone Lakes area, 5 to 10 km of submarine tholeiitic basalt and gabbro, the Katimiagamak formation¹ is folded in a broad, steeply plunging anticline

¹The term *formation* is used here in the informal sense (stratigraphically).

about the intrusive Kishkutena to the Sabaskong Batholith. The Phinash Lakes Complex, consisting of subvolcanic to line dacitic to rhyolitic volcanic rocks and clastic sedimentary rocks

and intrudes and overlies the Katimiagamak formation (Figure 2). The Katimiagamak formation and Phinash Lakes Complex (Figures 3,4 and 5) were defined by Hodder and Edwards (1980).

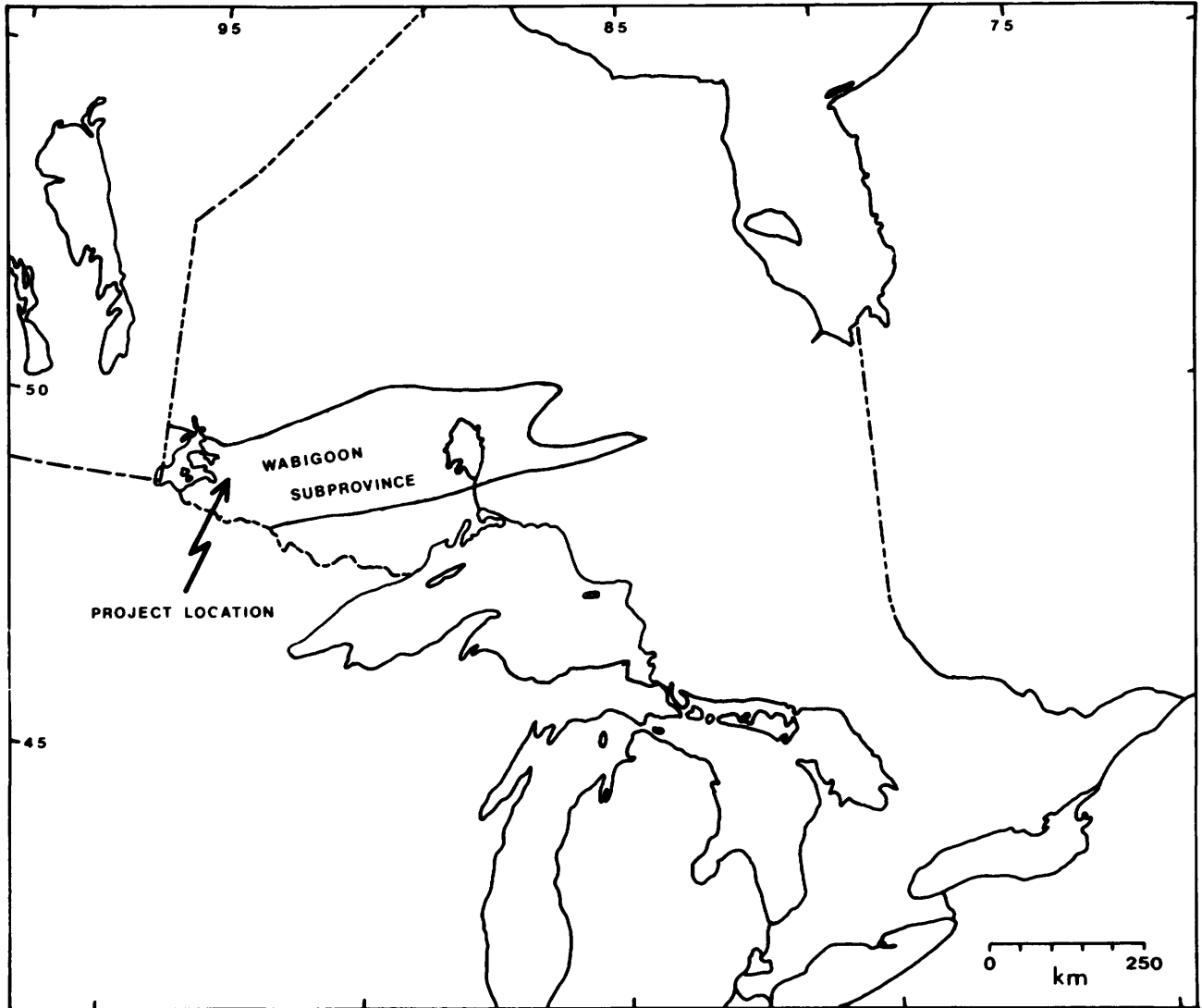


Figure 1—Location of the project and the Wabigoon Subprovince.

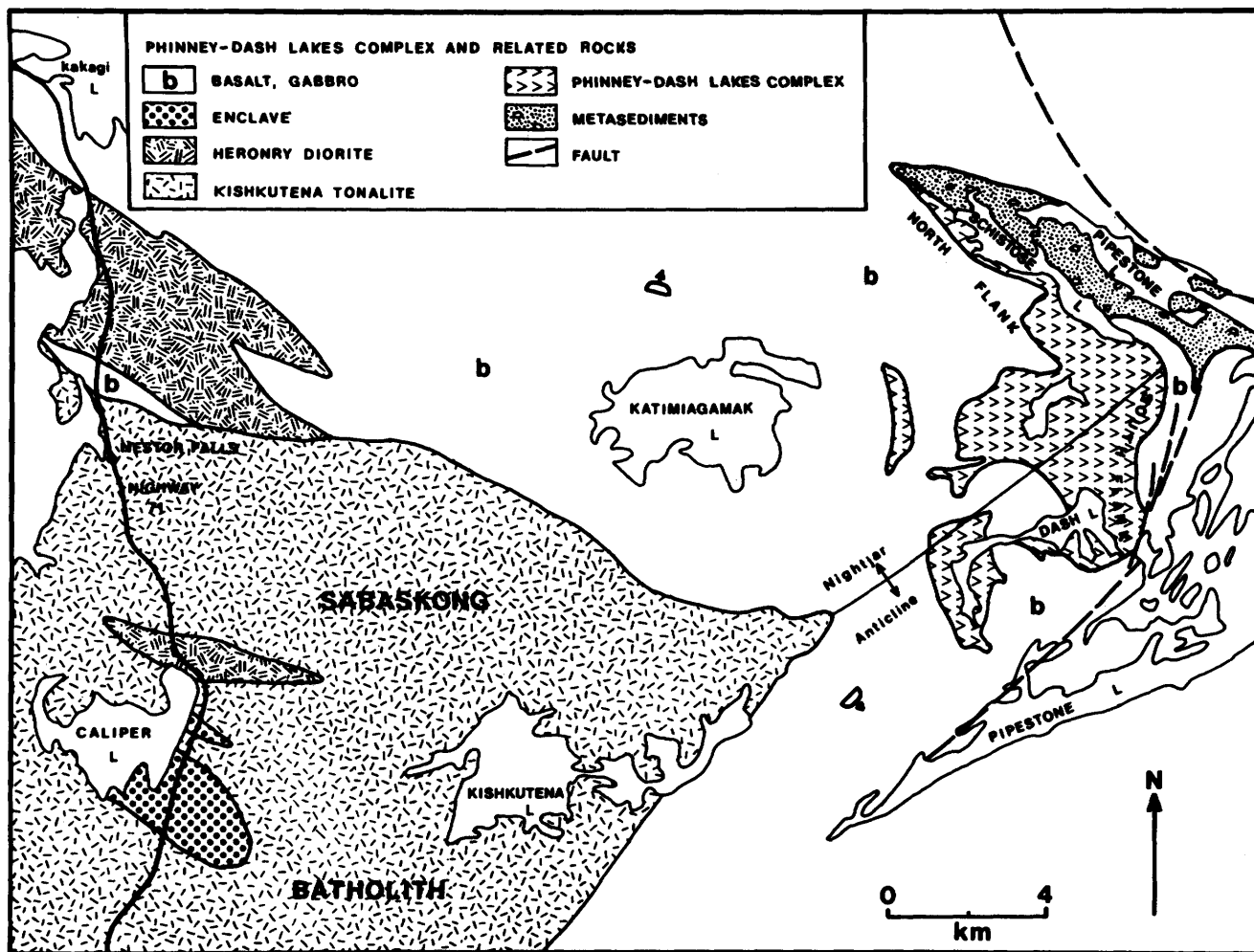


Figure 2—Phinney-Dash Lakes Complex and part of the Sabaskong Batholith.

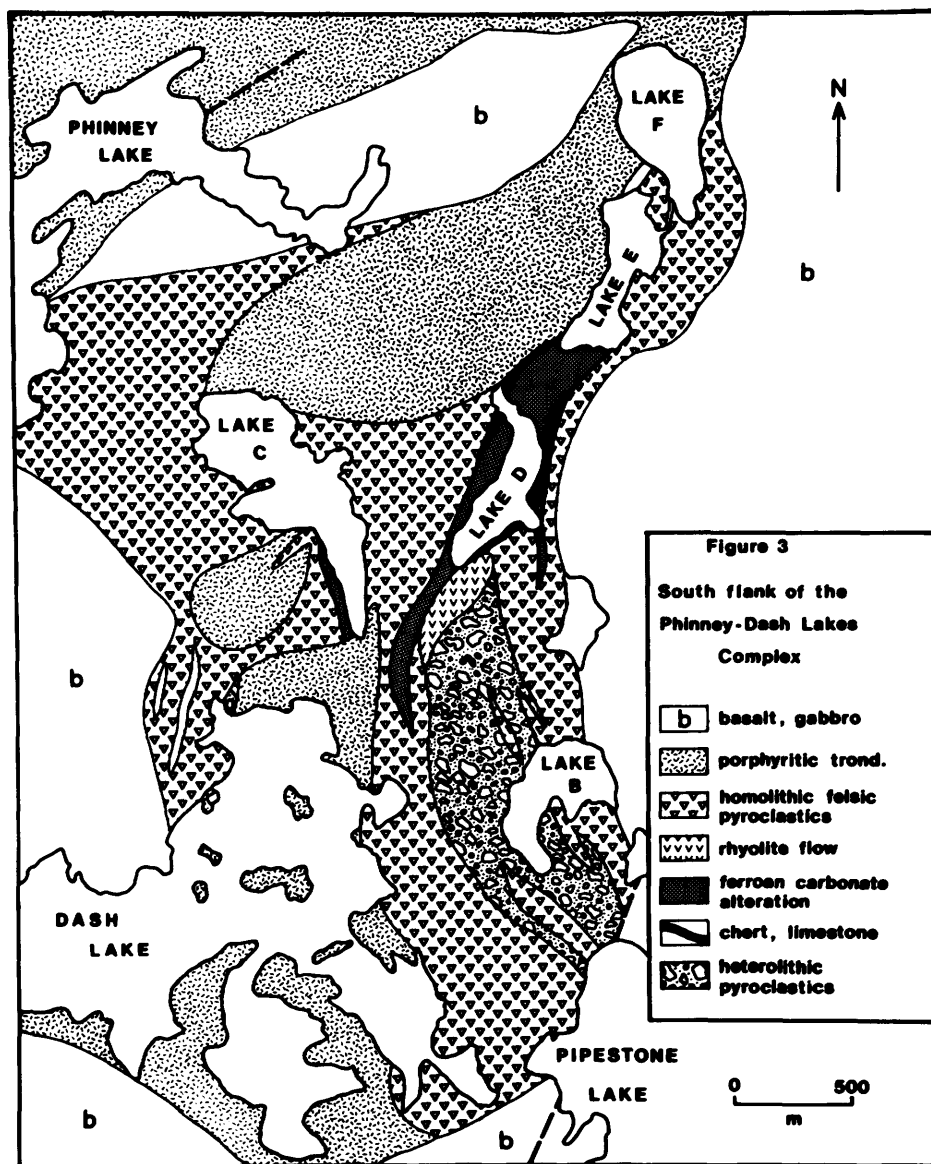


Figure 3—South flank of the Phinney-Dash Lakes Complex.

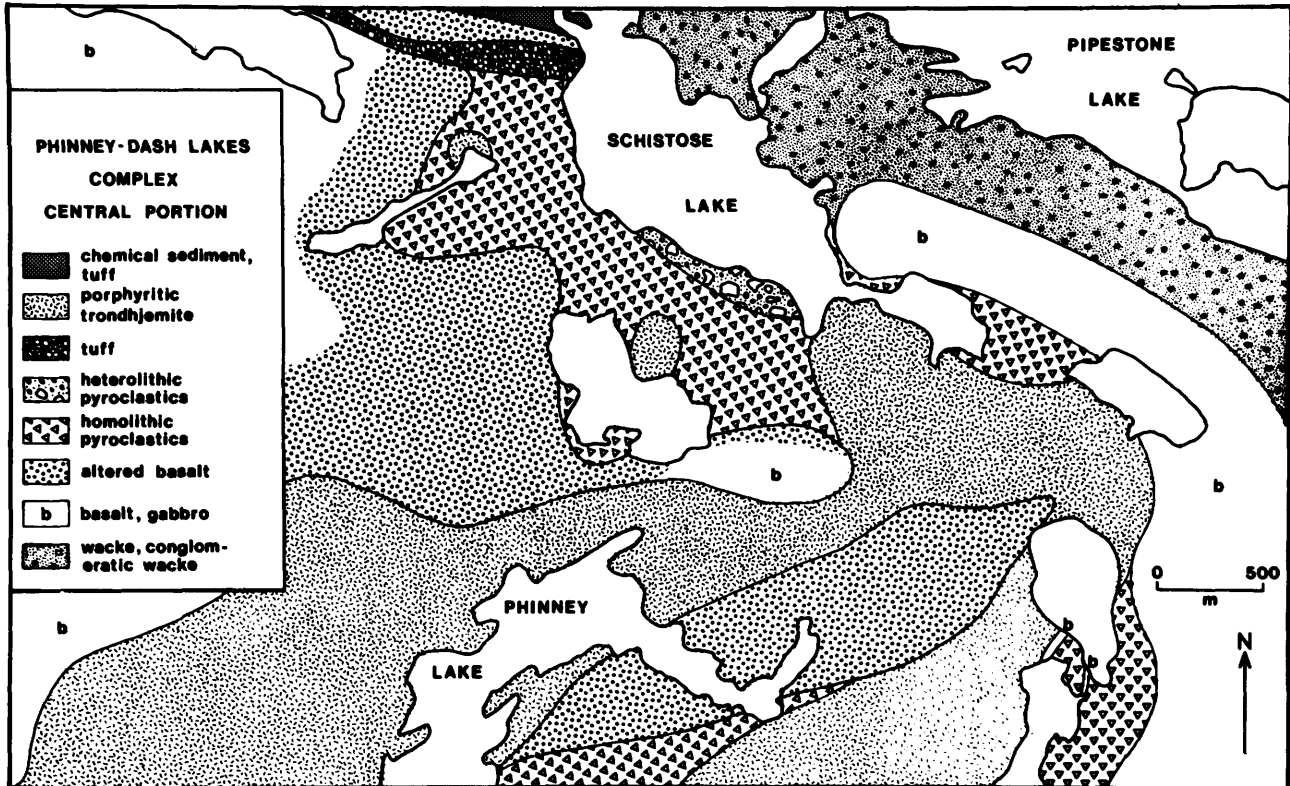


Figure 4—Central part of the Phinney-Dash Lakes Complex.

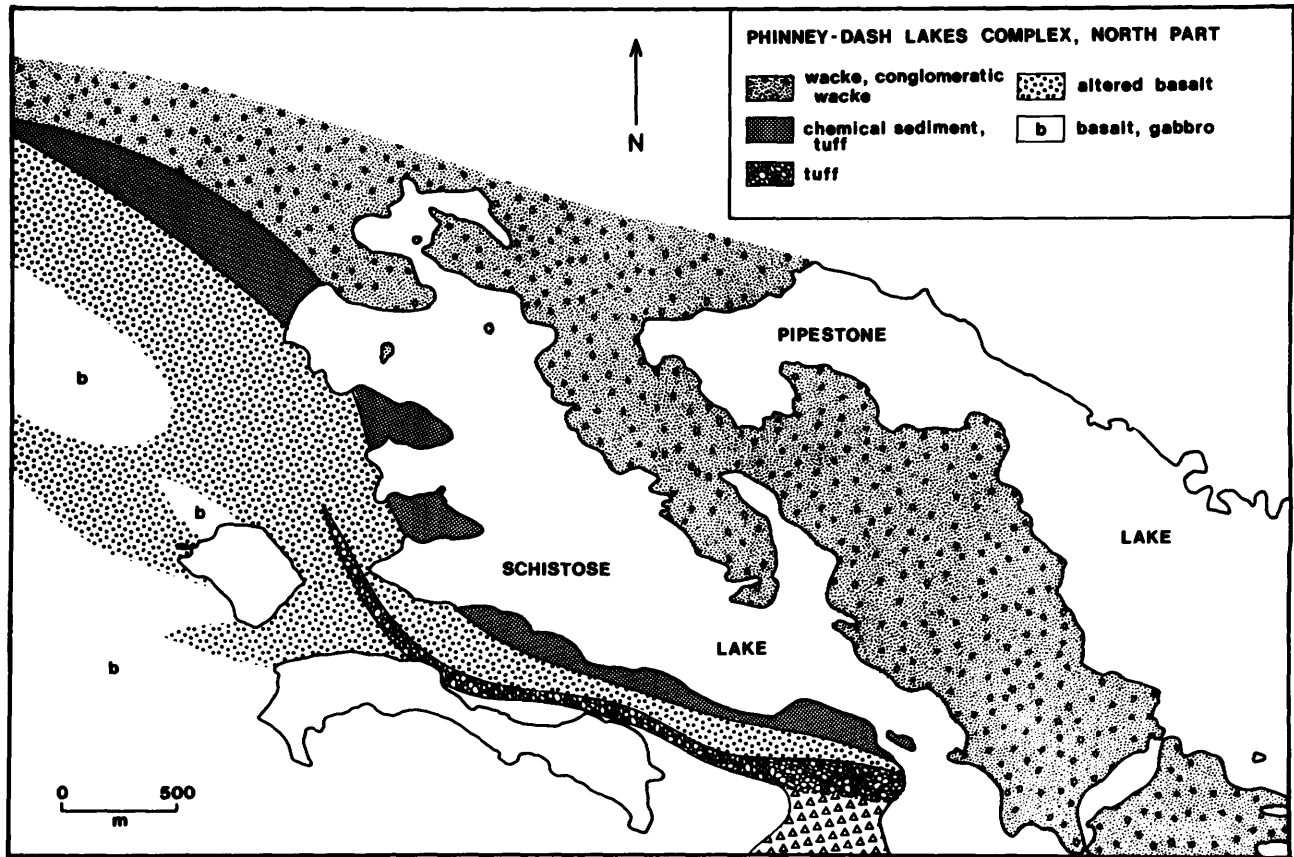


Figure 5—North flank of the Phinney-Dash Lakes Complex.

SABASKONG BATHOLITH

The Sabaskong Batholith is at the west end of a series of diapiric batholiths forming an axis approximately 350 km long by 60 km average width in the Wabigoon Subprovince. These diapiric batholiths consist of 1) tonalitic to granodioritic gneiss and gneiss domes with lesser massive segregations, 2) arcuate dioritic to monzonitic plutons occurring between the gneiss domes and the supracrustal rocks, and 3) later granitic plutons of various compositions (Schwerdtner *et al.* 1979).

Part of the Sabaskong Batholith, mainly east of Highway 71 was mapped to identify the plutonic analogues and precursors of the Phinney-Dash Lakes Complex. Three main groups of rocks are recognized.

1) The Kishkutena hornblende-biotite tonalite to biotite trondhjemite is exposed over at least 110 km² between the main mass of the Sabaskong Batholith to the west and the Katimiagamak formation to the north and east (see Figure 2). To the east the tonalite is massive, exhibiting a generally concordant, low grade metamorphic contact

with the Katimiagamak formation. At Highway 71, the tonalite is gneissic and has dips as low as 35° to the east and south. The adjacent Katimiagamak formation in this area is drag folded and boudinaged and is represented by lineated amphibole schist and gneiss. West of Highway 71 the tonalite merges with migmatitic rocks which received only cursory examination for this study.

2) The Heronry diorite, a lenticular intrusion consisting of massive to lineated biotite-hornblende diorite, quartz diorite, and hornblende gabbro with many inclusions and large enclaves of amphibolite, and irregular dikes and patches of fine grained trondhjemite and pegmatite, intrudes the Katimiagamak formation in the zone of amphibole schist and gneiss north of the Kishkutena tonalite (see Figure 2). It is separated from the tonalite by a semi-continuous septum of amphibolite and agmatite. Where the tonalite and diorite are in contact, the tonalite is locally brecciated and has a fine grained dioritic matrix.

3) In the Kishkutena tonalite at Caliper Lake (see Figure 2) is an enclave of talcose peridotite, amphibolitized talcose peridotite and amphibole intruded by melanocratic

gabbro, gabbro, diorite and tonalite. Locally there are agmatitic dikes, pegmatitic hornblende gabbro dikes, veins of apatite and magnetite, and veins of green to bluish green serpentine. The contact of the enclave and adjacent Kishkutena tonalite is generally marked by diorite or hybrid diorite-tonalite. Foliation in diorite and tonalite at the south margin indicates that the enclave dips approximately 40° S.

CHEMISTRY

Major element analyses of 158 samples were done by X-ray Assay Laboratories Limited using a fused disc X-ray fluorescence (XRF) technique. At the University of Western Ontario, 62 of these samples were analyzed for trace elements using a compressed powder pellet XRF tech-

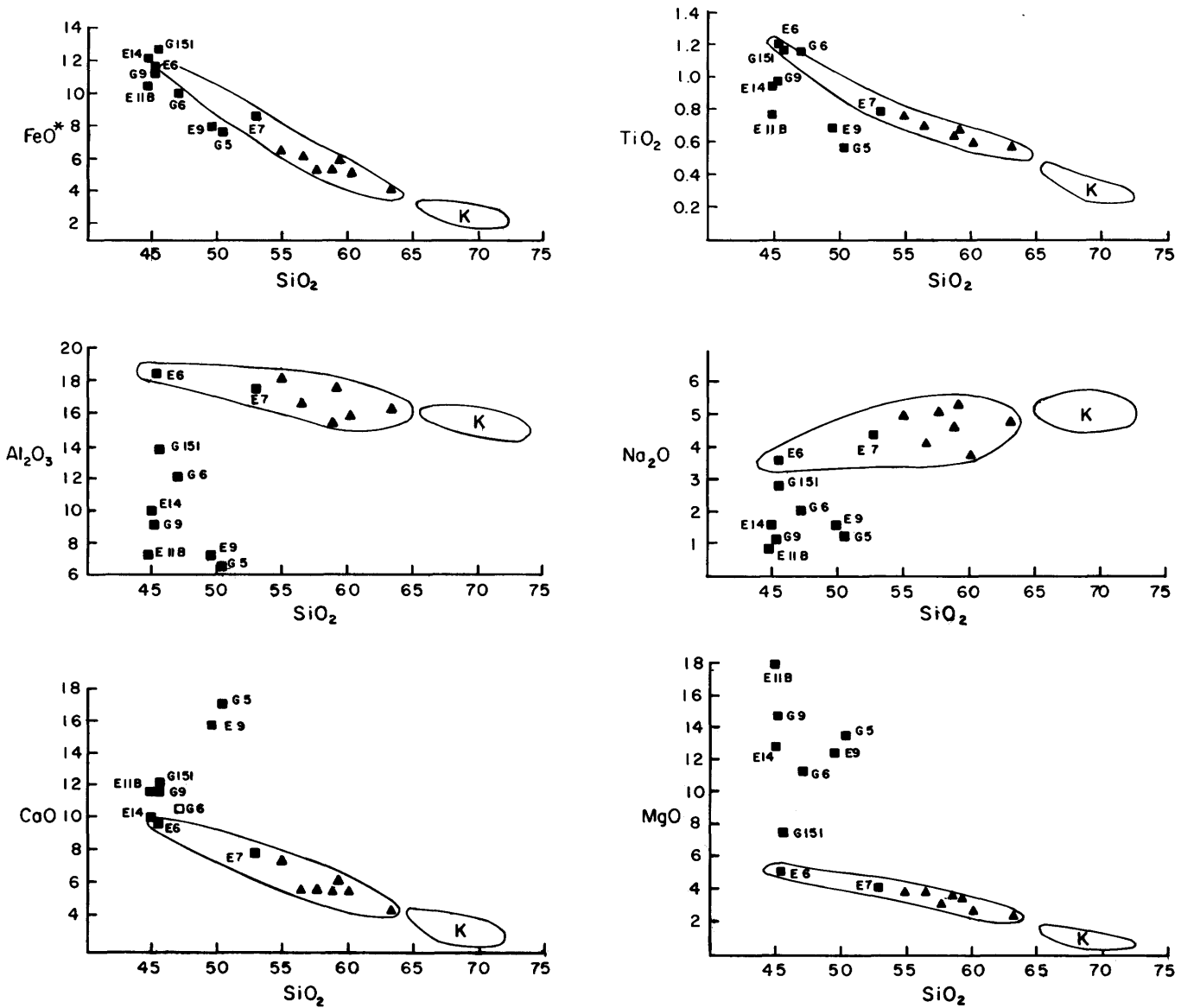


Figure 6—Harker variation diagrams showing trends for rocks of the Kishkutena tonalite (K), Heronry diorite (triangles) and the Caliper Lake enclave (squares).

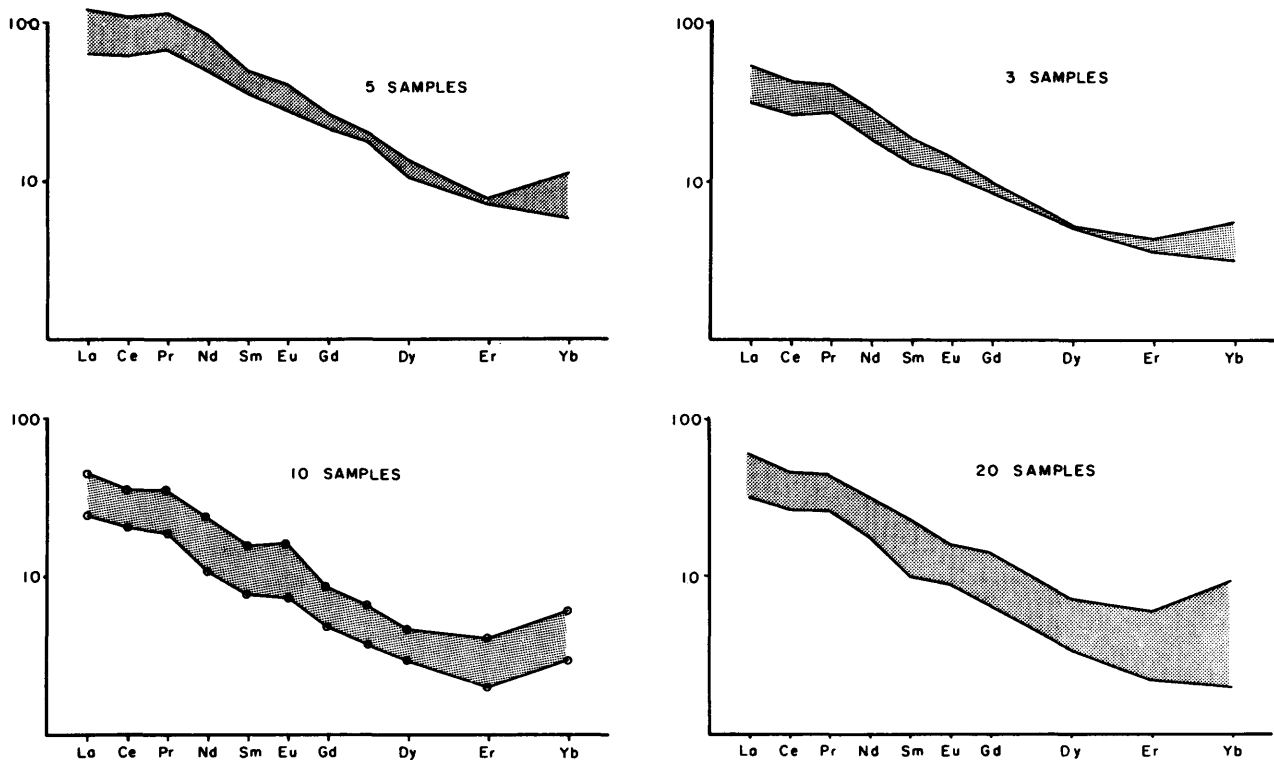


Figure 7—Chondrite-normalized rare earth element trends of samples from the Heronry diorite (upper left), the Dash Lake stock (upper right), the Kishkutena Tonalite (lower left), and the Phinney-Dash Lakes volcanic rocks (lower right).

nique and 92 samples were analyzed for rare earth elements using a slightly modified version (Fryer 1977) of the thin film XRF procedure of Eby (1972).

Major element trends of 24 samples of the Kishkutena tonalite, 5 samples of the Heronry diorite and 10 samples of diorite, gabbro and pyroxenite from the enclave at Caliper Lake are presented in Figure 6. Table 1 gives the average major element compositions of samples from the Kishkutena tonalite, the Heronry diorite and the Phinney-Dash Lakes Complex. Chondrite-normalized rare earth element trends of rocks from the Sabaskong Batholith and the Phinney-Dash Lakes Complex are displayed in Figures 7 and 8. Table 2 lists the average rare earth element abundances of samples from the Kishkutena tonalite, the Heronry diorite and the Phinney-Dash Lakes Complex.

Amphibole in the Kishkutena tonalite and Heronry diorite was analyzed using the Materials Analysis Company electron microprobe at the University of Western Ontario. Average results are tabulated in Table 3. Amphibole classification (Figure 9) is that of Leake (1978).

ANALYSIS OF CHEMICAL DATA

The Harker variation diagrams of Figure 6 show smooth

major element trends between Kishkutena tonalite and Heronry diorite with a small gap between 64 and 66 percent silica. This trend includes samples E7 (diorite) and E6 (hornblende gabbro) phases from the Caliper Lake enclave and can be qualitatively explained by the crystal accumulation of hornblende to form an orthocumulate. Samples G5 and E9 are gabbroic hornblende clinopyroxenite and are either restite or cumulate. They are anomalously low in alumina, reflecting their mineralogy. Samples E11B, E14, G6 and G9 are from mafic to ultramafic dikes which could be a late unrelated suite of rocks fortuitously intruding the enclave. They are interpreted here however, as fluidized restite because 1) they are apparently restricted to the enclave, 2) there is abundant water in the talc in nearby talcose peridotite in the enclave, and 3) some of these dikes have talc xenocrysts rimmed with opaque oxides and reacting to colourless amphibole. Sample G151 is from a gabbroid rock in an insitu, partially melted zone in an amphibolite enclave in the Heronry diorite east of Nestor Falls. On the variation diagrams (Figure 6), it generally plots between sample E6 of the diorite-tonalite trend and the restite samples E9 and G5.

The chondrite-normalized rare earth element trends of samples from the Sabaskong Batholith and volcanic and subvolcanic rocks of the Phinney-Dash Lakes Complex (see Figure 7) are essentially parallel but generally

Table 1—Average major element compositions of 52 samples from the Phinney-Dash Lakes Complex (P), 24 samples from the Kishkutena tonalite (K) and 5 samples from the Heronry diorite (H). Column 2 is anhydrous, recast to 100 percent in each case.

	P		K		H	
	1	2	1	2	1	2
SiO ₂	68.94	71.92	69.25	70.5	58.68	60.08
Al ₂ O ₃	14.55	15.18	15.55	15.83	16.86	17.26
TiO ₂	0.34	0.35	0.31	0.32	0.66	0.68
FeO*	2.83	2.95	2.49	2.54	5.41	5.54
MnO	0.09	0.09	0.05	0.05	0.10	0.10
MgO	0.72	0.75	0.86	0.88	3.29	3.37
CaO	2.78	2.90	3.17	3.23	5.77	5.91
Na ₂ O	3.81	3.97	5.09	5.18	5.00	5.12
K ₂ O	1.69	1.76	1.36	1.38	1.62	1.66
P ₂ O ₅	0.10	0.10	0.09	0.09	0.28	0.29
L.O.I.	3.33		0.57		0.51	
TOTAL	99.18	100	98.79	100	98.18	100

Table 2—Average rare earth element abundances in ppm of 32 samples from the Phinney-Dash Lakes Complex (P), 10 samples from the Kishkutena tonalite (K), 2 samples from the Heronry diorite (H) and 1 sample of cumulate hornblende gabbro (E6) from the enclave at Caliper Lake.

	P	K	H	E6
La	14.2	11.2	37.8	56.4
Ce	30.5	24.8	92.1	154.4
Pr	3.7	2.9	12.7	22.7
Nd	12.9	10.2	49.2	95.5
Sm	2.6	2.1	9.2	19.0
Eu	0.8	0.7	2.7	5.4
Gd	2.2	1.7	6.6	14.5
Dy	1.5	1.2	3.9	6.7
Er	0.7	0.6	1.5	2.7
Yb	0.8	0.6	1.7	2.2

Table 3—Average amphibole compositions of 21 samples from the Kishkutena tonalite (K) and 4 samples from the Heronry diorite (H).

Oxide	K	%	Oxide	H	%
SiO ₂		44.45	SiO ₂		44.94
TiO ₂		1.06	TiO ₂		0.95
Al ₂ O ₃		8.92	Al ₂ O ₃		9.40
Cr ₂ O ₃		0.10	Cr ₂ O ₃		0.03
FeO*		18.48	FeO*		17.91
MnO		0.47	MnO		0.31
MgO		10.64	MgO		11.18
CaO		11.64	CaO		11.44
Na ₂ O		1.30	Na ₂ O		1.55
K ₂ O		0.90	K ₂ O		1.03
Sum		97.96	Sum		98.73
Cations			Cations		
Si		6.708	Si		6.700
Al IV		1.292	Al IV		1.300
Al VI		0.295	Al VI		0.351
Ti		0.120	Ti		0.106
Fe		2.333	Fe		2.233
Mg		2.392	Mg		2.485
Mn		0.060	Mn		0.039
Cr		0.012	Cr		0.003
Na		0.379	Na		0.447
Ca		1.883	Ca		1.828
K		0.174	K		0.196

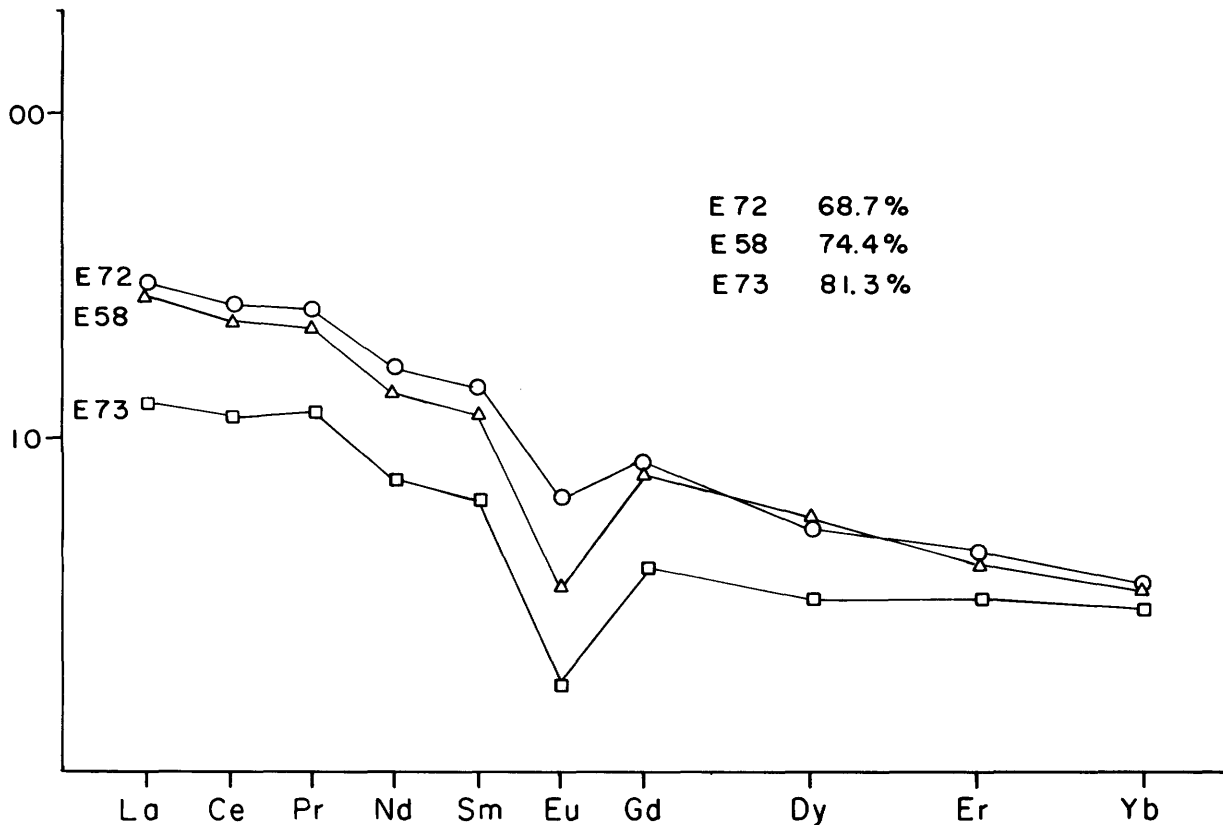


Figure 8—Chondrite-normalized rare earth element trends of three rhyolite samples from north and east of Dash Lake. Silica content of each sample is listed at the upper right of the diagram.

vary in total rare earth abundance according to the silica content of the rock. Arth *et al.* (1978) attributed similar trends in the gabbro-diorite-tonalite-trondhjemite suite of southwest Finland to hornblende fractionation or partial melting of basalt leaving a hornblende-rich residue. The rare earth element variations in rocks of the present study can be interpreted similarly but with some modification as discussed later.

Figure 8 is a plot of the chondrite-normalized rare earth element variations for three rhyolite samples of the Phinney-Dash Lakes Complex near Dash Lake. The rhyolites exhibit decreasing rare earth element abundance, increasing negative Eu anomaly and decreasing Ce/Yb ratio with increasing silica content. Hildreth (1979) suggested that a similar effect in silica-rich members of the Bishop Tuff in California may be controlled by thermogravitational diffusion. Fractionation of feldspar could also deplete the melt in light rare earth elements (LREE) and Eu relative to heavy rare earth elements (HREE) because the feldspar/melt distribution coefficient is higher for Ce than Yb. For the fractionation of feldspar to change Ce/Yb substantially, however, would require an increase in the distribution coefficient of LREE/liquid and Eu/liquid for feldspars in highly siliceous magmas.

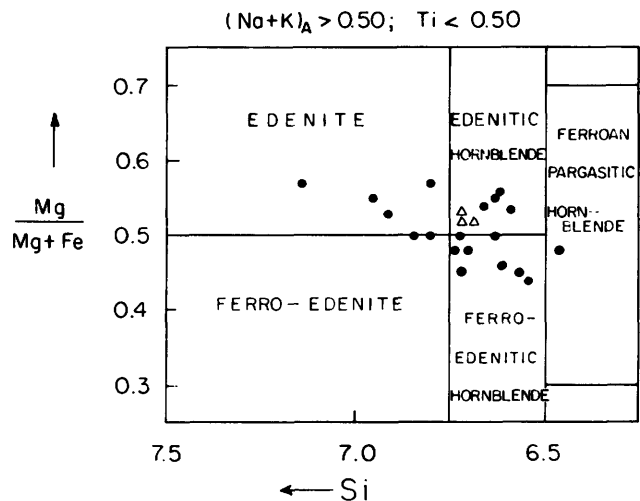


Figure 9—Mg/(Mg + Fe) vs. Si plot of amphiboles from the Kishkutena tonalite (solid circles) and the Heronry diorite (triangles). Classification from Leake (1978), based on 23 oxygens.

DISCUSSION

The experimental work of Helz (1973, 1976) has shown that the feldspar component of unaltered basalt starts to melt at P_{H_2O} of 5 kbar and 690°C. Hornblende however does not start to melt substantially until most of the plagioclase is melted at 950 to 1000°C. If the plagioclase-rich liquid is removed as fast as it is formed, aluminous trondhjemite melts would accumulate, and upon intruding overlying rock, would leave an amphibole-rich residue. In dynamic systems, amphibole will be carried up by convection. In this manner, partial melting of K-poor basalt could result in stratified plutons grading from restite to gabbro, diorite, tonalite and trondhjemite without attaining the temperature necessary to melt hornblende.

Evidence for this is in the amphiboles of the Heronry diorite and Kishkutena tonalite. The amphibole chemistry for both rocks is essentially identical in those samples studied (see Table 3, Figure 9) and suggests a common source for the amphiboles but not crystallization from dioritic or tonalitic magmas respectively.

In one of their models, Arth *et al.* (1978) invoked hornblende as a major fractionating or residual phase in the genesis of the gabbro-diorite-tonalite-trondhjemite suite of southwest Finland. The rare earth element trends in the rocks studied by them show a variation consistent with the changing mineral/melt distribution coefficient for rare earth elements in hornblende in equilibrium with melts from basaltic to rhyolite composition (Higuchi and Nagasawa 1969; Nagasawa and Schnetzler 1971; Arth and Barker 1976); the whole rock abundances reached a maximum in rocks with 59.5 percent SiO_2 . In tonalite to gabbro samples of the present study (see Table 2), whole-rock, rare earth element abundances increase steadily with decreasing silica and increasing modal amphibole suggesting that amphibole in the Heronry diorite (-gabbro) is xenocrystic, orthocumulative and was not in equilibrium with melts of basalt or andesite composition.

CONCLUSIONS

Field and chemical evidence suggests that the base of the Katimiagamak formation was partially melted yielding trondhjemite liquid containing xenocrystic amphibole which formed orthocumulate gabbro, diorite and tonalite. The enclave at Caliper Lake is interpreted as metamorphosed and partially melted Katimiagamak basalt because 1) the aeromagnetic anomaly associated with it is semicontinuous with basaltic rocks south of Kishkutena Lake, 2) basalt east of Kishkutena Lake is intruded by composite sills of gabbro with talcose peridotite similar to that observed in the enclave, 3) diorite and hornblende gabbro (E7 and E6 of Figure 6) with major and trace element abundances similar to the Heronry diorite are in and adjacent to the enclave and probably formed during partial melting of the enclave.

The overlapping rare earth element and major element trends of the Phinney-Dash Lakes Complex and the

Kishkutena lobe of the Sabaskong Batholith suggest their common origin by partial melting of basalt. Partial melting of basalt in this area resulted in the bimodal basalt-dacite association.

The lack of significant base metal deposition in the silica and iron-dominated chemical sedimentary units of the Phinney-Dash Lakes Complex could be accounted for as follows. 1) Leaching and deposition of iron from the generally Fe-rich Katimiagamak formation during hydrothermal processes associated with chemical sedimentary deposition diluted or inhibited the deposition of other base metals. 2) The Phinney-Dash Lakes Complex is peripheral to the major paleo-volcanic centre. The near vertical dip of the lithologies in the complex suggests considerable batholith diapirism after the emplacement of the present exposed section of the Phinney-Dash Lakes Complex. The dip of strata in the base-metal-rich Noranda area of Quebec is generally shallower, perhaps indicating that some of the exposed volcanic sections there are presently above some of their plutonic equivalents. 3) The Heronry diorite, Kishkutena trondhjemite and the Phinney-Dash Lakes Complex may have originated by relatively low temperature partial melting of basalt and therefore may not have had enough heat to maintain a hydrothermal flux in the adjacent host rock. Also consistent with the low temperature origin of the Phinney-Dash Lakes volcanic plutonic system is the lack of evidence for explosive activity normally associated with amphibole-crystallizing calc-alkaline volcanism.

REFERENCES

- Arth, J.G., and Barker, F.
1976: Rare-earth partitioning between hornblende and dacitic liquid and implications for the genesis of trondhjemitic-tonalitic magmas; *Geology*, vol. 4, p.534-536.
- Arth, J.G., Barker, F., Petermen, Z.E., and Freidman, I.
1978: Geochemistry of the gabbro-diorite-tonalite trondhjemite suite of southwest Finland and its implications for the origin of tonalitic and trondhjemitic magmas; *Journal of Petrology*, vol. 19, pt.2, p.289-316.
- Barker, F., and Arth, J.G.
1976: Generation of trondhjemitic-tonalitic liquids and Archean bimodal trondhjemite-basalt suites; *Geology*, vol. 4, p.596-600.
- Bowen, N.L.
1928: *The Evolution of Igneous Rocks*; University Press, Princeton.
- Eby, G.N.
1972: Determination of rare earth, yttrium and scandium abundances in rocks and minerals by ion-exchange-X-ray fluorescence procedure; *Analytical Chemistry*, vol. 44, p.2137.
- Edwards, G.R.
1976: *Geology of the Pipestone Lake (North) Area, District of Kenora*; Ontario Division of Mines, Open File Report 5194, 87p. Accompanied by Map P.1000.
- 1978: *Geology of the Pipestone Lake (South) Area, District of Rainy River*; Ontario Geological Survey, Open File Report 5247, 92p. Accompanied by map.

- Fryer, B.J.
1977: Rare earth evidence in iron-formations for changing Precambrian oxidation states; *Geochimica et Cosmochimica Acta*, vol. 41, p.361-367.
- Green, T.H., and Ringwood, A.E.
1968: Genesis of the calc-alkaline igneous rock suite; *Contributions to Mineralogy and Petrology*, vol. 18, p.105.
- Helz, R.T.
1973: Phase relations of basalts in their melting range at $P_{H_2O} = 5$ kb as a function of oxygen fugacity. Part 1. Mafic phases; *Journal of Petrology*, vol. 14, part 2, p.249-302.
1976: Phase relations of basalts in their melting ranges at $P_{H_2O} = 5$ kb. Part II. Melt compositions; *Journal of Petrology*, vol. 17, part 2, p.139-193.
- Higuchi, H., and Nagasawa, H.
1969: Partition of trace elements between rock-forming minerals and the host volcanic rocks; *Earth and Planetary Science Letters*, vol. 7, p.281-287.
- Hildreth, W.
1979: The Bishop tuff: Evidence for the origin of compositional zonation in silicic magma chambers; *Geological Society of America, Special Paper 180*.
- Hodder, R.W. and Edwards, G.R.
1980: Evolution of an Archean Felsic Volcanic Complex; Grant 55, p.101-110 in *Geoscience Research Grant Program, Summary of Research 1979-1980*, edited by E.G. Pye, Ontario Geological Survey, Miscellaneous Paper 93, 263p.
- Leake, B.E.
1978: Nomenclature of amphiboles; *The Canadian Mineralogist*, vol. 16, p.501-520.
- Morse, S.A., Lindsley, D.H., and Williams, R.J.
1980: Concerning intensive parameters in the Skaergaard intrusion; *American Journal of Science*, vol. 280A, p.159-170.
- Nagasawa, H., and Schnetzler, C.C.
1971: Partitioning of rare earth, alkalic and alkaline earth elements between phenocrysts and acidic igneous magma; *Geochimica et Cosmochimica Acta*, vol. 35, p.953-968.
- Osborn, E.F.
1959: Role of oxygen pressure in the crystallization and differentiation of basaltic magma; *American Journal of Science*, vol. 257, p.609-647.
- Osborn, E.F.
1962: Reaction series for sub-alkaline igneous rocks based on different oxygen pressure conditions; *American Mineralogist*, vol. 47, p.177-188.
- Schwerdtner, W.M., Stone, D., Osadetz, K., Morgan, J., and Stott, G.M.
1979: Granitoid complexes and the Archean tectonic record in the southern part of northwestern Ontario; *Canadian Journal of Earth Science*, vol. 16, p.1965-1977.

Grant 84 Sedimentology of the Matinenda Formation

P.W. Fralick and A.D. Miall

Department of Geology, University of Toronto

ABSTRACT

A comprehensive investigation of the sedimentation history of a rock unit must involve regional as well as detailed studies. This approach has been taken in the present investigation of the processes controlling deposition of the Matinenda Formation.

Hypotheses concerning the basin type in which the Matinenda Formation was deposited are limited because lithosphere plate interaction during the Precambrian is poorly understood. However, new data indicate that the Huronian Supergroup may have been deposited in a rifted margin. The Matinenda Formation appears to represent braided stream deposition; longitudinal and transverse bars form extensive deposits, but out-of-channel deposits are relatively rare. Uranium concentrations in the formation are limited to conglomeratic "packages". Three models may be used for the concentration of uraninite in these packages: 1) high water turbulence over openwork gravel stretches of the stream bed reduced the slope of the vertical velocity profile and caused preferential deposition of uraninite; 2) erosion of small point-sources made pulses of quartz pebbles and uraninite available for sedimentation by the braided streams; or 3) a combination of the previous two possible causes. Selection of the correct model must await further investigation.

INTRODUCTION

The basal Huronian Matinenda Formation contains more than half of Canada's reasonably assured resources of uranium. The economically important deposits within the rock mass have been the subject of much research. However, the vast majority of published work has dealt with the mineralogy and stratigraphy of the unit while a firm understanding of the sedimentology has remained lacking. We hope that the research effort of which this paper is the beginning will correct the deficiency.

A full understanding of the depositional processes operating during sedimentation of the Matinenda Formation entails viewing the problem at several different levels. The overall basin(s) type, shape, predepositional history, and postdepositional evolution must be known in order to fit the Matinenda Formation into a plausible sequence of events. The formation itself must be studied on a regional scale to ascertain both lateral and vertical changes. Finally, at the smallest scale, an in-depth investigation of

the sedimentology of individual units will lead to definition of possible depositional environments and subenvironments.

GENERAL GEOLOGY

The Matinenda Formation forms the lowermost unit of the Huronian Supergroup. The supergroup was deposited in a basin which formed sometime after the Kenoran Orogeny (2.7 Ga*, Morey and Sims 1976) and before intrusion of the Nipissing Diabase (2.15 Ga, Robertson 1973). The present outcrop area forms a wide belt curving from the north shore of Lake Huron to the Ottawa River. The succession itself is almost entirely composed of siliciclastic rocks. Mafic volcanic flows occur in a few places near the base, usually interlayered with coarse clastic rocks of the Matinenda Formation. The Espanola Formation is the only unit of the supergroup containing appreciable carbonate rocks.

The clastic rocks form four megacycles. Poorly sorted conglomerate and mudstone usually occur at the base of each cycle. The coarse fraction disappears vertically leaving mudstone and siltstone as the middle units. Quartzite caps the tripartite assemblages. Metamorphic grade varies from subgreenschist facies in the eastern and western parts of the belt to amphibolite facies, staurolite zone (Card 1978a), in the central part (Sudbury-Cutler area). A linear zone of high-grade metamorphism extending from Cutler to Sudbury is probably a result of shearing along the Murray Fault Zone which extends through this area. The major metamorphic event has been dated at 1.9 Ga, thus correlating it with the Penokean Orogeny (Card 1978a).

The sedimentology of the Huronian Supergroup is poorly understood because individual researchers have seldom been able to work on more than a small segment of the supergroup, and a truly regional synthesis has never been developed. Therefore, only a rough outline of the sedimentology of the Huronian Supergroup can be presented (Table 1).

A deep marine interpretation for the turbidite basin (McKim Formation) and glacio-marine lithofacies (Ramsey Lake, Bruce, and Gowganda Formations) results in marked fluctuations in the relative water-level curve (right-hand part of Table 1). Turbidites themselves do not al-

*Ga = billion years.

Table 1—Sedimentation history of the Huronian Supergroup. Compiled from: Theis (1979), Card (1978), Casshyap (1966), Chandler (1969), Palonen (1971), Long (1976), Young (1973), Lindsey (1971), Roscoe (1973), and Wood (1973).

Group	Formation	Depositional Environment	Deep Marine	Shallow Marine	Strand	Subaerial
Cobalt	Bar River	coastal-beach				
	Gordon Lake	tidal flat				
	Lorrain	fluvial to near-shore				
	Gowganda	glacial to glacio-marine				
Quirke Lake	Serpent	distal stream				
	Espanola	fluvial through deltaic and shallow marine to deeper marine				
	Bruce	glacial to glacio-marine				
Hough Lake	Mississagi	deltaic, fluvial and shallow marine				
	Pecors	turbidite basin				
	Ramsay Lake	glacial to glacio-marine				
Elliot Lake	McKim	turbidite basin				
	Matinenda	fluvial				

ways denote deep water deposition. However, in this case, where there seems to have been an abundance of coarse clastics in the transportation-deposition system, deep water seems the most likely environment for fine-grained turbidite deposits. The fluctuations in the relative water level follow a pattern. After an initial clastic influx, the lower half of the Huronian succession is dominated by deeper-water sedimentation. The only unit breaking this trend is the Mississagi Formation which may represent prograding deltas. The Espanola Formation signals the end of extensive deep water conditions. Above this unit, strandline-fluvial deposits dominate.

The division of the stratigraphic column into shallow-water and deep-water assemblages may be caused by either glaciation or tectonism. During glaciation, water tied up in the ice sheet causes worldwide depression of sea level. However, in the glaciated area this is counteracted by isostatic depression induced by glacial loading. In the waning stages of a glacial event sea level rises rapidly as the ice cap melts. After a period of time, rebound of the terrain previously in the area of the ice cap may outstrip sea level rise and a regression occurs. This scenario may be used to explain the Pecors-Mississagi couplet after Ramsey Lake glaciation. However, events following Bruce and Gowganda glaciation do not show this same relationship. Indeed the major change from deep-water to shallow-water sedimentation seems to be unrelated to the three glacial episodes.

The tectonic regime governing the sedimentary style of the Huronian Supergroup is considerably less understood than the rock units themselves. This may change in the near future as ideas developed by Morey and Sims (1976), Sims (1976), and Sims *et al.* (1980) are applied in more detail to the Huronian basin. These authors believe that a geosuture separates an older gneissic terrain in the north-central United States from the Superior Province. They further hypothesize that episodes of tension and compression occurred in the Great Lakes region as these two crustal segments separated and collided.

The Huronian Supergroup appears to have been deposited on a tectonically quiescent platform bordering an ocean to the south. This indicates that the southern craton was probably separated from the northern terrain during Huronian deposition. If this is the case the change-over from "deep" to "shallow" water deposition could have occurred when clastic influx and carbonate generation outstripped subsidence of the shelf area. In this model the Matinenda Formation would represent the earliest preserved infilling of the basins on the rifted margin.

DEPOSITIONAL ENVIRONMENT

DESCRIPTION

The depositional environment of the Matinenda Formation will be investigated in the field in the summer of 1981. The present description relies heavily on material published by other authors.

The Matinenda Formation (Figure 1) outcrops extensively at the nose of the Chiblow Anticline and along the southern margin of the Quirke Syncline. Other exposures tend to be small and scattered. The unit thickens to the south increasing from less than 1 m on the north shore of Quirke Lake to 210 m at Pronto Mine (Robertson 1976).

In most areas the Matinenda Formation may be divided into two lithofacies. Some basal sections of the unit consist of coarse, gritty sandstone interbedded with conglomerate (Roscoe 1969). Laterally and vertically gradational with the "grit" lithofacies is a unit consisting almost entirely of fine- to coarse-grained, poorly sorted subarkose, lithic arkose, and lithic subarkosic wacke (Parviainen 1973; Roscoe 1969). The position of both lithofacies in the sedimentary sequence appears to be strictly controlled by genesis; the grits tend to lie on or near basement and sometimes overlap arkosic units to the south. This relationship is caused by a combination of two

factors: progressive younging of basal units in a northerly direction (Roscoe 1969; Robertson 1976); and sporadic tectonic activity causing coarser grained units to prograde to the south over the finer arkoses. Positioning of grits and conglomerate units is also controlled by basement topography. Valleys eroded into less resistant rock tend to be filled with the "grit" lithofacies (Roscoe 1957; Pienaar 1963; Robertson 1976).

The presence of ore-grade uranium mineralization has made the quartz-pebble conglomerates by far the most thoroughly described units in the sedimentary package. Three ore zones occur: 1) the Pronto Zone, 2) the Nordic Zone, and 3) the Quirke Zone (see Figure 1). Clast size decreases from the Pronto Zone to the Nordic Zone to the Quirke Zone (Robertson 1976). The units also appear to become progressively younger to the north (Roscoe 1969; Robertson 1976). Where "grit" lithofacies directly overlies basement it usually consists of a gravelly, immature lag deposit (Figure 2, upper left). The lag is replaced vertically by extensive conglomerate and sandstone units. The conglomerates are composite containing lenses of a variety of lithofacies from subarkose through to tightly packed gravel-cobble conglomerate (Theis 1979; Peinaar 1963) (Figure 2, upper right; Figures 3, 4 and 5). The individual lenses tend not to be very

extensive. Crossbedding, both trough and planar, and ripple lamination dominate the sedimentary structures. At one location, large (amplitude 1 m), planar cross-sets with numerous reactivation surfaces were developed in a sandstone lens. Paleocurrent studies carried out by McDowell (1957) and Pienaar (1963) on the conglomerate packages indicate flow was towards the southeast.

The arkosic and subarkosic lithofacies has received less attention than the economically significant "grit" lithofacies. A range of grain sizes from fine to coarse sand dominates the "arkosic" assemblage (Parviainen 1973; Frarey 1977). Mudstone drapes are common between sandstone beds (see Figure 2, lower right). Aside from these drapes, siltstone and mudstone beds appear to be relatively rare in the western outcrop area but increase in importance in the east (Card 1978b). Occasional conglomerate lenses and thin sheets are interbedded with the sandstone. Ripple marks, scour and fill structures, parallel laminations, and both planar and trough crossbedding are common in the "arkose" lithofacies. Parviainen (1973) found that these structures indicate sediment transport was towards the south in the east and central outcrop area and towards the southeast in the western outcrop area.

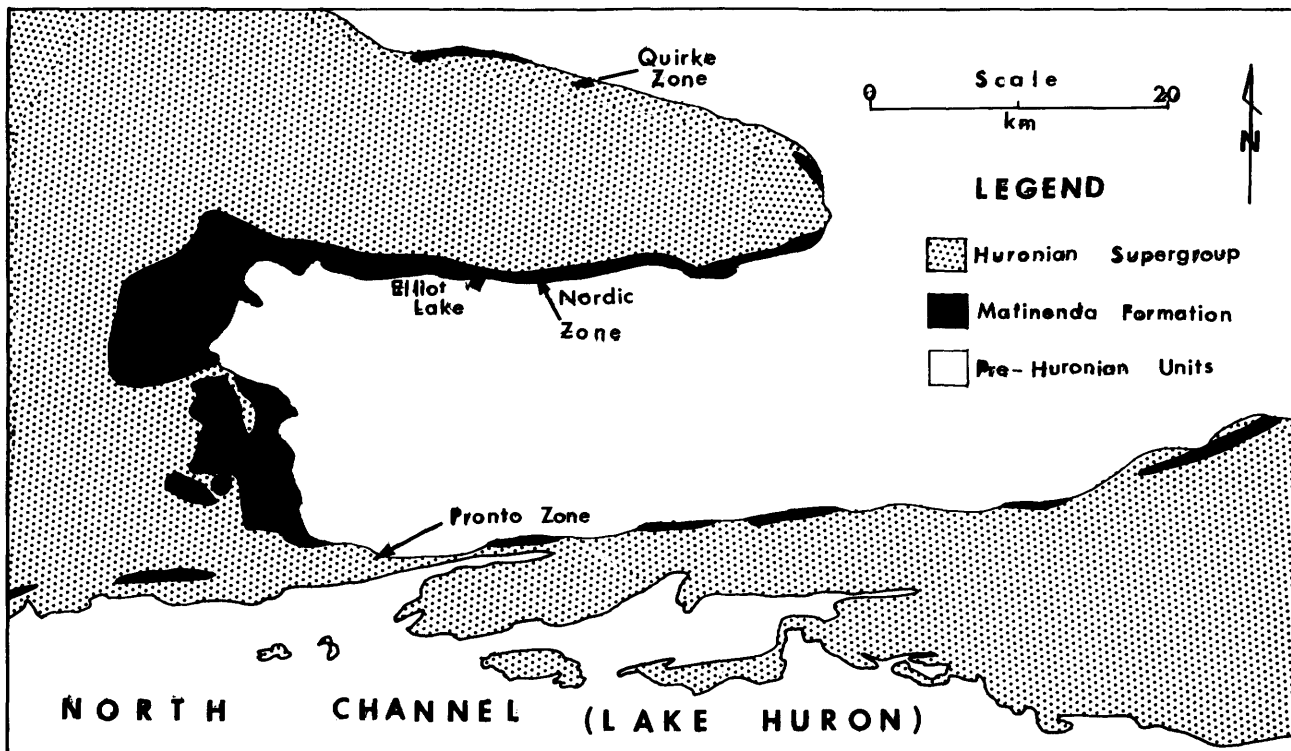


Figure 1—Location of outcrop area of the Matinenda Formation.

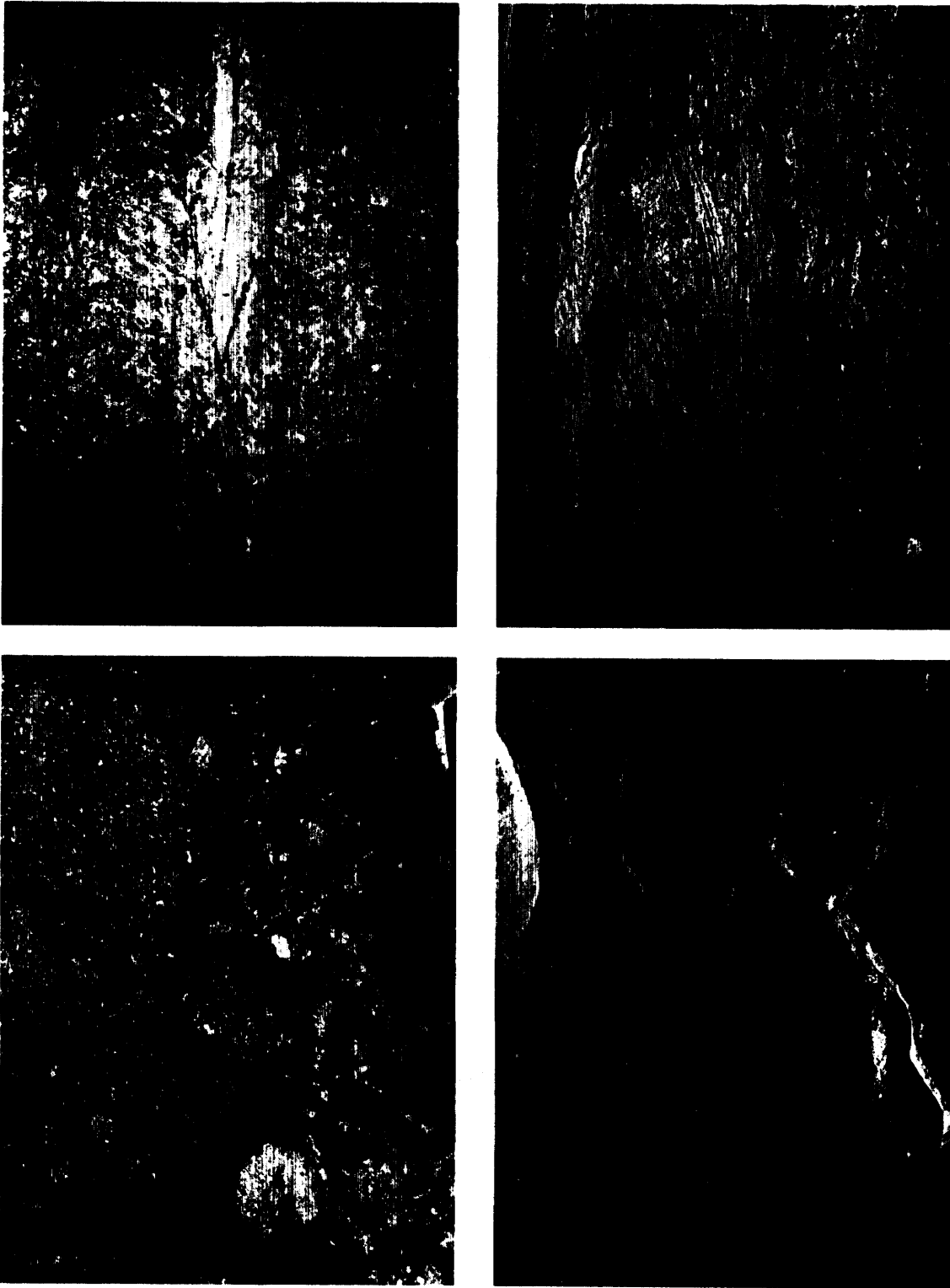


Figure 2—Upper left: basal contact of the Matinenda Formation (overturned). Upper right: quartz-pebble conglomerate (originally overlying granite, near Pronto Mine. Lower right: trough crossbedded arkose at Elliot Lake. Lower left: trough crossbedded arkose. A thin mud drape separates the units (Pronto Mine gate).

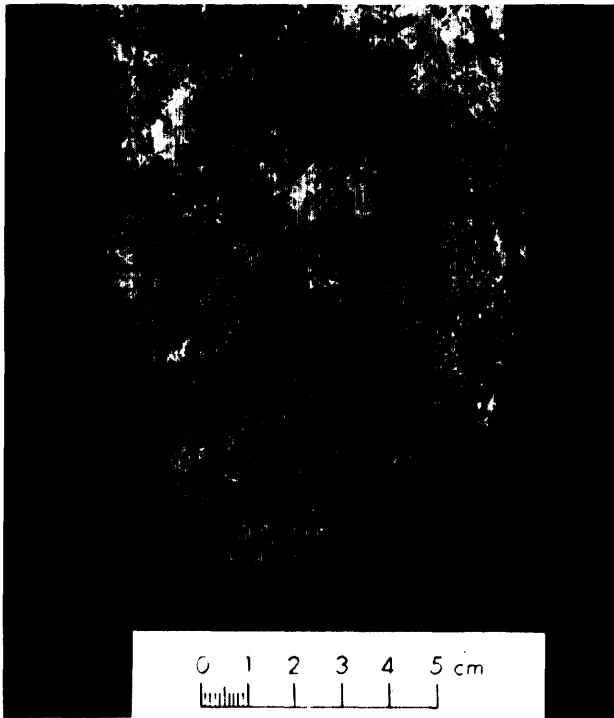


Figure 3—Typical uraniferous quartz-pebble conglomerate.

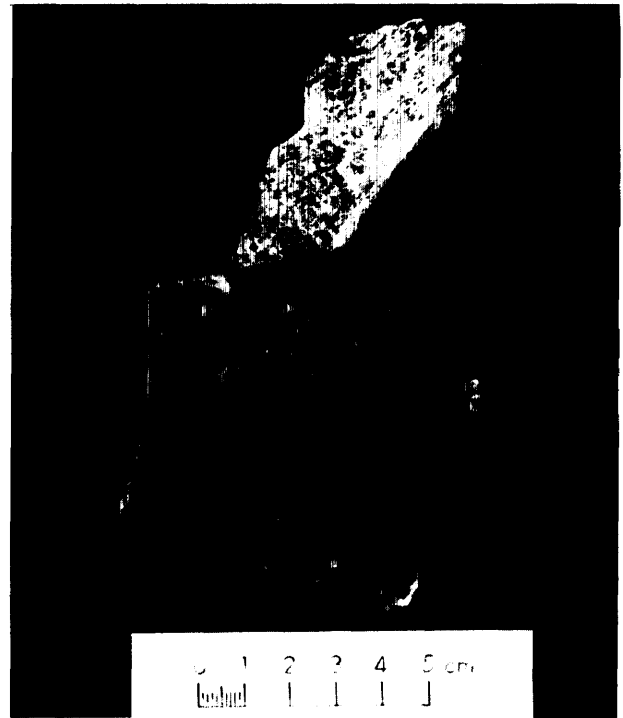


Figure 4—Uraniferous quartz-pebble conglomerate grading vertically into a barren quartzite. Note the rapid grain-size changes.

CONCLUSIONS

An in-depth analysis of the depositional environment must await the acquisition of further data. However, some rudimentary conclusions can be drawn from the work of other authors. Most authors (Theis 1979; Frarey 1977; Robertson 1976; Parviainen 1973; Roscoe 1969) consider the Matinenda Formation to have been deposited under fluvial conditions. In particular a braided stream model is suggested (Parviainen 1973; Theis 1979).

The sediments served to even the topography by infilling valleys. As the slope was reduced both by sedimentary buildup in low areas and erosive levelling of uplands, the Matinenda Formation overlapped to the north. Coarser "grit" lithofacies may have developed adjacent to isolated upland areas while the "arkose" lithofacies formed the more extensive, better-worked deposits. As the depositional edge of the Matinenda Formation progressively moved north, the argillites of the McKim Formation appear to progressively transgress the Matinenda in this direction. This relationship may not denote the lateral equivalence of Matinenda and McKim depositional environments as Parviainen (1973) believes an interval of nondeposition and intense weathering separates Matinenda and McKim deposition.

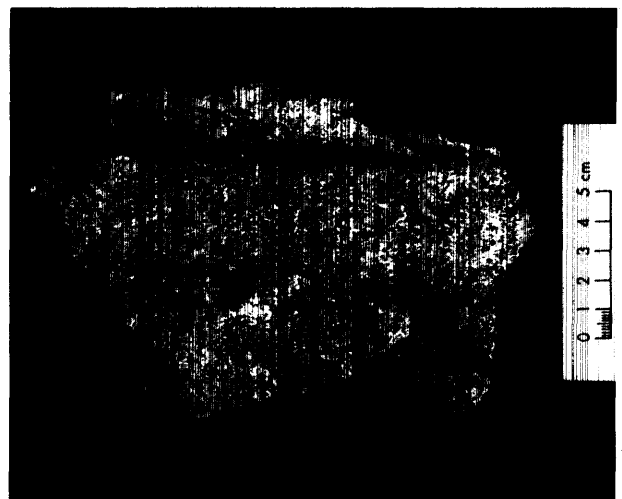


Figure 5—Barren quartzite with prominent, dark, cross-bedded heavy mineral layers.

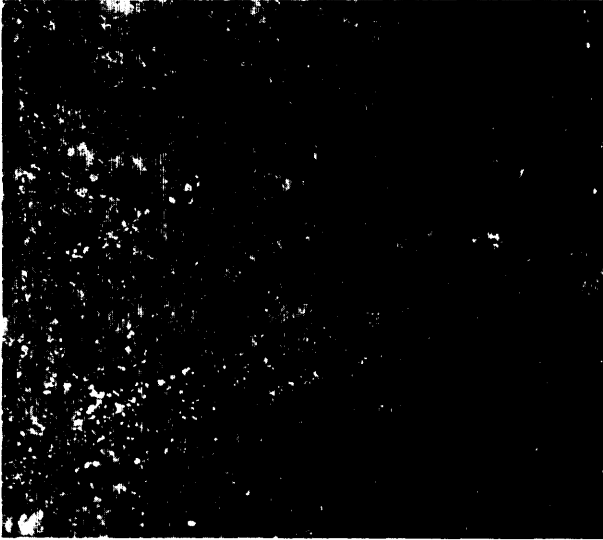


Figure 6—Pyrite accentuating ripple lamination in a small sandy area of a uraniferous ore reef, Denison Mine, (actual size).

HYDRAULIC CONTROLS ON URANIUM MINERALIZATION

URANIUM OCCURRENCES

Ore grade uraninite mineralization is limited to conglomerates in the lower portions of the Matinenda Formation. Quartzite interbeds separating conglomerate packages and quartzite lenses in the packages themselves do not contain uraninite mineralization (A.G. Robinson, Department of Geology, University of Toronto, personal communication, 1981). Fluvial control of mineralization has been demonstrated by Theis (1979). He believes that changes in the mineralogy of the ore zones reflect regional patterns in the depositional environment and that smaller scale zoning was caused by fluctuations in the depositional energy.

A similar situation exists in South Africa where uraninite and gold mineralization was concentrated in quartz-pebble conglomerates by fluvial sedimentation (Minter 1976). Here the uraninite values also drastically fall off outside conglomerate units (Koen 1961; Coetzee 1965). This is problematic as other accessory heavy minerals such as zircon and chromite, which are associated with uraninite in the ore "reefs", do not decrease in abundance in the quartzite. Koen (1961) concluded from this that the uraninite must be genetically linked to special conditions which operated during the formation of the ore conglomerates. As in the Witwatersrand, heavy minerals but not uraninite are concentrated outside of the conglomerates in the ore zones of the Matinenda Formation

(A.G. Robinson, personal communication, 1981) (Figure 6).

As previously noted, the uraniferous conglomerate packages in the Matinenda Formation are composed of a variety of lithologies. Conglomerates grade from clast- to matrix-supported and are transitional into pebbly quartzite and quartzite (Pienaar 1963). Scoured surfaces are common. A wide range of grain sizes exists: the maximum diameter of the clasts in conglomerates of the Quirke Zone averages 4.5 cm; interstitial poorly sorted sand averages 0.4 mm; and primary uraninite grains average 0.2 mm (Figure 7) (A.G. Robinson, personal communication, 1981). From this data some constraints on the hydraulic factors governing uranium mineralization can be developed.

EXPERIMENTAL PROCEDURE

Most authors have approached the problem of defining controls governing the hydraulic concentration of heavy minerals from a very theoretical standpoint. Investigations along these lines suffer from severe constraints: 1) Stokes Law and other equations derived from it are applicable

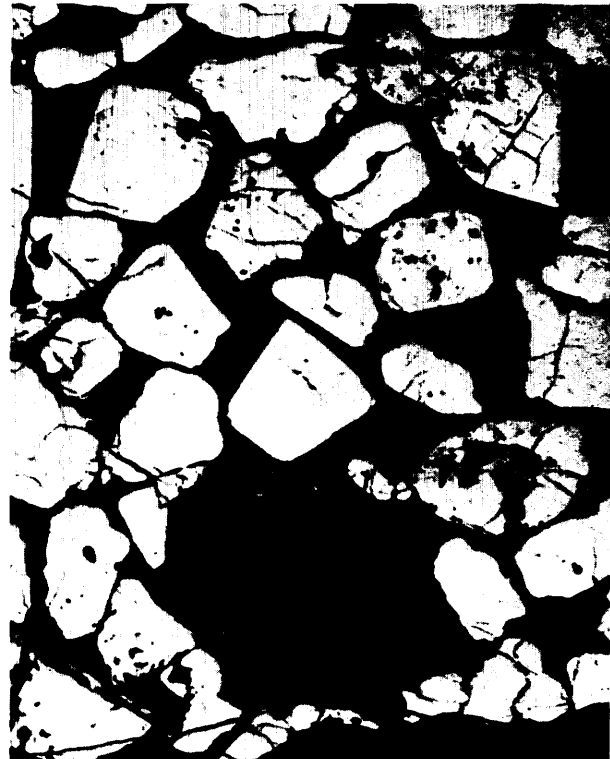


Figure 7—Photomicrograph of sub-angular uraninite grains (200 μ diameter) with a large (325 μ) uranothorite grain (bottom). Bar scale in upper right corner is 100 μ .

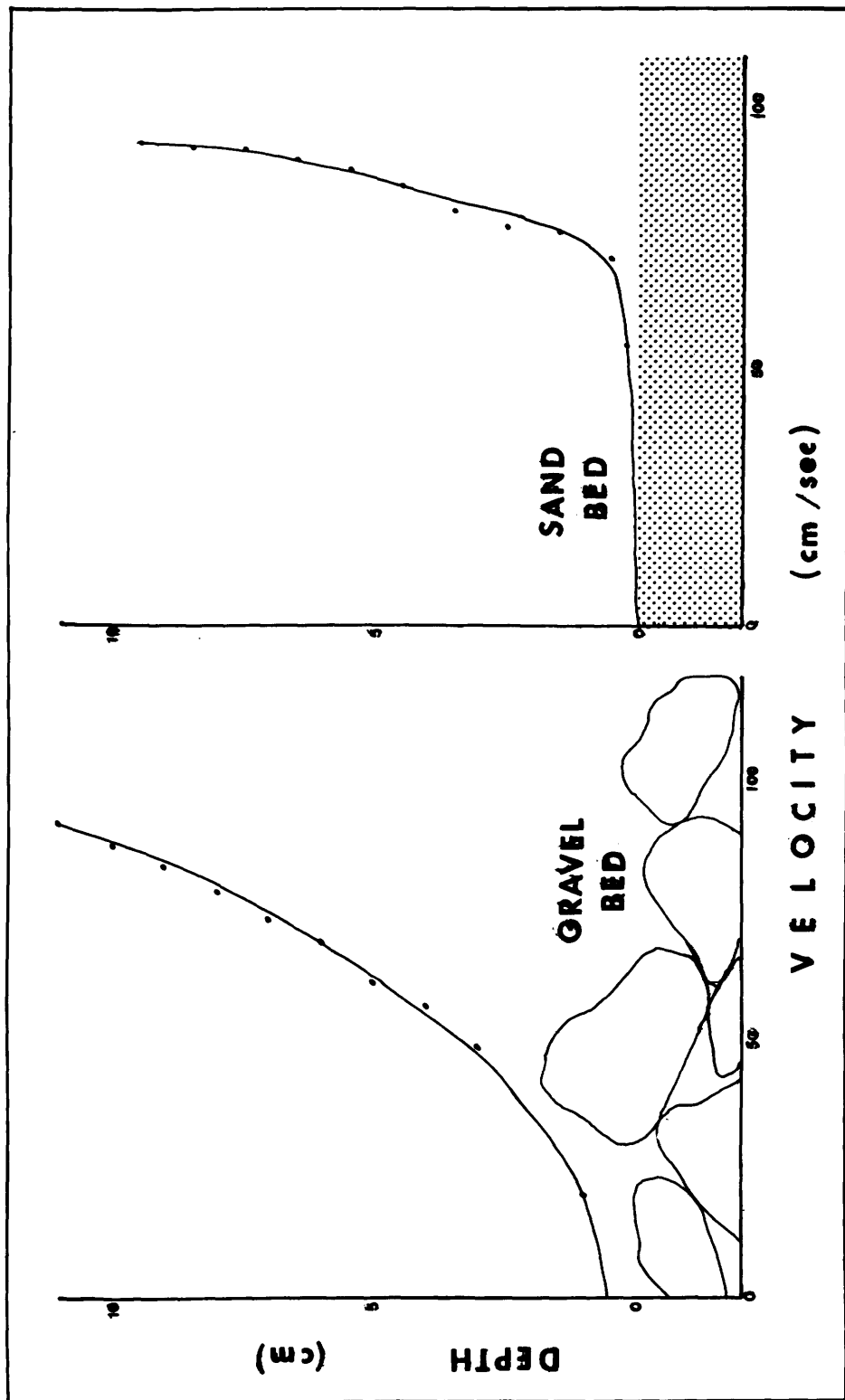


Figure 8—Velocity profile above a gravel bed (left) and a sand bed (right). The flume in which this data was generated measured 6.1 m by 0.3 m. $Q = 24.2$ l/sec, $T = 24^\circ\text{C}$, average grain size of sand = 0.25 mm, average maximum gravel diameter = 50 mm, average depth of water = 11.7 cm, average velocity = 0.66 m/sec, $Re = 36,500$, $Fr = 0.825$, Chezy $C = 21$, Manning $n = 0.03$; the bedforms were transitional between lower and upper flow regimes.

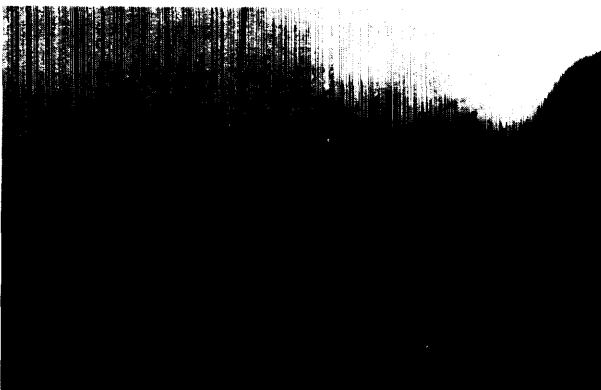
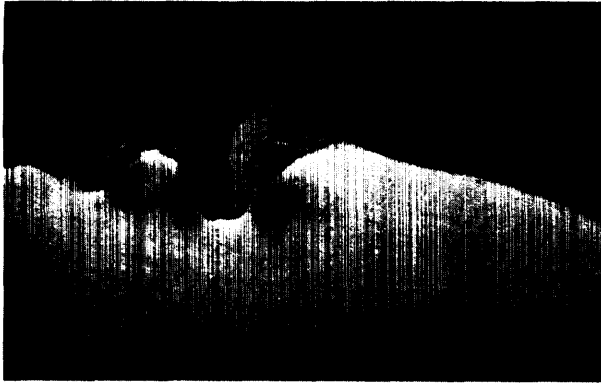


Figure 9—Sediment transport over a gravel bed. Top: The current is from left to right. Notice the high suspended sand concentration in the lee of the cobbles, the complete infilling of voids, and the development of wavy laminae. Middle: Flow is from right to left. A high concentration of sand is being carried close to the gravel bed. Bottom: Flow is from right to left. Notice the strong backflow near the bed as indicated by the dye. The two upper photographs are at flow conditions specified in Figure 8. The lower photograph represents flow conditions well into the upper flow regime. (flume length photographed = 20 cm)

only where viscous forces dominate (i.e. only for the equivalent of quartz grains less than 0.14 mm falling through still water of 16°C) (Tourtelot 1968); 2) Shield's criterion only approximately applies to a mixture of small, heavy minerals and quartz sand because of the shielding problem (Grigg and Rathbun 1969); 3) almost no reliable data exists for the threshold of sediment movement at high Grain Reynolds Number values (Miller *et al.* 1977); and 4) velocity fluctuations caused by eddying play a very important role in governing grain size of material deposited and these fluctuations are very poorly understood. Primarily because of the last problem listed, work carried out by such authors as White and Williams (1967), Lowright *et al.* (1972), and Slingerland (1977) is not applicable to the heavy mineral concentrations in the Matinenda Formation.

In order to shed light on the hydraulic controls of uraninite concentration, experiments were conducted on sand transport over a gravel bed. A 6.1 m by 0.3 m sediment-water recirculating flume was used. Approximately 1 m from the upstream end a 1.5 m by 0.05 m ramp was inserted. An openwork gravel-cobble bed was positioned at the end of the ramp and extended for 0.7 m downcurrent. Five runs were conducted using a sand with an average grain size of 0.25 mm. For three runs the Reynolds Number was 36,500 (fully turbulent flow) and the Froude Number was 0.825 (in transition from lower to upper flow regime). The other two runs were conducted at higher velocities in the upper flow regime.

At the transitional velocities, pores between the gravel clasts slowly accumulated sand until all available pore space was filled. At this point a thin (2 cm) sand blanket developed over the gravel with only larger cobbles protruding. The velocity profile above the gravel (early in run) and the sand blanket (late in run) proved very different (Figure 8). The high degree of turbulence which develops over the irregular gravel surface causes the velocity profile to increase gradually away from the bed of the stream. Compared to the gravel bed a sand bed is smooth and unable to create sufficient turbulence to impede the flow very far above the bed. The highly turbulent layer above the gravel bed is extremely important in controlling the transport and deposition of sand grains. This layer appears cloudy because of the high sediment concentration it contains (Figure 9). Combined with its high potential to carry sediment because of the periodic large upward forces operative in the layer the rapid velocity fluctuations in both space and time can produce intense sedimentation.

At slightly higher water velocity, sedimentation in the open work gravel proceeded much more rapidly. Only very patchy sand blankets developed in low-lying areas. The rapid increase in depositional speed probably reflects a great increase in the amount of material in suspension and available for sedimentation with only a minor increase in velocity. A run conducted at even higher velocity resulted in the development of up-current breaking surface waves and again rapid sedimentation in the openwork gravel. As the velocity was decreased during this run a ripple field migrated over the gravel bed. In all five runs the sand filling the spaces between clasts devel-

oped a very irregular lamination. The laminations were sometimes traceable over 0.3 m.

FACTORS CONTROLLING URANIUM CONCENTRATIONS

According to Rittenhouse (1943), who did pioneer work on heavy mineral concentrations, these concentrations are governed by 1) the mineral's relative availability in each size grade in the stream load, 2) the mineral's density, 3) the hydraulic conditions at the time and place of deposition, and 4) unknown factors. In the case of the uraniferous deposits in the Matinenda Formation uraninite accumulations are limited to the conglomerate units. This implies that the hydraulic conditions at the time and place of deposition, namely high turbulence induced by bed roughness, may have been the primary control of uraninite concentration. The lack of uraninite in quartzites of both the Matinenda Formation (A.G. Robinson, personal communication) and the Witwatersrand deposits (Koen 1961; Coetzee 1965) indicates that either the fairly constant velocity immediately above planar sand beds was too high (see Figure 8) to deposit uraninite or pulses of uraninite were derived along with quartz pebbles from isolated local sources. Experiments conducted by Minter and Toens (1970) indicate that heavy minerals (magnetite) are slightly depleted in sand deposited in openwork gravel and therefore are enriched in the sediment passing over the gravel. They hypothesized that further downstream, after the sediment in transport had become suitably enriched, it would be capable of forming a placer similar to those of the Witwatersrand. This unfortunately does not explain why the uraninite is limited to conglomerates, although magnetite's specific gravity is very much less than that of uraninite and their results may not be applicable.

Another problem arises in areas where sand deposition occurred over bedforms such as ripples and dunes. Turbulence and flow separation caused by these structures (Jopling 1964) is similar to that observed over gravel beds. Thus if degree of turbulence controlled uraninite deposition, ripple laminated and crossbedded units would be expected to contain concentrations of uraninite. They do not, though other heavy minerals behave in agreement with theory and experimental results (McQuivey and Keefer 1969). The uraninite may behave differently because of its very high specific gravity, or its concentration may have been controlled by sporadic inputs from point sources. Further experimentation is needed to choose between these two options.

FUTURE WORK

A great deal more remains to be done towards understanding the sedimentology of the Matinenda Formation. Defining the overall basin type and its development must await further research into forces operating during evolution of the Precambrian crust. On the local scale a study

of data collected from outcrop and core will be undertaken to gain more knowledge on the depositional environment and its variation through space and time. Further laboratory investigation of sediment transport in flumes will also be conducted. This should define the sedimentation characteristics of uraninite under turbulent flow.

ACKNOWLEDGMENTS

Grateful appreciation is extended to Mr. A.G. Robinson of the University of Toronto for the use of many photographs and for the extremely helpful discussions concerning the mineralogy of the deposits. Typing of the manuscript, done on short notice by Miss Sheilaigh McKeough, is also greatly appreciated. Dr. A.V. Jopling of the University of Toronto provided the flume for the experimental work.

REFERENCES

- Card, K.D.
1978a: Metamorphism of the Middle Precambrian (Aphebian) rocks of the eastern Southern Province; p.269-282 in, ed. Fraser, J.A., and Heywood, W.W., Metamorphism in the Canadian Shield, Geological Survey of Canada, Paper 78-10.
1978b: Geology of the Sudbury-Manitoulin area, Districts of Sudbury and Manitoulin; Ontario Geological Survey, Report 186, 238p.
- Casshyap, S.M.
1966: Sedimentary petrology and stratigraphy of the Huronian rocks south of Espanola, Ontario; Unpublished Ph.D. thesis, University of Western Ontario, London, Ontario, 232p.
- Chandler, F.W.
1969: Geology of the Huronian rocks, Harrow Township area, Ontario; unpublished Ph.D. thesis, University of Western Ontario, London, Ontario, 327p.
- Coetzee, F.
1965: Distribution and grain-size of gold, uraninite, pyrite, and certain other heavy minerals in gold-bearing reefs of the Witwatersrand Basin; Transactions and Proceedings of the Geological Society of South Africa, Vol. 68, p.61-88.
- Frarey, M.J.
1977: Geology of the Huronian belt between Sault Ste. Marie and Blind River, Ontario; Geological Survey of Canada, Memoir 383, 87p.
- Grigg, N.S., and Rathbun, R.E.
1969: Hydraulic equivalence of minerals with a consideration of the reentrainment process; United States Geological Survey, Professional Paper 650B, p.B77-B80.
- Jopling, A.V.
1964: Laboratory study of sorting processes related to flow separation; Journal of Geophysical Research, Vol. 69, p.3403-3418.
- Koen, G.M.
1961: The genetic significance of the size distribution of uraninite in the Witwatersrand blankets; Transactions and Proceedings of the Geological Society of South Africa, Vol.64, p.23-45.
- Lindsey, D.A.
1971: Glacial marine sediments in the Precambrian Gowganda Formation at Whitefish Falls, Ontario; Pal., Pal., and Pal., Vol.9, p.7-25.

- Long, D.G.F.
1976: The stratigraphy and sedimentology of the Huronian (Lower Apehebian) Mississagi and Serpent Formations; Unpublished Ph.D. thesis, University of Western Ontario, London, Ontario, 291p.
- Lowright, R., Williams, E.G., and Dachille, F.
1972: An analysis of factors controlling deviations in hydraulic equivalence in some modern sands; *Journal of Sedimentary Petrology*, Vol.42, p.635-645.
- McDowell, J.P.
1957: The sedimentary petrology of the Mississagi quartzite in the Blind River area, Ontario; Ontario Department of Mines, Geological Circular 6.
- McQuivey, R.S., and Keefer, T.N.
1969: The relation of turbulence to deposition of magnetite over ripples; *United States Geological Survey Professional Paper 650-D*, p.244-247.
- Miller, M.C., McCave, S.N., and Koman, P.D.
1977: Threshold of sediment movement under unidirectional currents; *Sedimentology*, Vol.24, p.507-527.
- Minter, W.E.L.
1976: Detrital gold, uraninite, and pyrite concentrations related to sedimentology in the Precambrian Vaal Reef placer, Witwatersrand, South Africa; *Economic Geology*, Vol.71, p.157-175.
- Minter, W.E.L.
1970: Experimental simulation of gold deposition in gravel beds; *Transactions of the Geological Society of South Africa*, Vol.73, p.89-98.
- Morey, G.B., and Sims, P.K.
1976: Boundary between two Precambrian W terrains in Minnesota and its geologic significance; *Geological Society of America, Bulletin*, Vol.87, p.141-152.
- Palonen, P.A.
1971: Stratigraphy and depositional environment of the Mississagi Formation, Ontario; Unpublished M.Sc. thesis, University of Calgary, Alberta, 103p.
- Parviainen, E.A.V.
1973: The sedimentology of the Huronian Ramsay Lake and Bruce Formations, north shore of Lake Huron, Ontario; Unpublished Ph.D. thesis, University of Western Ontario, London, Ontario, 426p.
- Pienaar, P.J.
1963: Stratigraphy, petrology and genesis of the Elliot Lake Group, Blind River, Ontario, including the uraniferous conglomerate; *Geological Survey of Canada, Bulletin 83*, 143p.
- Rittenhouse, G.
1943: The transportation and deposition of heavy minerals; *Geological Society of America, Bulletin*, Vol.54, p.1725-1780.
- Robertson, J.A.
1973: A review of recently acquired geological data, Blind River-Elliot Lake area; p.169-198 in, ed. Young, G.M., *Huronian Stratigraphy and Sedimentation*, Geological Association of Canada, Special Paper Number 12.
- 1976: The Blind River uranium deposits: the ores and their settings; Ontario Division of Mines, *Miscellaneous Paper 65*, 45p.
- Roscoe, S.M.
1957: Geology and uranium deposits, Quirke Lake-Elliot Lake, Blind River, Ontario; *Geological Survey of Canada, Paper 56-7*.
- 1969: Huronian rocks and uraniferous conglomerates in the Canadian Shield; *Geological Survey of Canada, Paper 68-40*, 205p.
- 1973: The Huronian Supergroup, a Paleoproterozoic succession showing evidence of atmospheric evolution; p.31-48 in, ed. Young, G.M., *Huronian Stratigraphy and Sedimentation*. Geological Association of Canada, Special Paper Number 12.
- Sims, P.K.
1976: Precambrian tectonics and mineral deposits, Lake Superior region; *Economic Geology*, Vol.71, p.1092-1118.
- Sims, P.K., Card, K.D., Morey, G.B., and Peterman, Z.E.
1980: The Great Lakes tectonic zone—a major crustal structure in central North America; *Geological Society of America, Bulletin*, Vol.91, p.690-698.
- Slingerland, R.L.
1977: The effects of entrainment on the hydraulic equivalence relationships of light and heavy minerals in sands; *Journal of Sedimentary Petrology*, Vol.47, p.753-770.
- Theis, N.J.
1979: Uranium-bearing and associated minerals in their geochemical and sedimentological context, Elliot Lake, Ontario; *Geological Survey of Canada, Bulletin 304*, 50p.
- Tourtlot, H.A.
1968: Hydraulic equivalence of grains of quartz and heavier minerals and implications for the study of placers; *United States Geological Survey, Professional Paper, 594-F*, 13p.
- White, J.R., and Williams, E.G.
1967: The nature of a fluvial process as defined by settling velocities of heavy and light minerals; *Journal of Sedimentary Petrology*, Vol.37, p.530-539.
- Wood, J.
1973: Stratigraphy and depositional environments of Upper Huronian rocks of the Rawhide Lake-Flack Lake area, Ontario; p.73-96 in, ed. Young, G.M., *Huronian Stratigraphy and Sedimentology*, Geological Association of Canada, Special Paper Number 12.
- Young, G.M.
1973: Origin of carbonate-rich Early Proterozoic Espanola Formation, Ontario, Canada; *Geological Society of America, Bulletin*, Vol.84, p.135-160.

Grant 49 Trace Element and Stable Isotope Geochemistry of Auriferous Iron Formations in the Timmins Area

J.A. Fyon, J.H. Crocket, H.P. Schwarcz, A. Kabir, and M. Knyf

Department of Geology, McMaster University

ABSTRACT

Trace element and stable isotopic characteristics of auriferous and non-auriferous, chert-magnetite iron formations, within the Deloro Group volcanic rocks south of Timmins, were compared with the objective of 1) defining gold exploration criteria for this environment, and 2) describing the hydrothermal history of the gold mineralization and carbonate alteration. The auriferous iron formations are enriched in gold, sulphur, tungsten, antimony and carbon dioxide. Both auriferous and non-auriferous iron formations have similar arsenic abundances. Gold in iron formation occurs in two ways: 1) as native gold and as inclusions in pyrite that envelops metamorphic quartz veins; and 2) as inclusions within pyrite and pyrrhotite grains that are disseminated throughout the iron formations, but are not spatially associated with metamorphic quartz veins.

Basalts, which contain the auriferous iron formations and have been altered at low temperatures by seawater, contain replacement calcite having a $\delta^{13}\text{C}$ isotope composition of -1 to -2% (PDB). Calcites from the outer edge and dolomites from the cores of pervasive carbonate alteration zones have $\delta^{13}\text{C}$ compositions of -2% and -4% respectively. This trend is consistent with higher-temperature carbonate precipitation in the core of the alteration zone. Replacement carbonates from the iron formations have a $\delta^{13}\text{C}$ compositional range from -2% to -5% which correlates with the abundance of magnetite. Syngenetic chert fragments and the replacement carbonates have exchanged oxygen with ubiquitous, oxygen-bearing metamorphic pore fluid.

INTRODUCTION

This report constitutes one phase of a larger, more comprehensive metallogenic study of certain types of gold deposits in the Timmins area. Emphasis is placed on defining the field characteristics of the gold mineralization, the host rock environment and associated rock alteration types to establish the timing of the various mineralization and alteration events. These field studies are being integrated with stable-isotope determinations of carbon, oxygen and ultimately hydrogen from mineralized and unmineralized environments in order to:

1) evaluate the stability of stable-isotope systematics in complexly polydeformed, Early Precambrian (Archean), volcano-sedimentary terrains;

2) better describe the ore forming processes, within the constraints imposed by the observed field relationships and the limitations of the stable-isotope data.

Epithermal instrumental neutron activation analysis of ores and associated host rocks for antimony, arsenic, gold and tungsten is being carried out to augment existing litho-geochemical, field, and stable-isotope criteria for gold exploration.

In other Early Precambrian terrains, banded iron formations have been host to significant concentrations of gold (e.g. Zimbabwe, Fripp 1976; Beardmore-Geraldton area, Pye 1951, Horwood and Pye 1951; Minas Gerais, Brazil, Fleischer and Routhier 1973, Tolbert 1964). Although regional stratigraphic syntheses of the Abitibi Belt in northeastern Ontario by Jensen (1978) and Pyke (1980) have illustrated that banded iron formations occur within and at the top of an older volcanic sequence (Lower Metavolcanic Group or Deloro Group), little gold production has come from these formations. Does this lack of gold production reflect insufficient exploration, or does it reflect more fundamental characteristics of the iron formations? Such characteristics include:

- 1) the environment in which the iron formation was formed;
- 2) the lateral and vertical scale of the iron formation;
- 3) its place within the volcano-sedimentary stratigraphy;
- 4) the intensity of diagenetic and metamorphic processes to which the iron formation has been subjected;
- 5) the structural regime in which the iron formation sits; and
- 6) the mineralogical constitution of the iron formation.

Not all of these questions can be answered by a cursory study of three iron-formation units: however, two small iron formations (Malga and Carshaw) (Figure 1) exposed in Carman and Shaw Townships are being studied in detail and serve as auriferous control units. For non-auriferous control, a preliminary suite of samples was collected from the Goose Lake iron formation, just west of Goose Lake in Shaw Township (Figure 1).

MALGA AND CARSHAW IRON FORMATIONS

GENERAL GEOLOGY

Mafic, pillowed flows (formation II, Deloro Group; Pyke 1980), which underlie the area, trend N25E and dip 25° E. Dikes and sills of quartz-feldspar porphyry and ultramafic

LEGEND

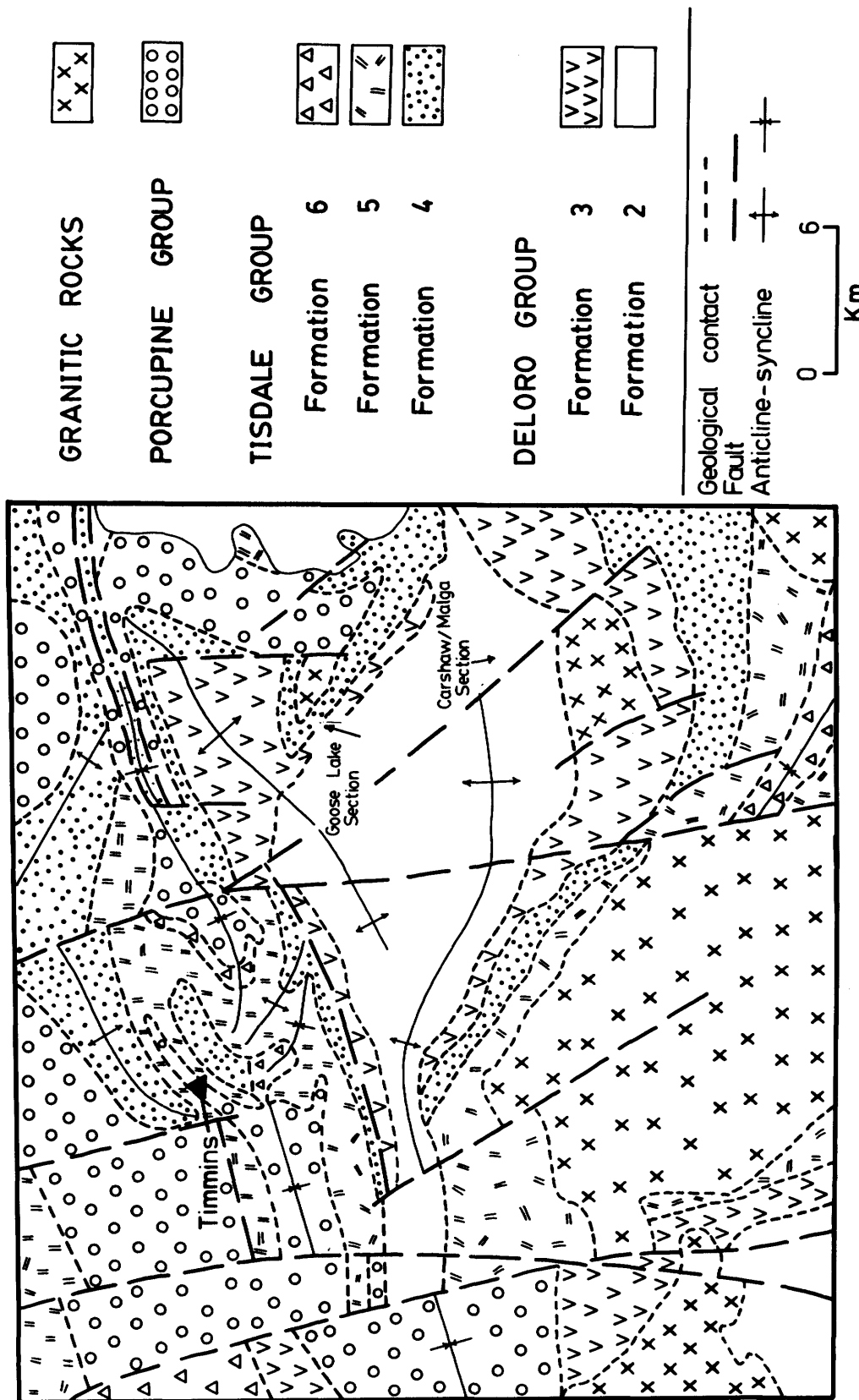


Figure 1—Regional stratigraphy of the Timmins area from Pyke (1980), illustrating the location of the Goose Lake and Carshaw-Malga iron-formation study areas.

komatiite, averaging 2 m in thickness, occur throughout the area and are interpreted to be subvolcanic equivalents of the overlying felsic and ultramafic volcanic rocks of formations III and IV respectively. A thin unit (100 m) consisting of siliceous, very fine-grained, massive to finely laminated tuff and a coarse-grained, matrix-supported, cherty debris flow conglomerate overlies the Malga iron formation. A regional metamorphic grade of greenschist facies has been attained.

IRON FORMATIONS

The Malga and Carshaw iron formation units average about 400 m in length, based on geophysical data. At its thickest, the Malga iron formation averages 30 m in thickness whereas the Carshaw iron formation does not exceed 15 m. Both iron formations consist predominantly of chert and magnetite mesobands (1-3 cm) with fewer carbonate and chlorite mesobands. Carbonate also occurs as an accessory phase present in the chert, magnetite and chlorite mesobands. Tentative carbonate identification by X-ray diffraction (XRD) reveals that dolomite predominates, although it may occur with admixtures of siderite. There appears to be no systematic correlation between carbonate type (as identified by XRD) and associated mesoband mineralogy. However, this observation remains to be tested by microprobe analyses of the carbonate mineralogy.

The iron formations are cut by late quartz veins (0.1 to 5 cm width) which are enveloped by pyrite. The pyrite envelopes, ranging in thickness from 1 to 5 cm, preferentially replace magnetite mesobands. It is noteworthy that accessory carbonate (up to 30 modal percent) occurs

in all magnetite mesobands, regardless of proximity to the megascopic quartz veins and that both carbonate-rich and carbonate-poor magnetite mesobands are replaced by the pyrite envelopes. Hence the introduction of carbonate into the iron formation appears to pre-date and to be unrelated to quartz-pyrite vein formation.

GOLD MINERALIZATION

Two types of gold mineralization are recognized. In the first, auriferous quartz veins, ranging in width from 1 mm to 5 cm, cut sub-orthogonally across and are restricted to the iron formation units. The larger of these quartz veins cut across many mesobands and can be traced over several metres. Within the pyrite envelopes about the quartz veins, metallic gold occurs in fractures and as blebs (0.03 mm) included within the pyrite.

Disseminated throughout the iron formations, not spatially associated with the megascopic quartz veining, are grains of pyrite and pyrrhotite. Significant geochemical correlations between gold and sulphur (see Table 4) show that gold is included within these disseminated sulphides. However, no metallic gold has been recognized petrographically in this type of sample material.

Of the sulphides present in the iron formations, pyrite predominates. It occurs invariably as euhedral grains 0.1 mm to 5 mm across which contain minute (<0.01 mm), blebby inclusions of chalcocopyrite, pyrrhotite and rarely gold where it occurs adjacent to quartz veins. Discrete grains of pyrrhotite also are present, although grain size rarely exceeds 0.1 mm. Pyrrhotite abundance varies from trace to nil in the chert and carbonate mesobands to nearly equal to that of pyrite in the magnetite mesobands.

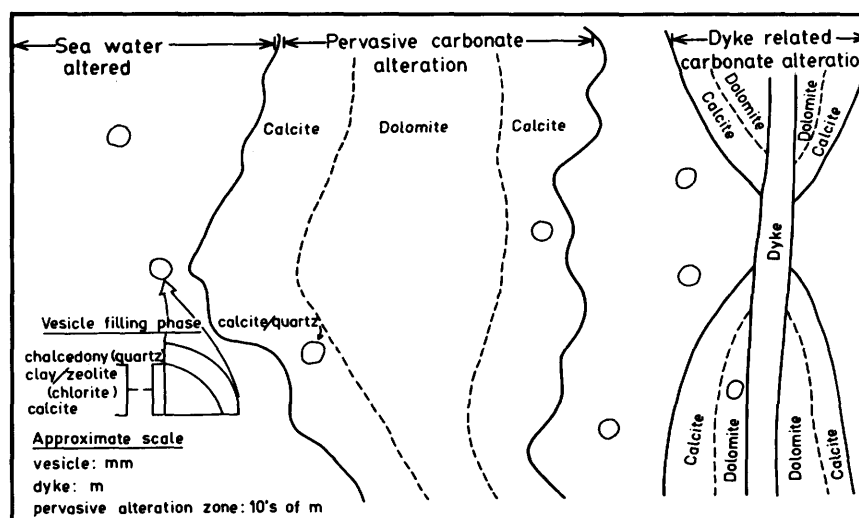


Figure 2—Alteration types recognized in the Malga and Carshaw study areas. Least altered volcanic rocks have been subjected to low temperature sea water alteration. Later, pervasive carbonate alteration zones, consisting of a dolomite core and a calcite-rich outer zone, occur throughout the volcanic stratigraphy and also envelop sub-volcanic dikes.

Table 1—Chemical and isotopic analyses of mesoband samples. Note, concentration units are as follows: Au, ppb; As, W, Sb, ppm; S, CO₂, weight percent.

Magnetite (minor chert and carbonate) Mesobands

Sample Number	Chert (minor magnetite and carbonate) Mesobands						Carbonates		Type
	Au	As	Sb	W	S	CO ₂	δ ¹³ C	δ ¹⁸ O	
81A	5.1	0.68	0.47	0.59	0.07	5.7	--	--	D
82	2.8	0.83	0.55	1.20	4.01	0.5	-5.36	11.87	N/D
88A	8.4	1.14	0.43	0.68	0.20	2.8	-5.44	10.59	N/D
89A	63	0.50	0.17	0.27	0.14	2.0	-4.78	11.03	D
121-1	390	0.55	0.34	0.66	1.72	11.4	-5.12	10.15	N/D
125-2	0.9	0.59	0.71	0.91	0.15	12.1	-4.95	12.10	S
127-2	95	1.48	1.22	0.89	0.36	12.1	-4.84	10.97	S
127-5	9.2	0.59	1.17	0.80	0.02	11.6	-4.70	10.73	D/S
128-1	30	0.53	0.59	0.48	1.50	6.0	-4.52	11.32	D/S
128-3	5900	0.16	0.34	0.89	1.74	15.1	-4.55	10.61	D/S
129-4	1.0	0.37	0.52	0.34	0.09	6.8	-4.55	10.61	D
130-4	700	1.45	0.55	0.46	1.27	6.4	-4.88	10.68	D
\bar{x}	600	0.72	0.59	0.68	0.61	6.92	-4.91	11.01	
σ	1610	0.41	0.30	0.26	0.69	4.49	0.30	0.57	
\bar{x}'	28.2	0.60	0.51	0.63	0.22	5.01			
σ'	1.14	0.27	0.22	0.18	0.72	0.42			

Chert (minor magnetite and carbonate) Mesobands

Sample Number	Chert (minor magnetite and carbonate) Mesobands						Carbonates		Type
	Au	As	Sb	W	S	CO ₂	δ ¹³ C	δ ¹⁸ O	
11	2.7	0.50	0.201	0.428	4.01	1.3	-6.05	14.01	N/D
12	3.7	0.25	0.058	0.087	0.04	0.18	--	--	N/D
13	0.77	0.58	0.024	0.009	4.01	0.17	-3.85	16.96	N/D
16	1.9	0.12	0.073	0.081	0.01	1.1	-3.25	12.56	N/D
17	6.6	0.63	0.312	0.641	0.14	5.9	-3.83	12.68	D
19	2.7	0.22	0.101	0.179	0.01	0.56	-3.72	11.52	N/D
21	4.9	0.03	0.076	0.020	0.06	0.55	-4.83	11.88	N/D
89B	3.6	1.76	0.489	0.272	0.02	4.0	-4.06	11.88	D
121-2	11.3	0.11	0.029	0.139	0.04	3.0	-3.65	10.59	D/D
127-1	125	0.21	0.131	0.729	0.37	3.3	-3.74	10.27	S/D
127-3	210	0.31	0.059	0.104	0.68	6.1	-4.32	10.62	S/D
127-4	1400	0.20	0.247	0.398	0.05	8.0	-3.72	11.10	S/D
127-6	20	0.15	0.077	0.012	0.43	5.8	-4.1	12.02	S/D
125-1	2.8	0.12	0.051	0.189	0.02	3.0	-4.41	10.94	S
128-2	14.5	0.45	0.057	0.123	0.85	3.0	-4.63	10.79	S
129-1	13	1.28	0.17	0.061	0.01	1.7	-4.63	10.79	D/S
129-3	33	1.28	0.512	0.374	0.50	6.7	-4.64	10.69	D
129-5	0.8	0.07	0.093	0.193	0.01	0.7	-4.80	11.11	N/D
130-3	11.6	0.23	0.072	0.132	0.02	1.80	-4.80	11.11	N/D
\bar{x}	98.4	0.39	0.143	0.219	0.17	3.35	-4.25	11.84	
σ	320	0.43	0.143	0.201	0.26	2.70	0.63	1.75	
\bar{x}'	9.8	0.28	0.10	0.13	0.05	1.95			
σ'	0.81	0.49	0.36	0.52	0.69	0.53			

Carbonate Mesobands

Sample Number	Carbonate Mesobands						Carbonates		Type
	Au	As	Sb	W	S	CO ₂	δ ¹³ C	δ ¹⁸ O	
85	1.6	0.27	0.052	0.654	4.01	15.7	-4.89	9.47	D
86	2.9	0.40	0.231	0.994	0.02	18.0	-4.19	10.24	D
88B	8.4	0.17	0.101	1.661	0.20	22.0	-4.84	10.68	S/D
89C	9.2	0.25	0.197	0.629	0.66	16.5	-4.67	9.96	D
90	2.8	0.18	0.142	0.933	0.22	27.2	-4.77	10.14	D
125-3	29.4	0.19	0.166	0.576	1.28	34.3	-3.90	11.40	D/S
128-4	80.4	0.61	0.102	0.438	3.02	33.5	0.72	11.42	D/S
129-2	9.6	0.22	0.115	0.175	0.29	22.0	-4.18	10.36	D/S
130-1	10.1	0.35	0.099	0.326	0.71	31.3	-4.18	10.59	D/S
130-2	660	0.96	0.072	0.496	1.36	25.3	-4.40	10.11	D
\bar{x}	81	0.36	0.128	0.688	0.78	24.78	-3.93	10.44	
σ	194	0.24	0.053	0.401	0.88	6.31	1.56	0.58	
\bar{x}'	13.18	0.30	0.12	0.32	0.30	23.99	-4.45	10.33	excluded
σ'	0.74	0.23	0.18	0.26	0.76	0.11	0.34	0.51	128-4, 89C value

KEY
 \bar{x} : Mean
 σ : Standard deviation } Arithmetic distribution
 \bar{x}' : Mean
 σ' : Standard deviation } Log transformed distribution

Carbonate types
 D: Dolomite
 S: Siderite

N/D: Not detected by XRD whole rock scan

ROCK ALTERATION

The volcanic rocks which host the Malga and Carshaw iron formations have been subjected to at least two distinct periods of hydrothermal alteration (Figure 2). The earliest alteration is characterized by the filling of vesicles by calcite, quartz and chlorite. Some of the vesicle-filling quartz is bladed and oriented perpendicularly to vesicle walls or more rarely, shows colliform banding. However, most of the vesicle-filling quartz consists of a polygonized to blocky grain array. Chlorite may be authigenic, or more likely, considering the regional greenschist metamorphic grade, is pseudomorphous after a zeolite or clay precursor. When two or more vesicle-filling phases are present, quartz always rims the outer edge, whereas calcite and chlorite occupy the core. About the perimeter of these vesicles, within the rock matrix, clinozoisite is concentrated and presumably is pseudomorphous after a pre-existing calcium-bearing clay phase. In some cases, the clinozoisite occurs within the vesicles. The matrix of the host basalt consists of chlorite, quartz and albite dendrites. Within this matrix, feldspar microlites, consisting of straight hollow needles, show overgrowths of curving skeletal feldspars (see also Dimroth and Lichtblau 1979, Figure 23). Similar textures have been described from basalts of the Tisdale Group, near Timmins (Fyon and Crocket 1981). The textural characteristics of these altered basalts are similar to those of Cenozoic and other Early Precambrian volcanic rocks (cf. Dimroth and Lichtblau 1979; Baragar *et al.* 1979) which have been subjected to low temperature, sea water alteration.

A second, later period of rock alteration is characterized by pervasive replacement of the volcanic rock and iron formation by carbonate, quartz and albite. The mineralogical zoning observed in these pervasive carbonate alteration zones is identical to that observed in the Timmins area (Fyon and Crocket 1981). The most intensely carbonatized zones consist of dolomite (ferroan), quartz, albite and traces of chlorite and sericite. Dolomite gives way to calcite in the less altered, more peripheral parts of the alteration zone (Figure 2). This pervasive carbonate alteration envelops parts of the sub-volcanic dikes and occurs as extensive zones cutting across the volcanic stratigraphy. It is superimposed upon the earlier seawater alteration assemblages described above.

That both the seawater-altered volcanic rocks and the pervasively carbonatized volcanic rocks bear the same tectonic fabric and that carbonate alteration zones envelop subvolcanic dikes indicates that the pervasive carbonate alteration took place very early in the development of the volcanic pile, prior to regional metamorphism, in a subvolcanic environment.

GOOSE LAKE IRON FORMATION

As a barren control area, that section of the Goose Lake iron formation (see Figure 1) just west of Goose Lake, located in north-central Shaw Township, was sampled, uti-

lizing the base map by Pyke *et al.* (1978; p.164). This iron formation lies within andesitic tuffs at the top of formation III (Deloro Group) and is overlain by komatiitic flows of formation IV (Tisdale Group). This section is part of a regionally continuous iron formation unit at the top of the Deloro Group and as such, contrasts with the limited strike length of the Malga and Carshaw iron formations which lie lower in volcanic stratigraphy (formation II).

Mild to moderate carbonate alteration of volcanic rocks is widespread in the Goose Lake area; however, no attempt was made to map this alteration during our sampling.

Since only eight oxide facies and one sulphide facies samples from the Goose Lake iron formation have been analysed, conclusions drawn at this time from geochemical comparison between the Goose Lake and Malga-Carshaw iron formations are speculative at best.

GEOCHEMISTRY OF THE MALGA AND CARSHAW IRON FORMATIONS

METHODOLOGY

Large blocks and hand samples were collected from the iron formation units. Each block was slabbed and from each slab, a number of mesobands were sampled indi-

Table 2—Replicate epithermal instrumental neutron activation analyses.

Sample Number	Reference	Au ppb	W ppm	As ppm	Sb ppm
12		3.7	0.1	0.3	0.06
12D		3.2	0.1	0.3	0.06
14		6.3	1.2	1.7	0.15
14D		5.4	1.8	1.6	0.19
17		6.6	0.2	0.6	0.31
17D		6.7	0.8	0.7	0.35
AGV-1		1.8	0.6	0.9	4.1
AGV-1		2.8	0.6	1.1	4.4
AGV-1	Abbey (1977)	—	—	—	4.3
AGV-1	Flanagan (1973, 1976)	0.44	0.55	0.8	4.17
W-1		3.9	0.5	2.1	0.92
W-1	Abbey (1977)	3.7	0.5	1.9	1.0
W-1	Flanagan (1973, 1976)	3.7	0.5	1.9	1.0
Pooled Statistics					
Variance (Sp ²)		4	0.05	0.01	0.01
Standard deviation (Sp)		2	0.22	0.09	0.11

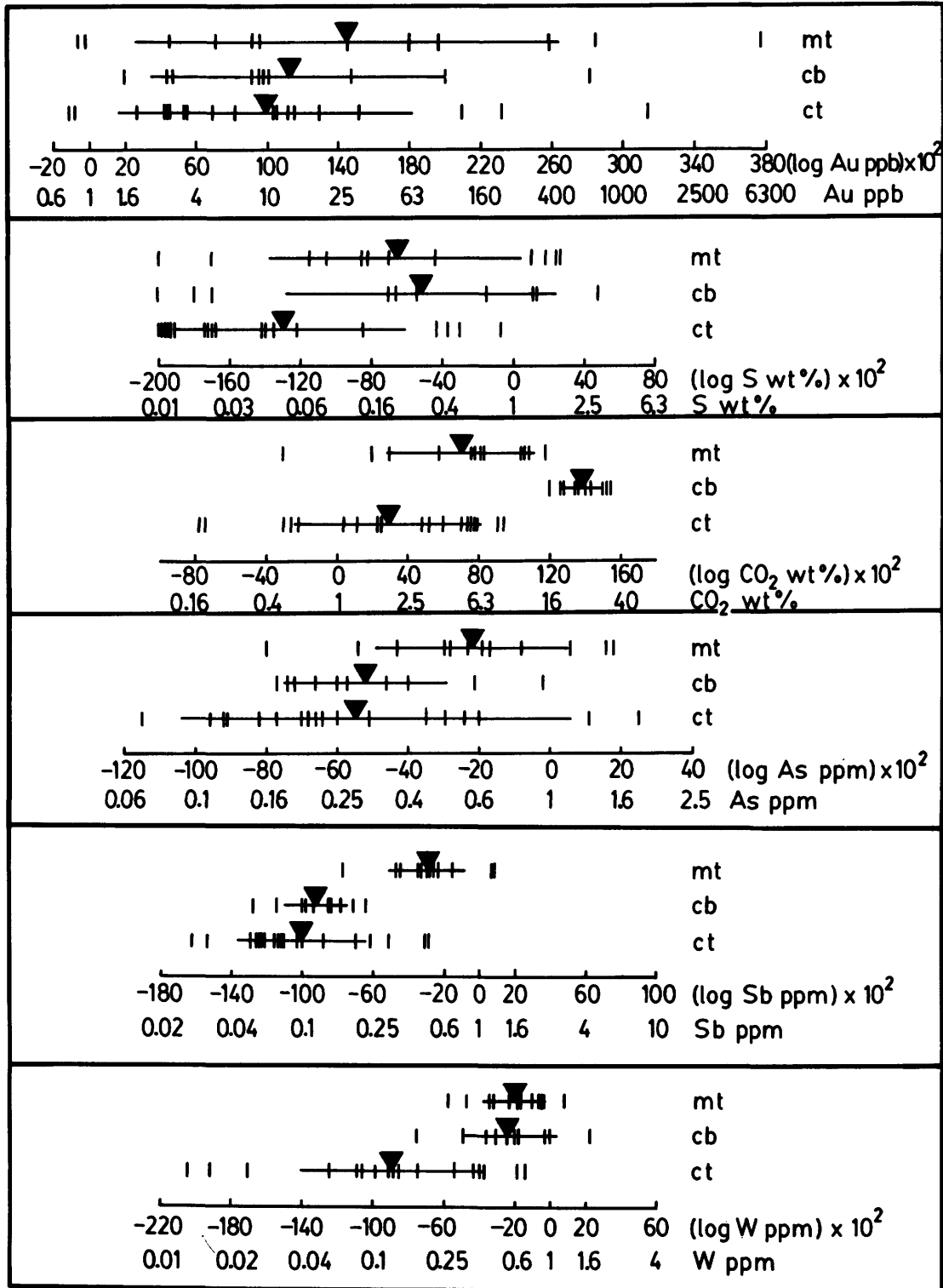


Figure 3—Geochemical data for the Malga and Carshaw iron formation mesoband analyses. Indicated are the mean (solid triangle), standard deviation (horizontal line) and sample values (vertical lines) for the log-transformed data populations. Analyses are arranged in magnetite (mt), carbonate (cb) and chert (ct) mesoband groups.

vidually. Approximately 1 g of mesoband sample was analysed by epithermal instrumental neutron activation for arsenic (As), antimony (Sb), tungsten (W) and gold (Au) and by Leco combustion for carbon dioxide (CO₂) and sulphur (S) (Table 1). No sample material from either the quartz veins or the adjacent pyrite envelopes has been analysed yet.

Prior to statistical treatment, the analytical data were grouped into three distinct mesoband types, based on the mineralogy of the mesoband sample. Chert mesobands consist of chert (20 to 100 modal percent), magnetite microbands (0 to 80 modal percent) and traces of carbonate. Magnetite mesobands consist of magnetite (80 to 100 modal percent) and traces of chert, carbonate and chlorite. The carbonate mesobands consist almost entirely of carbonate (>85 modal percent) with traces of chert and chlorite. Chlorite mesobands (>80 modal percent chlorite) also exist in the iron formation, but too few samples are available to constitute a statistically significant group.

These analyses, particularly for gold, are considered to be representative on a mesoband scale, but may not be representative on a larger, hand sample scale where dilution by inert components (chert) would tend to lower the trace element abundances. Although these analyses are appropriate to geochemically characterize the mesoband constituents, such a small sampling scale may not be suitable for gold exploration where larger samples are preferable. We are presently evaluating the geochemical departure between the mesoband analyses and analyses of larger sized hand samples.

ANALYTICAL ACCURACY AND PRECISION

Listed in Table 2 are the pooled variance and standard deviation estimates for the activation analyses based on replicate analyses of rocks and a standard, AGV-1. Data

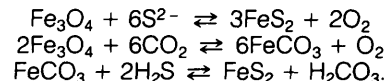
variance of W, As and Sb at low levels is good. Also there is good agreement between our standard determinations for AGV-1 and W-1 and those reported by Abbey (1977) and Flanagan (1973, 1976). The rather high variance for gold probably reflects sample heterogeneity at low gold concentrations in small (1 g) sample sizes.

MESOBAND ANALYSES FOR THE MALGA AND CARSHAW IRON FORMATIONS

Illustrated on Figure 3 are the log-transformed means, standard deviations and ranges of the mesoband data. To establish if significant geochemical differences exist between different mesobands types, a variance and mean equivalence test was applied (Table 3), assuming the log-transformed populations are approximately gaussian. Statistically significant intra-mesoband element correlations are summarized in Table 4.

Gold abundances in the chert, carbonate and magnetite mesobands are statistically equivalent (see Table 3), illustrating that gold is not preferentially enriched in any specific mesoband type (see Figure 3).

The higher abundances of sulphur in the magnetite and carbonate mesobands and CO₂ in the magnetite mesobands with respect to that of the chert mesobands might be attributed to the greater abundances of iron in the magnetite and carbonate mesobands available to fix S²⁻ as pyrite and CO₂ as iron-rich carbonates respectively:



To test this possibility, CO₂ and S abundances of the chert and magnetite mesobands were plotted against the modal proportion of magnetite microbands in each corresponding mesoband sample (Figure 4). It is apparent

Table 3—Inter-mesoband group variance and mean similarity tests for trace elements and isotope data.

Element	chert vs magnetite				chert vs carbonate				carbonate vs magnetite			
	variance		mean ¹		variance		mean ¹		variance		mean ¹	
	x ² calc	x ² (.05,1)	t calc	t (.1,29)	x ² calc	x ² (.05,1)	t calc	t (.1,27)	x ² calc	x ² (.05,1)	t calc	t (.1,20)
Au ²	1.35	3.84	-1.28	±1.70	0.03	3.84	-0.41	±1.70	1.82	3.84	-0.76	±1.73
S ²	0.04		-2.37		0.11		-2.69		0.03		0.43	
Sb ²	2.24		-6.00		3.38		-0.61		0.35		-6.96	
As ²	1.65		-2.80		2.44		-0.64		0.23		-2.58	
W ²	9.63		----		3.71		-3.61		1.24		-0.32	
CO ₂ ²	0.49		-2.16		14.55		----		14.25		----	
¹³ C	5.82		----		2.71		0.84		0.41		3.05	
¹⁸ O	10.78		----		7.22		----		0.14		-2.09	

¹, 2 tailed t-test
², Based on log-transformed distribution

Summary of inter-group similarity tests

Group Comparison	Similar Variances	Similar means	Statistically significant mean differences
Chert vs magnetite	Au, S, Sb, As, CO ₂	Au	¹³ C, ¹⁸ O, S, Sb, As, W, CO ₂
Chert vs carbonate	Au, S, Sb, ¹³ C, As, W	Au, Sb, As, ¹³ C	S, W, CO ₂ , ¹⁸ O
Carbonate vs magnetite	Au, ¹³ C, ¹⁸ O, S, Sb, As, W	Au, S, W	Sb, As, ¹³ C, ¹⁸ O, CO ₂

Table 4—Summary of statistically significant, intra-mesoband geochemical correlations for the Malga and Carshaw samples.

Mesoband	Elements	n	α	r
Chert	Au-CO ₂	18	.05	.48
	S-CO ₂	19	.025	.47
	W-CO ₂	18	.025	.47
	S-Au	17	.01	.79
	Sb-W	19	.01	.65
	Sb-As	19	.01	.54
Carbonate	Au-S	10	.01	.77
	Au-CO ₂	10	.05	.52
	S-CO ₂	10	.01	.80
	Au-As	10	.01	.71
Magnetite	Au-CO ₂	12	.05	.55
	S-CO ₂	11	.05	.56
	Au-S	12	.01	.73
	Au-As	11	.025	.59

n: number of samples
 α : level of significance
 r: correlation coefficient

that both CO₂ and S abundances in these mesobands are independent of magnetite abundance.

Because no arsenopyrite is present, arsenic is probably hosted in pyrite. However, arsenic abundance does not exactly follow that of sulphur (Figure 3). For example, the carbonate mesobands are enriched in sulphur with respect to chert mesobands, but both have equivalent arsenic concentrations. Furthermore, in no mesoband-type is there statistically significant correlation between sulphur and arsenic (see Table 4). Arsenic correlates with gold only in the carbonate and magnetite mesobands.

Antimony is enriched in the magnetite mesobands relative to the carbonate and chert mesobands, whereas tungsten is enriched in both magnetite and carbonate mesobands relative to the chert mesobands. Neither antimony nor tungsten abundances correlate with gold (see Table 4).

The following, statistically significant element correlations are common to the three mesoband types: Au-CO₂, Au-S, S-CO₂ (see Table 4). The Au-S correlation arises because gold is hosted in either pyrite or pyrrhotite. The Au-CO₂ and S-CO₂ are not as easily explained. Texturally, it appears as though the carbonate mineralogy formed prior to the gold-quartz veins. However, if a small amount of carbonate introduction accompanied the formation of gold-quartz veins, and if this carbonate were indistinguishable from the pre-existing carbonate mineralogy, a correlation could arise between Au and S, Au

and CO₂ and CO₂ and S. A second possibility could arise if gold was transported in solution by some type of sulphur complex. Interaction of iron-bearing carbonates with this hydrothermal fluid might break down the gold-sulphur complexes, and induce the precipitation of pyrite, which would scavenge gold from the solutions:



Such interaction between a sulphide-rich hydrothermal fluid and a carbonate mineral substrate could give rise to the observed, common, Au-S-CO₂ correlations. However, as noted previously (Table 3), all mesobands types have equivalent gold abundances, even though they have different CO₂ abundances.

A third possibility is that gold, sulphur and carbon dioxide were all consanguineously enriched in the iron formation at the time of carbonate mineral formation. Subsequently, gold and sulphur (and possibly silica) were locally remobilized within the iron formation during the post-carbonatization, quartz-fracture-filling event, giving

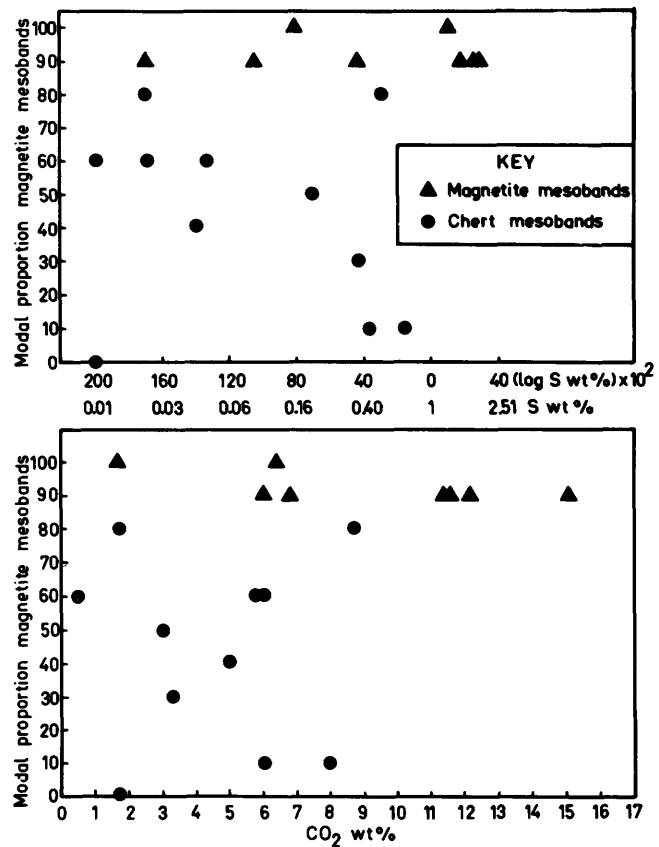


Figure 4—Covariance between sulphur (S) and carbon dioxide (CO₂) abundances and estimated modal proportion of magnetite microbands in corresponding mesoband samples from the Malga and Carshaw iron formations.

rise to the pyrite selvages adjacent to the quartz veins. That is, the iron formation acted as a closed system with respect to gold and sulphur (and possibly silica). In this case, the observed Au-S-CO₂ correlations would be artifacts of an earlier, pre-quartz-veining hydrothermal event.

Yet another possibility exists which cannot be evaluated at this stage. Perhaps the two types of gold mineralization, described previously, (gold in pyrite adjacent to quartz veins vs. gold in pyrite and pyrrhotite which are disseminated throughout the iron formation and are not spatially associated with quartz veins) are genetically unrelated. The disseminated, auriferous, pyrite-pyrrhotite mineralization could represent an early hydrothermal event whereas the later gold-quartz veining represents exotic material introduced locally into the iron formation.

Material from the gold-quartz veins and the associated pyritic selvage has not yet been analysed and hence we do not know if the two types of mineralization are geochemically distinct.

GEOCHEMICAL COMPARISON OF AURIFEROUS AND NON-AURIFEROUS IRON FORMATIONS

Because only nine samples have been analysed from the non-auriferous Goose Lake iron formation, only very general comparisons can be made with the auriferous Malga and Carshaw iron formations.

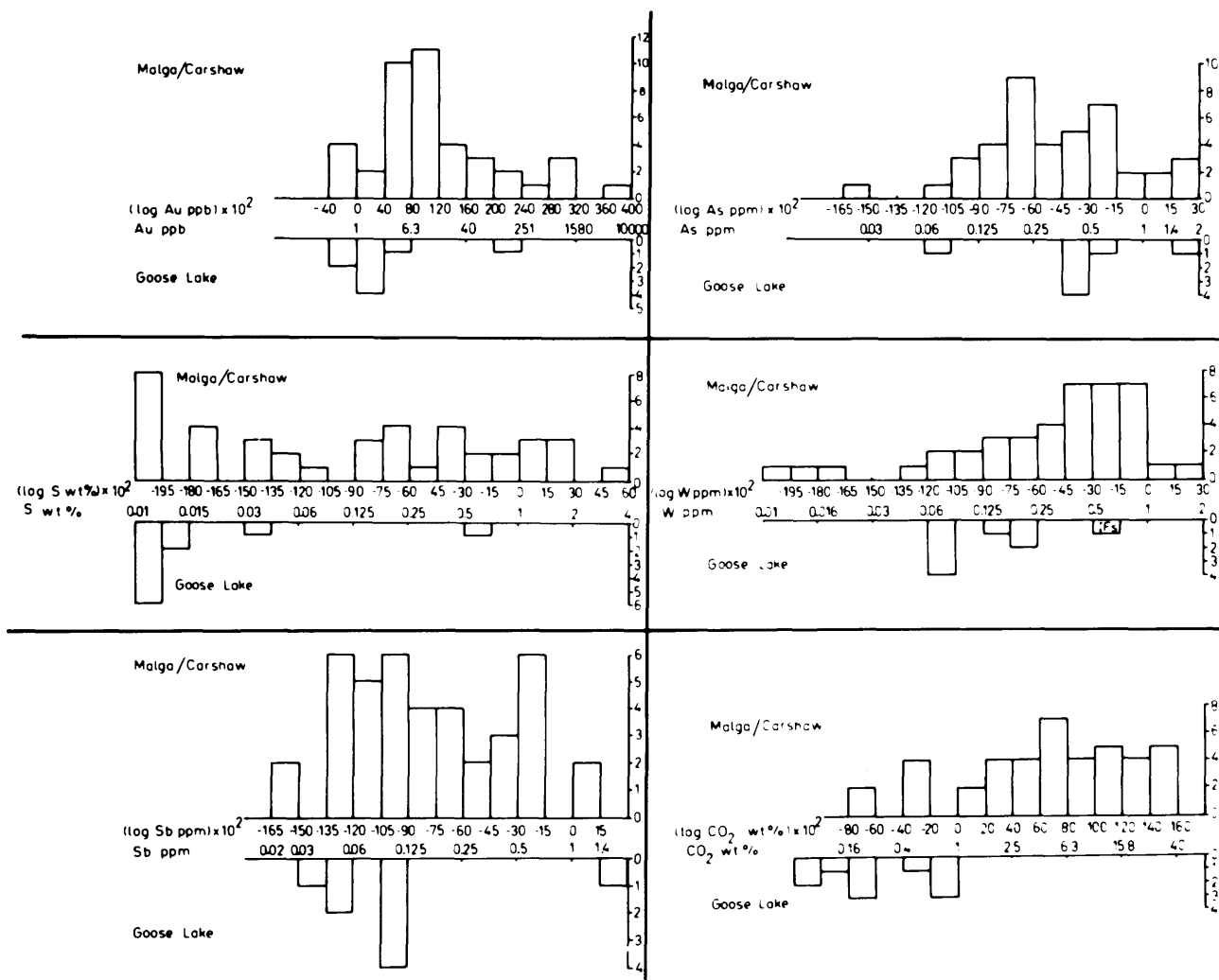


Figure 5—Comparison between arsenic (As), antimony (Sb), gold (Au), tungsten (W), sulphur (S) and carbon dioxide (CO₂) abundances of the non-auriferous Goose Lake and the auriferous Malga and Carshaw iron formations.

GOLD

The mean gold abundance of the auriferous iron formations exceeds that of the Goose Lake samples. In addition, a much greater range of data characterizes the auriferous iron formations (Figure 5).

SULPHUR

Like gold, a larger range of sulphur data and a higher mean characterizes the auriferous iron formations (Figure 5).

ARSENIC

The arsenic abundances of the auriferous and barren iron formations appear similar with respect to mean and possible range (Figure 5).

TUNGSTEN

A higher mean and greater data range characterize the auriferous iron formations (Figure 5).

ANTIMONY

Antimony distributions are similar to those of gold, sulphur and tungsten. The auriferous iron formations have a

larger mean and greater range with respect to the Goose Lake samples (Figure 5).

CARBON DIOXIDE

The Goose Lake iron formation has lower CO₂ abundances and a smaller range of data with respect to the Malga and Carshaw data (Figure 5).

SUMMARY

Tentatively, gold, sulphur, carbon dioxide, tungsten and antimony discriminate between gold-bearing Malga and Carshaw iron formations and the barren Goose Lake iron formation section. It should be emphasized that these iron formations are dominantly chert and magnetite. Additional tests would be required to establish effective screens for sulphide iron formations. Furthermore, additional samples from unmineralized iron formations must be collected to establish a significant data base.

STABLE ISOTOPE STUDIES

Oxygen and carbon isotope studies of quartz and carbonate minerals have been applied to provide further insight into the depositional and diagenetic history of the iron formations and the hydrothermal history of the gold mineralization and the altered volcanic rocks.

Measurements of isotope variations are reported in parts per thousand (‰) difference with respect to a standard. The standard used for oxygen is Standard Mean Ocean Water (SMOW) whereas the standard for carbon is the carbonate "PDB" (Craig 1957, 1961). Thus,

$$\delta^{18}\text{O} = \frac{(^{18}\text{O}/^{16}\text{O})_{\text{sample}} - (^{18}\text{O}/^{16}\text{O})_{\text{SMOW}}}{(^{18}\text{O}/^{16}\text{O})_{\text{SMOW}}} \times 1000$$

$$\delta^{13}\text{C} = \frac{(^{13}\text{C}/^{12}\text{C})_{\text{sample}} - (^{13}\text{C}/^{12}\text{C})_{\text{PDB}}}{(^{13}\text{C}/^{12}\text{C})_{\text{PDB}}} \times 1000$$

Carbon and oxygen isotope data on carbonates were obtained from CO₂ liberated by reaction with 100 percent phosphoric acid (McCrea 1950). The fractionation factors used for the phosphoric acid reaction were 1.01025 for calcite and 1.01110 for dolomite (Sharma and Clayton 1965). Oxygen from quartz was obtained by reaction with BrF₅ and converted to CO₂ (Clayton and Mayeda 1963). All CO₂ gases were analysed on a Nier-type mass spectrometer.

ACCURACY AND PRECISION

CARBONATES

Analytical accuracy and precision were estimated using replicate analyses of samples and standards. For carbonate minerals, an in-house standard, GCS (Grenville marble), was used as a reference gas and was run as an unknown sample. The carbon and oxygen isotope compositions were then corrected to PDB using the intermediary standard NBS-20. From the replicate data (Table 5) it is apparent that an experimental bias of -0.11‰ δ¹³C and -0.14‰ δ¹⁸O exists. The standard deviation

Table 5—Accuracy and precision of isotope analyses.

Carbonate Minerals						
Sample Material	δ ¹³ C (GCS)			δ ¹⁸ O (GCS)		
	\bar{X}	Sp ²	Sp	\bar{X}	Sp ²	Sp
GCS n=8	-0.11	0.01	0.08	-0.14	0.01	0.10
Whole rock samples n=37	—	0.023	0.15	—	0.063	0.25
Quartz						
Sample Material	δ ¹⁸ O (SMOW)			Literature values for NBS-28		
	\bar{X}	Sp ²	Sp			
NBS-28 Quartz	9.32	0.03	0.17	9.0 ^a , 9.5 ^b , 10.0 ^c , 9.17 ^d		
Samples	—	0.19	0.44			

a: Lipman and Friedman (1975)
 b: Matsuhisa (1974)
 c: Friedman and Gleason (1973)
 d: Longstaffe (1977)

of the carbon and oxygen determinations for GCS are 0.08 and 0.10 respectively. A pooled standard deviation estimate using 37 replicate analyses of whole rock samples for carbon ($\pm 0.15\%$) and oxygen ($\pm 0.25\%$) is slightly worse than for the GCS replicates (Table 5).

QUARTZ

Replicate analyses of NBS-28 yield a $\delta^{18}\text{O}$ mean of 9.32‰ (SMOW) and a pooled standard deviation of 0.17‰. This mean agrees well with reported literature values (Table 5). Replicate analyses of quartz samples give a slightly worse pooled standard deviation of 0.44‰.

ISOTOPIC RE-EQUILIBRATION

Because the carbonate replacement of the volcanic rocks and the iron formation took place very early in the history of the volcanic pile, interpretation of the stable isotope data rests on the premise that the isotope systematics were not disrupted by post-carbonatization regional metamorphic events. For example, oxygen isotope homogenization of certain minerals in metamorphosed rocks has been documented by Taylor *et al.* (1963): quartz, albite, white mica, kyanite, chlorite, biotite, ilmenite in peli-

tic schists over a 200 m scale; Anderson (1967): quartz in metasediments and iron formation on a metre scale; Taylor and Coleman (1968): quartz, glaucophane, muscovite, lawsonite and garnet in metasediments and metavolcanics and $\delta^{18}\text{O}$ lowering in cherts and limestone over a 25 m scale; and Perry *et al.* (1973): chert, magnetite and carbonate in iron formation over a 200 m scale. Carbon isotope systematics appear to be relatively stable at low metamorphic grades, although some diagenetic changes have been described (Perry *et al.* 1973; Perry and Tan 1972; Becker and Clayton 1972).

Four isotope homogenization phenomena are possible for layered or heterogeneous rock sequences (Figure 6).

1) No interaction has occurred and no exchange between layers is observed.

2) Partial exchange has occurred; the central part of a layer retains a primary isotope signature, but the margins have ratios resulting from exchange with adjacent rock.

3) Pervasive isotope exchange has occurred, but the process was incomplete so that an isotope gradient exists between the centre and margins of a layer.

4) Complete isotope exchange has occurred; the layer is

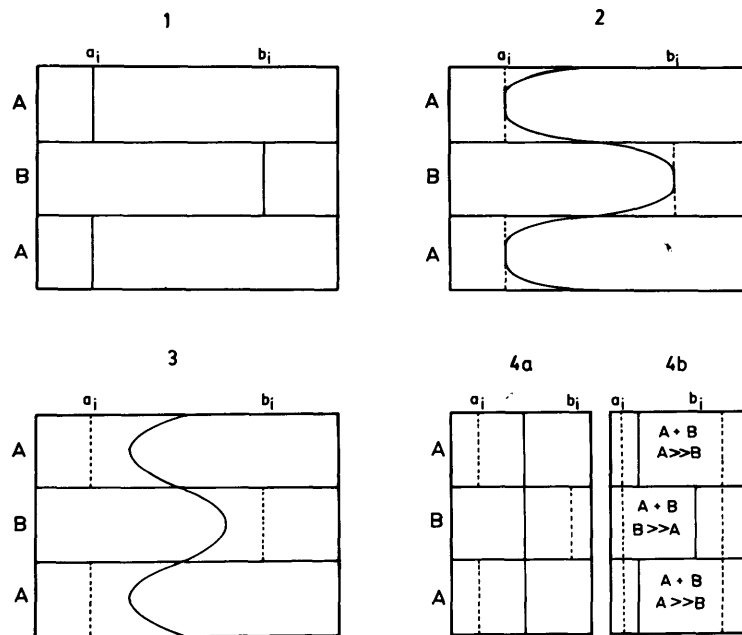


Figure 6—Four possible isotope equilibration phenomena in layered sequences. Layers A and B are monomineralic having initial isotopic compositions a_i and b_i respectively. Type 1: no isotope homogenization across boundary layers. Type 2: partial isotope exchange across boundary layers; margins have been altered, but cores of layers retain their initial isotope composition. Type 3: partial isotope exchange across boundary layers; margins and cores of layers have been altered such that no record of initial isotope composition is retained. Type 4a: complete isotope exchange throughout layered sequence, with no retention of initial isotope composition. Type 4b: partial, intraband isotope exchange between two phases, A and B, of differing initial isotope composition, a_i and b_i . The degree of intraband isotope exchange depends on the relative proportions of the two phases (A and B) present. Interband exchange is assumed to be negligible.

isotopically homogeneous and retains no record of its original isotope signature.

Several approaches have been adopted to test the stability of the isotope systematics and to identify the scales over which isotopes were homogenized. By sampling mesobands from individual, slabbed hand samples, it is possible to test for isotopic equilibrium on a centimetre scale. From samples collected across carbonate alteration zones developed adjacent to dikes, it is possible to test for isotopic equilibrium over a scale of several metres. Finally, by comparison of property-wide samples it is possible to test for isotopic equilibrium or homogenization over a scale of hundreds of metres.

MESOBAND SAMPLES

Between two and four adjacent mesobands were sampled from each hand sample, and each mesoband analysis is represented by one point on Figure 7. Because the minimum sample size needed was about 5 grams, detailed sampling from mesoband margin to core was impossible. Consequently, homogenization phenomena 2) and 3) above cannot be recognized. The mesobands range in thickness from 0.5 to 3 cm, but average 1 cm in thickness. The vertical stacking of the hand sample groups in Figure 7 (e.g. 121, 127, 125, 128, 130) is merely for representational purposes. No stratigraphic conti-

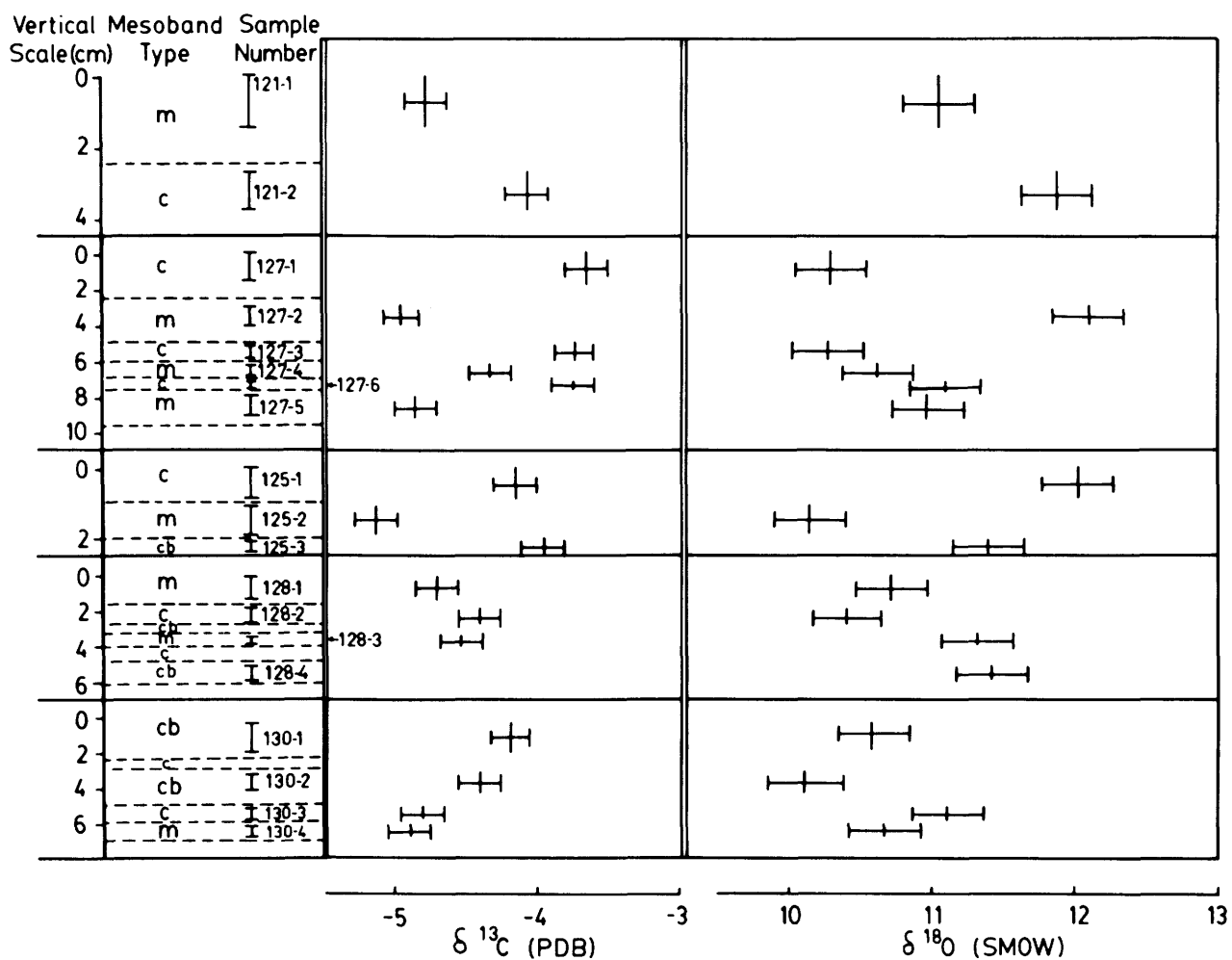


Figure 7—Carbon and oxygen isotope compositions of carbonates hosted in magnetite (m), chert (c) and carbonate (cb) mesobands from separate hand samples (121, 127, 125, 128, 130). No stratigraphic continuity exists between hand samples. All samples come from the Malga and Carshaw iron formations.

num exists between sample groups. In fact, because of the complex soft sediment folding, vertical stratigraphic sequences can be defined only on a scale of a metre or less. Lateral stratigraphic equivalence of discrete mesobands is recognizable over a similar horizontal scale.

CARBON ISOTOPES

A carbon isotope spread of about 2‰ exists between adjacent mesobands of a given hand sample (see Figure 7, sample 127). This variation is attributed to a correlation between $\delta^{13}\text{C}$ of the accessory carbonates and the estimated modal proportion of magnetite microbands in the chert and magnetite mesobands (Figure 8). Carbonates from the magnetite-rich bands have lighter $\delta^{13}\text{C}$ values with respect to those from chert mesobands.

That each mesoband type has a statistically different $\delta^{13}\text{C}$ mean (see Table 3, cf. Figure 11) suggests that carbon isotope homogenization across mesoband boundaries did not take place. However, types 2) and 3) homogenization cannot be recognized in this study nor could isotopic disruption during which the $\delta^{13}\text{C}$ of each carbonate mineral was changed by the same amount. This type of isotopic disruption would preserve the initial isotope trends, but would destroy the initial isotope compositions of the carbonates. In this regard, it is perhaps significant that the $\delta^{13}\text{C}$ of a thin (<1 m) marble exposed in the Timmins area at the base of the Tisdale Group has retained its marine isotopic signature of about 0‰ (Fyon *et al.* 1980), suggesting that the carbon isotope systematics are relatively stable through regional greenschist metamorphism.

OXYGEN ISOTOPES IN CARBONATES

Like $\delta^{13}\text{C}$, the $\delta^{18}\text{O}$ of the carbonates hosted by iron formation shows considerable variation (2‰) between adjacent mesobands (see Figure 7). However, no correlation exists between $\delta^{18}\text{O}$ of the carbonates and the modal proportion of magnetite microbanding (see Figure 8), nor does any consistent sense of $\delta^{18}\text{O}$ enrichment in the carbonates exist, except perhaps for the carbonate mesobands. For example, in sample 127 (see Figure 7) carbonates of some chert mesobands are depleted in ^{18}O relative to adjacent, accessory carbonates in magnetite mesobands, whereas in other adjacent mesobands the opposite sense of ^{18}O enrichment is observed. Furthermore, the $\delta^{18}\text{O}$ means of carbonates from the magnetite ($11.01 \pm 0.57\text{‰}$) and chert ($11.84 \pm 1.75\text{‰}$) mesobands are identical if three anomalously heavy ($\delta^{18}\text{O} > 13.5\text{‰}$) carbonate analyses are eliminated from the chert population ($\delta^{18}\text{O}$ grand mean = $11.84 \pm 1.75\text{‰}$ vs. condensed $\delta^{18}\text{O}$ mean chert population = $11.19 \pm 0.81\text{‰}$). These $\delta^{18}\text{O}$ means are slightly heavier (0.7‰) than the mean $\delta^{18}\text{O}$ composition of the carbonate mesobands ($10.33 \pm 0.50\text{‰}$).

The slight difference between $\delta^{18}\text{O}$ of carbonates from the magnetite and chert mesobands and those of the carbonate mesobands and the volcanic rock replacement carbonates might reflect compositional differences between the carbonates. All carbonate oxygen data was

corrected using a kinetic isotopic fractionation factor of 1.0110 for dolomite (Sharma and Clayton 1965), however no correction was made for admixture of siderite. Hence sideritic samples could be heavier by up to 0.75‰ with respect to the siderite-free dolomitic data. However, although the sample population is small, there is no systematic change to heavier $\delta^{18}\text{O}$ values in sideritic samples (Figure 9), except perhaps for the magnetite-associated carbonates. Appeal to local, closed system oxygen isotope exchange between the accessory carbonates and the coexisting chert is also unsatisfactory, for no correlation exists between chert abundance and $\delta^{18}\text{O}$ of the carbonate (see Figure 8; reverse of magnetite proportion scale).

Hence, although there are slight differences between mean $\delta^{18}\text{O}$ compositions of accessory carbonates in the mesoband groups, their overall similarity suggests two possibilities:

1) all carbonates were precipitated at the same temperature, from a fluid having a uniform $\delta^{18}\text{O}$ composition; or

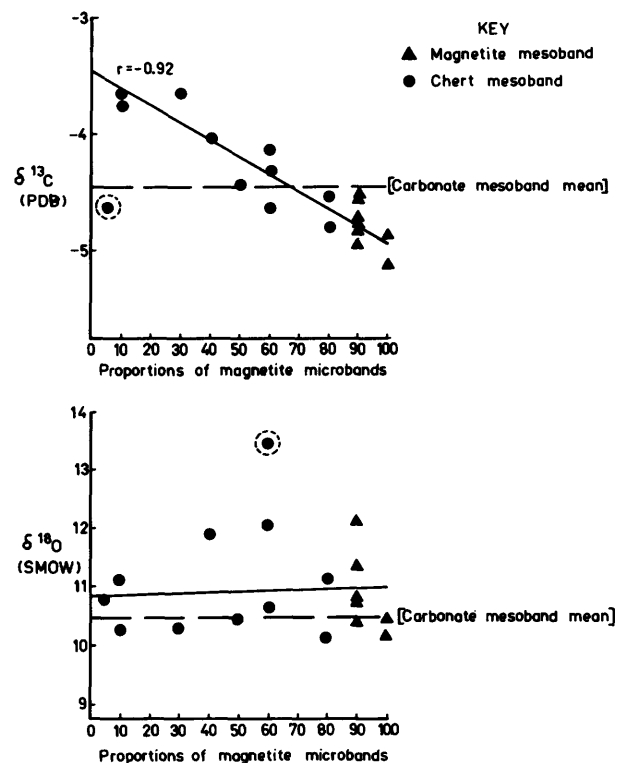
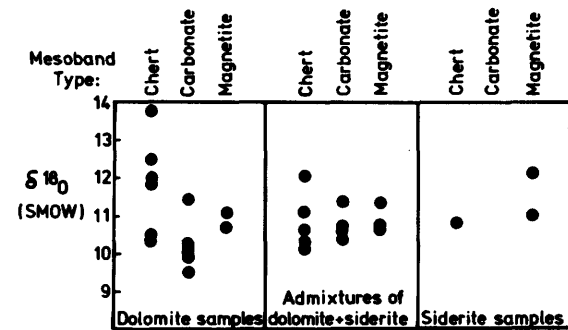


Figure 8—Correlations between carbon and oxygen isotope compositions of accessory carbonates hosted in magnetite and chert mesobands and modal proportion of magnetite microbands in corresponding mesobands. Mean isotopic compositions of carbonate mesoband data are illustrated for comparison. Circled samples have not been included in the regression and correlation calculations. All data from the Malga and Carshaw iron formations.

2) partial (in magnetite and chert mesobands) to complete (carbonate mesobands) oxygen isotope homogenization of carbonates took place during a post-carbonatization event over a scale larger than the mesoband and iron formation widths. Conversely, the carbon isotopes have not been homogenized across mesoband boundaries or throughout the iron formation.

DIKE PROFILES

Carbonate alteration zones envelop parts of felsic dikes which cut the volcanic rocks. Profiles of carbon and oxygen isotopes from the replacement carbonates and CO₂ abundances across three felsic dikes are presented in Figure 10. Initial sample locations with respect to the dikes differed so the relative sample positions have been plotted according to rock alteration assemblage type. Original distances between the dike edge and the sample, and a brief description of the alteration assemblage are given in Table 6.



Mesoband Type	Type of Carbonate		
	Dolomite	Dolomite and Siderite	Siderite
Chert	n = 6 X̄ = 11.78 σ = 1.28	n = 5 X̄ = 10.82 σ = 0.77	n = 1 X̄ = 10.79
Carbonate	n = 6 X̄ = 10.22 σ = 0.65	n = 4 X̄ = 10.76 σ = 0.45	n = 0
Magnetite	n = 2 X̄ = 10.87 σ = 0.26	n = 3 X̄ = 10.89 σ = 0.38	n = 2 X̄ = 11.54 σ = 0.80

n: Number of samples
 X̄: Sample mean
 σ: Standard deviation

Figure 9—Correspondence between oxygen isotope compositions of accessory carbonates and the carbonate mineralogy of mesoband samples from the Malga and Carshaw iron formations.

A symmetrical trend of decreasing δ¹³C toward the felsic dike exists (Figure 10). This trend could arise by precipitation of the replacement carbonates at increasingly higher temperatures towards the porphyry dike, consistent with present models of hydrothermal convective cooling of igneous bodies (cf. Taylor 1974; Parmentier and Schedl 1981) and the present symmetrical arrangement of alteration zones observed in the field. Note however that the δ¹⁸O compositions of the carbonates show a flat trend. This trend could arise if:

- 1) the carbonate was precipitated from a fluid having a uniform δ¹⁸O at a fixed temperature, contrary to the temperature relations deduced from the carbon isotope trends;
- 2) the carbonate was precipitated at higher temperatures towards the dike from a fluid whose δ¹⁸O composition was increasing;
- 3) the carbonate was precipitated at increasing temperatures towards the dike from a fluid whose δ¹⁸O composition was approximately uniform; during subsequent thermal events, the carbonate exchanged with an oxygen-

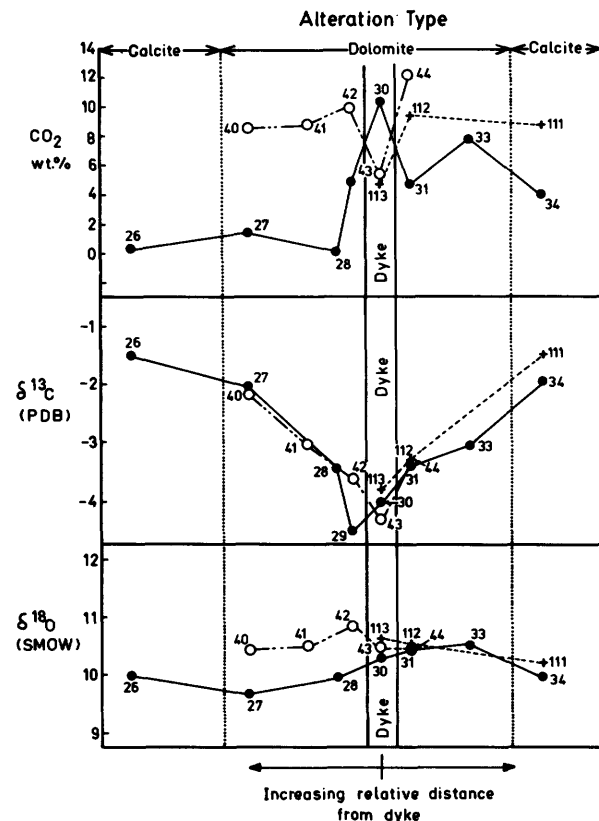


Figure 10—Carbon and oxygen isotope compositions of replacement carbonates collected from carbonate alteration zones developed about felsic dikes. All data from the Malga and Carshaw properties. See Table 6 for sample details.

Table 6—Description of the felsic dike and altered volcanic rock profile samples.

Dike Number	Dike Thickness	Sample number and distance from dike edge (00) in meters			
1	1 m	29 ^a (0.5)	28 ^a (2)	27 ^c (30)	26 ^c (50)
2	15 m	42 ^a (0.3)	44 ^a (0.5)	41 ^a (15)	40 ^b (30)
3	30 m	112 ^a (0.5)	111 ^c (15)		

Alteration assemblages:

- a. Dolomite, quartz, albite, trace sericite and chlorite
 - b. Calcite, quartz, albite, trace chlorite
 - c. Vesicle filling by quartz, calcite and chlorite
- Pervasive carbonate alteration zone

bearing fluid such that the initial $\delta^{18}\text{O}$ variations of the replacement carbonates were destroyed. The question is resolved by comparing the isotopic data of all carbonates, regardless of host rock.

REPLACEMENT CARBONATES IN VOLCANIC ROCK

OXYGEN ISOTOPES. Figure 11 illustrates that the mean $\delta^{18}\text{O}$ of the carbonate mesobands ($10.33 \pm 0.50\text{‰}$) is indistinguishable from those of the replacement carbonates in the felsic dikes ($10.27 \pm 0.40\text{‰}$) and in the volcanic rocks ($10.49 \pm 0.57\text{‰}$). The $\delta^{18}\text{O}$ compositions of these carbonates differ by only 0.5‰ from those of the magnetite ($11.01 \pm 0.57\text{‰}$) and restricted population of chert mesoband ($11.19 \pm 0.81\text{‰}$) carbonates. This strongly suggests that there was widespread oxygen exchange between all replacement carbonates and a common, oxygen-bearing pore fluid.

CARBON ISOTOPES. The $\delta^{13}\text{C}$ grand mean of the carbonatized volcanic rocks ($-2.84 \pm 0.92\text{‰}$) is heavier than that for the iron formation samples ($-4.48 \pm 0.57\text{‰}$). This is attributed to the much higher magnetite content (or that factor related to magnetite formation) in the iron formation (see Figure 8) with respect to the altered volcanic rocks.

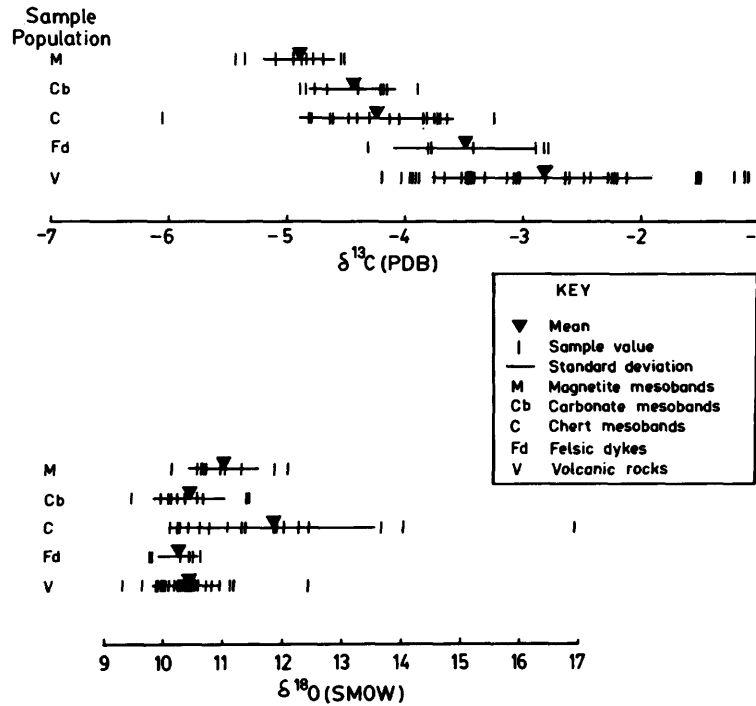
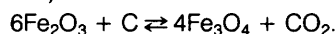


Figure 11—Carbon and oxygen isotope compositions of replacement carbonates from the Malga and Carshaw study areas.

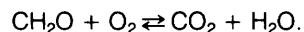
The rather large range of the carbon isotopic data (-1.0 to -4.3%) arises because the total population includes calcites from low-temperature-seawater-altered basalts as well as dolomites and calcites from the pervasive carbonate alteration zones. For example, calcites occupying vesicles from the seawater-altered basalts and those from the fringe zones of the pervasive carbonate alteration zones have the heaviest $\delta^{13}\text{C}$ values (-1.0 to -2.2%). The $\delta^{13}\text{C}$ of the replacement dolomites, all lighter than these calcites, vary depending on a sample's location within an alteration zone. For carbonate alteration zones enveloping dikes, the heaviest $\delta^{13}\text{C}$ values of dolomite occur adjacent to the dikes (see Figure 10). A similar trend from heavy to light $\delta^{13}\text{C}$ composition of dolomites is developed in the pervasive carbonate alteration zones in the Timmins area which are not related to dikes (Fyon *et al.* 1980, Figure 3). Such trends are consistent with dolomite precipitation at higher temperatures in the core of the alteration zone relative to the precipitation temperatures at the outer edge of the alteration zone.

INTERPRETATION OF THE CARBONATE ISOTOPE GEOCHEMISTRY

Carbon isotope trends are recognizable at small scales (centimetres) in the iron formation and on larger scales (metres) in the altered volcanic rocks. The small-scale trends appear to arise from compositional differences in the iron formation at the site of carbonate deposition. For example, a correlation exists between $\delta^{13}\text{C}$ composition of the iron formation carbonates and the modal proportion of magnetite. A similar correlation has been recognized in Middle and Early Precambrian iron formations (Perry *et al.* 1973; Perry and Tan 1972) where it is attributed to diagenetic reactions that produced magnetite (Perry *et al.* 1973):



Alternatively the correlation might arise simply by oxidation of organic material which was initially concentrated in iron-oxide layers:



In either case, the CO_2 produced would be isotopically light ($\delta^{13}\text{C} = -25\%$), and carbonates formed from this CO_2 would acquire very light $\delta^{13}\text{C}$ compositions. The limited spread of $\delta^{13}\text{C}$ compositions and the absence of extremely light carbonates in the iron formations suggests either a small amount of organic carbon was present in the iron formation when carbonatization began or the carbonates formed from a fluid rich in relatively heavy carbon ($\delta^{13}\text{C} = -4$ to -1) such that the organically derived CO_2 was much less significant in total carbon budget of the hydrothermal system.

Outside the iron formation environment in the volcanic rocks the $\delta^{13}\text{C}$ composition of the replacement carbonates appears to have been controlled largely by temperature effects. Calcites present within vesicles of basalts which petrographically appear to have undergone a low-temperature-seawater diagenesis, have $\delta^{13}\text{C}$ compositions of -1 to -2% , consistent with seawater

carbonate fixation at relatively low temperature (100 to 200°C). Replacement dolomites from the pervasive carbonate alteration zones can be up to 3% lighter ($\delta^{13}\text{C} = -4.4\%$) than the vesicle-filling calcites. Although this trend is consistent with higher temperature alteration, this temperature cannot be accurately constrained unless the $\delta^{13}\text{C}$ composition of the hydrothermal fluid is known.

The uniformity of the $\delta^{18}\text{O}$ compositions of the replacement carbonates, regardless of host-rock type or type of carbonate alteration, suggest that widespread, post-carbonatization oxygen exchange took place between the replacement carbonates and a ubiquitous, oxygen-bearing pore fluid. That is, the $\delta^{18}\text{O}$ composition of the replacement carbonates reflects the last, major thermal event, presumably regional metamorphism, and no record of the carbonate precipitation temperatures is retained.

^{18}O RELATIONS OF QUARTZ

Quartz from four different environments has been analysed: chert fragments present in flow top breccias; chert fragments present in a matrix-supported, chert fragment debris flow; cherty or chalcedonic material filling vesicles; and hydrothermal quartz veins which cut the iron formations and volcanic rocks (Table 7). Texturally all cherty samples, except for a very few chalcedonic vesicle fillings, consist of a polygonized array of strain-free quartz crystals which range in grain diameter from 0.1 to 2 mm. This texture and grain size of quartz strongly suggests that the chert clasts and vesicle fillings have been recrystallized. The chert clasts ranged from 1 to 10 cm in width. No chert from the iron formations has been analysed isotopically; however, all samples examined show a similar granular, polygonized texture, although grain size rarely exceeds 0.1 mm. The quartz veins cut all units which host the chert clasts and the cherty vesicle-filling material and hence, the quartz vein formation post-dates that of the chert formation.

The $\delta^{18}\text{O}$ of the quartz vein material ($10.86 \pm 0.43\%$) is somewhat lighter with respect to $\delta^{18}\text{O}$ composition of the cherty samples ($\delta^{18}\text{O} = 11.31 \pm 0.27\%$). However, the difference between these means is not statistically significant ($t_{\text{calculated}}(0.10, 10) = -2.78$; $t_{\text{critical}}(0.05, 19) = \pm 1.78$) indicating that the vein quartz and the cherty samples have equivalent $\delta^{18}\text{O}$ compositions. However, the field evidence clearly illustrates that the quartz veins are younger than the cherty materials, and the petrographic evidence suggests that the cherts have undergone wholesale recrystallization. Furthermore, the $\delta^{18}\text{O}$ composition of the most pristine Early Precambrian cherts generally exceeds $+20.0\%$ (Perry *et al.* 1973; Knauth and Lowe 1978). This is much heavier than the $\delta^{18}\text{O}$ compositions of the cherty material from the Malgashaw study areas. Lowering of the $\delta^{18}\text{O}$ composition of cherts is a common phenomenon (Perry *et al.* 1973; Knauth and Lowe 1978; Taylor and Coleman 1968) and is related to post-depositional oxygen isotope exchange between the chert and either ground waters or meta-

Table 7— ^{18}O analyses of quartz from the Malga and Carshaw study areas.

Sample Number	Description	^{18}O (SMOW)
Late quartz veins		
105	Quartz veins cutting felsic dikes	10.45
107		11.48
118		10.12
55	Quartz veins cutting basalts	11.13
58		11.13(2)
59		11.01
60		11.34
49	Quartz veins cutting ultramafic dikes	10.21
99		10.73(2)
79	Quartz veins cutting iron formation	10.89
91		10.71
92		11.07
	mean	10.86
	standard deviation	0.43
Syngenetic and vesicle-filling chert		
94	Chert clasts in debris flow	11.53
95		11.07(2)
96		10.79
64	Chert fragments in basalt flow top	11.44
65		11.49(3)
66		11.19(2)
67		11.55
77	Chalcedonic, quartz vesicle fillings	11.17
78		11.53(2)
	mean	11.31
	standard deviation	0.27
	Grand mean	11.05
	standard deviation	0.43

(): Number of replicates

morphic pore fluids. Hence it is concluded that property-wide oxygen isotope exchange took place between cherty material and the oxygen-bearing fluid from which the vein quartz was precipitated.

The quartz-water and dolomite-water oxygen isotope fractionation factors are quite similar (Clayton *et al.* 1972; Northrop and Clayton 1966), and hence cogenetic quartz and dolomite would have similar $\delta^{18}\text{O}$ compositions. However, as indicated previously, the quartz veins cut and therefore are younger than all units which host the replacement carbonates. Hence, the similarity between the oxygen isotope compositions of the late vein quartz ($\delta^{18}\text{O} = 10.86 \pm 0.43\text{‰}$) and the earlier replacement carbonates ($\delta^{18}\text{O}_{\text{grand mean}} = 10.91 \pm 0.75\text{‰}$) strongly suggests that the replacement carbonates exchanged oxygen with the same fluid reservoir from which the vein quartz precipitated. This exchange probably took place during the regional metamorphism to greenschist facies.

CONCLUSIONS

1) Low-temperature-seawater-altered basalts contain replacement calcites which have $\delta^{13}\text{C}$ composition of -1‰ to -2‰ (PDB). Dolomites and calcites from the pervasive carbonate alteration zones have $\delta^{13}\text{C}$ compositions ranging from -2‰ to -4‰ (PDB). The lighter dolomites were precipitated at higher temperatures in the cores of the carbonate alteration zones.

2) Chert fragments hosted in clastic sediments and flow top breccias and all replacement carbonates have exchanged oxygen with metamorphic pore fluids, destroying their initial $\delta^{18}\text{O}$ composition. This evidence demonstrates that in some Early Precambrian terrains of greenschist metamorphic grade, quartz, generally considered to resist oxygen isotope exchange, can readily exchange oxygen with metamorphic pore fluids during regional metamorphic events.

3) Carbon isotope systematics do not appear to have been severely disrupted during metamorphism, and hence the $\delta^{13}\text{C}$ of the replacement carbonates retains a record of the premetamorphic, carbonate alteration history.

4) Some gold mineralization hosted in the Malga-Carshaw iron formations is spatially associated with metamorphic quartz veins; however, it is still uncertain whether the gold (and sulphur, carbon dioxide, silica) has been remobilized from within the iron formations or if the iron formations served only as a suitable depository for metamorphic fluids.

5) Gold, sulphur, carbon dioxide, antimony and tungsten are enriched in the auriferous iron formations, although significant positive correlations, common to all mesoband types, exist only between gold-sulphur, gold-carbon dioxide and sulphur-carbon dioxide.

ACKNOWLEDGMENTS

Access to the former Malga Porcupine property and permission to publish the analytical data was granted by M. P. Ferderber of Prospecting Geophysics Limited, Val d'Or, Quebec, and is gratefully acknowledged.

Activation analyses were performed by A. Kabir; M. Knyf carried out some of the stable isotope analyses.

REFERENCES

- Abbey, S.
1977: Studies in "Standard Samples" for use in the General Analysis of Silicate Rocks and Minerals; Part 5: 1977 Edition of "Usable" Values, Geological Survey Canada, Paper 77-34, 31p.
- Anderson, A.T.
1967: The Dimensions of Oxygen Isotopic Equilibrium Attainment during Prograde Metamorphism; *Jour. Geology*, Vol. 75, p.323-332.
- Baragar, W.R.A., Plant, A.G., Pringle, G.J. and Schau, M.
1979: Diagenetic and Postdiagenetic Changes in the Composition of an Archean Pillow; *Canadian Jour. Earth Sci.*, Vol. 16, p.2102-2121.

- Becker, R.H. and Clayton, R.N.
1972: Carbon Isotopic Evidence for the Origin of a Banded Iron-Formation in Western Australia; *Geochim. Cosmochim. Acta*, Vol.36, p.577-595.
- Clayton, R.N. and Mayeda, T.K.
1963: The Use of Bromine Pentafluoride in the Extraction of Oxygen from Oxides and Silicates for Isotopic Analysis; *Geochim. Cosmochim. Acta*, Vol.27, p.43-52.
- Clayton, R.N., O'Neil, J.R. and Mayeda, T.K.
1972: Oxygen Isotope Exchange between Quartz and Water; *Jour. Geophys. Res.*, Vol.77, p.3057-3067.
- Craig, H.
1957: Isotopic Standards for Carbon and Oxygen and Correction Factors for Mass Spectrometric Analysis of Carbon Dioxide; *Geochim. Cosmochim. Acta*, Vol.12, p.133-149.
- 1961: Standard for Reporting Concentrations of Deuterium and Oxygen-18 in Natural Waters; *Science*, Vol.133, p.1833-1834.
- Dimroth, E. and Lichtblau, A.P.
1979: Metamorphic Evolution of Archean Hyaloclastites, Noranda Area, Quebec, Canada. Part 1: Comparison of Archean and Cenozoic Sea-Floor Metamorphism; *Canadian Jour. Earth Sci.*, Vol.16, p.1315-1340.
- Flanagan, F.J.
1973: 1972 Values for International Geochemical Reference Samples; *Geochim. Cosmochim. Acta*, Vol.37, p.1189-1200.
- 1976: Descriptions and Analyses of Eight New USGS Rock Standards; United States Geological Survey, Professional Paper 840, 192p.
- Fleischer, R. and Routhier, P.
1973: The Consanguineous Origin of a Tourmaline-Bearing Gold Deposit: Passagem de Mariana (Brazil); *Econ. Geol.*, Vol.68, p.11-22.
- Friedman, I. and Gleason, J.D.
1973: A New Silicate Inter-Comparison Standard for $\delta^{18}\text{O}$ Analysis; *Earth Planet. Sci. Lett.*, Vol.18, p.124
- Fripp, R.E.P.
1976: Gold Metallogeny in the Archean of Rhodesia; p. 455-466 in *Early History of the Earth*, ed. B.F. Windley, John Wiley and Sons, Toronto.
- Fyon, J.A. and Crocket, J.H.
1981: Gold Exploration in the Timmins Area Using Field and Litho-geochemical Characteristics of Carbonate Alteration Zones; Ontario Geological Survey, Open File Report 5339, 172p.
- Fyon, J.A., Schwarcz, H.P. and Crocket, J.H.
1980: Carbon and Oxygen Isotope Geochemistry of Replacement Carbonates from the Timmins-Porcupine Gold Camp; Grant 49, p.72-82 in *Geoscience Research Grant Program, Summary of Research, 1979-1980*, edited by E.G. Pye, Ontario Geological Survey, Miscellaneous Paper 93, 262p.
- Horwood, H.C. and Pye, E.G.
1951: Geology of Ashmore Township; Ontario Department of Mines, Annual Report, Vol. 60, pt.5, p.1-105; accompanied by Map 1951-2, scale 1 inch to 1000 feet.
- Jensen, L.S.
1978: Archean Komatiitic, Tholeiitic, Calc-Alkalic and Alkalic Volcanic Sequences in the Kirkland Lake Area; p.236-259 in *Toronto '78 Field Trips Guidebook*, edited by A.L. Currie and W.O. MacKasey, Geological Association of Canada, 361p.
- Knauth, L.P., and Lowe, D.R.
1978: Oxygen isotope geochemistry of cherts from the Onverwacht Group (3.4 billion years), Transvaal, South Africa, with implications for secular variations in the isotopic composition of cherts; *Earth Planet. Sci. Letters*, Vol.41, p.209-222.
- Lipman, P.W. and Friedman, I.
1975: Interaction of Meteoric Water with Magma: An Oxygen-Isotope Study of Ash-Flow Sheets From Southern Nevada; *Geological Society of America, Bulletin*, Vol.86, p.695-702.
- Longstaffe, F.J.
1977: The Oxygen Isotope and Elemental Geochemistry of Archean Rocks from Northern Ontario; unpublished Ph.D. thesis, McMaster University, 564p.
- Matsuhisa, Y.
1974: $^{18}\text{O}/^{16}\text{O}$ Ratios of NBS-28 and some Silicate Reference Samples; *Geochem. Jour.*, Vol.8, p.103-107.
- McCrea, J.M.
1950: On the Isotope Chemistry of Carbonates and a Paleotemperature Scale; *Jour. Chem. Physics*, Vol.18, p.849-857.
- Nesbitt, R.W., Sun, S.S. and Purvis, A.C.
1979: Komatiites: Geochemistry and Genesis; *Canadian Mineralogist*, Vol.17, p.165-186.
- Northrop, D.A. and Clayton, R.N.
1966: Oxygen-Isotope Fractionations in Systems Containing Dolomite; *Jour. Geology*, Vol.74, p.174-196.
- Parmentier, E.M., and Schedl, A.
1981: Thermal aureoles of igneous intrusions: some possible indications of hydrothermal convective cooling; *Jour. Geol.*, Vol.89, p.1-22.
- Perry, E.C. Jr. and Tan, F.C.
1972: Significance of Oxygen and Carbon Isotope Variations in Early Precambrian Cherts and Carbonate Rocks of Southern Africa; *Geological Society of America, Bulletin*, Vol.83, p.647-664.
- Perry, E.C. Jr., Tan, F.C. and Morey, G.B.
1973: Geology and Stable Isotope Geochemistry of the Biwabik Iron Formation, Northern Minnesota; *Econ. Geol.*, Vol.68, p.1110-1125.
- Pye, E.G.
1952: Geology of Errington Township, Little Long Lac Area; Ontario Department of Mines, Annual Report, Vol.60, pt.6, p.1-40.
- Pyke, D.R.
1980: Geology of the Timmins Area, District of Cochrane; Ontario Geological Survey, Open File Report 5281, 369p.
- Pyke, D.R., MacVeigh, J.G. and Middleton, R.S.
1978: Volcanic Stratigraphy and Geochemistry in the Timmins Mining Area, p.160-184 in *Toronto '78 Field Trips Guidebook*, edited by A.L. Currie and W.O. MacKasey, Joint Annual Meeting of GSA, GAC and MAC.
- Sharma, T. and Clayton, R.N.
1965: Measurement of $^{18}\text{O}/^{16}\text{O}$ Ratios of Total Oxygen of Carbonates; *Geochim. Cosmochim. Acta*, Vol.29, p.1347-1353.
- Taylor, H.P., Jr.
1974: The application of oxygen and hydrogen isotope studies to problems of hydrothermal alteration and ore deposition, *Econ. Geol.*, Vol.69, p.843-883.
- Taylor, H.P., Jr., Albee, A. and Epstein, S.
1963: $^{18}\text{O}/^{16}\text{O}$ Ratios of Coexisting Minerals in Three Assemblages of Kyanite-Zone Pelitic Schist; *Jour. Geology*, Vol.71, p.513-522.
- Taylor, H.P., Jr. and Coleman, R.G.
1968: $^{18}\text{O}/^{16}\text{O}$ Ratios of Coexisting Minerals in Glaucophane-bearing Metamorphic Rocks; *Geological Society of America, Bull.*, Vol.79, p.1727-1756.
- Tolbert, G.E.
1964: Geology of the Raposos Gold Mine, Minas Gerais, Brazil; *Econ. Geology*, Vol.59, p.775-798.

Grant 56 Part A Geochemistry and Field Relations of Lode Gold Deposits in Felsic Igneous Intrusions — Porphyries of the Timmins District

B. E. Gorman¹, R. Kerrich², and W. S. Fyfe²

¹Sulpetro Minerals Limited, Toronto

²Department of Geology, University of Western Ontario

ABSTRACT

Gold-bearing felsic igneous porphyries in the Timmins and Kirkland Lake areas exhibit anomalous enrichments of Na₂O, volatiles, and ¹⁸O compared to barren porphyries. The patterns reflect pervasive albitization and hydration, coupled with oxidation, which are characteristic of a process similar to large scale spilitization. The process was the result of thermally driven seawater convection in proximity to the seafloor at temperatures between 200°C and 335°C.

Geochemical studies suggest that the initial solutions causing alteration were oxidizing and carried a high chemical potential of Na₂O. With continued reaction the solutions were enriched in K, and eventually evolved into reducing, alkali-poor fluids. Quartz veins associated with these porphyries are of several generations, and gold is invariably found in quartz and coexisting sulphides which retain textural evidence of brittle fractures.

INTRODUCTION

In a comprehensive review paper, Gallagher (1940) noted the association between albitized felsic intrusive rocks and vein-hosted gold deposits. From examples spanning the geological column, he suggested that albitization preceded, and exercised a structural control on, gold deposition. Albitization in felsic intrusive rocks is akin to spilitization of ocean-floor basalts, resulting from an episode of low-temperature (<350°C) alteration by seawater during convection through felsic intrusions emplaced in proximity to the seafloor (Kerrich *et al.* 1980).

The purpose of this study is to determine the process of albitization in Archean felsic intrusions (porphyries), and its influence on the subsequent emplacement of auriferous quartz veins. Emphasis is placed on the structural and mechanical controls for the deposition and preservation of gold within, and adjacent to, albitized porphyries. We believe that this emphasis can lead to refined and effective exploration techniques.

Much of the analytical data in this paper is from samples collected underground at the Schumacher (McIntyre) and Dome Mines in the Timmins camp. Additional material was obtained from numerous producing and past-producing mines in northern Ontario, from graduate

students, and from the Gordon Suffel Collection at the University of Western Ontario.

MINERAL ASSEMBLAGES AND ALTERATION OF GOLD-BEARING PORPHYRIES

A petrographic study of over 100 thin sections of porphyries from the Timmins camp revealed a number of mineral assemblages which can be synthesized into a model for a coherent alteration process. These assemblages are listed in Table 1, and their chemical compositions (determined by reconnaissance microprobe studies) are listed in Appendix 1. Whole-rock analyses of the porphyries are given in Appendix 2.

A chemographic portrayal of these mineral assemblages can be constructed by considering five components: Na₂O, Al₂O₃, Fe₂O₃, FeO, and MgO. SiO₂ and H₂O are considered to be in excess. CaO as well as CO₂ and SO₂ are left out of this system, since calcite (and/or anhydrite) can be found in all assemblages. Due to the extreme mobility of Na₂O and the observed variations in the oxidation state of iron (*viz.* the stilpnomelane + hematite assemblage in Table 1), we chose to display the constituent minerals as functions of the chemical potentials of soda and oxygen ($\mu_{\text{Na}_2\text{O}}-\mu_{\text{O}_2}$) in Figure 1a, modified after Dobretsov *et al.* (1973). An AFM (Al, Fe, Mg) projection of key minerals is shown in Figure 1b. It is apparent that assemblages containing stilpnomelane and assemblages containing chloritoid lie at opposite ends of the diagram (high $\mu_{\text{Na}_2\text{O}}$ and μ_{O_2} , and low $\mu_{\text{Na}_2\text{O}}$ and μ_{O_2} , respectively). For example, such assemblages could be in equilibrium with a solution which evolves from one that is oxidizing and sodic to one that is fairly reducing and depleted in soda.

The presence of albite and paragonite (+ muscovite) in these porphyries points to equilibrium with solutions for which $\log \text{Na}^+/\text{H}^+ > \log \text{K}^+/\text{H}^+$ (Figure 2), $\text{Na}^+/\text{K}^+ > 5$ (Orville 1963), and $\text{Na}^+/\text{Ca}^{++} \geq 40$ (Orville 1972). These parameters are consistent with seawater compositions (Fyfe *et al.* 1978).

Alteration of felsic igneous rocks by seawater would thus stabilize albite as the sole feldspar (or paragonite + quartz at temperatures greater than 335°C: Chatterjee 1973) and induce precipitation of sulphate (as anhydrite,

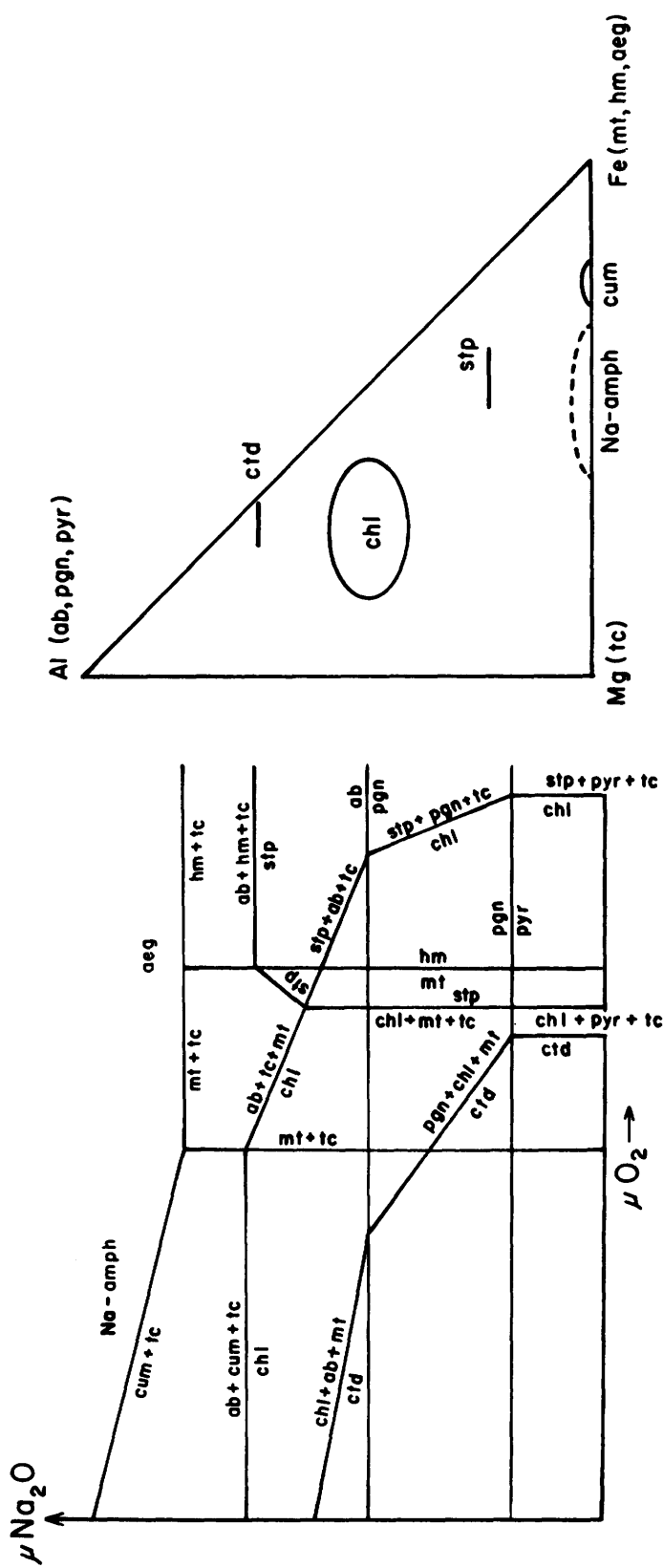


Figure 1—(left) Schematic representation of mineral stabilities for the system Na_2O , Al_2O_3 , Fe_2O_3 , FeO , and MgO (SiO_2 and H_2O in excess) as functions of $\mu\text{Na}_2\text{O}$ and μO_2 (or $\mu\text{Fe}_2\text{O}_3$) at constant T and P . Diagram modified after Dobretsov et al. (1973). (right) The projections of key minerals in the sub system Al-Mg-Fe . Abbreviations: ab = albite, pgn = paragonite, pyr = pyrophyllite, chl = chlorite, ctd = chloritoid, tc = talc, mt = magnetite, hm = hematite, cum = cummingtonite, stp = stilpnomelane.

Table 1—Key mineral assemblages in Timmins area felsic intrusions.

ROCK TYPE	MINERAL ASSEMBLAGE ¹
Ottrelite schists ²	chloritoid + paragonite/muscovite + chlorite + calcite + magnetite + quartz (tourmaline, sphene, apatite)
Albitized porphyry	quartz + albite + paragonite/muscovite + chlorite + calcite + pyrite ± talc ± anhydrite (tourmaline, sphene, apatite, sphalerite, leucoxene)
Pearl Lake Porphyry, near Copper Zone	quartz + albite + paragonite/muscovite + chlorite + anhydrite + calcite + hematite ± talc + pyrite ± K-feldspar (chalcopyrite, bornite, tetrahedrite, sphalerite, tourmaline, apatite, sphene ± rutile)
Stilpnomelane-bearing Paymaster Porphyry ³	quartz + albite + paragonite/muscovite + talc + stilpnomelane ± chlorite + hematite (pyrite, apatite, tourmaline, sphene + rutile)

¹minerals in parenthesis are present in minor amounts

²Two specimens (HOLL 2950 and HOLL 2951), from the 2750 and 3650 levels of the Hollinger Mine, respectively. Whole-rock analyses in Appendix 2

³Two specimens (PM 1A and PM 2) from surface exposures of Paymaster Porphyry. Whole-rock analyses in Appendix 2

barring excessive interaction with iron silicates which reduces SO_4^{2-} to S^{2-} : Fyfe and Lonsdale in press). The evolved fluids would have decreased Na^+/K^+ ratios similar to thermal discharges in Iceland (Tomasson and Kristmannsdottir 1972). The concentration of Ca^{++} in NaCl solutions heated from 25°C to 400°C in equilibrium with albite + quartz would drop some five orders of magnitude, whereas the co-existence of albite + calcite at 400°C requires $fCO_2 \sim 100$ bars (at $P_{fluid} = 2000$ bars: Helgeson 1974).

In summary, the progressive alteration of a felsic intrusion by seawater can be visualized as follows.

1) Sodic or albitic alteration. The stability of albite (or paragonite + quartz) replacing igneous feldspar or in veinlets (rare) increases with the addition of quartz (silicification). The progressive heating of seawater results in widespread oxidation of iron (stilpnomelane + hematite assemblages?) and deposition of anhydrite and calcite. With regard to calcite deposition, Eugster and Skippen (1967) note that CO_2 is the dominant gas species in the C-O-H system with fH_2 buffered by magnetite-hematite. It is of interest to note that albite + paragonite + Na-montmorillonite alteration has been reported in porphyry copper system in Indonesia (Lower and Dow 1978).

2) Sericitic or propylitic alteration. The continued interaction with seawater results in decreased Na^+/K^+ and stability of muscovite in addition to paragonite. Reaction with iron silicate causes reduction of SO_4^{2-} to sulphide.

Lower chemical potentials of alkalis and alkaline-earth metals due to leaching in hydrolysis reactions would act to stabilize chlorite and chloritoid.

GEOCHEMISTRY OF ALTERATION OF GOLD-BEARING PORPHYRIES

Early in the study, the geochemistry of several granitic rocks was examined by means of R- and Q- mode factor analysis or correspondence analysis (David *et al.* 1977). It was noted that Archean felsic intrusions containing gold deposits, such as the Pearl Lake Porphyry, exhibited an unusual antipathetic behavior between K_2O and Na_2O (Gorman 1980). In most normal or barren intrusions, such as the Bourlamaque batholith in Quebec, and in Cenozoic granitic rocks, K_2O and Na_2O behave sympathetically. It was noted on factor analysis plots that where the Na_2O trend had a different direction than the K_2O trend, samples clustering near the Na_2O trend were generally enriched in trace elements (Au, Ag, Cu, Zn, Cr, Ni, and Li).

A more quantitative examination of the geochemistry of alteration in the Pearl Lake, Northern, and Millerton-Miller Lake Porphyries (43 analyses) and the Preston and Paymaster Porphyries was undertaken. The most efficient

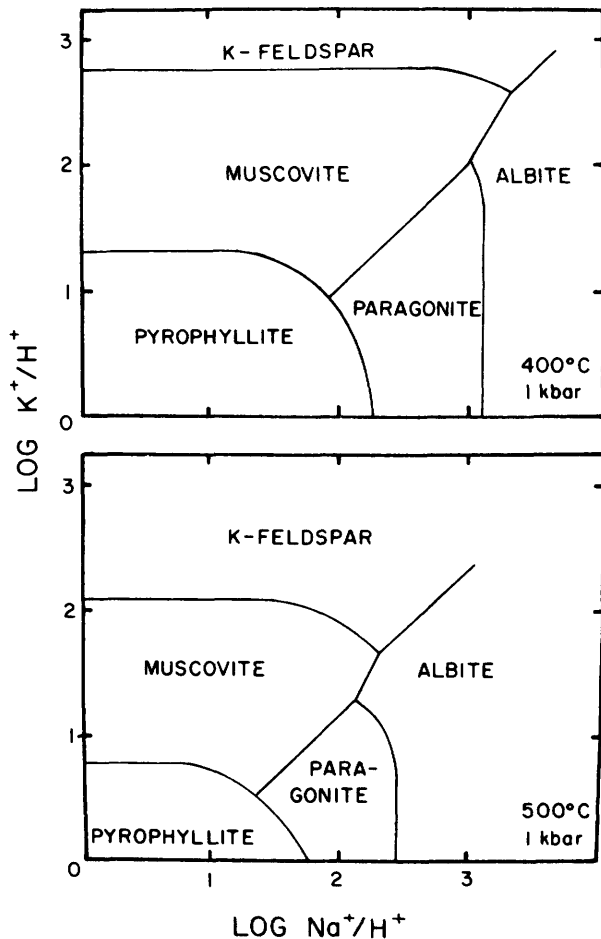


Figure 2—Stability relations of alkalic feldspars, mica, and pyrophyllite in the system $KAISi_3O_8-NaAlSi_3O_8-Al_2SiO_5-SiO_2-H_2O-HCl$ at $P_1 = 1000$ bars ($a_{H_2O} \sim 1$), expressed as functions of $\log K^+/H^+$ versus $\log Na^+/H^+$. Equilibrium temperatures of $400^\circ C$ (upper diagram) and $500^\circ C$ (lower diagram). After Wintsch (1975). In the presence of Al_2SiO_5 polymorphs, the stability field of paragonite would be considerably reduced.

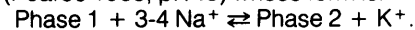
approach is to use molar ratio diagrams (Pearce 1968). These diagrams portray the variation of two elements or oxides, each divided by the abundance of a common element or oxide (e.g. Al_2O_3/Na_2O vs. SiO_2/Na_2O ; see Davies and Luhta 1978). An interesting and useful property of molar ratio diagrams is that if the divisor element is mobile, it can generate a straight line projecting through the origin.

Our investigations confirm Davies and Luhta's (1978) conclusions that all oxides, apart from combinations of Al_2O_3 , SiO_2 , and TiO_2 , were mobile as a result of the pervasive alteration of the porphyries. Further, it was noted that the molar ratio Al_2O_3/SiO_2 derived from plots of

Al_2O_3 vs. SiO_2 using various combinations of nine elements as divisors (FeO^* , MgO , CaO , Na_2O , K_2O , CO_2 , Rb , Sr , and Ba), remained constant at 0.145 (range of 0.127 to 0.162). This feature suggests that the Al_2O_3/SiO_2 ratio in the porphyries remained approximately constant throughout the episode of alteration.

This relationship may be represented as a metasomatic process whereby the Timmins area porphyries were altered due to the "fractionation" (viz. dissolution and/or precipitation) of one or more phases whose overall Al_2O_3/SiO_2 molar ratio was approximately 0.15. Considering the mineralogy of these rocks, such a process could involve a mixture of albite ($Al_2O_3/SiO_2 = 0.33$), mica ($Al_2O_3/SiO_2 \sim 0.5$), or chlorite ($Al_2O_3/SiO_2 \leq 1$) with quartz ($Al_2O_3/SiO_2 = 0$) and talc ($Al_2O_3/SiO_2 \sim 0$).

On the assumption that Al_2O_3 (and TiO_2) were, to a first approximation, immobile, they were used as divisors to compare the behavior of alkalis (plots of K_2O/Al_2O_3 vs. Na_2O/Al_2O_3). Such diagrams generate negative slopes between -0.22 and -0.34 , consistent with an exchange reaction (Pearce 1968, p. 149) whose form is:



In other words, one can visualize the Timmins area porphyries as giant ion-exchange columns subjected to a solution with at least a three-fold excess of Na^+ over K^+ . The lack of widespread potassic alteration is simply due to the deficiency in K^+ .

OXYGEN ISOTOPE RELATIONS

Data from a reconnaissance oxygen-isotope study of the various mineralization types in the Pearl Lake Porphyry is presented in Table 2. The $\delta^{18}O$ of quartz from disseminated chalcopyrite veinlets is relatively uniform at $+8$ to $+11\text{‰}$, but co-existing K-feldspar is more variable, such that Δ quartz-K-feldspar ranges from $+2\text{‰}$ to $+4\text{‰}$. The minimum quartz-feldspar fractionation corresponds to a temperature of about $400^\circ C$, and a $\delta^{18}O$ fluid of $\sim 6\text{‰}$, within the "magmatic" range.

In the anhydrite-dominated envelope surrounding copper mineralization, quartz, albite, and chlorite fractionations are isotopically concordant, signifying a temperature of about $200^\circ C$ and a $\delta^{18}O$ fluid of -1‰ , close to Archean marine water. These data collectively are interpreted as follows. A high temperature "magmatic" fluid, associated with the disseminated copper deposit, mixed with cooler seawater which had penetrated downwards to the "magmatic" fluid reservoir. The low temperature, oxidative, sodium-dominated alteration by the same marine water which albitized the porphyry, is consistent with previous results for high-Na porphyries hosting gold deposits (Kerrick *et al.* 1980).

Gold-bearing veins have a $\delta^{18}O$ of $\sim 14\text{‰}$ and quartz-chlorite fractionations of 6.5‰ , indicating fluids with $\delta^{18}O$ of 9‰ , i.e., in the "metamorphic" range, at about $400^\circ C$. Hence at the Pearl Lake Porphyry three distinct hydrothermal reservoirs can be identified on the basis of metal association, alteration, temperature and isotopic characters.

FeO^* is total Fe expressed as FeO .

Table 2—The oxygen isotope composition of minerals isolated from albitized quartz/feldspar porphyries.

Sample number	Sample description	$\delta^{18}\text{O}$ quartz	$\delta^{18}\text{O}$ feldspar	$\delta^{18}\text{O}$ chlorite
35L	albitized QFP	13.78	11.83(a)	
PM1A	albitized QFP	11.07	12.18(a)	
P11	albitized QFP	11.96	10.66(a)	
38 SyB	albitized QFP	11.19	10.82(a)	
2 ΔH	albitized QFP	12.88	12.32(a)	
4 B2	albitized QFP	12.36	10.39(a)	
9 A	albitized QFP	11.70	12.09(a)	
PLA	quartz ksp chalcopyrite	8 to 11	7.1 to 8.5(k)	
PLB	anhydrite-albite quartz-chlorite	12.4	8.6(k)	1.3

a - albite, k - K-feldspar.

QFP - quartz-feldspar porphyry

THE ROLE OF ALBITIZED FELSIC INTRUSIONS AS HOSTS TO GOLD-BEARING VEINS

Our investigations lead us to conclude that the albitized (or "spilitized") felsic intrusions in gold-producing districts represent ideal mechanical host rocks for subsequent auriferous hydrothermal solutions, regardless of the origin of the porphyries (igneous or syntectic) or the ultimate source of the mineralizing fluids.

The majority of porphyries in the Timmins area are essentially tabular in shape and subconcordant to the regional stratigraphy (e.g. Ferguson *et al.* 1968). From a mechanical viewpoint, they can be considered as sheet-like bodies whose physical properties differ markedly from those of enclosing metavolcanic (and dominantly mafic) rocks and their derivatives.

The room temperature permeability of a granitic rock is of the order of 10^{-7} to 10^{-8} darcies, some 2-4 orders of magnitude greater than permeabilities of gneisses or gabbros (Trimmer *et al.* 1980). This initial permeability may be enhanced by a factor of 20 by heating granites to 400°C (Summer *et al.* 1978), or by a factor of 4 by applying differential stresses to approximately 75-90 percent of the fracture strength (Zoback and Byerlee 1975). It is thus apparent that a combination of temperature change and non-uniform stress (viz. the emplacement and cooling of an intrusion) would likely result in the rock behaving as both heat source and aquifer to thermal convection of fluid.

Experiments have demonstrated that the flow of water through a 4 cm core of granite effectively ceased

within hours for temperatures in excess of 200°C (Summers *et al.* 1978). The granite was simply plugged due to the deposition of quartz, feldspars, mica, and calcite.

We suggest that a similar process was operative in felsic intrusions undergoing "spilitization": a cooling aquifer was rapidly transformed into an impermeable and brittle rock mass enclosed within contorted, heterogeneous metavolcanics and metasediments. The effects of such a sudden disruption of the hydraulic regime could be spectacular, resulting in hydraulic fracturing of the brittle porphyry and focussing of fluid flow along the porphyry contacts. Since felsic intrusive rocks have lower tensile fracture strengths than most volcanic and sedimentary rocks, hydraulic fracturing would likely be concentrated within the porphyries.

CHARACTERISTICS OF GOLD-BEARING VEIN SYSTEMS IN ARCHEAN FELSIC INTRUSIONS

A review of the literature on gold-bearing vein systems in the Archean of Ontario confirms that gold was one of the last elements to be deposited in vein systems, and is almost invariably found within fractures in associated minerals. For convenience, these findings are summarized in Table 3.

With specific reference to the Pearl Lake and associated porphyries, the following sequence of alteration and mineralization has been synthesized from numerous studies in the Hollinger and McIntyre (Schumacher) Mines.

Table 3—Mineralogy of gold-bearing systems in Archean felsic intrusions of Ontario.

REGION	HOST ROCK	SEQUENCE OF VEIN MINERALIZATION	PETROGRAPHY OF GOLD-BEARING VEINS	REFERENCE
Straw-Manitou Lake, Kenora	quartz porphyry	py-mt,qtz,carb-sph,gs-tell-cpy,Au	Au + tell in fractured (creamy-white) quartz	Thomson (1934)
Matichewan-Kenogami, Timiskaming	albitized porphyry in conglomerates	py,mt,qtz,carb-sph,Au	Au in fractures in coarse-grained py, and with cpy in fractured quartz	Dyer (1936)
Little Long Lac, Thunder Bay	greywackes	carb,qtz,asp,py-qtz-bour-Au	Au in fractured qtz, and as blebs in py and bour. Late qtz veins low-grade	Bruce (1935)
Lake of the Woods	schistose basalt	qtz(1)-carb,qtz(2)-py-tour, cpy-ga-tell-Au,glassy qtz(3)	Au as veinlets and blebs in second generation of quartz (with py-tour)	Thomson (1937)
Red Lake	quartz porphyry	qtz(1)-auriferous py,qtz(2)-sph-ga-tour-Au	Au in brecciated qtz at intersection of two vein systems	Hurst (1936)
Michipicoten	Algoman intrusives	qtz(1),ab,asp,tour,bt,qtz(2)	"A prerequisite for the [Au] mineralization of the veins has been a mechanical deformation of the quartz. In barren quartz veins (qtz(2)), such signs of deformation are absent" (p. 73)	Fronberg (1937)
Argosy Mine, Kenora	greywackes	qtz,asp,po-cpy-py-sph,ga,Au	Au in fractures and along quartz grain boundaries, and in fractured asp	Horwood (1938a)
Sturgeon Lake, Kenora	basalt-andesite	qtz(1)-Au,py-asp,qtz(2)-tour-Au,qtz(3)	Au disseminations in qtz(1), mainly in fractured qtz(1) along with qtz(2)-tour-sulphides	Horwood (1938b)
Uchi-Slate Lakes, Kenora	greenstone-gabbro	banded qtz(1),qtz(2) stringers-py-po-cpy,ga-sph,Au	Au in sutured, micro-brecciated qtz(1 and 2) especially when both banded and stringer qtz veins are found together	Baleman (1940)
Goudreau-Lochalsh, Algoma	granodiorite	glassy qtz(1),grey qtz(2)-py-po-asp-Au,qtz(3)	Au in quartz "in lines as if following some obscure fracture" (p. 40), esp. adjacent to py. Au as blebs in and on py, with ga	Bruce (1942)
Ashmore Township, Thunder Bay	albite porphyry, greywacke, iron formation	grey qtz(1)-asp-py-po-sph-cpy-ga-ank-Au, fine-grained qtz(2)-tour-carb-asp-py-Au, milky qtz(3)-calcite	Au-bearing qtz (1 and 2) fractured and cataclastic. Qtz(3) is milky and coarse-grained, generally low-grade	Horwood and Pye (1955)
Errington Township, Little-Long Lac	volcanic-sedimentary contact albite porphyry, sheared gabbro	cherty qtz(1), glassy coarse qtz(2)-sulphides-Au, fine-grained qtz(3)-py-tour-carb-Au, grey qtz(4), milky coarse qtz(5)	Au in qtz (2 and 3); higher assays associated with increased granulation and fragmentation	Pye (1952)
Hollinger Mine, Timmins	quartz porphyry in metavolcanic rocks	qtz(1)-ank-tour-scheelite, qtz(2)-ab-py, qtz(3)-po-sph-ga-Au, qtz(4)-carb-sph-cpy-minor Au, qtz(5)+calcite	Au filling fractures in ankerite, in strained and recrystallized qtz (3 and 4), and as blebs in qtz (3 and 4) connected by empty fractures	Keys (1940)
Porcupine area, Timmins	quartz-albite porphyry	qtz(1)-tour-py-po-ank, qtz(2)-Au, qtz(3)-calcite	Au in qtz(1)-ank veins: ore shoots caused by "creation and filling of open spaces during the interval of gold mineralization" (p. 126)	Hurst (1935)
Kirkland Lake	syenites	early coarse-grained milky quartz, later finer-grained dark quartz	Au as fine particles in py and tellurides. Au has been noted replacing, veining, following cleavages in, and rimming many of the previously described minerals (sulphides and tellurides), including quartz, and in fractures in various types of wall rocks" (p. 119)	Thomson et al. (1950)

Abbreviations: ab-albite, ank-ankerite, asp-arsenopyrite, Au-gold, bour-bourmonite, bt-biotite, carb-carbonate minerals, cpy-chalcopyrite, ga-galenite, mc-magnetite, po-pyrrhoite, py-pyrite, qtz-quartz, sph-sphalerite, tell-telluride minerals, tour-tourmaline

1) The earliest episode of alteration is recognized by the introduction of soda (albitization), quartz (silicification), and early quartz veins, with tourmaline, axinite, scheelite, and scarce epidote minerals (Bain 1933; Allen and Folinsbee 1944; this study). The main carbonate mineral is ankerite, whose composition is apparently independent of host-rock compositions (Charlewood 1935). Allen and Folinsbee (1944) noted that scheelite is found in a vein system in the Millerton Porphyry which extends some 4000 feet vertically; and that the ratio gold/scheelite increases towards the margins of the porphyry.

2) Coarse-grained pyrite and arsenopyrite was deposited in both quartz veins and porphyry wall-rock, and are considered essentially non-gold-bearing at this stage (Keys 1940). The precipitation of anhydrite in the Pearl Lake Porphyry followed the period of ankerite deposition (Langford and Hancox 1936). The development of micas (paragonite/muscovite) was widespread, whether contemporaneous with (Bain 1933) or following (Keys 1940) the introduction of gold. Bain (1933) noted that extensive "sericitization" is restricted to low-grade or non-productive porphyries in Ontario. This generalization appears to be true in the Timmins area, based on the present study, but may not hold for all sericitized porphyries (e.g. Pye 1952).

3) A period of fracturing and re-opening of quartz-ankerite-pyrite veins resulted in the introduction of quartz, pyrrhotite, sphalerite, minor galena and tellurides, and gold (Dougherty 1925; Graton *et al.* 1933; Hurst 1935; Keys 1940). These workers reported gold as fracture-fillings in ankerite, quartz, and pyrite. Gold values are highest where vein systems contain abundant pyrite and ankerite as the dominant carbonate. Bain (1933) noted that high-grade lodes are characterized by chlorite overgrowths on pyrite, in contrast to the more common presence of quartz overgrowths.

4) Late quartz-calcite veins, especially near the margins of the porphyries, are generally barren (Bain 1933; Hurst 1935; Keys 1940).

In summary: more than 50 years of work on Ontario gold deposits in porphyries points to the following factors as important to the localization of ore:

1) the nature of pre-mineralization alteration: albitization and silicification (Bruce 1933; Gallagher 1940), chloritization (Bain 1933), and ankerite as the dominant carbonate mineral (Hurst 1935; Keys, 1940);

2) as a corollary of 1): the availability of a competent wall-rock (Bain 1933; Gallagher 1940);

3) periods of repeated fracturing during the ingress of gold-bearing solutions (Keys 1940; Table 3); and

4) the stress regime and its influence on the mechanics of veining.

A number of workers have noted that gold-bearing veins are found in rocks that have been subjected to simple shear rather than non-displacing tensile stresses (Hulin 1929). Such a simple shear regime can be inferred from wall-rock displacement (Bateman 1940), rotation of pyrite crystals with appended trails of chlorite, quartz, or mica (Bain 1933), wall-rock slabs in veins (often considered as evidence for replacement: Dougherty 1925), ribbon structures in quartz (McKinstry and Ohle 1949), inter-

mineralization brecciation and low-angle vein intersections (Hulin 1929), multiple generations of quartz (Stone 1937), and the congruency of vein systems with shear fractures during folding and faulting (Preston East Dome: J. W. Ambrose, unpublished data on file at Queen's University, Kingston).

RECOGNITION OF POTENTIALLY GOLD-BEARING VEINS

Inspection of Table 3 illustrates the importance of brittle fracturing with respect to vein systems emplaced prior to, and during, the availability of gold-bearing solutions. Late (post-ore) quartz veins, variously described as milky, glassy, mottled, or bull quartz are generally barren.

A number of workers have attempted to distinguish "live" (auriferous) quartz from "dead" quartz on the basis of textures in thin section (Adams 1920; Ferguson and Gannett 1932; White 1943). We believe that their lack of success was due, in part, to incorrect identification of the mechanical origin of observed textures in quartz. Terms such as cataclastic, microbrecciated, and anhedral replacement were applied to quartz which had undergone dynamic recrystallization (a rather high-temperature ductile or plastic deformation) rather than dominantly brittle fracturing (a low-temperature, high-stress deformation). When gold was seen in fractures superposed on "microbrecciated" quartz, the distinction between which episode of "fracture" characterized "live" quartz was, at best, uncertain.

The distinction between ductile deformation of quartz (and sulphide minerals) and brittle fracture is important in examining vein systems, as exemplified by Pye (1952) while examining the gold deposits of Errington Township (Little Long Lac area). He noted that two phases of quartz were present: coarse-grained milky quartz (in part fractured), and a fine-grained mosaic of anhedral quartz grains. The latter quartz is (Pye 1952, p. 55):

"a phase of the coarse-grained quartz, which has been partly granulated and possibly recrystallized in consequence of inter-mineralization fracturing. Such a hypothesis explains the general intimate association of the two varieties of quartz, the gradations in type between them, and the absence of definite cross-cutting relationships. Where only the coarse-grained quartz is present, the veins are glassy and white in colour, but where the two varieties are intimately associated, as in the Little Long Lac ores, the veins generally possess a greyish to bluish colour and exhibit an ill-defined fragmental appearance. Sampling has demonstrated that, where the quartz at the Little Long Lac mine is distinctly fragmental, the values in gold are higher than where the quartz appears to be glassy and massive."

The common association of gold with fractured quartz, pyrite, and arsenopyrite suggests to us that, on a microscopic scale, it is the mechanical properties of these minerals (i.e. the predominance of brittle over ductile deformation) that governs the deposition and preservation of gold mineralization. This conjecture may be evaluated by considering the strengths of quartz and sul-

phide minerals over a geologically-reasonable temperature range (Figure 3). It is apparent that quartz and pyrite (and likely arsenopyrite) are significantly stronger than other sulphide minerals at temperatures around 400°C. As such, gold can be introduced into quartz-pyrite-arsenopyrite veins at 400°C along fractures within these phases. Should regional temperatures and stresses persist long after the introduction of gold, quartz can anneal and recrystallize, thereby expelling gold from healing fractures. The remobilized gold would either find refuge in brittle sulphides or be lost from the system. This process may explain the observation that bull quartz in metamorphic terrains is generally barren. Where quartz veins contain a significant amount of a second phase (apart from sulphides), such as mica, gold may be preserved along micaceous grain boundaries. This feature has

been recognized in amphibolite-facies quartz + biotite veins in the Grenville Province.

Many of the described textures of barren and auriferous quartz veins are shown in Figures 4-7 (Appendix 3).

CONCLUSIONS

1) The alteration ("spilitization") of felsic intrusions in the Timmins area occurred as the result of the formation of phases whose overall $\text{Al}_2\text{O}_3/\text{SiO}_2$ molar ratio was approximately 0.15. The spectrum of alteration can be approximated by considering the precipitation of albite ($\text{Al}_2\text{O}_3/\text{SiO}_2 = 0.33$) and quartz ($\text{Al}_2\text{O}_3/\text{SiO}_2 = 0$) in a ratio of 1/1.

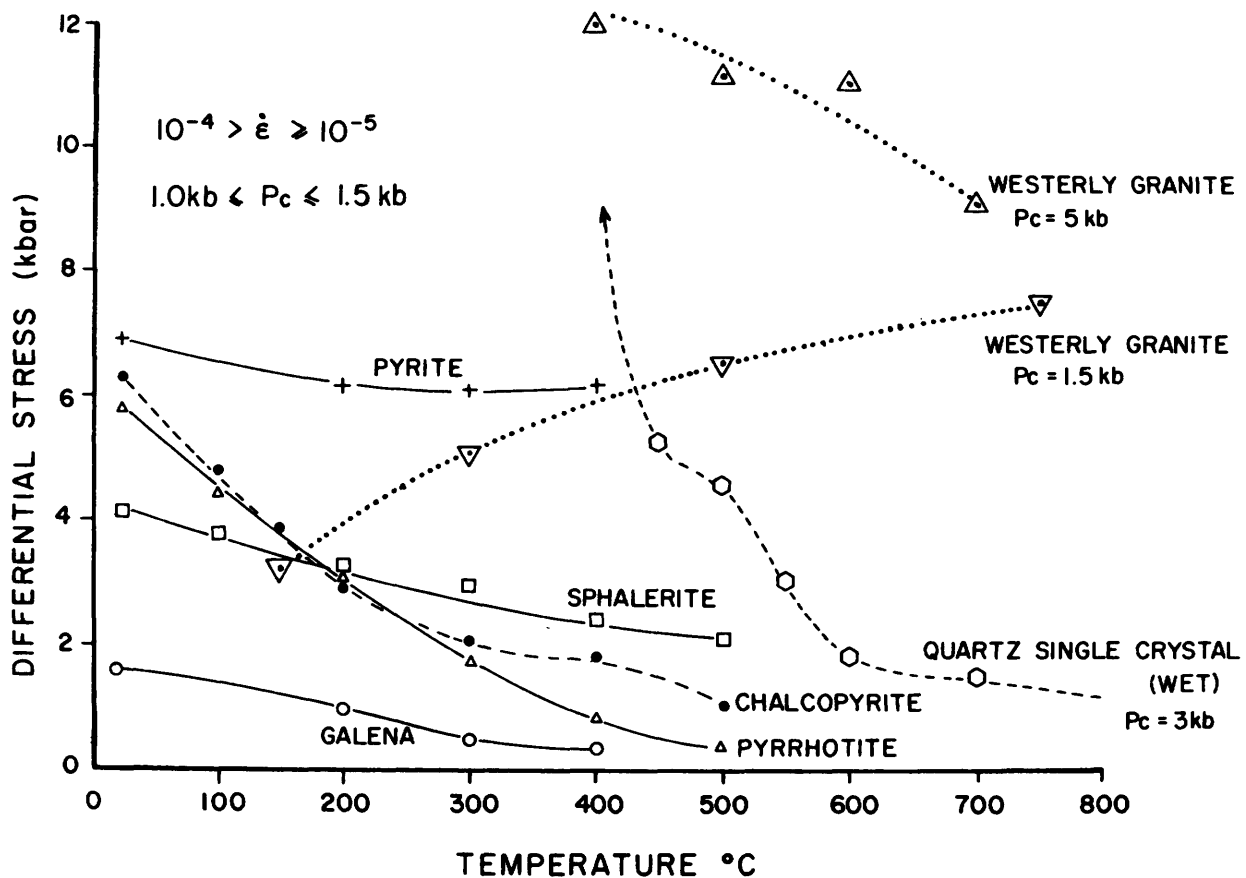


Figure 3—Strengths of rocks and minerals as a function of temperature. The points represent experimentally determined strengths recorded at 10 percent strain if stress levels are still rising, or the ultimate strengths if stress levels are falling. Experimental strain rates ($\dot{\sigma}$) vary between 10^{-4} and 10^{-5} sec^{-1} . Confining pressures are between 1000 and 1500 bars (except where noted otherwise). Sources of data: Westerly granite from Tullis and Yund (1977); quartz (Hobbs et al. 1972); pyrite (Atkinson 1975), sphalerite and pyrrhotite (Clark and Kelly 1973); chalcopyrite (Roscoe 1975; Kelly and Clark 1975); galena (Salmon et al. 1974; Atkinson 1976).

2) The initial solutions causing the alteration were oxidizing and carried a high chemical potential of Na₂O (reflected in stilpnomelane + hematite assemblages). With continued reaction, the solutions were enriched in K⁺ (paragonite + muscovite assemblages), and ultimately evolved into reducing, alkali-poor fluids which formed peraluminous chloritoid-bearing assemblages.

3) The co-existence of albite, paragonite, and quartz suggests a maximum alteration temperature of 335°C.

4) This episode of alteration effectively transformed the felsic intrusions into competent and impermeable masses, which exercised a strong structural control on subsequent gold mineralization. It is possible that tabular, sub-concordant porphyries represent structurally favourable hosts, as compared to cross-cutting plugs or stocks.

5) Numerous gold-bearing vein systems appear to have been emplaced under conditions of simple shear, rather than tensile fracturing in host rocks. Regional structural studies will be useful in localizing such favourable structures and their possible congruency with folding and faulting.

6) Petrographic examination of several generations of quartz veins (in conjunction with 5, above) can be used

as an exploration tool, as gold is invariably found in quartz and associated sulphides which retain textural evidence of brittle fractures. Such a technique may be most useful in a negative way when examining metamorphic terrains: *the absence of any evidence of brittle fracturing in any given vein system indicates a low potential for the introduction or preservation of gold.*

ACKNOWLEDGMENTS

We wish to express our appreciation for the co-operation and hospitality given to us by Pamour Porcupine Mines Limited (W. W. Holmes, manager; Denis Caron, W. Wayne Gennings, and Peter Mathias, geologists) and by Dome Mines Limited (H. V. Pyke, manager, and D. S. Rogers, senior geologist).

John Forth provided technical assistance and advice concerning rock preparation and quality thin sections. Photography and reproduction was done by Alan Noon and F. W. Graves. R.L. Barnes provided expertise in mineral identification, textural interpretation, electron micro probe studies, and invaluable critical discussion.

APPENDIX 1. Mineral Compositions from Timmins Area Porphyries Determined by Electron Microprobe

A. CHLORITOID-BEARING ROCKS

	Sample HOLL 2950		Sample HOLL 2951		
	1	2	3	4	5
SiO ₂	24.83	47.51	24.55	47.80	37.00
TiO ₂	.00	.04	.00	.00	.14
Al ₂ O ₃	41.19	38.19	39.75	38.58	33.50
FeO*	25.01	.17	25.93	.23	7.40
MnO	.20	.00	.18	.00	.00
MgO	1.90	.17	1.52	.07	5.18
CaO	.00	.64	.00	.12	.16
Na ₂ O	.00	4.25	.00	4.48	1.59
K ₂ O	.00	3.06	.01	3.97	.04
Cr ₂ O ₃	.04	.04	.06	.00	.00
TOTAL	93.12	94.05	91.94	95.25	84.67
n	4	3	3	1	2
1: chloritoid					
2: mica					
3: chloritoid					
4: mica					
5: tourmaline					

B. STILPNOMELANE-BEARING ROCKS

	Sample PM1A				Sample PM2		
	1	2	3	4	5	6	7
SiO ₂	49.49	60.12	69.82	25.63	48.50	59.11	26.31
TiO ₂	.00	.00	.00	.00	.00	.00	.00
Al ₂ O ₃	4.91	.00	19.86	21.70	5.14	.00	21.19
FeO*	20.29	8.60	.32	20.95	24.59	9.75	22.41
MnO	.30	.07	.00	.11	.19	.04	.12
MgO	12.31	24.95	.00	17.29	9.06	24.06	17.43
CaO	.04	.00	.00	.00	.13	.00	.00
Na ₂ O	.09	.00	11.85	.03	.10	.00	.00
K ₂ O	1.08	.00	.00	.01	.30	.00	.00
Cr ₂ O ₃	.01	.00	.00	.04	.00	.00	.08
TOTAL	88.52	93.72	101.84	85.74	88.09	92.96	87.53
n	3	2	1	2	2	3	2
1. stilpnomelane							
2. talc							
3. albite							
4. chlorite							
5. stilpnomelane							
6. talc							
7. chlorite							

C. PEARL LAKE PORPHYRY

	PL23-08		PL23-10	PL46-22
	1	2	3	4
SiO ₂	25.02	47.28	48.25	46.94
TiO ₂	.04	.08	.09	.06
Al ₂ O ₃	21.98	36.09	32.81	38.07
FeO*	25.85	.85	2.37	.51
MnO	.10	.00	.00	.00
MgO	14.36	.55	1.20	.55
CaO	.00	.05	.00	.01
Na ₂ O	.12	1.60	.50	2.90
K ₂ O	.00	8.48	10.14	7.21
Cr ₂ O ₃	.04	.08	.09	.06
TOTAL	87.55	95.02	95.38	96.35
n	3	8	3	5
1. chlorite				
2. mica				
3. mica				
4. mica				

D. NORTHERN PORPHYRY

	NP53-34A		NP38-18
	1	2	3
SiO ₂	46.82	25.23	47.24
TiO ₂	.13	.00	.07
Al ₂ O ₃	36.96	21.22	35.48
FeO*	.79	28.44	.69
MnO	.00	.01	.00
MgO	.96	13.29	.60
CaO	.00	.00	.05
Na ₂ O	.75	.24	2.39
K ₂ O	10.55	.00	7.57
Cr ₂ O ₃	.08	.10	.03
TOTAL	97.03	88.54	94.13
n	3	3	3
1. mica			
2. chlorite			
3. mica			

APPENDIX 2. Selected Whole Rock Analyses of Timmins Area Porphyries

	CHLORITOID-BEARING ROCKS		STILPNOMELANE-BEARING ROCKS	
	Holl 2950	Holl 2951	PM 1A	PM 2
SiO ₂	54.70	46.10	66.60	69.50
TiO ₂	0.69	0.76	0.32	0.44
Al ₂ O ₃	12.30	13.10	15.90	12.40
FeO ₁	6.97	8.80	2.40	3.72
MnO	0.18	0.15	0.04	0.03
MgO	3.86	4.13	1.70	3.83
CaO	8.10	10.60	0.82	0.52
Na ₂ O	1.12	1.04	8.76	6.35
K ₂ O	0.83	0.89	0.28	0.19
P ₂ O ₅	0.07	0.06	0.14	0.12
H ₂ O ⁺	10.00	15.08	0.60	1.39
CO ₂	n.d.	n.d.	0.50	0.30
S	n.d.	n.d.	n.d.	n.d.
Total:	98.82	100.71	98.06	98.79

APPENDIX 3. Textures of Barren and Auriferous Quartz Veins

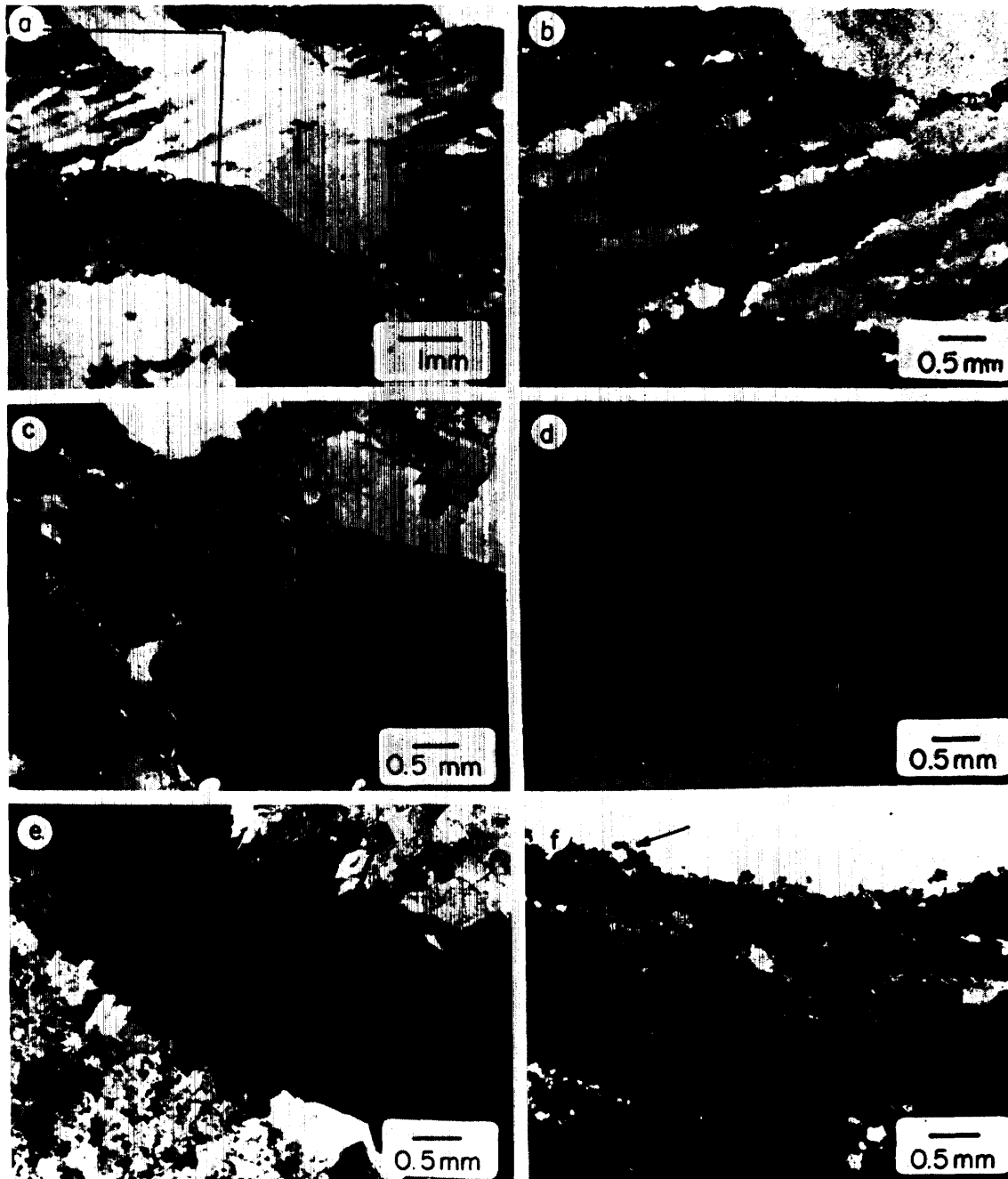


Figure 4—Dome Mine, Timmins. **a,b.** Quartz-ankerite vein, 1200 level. Elongate subgrains are forming within the large quartz crystals. Note the initiation of dynamic recrystallization which is healing transgranular fractures and closing grain boundaries (arrows.) **c,d.** "Dacite ore", 1200 level. Quartz records minor strain seen as undulatory extinction. Grain boundaries and transgranular fractures are outlined by seams of mica and traces of sulphides. **e.** Late "mottled quartz" veinlet in ankerite layer, 1200 level. Note growth rings in quartz outlined by concentric layers of fluid inclusions. The quartz is totally undeformed. **f.** "Conglomerate ore" vein stockwork, 1257 stope. Note the comb structure preserved in the large quartz crystal. Small fractures are healing due to recrystallization, and recrystallization as a result of grain boundary migration (bulging) is seen at the upper contact (arrow).

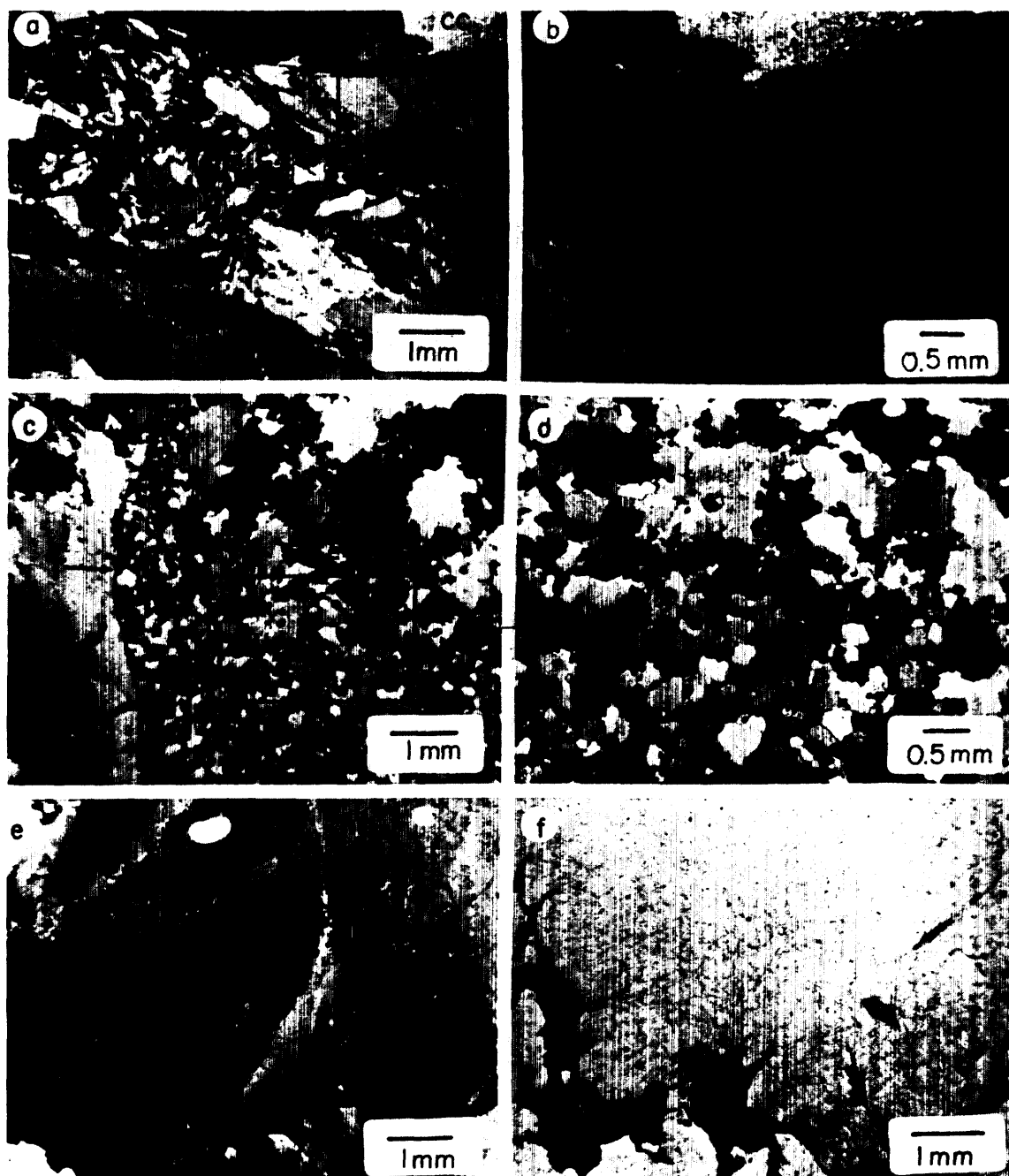


Figure 5—Dome Mine, Timmins. **a,b.** "Conglomerate ore" vein stockwork, 1257 stope. Quartz records the effects of brittle fracturing and brecciation, with transgranular fractures veined by auriferous pyrite. **c,d.** Quartz-tourmaline vein, 1220 stope. Tectonic grain-size reduction and dynamic recrystallization (note the approach to an equilibrium foam texture) to the right of the tourmaline layer (t). The tourmaline layer has preserved an "augen" of low deformation in quartz at the left extremity of (c). **e,f.** Quartz vein from the margin of the Preston Porphyry, 1200 level. Pyrite and native gold filling fractures in quartz. Crossed nicols (e) and plane light (f).

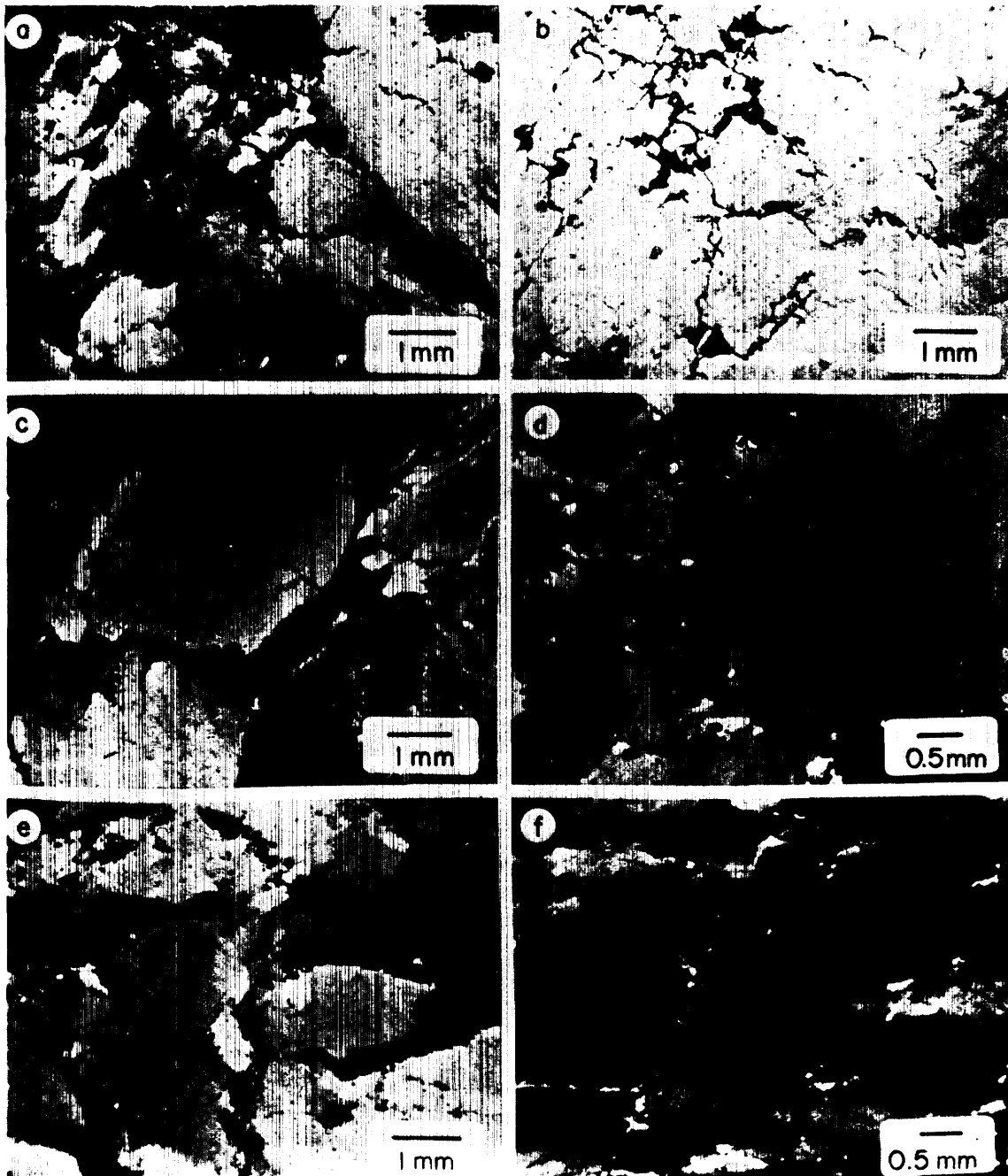


Figure 6—Dome Mine, Timmins. **a,b,c.** Quartz vein from the margin of the Preston Porphyry, 1200 level. Native gold and minor pyrite along transgranular fractures and grain boundaries in quartz. (a) and (b) are crossed nicols and plane light for the same field of view. **d,e.** Barren "mottled quartz" veins in the Preston Porphyry, 1200 level. Note the clean interlocking and sutured grain boundaries. In (d) the large quartz crystal is unfractured, whereas (e) records the effects of incipient recrystallization along clean grain boundaries. **f.** Quartz/tourmaline vein in highly-altered (HA) zone, 1200 level. The large quartz crystals are highly strained and developing a subgrain structure. Transgranular fractures (arrows) are partially healed.

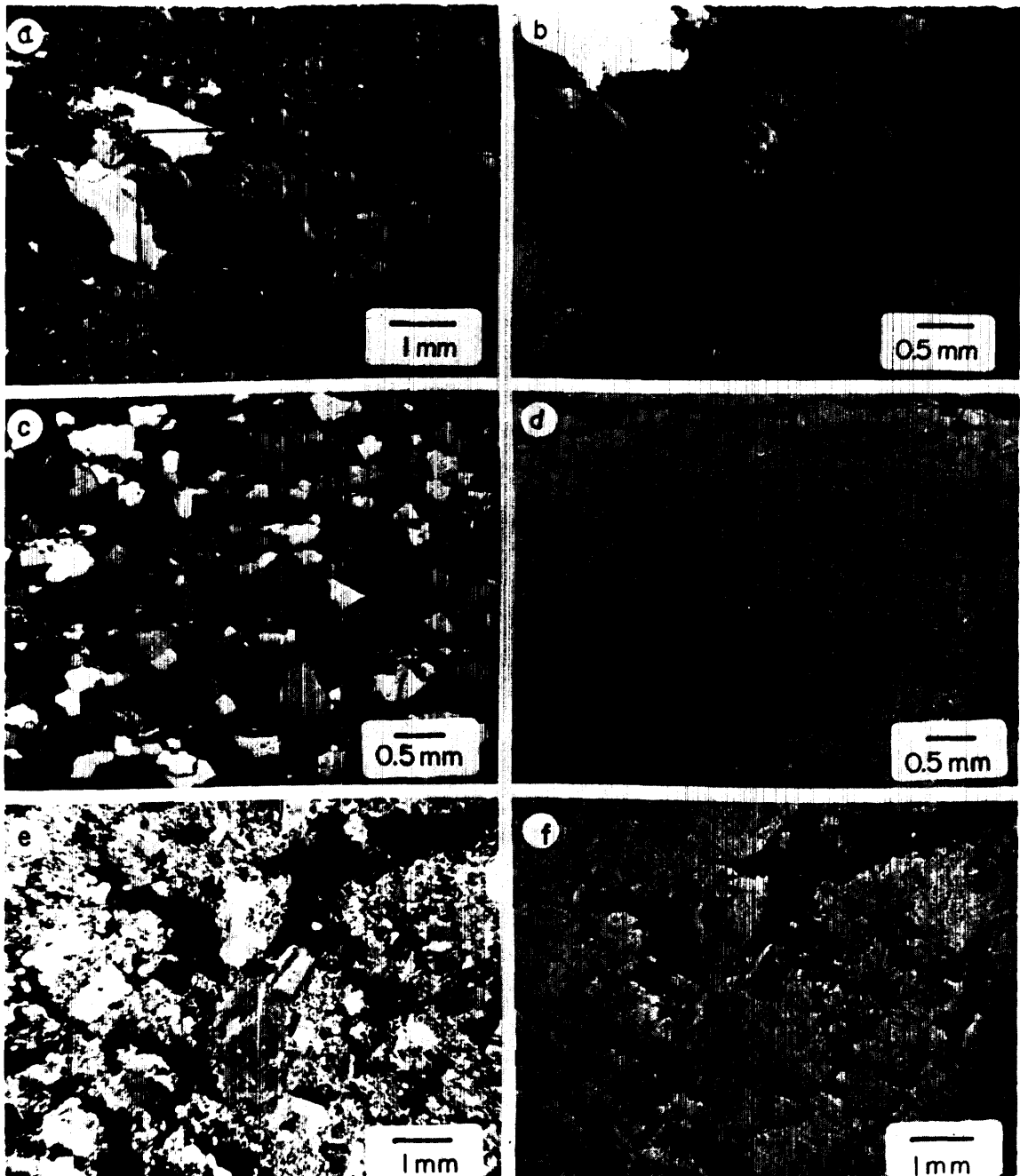


Figure 7—Gauthier Township, Larder Lake. **a,b.** Quartz vein in “dolomite” along Larder Lake Break. Quartz crystals are being replaced by a mosaic of elongate subgrains, likely bounded by fractures. These fractures (arrow) are filled with fine-grained fuchsite and carbonate. Au, 100 ppb.
 Kaladar Township, Hastings-Madoc area. **c,d.** Quartz lenses in biotite quartzite of the Flinton Group. Amphibolite-facies metamorphism is recorded by the assemblage biotite/staurolite/quartz. The quartz has recrystallized to an equilibrium foam texture. The layers consist of biotite and pyrite, which have acted to retain gold. This rock assays 2.26 ounces Au per ton.
 Schumacher (McIntyre) Mine, Timmins. **e,f.** Pearl Lake Porphyry adjacent to copper zone, 3375 level. Brittle fractures in albitized porphyry are filled by pyrite and chalcopyrite.

REFERENCES

- Adams, S. F.
1920: A microscopic study of vein quartz; *Econ. Geol.* Vol. 15, p.623-664.
- Allen, C. C. and Folinsbee, R. E.
1944: Scheelite veins related to porphyry intrusives, Hollinger Mine; *Econ. Geol.* Vol. 39, p.340-348.
- Armstrong, H. S.
1943: Gold ores of the Little Long Lac area. Ontario; *Econ. Geol.* Vol. 38, p.204-252.
- Atkinson, B. K.
1975: Experimental deformation of polycrystalline pyrite: effects of temperature, confining pressure, strain rate, and porosity; *Econ. Geol.* Vol. 70, p.473-487.
- 1976: The temperature and strain rate dependent mechanical behavior of a polycrystalline galena ore; *Econ. Geol.* Vol. 71, p.513-525.
- Bain, G. W.
1933: Wall-rock mineralization along Ontario gold deposits; *Econ. Geol.* Vol. 28, p.705-743.
- Bateman, J. D.
1940: Geology and gold deposits of the Uchi-Slate Lakes area; Ontario Dept. Mines, Ann. Rept. Vol. 48, Pt.8, p.1-43.
- Bevington, P. R.
1969: *Data Reduction and Error Analysis for the Physical Sciences*; McGraw-Hill Book Company, New York, 336p.
- Bruce, E. L.
1933: *Mineral Deposits of the Canadian Shield*; Macmillan Co., Toronto.
1935: Little Long Lac gold area; Ontario Dept. Mines, Ann. Rept. Vol. 44, Pt.3, 60p.
1942: Geology of the Goudreau-Lochalsh area, Algoma District; Ontario Department Mines, Annual Report, Vol. 49, Pt.3.
- Burrows, A. A.
1924: The Porcupine gold area; Ontario Dept. Mines, Ann. Rept. Vol. 33, Pt.2, 112p.
- Campiglio, C.
1977: Bourlamaque batholith; *Ministere des Richesses Naturelles du Quebec, Etude Speciale 26*, 211p.
- Charlewood, G. H.
1935: The nature and occurrence of carbonates on veins; *Econ. Geol.* Vol. 30, p.502-517.
- Chatterjee, N. D.
1973: Low-temperature compatibility relations of the assemblage quartz-paragonite and the thermodynamic status of the phase rectorite; *Contrib. Mineral. Petrol.* Vol. 42, p.259-271.
- Clark, B. R. and Kelly, W. C.
1973: Sulphide deformation studies: I. Experimental deformation of pyrrhotite and sphalerite to 2000 bars and 500°C; *Econ. Geol.* Vol. 68, p.332-352.
- David, M., Dagbert, M., and Beauchemin, Y.
1977: Statistical analysis in geology: correspondence analysis; *Quarterly of the Colorado School of Mines*, Vol. 72, No. 1, 60p.
- Davies, J. F. and Luhta, L. E.
1978: An Archean "porphyry-type" disseminated copper deposit, Timmins, Ontario; *Econ. Geol.* Vol. 73, p.383-396.
- Dobretsov, N. L., Khlestov, V. V. and Sobolev, V. S.
1973: The Facies of Regional Metamorphism at Moderate Pressures; D. A. Brown, trans. Canberra: Australian National University, 297p.
- Dougherty, E. Y.
1925: Mode of formation of the Porcupine quartz veins; *Econ. Geol.* Vol. 20, p.660-670.
- Dyer, W. S.
1936: Geology and ore deposits of the Matachewan-Kenogami area; Ontario Dept. Mines, Ann. Rept. Vol. 44, Pt.2, p.1-55.
- Eugster, H. P. and Skippen, G. B.
1967: *Igneous and Metamorphic Reactions involving Gas Equilibria*; in P. H. Abelson, Editor, *Researches in Geochemistry*, Vol. 2, Wiley: New York, 492p.
- Evans, J.E.L.
1944: Porphyry of the Porcupine district, Ontario; *Geol. Soc. America, Bull.* Vol. 55, p.1115-1142.
- Ferguson, H. G. and Gannett, R. W.
1932: Gold quartz veins of the Alleghany District, California; United States Geological Survey, Professional Paper 172, 139p.
- Ferguson, S. A. and associated geologists
1968: Geology and ore deposits of Tisdale Township, District of Cochrane; Ontario Department of Mines, Geological Report 58, 177p.
- Frohberg, M. H.
1935: The ore deposits of the Michipicoten area; Ontario Dept. Mines, Ann. Rept. Vol. 44, Pt.8, p.39-83.
- Fyfe, W. S. and Lonsdale, P.
in press: Ocean floor hydrothermal activity.
- Fyfe, W. S. Price, N. J. and Thompson, A. B.
1978: *Fluids in the Earth's crust*; Elsevier, Amsterdam, 383p.
- Gallagher, D.
1940: Albite and gold; *Econ. Geol.* Vol. 35, p.698-736.
- Gorman, B. E.
1980: The Application of Factor Analysis and Quartz Microstructures to Gold Exploration in Felsic Igneous Intrusions; in *Geoscience Research Abstracts*, edited by E. G. Pye, Ontario Geol. Surv., 21p.
- Graton, L. C., McKinstry, H. E. and others
1933: Outstanding features of Hollinger geology; *Canadian Inst. Min. Met., Bull.* 249.
- Gustafson, J. K.
1945: The Porcupine porphyries; *Econ. Geol.* Vol. 40, p.148-152.
- Helgeson, H. C.
1974: Chemical interactions of feldspars and aqueous solutions; p.184-217 in W. S. MacKenzie and J. Zussman, Editors, *The Feldspars*, Manchester University Press.
- Hobbs, B. E., McLaren, A. C. and Paterson, M. S.
1972: Plasticity of Single Crystals of Synthetic Quartz; in H. C. Heard and others, Editors, *Flow and Fracture of Rocks*, American Geophys. Union, Monograph, Ser. 16.
- Horwood, H. C.
1938a: Geology of the Casummit Lake area and the Argosy Mine; Ontario Dept. Mines, Ann. Rept. Vol. 46, Pt.7, 33p.
1938b: Geology of the Superior Junction - Sturgeon Lake Area, Kenora District; Ontario Department of Mines, Annual Report, Vol. 46, part b, p.1-25.
- Horwood, H. C. and Pye, E. G.
1955: Geology of Ashmore Township; Ontario Dept. Mines, Ann. Rept. Vol. 60, Pt.5, 105p.
- Hulin, C. D.
1929: Structural controls of ore deposition; *Econ. Geol.* Vol. 24, p.15-49.
- Hurst, M. E.
1935: Vein formation at Porcupine, Ontario; *Econ. Geol.* Vol. 30, p.103-127.
1936: Gold deposits in the vicinity of Red Lake; Ontario Dept. Mines, Ann. Rept. Vol. 44, Pt.6, p.1-52.

GRANT 56 PART A PORPHYRIES OF THE TIMMINS DISTRICT

- Kelly, W. C. and Clark, B. R.
1975: Sulfide deformation studies. III. Experimental deformation of chalcopyrite to 2000 bars and 500°C; *Econ. Geol.* Vol. 70, p.431-453.
- Kerrich, R., Gorman, B. E., and Fyfe, W. S.
1980: Geochemistry and field relations of lode gold deposits in felsic igneous intrusions; p.136-141 in E.G. Pye, Editor, *Geoscience Research Grant Program, Summary of Research 1979-1980*, Ontario Geol. Surv., Miscellaneous Paper 93.
- Keys, M. R.
1940: Paragenesis in the Hollinger veins; *Econ. Geol.* Vol. 35, p.611-628.
- Langford, G. B. and Hancox, E. G.
1936: Hypogene anhydrite from McIntyre Mine, Porcupine District, Ontario; *Econ. Geol.* Vol. 31, p.600-610.
- Lowder, G. G. and Dow, J.A.S.
1978: Geology and exploration of porphyry copper deposits in North Sulawesi, Indonesia; *Econ. Geol.* Vol. 73, p.628-644.
- McKinstry, H. E. and Ohle, E. L., Jr.
1949: Ribbon structure in gold-quartz veins; *Econ. Geol.* Vol. 44, p.87-109.
- Orville, P. M.
1963: Alkali ion exchange between vapour and feldspar phases; *American Jour. Sci.* Vol. 261, p.201-237.
1972: Plagioclase cation exchange equilibria with aqueous chloride solution: results at 700°C and 2000 bars in the presence of quartz; *American Jour. Sci.* Vol. 272, p.234-272.
- Pearce, T. H.
1968: A contribution to the theory of variation diagrams; *Contrib. Mineral. Petrol.* Vol. 19, p.142-157.
- Pye, E. G.
1952: Geology of Errington Townships, Little Long Lac area; Ontario Dept. Mines, Ann. Rept. Vol. 60, Pt.6, 140p.
- Roscoe, W. E.
1975: Experimental deformation of natural chalcopyrite at temperatures up to 300°C over the strain rate range of 10^{-2} to 10^{-6} sec⁻¹; *Econ. Geol.* Vol. 70, p.454-472.
- Salmon, B. C., Clark, B. R., and Kelly, W. C.
1974: Sulfide deformation studies. II. Experimental deformation of galena to 2000 bars and 400°C; *Econ. Geol.* Vol. 69, p.1-16.
- Stone, J. B.
1937: The structural environment of the Bendigo goldfield; *Econ. Geol.* Vol. 32, p.867-895.
- Summers, R., Winkler, K., and Byerlee, J.
1978: Permeability changes during the flow of water through westerly granite at temperatures of 100°-400°C; *Jour. Geophys. Res.* Vol. 83, p.339-344.
- Thomson, J. E.
1934: Geology of the Straw-Manitou Lakes area; Ontario Dept. Mines, Ann. Rept. Vol. 43, Pt.4, 32p.
1936: Gold deposits on the Lake of the Woods; Ontario Dept. Mines, Ann. Rept. Vol. 44, Pt.4, p.29-47.
1937: Geology of the North Central part of the Lake of the Woods; Ontario Dept. Mines, Ann. Rept. Vol. 45, Pt.3, p.1-43.
- Thomson, J. E., Charlewood, G. H., Griffin, K., Hawley, J. E., Hopkins, H., MacIntosh, C. G., Ogrizlo, S. P., Perry, O. S., and Ward, W.
1950: Geology of the main ore zone at Kirkland Lake; Ontario Dept. Mines, Ann. Rept. Vol. 577, Pt.5, p.54-188.
- Tomasson, J. and Kristmannsdottir, H.
1972: High-temperature alteration minerals and thermal brines, Reykjanes, Iceland; *Contrib. Mineral. Petrol.* Vol. 36, p.123-134.
- Trimmer, D., Bonner, B., Heard, H. C. and Duba, A.
1980: Effects of pressure and stress on water transport in intact and fractured gabbro and granite; *Jour. Geophys. Res.* Vol. 85, p.7059-7071.
- Tullis, J. and Yund, R. A.
1977: Experimental deformation of dry westerly granite; *Jour. Geophys. Res.* Vol. 82, p.5705-5718.
- Turner, F. J.
1981: *Metamorphic Petrology: Mineralogical, Field and Tectonic Aspects*; 2nd edition, McGraw-Hill Book Company, New York, 524p.
- White, W. H.
1943: The mechanism and environment of gold deposition in veins; *Econ. Geol.* Vol. 38, p.512-532.
- Wintsch, R. P.
1975: Solid-fluid equilibria in the system $\text{KAlSi}_3\text{O}_8\text{-NaAlSi}_3\text{O}_8\text{-Al}_2\text{SiO}_5\text{-H}_2\text{O-HCl}$; *Jour. Petrol.* Vol. 16, p.57-79.
- Zoback, M. D. and Byerlee, J. D.
1975: The effect of microcrack dilatancy on the permeability of westerly granite; *Jour. Geophys. Res.* Vol. 80, p.752-755.

Grant 76 Speciation of Free Gold in Glacial Overburden

D.L. Guindon and I. Nichol

Department of Geological Sciences, Queen's University

ABSTRACT

The investigation is designed to 1) test the hypothesis that gold particles from varying types of mineralization contain distinct suites of trace elements, 2) determine if gold grains maintain their diagnostic trace element assemblage in overburden, and 3) evaluate the feasibility of distinguishing the provenance of gold on the basis of element associations as an exploration guide.

Previous investigations have concluded that regional variations in trace element content exist and that gold from a metallogenic province or zone has a characteristic assemblage. Information regarding variations due to vein type differences within a metallogenic province is not available.

Analyses of gold grains from 18 mines are summarized. In most cases, species of gold cannot be recognized simply by the presence or absence of certain trace elements, but gold from different vein types can be identified by discriminant-function analysis of the trace element contents. Further analyses of gold from mineralized veins and from overburden are required to support the findings to date.

INTRODUCTION

The investigation is designed to 1) test the hypothesis that gold particles from varying types of mineralized veins contain distinct suites of trace elements, 2) determine if gold grains maintain their diagnostic suite of trace elements in overburden, and 3) evaluate the feasibility of distinguishing the provenance of gold on the basis of element associations as an exploration guide.

Samples were collected from producing and past producing mines as well as several mineral prospects in the Larder Lake, Kirkland Lake, Matheson, Timmins, and Matachewan areas of northeastern Ontario. Samples were classified in the field according to the vein material: quartz, quartz-carbonate, quartz-green carbonate (containing fuchsite), quartz-albite, pyrite-mafic volcanic rock, and graphite. Different vein types were collected in each area to determine if regional variation as well as vein type variation occurs.

PREVIOUS WORK

Original work by Warren and Thompson (1944), using emission spectrography to investigate the application of

gold as a pathfinder for other metals, demonstrated the presence of trace elements in gold grains. A large suite of elements, Ag, Cu, Fe, Mn, V, Ti, Pb, Bi, Te, As, Sb, Zn, Cd, Sn, Pd and Pt were found to be present in gold grains from different areas. Other elements reported by these workers, Si, Ca, Al, Mg and Na, were attributed to minerals derived from the gangue, presumably within or adhering to the gold grains. They concluded that variations in the content and assemblage of trace elements is controlled by metallogenic provinces rather than deposit types. Brief consideration was given to the contribution to the trace element suite by mineral inclusions in the gold. It was concluded that in general trace elements could be correlated with other minerals known to be present in the ore although there were exceptions.

Steele and Carlton (1961, *in* Gay 1963) analysed samples of visible gold from the Barberton Mountain Land of South Africa using a spectrographic technique. Their results as well as others reported in Gay (1963) confirmed the conclusions reached by Warren and Thompson (1944).

Sakharova (1969) demonstrated that the composition of gold grains could be influenced by the metal content of adjacent minerals. Using an electron microprobe, he showed that Fe and Cu diffused 3 to 12 μm into gold from metallic minerals in contact with the gold. Sakharova's statement that Te, Sb and As do not diffuse into the gold may be a result of the relatively high detection limits for these elements. It is noteworthy that the mineral inclusions in or on gold grains may provide a source for trace elements that subsequently migrate into the gold after its deposition.

Gay (1964) completed a regional study of gold in the Barberton Mountain Land, South Africa, as well as a detailed study of the Zwarkopji shoot of the Sheba Mine. Trace elements were determined by atomic absorption or by spectrographic analyses. He concluded that Al, Ca, Mg and Si are present as mineral impurities, that Be, Bi, Co, Mn, Hg, Mo, Pd, Pt, Ag, Sn and V are in solid solution with the gold, and that Sb, Cu, Fe, Pb, Ni, Ti and Zn may be present either in the gold lattice or as mineral inclusions. The composition of gold will depend largely on local conditions prevailing at the time of deposition (Gay 1964). The pressure and temperature may be assumed to control the fineness* but local conditions, such as concentration of Ag and minor elements in the ore fluids, the mineralogical environment, and the nature of the wall

*Fineness = $\text{Au}/(\text{Au} + \text{Ag}) \times 1000$.

rock, will affect the composition of the gold at a particular point. Gold samples with high Cu contain chalcopyrite, gold samples with Sb are rich in stibnite. These conclusions tend to support the conclusions of Warren and Thompson (1944).

Denisov *et al.* (1966) spectrographically analysed samples from lode and placer sources in the Amur region of the USSR. They concluded that characteristic trace element assemblages are present in gold from different sources in this area. Gold from hypothermal zones contains Bi, As, Pd and Cu, and has Cu and Pb content two to three times greater than that of epithermal areas. Mesothermal and epithermal regions contain Sb and Zn, but the epithermal regions are characterized by the absence of As and Bi.

Antweiler and Sutton (1970) spectrographically detected Ag, Cu, Fe and Ti most often in gold samples; Pb, Pd, Bi, V, Ni and Co were found to be accessories in lode deposits, and Ti, Zr, La, Y and Cr in placer deposits.

Antweiler and Campbell (1977) applied a method involving panning and hand sorting to concentrate gold grains. Using the emission spectrographic method of Mosier (1975), gold grains were placed in carbon electrodes and packed with an aluminum oxide flux prior to ignition. They detected As, Bi, Cd, Co, Cr, Mo, Ni, Pb, Pd, Pt, Sb, Sn, Te, W and Zn. Detection limits for the method were commonly less than 20 ppm and some were less than 100 ppm. They concluded that 1) hypothermal deposits contain low concentrations of Ag and high Cu and As together with Bi, Ni and Pb, 2) mesothermal deposits have Cu, Bi and Pb as trace elements, 3) epithermal deposits have high Ag, along with Cu, Pb and Sb as characteristic trace elements, and 4) gold from porphyry Cu deposits contain Pb, Bi, Sb and Zn. These assemblages are similar to those determined by Denisov *et al.* (1966). Gold signatures from deposits of ambiguous hypothermal-epithermal classification were also ambiguous.

Gold signatures may be used to search for the sources of placer gold. Denisov *et al.* (1966) detected an increased fineness of gold in placer deposits with distance from bedrock source, along with a decrease in trace element content. They explain this by leaching and the loss of minerals which occur as inclusions in the gold. A well documented example was described by Antweiler and Campbell (1977) who related placer gold to its source area in the Tarryall district of Colorado. In the Tarryall district, placer gold averaged 9.1 percent Ag. Samples collected by Antweiler and Campbell (1977) ranged from 4.3 percent to 19.9 percent Ag, but from the most productive areas, Ag concentration was 9-10 percent. Early prospectors were unable to locate significant amounts of gold in bedrock, partly due to poor outcrop as a result of glaciation and landslide. Antweiler and Campbell sampled old prospects and areas recently exposed by road construction. Special attention was given to sampling ground about a granitic intrusive stock. Several areas were located which had apparently been little prospected in the past yet yielded gold of the composition found in the productive placers. Following Warren and Thompson's (1944) proposition that gold could be used

as a pathfinder mineral for other metals, Antweiler and Campbell (1977) found platinum group metals in gold from the New Rambler platinum mine in Wyoming, and found Sn, W and Mo in gold panned downstream from the Urad molybdenum mine in Colorado.

To date, very limited trace element composition data for gold have been obtained from Ontario (Boyle 1979) and efforts to apply the available information in prospecting appear minimal. Detailed studies to determine if differences exist in the trace element composition of gold from different vein types in one area have not been attempted.

SAMPLE PREPARATION AND ANALYSES

Polished sections of hand samples were prepared, and gold grains were located using a reflected-light microscope and marked. We suspected that the top microlayer of the gold would be affected by smearing and inclusions entrapped in polishing. A simple test was devised to confirm the need for further preparation. A grain mount of 99.999 percent gold and 99.999 silver was prepared and analysed. The grains were about 0.5 mm in diameter and were located about 3 mm apart. The gold analysed 0.5 weight percent silver and the silver up to 2.0 weight percent gold. The sample was then etched in an aqueous solution of 3 percent potassium cyanide and 3 percent ammonium persulphate for 2 minutes, rinsed in water, and finally cleaned using an ultrasonic bath. The respective grains analysed 100 percent Au and 100 percent Ag after treatment, indicating the disturbed layer had been removed. As revealed by a reflected light microscope, the etch uncovered the crystallographic structure of the gold and the roughening of the surface had no apparent effect on the analyses.

For this project, the best analytical tool appears to be the electron microprobe so that lattice-held trace elements and mineral inclusions can be studied independently. The electron microprobe operates in two modes. "Energy dispersive analysis" provides a multi-element analysis with poor detection limits, and "wavelength dispersive analysis" obtains individual element analyses with better detection limits. In the past, analyses of gold by Viljoen (1971), Desborough (1970) and others have been limited to the determination of Ag, Cu and Fe as trace elements probably due to high detection limits. This problem has now been overcome to a great extent.

The conditions for analyses, count times for peak and background and detection limits are listed in Table 1. Detection limits (D.L.) were calculated for the worst case using the formula given in Table 1.

DISCUSSION OF RESULTS

Minimum, maximum and mean values for 10 trace elements and the fineness of the associated gold grains are

Table 1—Conditions for analyses of trace elements in gold grains, by electron microprobe.

Beam Current 100 nA		20 KeV	
Count Time (sec.)			
Element	Peak	Background	Detection Limits wt % *
Cu	50	C	0.013
Ni	30	C	0.013
Fe	30	C	0.010
Co	110	C	0.006
Au	30	10	--
Hg	30	C	0.025
Pb	30	C	0.016
Pd	30	C	0.013
Ag	30	10	--
Sb	30	C	0.012
Zn	50	C	0.010
As	170	C	0.004

C - background corrected for fineness

* - detection limit calculated by

$$D.L. = \frac{\% \text{ concentration of standard} \times 2 \sqrt{\text{background counts}}}{\text{peak counts}}$$

listed in Table 2. The table is arranged so that the data for each vein type is followed by the data for each mine in the vein type for ease of comparison. Heavy minerals identified in polished section are also listed.

A number of aspects are apparent. 1) There is apparently little correlation between heavy minerals in the sample and the trace element composition of the gold, for example the Timmins quartz veins contain galena, yet have approximately the same average content of Pb as the Canadian Arrow Mine where no Pb minerals were identified. 2) On the basis of a simple visual inspection of the data, most vein types cannot be distinguished by the presence or absence of one or more elements. Some can: e.g., the Canadian Arrow Mine is the only mine with Cu below detection limits in all case. 3) Within a mine, one analysis may have a disproportionate effect on the mean abundance of an element, e.g., in the Ross Mine, for 13 analyses the mean Fe content is 1.227 but for 12 analyses the mean is 0.497. This may be due to undetected

mineral inclusions in the gold or to analytic problems caused by interference from surrounding minerals in the case of <10 μ m diameter grains.

The majority of the vein types cannot be easily separated on the basis of elements present or absent; therefore another technique of interpretation is required. The method chosen is discriminant-function analysis (Klovan and Billings 1967). In brief, this is a statistical method to determine a function which best separates previously established groups. The discriminant function is established by comparing the abundances of each element in samples representing each group. The function is then tested by using it to classify each sample. The number of correctly identified samples is a measure of the effectiveness of the discrimination.

To avoid a bias in the results, gold, silver and hence fineness were not considered in the calculations since the silver content may be dependent on temperature-pressure conditions during formation and thus may vary

GRANT 76 SPECIATION OF FREE GOLD IN GLACIAL OVERBURDEN

Table 2—Summary of electron probe analyses of gold grains, arranged by vein type and mine (or deposit). Average of 3 analyses per grain. Analyses below detection limits were assigned a value of half the detection limit for calculation of the mean.

Mine	No. Samples	No. Analyses	Value	Cu	Ni	Fe	Co	Hg	Pb	Pd	Sb	Zn	As	Fin	Associated Heavy Minerals
Larder Lake Quartz Green Carbonate															
average	4	47	min	<.013	<.013	<.010	<.006	.058	<.016	<.013	<.012	<.010	<.004		
			max	.487	.018	.133	<.006	.447	.395	.033	.033	.075	.041		
			mean	.077	.007	.011	.003	.284	.021	.012	.008	.021	.021		
Davey Lowe	1	12	min	.058	<.013	<.010	<.006	.058	<.016	<.012	<.012	<.010	.015	950	Pyrite
			max	.086	<.013	<.010	<.006	.128	.026	.033	.033	.044	.041	952	
			mean	.074	.007	.005	.003	.094	.017	.020	.013	.022	.030	951	
Martin Bird	1	13	min	<.013	<.013	<.010	<.006	.150	<.016	<.013	<.012	<.010	<.004	943	
			max	.091	.018	.133	<.006	.401	.046	.021	<.012	.046	.041	956	
			mean	.040	.007	.022	.003	.321	.012	.010	.006	.018	.017	946	
Kerr Addison	2	22	min	.048	<.013	<.010	<.006	.229	<.016	<.013	<.012	<.010	<.004	939	Pyrite, chalcopyrite
			max	.487	<.013	.034	<.006	.447	.395	.025	.021	.075	.038	950	
			mean	.100	.007	.007	.003	.365	.028	.009	.007	.022	.019	944	
Kirkland Lake Quartz															
average	8	61	min	<.013	<.013	<.010	<.006	<.025	<.016	<.013	<.012	<.010	<.004		
			max	.087	.014	.173	.011	1.740	4.964	.265	.037	.042	.061		
			mean	.032	.007	.018	.003	.198	.179	.013	.009	.013	.017		
Lakeshore	1	13	min	<.013	<.013	<.010	<.006	.029	<.016	<.013	<.012	<.010	<.004	937	Pyrite
			max	.059	<.013	<.010	.008	<.116	<.016	.019	<.012	.040	.033	951	
			mean	.028	.007	.005	.004	.077	.008	.010	.006	.015	.020	947	
Toburn	3	17	min	<.013	<.013	<.010	<.006	<.025	<.016	<.013	<.012	<.010	<.004	942	Pyrite, altaite, melonite
			max	.079	.014	<.010	.011	.098	.223	.021	<.012	.022	.034	954	
			mean	.045	.007	.005	.004	.048	.037	.008	.006	.008	.013	949	
Macassa	2	17	min	<.013	<.013	<.010	<.006	<.025	<.016	<.013	<.012	<.010	<.004	931	Pyrite, altaite
			max	.087	<.013	.075	.008	1.155	4.964	.265	.017	.042	.044	948	
			mean	.035	.007	.020	.003	.110	.521	.022	.008	.019	.022	940	
Baldwin Consolidated	2	14	min	<.013	<.013	<.010	<.006	.052	<.016	<.013	<.012	<.010	<.004	901	Pyrite, altaite, calaverite
			max	.065	<.013	.173	<.006	1.740	.566	.032	.037	.030	.061	926	
			mean	.018	.007	.044	.003	.598	.097	.011	.015	.010	.031	914	
Timmins Quartz															
average	5	96	min	<.013	<.013	<.010	<.006	<.025	<.016	<.013	<.012	<.010	<.004		
			max	.047	.025	.626	.009	.131	1.818	.036	.024	.071	0.046		
			mean	.018	.007	.026	.003	.048	.041	.010	.007	.029	.030		
McIntyre	1	20	min	<.013	<.013	<.010	<.006	<.025	<.016	<.013	<.012	<.010	<.004	899	Galena, pyrite
			max	.037	.013	.626	.007	.078	.087	.036	.012	.060	.046	902	
			mean	.014	.007	.040	.003	.037	.040	.012	.006	.026	.029	900	
Hollinger	3	61	min	<.013	<.013	<.010	<.006	<.025	<.016	<.013	<.012	<.010	<.004	893	Galena, sphalerite pyrite
			max	.029	.025	.125	.009	.131	1.818	.024	<.012	.071	0.046	905	
			mean	.016	.007	.024	.003	.047	.047	.009	.006	.033	.030	900	
Dome	1	15	min	<.013	<.013	<.010	<.006	.039	<.016	<.013	<.012	<.010	<.004	920	
			max	.047	<.013	.067	<.006	.084	.035	.016	.024	.031	.035	926	
			mean	.026	.007	.013	.003	.064	.015	.010	.009	.016	.021	923	
Larder Lake Pyrite-Mafic Volcanic															
average	3	18	min	<.013	<.013	.392	<.006	.137	<.016	<.013	<.012	<.010	<.004		
			max	.798	.026	8.698	.008	.580	.048	.026	.014	.051	.052		
			mean	.099	.009	1.681	.003	.408	.012	.009	.006	.022	.037		
Barber Larder	1	4	min	<.013	<.013	.392	<.006	.499	<.016	<.013	<.012	<.010	.029	890	Pyrite, chalcopyrite
			max	.173	<.013	2.286	<.006	.580	.022	<.013	<.012	<.010	.047	901	
			mean	.077	.007	1.002	.003	.536	.012	.007	.006	.005	.036	898	
Kerr Addison	2	14	min	<.013	<.013	.788	<.006	.137	<.016	<.013	<.012	<.010	<.004	908	Pyrite, chalcopyrite
			max	.798	.026	8.698	.008	.477	.048	.026	.014	.051	.052	936	
			mean	.105	.010	1.876	.004	.372	.012	.010	.007	.027	.037	918	
Pamour Quartz-Carbonate															
Pamour	2	14	min	<.013	<.013	.076	<.006	.076	<.016	<.013	<.012	<.010	<.004	923	Pyrite
			max	.026	<.013	.941	.006	.228	.073	.026	.018	3.097	.028	939	
			mean	.009	.007	.282	.003	.114	.019	.011	.009	.287	.012	932	
Canadian Arrow Quartz															
Canadian Arrow	1	7	min	<.013	<.013	1.368	<.006	<.025	.019	<.013	<.012	<.010	.021	713	Pyrite, chalcopyrite
			max	<.013	<.013	8.480	<.006	.201	.069	.050	<.012	.080	.071	886	
			mean	.007	.007	3.013	.003	.080	.044	.017	.006	.041	.047	799	
Ross Quartz Carbonate															
Ross	2	13	min	<.013	<.013	.205	<.006	<.025	<.016	<.013	<.012	<.010	<.004	616	Pyrite, chalcopyrite
			max	.220	<.013	9.999	<.006	.157	.089	.022	.077	.093	.248	710	tenanite, native silver
			mean	.040	.007	1.227	.003	.072	.016	.008	.014	.042	.051	658	
Quartz-Albite															
average	3	17	min	<.013	<.013	.246	<.006	<.025	<.016	<.013	<.012	<.010	.012		
			max	1.063	<.013	4.191	<.006	.378	.037	.024	.030	.036	.031		
			mean	.196	.007	1.146	.003	.133	.015	.013	.007	.021	.022		
Buffonta	1	11	min	.039	<.013	.246	<.006	<.025	<.016	<.013	<.012	<.010	.023	938	Pyrite
			max	.087	<.013	4.191	<.006	.029	.037	.024	.030	.036	.031	955	
			mean	.060	.007	1.046	.003	.017	.018	.016	.008	.025	.026	948	
Kerr Addison	2	6	min	<.013	<.013	1.139	<.006	.316	<.016	<.013	<.012	<.010	.012	929	Pyrite, chalcopyrite
			max	1.063	<.013	1.657	<.006	.378	<.016	<.013	<.012	.036	.024	936	
			mean	.444	.007	1.329	.003	.347	.008	.007	.006	.014	.016	932	
Moffat Hall Unknown Vein type															
Moffat Hall	1	8	min	<.013	<.013	<.010	<.006	.033	<.016	<.013	<.012	<.010	.016	924	
			max	.057	<.013	<.010	<.006	.132	.051	.030	.013	.032	.054	943	
			mean	.037	.007	.005	.003	.075	.021	.014	.007	.013	.033	931	

Table 3—Discriminant-function analysis of trace element abundances in gold grains. The pairs of numbers are percentages of samples correctly classified for each vein type when compared with another vein type (see text). The elements listed are those that contribute most to the discrimination. The small number of samples in some groups greatly affects the percentage classified.

	Kirkland Quartz	Timmins Quartz	Larder Pyrite	Pamour Qtz-Carb	Can. Arrow Quartz	Ross Qtz-Carb	Quartz- Albite
Larder Qtz-G. Carb	70/87 Cu,Zn,Co,Hg	83/100 Hg,Pd,Cu,Zn	100/100 Fe,As,Hg	100/93 Fe,Hg,As	100/86 Fe,As	100/100 Hg,Pd,As,Fe	100/77 Fe,Hg
Kirkland Quartz		71/93 Zn,Cu,Hg,Pb	98/94 Fe,As,Hg,Pd	100/50 Fe,Cu,Zn,Hg,Pb,Pd	100/86 Fe,Zn	100/54 Zn	100/71 Fe,Cu,Hg
Timmins Quartz			100/100 Hg,Fe	99/79 Hg,Fe,Zn,Ni	100/86 Hg,Pb	100/23 Fe,Cu	100/71 Fe,Cu,Pd, Zn,Sb
Larder Pyrite				100/100 Hg,Fe,As	100/100 Hg,Pb	100/100 Hg,Zn	89/100 Hg,As,Fe
Pamour					100/100 As,Fe	100/77 Hg,Fe,As	93/94 As,Fe,Cu
Can. Arrow						100/100 Pb,Pd,Zn,Fe,Hg	100/100 As,Fe,Zn
Ross							92/94 Zr,Pd,Hg,Fe

with depth in the same vein as suggested by Gay (1964). All other elements were given equal priority to enter into the sequence of calculations which determines the discriminant function. The probability of a sample being assigned to a particular group during the second stage of the analysis was equal to the proportion of samples originally defined as belonging to that group. Vein types were compared in pairs to maximize the discrimination, e.g. Larder Lake quartz-green carbonate vs. Kirkland Lake quartz, Kirkland Lake quartz vs. Timmins quartz, etc. The results of the analysis are listed in Table 3 along with the elements responsible for most of the discrimination. The percentages refer to the samples correctly identified in each pair of vein types e.g. Larder Lake quartz-green carbonate 70 percent correctly classified, Kirkland Lake quartz 87 percent correctly classified. Therefore 30 percent of the Larder Lake samples were classified as belonging to Kirkland Lake and 13 percent of the Kirkland Lake samples as belonging to Larder Lake. In 25 of the 28 cases, more than 70 percent of the samples were correctly classified and in 14 cases more than 90 percent were correctly classified. It is also important to note the number of samples in each vein type because for vein types with few analyses, one improperly classified sample may contribute up to 15 percent of the incorrect classifications.

Discriminant-function analysis was also used to test if individual mines within a given vein type could be separated. The results of these tests are given in Table 4. One mine is usually different from the remainder, e.g., in the Larder Lake quartz-green carbonate veins the Davey

Lowe property can easily be separated from the other two but the Kerr Addison is not easily separated from the Martin Bird. It must be noted that there is a higher proportion of Kerr Addison samples properly classified because of a greater number of analyses (see Table 2) therefore a higher probability of any one sample being classified in that group as noted above.

The initial data indicates that there are significant differences in the trace element composition of gold from different sources. It is possible that subgroups exist within vein type groups as suggested by discriminant-function analysis of individual mines or deposits within a given vein type. However, this does not mean that gold cannot be identified with respect to vein type on the basis of trace element composition.

FUTURE PLANS

To reinforce the preliminary findings further sampling of certain vein types is required in some areas. Separation of gold grains by crushing and panning will release more grains for analysis and eliminate any interference and contamination from surrounding minerals during analysis. In some mines detailed sampling is required to study the variation of the trace element content of gold due to different lithologies which are cross-cut by the gold-bearing veins, and to study the natural spatial variations within a mine. Overburden samples are required to test the effects on trace elements composition by the secondary environment.

GRANT 76 SPECIATION OF FREE GOLD IN GLACIAL OVERBURDEN

Table 4—Discriminant-function analysis of trace element abundances in gold grains. The numbers are the percentages of samples correctly classified for each deposit when compared with another deposit of the same vein type.

Timmins Quartz Veins				
	McIntyre	Hollinger	Dome	
McIntyre	35	60	5	
Hollinger	3	90	7	
Dome	7	20	73	

Kirkland Lake Quartz Veins				
	Toburn	Lakeshore	Macassa	Baldwin Con.
Toburn	82	18	0	0
Lakeshore	31	46	23	0
Macassa	29	12	59	0
Baldwin Con.	14	7	0	77

Quartz Albite Veins		
	Kerr Addison	Buffonta
Kerr Addison	100	0
Buffonta	0	100

Larder Lake Quartz Green Carbonate Veins			
	Kerr Addison	Davey Lowe	Martin Bird
Kerr Addison	73	0	27
Davey Lowe	0	100	0
Martin Bird	54	0	46

	Martin Bird	Davey Lowe
Martin Bird	100	0
Davey Lowe	0	100

	Kerr Addison	Martin Bird
Kerr Addison	91	9
Martin Bird	54	46

ACKNOWLEDGMENTS

We are indebted to numerous people for their help in the collection and donation of samples. We would particularly like to thank Mr. T.N. Solberg of Virginia Polytechnic Institute for his suggestions and the time he devoted to overcome many of the analytical difficulties.

REFERENCES

- Antweiler, J.C. and Campbell, W.L.
1977: Application of gold compositional analyses to mineral exploration in the United States: Jour. Geochem. Exploration vol. 8, p.17-29.
- Antweiler, J.C. and Sutton, A.L.
1970: Spectrochemical analysis of native gold samples; Chem. Abstr. vol. 75, p.8625.
- Boyle, R.W.
1979: The geochemistry of gold and its deposits, Geological Survey of Canada, Bull.280, 584p.
- Denisov, S.V., Koshman, P.N. and Yugay, T.A.
1966: Trace elements in gold from some districts of the Amur region; Geochem. Int., vol. 3, p.904-908.
- Desborough, G.A.,
1970: Silver depletion indicated by microanalysis of gold from placer occurrences, western United States; Econ. Geol., vol. 65, p.304-311.
- Gay, N.C.
1963: A review of the geochemical characteristics of gold in ore deposits; Univ. Witwatersrand, Econ. Geol. Res. Unit, Inform. Cir. 12, 70p.
- 1964: The composition of gold from the Barberton Mountain Land; Univ. Witwatersand, Econ. Geol. Res. Unit, Inform. Circ. 19, 53p.
- Klován, J.E. and Billings, G.K.
1967: Classification of geological samples by discriminant-function analysis; Bull. of Can. Pet. Geol., vol. 15, p.313-330.
- Mosier, E.L.
1975: Use of emission spectroscopy for semiquantitative analyses of trace elements and silver in native gold; United States Geol. Survey, Bull.1408, p.97-105.
- Sakharova, M.S.
1969: Study of the composition of gold by X-ray spectral microanalysis; Akad. Nauk. SSSR, Dokl., vol. 186. no.2, p.430-433.
- Viljoen, E.A.
1971: An electron-microprobe analysis of gold in the Witwatersrand banket and in ores from the Barberton Mountain Land; Natl. Inst. Metal., S. Afr., Rep., no.1361, 7p.
- Warren, H.V. and Thompson, R.M.
1944: Minor elements in gold; Econ. Geol., vol. 39, p.457-471.

Grant 11 Gold Ore Formation at the Campbell and Dickenson Mines, Red Lake Area

C.J. Hodgson and P.J. MacGeehan

Department of Geological Sciences, Queen's University

ABSTRACT

The ore zones of the Campbell and Dickenson Mines are the product of a sequence of gold-enriching processes which operated in a lithologically distinctive volcanic setting. Mobilization of gold first occurred during sub-seafloor geothermal activity which caused spilitization (albitization, variable silicification and Fe, Mg, Ca, Au and As leaching) throughout the rocks now underlying Balmer Township, and carbonatization and feldspar-destructive alteration (Na leaching, Au, As, variable Si, and Ca-Mg-Fe carbonate enrichment) in a 1 km wide, 2 km long zone centered on the mines. The feldspar-destructive alteration occurred within a major discharge zone of the geothermal system, which coincided with a local centre of felsic extrusive activity within the dominantly mafic volcanic sequence. Iron formation was the main exhalative product of the geothermal system, though minor amounts of low grade exhalative gold ore were formed in close spatial association with rhyolitic extrusion. In the second period of gold mobilization during the main period of metamorphism and deformation, deformation was focussed, and fissure-filling gold-bearing veins (the major ore-type in the mines) were formed within the previously formed feldspar-destructive alteration zone. Finally, a third period of gold mobilization resulted in high-grade siliceous replacement zones being superimposed on the veins after the cessation of most of the deformation, probably as a result of geothermal activity associated with the emplacement of late felsic porphyry and mafic dikes.

INTRODUCTION

This report summarizes briefly the results of our research in the past year. Background information, and a more detailed presentation of the data is given by Hodgson *et al.* (1980), MacGeehan and Hodgson (1980), Rigg and Helmstaedt (1980), Rigg (1980), Sutherland (1980), MacGeehan *et al.* (in press), MacGeehan and Hodgson (in press) and Hodgson and MacGeehan (in press).

GEOLOGICAL SETTING

The geological setting of the mines is described by MacGeehan and Hodgson (1980) and Rigg and Helmstaedt (1980), and is briefly summarized by Hodgson *et al.* (1980). The mines are located in a restricted strati-

graphic zone within a major mafic, predominantly volcanic complex (Western Volcanic Complex in Figure 2 of Hodgson *et al.* 1980) in close association with two small rhyolitic domes (unit "Vr" and the southernmost "Val" unit in Figure 7 of Hodgson *et al.* 1980), near the contact of the mafic complex with an adjacent and synchronously formed sedimentary sequence (Central Sedimentary Belt in Figure 2 of Hodgson *et al.*, 1980) composed mainly of siliceous oxide, carbonate and sulphide iron formation. The rocks have been tilted to subvertical attitudes, and deformed to variable degrees, the extent of deformation depending mainly on the original lithology of the rocks (Rigg and Helmstaedt 1980). Most deformed are mafic volcanic rocks strongly affected by synvolcanic, feldspar-destructive hydrothermal alteration in the area of the mines (see below), and sedimentary rocks. Much less deformed are ultramafic-mafic intrusive rocks and felsic volcanic rocks. One main schistosity which strikes east to S55°E and dips subvertically, subparallel to stratigraphic contacts, predominates in the area, although locally in the more fissile and deformed rocks, a second cleavage striking S60°E to S40°E and also dipping subvertically, is present (Rigg and Helmstaedt 1980). A conspicuous feature of the area is the high intensity of deformation, and marked fissility of the mafic flow rocks in the mines area, relative to that in Balmer Township as a whole.

Following the major deformation, but before the cessation of metamorphism, a series of felsic porphyry and mafic dikes were emplaced.

Hydrothermal alteration and gold-ore formation appear to have occurred at least three times during the geological evolution of the area: during synvolcanic geothermal activity, during the main period of deformation and metamorphism, and after most of the deformation but before the emplacement of the late dikes. The alteration and mineralization which formed in each of these events is described briefly in the following sections.

SYNVOLCANIC ALTERATION AND MINERALIZATION

Two types of alteration which formed in a synvolcanic hydrothermal system have been distinguished (MacGeehan *et al.*, in press). These are termed "spilitic" and "feldspar-destructive" alterations, from their most distinctive mineralogical and chemical properties.

SPLITITIC ALTERATION consists of bleached domains of Na and variable Si enrichment, and Fe, Mg, Ca, Au and As depletion which are localized around zones of primary permeability, such as pillow margins, and quartz-epidote-carbonate-filled fissures and pipe-shaped zones in mafic volcanic rocks. This alteration type is widely, though unevenly developed in the mafic rocks of Balmer Township, with the most extensive spilitization generally occurring in pillowed flows, and particularly in pillowed flows directly overlain by exhalative iron formation. On Figure 1 is shown the variation in chemistry with degree of spilitization, as measured by the normative differentiation index (normative quartz plus alkali feldspar) (Thor-

ton and Tuttle 1960) of basalts in unit "GB" in the volcanic rocks east of the mines (Eastern Volcanic Belt in Figure 2 of Hodgson *et al.* 1980). The least altered samples are normal iron-rich tholeiites (cf. Figure 5, MacGeehan *et al.* in press) with a normative differentiation index of 20-25 percent, whereas the most altered samples have the silica content of andesite, and a differentiation index of 50-60 percent (Figure 1; cf. Hodgson *et al.* 1980, Table 1).

FELDSPAR-DESTRUCTIVE ALTERATION is confined mainly to an area within and immediately adjacent to the mines, and includes, but extends outside of the zone of

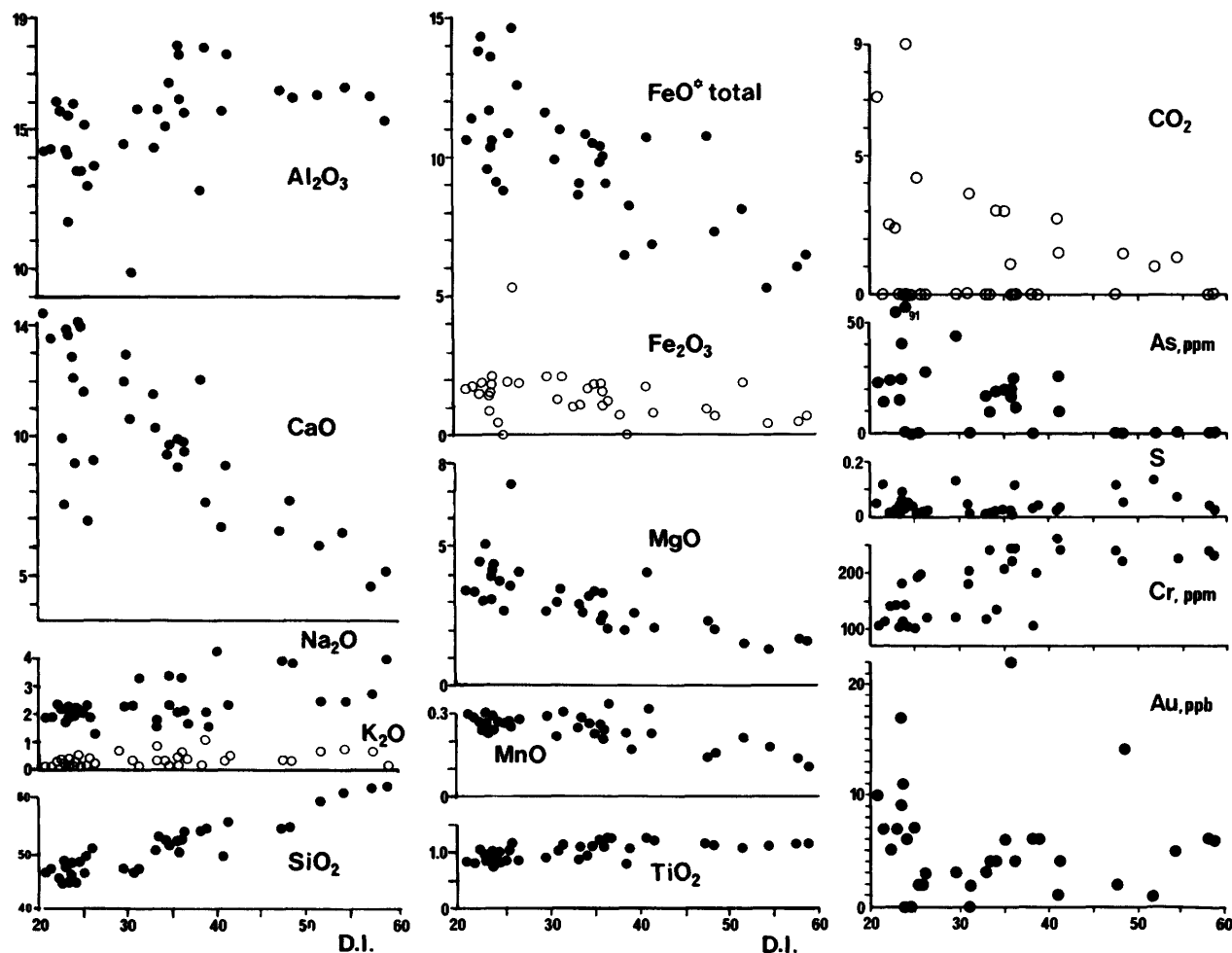


Figure 1—Major and trace elements against normative differentiation index (D.I.) plot of least altered (D.I. 20-25 percent) and variably spilitized samples of Unit GB. The major element oxides were analysed by X-ray fluorescence (XRF) and Au was determined by neutron activation analysis by X-Ray Assay Laboratories Limited, Don Mills, Ontario. As, S and Cr were determined by XRF on powder pellets at Queen's University. From MacGeehan *et al.* (in press). All abundances, except of Au, Cr, and As, are given in weight percent.

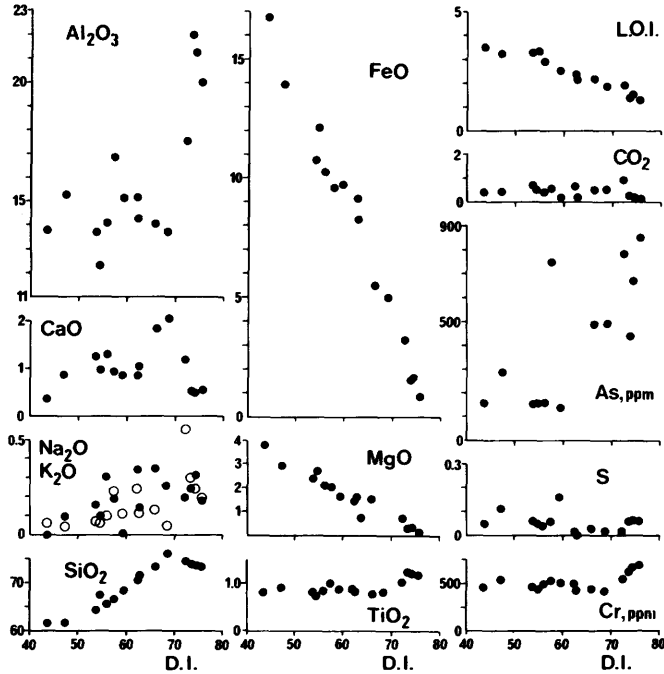


Figure 2—Plot of major and trace elements against differentiation index (D.I.) of variable bleached pillows in basalt from the zone of feldspar-destructive alteration hosting the orebodies of the Campbell and Dickenson mines. Analytical details as noted in Figure 1. From MacGeehan *et al.* (in press).

highly fissile and strongly deformed rocks which host the orebodies. Though a number of alteration types occur within the zone, all are characterized by a lack of feldspar, which is chemically indicated by their very low Na content. Other conspicuous features of the altered zone are: abundant (averaging about 20 percent of the rocks on the outcrop scale), variably transposed carbonate (dolomite-ferrodolomite-ankerite)-quartz veinlets; variable bleaching related to zones of primary permeability in the rocks; and a high ratio of chlorite/amphibole, relative to rocks outside of the zone. On Figure 2 is shown the chemistry of variably bleached pillows from one outcrop within the feldspar-destructive alteration zone. Although the morphology of the alteration effects is essentially identical to that of the spilitic alteration, all of the samples, even those of unbleached rocks, are significantly more siliceous, and their Na content is uniformly low, compared to that of samples of spilitic altered rocks. Furthermore, the As content of the rocks increases, rather than decreases, with increasing degree of bleaching and silicification.

The regional distribution and intensity of the two alteration types can be defined by three lithogeochemical parameters: peraluminosity index (P.A.I.: mole percent

$\text{Al}_2\text{O}_3/(\text{CaO} + \text{Na}_2\text{O} + \text{K}_2\text{O})$; Spitz 1973; Spitz and Darling 1975), which essentially measures the extent of feldspar-destructive alteration (Figure 3; cf. Hodgson *et al.*, 1980; As content, which decreases with intensity of spilitic alteration, but increases with intensity of feldspar-destructive alteration (Figure 4), and Au content (Figure 5). The feldspar-destructive alteration zone also coincides approximately with a zone of abundant, variably transposed carbonate veinlets, even though rock samples free of vein material generally contain less Ca and CO_2 than rocks from outside the zone.

Two main types of exhalite were formed during the synvolcanic activity. Most widespread and abundant are siliceous, slightly auriferous (Figure 6) iron oxide, carbonate and sulphide formations which comprise most of the Central Sedimentary Belt, and also occur as layers between flow units in the Western Volcanic Complex and Eastern Volcanic Belt (cf. Hodgson *et al.* 1980, Figure 2). Most of the rocks in the Central Sedimentary Belt are turbidites. Lateral variations in the lithology of sedimentary rocks in the Central Sedimentary Belt indicate that the main source area of the constituents in the sedimentary sequence was the Western Volcanic Complex (Hodgson *et al.* 1980), which in turn indicates that iron formation was the main exhalative product deposited in the hot-spring vent area defined by the feldspar-destructive alteration described above. Within the mines, and closely associated spatially with two rhyolitic domes, two zones of a second type of exhalite which constitute low-grade gold ores have been identified. One of these zones, the "North L-Zone" in the Campbell Mine, consists of fine disseminated native gold and up to 1 percent total sulphides which are essentially restricted to thin bands of rhyolitic tuff and chert in a sequence of rhyolitic agglomerate, tuff and chert which overlies and flanks the Campbell Rhyolite (Unit Vr in Figure 7 of Hodgson *et al.* 1980). The other zone, the "H-Zone" in the Dickenson Mine, is a 1 m thick sequence of alternating chert and banded pyritic iron formation, within a sequence of rhyolitic tuff flanking the Dickenson rhyolite dome (southernmost Val Unit in Figure 7 of Hodgson *et al.*, 1980).

Closely associated with these auriferous exhalites are minor small auriferous carbonate-chert veins which appear to predate all of the deformational structures, and are widely distributed through the mines area.

"METAMORPHOGENIC" MINERALIZATION AND ALTERATION

Most of the ore in the mines occurs in large fissure-filling veins. The morphology, mineralogy and mineralogical and chemical zoning in these has been described in detail by MacGeehan and Hodgson (in press), and only their essential features will be outlined here.

Three main types and ages of vein are distinguished. In order from oldest to youngest, these are as follows. 1) Breccia veins, consisting of tabular fragments of foliated

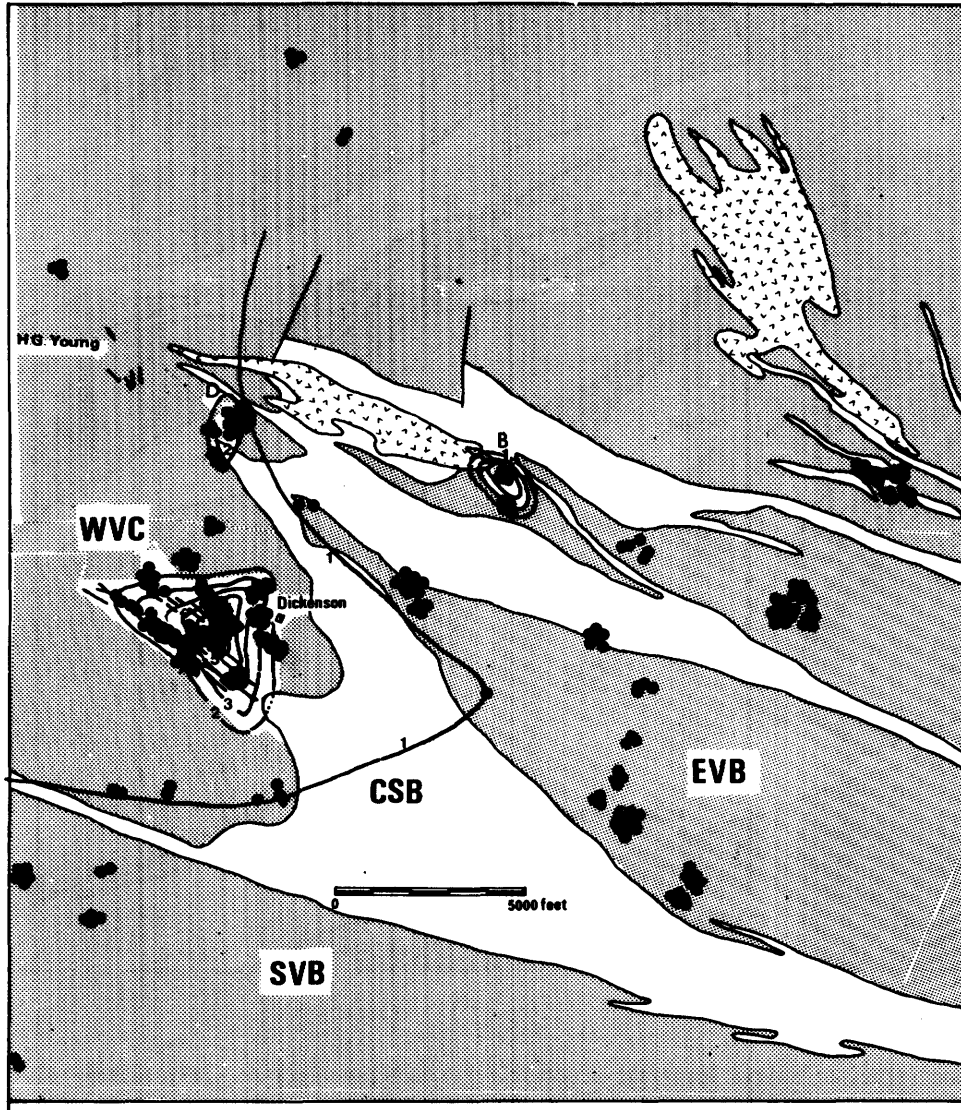


Figure 3—Peraluminosity index in basalts, Balmer Township. Contours are in mole percent $Al_2O_3/(CaO + Na_2O + K_2O)$. Dots represent analyses; white areas are sedimentary rocks; shaded areas are volcanic rocks and their intrusive equivalents; patterned areas are mainly felsic intrusive rocks. WVC — Western Volcanic Complex, EVB — Eastern Volcanic Belt, SVB — Southern Volcanic Belt, CSB — Central Sedimentary Belt. From MacGeehan et al. (in press).

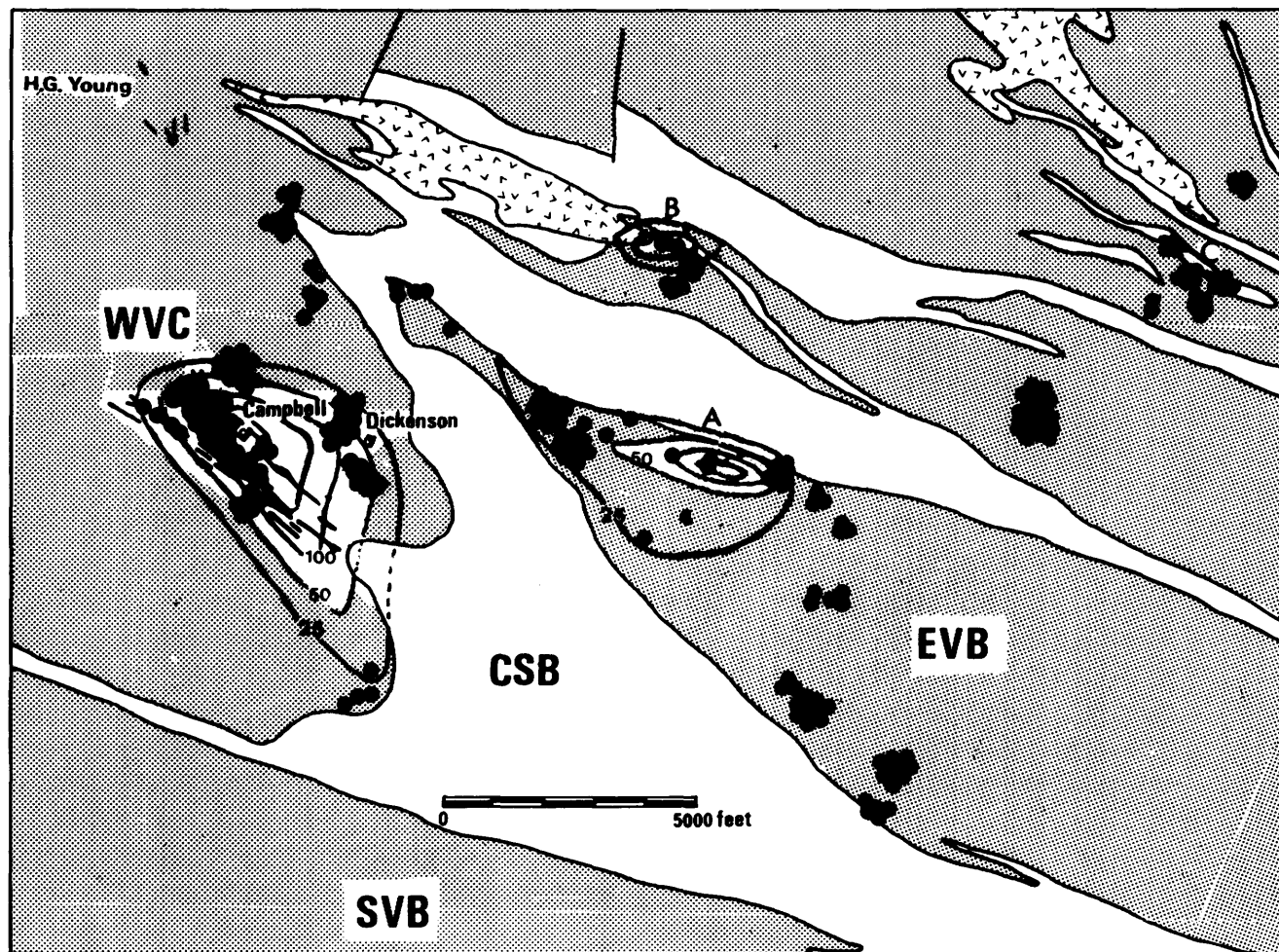


Figure 4—Arsenic in basalts, Balmer Township. Contours are in parts per million As. Ornamentation as for Figure 3. From MacGeehan et al. (in press).

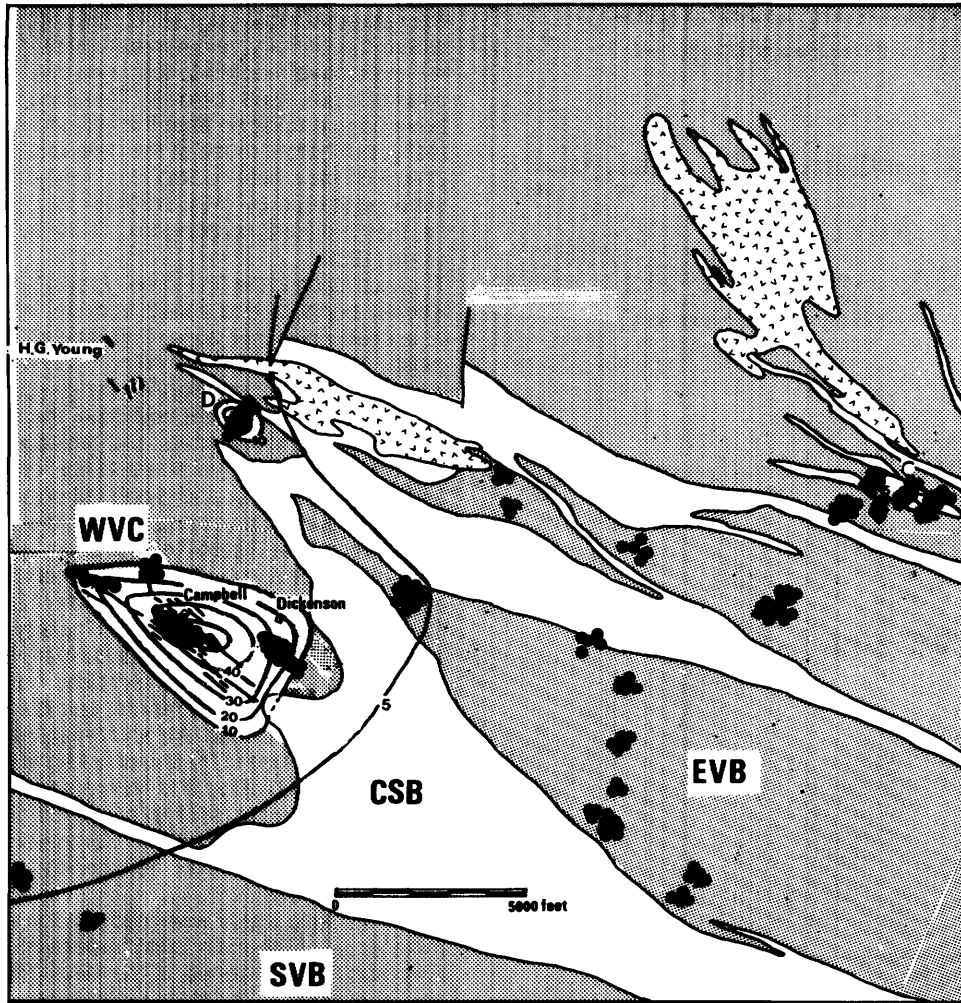


Figure 5—Gold in basalt, Balmer Township. Contours are in parts per billion Au. Ornamentation as for Figure 3. From MacGeehan et al. (in press).

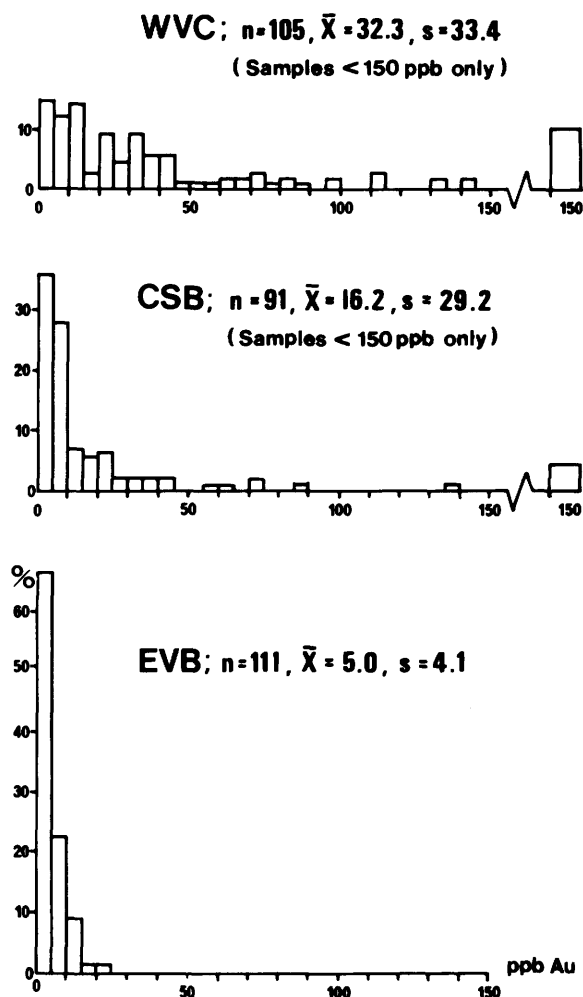


Figure 6—Frequency distribution of gold contents of basalts in Eastern Volcanic Belt (EVB) and the Western Volcanic Complex (WVC), and sedimentary rocks in the Central Sedimentary Belt (CSB). Analytical details as noted in Figure 1. From MacGeehan *et al.* (in press).

wall rock in a matrix of carbonate and chert, range up to a few metres long, and are most abundant at the east end and near the major foliation-parallel vein systems. 2) Foliation-parallel carbonate-chert veins range up to 200 m long and form an echelon vein systems of great lateral (up to 1.5 km) and vertical (up to at least 1 km) continuity. 3) Foliation-oblique carbonate-chert veins are thicker, but shorter than the foliation-parallel vein systems, and occur mainly in the Campbell Mine. 4) Foliation-parallel quartz-arsenopyrite veins occur only in the western part of the Campbell Mine. Though these veins are either oriented parallel or subparallel to the dominant mine schistosity (foliation-parallel veins and breccia veins), or occur in

faults which cut the schistosity (foliation-oblique veins), they show variable degrees of deformation. Furthermore, where the primary vein mineralogy was appropriate, the minerals have reacted to form new metamorphic mineral assemblages (see below). Therefore, the veins must have been emplaced after the initial formation of a schistosity, but before much of the deformation and metamorphism of their host rocks. This indicates that the veins were generated by metamorphic-deformational process, i.e. they are metamorphogenic, in the terminology of Karvinen (1980).

The vein filling in the first three types of veins is characteristically banded, and zoned from a carbonate-rich outer to a chert-rich inner zone. The gold in the veins occurs mostly in the siliceous vein filling (Figure 7). Bleached, siliceous alteration envelopes are irregularly developed along the veins. The last vein-type, the quartz-arsenopyrite veins, are not banded, and lack bleached alteration envelopes. All of the veins are almost entirely confined to basalt and andesite, and pinch out where they strike into rhyolite, sedimentary rocks, or altered ultramafic-mafic intrusive rock (see Figure 7 of Hodgson *et al.* 1980).

In addition to the above auriferous vein types, altered ultramafic-mafic intrusive rocks in the Campbell Mine (altered rock in Campbell Mine terminology, Hodgson *et al.*, 1980) locally are cut by foliation-parallel sheeted vein systems to stockwork vein systems consisting of gold-free, quartz-carbonate-chlorite veinlets. These veinlets appear to have formed at about the same time as the carbonate-chert veins in the basalt and andesite (Sutherland 1980; Rigg 1980; Rigg and Helmstaedt 1980). Also interpreted as being the result of metamorphic processes are the small, gold-free carbonate-quartz veinlets which characterize the zone of feldspar-destructive alteration described above.

A detailed study was made of the morphology and mineralogy of the main foliation-parallel vein system, the F, A, and South C zones, in the mines (Figure 7 of Hodgson *et al.*, 1980). The main results of this study, which is described in detail by MacGeehan and Hodgson (in press) are shown in Figure 7. The system occurs within a 1-3 m wide, 1.5 km long, and over 1 km deep zone across which there is a sinistral strike displacement of 5 m. The system in most areas is composed of from one or two, 10-200 m long individual veins, though locally up to eight veins are present. The displacement across the system appears to have occurred in increments during vein emplacement, since in areas of multiple vein-units, drag-folded older veins are cut by less deformed or undeformed younger veins (Figure 7). All of the individual veins are conspicuously banded, the vein fill consisting of bilaterally symmetrical outer zones of banded carbonate, and an inner chert-rich zone which, where the veins are wide, commonly contains fragments of vein-wall carbonate, and/or chert, and/or banded carbonate orbicules. In general, there is a progression from lower to higher Fe/Mg ratio in individual carbonate bands, and through the succession of bands in the vein-wall fill towards the cherty vein centre.

No systematic differences were detected among individual veins of different ages at one location in the system. However, there is a striking zonal variation in miner-

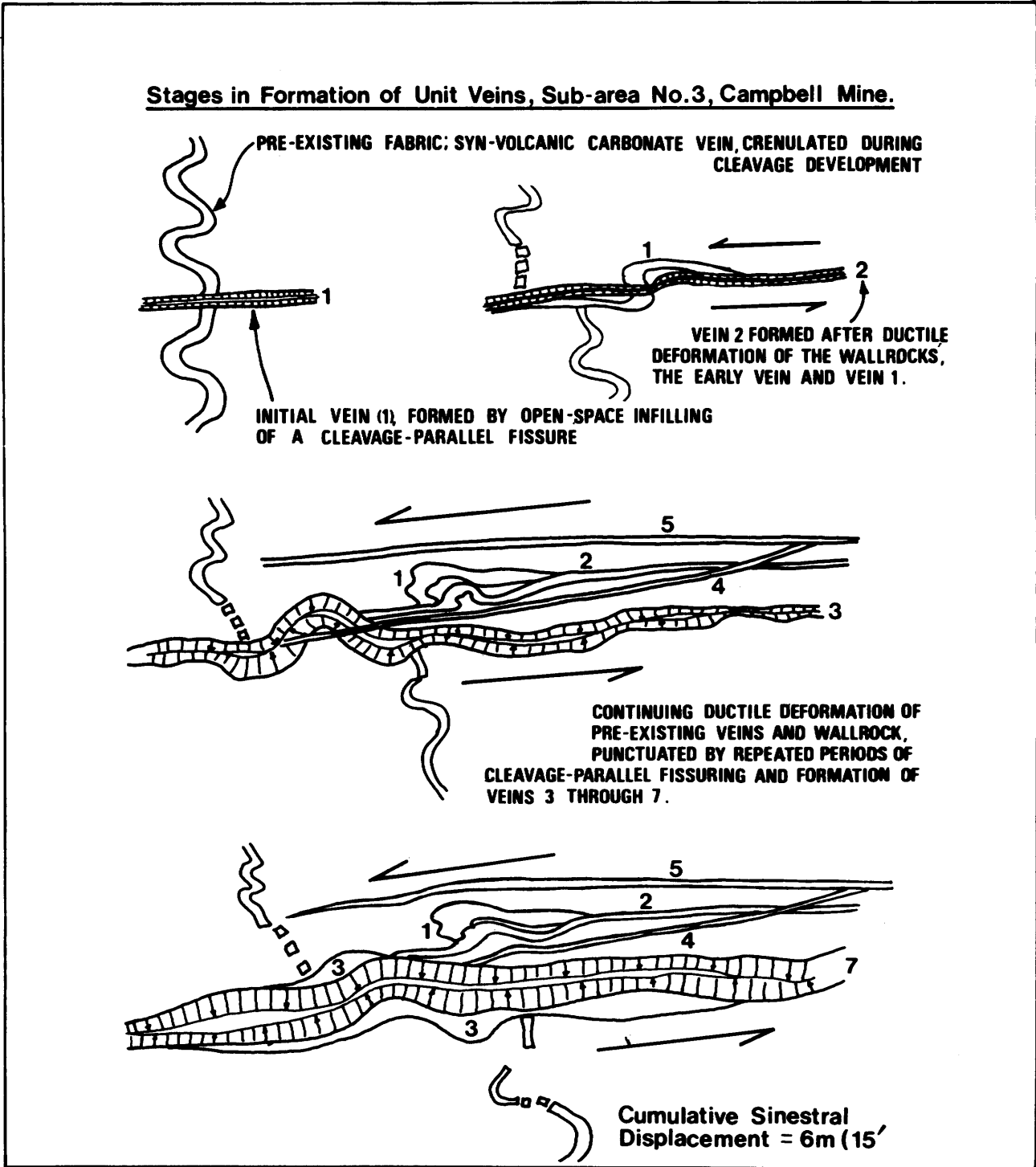


Figure 7—Interpretation of sequence of events in sub-area 3, A-Zone, Campbell Mine, (see Hodgson et al. 1980, Figure 7 for location of A-Zone. From MacGeehan and Hodgson (in press).

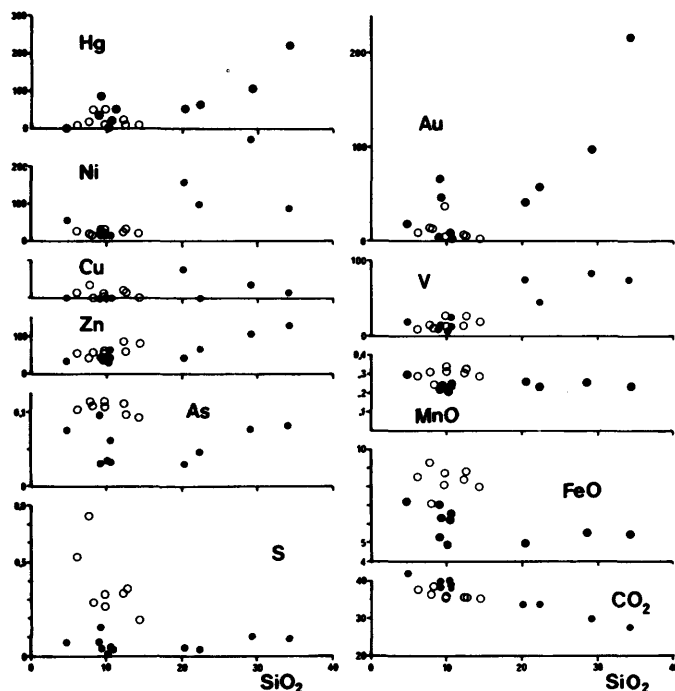


Figure 8—Chemistry of vein fill from main vein in South C-Zone, Dickenson Mine (see Hodgson *et al.*, 1980, Fig. 7 for location). Open and filled circles are samples comprised dominantly of vein-wall carbonate and vein-center cherty fill, respectively. From MacGeehan and Hodgson (*in press*).

alogy and composition along the system where it was studied on the 14 level, Campbell Mine and 15 level, Dickenson Mine. The essential features of this zonation are shown in Figures 8 and 9. The veins in the east end of the system have a higher chert/carbonate ratio, the cherty vein core is carbonate-rich, the carbonate is dolomite-ferrodolomite, and alteration envelopes contain magnetite. Westwards, the chert/carbonate ratio of the veins decreases, the carbonate content of the cherty core decreases, the Fe/Mg ratio of the carbonate increases, and magnetite is absent from the alteration envelopes. In the western part of the system where the veins have a high Fe/Mg ratio, iron silicate minerals (grunerite, anthophyllite) are present. These are interpreted to have formed by the metamorphic reaction of a primary sideritic carbonate with the cherty vein fill. The zonation in ore elements in the vein system is complex, but in general terms the veins are most gold-rich at the eastern end of the system in the Dickenson Mine, which is consistent with the close association of gold with chert. Mercury, though present in only low concentrations in the system as a whole (<100 ppm), is moderately abundant in the east end, rises to a maximum in the central part, then drops to low levels in the west end of the system. Tungsten is low in the east end of the system (<400 ppm W), increases

westwards to a maximum of about 0.3 percent WO_3 in the central part, then decreases rapidly further to the west.

The foliation-oblique veins, though broadly similar to the foliation-parallel veins, generally have much more complex banding, with evidence in several areas of repeated cyclic deposition of carbonate-chert fill, either in successively stacked layers, or in multiple separately emplaced veins which results in a well developed ribbon structure. In some foliation-oblique veins, unconformities, slump-like structures, and conformable breccia zones are present, and are strikingly similar to structures in sedimentary rocks.

SILICEOUS REPLACEMENT-TYPE MINERALIZATION

In the Campbell Mine, particularly on the deeper levels, are a number of subvertically-oriented, pod- to pipe-shaped zones of spectacularly high grade siliceous replacement-type mineralization. Within these zones, the host rocks and "metamorphogenic" veins are replaced by fine grained quartz, arsenopyrite, pyrite and native gold. The mineralization is superimposed on the dominant mine schistosity (striking east to $\text{S}55^\circ\text{E}$), several ages of faults which cut this foliation, and the metamorphogenic veins, but is overprinted by, or formed contemporaneously with a late cleavage striking $\text{S}25\text{--}45^\circ\text{E}$. Because the late felsic porphyry and mafic dikes in the mines also post-date most of the deformation, but have been thoroughly metamorphosed and locally hydrothermally altered, we have tentatively suggested that the dikes and replacement-type mineralization are approximately contemporaneous, even though the dikes post-date the mineralization.

The siliceous replacement zones are all spatially related to bodies of altered ultramafic-mafic intrusive rock (altered rock in Campbell Mine terminology, Hodgson *et al.*, 1980), occurring either in altered rock or basalt or both near their contact, particularly near rolls in this contact, or where the two rock types have been juxtaposed by faulting (Rigg 1980; Sutherland 1980; Rigg and Helmstaedt 1980).

SUMMARY AND SIGNIFICANCE FOR EXPLORATION

The gold ore zones of the Campbell and Dickenson Mines are polygenetic, having formed during at least three of the major geological events which affected the area. The first period of gold redistribution occurred during volcanism, as a result of sub-seafloor geothermal activity. Products which formed at this time provide the largest-scale indication of possible gold mineralization. On the township scale, the presence of abundant exhalative iron formation and Au- and As-leaching spililitic alteration in the mafic volcanic rocks indicate that gold-mobilizing

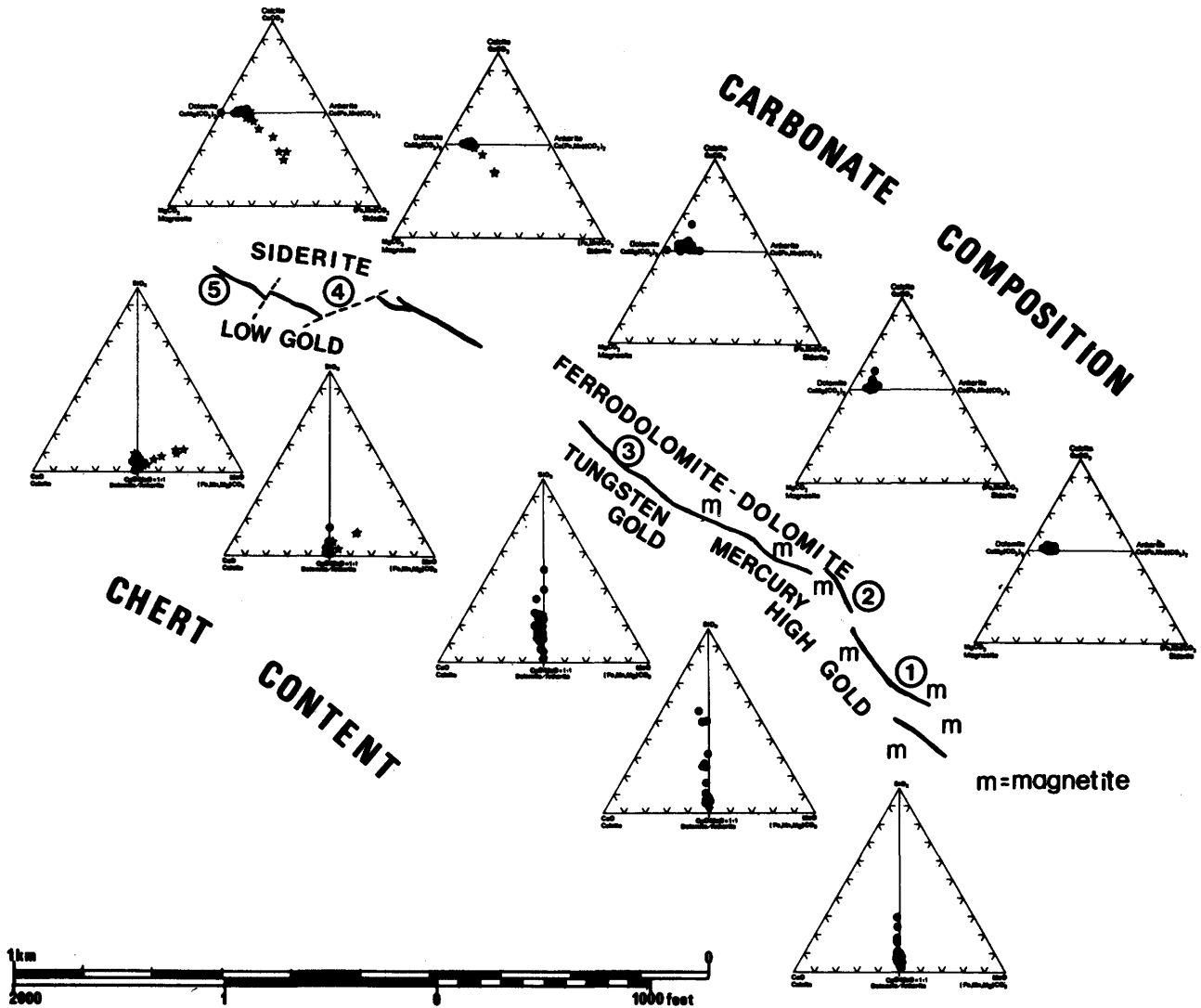


Figure 9—Zoning in major element composition (carbonate composition plotted as molecular ratio CaO, top apex, MgO, left apex, and FeO + MnO, right apex; chert content plotted as molecular ratio SiO₂, top apex, CaO, left apex, and FeO + MnO + MgO, right apex, mineralogy, and gold and tungsten content of the F-A-South C vein system. Based on mapping of five sub-areas (circled numbers) and analysis of hand and channel samples from these. Analyses plotted as star symbols are of samples which contain an iron silicate metamorphic mineral assemblage (see text). Magnetite in alteration selvages occurs in areas marked 'm'. From MacGeehan and Hodgson (in press).

geothermal activity affected the rocks. The mine or claim group scale target is indicated by the distinctive chemistry (high Au and As; high ratio of mole percent $Al_2O_3/(CaO + Na_2O + K_2O)$ in vein-free rocks; and abundant Fe-Mg-rich carbonate in "metamorphogenic" veinlets) of the altered rocks which formed at the time the area was a major hot spring discharge zone. The presence of small rhyolitic extrusive bodies in the mines area is also considered genetically significant, and therefore of importance at this scale of exploration, since felsic intrusions or extrusions are associated, on a mine scale, with almost all of the larger gold mines in the Superior Province of the Canadian Shield (Hodgson and MacGeehan, in press). In this case, the rhyolitic extrusions probably mark the site of fissures which also were the main discharge conduits for auriferous solutions, though it is also possible that magmatic hydrothermal fluids were involved in the mineralizing process.

Certain features caused by later deformation and metamorphism, but which only formed because of the effects of synvolcanic processes, also are useful claim group scale exploration criteria. The most obvious of these is the highly deformed state, and highly fissile nature of the rocks in the target area, relative to rocks in the area as a whole. This effect we ascribe to the focussing of deformation in the mineralogically and chemically altered (and thus mechanically weakened) feldspar-destructive alteration zone formed at the time of synvolcanic hydrothermal activity. Also conspicuous is the abundance of Fe-Mg-rich carbonate-quartz veinlets, which are transposed to a variable extent into parallelism with the cleavage, and which we have interpreted as having formed by metamorphic mobilization and concentration of carbonate, originally dispersed through the altered rocks, during deformation and metamorphism.

Finally, a number of exploration criteria of use on the orebody scale of exploration derive from the recognition of the three main types of gold mineralization in the mines, and their morphological and mineralogical characteristics. The earliest, or synvolcanic exhalative type of ore is stratiform, and appears to be closely associated, spatially, with rhyolite domes and their associated pyroclastic-hyaloclastic aprons, indicating that areas flanking rhyolitic bodies are good places to look for this ore type. The "metamorphogenic" fissure-filling veins, while mainly oriented parallel to major lithological contacts and foliation, may also be inclined to foliation, which means that too-widely-spaced drill holes oriented normal to foliation can miss significant orebodies of the foliation-oblique vein type. The zonation in mineralogy, and in particular, in gold content which we have documented in the F-A-South C vein system, if generally present in this vein type, could provide an important guide to which way to go in exploring such veins, and is particularly significant considering the fact the barren carbonate-rich veins (snow-bank veins, in Campbell Mine terminology) occur in the mines.

One of the most profitable of the orebody types in the mines is the small, pod to pipe-shaped siliceous replacement zone type. These appear to be spatially associated

with altered ultramafic-mafic intrusions, and with faulted contacts, or rolls in the contact of these rock bodies with basalt. They represent particularly difficult targets in orebody scale exploration. Although these replacement-type orebodies appear to be localized at structural sites, which perhaps in turn are related to competency contrasts between rocks being deformed together, their possible temporal and thus genetic relationship to late dike sets raises the possibility that zones of this type may, on a large scale, show some relationship to the igneous centers from which the dikes emanated.

ACKNOWLEDGEMENTS

We would like to thank S.M. Reid, Cal Mark and Ray Church of Campbell Red Lake Mines Limited, and R. Tapper, Cal Mark, Lloyd Koskitalo and Mike Chowainec of the Dickenson Mines Limited for free access to the mine workings, and for help, encouragement and thoughtful discussion during the course of the study.

REFERENCES

- Hodgson, C.J., Helmstaedt, H., MacGeehan, P.J. and Rigg, D.M.
1980: Grant 11 Gold Ore Formation of the Campbell and Dickenson Mines, Red Lake Area; Ontario Geological Survey, Miscellaneous Paper 93, p.111-121.
- Hodgson, C.J. and MacGeehan
in press: Geological Characteristics of Gold Deposits in the Superior Province of the Canadian Shield; Canadian Institute of Mining and Metallurgy, Special Volume on Timmins—Val d'Or Gold Symposium
- Karvinen, W.O.
1980: Geology and Evolution of Gold Deposits, Timmins Area; p. 1-43 in Genesis of Archean, Volcanic-Hosted Gold Deposits, Roberts, R.G. (ed.), Ontario Geological Survey Open File Report 5293, 387p.
- MacGeehan, P.J. and Hodgson, C.J.
1980: The Relationship of Gold Mineralization to Volcanic and Alteration Features in the Area of the Campbell and Dickenson Mines, Red Lake District, Western Ontario; p. 212-241 in Genesis of Archean, Volcanic-Hosted Gold Deposits, Roberts, R.G. (ed), Ontario Geological Survey Open File Report 5293, 387p.
- in press: Environments of Gold Mineralization in the Campbell Red Lake and Dickenson Mines, Red Lake District, Ontario. Canadian Institute of Mining and Metallurgy Special Volume on Timmins-Val d'Or Gold Symposium.
- MacGeehan, P.J., Sanders, T. and Hodgson, C.J.
in press: Meter-Wide Veins and a Kilometer-Wide Anomaly: Wall Rock Alteration at the Campbell Red Lake and Dickenson Gold Mines, Red Lake District, Ontario; Bulletin Canadian Institute of Mining and Metallurgy.
- Rigg, D.M.
1980: Relationship Between Structure and Gold Mineralization in Campbell Red Lake and Dickenson Mines, Red Lake District, Ontario; Unpublished M.Sc. Thesis, Queen's University, Kingston. 153p.

Rigg, D.M. and Helmstaedt, H.

1980: Relationships Between Structures and Gold Mineralization in Campbell Red Lake and Dickenson Mines, Red Lake District, Ontario; p. 243-279 in Genesis of Archean, Volcanic-Hosted Gold Deposits, Roberts, R.G. (ed.), Ontario Geological Survey Open File Report 5293, 387p.

Spitz, G.

1973: Etude Pétrographique et Pétrochimique des Roches Volcanique autour du Gisement de Louvem; Thèse de Maîtrise, Ecole Polytechnique, Université de Montréal.

Spitz, G. and Darling, R.

1975: The Petrochemistry of Altered Volcanic Rocks Surrounding the Louvem Copper Deposit, Val d'Or, Quebec, Canadian Journal Earth Sciences, vol. 12, p.1820-1829.

Sutherland, K. S.

1980: The Geology of the 1958W. Dr., Campbell Red Lake Mines Limited, Balmertown, Ontario; Unpublished B.Sc. Thesis, Queen's University, Kingston, 24p.

Thorton, C.P. and Tuttle, O.F.

1960: Chemistry of Igneous Rocks, Part 1: Differentiation Index; American Journal Science, vol. 258, p.664-684.

Grant 7 Field Investigation of Use of Horizontal Deep Drains to Stabilize Clay Slopes

T.C. Kenney and K.C. Lau

Department of Civil Engineering, University of Toronto

ABSTRACT

To investigate the effectiveness of horizontal deep drains in clay slopes to reduce groundwater pressures and thereby increase the stability of such slopes, a full-scale field test is being conducted at Wabi Creek near New Liskeard, Ontario. Five horizontal deep drains, about 50 mm in diameter and 35 m long, were constructed and installed in the slope at spacings of about 13 m between adjacent drains. The effectiveness of the drains in reducing groundwater pressures is being monitored with piezometers.

For purposes of predicting the influence of horizontal drains in slopes, an analytical procedure was developed based on the theory of consolidation. Changes of groundwater pressures with time were calculated using measured soil properties and measured hydraulic boundary conditions at the site. Comparisons between measured and predicted values indicated that the analytical procedure can be used with confidence.

The field results showed that horizontal deep drains do decrease groundwater pressure. At the test site, these reductions were small due to the small diameter of the drains and the comparatively large spacing between the drains. Another contributing factor was that the drains were installed at a level close to the top of the slope.

It is concluded that deep horizontal drains can be effective in increasing the stability of clay slopes. The economic viability of this approach to stabilize clay slopes has not been adequately studied and is still unknown at present.

INTRODUCTION

There are many regions in Ontario which have problems with instability of clay slopes, particularly along rivers. In the past a great deal of research effort has been directed towards the understanding of the mechanics of landslides. Comparatively little effort has been made to develop technology which could be used to prevent landslides.

Water was found to be almost always the agent that contributed most to instability of slopes and, therefore, drainage of surface and subsurface water appeared to be an effective means for improving stability.

During the past few decades, the installation of hori-

zontal deep drains from the base of slopes to reduce groundwater pressures in pervious materials has been found to be very effective. However, with a few exceptions (La Rochelle *et al.* 1977), attempts have not been made to use horizontal deep drains in clay slopes. The probable reason is that many people believe that because little water drains out of clay soils, little improvement of stability of a clay slope will result. This concept is incorrect — under identical hydraulic boundary conditions, horizontal drains should be as effective in reducing groundwater pressures in slopes in clay soils as in more pervious soils, although a longer period of time would be required for the drains in clay soils to become fully effective.

To determine the effectiveness of horizontal deep drains in reducing the groundwater pressures in clay slopes, a full-scale field test is being conducted. The test site is located 1.5 km north of New Liskeard, Ontario.

The slope consists mainly of varved clay and the groundwater pressure pattern within the slope has been monitored regularly over a period of ten years (every two weeks with more than 60 piezometers). The effectiveness of the five horizontal deep drains is being monitored by determining changes in groundwater pressure resulting from the installation of the drains.

1978-1980 RESEARCH PROGRAM

(a) **SETTING UP A GROUNDWATER PRESSURE MONITORING SYSTEM.** The change in groundwater pressures in the slope due to the installation of horizontal drains was monitored with piezometers. For an earlier research project, 63 piezometers were installed in 1970 in a section of the bank of the Wabi Creek on the property of the New Liskeard Agricultural College of Technology. This slope is now being used for research on horizontal deep drains. To make the most effective use of the existing piezometers, those piezometers which were not suitably located were removed and installed at new sites for the purpose of this research program. About 300 m of piezometer pipes were removed from the ground; the holes were sealed and the pipes were re-installed to form 25 new piezometer points.

(b) **DESIGN AND INSTALLATION OF HORIZONTAL DEEP DRAINS.** The drains consist of 5 cm diameter slotted plastic pipe with 5.6 cm diameter couplings and wrapped in filter cloth. In March 1979, five horizontal deep drains, each 36 m long, were installed. Each drain

Table 1—Packers tests to determine if filter cloths were clogged around drains

Distance from the outlet (m)	Rate of water discharge from the packer (cm ³ /min)* installed in drains		
	Drain #3	Drain #4	Drain#5
3.0	55.7	—	51.0
6.1	58.2	54.8	—
9.2	57.1	—	48.9
12.2	53.6	57.6	53.4
15.3	54.7	—	—
18.3	57.3	49.7	60.2
21.3	59.2	—	—
24.4	53.4	54.2	57.3
27.5	56.3	—	—
30.5	55.1	57.3	56.4
33.5	55.7	—	—
35.0	57.9	53.3	—

Rate of water discharge from packer only

(a) Before use in drain pipes — 57.4 cm³/min*

(b) After use in drain pipes — 56.7 cm³/min*

*Under a pressure head of 14 KPa at the inlet of the inflow line.

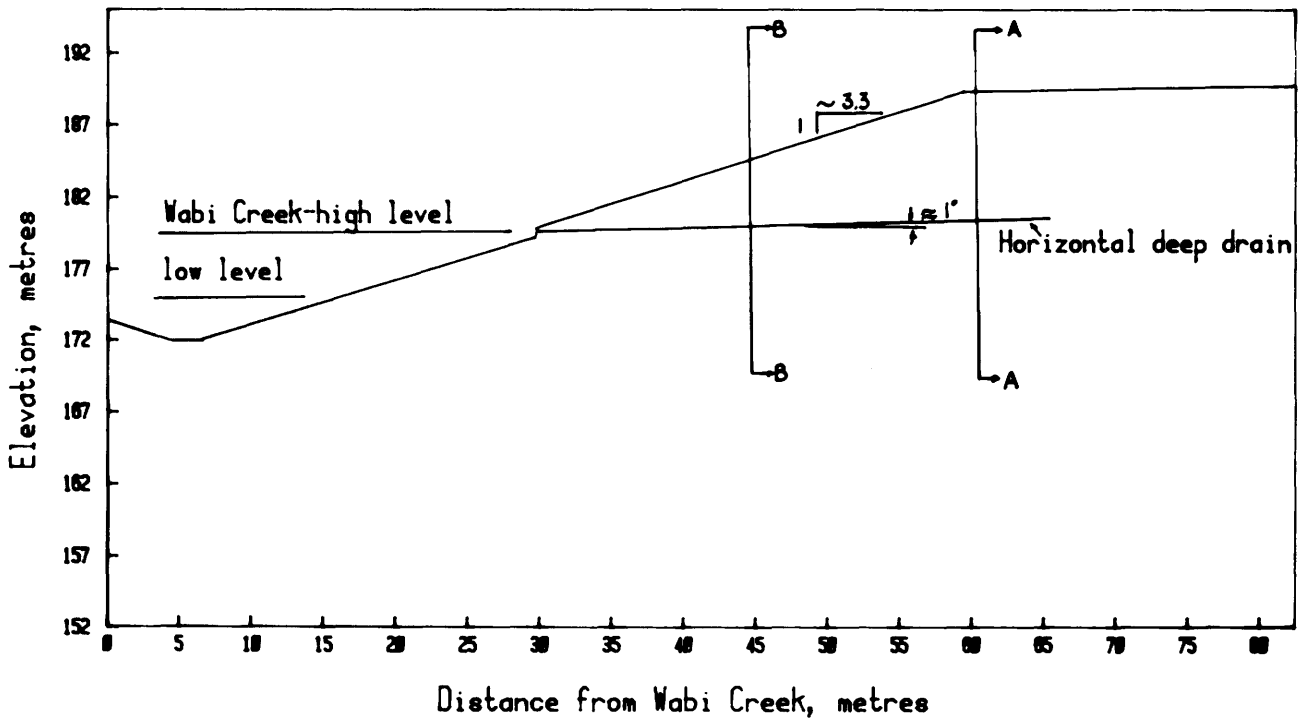


Figure 1—Cross-section of the test site. Piezometers were located on sections A and B.

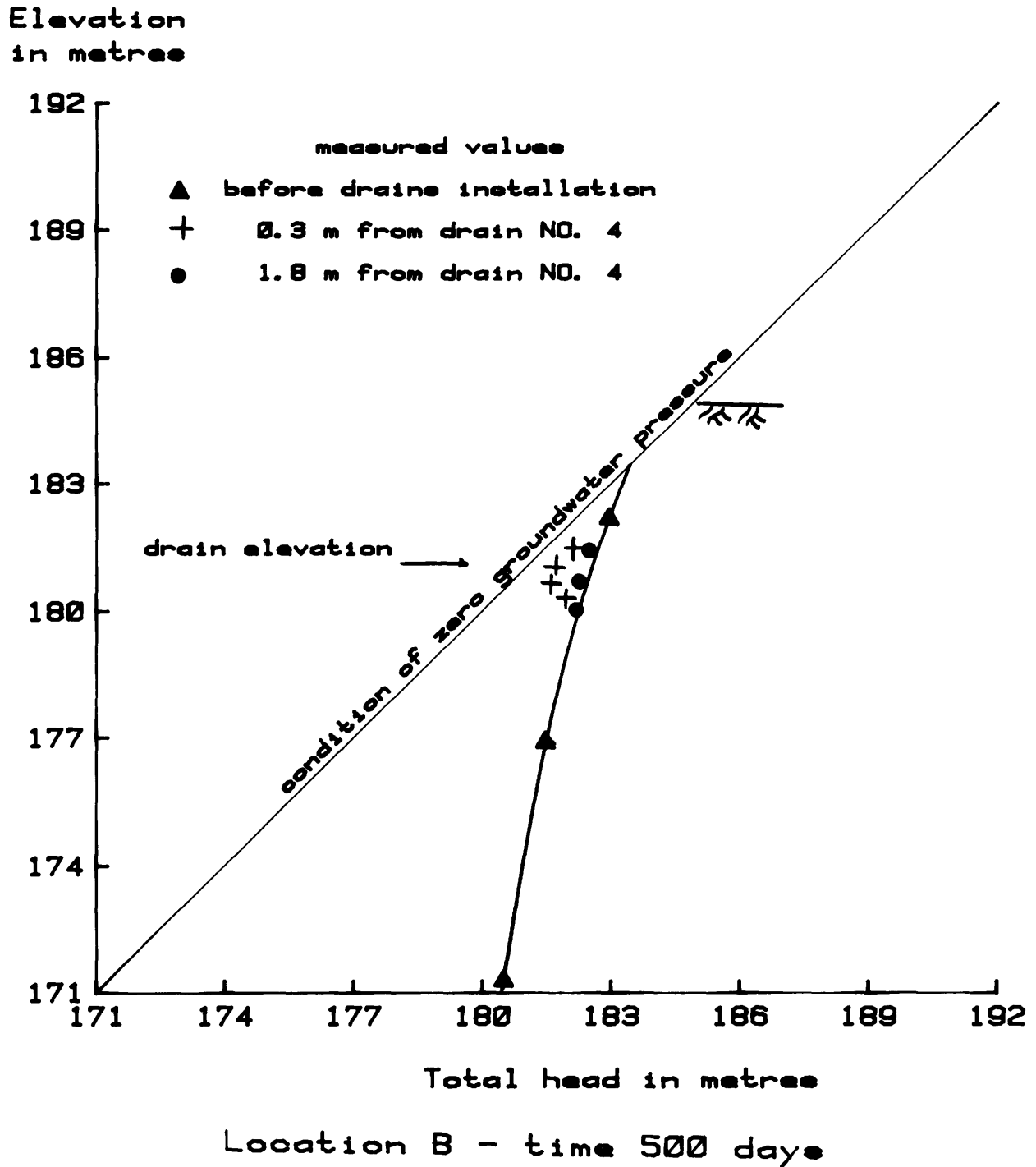


Figure 2—Measured groundwater pressure distribution along section B-B at different distances from drain No. 4.

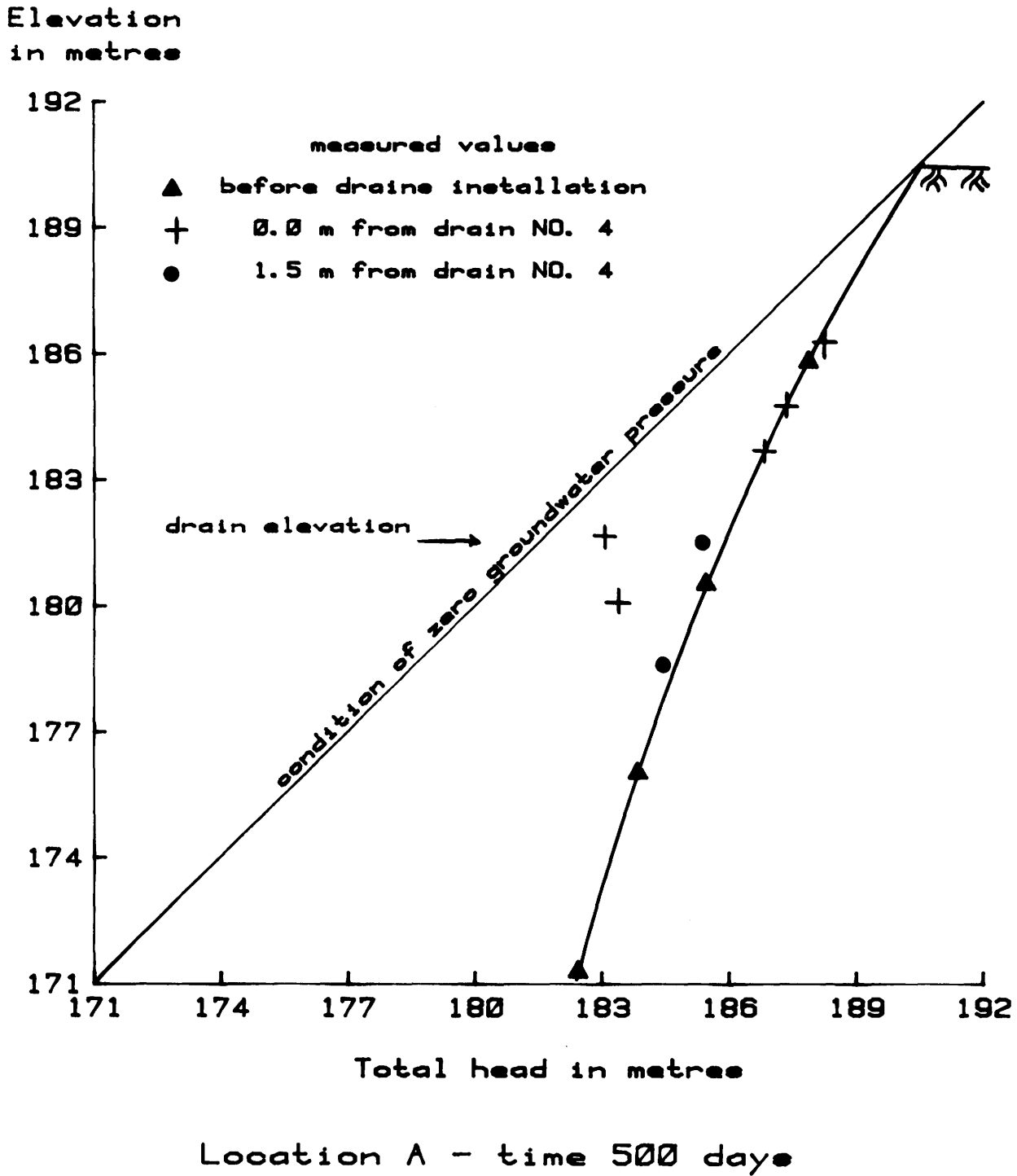
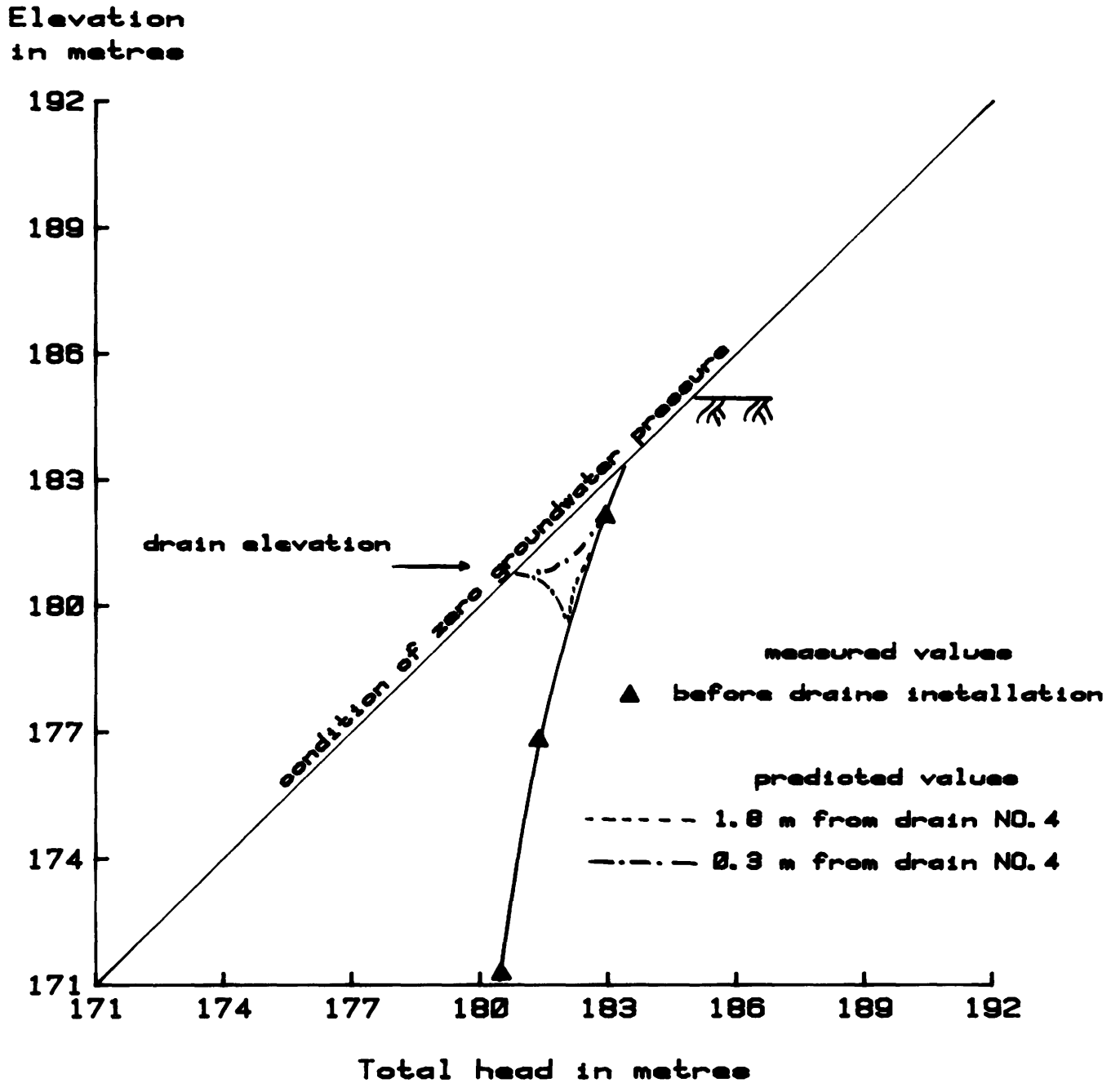
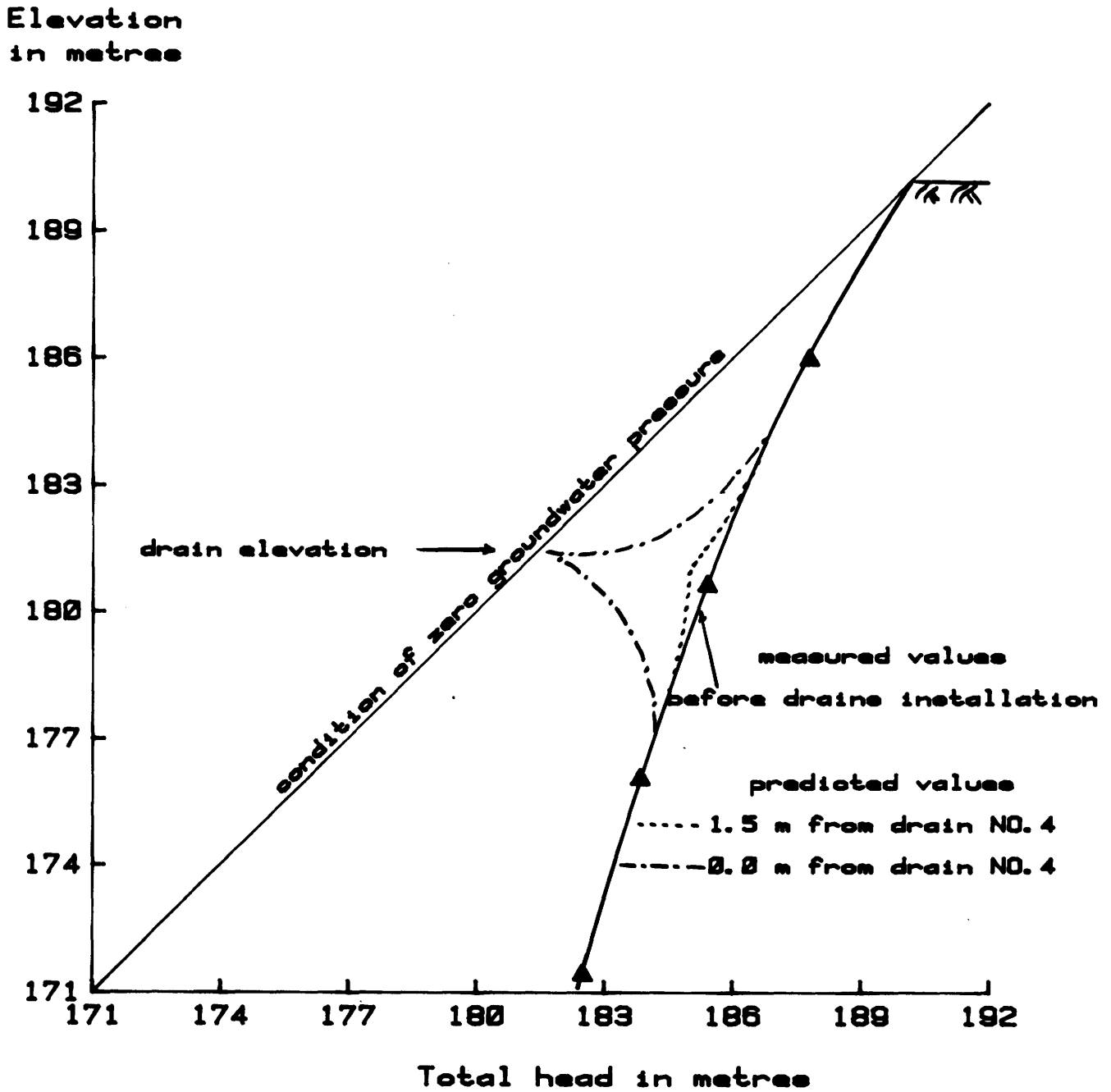


Figure 3—Measured groundwater pressure distribution along section A-A at different distances from drain No. 4.



Location B - time 500 days

Figure 4—Predicted groundwater pressure distribution along section B-B at different distances from drain No. 4.



Location A- time 500 days

Figure 5—Predicted groundwater pressure distribution along section A-A at different distances from drain No. 4.

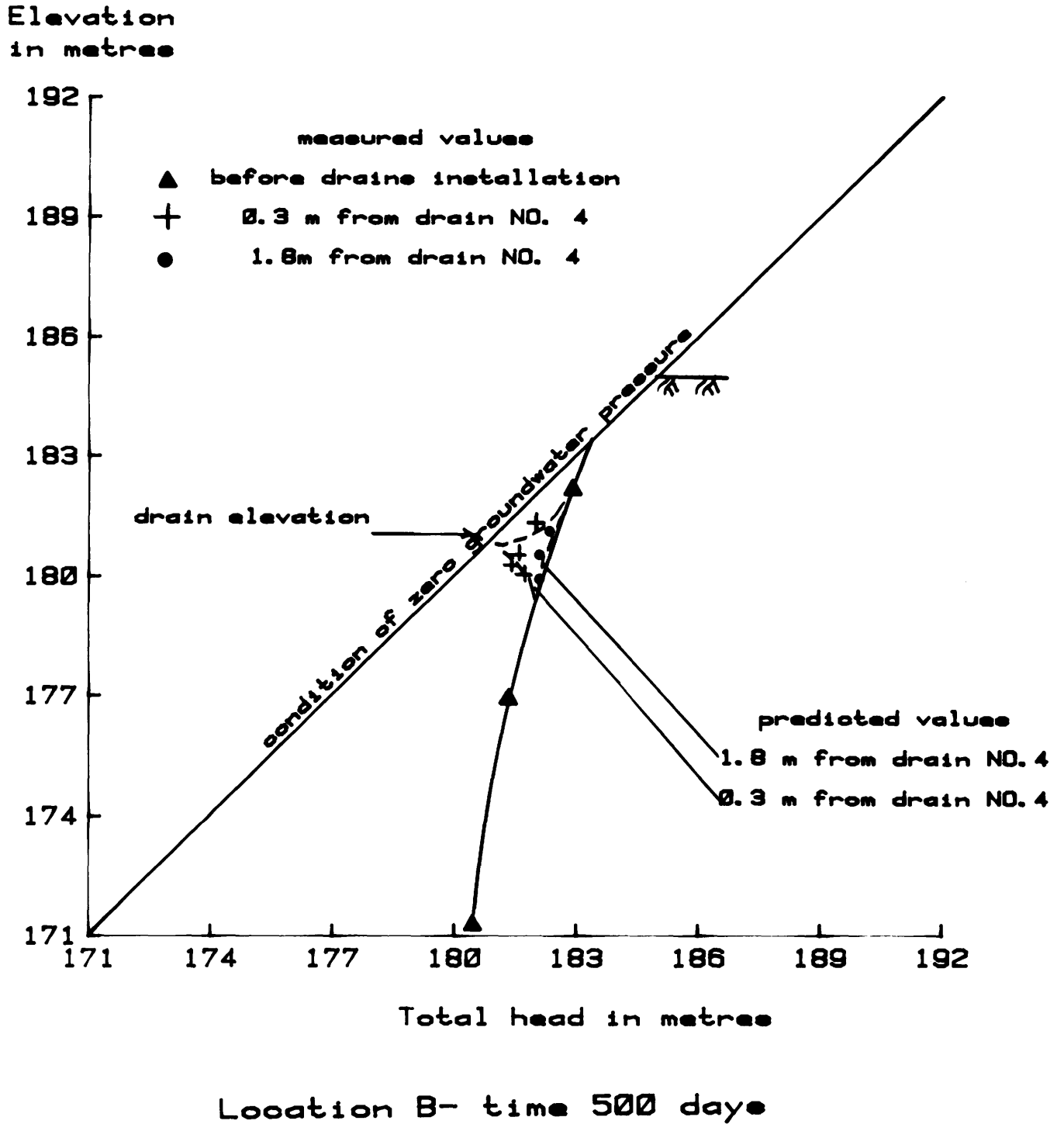


Figure 6—Comparison between measured and predicted groundwater pressure distribution along section B-B at different distances from drain No. 4.

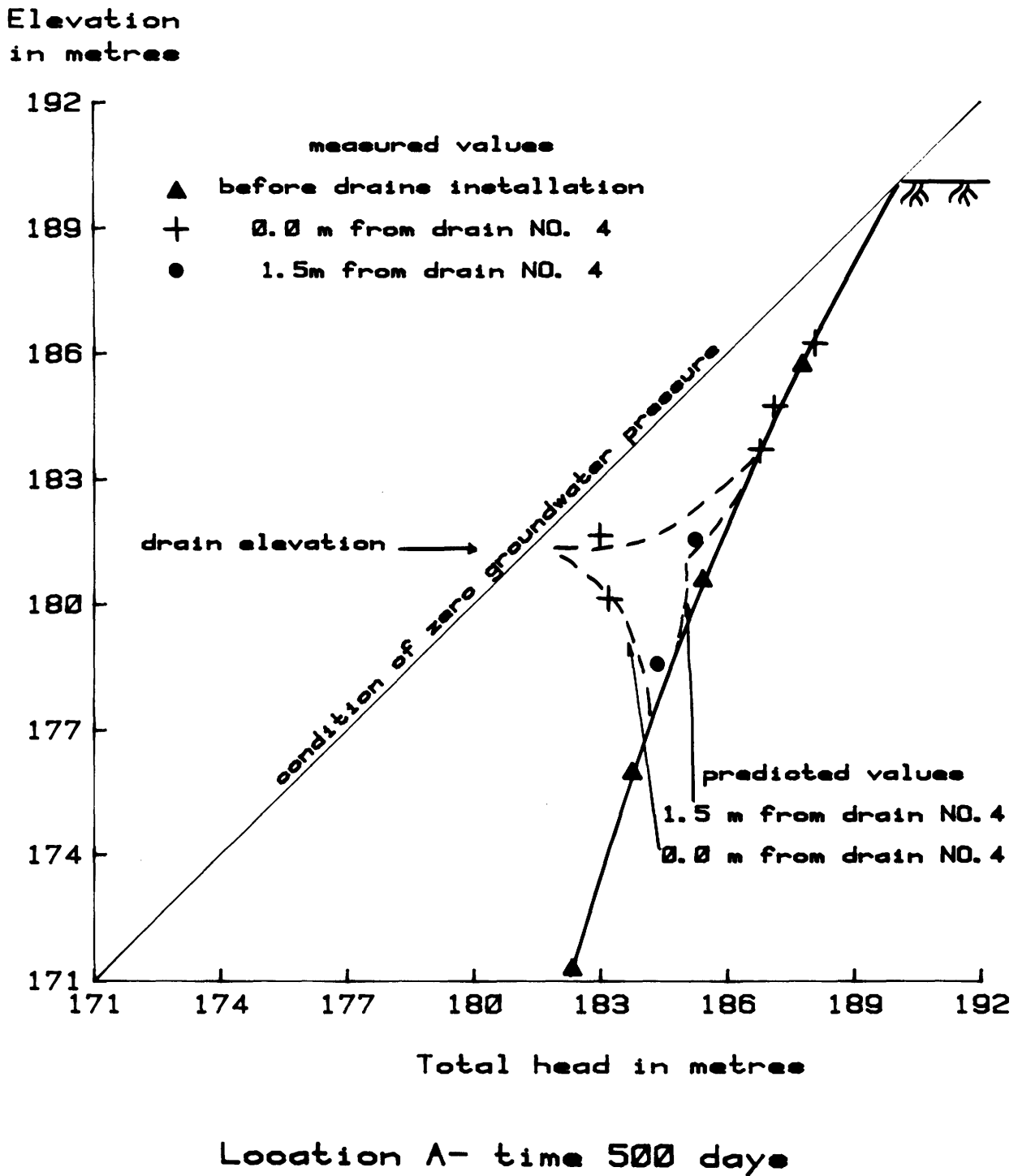


Figure 7—Comparison between measured and predicted groundwater pressure distribution along section A-A at different distances from drain No. 4.

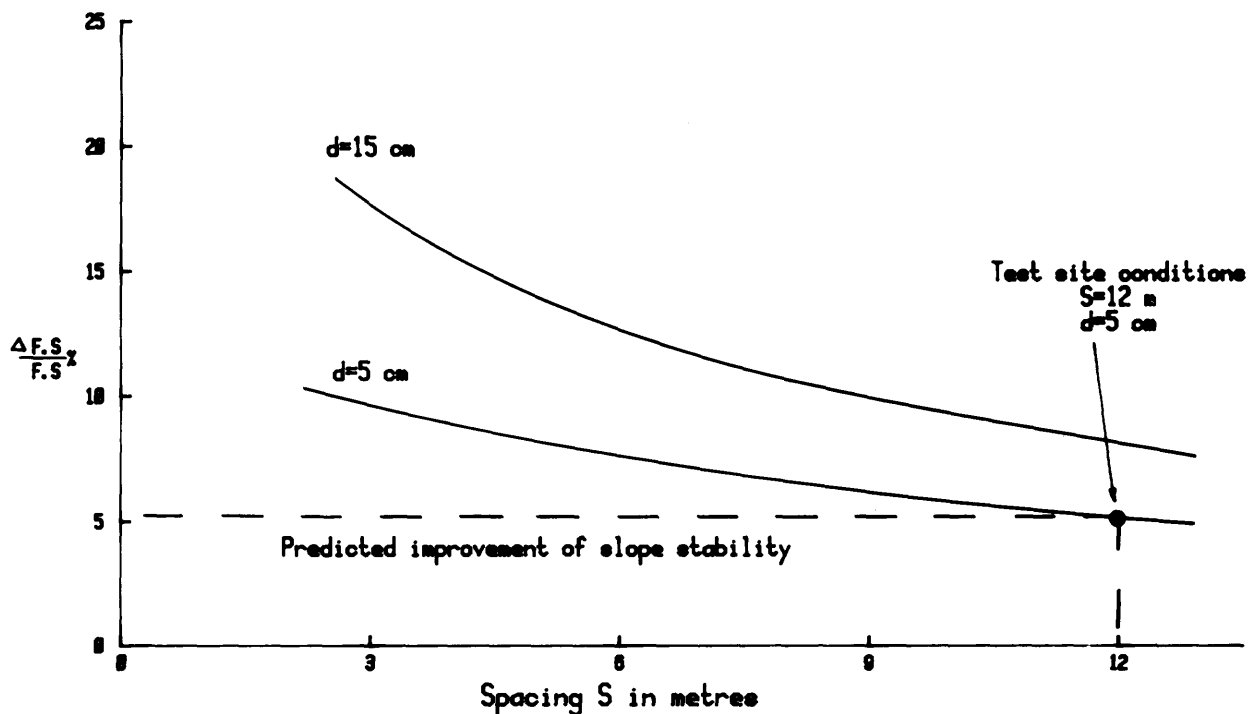


Figure 8—Predicted ultimate improvement of safety factor (F.S.) of Wabi Creek slope showing influences of drain spacing S and drain diameter d .

was installed by first drilling a hole with standard diamond drill casing (B-size casing) and then inserting the drain. The holes were inclined at a slope of about 1 degree upward into the slope. The final alignments of the drains were determined with a borehole directional inclinometer and the maximum deviation from the desired location was about 0.6 m.

(c) **MONITORING OF GROUNDWATER PRESSURES.** After the installation of the drains, groundwater pressures in the slope were monitored on a weekly basis for six months and, thereafter, the interval between readings was extended to two weeks.

(d) **DEVELOPMENT OF PREDICTIVE METHOD.** A modified integrating finite-difference computer program from the University of California (Narasimhan 1975) was used to model the slope and the drains. The numerical model was based on the theory of consolidation by which changes in groundwater pressures with time could be calculated using measured soil properties and measured hydraulic boundary conditions at the site. In conjunction with the integrating finite-difference program, a slope stability program, which can handle the groundwater pressure output from the integrating finite-difference program directly, was used to analyse slope stability. With this type of input, the groundwater pressure changes around the drain may be accurately represented and thereby will give an accurate analysis of slope stability.

1980-1981 RESEARCH PROGRAM

(a) **SOIL SAMPLING AND TESTING.** In August 1980, two borings were made to obtain undisturbed clay samples. Laboratory tests were conducted on these samples to determine the consolidation properties of the soils in the slope.

(b) **DETERMINATION OF THE EFFICIENCY OF THE DRAINS.** A special pressure packer was designed at the University of Toronto and was used to determine if the filter cloth was being clogged around the drains and if there was reduction in permeability of the filter cloth due to the soil pressures against the drainpipe. The test results are presented in Table 1. By comparing the rate of water flowing through the drainpipe in the slope and the rate of water flowing through the drainpipe without soil around it, it can be concluded that the filter cloth around the drains in the slope is not clogged and that the drains are performing as designed.

(c) **DETERMINATION OF GROUNDWATER PRESSURES AROUND DRAINS.** In August 1980, groundwater pressure distribution around the horizontal drains was determined by installing lines of electrical piezometers at locations close to the drains. The locations of these electrical piezometers are given in Figure 1. The results of the measurements are presented in Figure 2 and 3.

(d) COMPARISON BETWEEN MEASURED AND PREDICTED CHANGES IN GROUNDWATER PRESSURE.

The changes in groundwater pressure in the test site due to the installation of horizontal drains was studied with the analytical procedure using soil properties obtained from laboratory tests and measured hydraulic boundary conditions at the site. For simplicity, a two-dimensional model was used. The predicted groundwater pressure distribution along cross-sections A and B (see Figure 1) is presented in Figures 4 and 5.

A comparison between measured and predicted changes in groundwater pressure along these two sections is given in Figures 6 and 7. This comparison clearly shows that changes in groundwater pressures in slopes due to horizontal drains can be predicted with confidence, using the analytical procedure.

(e) INFLUENCE OF DRAIN SIZE AND DRAIN SPACING.

To determine the influence of drain size and spacing on the effectiveness of horizontal deep drains in reducing groundwater pressures, and thereby increasing the stability of the slope at the test site, an analysis of parameters has been conducted using the computer program from the University of California. The results of this study are presented in Figure 8.

DISCUSSION

After the installation of the horizontal drainage system, groundwater pressures in the slope were monitored with piezometers. These measurements indicate that the drains have not caused groundwater pressure decreases of the magnitude expected. The reason for this is that the drains installed in the test site are too small in diameter and the spacings between the drains are too large. Figure 8 clearly shows that by increasing the drain size and/or reducing the spacing between drains, the stability of the slope could be further improved.

Comparisons between the measured and the predicted groundwater pressures at the test site (Figures 6 and 7) indicate that the analytical procedure that was adopted can be used with confidence.

The measured and predicted changes in groundwater pressures in the slope clearly indicate that the effectiveness of horizontal drains to reduce groundwater pressures in slopes in clay soil is very local and can be predicted with a two-dimensional model. This implies that the length of the drain is not important as long as the drain extends beyond the critical slip surface of the slope.

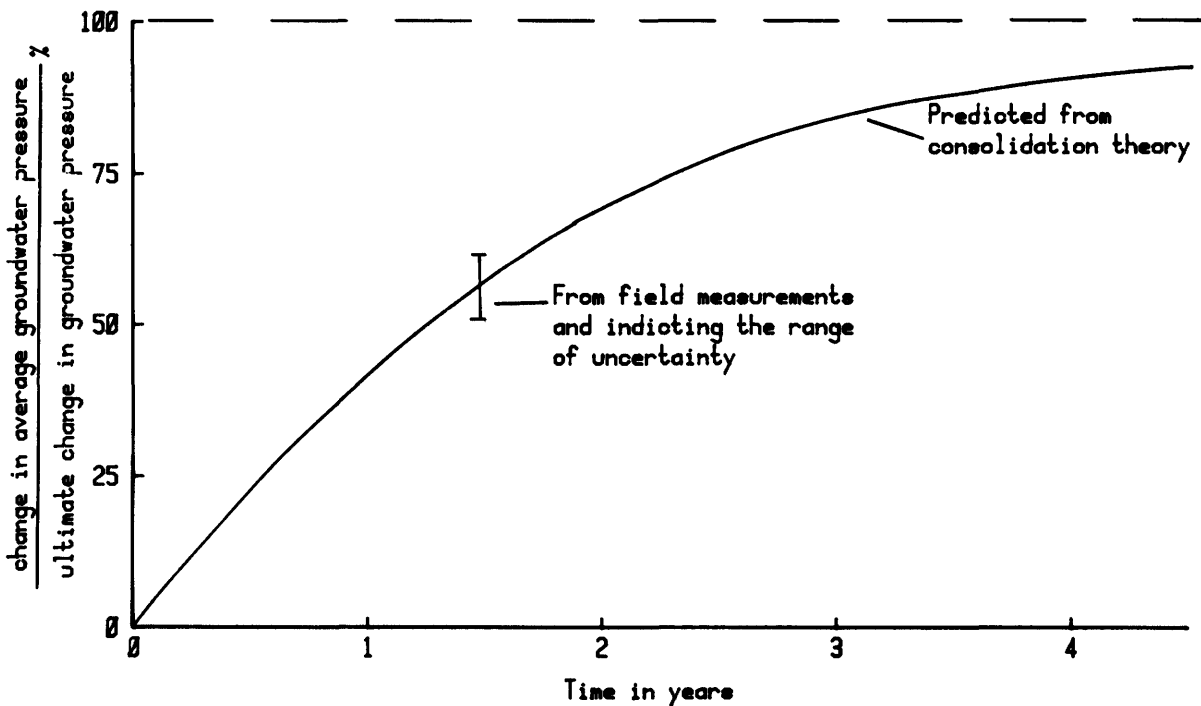


Figure 9—Rate of average changes in groundwater pressure of Wabi Creek slope due to installation of drains

CONCLUSIONS

- 1) Horizontal deep drains can be used to reduce groundwater pressures in clay slopes.
- 2) The effectiveness of horizontal deep drains to reduce groundwater pressures in clay slope and, thereby, to increase the stability of slopes can be improved by increasing the diameter of the drainpipes and/or reducing the spacings between drains.
- 3) The analytical procedure adopted in this research program can be used to predict the influence of horizontal drains in slopes and to design the dimensions and spacing of horizontal drainage systems for slope stability.
- 4) The economic viability of this approach to stabilize clay slopes has not been adequately studied and remains in question at this time. The development of a more economical way to construct and install horizontal drains is necessary.

5) About four years is required for the horizontal drainage system at the test site to become 90 percent effective (Figure 9). This gives a good idea of the time required for horizontal drains to become effective in soft clay soils because the clay soil at Wabi Creek is typical of the soft soils which have a small value of coefficient of consolidation.

REFERENCES

- La Rochelle, P. Lefebvre, G. and Bilodeau P.M.
1977: The stabilization of a slide in Saint-Jerome, Lac Saint-Jean; Canadian Geotechnical Journal, Vol. 14, p 340.
- Narasimhan, T.N.
1975: A unified numerical model for saturated-unsaturated groundwater flow; Unpublished Ph.D thesis, Department of Civil Engineering, University of California, Berkeley.

Grant 27 Field Relations and Geochemistry of Gold, Nickel, and Chromium Deposits in Ultramafic-Mafic Volcanic Rocks

R. Kerrich, D.J. Robinson, and R.L. Barnett

Department of Geology, University of Western Ontario

ABSTRACT

Silicate-facies iron formation, composed of manganese garnet, stilpnomelane and ferro-tschermakitic hornblende, flanks and in places is footwall to a stratabound massive nickel sulphide deposit at Redstone River, near Timmins. Garnet-stilpnomelane rocks represent a mixture of pyroclastic material and chemical sediment whereby all the Al, Ti, Zr, V, and P have a volcanoclastic origin, most of the Fe, Mn, Ca, Mg, Co, Y and Rb have been chemically precipitated, and Cr, Ni, Sr, Na, Nb, Ba and K have been leached from a volcanic precursor. Garnets are extensively zoned with respect to Mn, Fe, Ca and Mg, and display normal, reverse and oscillatory patterns. The maximum Mn/Fe ratio in garnet at the Redstone deposit is coincident with the nickel sulphide zone whereas minimum Mn/Fe ratios were observed in garnet-bearing samples laterally away from the deposit. Manganese garnet horizons are coincident with several gold and base metal sulphide deposits and represent key exploration guides to ore.

INTRODUCTION

The objective of the study is to investigate, on a broad comprehensive basis, the rocks and types of mineralization that are associated with metavolcanics and metasediments in the stratigraphically lower parts of Archean greenstone belts of Ontario. Deposits of Au and Ni are included. Studies of gold-enriched environments have been conducted at the Dome Mine in the Timmins area, the Dickenson Mine in the Red Lake area, and the Kerr Addison Mine in the Larder Lake area. Evaluation of Ni has been conducted at Redstone in the Timmins area.

At these deposits detailed geochemical evaluation, including major element analysis, trace and transition metal analysis, mineral chemistry and oxygen isotope determinations, have been applied to elucidating the environment of ore deposition in terms of temperature, pressure, hydrological regime, and the nature and magnitude of fluid-rock interaction.

PART A. GOLD

In two previous reports data for the chemical composition of gold-bearing chemical sedimentary rocks and their enclosing volcanic rocks at the Dome and Dickenson Mines were reported, together with oxygen isotope studies and redox patterns associated with gold enrichments (Kerrich *et al.* 1979, 1980). This report adds to the previous geochemical results with data for "flow" ore at the Kerr Addison Mine. All data from the three deposits are here treated in terms of rigorous chemical mass balance in order to establish patterns of alteration. In addition, a summary of the patterns of metal distribution in lode gold deposits is presented, and compared to metal distribution patterns in massive base metal sulphide deposits.

PATTERNS OF ALTERATION

The abundance of major element oxides and selected trace elements for flow ore at the Kerr Addison Mine is presented in Tables 1 and 2. Samples were collected from the footwall to the hanging wall of the 3821-50½ stope, cut 5 (KA 1 - KA 5), 3821-50½ cuts 13 (KA 6 - KA 10) and 38.

"Flow" ore is composed principally of pyritic tuff and mafic pillowed flows (Downes 1979). Electron microprobe analyses of minerals present in selected samples from the ore are compiled in Tables 3, 4 and 5. Albite (Ab > 92), chromian muscovite, and carbonates ranging in composition from dolomite through ankerite to magnesite-siderite are present. Inspection of Tables 1 and 2 reveals that both sodic and potassic-CO₂ patterns of alteration are present. Samples FA, FB, and the KA sample suite, exemplifying sodium enrichment (7.9 weight percent Na₂O, 0.18 weight percent K₂O), possess about ten times the Na₂O and one tenth the K₂O of the potassic, Fe, Mg, Ca-carbonate enriched samples (FC, WA, WB, WC). Note that the abundances of several of the diagnostic, relatively immobile, elements simultaneously indicate a probable primary dacitic or trondhjemitic igneous parentage for the first two samples in Table 2 (Ti/Zr 20-29, Sc 15-22 ppm, Nb 31-42 ppm), and a basaltic parentage for the latter four samples (Ti/Zr 36-58, Sc 21-40 ppm, Nb 0.4-11 ppm). If interpretation of the igneous parentage is correct, then absolute abundances of Si, Fe, Mg, Cr and

GRANT 27 AU, NI, AND CR IN ULTRAMAFIC-MAFIC VOLCANIC ROCKS

Table 1—Abundances of major and selected trace elements in "flow" ore at the Kerr Addison Mine.

	KAB1-1	KAB1-2	KAB1-3	KAB1-4	KAB1-5	KAB1-6	KAB1-7	KAB1-8	KAB1-9	KAB1-10
SiO_2	30.1	45.4	38.9	48.7	11.3	45.3	45.9	62.5	56.7	71.2
TiO_2	0.26	1.67	1.52	1.59	0.37	1.71	1.02	1.01	1.16	0.78
Al_2O_3	17.1	13.3	11.0	14.1	4.49	11.1	9.54	7.15	10.6	7.43
Fe_2O_3	15.69	13.47	20.70	12.24	11.80	14.80	9.54	9.34	9.26	5.05
MnO	0.17	0.24	0.23	0.13	0.35	0.21	0.28	0.23	0.13	0.06
MgO	24.8	4.40	3.31	3.40	16.2	3.87	3.79	3.10	3.05	2.32
CaO	0.09	6.16	7.04	5.83	21.7	8.88	12.2	6.69	5.54	3.55
K_2O	0.01	0.39	0.12	0.07	0.10	0.40	0.20	0.15	0.04	0.04
Na_2O	0.22	7.04	6.78	7.74	0.94	4.69	4.94	3.59	6.08	4.26
P_2O_5	0.01	0.03	0.03	0.03	0.01	0.09	1.54	0.11	0.03	0.01
L.O.I.	11.23	6.85	11.31	6.39	32.39	7.39	9.39	5.23	6.47	3.70
Total	99.6	99.0	101.0	100.2	99.7	98.4	98.4	99.1	99.0	98.4
Ag										
Au	6	<5	8	<5	<5	<5	<5	<5	<5	<5
Be	<.1	.2	<.1	<.1	.4	.4	<.1	.3	<.1	<.1
V	81.3	92.5	52.7	45.5	167	373	103	180	45.4	33.4
Cr	51.3	32.1	27.3	31.6	1860	39.6	23.5	23.4	22.5	95.8
Co	18	16	16	16	69	20	16	18	<3	17
Ni	80	51	54	51	870	53	36	46	46	66
Cu	70.4	385	553	119	62.0	152	219	380	796	37.5
Zn	70	41	25	17	46	63	44	28	17	10
Mo	<30	<30	<30	<30	<30	<30	<30	<30	<30	<30
Pb	<5	5	10	<5	<5	<5	<5	<5	<5	<5
Th	<6	<6	<6	<6	<6	<6	<6	<6	<6	<6
Sr	73.7	170	147	153	331	81.7	140	132	142	133
Zr	101	43	35	44	8	47	19	20	16	8
Cd	<7	<7	<7	<7	<7	<7	<7	<7	<7	<7

Ni are not useful for deducing parent rock-types for these examples of alteration.

An essential problem to be resolved and interpreted is why the low temperature, oxidative, sodic, seawater-induced alteration is spatially associated with, but distinct from, the reduced, potassic-CO₂ alteration. Kerrich and Hodder (in press) have addressed this question, and suggest that mixing of two fluids in permeable volcanic aquifers on the seafloor is implicated. One fluid was auriferous, relatively hot (350-450°C), reduced, and of probable metamorphic origin, possessing elevated CO₂ to stabilize carbonate and a K/Na ratio ~1 such that muscovite was stable. The second fluid was cool (<250°C), oxidized and of probable marine origin, possessing low CO₂ and a Na/K ratio ~27 (~seawater ratio) such that albite

formed from the hydrolysis of plagioclase.

Recognition of large low-temperature, sodium-dominated oxidative alteration patterns around stratabound volcanic-hosted gold concentrations may present a useful pathfinder in exploration. Significant additions of Mn accompany K + CO₂ fixation in the higher temperature, reducing alteration environment. Conversely, Mn is stripped from rocks during the low-temperature, sodic oxidizing alteration.

The two types of alteration patterns are illustrated in Figures 1 and 2. Calculations of mass balance were conducted according to the method of Gresens (1967) using an average of analyses of five relatively fresh tholeiitic basalts and an analysis of a fresh quartz-feldspar porphyry of trondhemitic composition as parent rocks.

Table 2—Chemical analyses of "flow" ore at the Kerr Addison Mine. Major elements in weight percent, trace elements in ppm. Sodic and potassic-CO₂ categories are alteration types.

	Sodic		Potassic - CO ₂			
	FA	FB	FC	WA	WB	WC
SiO ₂	55.71	55.25	25.81	27.35	20.26	11.33
TiO ₂	0.86	0.86	0.37	0.41	0.37	0.25
Al ₂ O ₃	14.92	15.10	8.47	6.70	6.37	5.08
Fe ₂ O ₃	6.20	5.82	7.95	9.83	9.96	9.31
MnO	0.18	0.13	0.49	0.30	0.30	0.35
MgO	1.96	2.43	9.27	12.24	16.37	16.70
CaO	4.41	4.55	17.54	16.37	15.36	20.70
K ₂ O	0.18	0.15	0.92	1.00	1.19	0.95
Na ₂ O	7.95	7.85	2.25	0.68	0.68	0.45
P ₂ O ₅	-	-	-	-	-	-
LOI*	6.38	6.23	25.62	26.35	30.47	35.19
Total	98.75	98.37	98.70	101.23	101.33	
S%	3.30	2.94	0.27	0.35	0.15	0.35
Au	6.70	25.0	0.63	0.16	0.20	0.10
Ag	1.4	3.8	-	-	-	-
As	350	280		1700	1850	1700
Sb	4.6	6.1		22	15	15
Sc	15	22	40	26	30	21
V	81	79	188	149	174	127
Cr	130	270	2170	2870	2490	1750
Co	90	44	148	104	139	106
Ni	99	175	1280	977	997	799
Cu	217	468	89	51	142	59
Zn	389	664	55	55	47	46
W	40	90		14	25	27
Pb	-	-	-	-	10	-
Th	-	8	-	-	-	-
Rb				20	26	19
Sr	64	77	180	106	151	213
Y				8	6	5
Zr	174	251	43	43	42	41
Nb	31	42	10	11	0.4	8
Cd	-	-	-	-	-	-
Ba				219	227	225
Ti/Zr	29	20	51	58	52	36

*Weight percent loss on ignition at 1100°C. Blank space indicates no analysis, - signifies below detection limit.

GRANT 27 AU, NI, AND CR IN ULTRAMAFIC-MAFIC VOLCANIC ROCKS

Table 3—Analyses of albite grains by electron microprobe, "flow ore", Kerr Addison Mine.

	Sample 010					Sample 1130		
	1A	2A	3A	4A	$\bar{X}A$	1B	2B	$\bar{X}B$
SiO ₂	69.02	69.02	69.80	68.64	69.12	69.53	68.06	68.80
Al ₂ O ₃	19.49	19.89	19.75	19.84	19.74	19.05	19.70	19.38
CaO	0.17	0.05	0.04	0.02	0.07	0.04	0.32	0.18
Na ₂ O	11.46	10.80	10.75	11.60	11.15	11.34	11.54	11.44
K ₂ O	0.03	0.04	0.02	0.05	0.04	0.07	0.04	0.06
Total	100.17	99.80	100.36	100.15	100.12	100.03	100.03	99.84
Si	12.016	12.019	12.074	11.960	12.017	12.104	11.933	12.019
Al	3.998	4.082	4.026	4.073	4.045	3.908	4.070	3.989
Na	3.868	3.646	3.605	3.919	3.759	3.827	3.923	3.875
Ca	0.032	0.009	0.007	0.004	0.013	0.007	0.060	0.034
K	0.007	0.009	0.004	0.110	0.008	0.016	0.009	0.012

	Sample 028						
	1C	2C	3C	4C	5C	6C	$\bar{X}C$
SiO ₂	69.39	68.65	68.76	68.97	69.15	69.88	69.13
Al ₂ O ₃	19.33	19.14	19.50	19.51	19.60	19.61	19.45
CaO	0.00	0.14	0.01	0.02	0.00	0.09	0.04
Na ₂ O	11.95	11.86	12.44	12.33	11.91	11.48	12.00
K ₂ O	0.05	0.05	0.07	0.03	0.07	0.11	0.06
Total	100.72	99.84	100.78	100.86	100.73	101.17	100.68
Si	12.030	12.016	11.951	11.967	11.991	12.040	12.040
M	3.949	3.948	3.994	3.989	4.005	3.981	3.981
Na	4.017	4.025	4.192	4.148	4.004	3.835	3.835
Ca	0.000	0.026	0.002	0.004	0.000	0.017	0.017
K	0.011	0.011	0.016	0.007	0.015	0.024	0.024

Table 4—Analyses of muscovite grains by electron microprobe, "flow ore", Kerr Addison Mine.

	Sample 010				
	1	2	3	4	\bar{X}
SiO ₂	48.91	47.00	47.89	47.64	47.86
Al ₂ O ₃	29.37	31.51	32.09	31.92	31.22
TiO ₂	0.17	0.14	0.11	0.04	0.12
Cr ₂ O ₃	1.57	2.93	2.85	2.42	2.44
FeO	0.80	0.63	0.66	0.74	0.71
MgO	2.99	1.52	1.57	1.50	1.90
MnO	0.00	0.00	0.00	0.11	0.03
CaO	0.01	0.04	0.02	0.00	0.02
Na ₂ O	0.23	0.00	0.00	0.00	0.06
K ₂ O	9.55	9.59	9.12	9.98	9.56
Total	93.60	93.36	94.31	94.35	93.90
Si	6.588	6.369	6.393	6.392	6.435
Al IV	1.412	1.631	1.607	1.608	1.565
	8.000	8.000	8.000	8.000	8.000
Al Vi	3.250	3.400	3.441	3.439	3.383
Ti	0.017	0.014	0.011	0.004	0.012
Cr	0.167	0.314	0.301	0.257	0.260
Fe	0.090	0.071	0.074	0.083	0.080
Mg	0.600	0.307	0.312	0.300	0.380
Mn	0.000	0.000	0.000	0.013	0.003
	4.125	4.107	4.139	4.095	4.116
Ca	0.001	0.006	0.003	0.000	0.003
Na	0.060	0.000	0.000	0.000	0.015
K	1.641	1.657	1.553	1.708	1.640
	1.702	1.663	1.556	1.708	1.657
Fe/Mg	0.150	0.233	0.236	0.318	0.218

 \bar{X} = average of analyses

GRANT 27 AU, NI, AND CR IN ULTRAMAFIC-MAFIC VOLCANIC ROCKS

Table 5—Analyses of carbonate minerals by electron microprobe, "flow ore", Kerr Addison Mine.

Sample 010									
	1	2	3	4	5	6	7	8	9
MgO	18.57	17.98	18.22	10.34	33.96	17.77	17.28	32.98	29.00
MnO	0.11	0.27	0.09	0.75	0.02	0.20	0.31	0.01	0.30
FeO	5.09	6.07	5.55	14.62	20.84	5.46	6.68	16.97	24.96
CaO	30.15	29.88	29.94	30.69	0.17	29.29	29.41	4.59	0.20

Sample 1130							
	1	2	3	4	5	6	7
MgO	8.85	18.20	9.65	8.85	10.29	10.34	18.20
MnO	1.06	0.08	1.96	1.06	0.71	0.75	0.08
FeO	18.34	5.59	14.81	18.34	15.25	14.62	5.59
CaO	29.09	29.49	27.87	29.09	30.33	30.69	29.49

Sample 028						
	1	2	3	4	5	6
MgO	16.04	12.11	13.54	14.14	13.15	14.82
MnO	0.46	0.33	0.52	0.82	1.05	0.58
FeO	7.66	41.77	44.84	43.12	12.21	8.55
CaO	27.83	2.51	0.50	0.31	28.80	28.46

Percentage gains and losses relative to parent

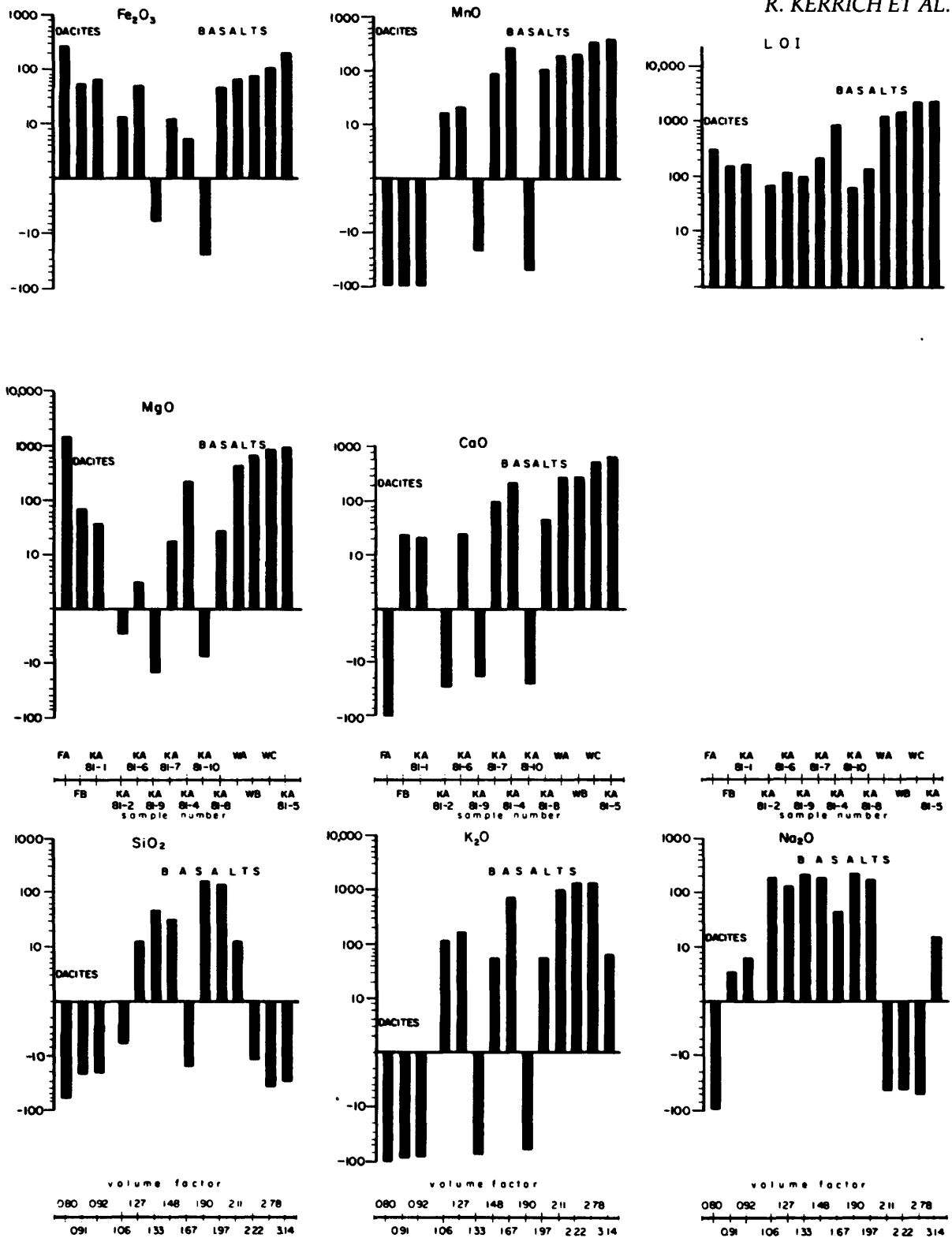


Figure 1—Calculated gains and losses of major element oxides for transformation of dacitic and basaltic precursors to hydrothermally altered products during gold mineralization in the "flow" ore, Kerr Addison Mine. Gains and losses expressed as a percentage relative to abundance in the assumed parent. Sources of data, Tables 1 and 2.

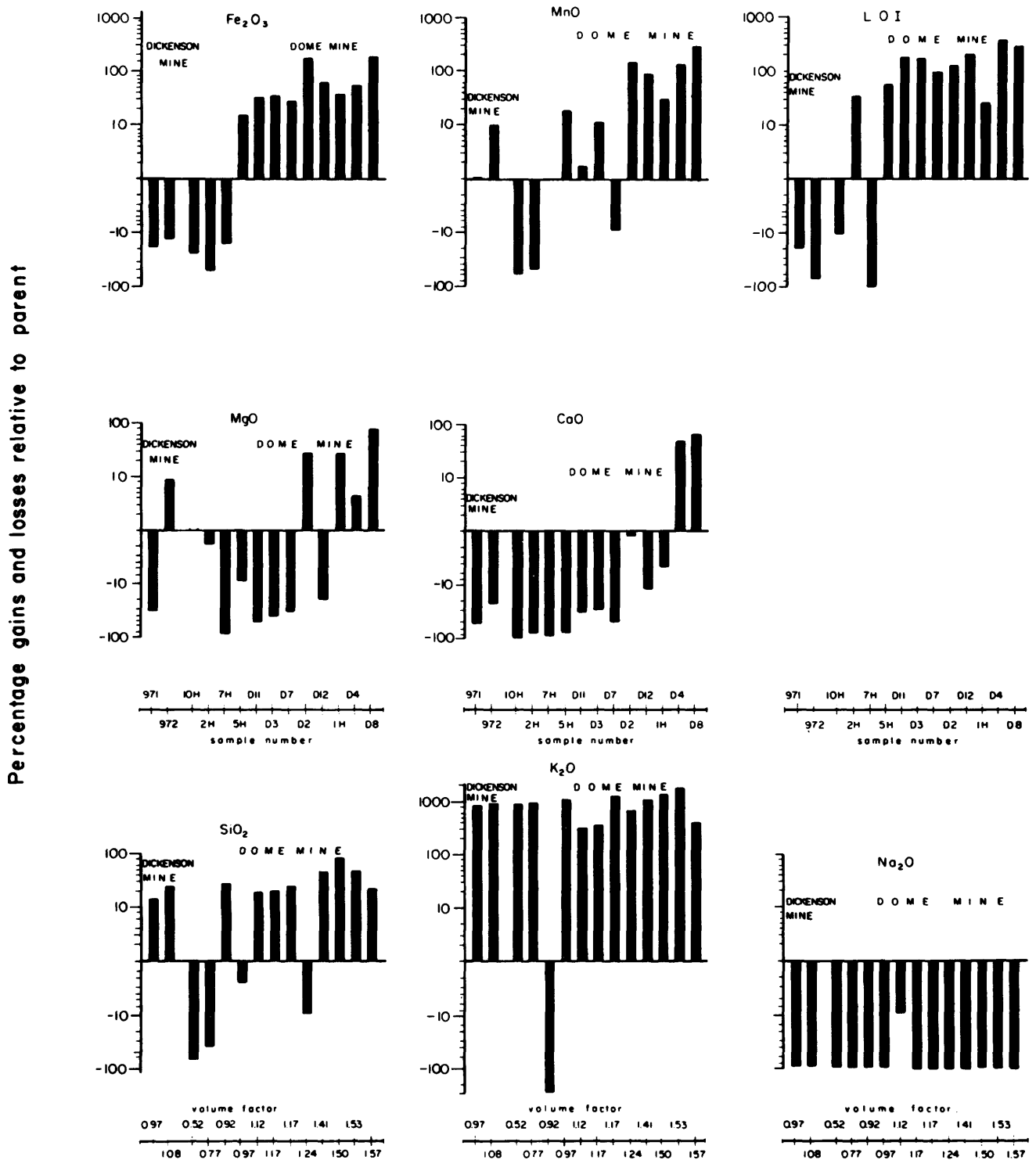


Figure 2—Calculated gains and losses of major element oxides for transformation of basaltic precursors to hydrothermally altered products during gold mineralization in the Dickenson Mine (host rocks to sedimentary ore, East South C zone) and Dome Mine (host rocks to “ankerite” sedimentary ore). Sources of data, Kerrich et al. (1979, 1981).

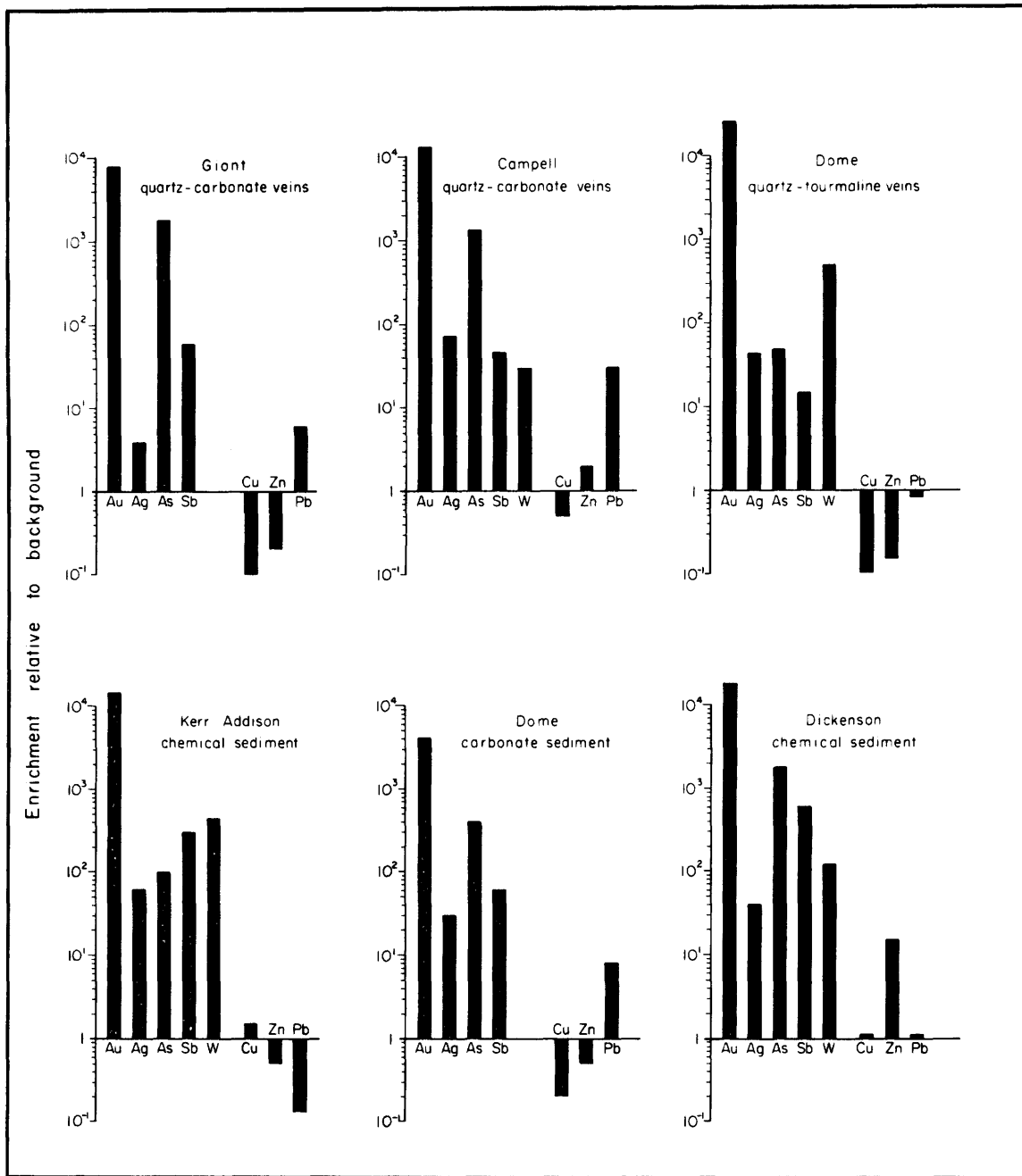


Figure 3—Enrichment of selected elements in Archean lode gold deposits. The upper three graphs are for vein-type orebodies, whereas the lower three represent gold-bearing chemical sedimentary rocks. Note logarithmic coordinate.

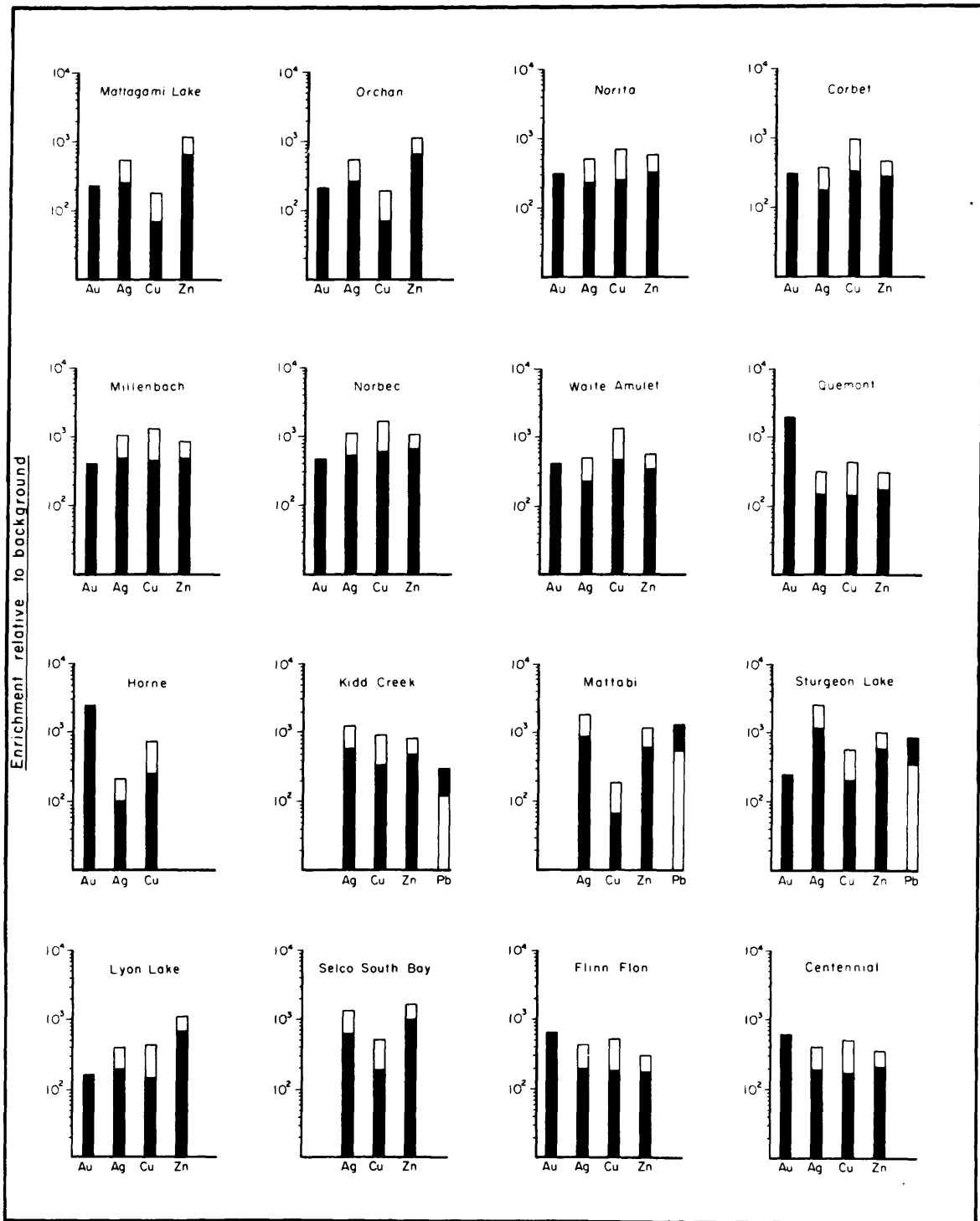


Figure 4—Enrichments of Au, Ag, Cu, Zn and Pb where recovered in some Precambrian base metal massive sulphide deposits. Solid bars represent enrichments relative to background abundance in unaltered mafic volcanic rocks, open bars signify enrichments relative to abundances in primary felsic igneous rocks. Note logarithmic coordinate.

METAL DISTRIBUTION

Compilation of the abundances of metals in Archean lode gold deposits reveals that both vein and chemical sedimentary types possess extreme enrichments of a suite of rare elements (Au, As, Sb, W, B, Se, Te, Bi) coupled with low concentrations of the more abundant and mobile base metals (Cu, Pb, Zn), whereas in massive base metal sulphide deposits Au, Ag, Cu, and Zn are all enriched by a factor of 200 to 2000 and there is no large separation of gold relative to base metals (Kerrich and Fryer 1981; Kerrich and Hodder in press). These relations are illustrated in Figures 3 and 4.

Separation of base metals out of auriferous systems could be accounted for by generation of fluid reservoirs during metamorphic dehydration at 350 to 480°C, when the water to rock ratio is low and halogen availability is limited by crustal abundance (60 ppm). These two factors may constrain the uptake of abundant base metals into solution, but the solute concentration of rare elements is not limited by solubility. By contrast, in base metal systems, which are the product of thermally driven seawater convection, fluid to rock ratio is high and total seawater halogens (19,000 ppm) exceed dissolved metals, such that there is no constraint on the uptake of either base metals or rare elements into solution.

Many lode gold deposits are characterized by K, CO₂, Si alteration of their enveloping rocks, whereas base metal deposits typically exhibit fixation of Fe, Mg, Si and S in footwall rocks. The fluids from which gold was precipitated had significant CO₂ and K≅Na, whereas the fluids which generated base metal deposits had much less CO₂ than H₂O and much more Na than K. Lode gold deposits may also have a relatively large halo of low-temperature, oxidative, sodic spilitization in enclosing volcanic rocks as described above, where seawater has streamed into cooling stocks or flows that have acted to focus the mineralization by metamorphic discharge along thermal contraction fractures. The submarine environment is one hydrologically appropriate for the mixing of fluids from two initially independent hydrothermal reservoirs, and hence the blending of their separate characteristics.

We believe that those major differences in the metal distribution and patterns of alteration associated with lode gold and base metal massive sulphide deposits should be taken into consideration in models for exploration.

PART B. NICKEL

Numerous stratiform volcanic-hosted gold and massive base metal sulphide deposits are accompanied by iron and manganiferous chemical sedimentary rocks. Recently, compositionally zoned manganese garnets have been recognized within metamorphosed chemical sedimentary units and alteration zones enveloping and coincident

with massive sulphide deposits at Ducktown, Tennessee (Addy and Ypma 1978), and Pegmont, Australia (Stanton and Vaughan 1979), and stratigraphically underlying stratiform gold orebodies at Bousquet and Dumagami, Quebec (Valliant 1981). The garnetiferous units at each of these deposits are enriched in Mn with respect to the surrounding rocks; the maximum Mn/Fe ratios in garnet and in whole rock are often coincident with the ore zones, and the Mn/Fe ratio decreases systematically along strike into barren country rock.

A stratabound massive nickel sulphide deposit near Redstone River, in the Timmins area, is locally underlain and flanked by a laterally continuous chemical sedimentary unit composed of manganese garnet, stilpnomelane, and ferro-tschermakitic hornblende. Chemical analyses of whole rocks and minerals were used to evaluate the chemical variation of Mn in garnet and in whole rock with respect to the nickel sulphide zone.

GEOLOGICAL SETTING OF THE REDSTONE DEPOSIT

Detailed descriptions of the Redstone deposit geology are presented by Robinson and Hutchinson (1981) and Kerrich *et al.* (1980) and emphasis here is restricted to the sequence of garnetiferous chemical sedimentary rocks which occur as a laterally continuous stratigraphic marker horizon, below sulphide-facies iron formation, flanking and in places forming the footwall to the Fe-Ni-Cu sulphide layer, referred to as the R-zone (Figures 5, 6). The garnet-stilpnomelane rock is interbedded with massive to well-bedded dacitic ash layers and with chert at the base of the sulphide iron formation. Garnet forms banded layers, semi-continuous lenses and disseminated megacrysts, with green to brown radiating stilpnomelane sheaves, within a blue-green ferro-tschermakitic hornblende matrix. Chlorite, biotite, quartz, albite, calcite, epidote, sphene, pyrite, pyrrhotite and minor sphalerite are accessory minerals. The habit and inclusion pattern of garnet in these rocks is apparently a function of the mineral assemblage. Individual garnet crystals occur as anhedral to subhedral, ragged poikilitic grains, 0.25 to 3.0 mm, within an amphibole-quartz-feldspar matrix, and as subhedral to euhedral non-poikilitic metacrysts within chlorite-biotite-epidote bands.

GEOCHEMISTRY AND MASS BALANCE

Garnet-stilpnomelane rocks are interbedded with dacitic tuff and appear megascopically and microscopically to represent a mixture of pyroclastic material and chemical sediment. Consequently, major and trace elements of 18 garnet-stilpnomelane rocks were compared to the average dacitic tuff composition, utilizing Gresen's (1967) mass balance equations, to differentiate between the chemical signature of the pyroclastic component versus that of the hydrothermal precipitate. Garnet-stilpnomelane rocks are extremely rich in FeO, ranging from 17.7 to 54.3 weight percent (Table 6) and are iron formation *sensu stricto* with >15 percent Fe (Gross 1965).

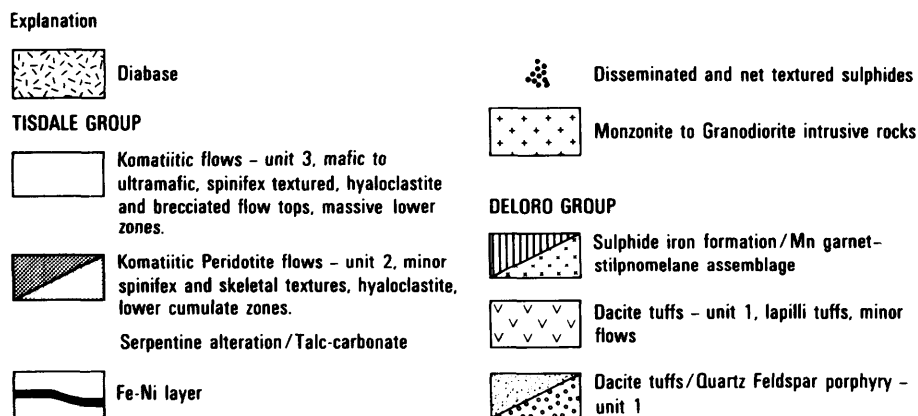
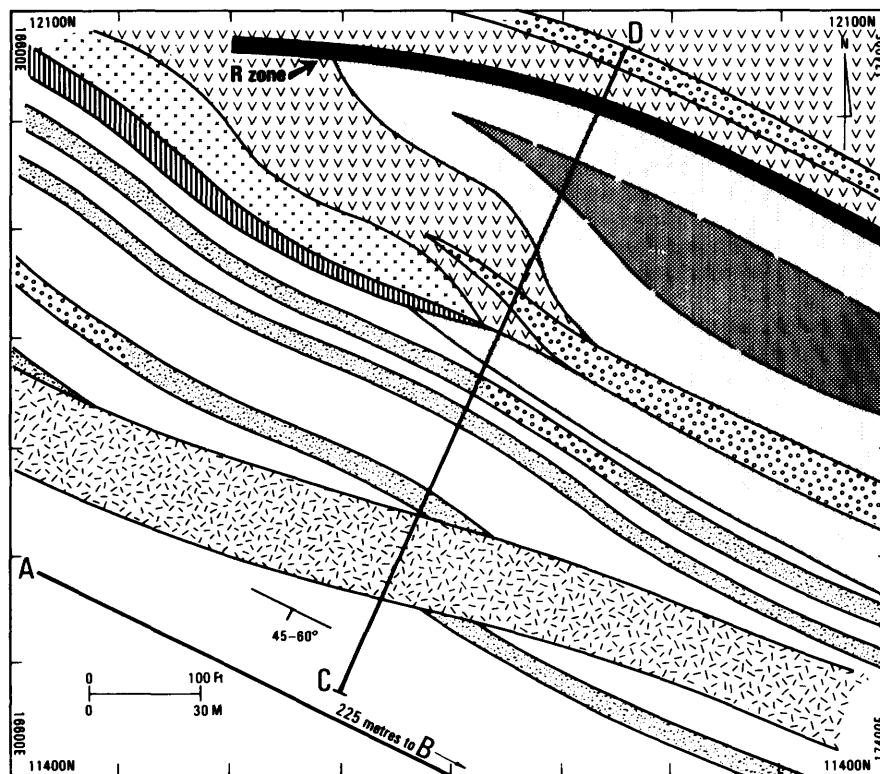
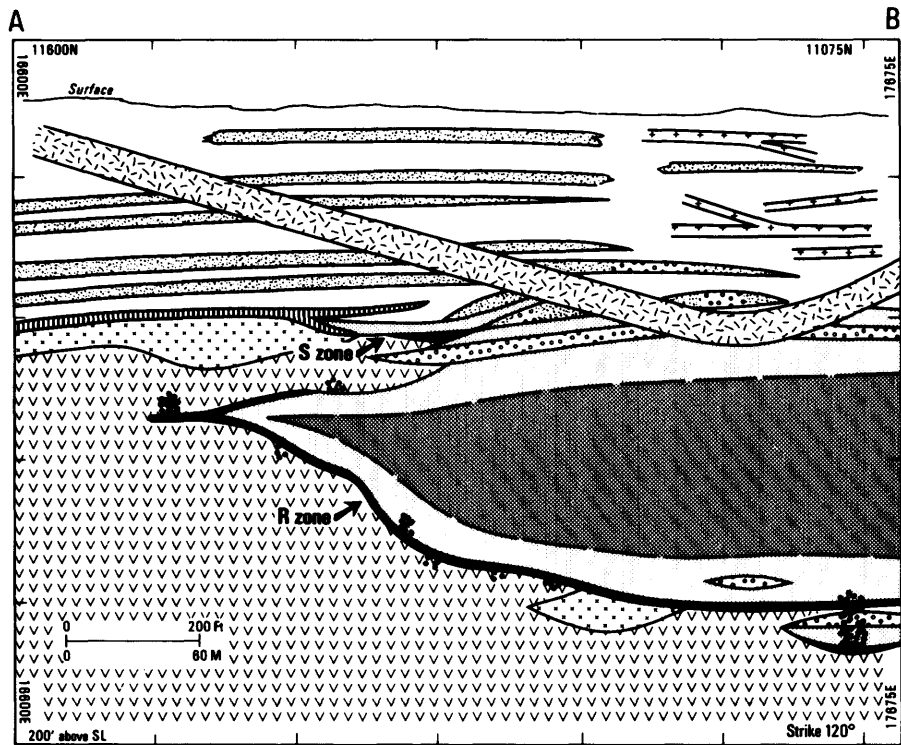


Figure 5—Plan view of Redstone geology. Manganese garnet-stilpnomelane rocks underlie sulphide-facies iron formation and flank the nickel sulphide (R) zone.



Explanation

- | | | | |
|-------------------------------------------------------------------------------------|---------------------------------------------------------------------------------------------------------------------------------|-------------------------------------------------------------------------------------|------------------------------------------------------------|
|  | Diabase |  | Disseminated and net textured sulphides |
| TISDALE GROUP | | | |
|  | Komatiitic flows - unit 3, mafic to ultramafic, spinifex textured, hyaloclastite and brecciated flow tops, massive lower zones. |  | Monzonite to Granodiorite intrusive rocks |
|  | Komatiitic Peridotite flows - unit 2, minor spinifex and skeletal textures, hyaloclastite, lower cumulate zones. | DELOORO GROUP | |
| | Serpentine alteration/Talc-carbonate |  | Sulphide iron formation/Mn garnet-stilpnomelane assemblage |
|  | Fe-Ni layer |  | Dacite tuffs - unit 1, lapilli tuffs, minor flows |
| | |  | Dacite tuffs/Quartz Feldspar porphyry - unit 1 |

Figure 6—Vertical longitudinal section of the Redstone deposit. Garnet-stilpnomelane rocks laterally flank R and S zones and footwall to the R zone.

Table 6—Chemical analyses of garnet stitipnomelane rocks at Redstone deposit.

Sample Number	R1-21	R3-5	R4-6	R5-6	R11-7	R12-19	R13-12	R14-11	R15-6	R16-8
SiO ₂	44.4	21.8	49.4	39.5	42.5	40.1	35.5	37.1	44.2	39.1
TiO ₂	0.35	0.10	0.41	0.20	0.35	0.32	0.35	0.39	0.32	0.35
Al ₂ O ₃	9.89	2.90	12.2	5.98	10.5	9.24	8.90	10.3	8.60	10.7
FeO	23.0	54.3	21.6	31.3	26.1	28.7	31.0	23.2	26.9	20.4
MnO	1.24	0.70	1.59	3.45	0.94	1.20	1.87	1.80	1.66	1.24
MgO	4.24	3.10	4.09	4.96	4.29	4.29	4.70	3.85	3.70	3.41
CaO	9.48	8.50	4.85	9.25	7.31	5.43	7.36	9.61	5.09	16.2
Na ₂ O	0.16	0.00	0.03	0.00	0.03	0.33	0.00	0.00	0.44	0.35
K ₂ O	0.93	0.60	1.18	0.58	1.27	2.80	2.17	3.02	1.14	0.48
P ₂ O ₅	0.09	0.10	0.09	0.04	0.08	0.06	0.09	0.08	0.06	0.08
L.O.I.	5.08	1.54	1.70	3.00	4.16	2.87	6.23	7.47	2.87	4.93
Total	101.4	99.7	99.5	101.8	100.5	98.5	101.5	99.5	97.9	99.5
S	n.d.	n.d.	0.25	5.75	3.55		3.45	5.05		1.90
Sc	29	14	12	14	45		26	12		48
V	68	28	63	42	118	52	52	54	45	101
Cr	65	11	43	28	42	80	23	14	40	40
Co	82	136	78	108	106	85	99	78	78	87
Ni	33	150	29	19	40	59	12	25	28	32
Cu	23	256	n.d.	64	217	260	57	70	46	107
Zn	62	167	54	85	71	37	24	39	23	48
Rb	45	19	48	32	50	92	90	94	71	15
Sr	25	20	41	14	14	25	36	31	23	44
Y	21.9	15.7	13.3	25.2	22.8	25.2	21.6	18.9	19.8	23.7
Zr	82	29	97	49	90	75	76	76	83	82
Nb	3.0	9.6	3.5	7.6	4.9	12	2	3.9	5.5	2.4
Ba	92	159	170	45	190	276	435	247	182	64
Pb	17	18	21	17	15	19	n.d.	11	17	5
Al/Ti	28	29	30	30	30	29	25	26	27	31
Ti/Zr	43	35	42	41	39	43	46	51	39	43
Ti/Y	160	64	308	79	154	127	162	206	162	148
Zr/Y	3.7	1.85	7.3	1.94	3.95	2.98	3.52	4.02	4.19	3.46
Zr/V	2.93	1.04	1.54	0.86	0.76	1.44	1.46	1.41	1.84	0.81
Mn/Fe	.054	.013	.074	.110	.074	.042	.060	.078	.062	.061
S.G.	2.973	3.938	3.025	3.395	3.027	3.100	3.116	3.113	2.972	3.188

Sample Number	R22-12	R26-8	R29-1	R34-10	R37-5	R44-17B	R49-19	R50-6	Avg. Dacite
SiO ₂	50.7	37.2	39.3	45.4	29.7	41.0	42.6	48.9	65.3
TiO ₂	0.42	0.25	0.37	0.37	0.15	0.38	0.41	0.40	0.49
Al ₂ O ₃	12.6	8.49	11.1	10.3	4.12	11.3	12.3	11.7	16.4
FeO	17.7	26.9	23.4	26.8	27.0	26.7	23.1	22.9	2.79
MnO	1.09	2.40	2.21	2.43	2.04	1.14	1.95	1.99	0.09
MgO	3.76	4.34	2.97	3.44	2.49	3.12	3.32	3.59	1.20
CaO	6.65	11.0	11.1	3.10	19.9	9.02	8.55	5.24	5.38
Na ₂ O	0.30	0.11	0.00	0.04	0.12	0.23	0.41	0.00	3.03
K ₂ O	0.92	1.62	0.85	1.62	1.03	0.69	0.87	1.84	1.97
P ₂ O ₅	0.11	0.05	0.07	0.06	0.03	0.10	0.08	0.09	0.11
L.O.I.	2.16	6.31	6.08	3.85	11.23	3.38	3.70	0.07	2.93
Total	98.3	101.6	100.0	100.3	100.8	100.1	99.9	101.8	99.69
S	0.15	1.45	2.35	2.35	3.08	0.30	2.35	2.20	
Sc	39	30	11	9	8	16	16	45	
V	111	40	69	54	28	63	67	93	85
Cr	45	76	112	26	15	75	19	67	114
Co	81	92	95	99	98	90	71	101	45
Ni	38	23	49	27	16	45	26	103	101
Cu	31	69	100	86	167	268	37	53	31
Zn	43	21	40	59	20	98	60	54	34
Rb	38	70	39	81	64	31	46	64	54
Sr	37	29	68	13	50	20	106	130	140
Y	19.3	18.6	25.7	16.4	26.9	38.3	17.1	24.4	19
Zr	92	51	90	81	36	97	100	104	139
Nb	1.8	4.8	2.6	9.4	12.3	15	6.4	3.1	10.7
Ba	121	236	207	235	140	316	90	273	436
Pb	7	12	14	7	n.d.	13	17	12.5	7
Al/Ti	30	34	30	28	28	30	30	29	33
Ti/Zr	46	49	41	46	42	39	41	39	36
Ti/Y	218	134	144	226	56	99	240	164	258
Zr/Y	4.77	2.74	3.50	4.94	1.34	2.53	5.85	4.26	7.37
Zr/V	0.83	1.28	1.30	1.50	1.29	1.54	1.49	1.12	1.65
Mn/Fe	.062	.089	.094	.091	.076	.043	.084	.087	.032
S.G.	3.116	3.011	3.101	3.058	2.873	3.075	3.120	3.280	2.766

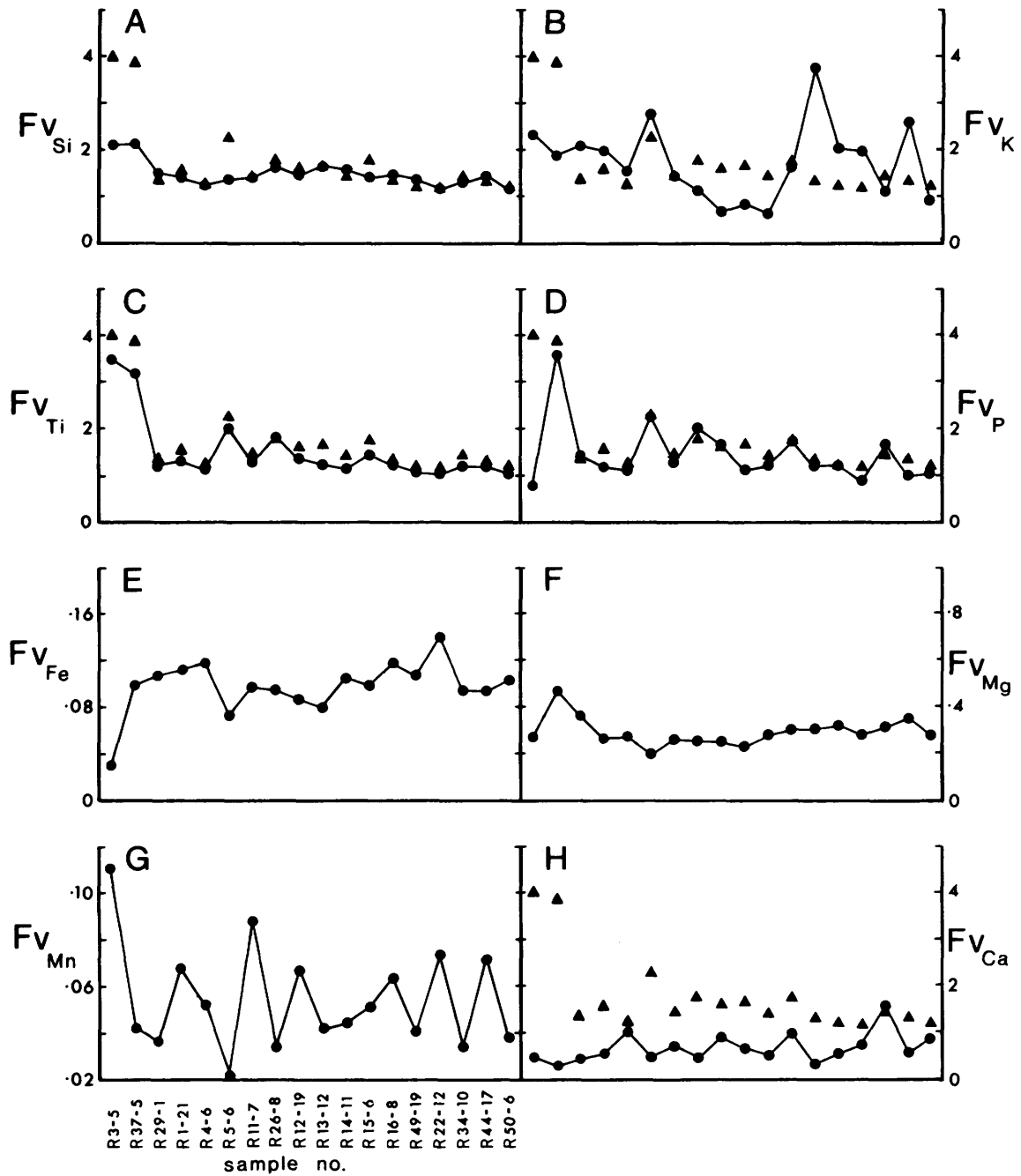


Figure 7—Volume-factor profiles for Si, K, Ti, P, Fe, Mg, Mn, and Ca, calculated from Gresen's (1967) mass balance equations. Sample numbers correspond to Table 1 and are arranged generally from W to E with respect to the R-zone. The volume factor of Al is shown in triangles and represents the proportion of volcaniclastic material. A volume factor less than F_{vAl} generally represents a chemical sedimentary component.

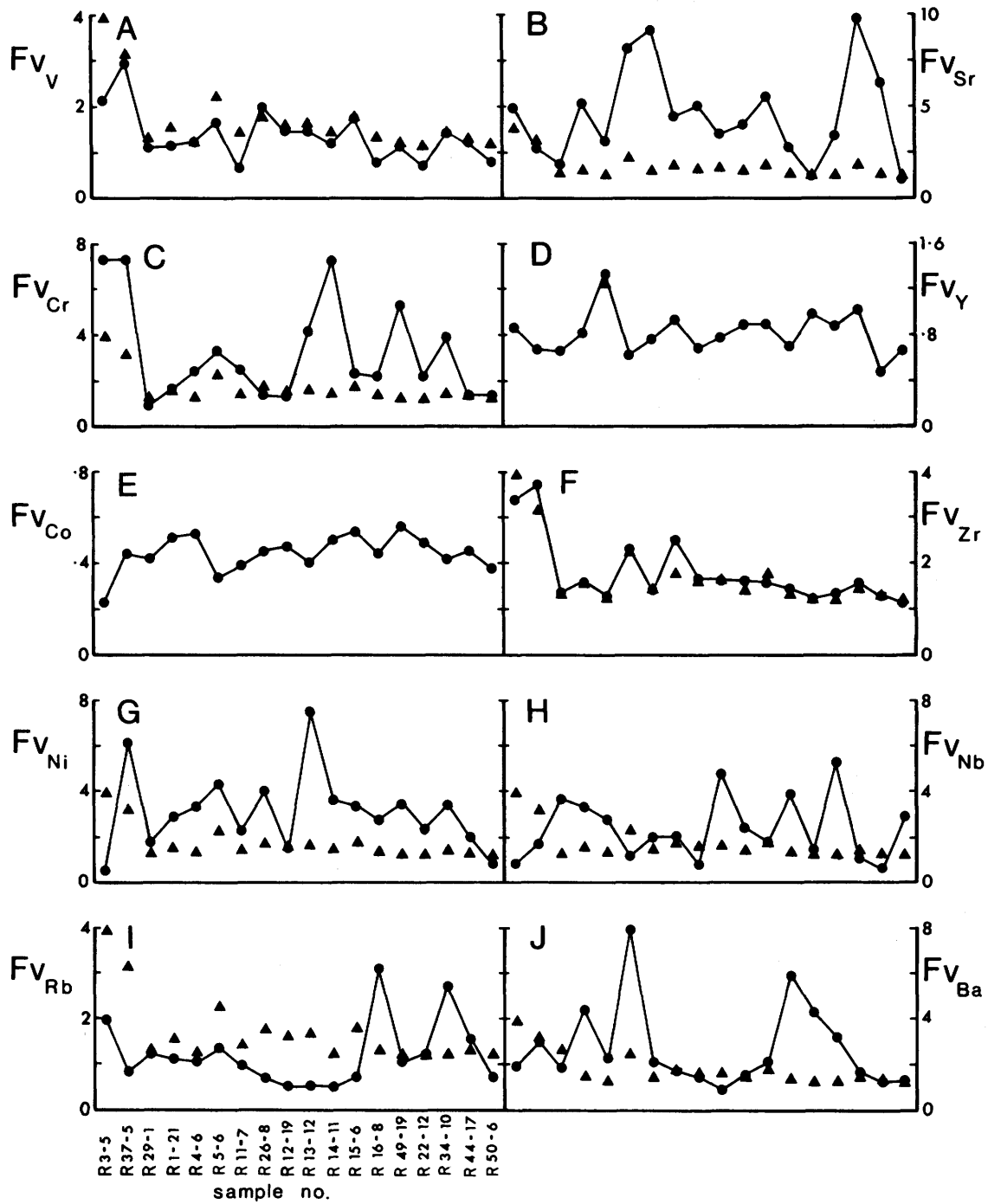


Figure 8—Volume-factor profiles for V, Sr, Cr, Y, Co, Zr, Ni, Nb, Rb, and Ba. See Figure 7 for explanation.

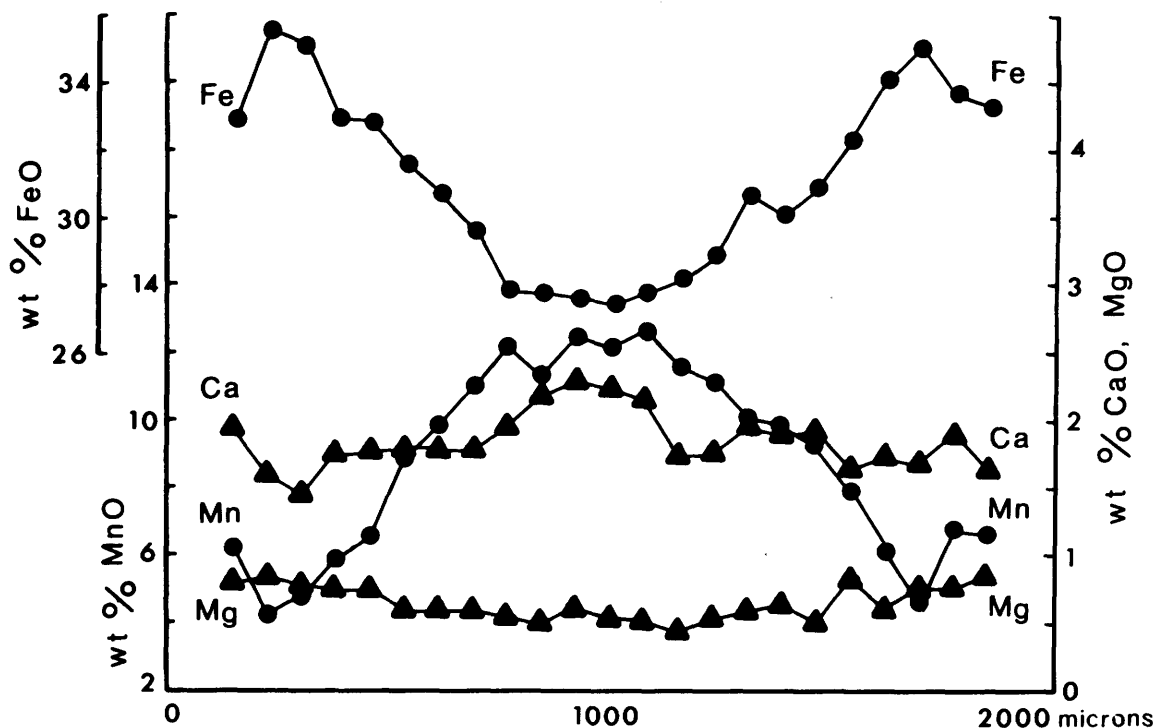


Figure 9—A detailed traverse by electron microprobe across a normally zoned garnet, sample R49-19. A symmetrical distribution of Mn and Fe is apparent from core to rim.

These rocks are of basic to ultrabasic composition, contain 21.8 to 50.7 weight percent SiO_2 , and contain less Al, Ti, Na, K, Zr, Cr, Ni, Nb, Ba and Sr in comparison to the average composition of the surrounding dacitic tuffs (column 19, Table 6). Absolute concentrations of major and trace elements of this unit are variable, however element ratios of Al, Ti and Zr are relatively constant.

Volume factors illustrating the mixture of volcanoclastic and chemical sedimentary rocks are illustrated in Figures 7 and 8. The volume factor of aluminum, $F_{V_{Al}}$, has been superimposed on most of the major and trace element profiles to compare the behaviour of those elements with that of aluminum. Volume factor profiles of Al, Ti, Zr and to a lesser extent P, V and Si are coincident and mimetic after each other, and vary inversely with $F_{V_{Fe}}$. As Al, Ti and Zr are commonly regarded as immobile elements (Kerrick *et al.* 1981; Davies *et al.* 1979; Nesbitt *et al.* 1979; and others), and given their convergent F_v profiles (Figures 7c, 8f), it is assumed that $F_{V_{Al}}$ approximates the proportion of pyroclastic component contributed to the garnet-stilpnomelane assemblage. Accordingly, if $F_{V_n} < F_{V_{Al}}$, then $X_n^A < X_n^B$, where X_n^A is the concentration of component n in dacitic tuff and X_n^B the concentration in garnet-stilpnomelane rock, at $\Delta X_{Al} = 0$. Here component n

is enriched in garnet-stilpnomelane rock relative to a dacitic parent. Therefore component n was added to the dacitic precursor and represents a chemical sedimentary precipitate. Conversely, if $F_{V_n} > F_{V_{Al}}$, the concentration of n is depleted in the garnet-stilpnomelane rock due to hydrothermal leaching.

The oscillating F_v profiles illustrated by the majority of major and trace elements is indicative of the heterogeneous proportions of pyroclastic material and chemical sediment from one sample to the next (Figures 7, 8). Volume factor profiles for Si, Ti, Al, P, Na, V, Cr, Ni, Zr, Sr, Nb and Ba are greater than one (constant volume) for most samples, and these large volume factors are a function of dilution by chemical sedimentary components. A volume factor of one would correspond to pure dacitic tuff, whereas a volume factor of 2, for example, signifies a combination of one part tuff plus one part chemical sediment (Kerrick *et al.* 1981). Cr, Ni, Sr, Na and to a lesser extent Nb, Ba and K, are depleted in the garnet-stilpnomelane assemblage relative to Al, as a result of hydrothermal leaching. Fe, Mn, Ca, Mg, Co, Y and Rb display volume factors less than $F_{V_{Al}}$, and are enriched within the garnet-stilpnomelane assemblage and in part represent chemical sedimentary components.

COMPOSITIONAL VARIATION WITHIN GARNET

Garnets at the Redstone deposit are members of the pyralspite series and display a wide compositional range in MnO, 2.0 to 20.0 weight percent, FeO, 12.0 to 36.0 weight percent, CaO, 3.0 to 12.0 weight percent, and MgO, 0.05 to 3.0 weight percent. These garnets are extensively zoned with respect to Mn, Fe, Ca and Mg, and display normal, reverse and oscillatory patterns. A normal distribution pattern contains the maximum amount of MnO at the centres of the grains and decreasing amounts of MnO toward the rims (Figure 9; Hollister 1966, 1969). Conversely, FeO contents vary inversely with MnO, from a minimum amount of FeO at the centre to a maximum at the rim. These grains often display a coupled substitution pattern of MnO + CaO for FeO + MgO. Hollister (1966) and Atherton (1968) attribute this normal distribution pattern to a fractionation-depletion growth model which formed during a prograde metamorphic event.

A reverse distribution pattern contains a minimum

amount of MnO at the centres of the grain and a maximum MnO content at the rim (Figure 10). At the Redstone deposit, MnO-rich rims are developed both symmetrically about MnO-depleted cores or preferentially developed at one or more edges. Woodsworth (1977), Amit (1976) and others have attributed Mn-rich rims to a retrograde metamorphic phenomenon, whereby garnet was partially re-sorbed, resulting in Mn diffusion back into the remaining garnet. This mechanism is not favoured here as normal- and reverse-zoned garnets occur in the same rock, and the coexisting mineral assemblage is typical of lower greenschist metamorphic grade. Further there appears to be a directional growth aspect to the Mn-rich rims, to some extent related to the actual mineral phase in direct contact with the garnet. Chlorite, stilpnomelane and to a lesser extent calcic amphibole contain accessory Mn, from 0.50 to 3.00 weight percent. However, a systematic Mn diffusion from the coexisting phases into garnet was not substantiated. Redstone pyralspite garnets also display heterogeneous patterns of MnO and FeO contents from core to rim which are referred to as oscillatory zoning. Here, similar substitutions of Mn, Fe, Ca and Mg oc-

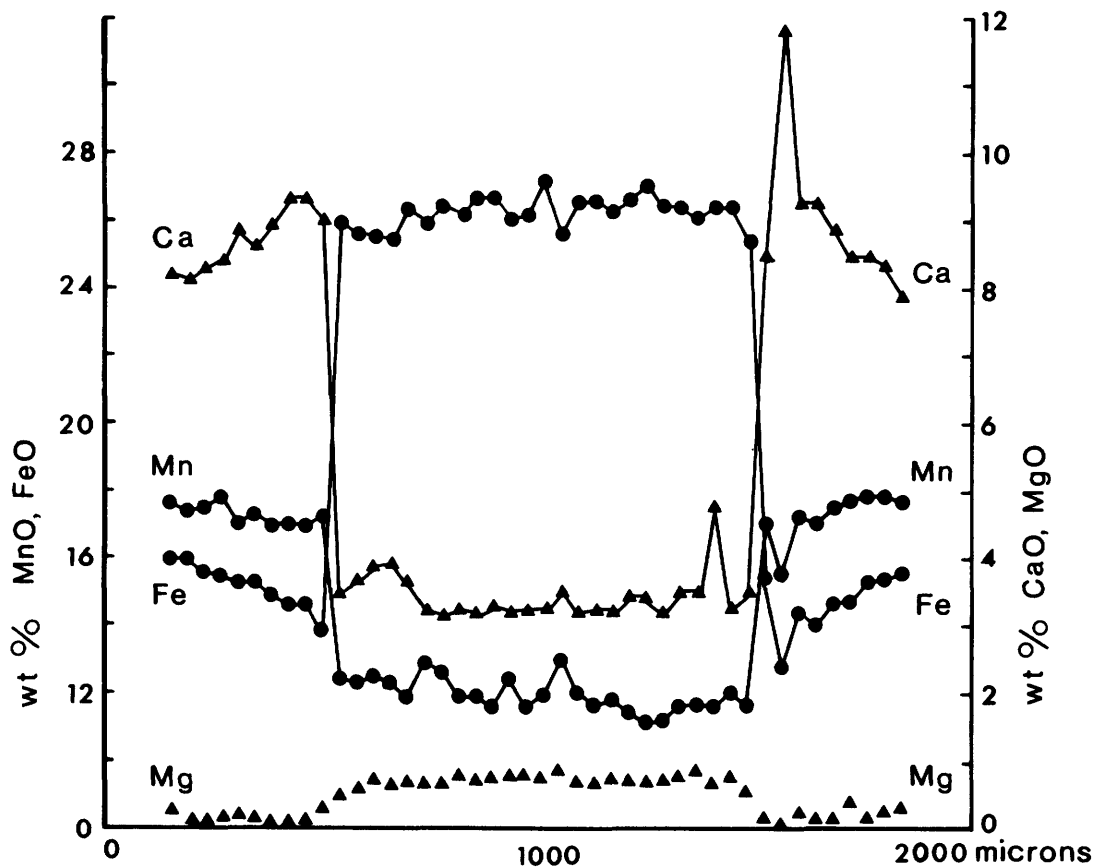


Figure 10—Reverse-zoned garnet with Mn-rich rims, sample R11-7. A coupled substitution of Mn + Ca and Fe + Mg is apparent.

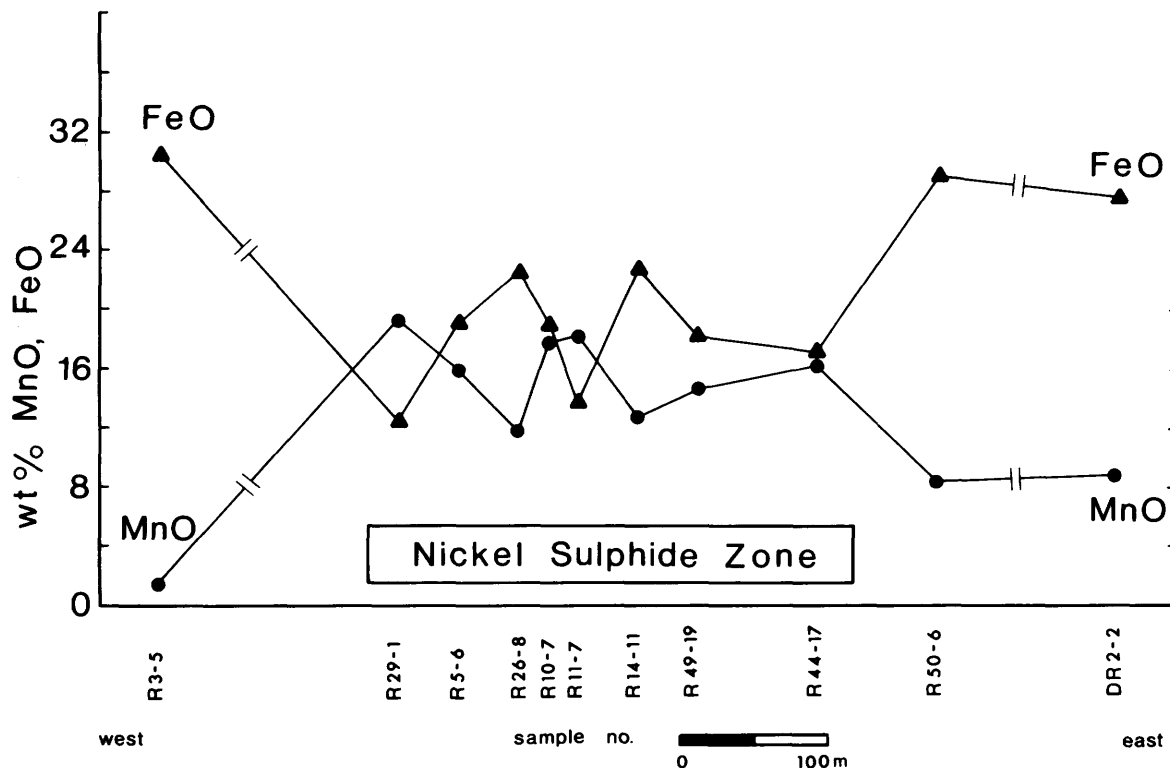


Figure 11—Lateral variation of MnO and FeO in garnet with respect to the nickel sulphide zone. Maximum MnO in garnet is coincident with the deposit, whereas samples R50-6, DR2-2 and R3-5 located in barren country rocks contain less MnO in garnet. The locations of samples R3-5 and DR2-2 are not to scale.

cur; however the distribution of MnO from core to rim is undulatory.

The garnet-stilpnomelane assemblage was sampled along strike in order to ascertain the chemical variation in garnet with respect to the Redstone deposit. A systematic variation of MnO and FeO content in garnet was not observed laterally away from the nickel sulphide zone (Figure 11). However, the maximum amounts of MnO in garnets are enriched spatially coincident with the nickel sulphide zone, whereas garnets contain less MnO in samples laterally away from the deposit (Figure 11).

DISCUSSION AND CONCLUSIONS

The chemical composition of the garnet-stilpnomelane assemblage represents a mixture of dacitic volcanoclastic detritus and chemical precipitates from hydrothermal discharge. Al, Ti, Zr, V and P have a volcanoclastic origin, whereas most of the Fe, Mn, Ca, Mg, Co, Y and Rb are introduced via chemical precipitation. Cr, Ni, Sr, Na and to a lesser extent Nb, Ba and K have been leached from a dacitic precursor.

Valliant (1981), identified a stratabound laterally continuous manganiferous garnet horizon stratigraphically underlying the Bousquet gold deposit, Quebec. A systematic increase in Mn/Fe ratio in garnet and in whole rock, from the periphery to the centre of the garnet member, was reported. The highest Mn/Fe ratio in garnet and whole rock is coincident with high grade gold ore and thickest portion of the garnet member, on the flanks of the orebody. A similar manganiferous garnet horizon is also present within the footwall rocks at the Dumagami gold deposit, located along strike from Bousquet. Mn garnets are also described by Addy and Ypma (1978), which show strong compositional zoning of Mn and Fe in alteration zones enveloping the massive sulphide deposits at Ducktown, Tennessee. Mn garnets are similarly described by Stanton and Vaughan (1979), within a thin phosphatic and manganiferous silicate-facies iron formation enclosing a Pb-Zn massive sulphide deposit at Pegmont, Australia. Here the MnO content in garnet is also highest coincident with the orebody, and decreases systematically along strike and vertically into non-mineralized rocks. Garnets spatially near the orebody are zoned

with Mn-rich cores and depleted rims, whereas garnets within barren country rocks are not chemically zoned.

Iron and manganese chemical sedimentary rocks and associated pyroclastic garnets represent key exploration guides to a variety of ores. Firstly, Fe- and Mn-rich chemical sedimentary units are often laterally more extensive than a given orebody and hence present a larger exploration target. Secondly the maximum Mn/Fe ratio in garnet and in whole rock is generally coincident with the ore zones and decreases systematically into barren country rock with low Mn/Fe ratios and less pronounced zoning in garnet.

REFERENCES

- Addy, S.K. and Ypma, P.J.M.
1978: Chemical zoning in garnets from rocks around the massive sulphide deposits at Ducktown, Tennessee, and its implications; *Journal of Geology*, vol. 86, p.385-392.
- Amit, O.
1976: Retrograde zoning in garnets of Elat-Wadi Magrish metamorphic rocks; *Lithos*, vol. 9, p.252-262.
- Atherton, M.P.
1968: The variation in garnet, biotite and chlorite composition in medium grade pelitic rocks from the Dalradian, Scotland, with particular reference to the zonation in garnet; *Contributions to Mineralogy and Petrology*, vol. 18, p.347-371.
- Davies, J.F., Grant, R.W.E. and Whitehead, R.E.S.
1979: Immobile trace elements and Archean volcanic stratigraphy in the Timmins mining area, Ontario; *Canadian Journal of Earth Sciences*, vol. 16, p.305-311.
- Downes, M.J.
1979: Kirkland Lake Area, Stratigraphic Mapping, District of Timiskaming; p. 121-125 in *Summary of Field Work, 1979*, by the Ontario Geological Survey, edited by V.G. Milne, O.L. White, R.B. Barlow and C.R. Kustra, Ontario Geological Survey Miscellaneous Paper 90, 245p.
- Gresens, R.L.
1967: Composition-volume relationships of metasomatism; *Chemical Geology*, vol. 2, p.47-65.
- Gross, G.A.
1965: Origin of Precambrian iron formations, discussion; *Economic Geology*, vol. 60, p.1063-1065.
- Hollister, L.S.
1966: Garnet zoning: an interpretation based on the Rayleigh fractionation model; *Science*, vol. 154, p.1647-1651.
- Hollister, L.S.
1969: Contact metamorphism in the Kwoiek area of British Columbia: an end member of the metamorphic process; *Geological Society of America, Bulletin*, vol. 80, p.2465-2494.
- Kerrich, R. and Fryer, B.J.
1981: The separation of rare elements from abundant base metals in Archean lode gold deposits: implications of low water/rock source regions; *Econ. Geol.*, vol. , p.160-166.
- Kerrich, R., Fryer, B.J., Milner, K.J. and Peirce, M.G.
1981: The geochemistry of gold-bearing chemical sediments, Dickenson Mine, Red Lake, Ontario: a reconnaissance study; *Canadian Journal of Earth Science*, vol. 18, p.624-637.
- Kerrich, R. and Hodder, R.W.
in press: Archean lode gold and base metal deposits: chemical evidence for metal separation into independent hydrothermal reservoirs; *C.I.M. Bulletin*.
- Kerrich, R., Robinson, D.J., Hodder, R.W. and Hutchinson, R.W.
1979: Field relations of Au, Ni and Cr Deposits in Ultramafic-Mafic Volcanic Rocks; p. 12 in *Geoscience Research Seminar, Abstracts*, and E.G. Pye, Ontario Geological Survey, 23p.
- Kerrich, R., Robinson, D.J., Hutchinson, R.W. and Hodder, R.W.
1980: Field Relations and Geochemistry of Au, Ni and Cr Deposits in Ultramafic-Mafic Volcanic Rocks; Grant 27, p. 144-162 in *Geoscience Research Grant Program, Summary of Research, 1979-1980*, edited by E.G. Pye, Ontario Geological Survey, Miscellaneous Paper 92, 262p.
- Kretz, R.
1973: Kinetics of the crystallization of garnet at two localities near Yellowknife; *Canadian Mineralogist*, vol. 12, p.1-20.
- Nesbitt, R.W., Sun, Shen-Su and Purvis, A.C.
1979: Komatiites: geochemistry and genesis; *Canadian Mineralogist*, vol. 17, part 2, p.165-186.
- Robinson, D.J. and Hutchinson, R.W.
1981: Evidence for a volcanogenic-exhalative origin of a massive nickel sulphide deposit at Redstone, Timmins, Ontario; in *H.S. Robinson Memorial Volume Hutchinson, R.W., Spence, C.D. and Franklin, J.M., eds., Geological Association of Canada Special Paper*.
- Stanton, R.L. and Vaughan, J.P.
1979: Facies of ore formation: a preliminary account of the Pegmont deposit as an example of potential relations between small "iron formations" and stratiform sulphide ores; *Australasian Institute of Mining and Metallurgy*, no. 270, p.25-38.
- Valliant, R.
1981: The geology, stratigraphic relationships and genesis of the Bousquet gold deposit, Northwest Quebec; Unpublished Ph.D. thesis, University of Western Ontario.
- Woodsworth, G.J.
1977: Homogenization of zoned garnets from pelitic schists; *Canadian Mineralogist*, vol. 15, p.230-242.

Grant 75 Asbestos Fibre Degradation in Laboratory Solution

N. D. MacRae, M. Hyatt, and H. W. Nesbitt

Department of Geology, University of Western Ontario

ABSTRACT

The group of fibrous minerals collectively called "asbestos" is readily dispersed in the environment by air or water transport. Because these minerals are recognized carcinogens, fibre numbers in a mining or manufacturing work area are limited, usually by various mechanical traps. This study investigates the possibility of altering the habit of a common variety of asbestos, chrysotile, through experimental runs with simple chemical reagents. In the first series of experiments attempts were made to degenerate the chrysotile with different solution strengths of HCl, Na₂CO₃ and CO₂-saturated water. In the second set, crystals of anhydrite were nucleated and grown about fibres. The applicability of experimental results to environmental controls is discussed.

INTRODUCTION

The fibrous varieties of amphibole and serpentine minerals collectively known as "asbestos" have been the subject of much research and debate in recent years. The serpentine mineral chrysotile [Mg₃Si₂O₅(OH)₄], which is used in this study, is the most common form of asbestos, accounting for over 90 percent of all the fibre consumed (Gibbs 1979). The unique properties exhibited by asbestos which make it industrially desirable, also make it completely stable in the natural environment and readily dispersed by either water or air.

Several types of pulmonary lesions, primary lung and abdominal cancer and asbestosis or fibrosis are diseases cited in reference to asbestos-induced illnesses. A high death rate due to malignant tumors among occupationally exposed workers has been known for decades, however recent discoveries of malignant tumors among those not occupationally exposed indicates a high risk potential to the general population (Coffin and Stockinger 1977).

Sources of asbestos which can lead to increases of fibres in the environment may be as simple as the weathering of asbestos-bearing rocks or they may be man-induced. In the latter category, disposal of fibre-bearing wastes from mining or milling operations and the wear of such commercial asbestos products as brake linings and certain heat shields are noteworthy.

The purpose of our study was to determine if certain

simple chemical reagents might affect chrysotile fibres under laboratory conditions such that the results could be applicable to some fibre control situations.



Figure 1—Chrysotile fibres treated with 100°C 2N HCl for 20 minutes. Dissolution and fibre breakage are readily evident. Scanning electron microscope, magnification 1000X.

Table 1—Experimental conditions for investigation of chrysotile fibres.

EXPERIMENTS		Reagent Concentration	Run Duration	Run Temperature(°C)	Chrysotile Weight(gm)	Solution Volume(ml)
Degeneration Runs	HCl	2N	2 weeks	21	.143	20
		1N	2 weeks	21	.145	20
	Na ₂ CO ₃	2N	2 hrs	50	.136	20
		2N	20 min	100	not meas.	not meas.
		.5M	2 weeks	21	.070	20
		1M	2 weeks	21	.072	20
		2M	2 weeks	21	.071	20
		2M	2 hrs	50	.09	20
	CO ₂ -saturated H ₂ O	dry	20 min	100	.12	100
		ice loaded	3 weeks	21	.142	80
Fibre Coating		3M CaCl ₂ 0.2M Na ₂ SO ₄	approx. 5 min.	21	0.58	3.05 titr. into 50
		3M CaCl ₂ 0.2M Na ₂ SO ₄	5 min.	56	0.56	100 into 200

**Figure 2**—Anhydrite crystals grown from 100°C seawater along the length of a chrysotile fibre. Scanning electron microscope, magnification 1000X.

EXPERIMENT AND RESULTS

Chrysotile asbestos from Munro Township in northern Ontario was used for all experiments in this study.

Conflicting values for length and diameter for the environmentally critical dimensions of asbestos are found in the literature. For example, Kaschner and Wright (1977) found that fibres of asbestos and glass greater than 10 μm were hazardous while Stanton (1978) outlined evidence to indicate fibres less than 2 μm were most hazardous. Lengths of fibres in air around an asbestos mill as measured by Gibbs and Hwang (1975) ranged from 0.22 to 14.88 μm . Since this study investigates the possibility of treatment of asbestos waste within tailings of such operations, similar fibre length distributions were deemed desirable.

Preliminary work was done on long fibres (approximately 1 mm) chiefly because they are more readily resolved optically. To obtain fibres of this length, hand-picked samples with clean 50 to 10 mm wide veins of chrysotile were selected, the chrysotile chopped into 1 mm long bundles and the cut blocks then ground under alcohol to disperse the fibres. The 1 mm fraction was further ground mechanically for subsequent experiments, most fibres finally falling within the 0.22-14.88 μm range.

Two types of experiments were conducted: the first to chemically react the fibres and the second simply to coat the fibres.

Untreated fibres were examined by scanning electron microscope (SEM) to establish initial morphology. Also, fibres from each experimental run were similarly examined. SEM sample preparation was the same for both types of experiment; at the end of each run solution was spun out by centrifuge, the fibre residue rinsed then re-centrifuged repeatedly to remove any occluded solution. Electron micrographs of the gold/palladium-coated dried samples were taken at magnifications ranging from 700X to 7000X (Hyatt 1981).



Figure 3—Gypsum plates randomly interspersed with chrysotile fibres. Scanning electron microscope, magnification 3000X.

DEGENERATION RUNS

Weighed amounts of chrysotile fibre were placed in known volumes of HCl, Na_2CO_3 and CO_2 -saturated water, then sealed in either glass or plastic vials. Duplicate charges were loaded and sealed for each series. Most runs involved placing the vials in a continually rocking furnace which was set for either room temperature (approximately 21°C) or 50°C . The motion of the furnace ensured continual agitation of the fibre solution over the duration of the runs. Experimental run times ranged up to three weeks (Table 1). In addition to the sealed runs, Na_2CO_3 and HCl solutions plus asbestos were boiled (approximately 100°C) for 20 minute runs in open beakers over a bunsen burner.

It has long been recognized that chrysotile is attacked by acids, particular HCl. Since the degree and rate of dissolution depend upon many factors, including the exact fibre composition, three experiments with the

test chrysotile and HCl were conducted in an effort to characterize the fibre used (see Table 1). SEM examination of the untreated fibres and residue from the two week room temperature runs of 2N and 1N HCl solutions showed no apparent change. The runs at 50°C showed significant dissolution and fibre breakage, and the 20 minute runs at 100°C showed extreme acid attack (Figure 1) and a loss of 50 weight percent of fibre.

The next two sets of experiments (Na_2CO_3 and CO_2 -saturated water plus chrysotile) were aimed at degrading chrysotile by forming a solid by-product of non-fibrous habit. An analogous situation is that of tremolite (an amphibole that can have a fibrous habit) which can be coaxed to grow talc plates from the (110) cleavage of the fibres (MacRae *et al.* 1976). No visible evidence of fibre reaction was determined for any of the runs listed in Table 1 for either set of runs.



Figure 4—Abundant anhydrite crystals grown on and about chrysotile fibres from 12 hour experimental run. Scanning electron microscope, magnification 3000X.

FIBRE-COATING RUNS

Experiments aimed at coating asbestos fibres with a common salt, anhydrite (CaSO_4) in this case, were carried out in an attempt to alter the fibrous dimensions of the material. As a preliminary step, chrysotile fibres were boiled (approximately 100°C) in seawater for 20 minutes. SEM inspection of the product revealed that a few anhydrite crystals had nucleated and grown along the length of several fibres (Figure 2). Anhydrite, the high temperature dehydrated equivalent of gypsum ($\text{CaSO}_4 \cdot 2\text{H}_2\text{O}$), crystallizes from seawater as the temperature is raised because the solubility of the salt decreases rapidly with increasing temperature in any solution.

The first controlled experiment consisted of titrating 3M CaCl_2 into 0.2M Na_2SO_4 plus chrysotile at room temperature (see Table 1). The system was continually stirred during the slow titration, and titration was stopped at the first visible precipitation. As seen in Figure 3, abundant monoclinic, plate-like gypsum crystals were formed, but they did not nucleate on the asbestos and, in fact, showed no relationship to the fibres.

In the second experiment of this series, the molar strength of Na_2SO_4 was reduced to 0.02M to bring it well below the concentration which would yield CaSO_4 from the solution at room temperature. The mixture was heated slowly to 56°C (see solubility data from Innorta *et al.* 1980) and held there for 12 hours. SEM examination of the run product revealed hundreds of tiny anhydrite crystals, a large proportion of which had nucleated on the asbestos fibres (Figure 4).

DISCUSSION

A problem of this investigation has been to choose reagents and methods of treatment which are not themselves more environmentally harmful than the chrysotile. Additionally, previous experimental work related to chrysotile has indicated that resistance to attack by reagents other than strong acids is in general excellent at temperatures below 100°C (Chatfield 1979). Strong bases, for example, were not tried in this study because they are routinely used to dissolve the tissue surrounding fibres in lung or other organ samples, leaving the fibres virtually unaffected. Nevertheless, in view of the fact that much of the research on the reactivity of chrysotile deals with dissolution of magnesium from the chemical structure of the serpentine mineral, it was considered valid to determine if magnesium carbonates could be formed from Na_2CO_3 or CO_2 -saturated water. The results, as recorded above, proved negative.

As indicated previously, chrysotile reactivity in HCl was observed primarily to provide a working case example of fibre degeneration; acid decomposition of chrysotile is not, however, an environmentally appropriate method of dealing with fibre-bearing wastes. Due to lack of comparable fibre breakdown in Na_2CO_3 or CO_2 -saturated water runs (which are environmentally harmless reagents), it can be concluded from the results of this and other studies that low temperature chemical

degradation of chrysotile fibres as a mode of environmental control is most likely impractical.

Current opinion, particularly in relation to health problems, is that fibre dimensions may be more important than other physical or chemical properties (Gibbs 1979). Thus, the aim of coating chrysotile fibres with chemically grown crystals is directed more toward preventing the initial spread and corresponding ingestion of waste fibrils. Slow growth of anhydrite is indicated to be the best way of inducing nucleation on the fibres, rather than forcing quick precipitation, as in our first experiment. As the SEM micrographs show, the anhydrite crystals maintained their habit despite repeatedly rinsing in the sample preparation method. This is important since resistance to solution would be a necessary characteristic for application of this or a similar coating principle to real conditions.

In general, the results of this study tend to develop some of the possibilities and difficulties of crystal coating rather than prove the validity of actual application to waste control. Wastes would have to be treated in a manner such that nucleation about a high percentage of fibres would occur. In the long run, isolation of fibres by chemical coating may prove to be desirable primarily because of the dimension-altering effects imposed on the product.

REFERENCES

- Chatfield, E.J.
1979: Measurement of asbestos fibres in the work place and general environment; Mineralogical Association of Canada Short Course in Mineralogical Techniques of Asbestos Determination, p. 111-163.
- Coffin, D.L. and Stockinger, E.
1977: Asbestos Air Pollution; Vol II. The Effects of Air Pollution, ed. A.C. Stern, p. 316-326. Academic Press.
- Gibbs, G.W.
1979: Techniques of asbestos determination — research prospective; Mineralogical Association of Canada Short Course in Mineralogical Techniques of Asbestos Determination, p. 253-279.
- Gibbs, G.W. and Hwang, C.Y.
1975: Physical parameters of air borne asbestos fibres; Abstracts, 3rd Int. Conf. Phys. and Chem. of Asbestos Minerals, Quebec. Paper 8.37.
- Hyatt, M.
1981: Chemical treatment of chrysotile in laboratory solutions; Unpublished B.Sc. thesis; Department of Geology, University of Western Ontario, 33 p.
- Innorta, G., Rabbi, E., and Tomadin, L.
1980: The gypsum-anhydrite equilibrium by solubility measurements; *Geochim. Cosmochim. Acta*, vol. 44, p. 1931-1936.
- Kaschner, M. and Wright, G.W.
1977: The influence of varying lengths of glass and asbestos fibre on tissue response in guinea pigs; *Inhaled Particles IV*, vol. 2, p. 455-474.
- MacRae, N.D., Grant, M., and Kullerud, G.
1976: A note on the sulphurization of Fe-tremolite; *Geol. Mag.*, vol. 113, p. 575-578.
- Stanton, M.F.
1978: The carcinogenicity of fibrous materials; National Bureau of Standards, Sp. Publ. 506. Proceedings of the Workshop on Asbestos: Definitions and Measurement methods, p. 143-150.

Grant 46 Origin of Chromian Spinel in the Crystal Lake Intrusion, Pardee Township, Ontario

Paul R. Mainwaring and David H. Watkinson

Department of Geology, Carleton University

ABSTRACT

The lower part of the Crystal Lake gabbroic intrusion can be divided into three zones: 1) a contact zone of contaminated gabbro containing numerous xenoliths of slate which are rimmed with fine-grained sulphide minerals; 2) a chaotic zone of cognate gabbroic xenoliths in a mixture of "pegmatitic" and fine-grained gabbro, overlain by gabbro containing disseminations and veinlets of Cr-spinel; and 3) an upper zone consisting of coarse-grained anorthosite, gabbro, and several Cr-spinel-rich layers.

Cr-spinels from the chaotic zone occur as inclusions in poikilitic plagioclase and olivine, and have a wide variation in chemical composition. Cr-spinels in the stratiform upper zone are much more restricted in composition, perhaps due to the more quiescent crystallization conditions. The variable compositions of Cr-spinels in the chaotic zone may have resulted from reaction of early cumulus spinels with gabbroic liquids which underwent contamination by assimilation of aluminous country rock.

INTRODUCTION

During the final year of this project we have undertaken a detailed study of the chromian spinel which occurs in the Crystal Lake gabbroic intrusion, near Thunder Bay. Previous years' work has concentrated largely on the occurrence and chemistry of solid inclusions, especially of sodic minerals, in Cr-spinel. No such solid inclusions were found in this study. However, the compositions and the compositional diversity of Cr-spinel in a single thin section is interpreted as evidence that its origin did not involve simple crystallization and accumulation.

The Crystal Lake Intrusion is located in Pardee Township, Ontario, approximately 42 km southwest of Thunder Bay (Figure 1). Extensive drilling of the body by mining companies to test its Cu-Ni potential has indicated that it is a stratiform-type layered intrusion of essentially gabbroic composition, with few or no extreme differentiates developed. The Crystal Lake Intrusion was emplaced into Proterozoic slate, argillite and greywacke (Geul 1973).

Although the intrusion consists mostly of gabbro, with only minor troctolite, there are striking similarities with the Duluth Complex. Some of these are 1) presence and type of sulphide mineralization, 2) occurrence of Cr-spinels, 3) evidence of contamination at the base, 4) similarity of rock types, 5) age, and 6) similar and correlatable country rocks. The intrusion has been dated at 1045 Ma (Geul 1973) which is similar to dates of 1100 Ma obtained for the Duluth Complex in nearby northeastern Minnesota (Silver and Green 1963).

This study concerns the lower 60 m of the intrusion which is about 750 m thick in its center. The basal zone, shown schematically on Figure 2 contains the lower contact zone, Cu-Ni mineralization, disseminated Cr-spinel and two uppermost Cr-spinel layers.

Contact relationships at the base are obscured from view in the field, however drill holes which penetrated the underlying country rock demonstrate that thermal metamorphism and anatexis of the slate and greywacke has been extensive. This zone is characterized by numerous inclusions and xenoliths of sulphide-bearing slate which exhibit vein-like development of quartz and feldspar anatectic melts.

Above the contact zone is a chaotic and inhomogeneous zone of mixed fine-grained and pegmatitic gabbro, the latter commonly containing crystals of clinopyroxene and plagioclase up to 5 cm in length. The dominant feature in this zone other than the contrasting grain sizes and textures, is the presence of many fine-grained cognate xenoliths which exhibit internal mineral grading. These xenoliths are commonly closely-packed and, at the margins of the intrusion, are supported by plagioclase-rich pegmatitic gabbro (Figure 2). On weathered surfaces the presence of sulphides within the matrix and absence of sulphides in the xenoliths emphasizes the chaotic internal structure of this zone.

The upper portion of the chaotic zone is composed of gabbroic rocks containing discontinuous disseminations of Cr-spinel. Macroscopically, the Cr-spinel disseminations occur in two common forms: 1) euhedral to subhedral grains enclosed poikilitically in all or most minerals in the rock imparting a dusty grey or dull black appearance to the rock, and 2) fine veinlets, again discontinuous, forming complex anastomosing networks throughout the rock (see Figure 2). The latter type attain widths of up to several centimetres and are continuous for perhaps 1 m, although commonly much less.

Overlying the disseminated Cr-spinel zone is a coarse-grained anorthosite layer which is continuous along strike for several hundred metres although of widely varying thickness. A spinel-rich layer is located at the base of this anorthosite in several places; however, the layer appears to be discontinuous. Grain size of silicate minerals increases toward the top of the basal zone, and this, together with the occurrence of the spinel layers, defines the upper limit of the basal zone. Cr-spinel does not occur above the basal zone in the area studied.

PETROGRAPHY

CONTACT ZONE

Within a 2 m contact aureole below the intrusion the Rove Formation has undergone incipient partial melting. In thin section this is observed as veinlets up to 1 cm wide of quartz and alkali feldspar in myrmekitic intergrowths with euhedra of orthopyroxene in the matrix (Figure 3). The latter mineral is crowded with inclusions, mostly opaque

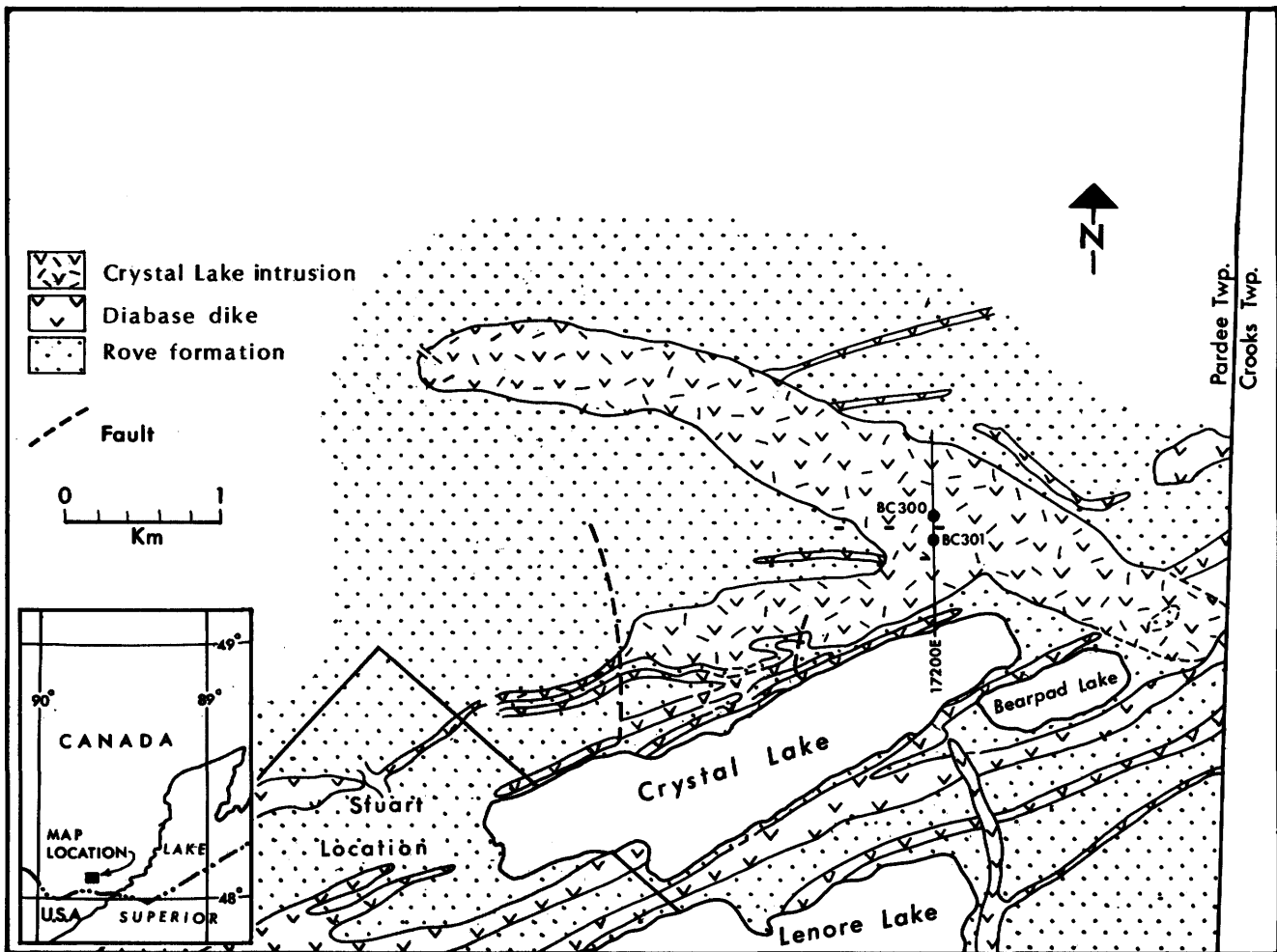


Figure 1—General geology and location of the Crystal Lake Intrusion. BC numbers show locations of drillholes from which samples were obtained.

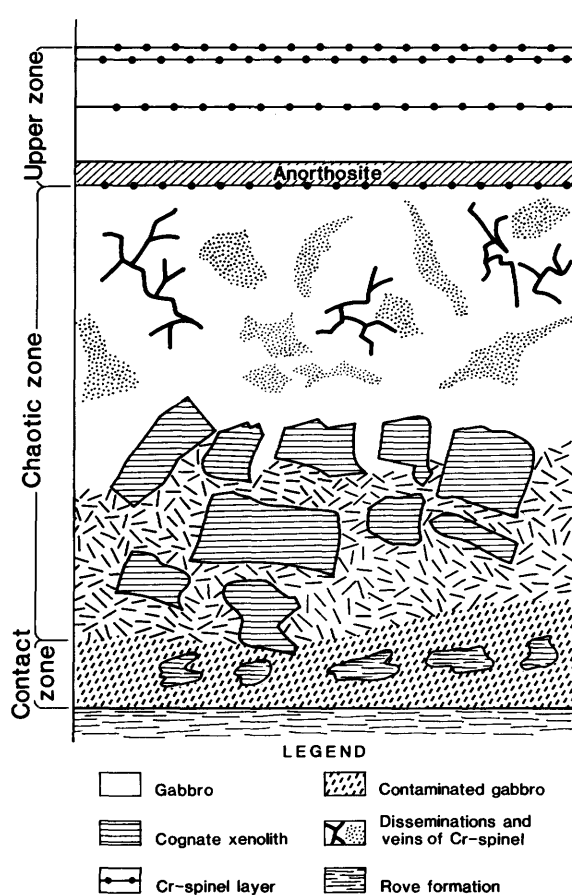


Figure 2—Schematic section of basal zone of the Crystal Lake Intrusion. Note: the cross-hatch pattern in the lower part of the chaotic zone represents "pegmatitic" gabbro.

ilmenite, and commonly contains graphite flakes. Fine needles of apatite occur in the more quartz-rich segregations in the rock. Xenoliths of Rove Formation which are included in the gabbro developed a rim of fine-grained sulphide minerals; sulphide grains within the xenoliths are disseminated and fine grained. Gabbro adjacent to the xenoliths is contaminated and characterised by the development of interstitial cordierite, alkali feldspar and apatite together with highly corroded plagioclase and interstitial orthopyroxene. Opaque oxides consist of magnetite and ilmenite while chalcopyrite and pyrrhotite are the common sulphides.

CHAOTIC ZONE

Within the chaotic zone are blocks of crudely mineral-graded gabbro set in an inhomogeneous mixture of massive gabbro and "pegmatitic", biotite-rich gabbro (Figure 4). The mineral-graded blocks and the massive gabbro

are mineralogically very similar, both being orthocumulate with intercumulus clinopyroxene. Biotite occurs only in trace quantities, in sharp contrast with its abundance in the pegmatitic gabbro. Mineral-grading in the xenoliths is defined by the increased proportion of olivine with respect to plagioclase. The latter mineral often forms planar laminations, a feature not seen in the adjacent massive gabbros. Cr-spinel has not been identified as a component of the gabbros of the chaotic zone.

Disseminated Cr-spinel occurs in two modes in this zone: 1) disseminated, discontinuous plagioclase-olivine-Cr-spinel rich pods or bodies, several centimetres to about a metre in size, and 2) discontinuous veins of almost massive Cr-spinel and plagioclase up to about 2 cm wide and up to several metres in maximum extent.

The irregularly shaped spinel-rich zones shown schematically in Figure 2 are composed of euhedral plagioclase, and olivine which is rarely euhedral but more commonly forms large oikocryst-like grains up to about



Figure 3—Photomicrograph (crossed nicols, 11X) of myrmekitic intergrowth of quartz and alkali feldspar. Veinlet of anatectic melt in contaminated Rove greywacke.

5 mm in diameter (Figure 5). Plagioclase occurs as equant to lath-like crystals up to 5 mm in maximum dimension; it is unzoned and appears to be cumulate in origin. As Figure 5 shows, fine-grained Cr-spinel is disseminated throughout both the plagioclase and olivine as poikilitic inclusions.

UPPER ZONE

The upper zone is composed of gabbro, an anorthosite layer about 1 m thick, and three persistent Cr-spinel layers. Neither gabbroic rocks nor anorthosite contain more than trace quantities of Cr-spinel.

Upper Cr-spinel layers consist of up to 80 percent Cr-spinel as subhedral to euhedral grains less than 2 mm in maximum dimension. The spinel layers vary in thickness from about 1 cm to about 2 cm and have sharp

lower contacts with more diffuse upper contacts with the overlying gabbroic rock.

MINERAL CHEMISTRY

CR-SPINELS

Cr-spinels in the chaotic zone and uppermost spinel layers have been analysed with the electron microprobe. There are three salient points which have arisen from these determinations: 1) there is a wide variation in composition of spinel from the chaotic zone, 2) individual spinel grains poikilitically enclosed in a single silicate crystal exhibit a wide compositional variation, and 3) compositions of spinels from the uppermost spinel layers exhibit little variation.



Figure 4—Cognate xenoliths of gabbro in matrix of pegmatitic, biotite-rich gabbro. Chaotic zone of the Crystal Lake Intrusion.



Figure 5—Photomicrograph (plane light, 40X) of Cr-spinel-rich zone in chaotic zone, showing large olivine oikocryst (centre of photo) and large plagioclase laths, both with abundant euhedral Cr-spinel inclusions.

Table 1—Forsterite composition of olivines containing Cr-spinel and free from Cr-spinel; electron microprobe analyses of Cr-spinels from the Crystal Lake intrusion.

OLIVINE COMPOSITION			CHROMIAN SPINEL COMPOSITION				
Sample #	Mole % Forsterite With included spinel		Cr2O3	TiO2	Al2O3	MgO	Fe2O3
	Yes	No					
BC300-2155A	75	69	25.5	2.7	27.1	9.6	11.1
2155B		68					
2155D		63					
2155E		64					
2161	75		22.6	7.8	11.4	5.8	15.8
2199		59					
2201		68					
2205	75		26.6	6.2	15.0	6.3	14.9
2217		64					
2219		70					
2223	79	72	22.5	10.4	8.2	4.0	16.9
2232.5	79	72	28.2	10.7	5.8	3.8	13.8
2336	78	72	27.4	4.8	16.1	4.6	18.3

Table 1 presents compositions of spinels which are poikilitically enclosed in olivine and plagioclase in the chaotic zone. Spinel in both silicate mineral hosts exhibit a similar range in composition and are again similar to spinels included in intercumulus augite.

As Figure 6 illustrates, Cr-spinels from the upper layers define a narrow compositional field (B) while those from the chaotic zone (A) exhibit a large variation in $Cr/(Cr+Al)$ ranging from 0.75 to 0.3 and $Mg/(Mg+Fe)$ ranging from about 0.1 to 0.4.

Compositional zoning of spinel grains was not evident during microprobe analysis.

OLIVINE

Olivines from both Cr-spinel-bearing and Cr-spinel-free rocks have been analysed. The forsterite contents are presented in Table 1. In general poikilitic olivine crystals that contain inclusions of chromian spinel are richer in forsterite than those which do not contain spinel. Commonly this enrichment is about 6 mole percent forsterite. Overall variation in forsterite content of olivine in the basal zone of the intrusion is about 20 mole percent.

The composition of olivine in the uppermost spinel layer is 75 mole percent forsterite. Again, this olivine contains abundant Cr-spinel.

DISCUSSION AND CONCLUSIONS

The following important observations form the basis of a model of genesis and distribution of the Cr-spinels in the lower part of the Crystal Lake Intrusion: 1) the contact of the basal zone consists of a high proportion of cognate xenoliths; 2) Cr-spinel occurs as both disrupted anastomosing veins and disseminations in the chaotic zone; 3) the chaotic zone is overlain by several laterally persistent Cr-spinel layers; 4) compositions of Cr-spinels in the chaotic zone are highly variable whereas those in the uppermost spinel layers are not; 5) the variation in the Cr-spinel compositions of the chaotic zone is largely in the $Cr/(Cr+Al)$ ratio and is in the order of 50 percent; and 6) poikilitic olivine compositions are a function of the presence of inclusions of Cr-spinel. Those grains containing spinel invariably have higher $Mg/(Mg+Fe)$ ratios than those that do not.

The gross structure of the basal zone of the intrusion, consisting of a cognate xenolith-rich contact facies and a chaotic zone, is interpreted to mean that a high proportion of solid xenolithic material existed at the time of intrusion. The absence of Cr-spinel in the cognate xenoliths indicates that this mineral was not on the liquidus during

initial stages of crystallization of the liquid. If these xenoliths are taken as representative of the earlier stages of crystallization, then both olivine and plagioclase were probably on the liquidus. This gains support from evidence derived from detailed studies in the Duluth Complex, Minnesota (Mainwaring and Naldrett 1977), where rocks similar to those in the Crystal Lake Intrusion have been documented as olivine and olivine + plagioclase cumulates occurring in repetitive cyclical units. The basal zone of the Crystal Lake Intrusion is characterized by a disrupted chaotic zone probably produced during intrusion of magma with a high solid content.

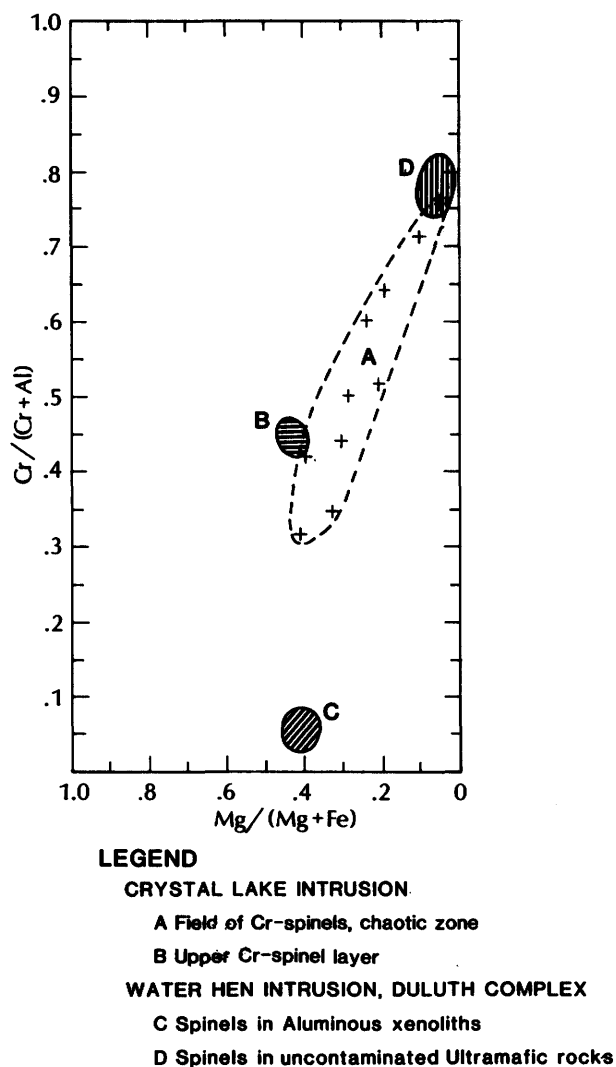


Figure 6—Compositional variation in Cr-spinels from the Crystal Lake Intrusion. Compositions from the Duluth Complex are shown for comparison.

The uppermost stratiform layers of the basal zone must represent a return to quiescent conditions following intrusion and deposition of the chaotic zone. Textures in the Cr-spinel-rich chaotic zone strongly suggest that plagioclase crystallized before olivine. Furthermore, the chaotic zone is characterized by the juxtaposition of both cumulus olivines which contain spinel euhedra and olivines that do not. Moreover, the compositional difference between these olivines suggests that they did not crystallize from the same liquid and had been brought together by other processes during intrusion.

Cr-spinel of compositions similar to those found in the Crystal Lake Intrusion have been described from several occurrences, most of which are in volcanic rocks. Eales and Snowden (1979) have described spinels of similar composition from the Elephant's Head dike. These spinels are typically rich in TiO_2 , although this is highly variable. In general, Cr-spinels included in olivine phenocrysts are TiO_2 -poor, containing less than 1 percent TiO_2 . The TiO_2 enrichment has been attributed to reaction with increasingly fractionated liquids which results in a progressive increase in TiO_2 and Fe_2O_3 and decrease in Cr_2O_3 , to result in a titaniferous magnetite. Similar variations have been described by Ridley (1977) in compositions of spinel from the Rhum Intrusion, northwestern Scotland, and these have been ascribed to reaction with differing amounts of trapped intercumulus liquid.

The highly variable compositions of the unzoned spinels in poikilitic olivine in the chaotic zone contrast strongly with the more restricted variation in the upper spinel layer. Furthermore, such wide variation in a single Cr-spinel layer is uncommon in mafic and ultramafic intrusions. The existence of such variation in the spinels is strong evidence that they formed under different physical and chemical conditions prior to inclusion. As discussed above, reaction with liquids of different compositions could result in the variable spinel compositions, although such reaction may normally be expected to result in zoned grain boundaries similar to those described by Henderson (1975). The euhedral, unzoned, nature of the spinel inclusions may be interpreted to mean that these spinels have crystallized from liquids of different compositions, and as such, represent cumulus spinel compositions.

Some compositional and textural diversity is to be expected in the "crop" of cumulus Cr-spinel crystals which crystallize from a silicate-rich liquid (Hamlyn and Keays 1979). However, such variation is commonly small, especially for those crystals poikilitically enclosed in a single olivine grain. Such fully enclosed spinels at the margin of the Elephant's Head dike show less than 10 percent variation in $\text{Fe}^{+3}/(\text{Fe} + \text{Cr} + \text{Al})$ (Eales and Snowden 1979). In contrast, those olivine-enclosed spinels from the chaotic zone show more than a 50 percent variation in this ratio. Spinel grains from the upper layer show variations in compositions more in keeping with those reported from other localities and probably represent a more normal, small, diversity of cumulus compositions.

In summary, the Cr-spinel compositions found in olivine grains in the chaotic zone are interpreted to have formed by fractionation from liquids of substantially

different compositions with minimal post-cumulus modification. Coexisting cumulus olivines which do not contain Cr-spinel are about 6 mole percent forsterite poorer than those that do enclose spinel. These facts, taken together with the xenolith-rich and disrupted nature of the chaotic zone and the existence of the upper Cr-spinel layers, strongly suggest that Cr-spinel crystallization may have been induced by contamination of the magma during final emplacement.

In support of this are the following: 1) spinel-free cognate xenoliths contain cumulus olivine and plagioclase, 2) both the chaotic zone and the upper stratiform layers have cumulus plagioclase and intercumulus olivine with cumulus Cr-spinel, and 3) compositions of spinels included in olivines show a remarkable variation which must reflect the variation in liquid compositions from which they formed.

The production of Cr-spinel in stratiform intrusions has been the object of recent study by Cameron (1977, 1980), Hill and Roeder (1974) and Irvine (1977). Irvine (1977) has demonstrated that Cr-spinel may be formed either by salic contamination (of the mafic magma) or magma mixing under certain circumstances. Mainwaring and Naldrett (1977) and Mainwaring and Watkinson (1980) have described the production of sulphide minerals and spinels in contaminated mafic rocks through assimilation of adjacent slates in the western Lake Superior region. The Crystal Lake Intrusion is similar in petrography, chemistry and layering to the Duluth Complex in northeastern Minnesota and similar to large associated dike-like intrusions in which are visible cordierite-bearing xenoliths of the Rove slates.

Compositions of spinels associated with cordierite-bearing troctolitic rocks in the Duluth Complex (Mainwaring and Naldrett 1977) are plotted in Figure 6, field C. Spinel compositions in field D are those from grains in associated but uncontaminated dunitic rocks. The highly variable compositions of spinels from the chaotic zone of the Crystal Lake Intrusion (field A) may be interpreted to have resulted from reaction of early cumulus spinels with gabbroic liquids which had undergone contamination by assimilation of aluminous country rocks. Spinels from the stratiform upper layer (field B) are less variable in composition than those from the chaotic zone. This is perhaps due to the more quiescent crystallization conditions with accompanying layer formation.

REFERENCES

- Cameron, E.N.
1977: Chromite in the central sector of the Eastern Bushveld Complex, South Africa; *Amer. Mineral.* Vol. 62, p.1082-1096.
1980: Evolution of the Lower Critical Zone, Central Sector, Eastern Bushveld Complex, and its Chromite Deposits; *Econ. Geol.*, Vol. 75, p.845-871.
- Eales, H.V. and Snowden, D.V.
1979: Chromiferous spinels of the Elephant's Head Dike; *Mineral. Deposita*, Vol. 14, p.227-242.
- Geul, J.J.C.
1973: Geology of Crooks Township, Jarvis and Prince Locations and Offshore Islands, District of Thunder Bay; Ontario Div. Mines, GR102, 46p.
- Hamlyn, P.R. and Keays, R.R.
1979: Origin of chromite compositional variation in the Panton Sill, Western Australia; *Contrib. Mineral. Petrol.*, Vol. 69, p.75-82.
- Henderson, P.
1975: Reaction trends shown by chrome-spinels of the Rhum layered intrusion; *Geochim. et Cosmochim. Acta*, Vol. 39, p.1035-1044.
- Hill, R. and Roeder, P.L.
1974: The crystallization of spinel from basaltic liquid as a function of oxygen fugacity; *Jour. Geology*, Vol. 82, p.709-729.
- Irvine, T.N.
1977: Origin of chromite layers in the Muskox intrusion and other stratiform intrusions: a new interpretation; *Geology*, Vol. 5, p.273-277.
- Mainwaring, P.R. and Naldrett, A.J.
1977: Country rock assimilation and the genesis of Cu-Ni sulfides in the Water Hen Intrusion, Duluth Complex Minnesota; *Econ. Geol.* Vol. 72, p.1269-1284.
- Mainwaring, P.R. and Watkinson, D.H.
1980: Distribution and Genesis of the Crystal Lake chromites, Pardee Township, Ontario; (Abstract) *Geoscience Research Seminar*, Ontario Geol. Survey, p.111.
- Ridley, W.Z.
1977: The crystallization trends of spinels in Tertiary basalts from Rhum and Nuck and their petrogenetic significance; *Contrib. Mineral. Petrol.* Vol. 64, p.243-255.
- Silver, L.T. and Green, J.C.
1963: Zircon ages for Middle Precambrian rocks of Lake Superior region; *American Geophys. Union Trans. (Abstract)*, Vol. 44, p.107.

Grant 92 Impact of Groundwater on Mining Activities in the Niagara Escarpment Area

R.L. Nadon and J.E. Gale

Department of Earth Sciences, University of Waterloo

ABSTRACT

A field, laboratory, and numerical modelling study has been undertaken to determine the impact of groundwater on mining activities and underground space development in the Paleozoic rock units of the Niagara Escarpment in southern Ontario. Five boreholes have been drilled at a site next to the Dufferin quarry near Milton. Core samples from three of the boreholes provided details of the lithology and fracture distribution and orientation for each geologic formation intersected. A total of 69 packer injection tests were performed in four of the boreholes. From these tests, a profile of hydraulic conductivity values and in situ groundwater pressures was obtained for the entire geologic section of the Niagara Escarpment. In addition to this, pump tests were conducted in the more permeable units to evaluate the larger-scale hydrogeologic characteristics of the rock masses. This data base has been used to assess, using two- and three-dimensional computer models, the hydrogeological consequences of mining within different geologic formations at the Dufferin quarry site.

INTRODUCTION

The mining of bedrock for aggregate is a major industry in south-central Ontario. With the depletion of existing sand and gravel deposits and with increasing demand for mineral aggregate in the Toronto area, more attention is being focussed on the expansion of the mining of the bedrock units in the immediate Niagara Escarpment area (Figure 1). A number of active and abandoned quarries already exist in this area. However, there is growing concern over the environmental consequences of further expansion of quarrying operations along the Niagara Escarpment. This concern has generated much interest in the possibilities of underground mining within the Niagara Escarpment for mineral aggregate production. This interest is documented in reports by Proctor and Redfern (1974), Acres (1974, 1976), and the Ontario Mineral Aggregate Working Party (1976) where underground aggregate mining is identified as a possible alternative to aggregate extraction by large scale open pit mining. The argument put forward in this case is that underground mining provides for the protection of the Niagara Escarpment's unique natural environment and at the same time

allows access to a large source of raw material of vital importance to this highly urbanized region.

Although it is more costly to produce aggregate material by underground mining techniques, the economies of such a scheme become attractive when subsequent use of the mined space for suitable commercial and industrial purposes is introduced. The successful conversion of over 2 km² of abandoned limestone mines below Kansas City into serviced, climate controlled, office, warehousing, and light industrial facilities serves as a good example of the many benefits to be derived by efficient use of the subsurface environment. A major factor in the economics of underground space is the energy efficiency of these facilities as described by McCreath and Mitchell (1978) and Stauffer (1975). These authors report on a number of examples where energy savings of 50 to 90 percent have been achieved by relocating commercial operations such as cold storage facilities in the subsurface.

Legget (1978) points out that the use of underground space could also help solve a serious problem which exists in the Niagara Peninsula. Fertile irreplaceable fruitlands below the escarpment in this area are being lost at an alarming rate, particularly near Hamilton, by the erection of single story industrial buildings. Legget suggests that underground mining of a suitable limestone or dolostone unit in the escarpment could provide the much needed supply of mineral aggregate material in such a way as to minimize the damage to the surface environment and at the same time create space for industrial use. Great energy savings would be achieved in this way, especially for cold storage facilities such as those used by the fruit producing industry.

NIAGARA ESCARPMENT FIELD STUDY

The technical feasibility of underground mining in the Paleozoic rock units of the Niagara Escarpment is the subject of a three-year field and laboratory testing program initiated by the University of Waterloo in 1979. This study involved initially the selection of three sites on the escarpment between Milton and Niagara Falls where detailed hydrogeological and engineering studies of the rock units would take place. The first phase of this field program, supported by the Ontario Geoscience Research Grant Program, has been completed. The purpose of this report

is to present the results and conclusions of eight months of hydrogeological field studies carried out at the first site.

DUFFERIN QUARRY SITE

The first site chosen for field testing is located 7 km west of Milton, on the Niagara Escarpment between the Dufferin quarry and the Indusmin quarry (Figure 2). Five boreholes, DQ-1 to DQ-5, were drilled for the hydrological study at this site. The orientation, length and diameter of the holes are tabulated at the top right corner of Figure 2. Four of the boreholes penetrated the ground to a depth greater than 50 m intersecting all of the escarpment's geologic units. Diamond core-drilling of three of these boreholes (DQ-1, DQ-3, DQ-5) provided core samples over the entire thickness of the stratigraphic section of the escarpment.

GEOLOGIC SETTING

The Niagara Escarpment consists of interbedded dolostone, shale, and sandstone beds of Upper Ordovician and Silurian age. A comprehensive discussion of the Paleozoic geology of southern Ontario is found in Bolton (1957, 1964), Caley (1940), and Telford (1978). Geologic maps of this region by Telford (1976) and Sanford (1969) are available at scales of 1:50,000 and 1:250,000 respectively.

The study area lies on the northeast edge of the Michigan Basin. The Niagara Escarpment represents the outer rim of this saucer-shaped structure. The cap rock of the escarpment is a massive resistant bed of dolostone varying in thickness from 20 to 30m along its outcropping face throughout southern Ontario. This unit, the Lockport-Amabel dolostone, is quarried extensively for the production of crushed stone. Underlying the dolostone is

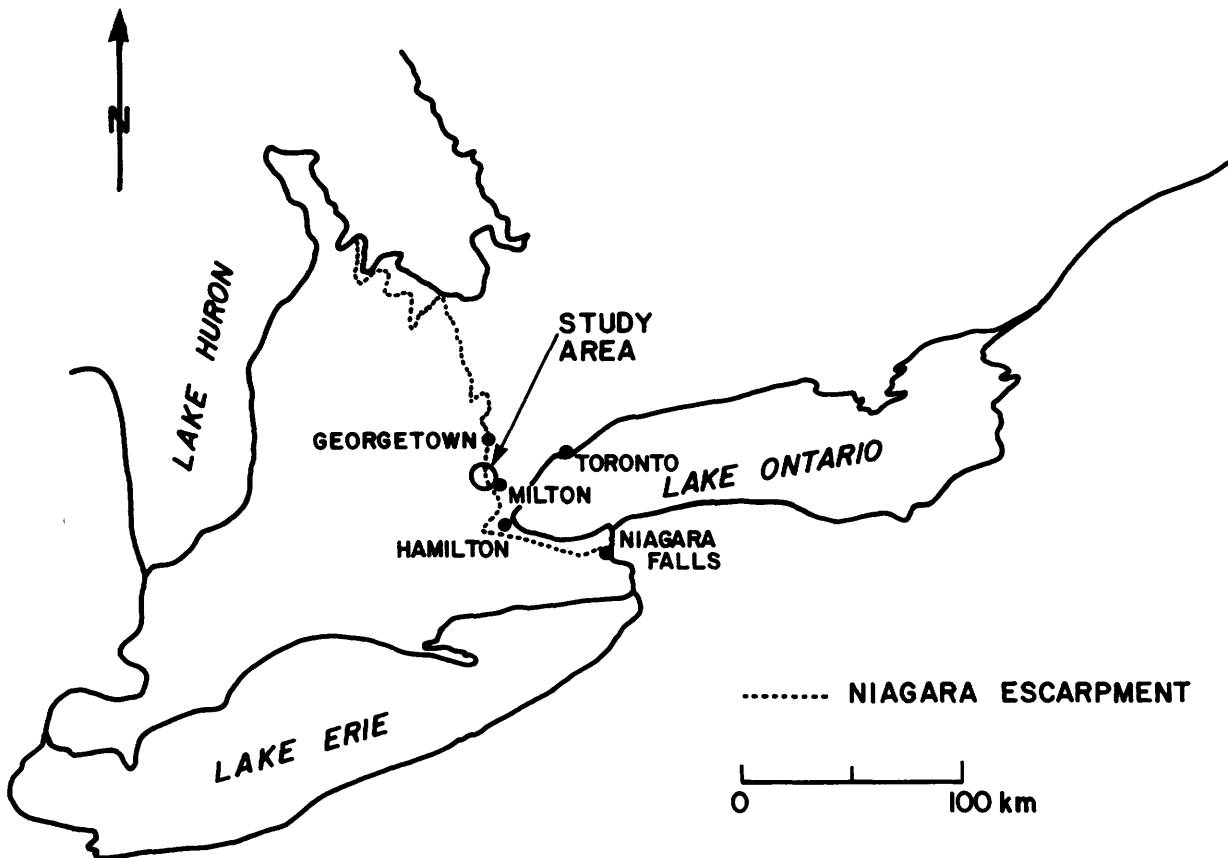


Figure 1—Location of Niagara Escarpment and study area.

a sequence of thinner beds of shale, dolostone, and sandstone.

The geology and topography of the Niagara Escarpment in the study area are illustrated by the cross-section in Figure 3. Figure 4 shows the rock formations intersected by the boreholes at the Dufferin quarry site. Six geologic formations are present. These are 1) the Amabel dolostone cap rock, 2) the Reynales argillaceous dolostone, 3) the Cabot Head shale, 4) the Manitoulin argillaceous limestone, 5) the Whirlpool sandstone, and 6) the Queenston shale.

AMABEL DOLOSTONE

The dolostone cap rock has a total thickness of about 24m in this section of the Niagara Escarpment. Most of this unit is characterized by massive beds of light grey-buff, fine to medium crystalline dolomite. The beds are highly fossiliferous, composed largely of bioclastic material forming in some sections a highly porous rock matrix. The top 7 m of this unit are more thinly bedded and slightly darker in colour than the rest of the unit and are generally of finer texture and less fossiliferous.

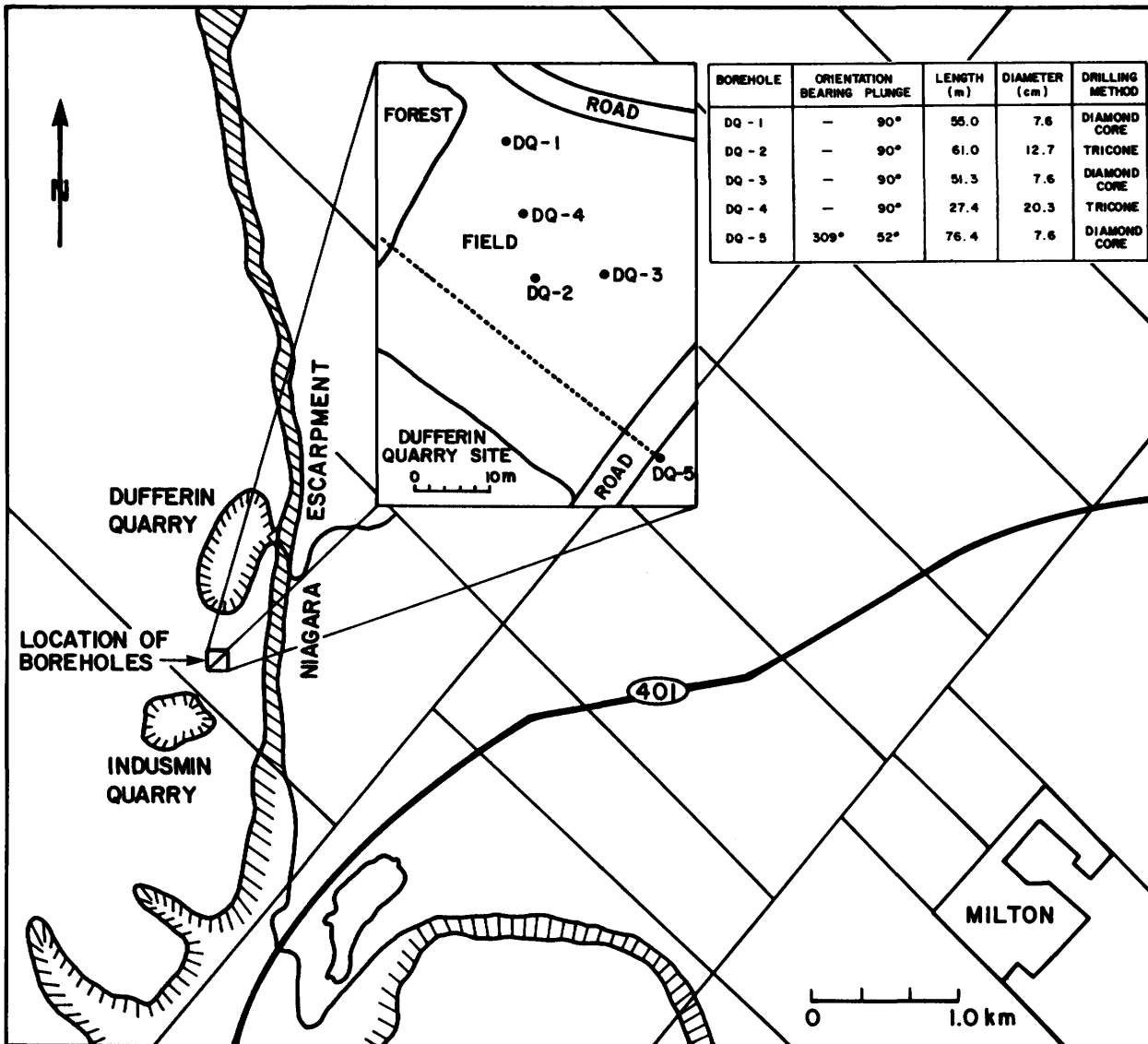


Figure 2—Location of Dufferin quarry site; inset map and table show location and details of boreholes.

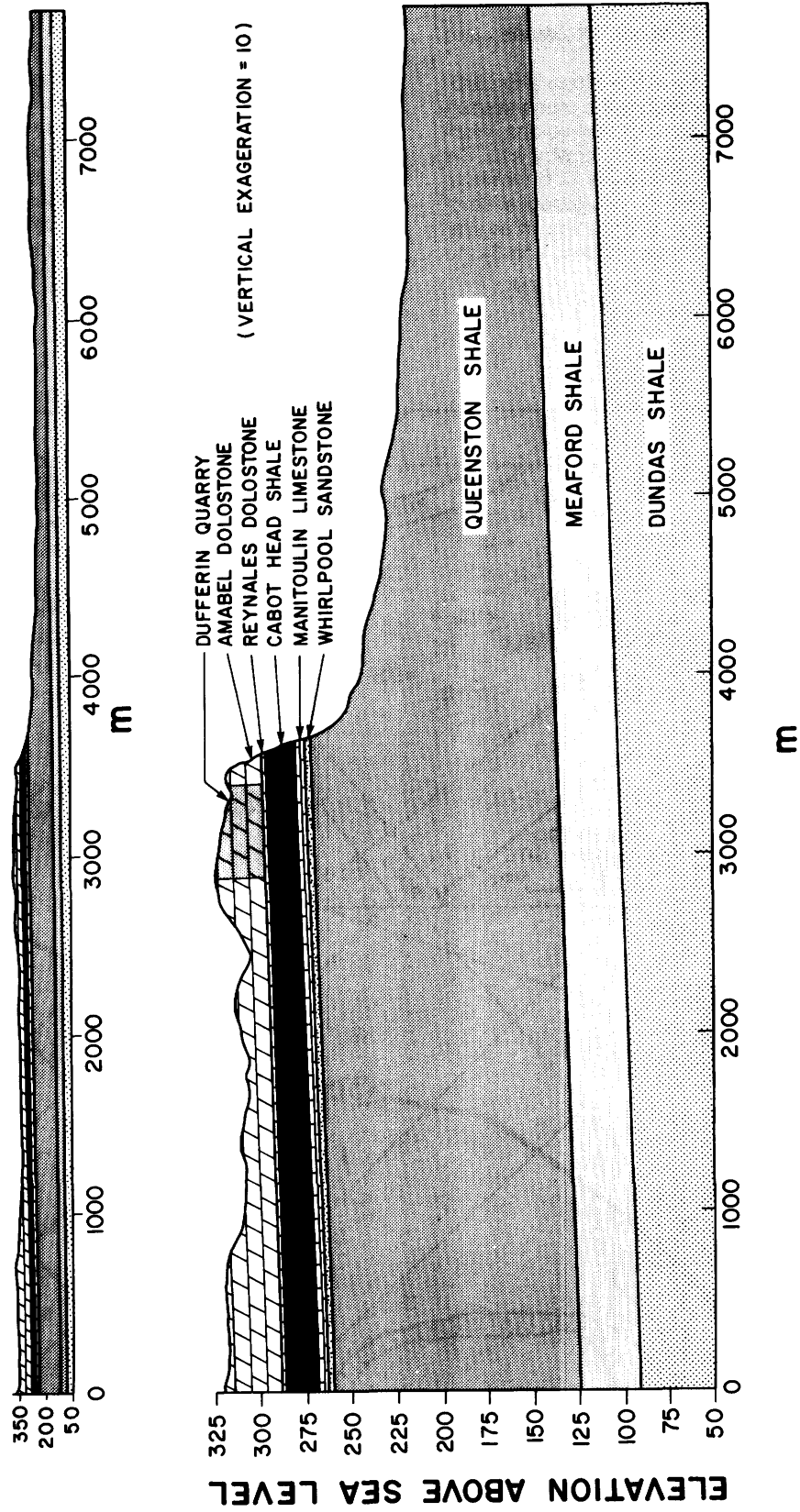


Figure 3—Vertical cross-section of the Niagara Escarpment at the Dufferin quarry site. Top diagram shows actual vertical scale.

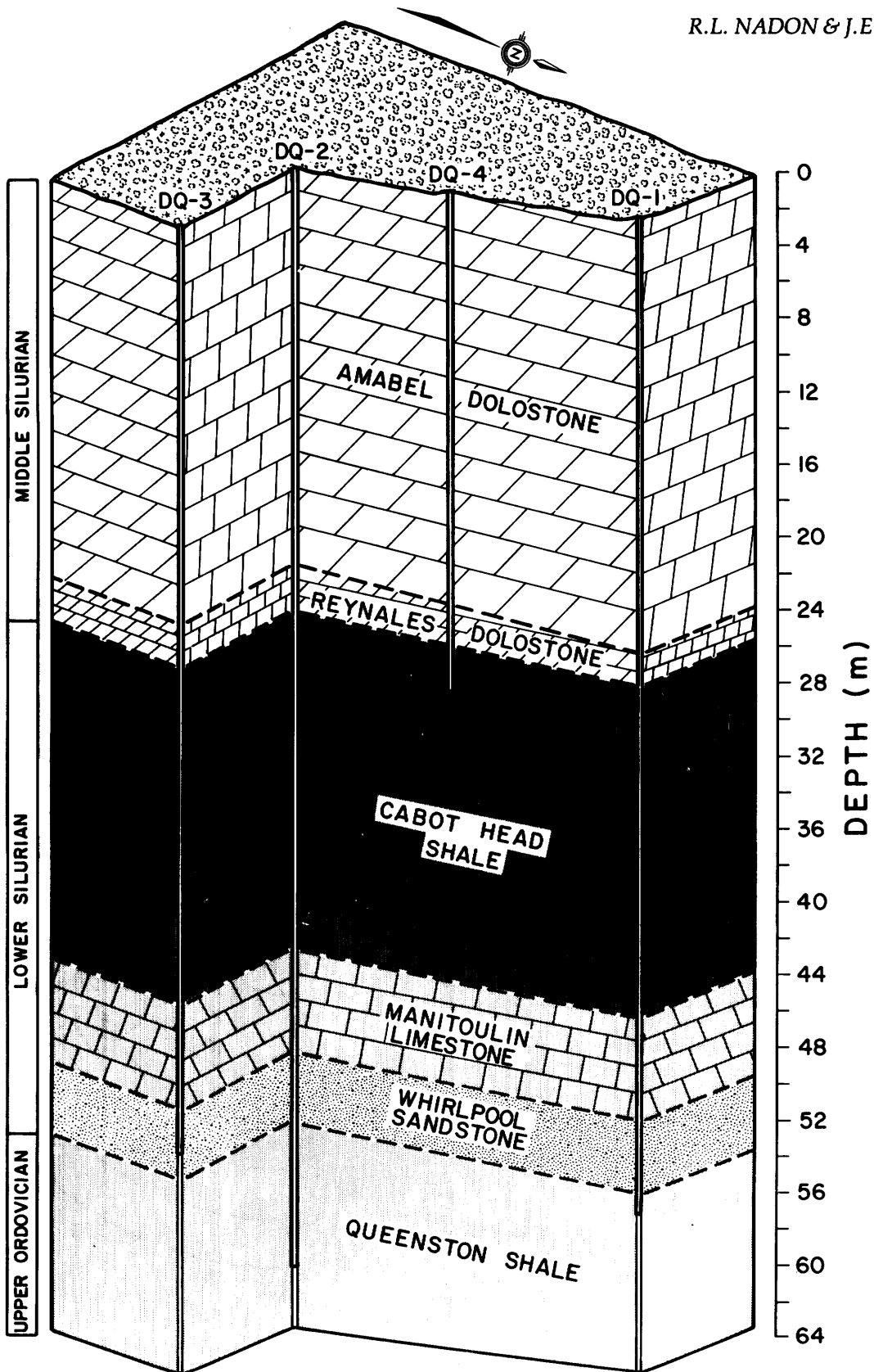


Figure 4—Geologic section drawn through the boreholes at the Dufferin quarry site.

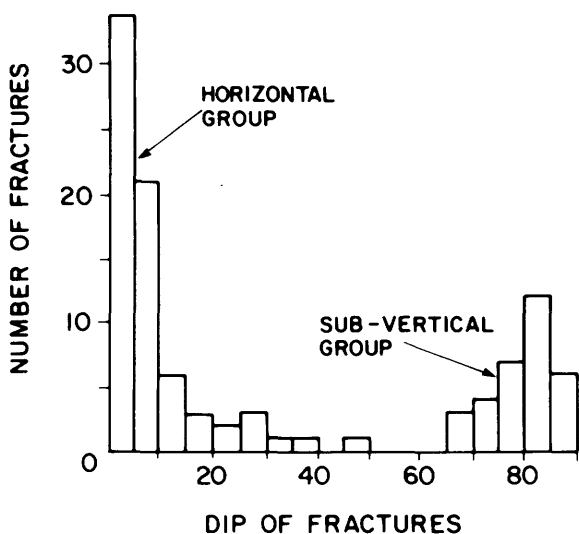


Figure 5—Histogram showing horizontal and sub-vertical fracture groups in Amabel dolostone identified in core from borehole DQ-5.

Fractures observed in this formation can be divided into two main groups: 1) horizontal bedding discontinuities, and 2) vertical and sub-vertical fractures. This is illustrated by the histogram of dips of fractures intersected in borehole DQ-5 (Figure 5). Fracture mapping of exposed faces in the Dufferin quarry and along the escarpment has revealed that there are two dominant trends for the orientation of the vertical fractures: 1) striking between S70°E and S50°E degrees, and 2) striking between N50°E and N80°E (Figure 6).

Typical spacings of horizontal fractures in this formation are 10 to 20 cm for the top 7 m and 20 to 60 cm for the lower section. In some locations within this more massive lower zone continuous cores of lengths greater than 1.5 m were recovered. Spacing of vertical fractures is variable but generally in the range of 0.5 to 1.0 m and often much greater.

Fractures in the Amabel dolostone are mostly clean, containing little gouge material. However, the fracture surfaces often have red-brown iron-oxide stains indicating that there has been flow of water through the fractures.

REYNALES DOLOSTONE

The Reynales dolostone is 2 m thick and consists of very fine crystalline, grey-brown, argillaceous, thinly bedded dolostone. The rock mass contains several shale bands generally less than 5 cm thick interbedded with the dolostone.

This formation is not exposed near the study area and therefore only the cores recovered from drilling provide information on the fractures. All fractures encoun-

tered were horizontal bedding discontinuities. The spacing of these fractures varied from 1 cm to 20 cm. Most fractures are filled with shale or clay gouge. There is no staining or signs of weathering on the fracture surfaces which suggests that no significant flow occurs through these fractures.

CABOT HEAD SHALE

The Cabot Head Formation is 18.5 m thick and consists predominantly of grey-green, finely laminated shale. Near the top of this unit, a section of interbedded, thin, red, calcareous shale and grey-green shale grading into a more massive, sandy, red, shaly limestone occurs over a thickness of about 4 m. In several locations below this, the

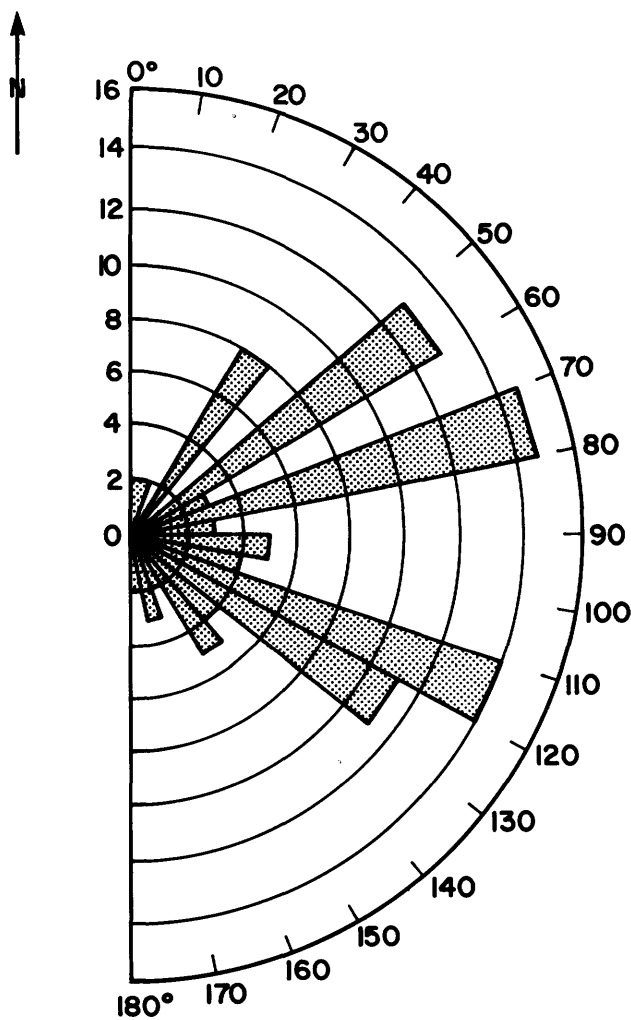


Figure 6—Rose diagram showing orientation of vertical and sub-vertical fractures in Amabel dolostone.

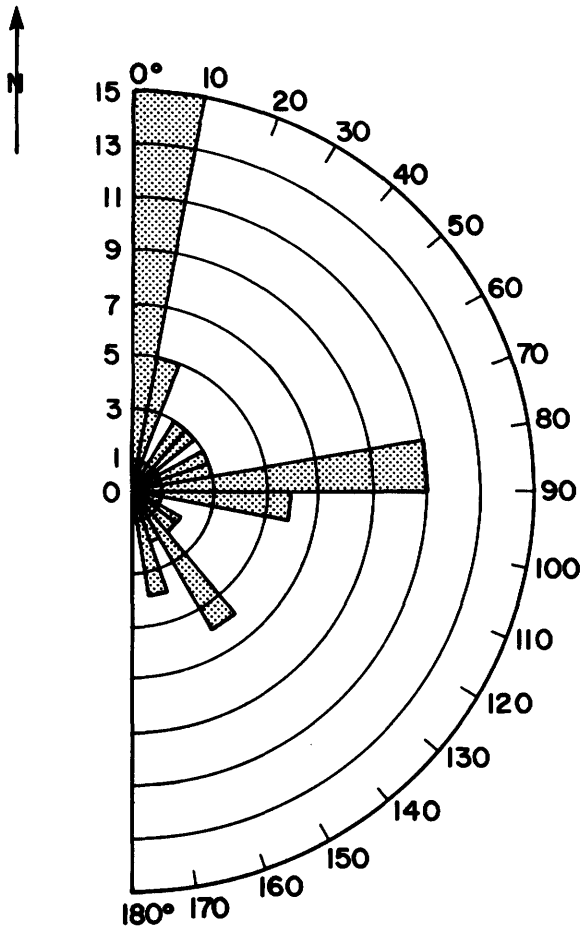


Figure 7—Rose diagram showing orientation of vertical fractures in Whirlpool sandstone.

shale is very soft, approaching the consistency of a plastic clay.

Virtually all of the discontinuities encountered in this formation are planes of weakness parallel to the bedding direction. These include shale lamination partings and discontinuities at contacts of soft and more rigid layers. The fractures are very tight and in the undisturbed state would not likely increase the rock mass permeability.

MANITOULIN ARGILLACEOUS LIMESTONE

At the base of the Cabot Head Formation, the soft shale becomes increasingly calcareous to a point where the rock is more suitably called argillaceous limestone. This somewhat arbitrary point is considered the upper contact of the Manitoulin Formation. This formation is about 5.7 m thick and consists of fine crystalline, argillaceous, dolomitic limestone beds 5 to 60 cm in thickness separated by several thin shale beds.

No vertical or inclined fractures were found in the cores from the Manitoulin Formation recovered from the three diamond drill holes. All fractures intersected by the boreholes are horizontal bedding discontinuities. Most breaks occur at shale-limestone contacts. In situ, these would be closed and tight and would not increase the permeability of the rock mass.

WHIRLPOOL SANDSTONE

This unit consists of thickly bedded, light brown-grey, fine-grained, well sorted, quartz sandstone. The Whirlpool Formation has sharp upper and lower contacts and is 4.1 m thick at the Dufferin quarry site. Very thin, dark grey to black shale seams occur throughout the sandstone.

Most fractures observed in this formation consist of horizontal bedding discontinuities at the contact of sandstone and thin shale seams. In the undisturbed state, these would be closed and would not tend to increase the permeability of the rock mass. No vertical fractures were intersected by any borehole but some were observed in an exposure near the Indusmin quarry. The rose diagram for the vertical fractures (Figure 7) shows that there are two dominant trends: 1) striking between N80°E and S80°E, and 2) striking between north and N10°E. The



Figure 8—Enlarged fractures caused by solution weathering of Amabel dolostone.

spacing of these fractures in the sandstone is variable but sections of continuous rock 2 to 5 m in length are very common. Most of the vertical fractures observed are very tight and clean. Some seepage of water through these thin vertical cracks was observed in a quarry exposure.

QUEENSTON SHALE

The Queenston shale is reported to be over 130 m thick in the Milton region (Bolton 1957). Only the top 7 m of the Queenston Formation was intersected by the boreholes at the Dufferin quarry site. This unit consists mostly of dark red, hematitic, fissile, calcareous shale interbedded with very finely crystalline, grey-green, highly argillaceous limestone.

For the most part, fractures in this unit are bedding plane discontinuities. In some more dense calcareous zones, very thin and tight inclined fractures are found. The extent of these is unknown as only core samples of this unit were available for examination.

TOPOGRAPHY

On top of the escarpment, the surface is irregular consisting of several small hills and depressions 200 to 1000 m in diameter and with a vertical relief of 10 to 20 m. The overburden material varies in composition from a sandy clay till to a sandy gravel till across the study area. Generally, outcrops of the Amabel dolostone occur at the top of the hills while in the depressions, the rock is covered by up to 8 m of overburden. This hummocky terrain reflects the numerous domed reef structures found throughout the Amabel Formation. Where exposed, the dolostone unit shows signs of extensive solution weathering. Large vertical crevices up to 1 m in width dissect the dolostone forming a blocky, highly permeable rock mass. These enlarged fractures narrow with depth and are often filled with till and organic material (Figure 8). Large crevices reaching depths of over 15 m and over 1 m in width are found near the edge of the escarpment in the Amabel dolostone on the Milton outlier 4 km south of the study area. These are oriented parallel to the face of the escarpment and have continuous lengths of over 50 m.

Near the field site, the exposed vertical face of the escarpment is about 20 m in height. A talus slope begins near the lower contact of the Amabel Formation and extends eastward for about 1000 m, dipping steeply at first then gradually levelling off until it blends into the flat-lying fields below the escarpment under which lies the easily eroded Queenston shale (see Figure 3).

HYDROGEOLOGY

From the above discussion of the geology of the Dufferin quarry site, it is apparent that there are two horizons within the vertical section of the Niagara Escarpment in which underground mining may be feasible. These are 1) at the base of the Amabel dolostone cap rock formation,

and 2) within the Whirlpool sandstone and Manitoulin limestone.

The hydrogeological setting of these two horizons differs greatly. The Amabel Formation is exposed at the surface and is therefore subject to direct recharge from surface water, whereas the Whirlpool and Manitoulin Formations are bounded above and below by thick shale beds which should impede groundwater movement. To

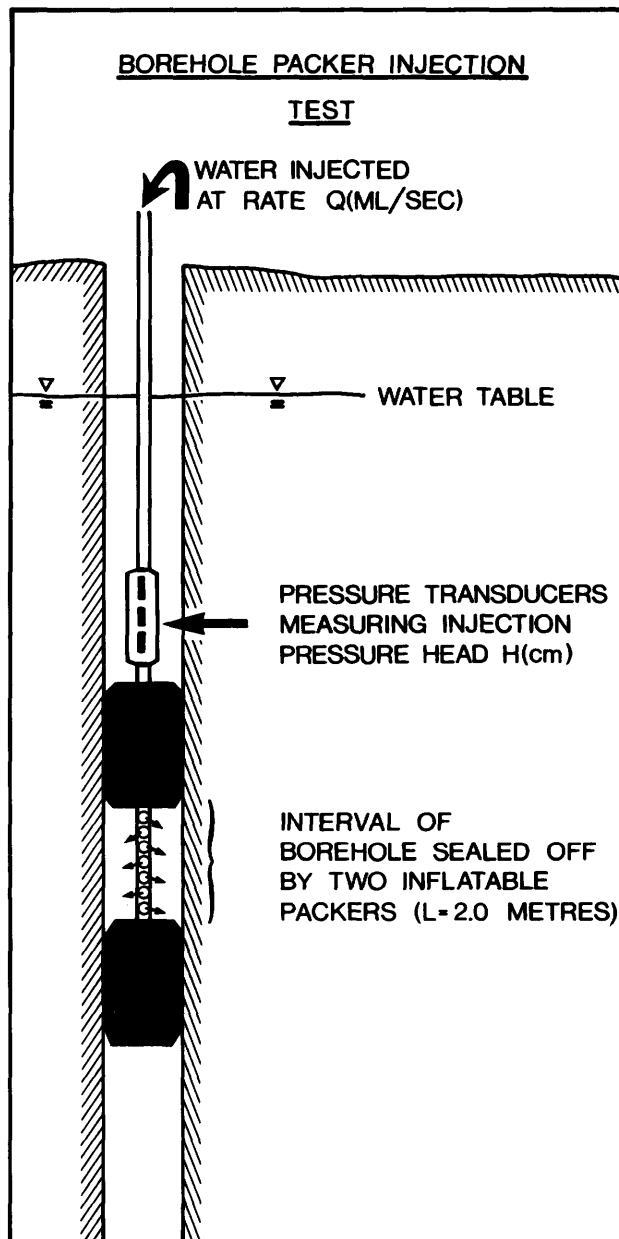


Figure 9—Principle of a borehole packer injection test.

evaluate the potential, from a hydrogeological perspective, of these two candidate horizons for the development of underground mining for aggregate production and/or space utilization, the hydrogeological properties of each of the rock units have been measured and this data has been combined with the distribution of hydraulic heads and recharge and discharge areas in order to define the overall groundwater flow system in the Dufferin quarry area.

HYDROGEOLOGICAL PROPERTIES

DOLOSTONE CAP ROCK UNIT

Hydraulic conductivity values determined from 22 packer injection tests (Figure 9) in the dolostone cap rock unit, which includes the Amabel and Reynales Formations, ranged from 1.1×10^{-5} cm/sec to 5.7×10^{-3} cm/sec. The distribution of hydraulic conductivity values as a function of depth, as determined from these tests, for the cap rock unit as well as for the other rock units intersected by each borehole, are presented in Figures 10a, b. Five laboratory tests on dolostone core samples gave a range of matrix hydraulic conductivity from 1×10^{-8} cm/sec to 5×10^{-5} cm/sec (squares on Figures 10a, b). The much lower intergranular permeability of the dolostone compared to the permeability of the rock mass indicates the importance of fractures to groundwater flow in this unit.

Plots showing the frequency of fractures intersected along the length of boreholes DQ-1, DQ-3, and DQ-5 are also shown in Figures 10a, b. Both horizontal and vertical fractures are included in these plots. In the dolostone cap rock unit, it is the distribution and character of these fractures that control the permeability of the rock mass. The importance of fractures is demonstrated in borehole DQ-3 where in four consecutive test intervals between 14 and 22 m (Figure 10a), the hydraulic conductivity varies by more than two orders of magnitude. Open horizontal fractures with iron oxide stained surfaces, indicating flow of groundwater, were observed in cores from the more permeable intervals while fractures in the less permeable intervals were generally much cleaner showing little or no sign of weathering or discoloration. Also, the hydraulic conductivity of an interval of rock in borehole DQ-1 (18.0 to 20.0 m) containing an open sub-vertical fracture is over ten times greater than the conductivity of the test intervals above and below in which only closed horizontal fractures are present. More evidence of the permeable nature of fractures is found in the Dufferin quarry where in several locations large vertical and horizontal fracture surfaces are exposed showing extensive red-brown iron oxide staining caused by groundwater flow.

For two pump tests performed in the Amabel dolostone, transmissivity values ranging from 1.2 to 3.6 cm²/sec (700 to 2100 imperial gallons/day/foot) were calculated using the Neuman type curve method for unconfined aquifers (Neuman 1975). Figure 11 shows the drawdown curve for well DQ-1 fitted to a β -0.001, type-A curve. For a saturated thickness of 12 m, the transmissivity values obtained correspond to a range of hydraulic conductivity values from 1×10^{-3} to 3×10^{-3} cm/sec

which agrees very well with the average conductivity calculated from injection tests (1.4×10^{-3} cm/sec).

In this study, concern is mainly with establishing the total flux of groundwater through the rock formation as opposed to determining the velocity at which groundwater moves. Therefore the permeability of the fracture system of the rock formation as a whole is of more interest than the ability of an individual fracture to transmit water. Although it is known that flow in the dolostone cap rock unit occurs primarily through discrete fractures, results from the pump tests indicate that the rock mass contains a sufficient number of well interconnected fractures so that over large distances, the rock mass responds in a way similar to a porous media.

CABOT HEAD - MANITOULIN UNIT

Below the dolostone cap rock unit there are 21 m of shale and argillaceous limestone for which hydraulic conductivity values ranging from 10^{-7} to 10^{-9} cm/sec were obtained from borehole injection tests (see Figures 10a, b). A similar range of matrix conductivity values were obtained for core samples from this zone (Table 1) indicating that the fractures observed in these formations are in fact closed or sealed with clay gouge and do not increase the rock mass permeability.

Given the presence of bedding stratification and the apparent lack of vertical fractures in this rock unit, it is reasonable to expect that the vertical conductivity of the shale and limestone is at least one or two orders of magnitude lower than the horizontal conductivity. Maximum vertical groundwater velocities through this unit would be less than 1 cm in 30 years assuming a hydraulic conductivity of 10^{-9} cm/sec and a unit gradient. Therefore the Cabot Head-Manitoulin unit should form an effective barrier to vertical groundwater movement.

WHIRLPOOL SANDSTONE UNIT

Intergranular hydraulic conductivity values of 2.8×10^{-5} cm/sec and 5.2×10^{-6} cm/sec were obtained for two core samples of the Whirlpool sandstone. Hydraulic conductivity values of the same magnitude were calculated from borehole injection tests performed in this formation. Similar field and laboratory results are not surprising since very few fractures were encountered in the sandstone. It may be incorrect, however, to conclude that groundwater flow in this unit is predominantly intergranular. As discussed earlier, widely spaced vertical fractures were observed in outcrops of the Whirlpool sandstone. The fact that none of these fractures were encountered in any borehole may only reflect the limited horizontal extent of the boreholes at the Dufferin quarry site. A high permeability zone discovered at the upper contact of the Whirlpool sandstone in borehole DQ-5, suggests that fractures may in fact increase significantly the rock mass permeability. An injection test in this zone gave a hydraulic conductivity of 6×10^{-4} cm/sec. Several closely spaced horizontal fractures and a 10 cm rubble zone are found near the contact in core from DQ-5. These horizontal fractures may provide communication between the borehole and vertical fractures in the sandstone.

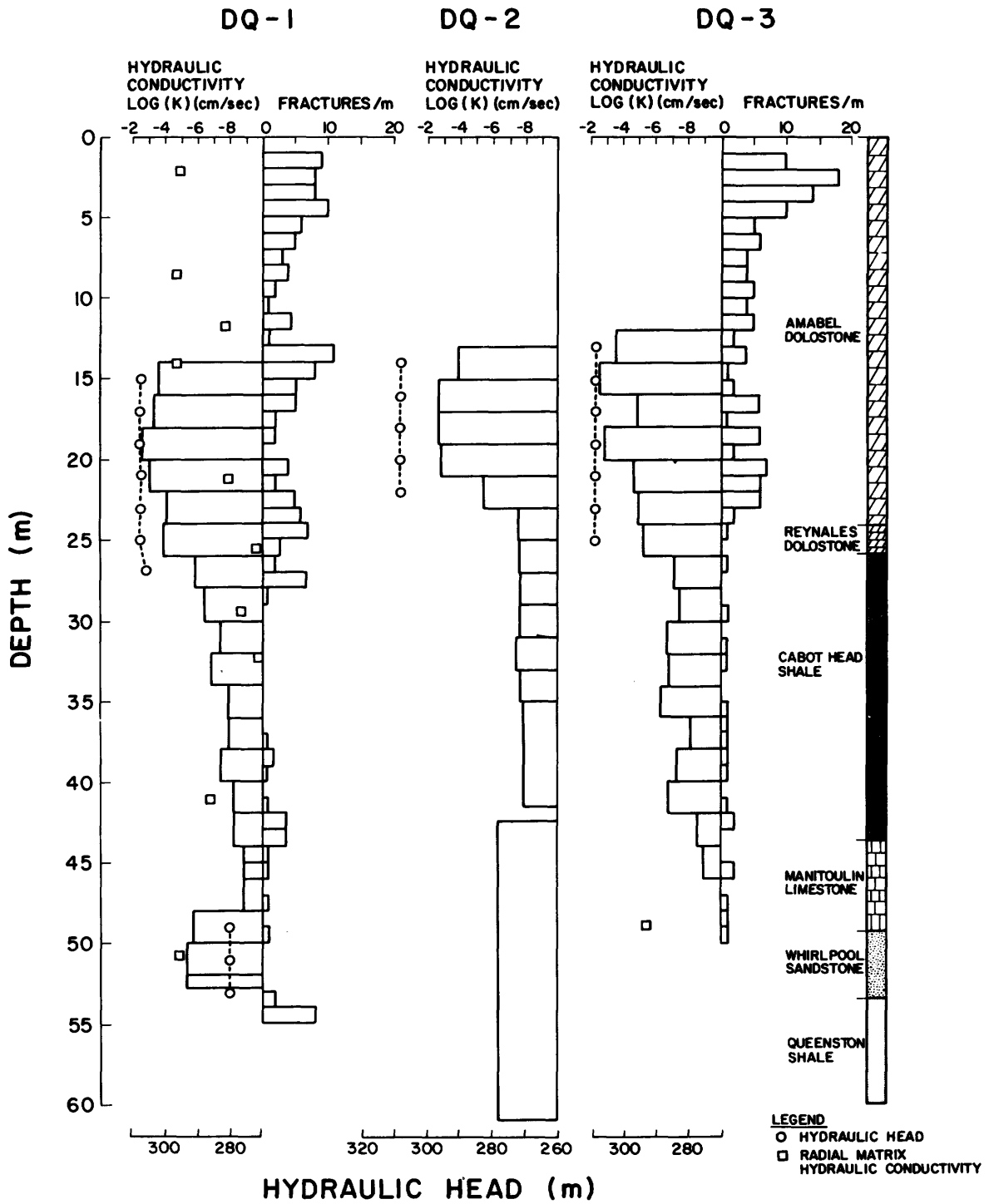


Figure 10a—Hydraulic conductivity determined by borehole injection tests, and fracture densities for DQ-1, DQ-2 and DQ-3.

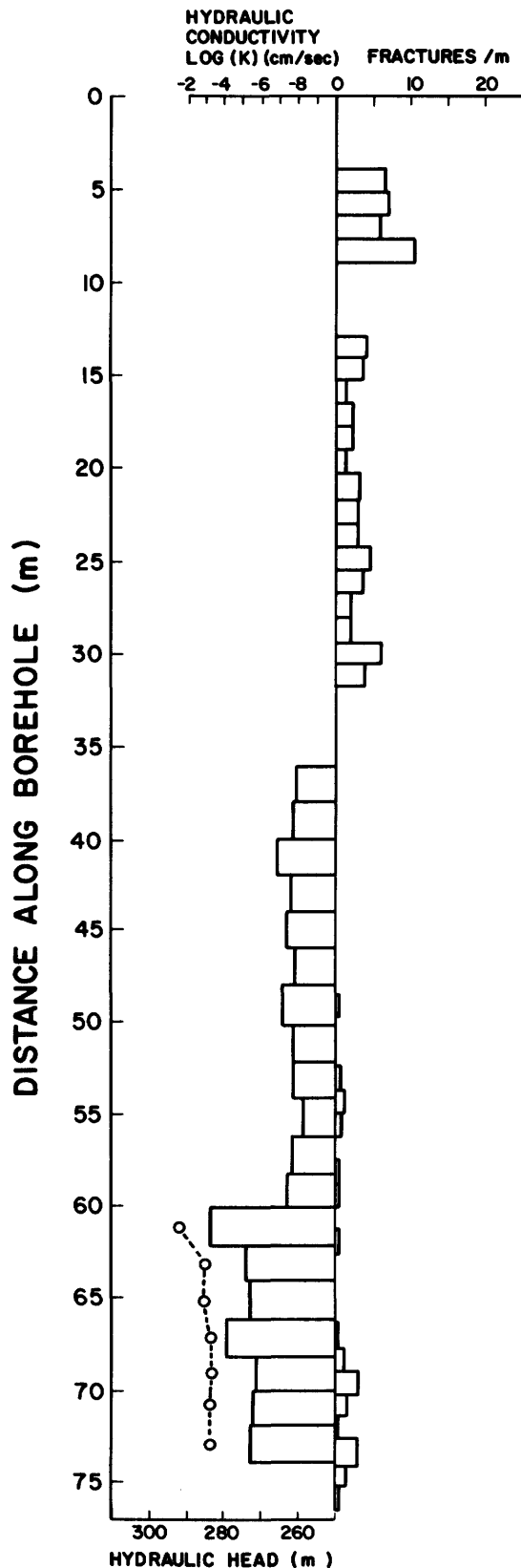


Figure 10b—Hydraulic conductivity determined by borehole injection tests, and fracture densities for borehole DQ-5.

Results from a 5-hour, constant flow-rate injection test conducted in the Whirlpool and upper Queenston Formations provide more evidence suggesting that vertical fractures may affect significantly the permeability of the sandstone rock mass. Water level responses in observation wells during this test indicate that permeability is highly anisotropic. The permeability of the rock mass is greatest in a north-south direction, which coincides with the orientation of the main vertical fracture set identified in the Whirlpool Formation (see Figure 7). Preferred flow along these fractures could account for the anisotropy observed. Based on available data, it is difficult to make any firm conclusions on the importance of vertical fractures to the permeability of the sandstone rock mass. The only conclusion that can be made at this point is that there are fractures in this formation of significantly higher permeability than the sandstone matrix and that these fractures increase significantly the overall rock mass permeability.

QUEENSTON SHALE UNIT

The average hydraulic conductivity of the upper few metres of the Queenston shale unit, as determined from packer injection tests, is 3×10^{-6} cm/sec. No intact core of sufficient length was recovered to obtain a measure of the intergranular hydraulic conductivity of the shale, however, by comparison with other samples tested, the conductivity is probably very low, certainly less than 10^{-8} cm/sec. The much higher conductivity values obtained from injection tests indicate that the fractures observed in this upper part of the Queenston formation increase significantly the permeability of the shale. More evidence of the ability of fractures in the shale to transmit water can be seen in core samples from this interval of rock, where greenish discoloration is found along several thin fractures. Caley (1940) suggested that the discoloration is probably due to bleaching of the shale by percolating waters charged with organic acids in solution.

The lower part of the Queenston shale was not penetrated by any borehole at the Dufferin quarry site and therefore the hydrogeologic properties of this section of rock could not be measured. Water well records, however, indicate that only the upper part of the Queenston Formation produces fresh water and that below this zone, only low yields are obtained and the groundwater is highly mineralized. It is therefore reasonable to expect that the permeability of the lower part of the Queenston shale is very low and probably no greater than 10^{-8} cm/sec.

GROUNDWATER FLOW SYSTEM

Figure 12 shows the idealized groundwater flow system of the Niagara Escarpment at the Dufferin quarry site (excluding the effects of drainage into the quarry) as interpreted from field observations and from a knowledge of the hydrogeologic properties of each rock type. It must be emphasized that the flow system presented is highly simplified and shows only the main features of a system which in reality is much more complex. Such simplifica-

Table 1—Porosity and permeability measurements of core samples.

SAMPLE NO.	DEPTH (m)	ROCK TYPE	POROSITY (%)	HYDRAULIC CONDUCTIVITY (CM/SEC)	
				RADIAL	AXIAL
1-1	2.05	DOLOSTONE	7.0	1.6×10^{-5}	2.2×10^{-8}
1-2	8.50	DOLOSTONE	9.0	5.3×10^{-5}	1.2×10^{-6}
1-3	11.70	DOLOSTONE	4.3	4.0×10^{-8}	$<10^{-10}$
1-4	14.10	DOLOSTONE	8.3	3.2×10^{-5}	2.5×10^{-7}
1-5	21.15	DOLOSTONE	3.9	1.2×10^{-8}	3.3×10^{-9}
1-10	55.55	DOLOSTONE	1.5	4.0×10^{-10}	$<10^{-10}$
1-6	29.35	ARGILLACEOUS DOLOSTONE	7.7		4.1×10^{-9}
1-7	32.10	DOLOMITIC SHALE	6.8	1.2×10^{-10}	9.4×10^{-10}
1-8	41.00	ARGILLACEOUS DOLOSTONE	5.5	1.5×10^{-7}	1.3×10^{-9}
1-9	50.65	SANDSTONE	13.4	2.8×10^{-5}	1.1×10^{-7}
3-1	48.75	SANDSTONE	11.1	5.2×10^{-6}	2.0×10^{-6}

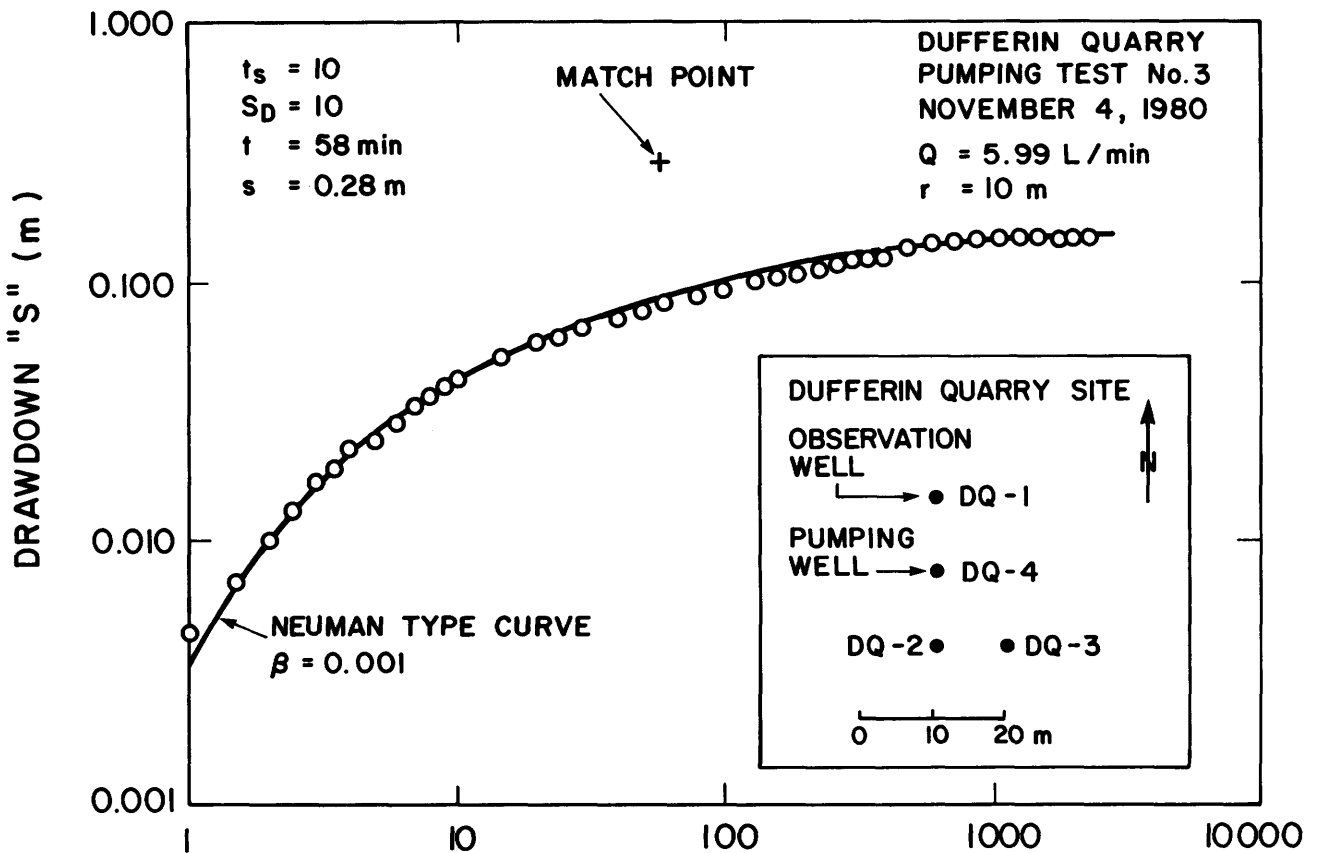


Figure 11—Drawdown curve for observation well DQ-1 during pump test No. 3. X axis represents time in minutes.

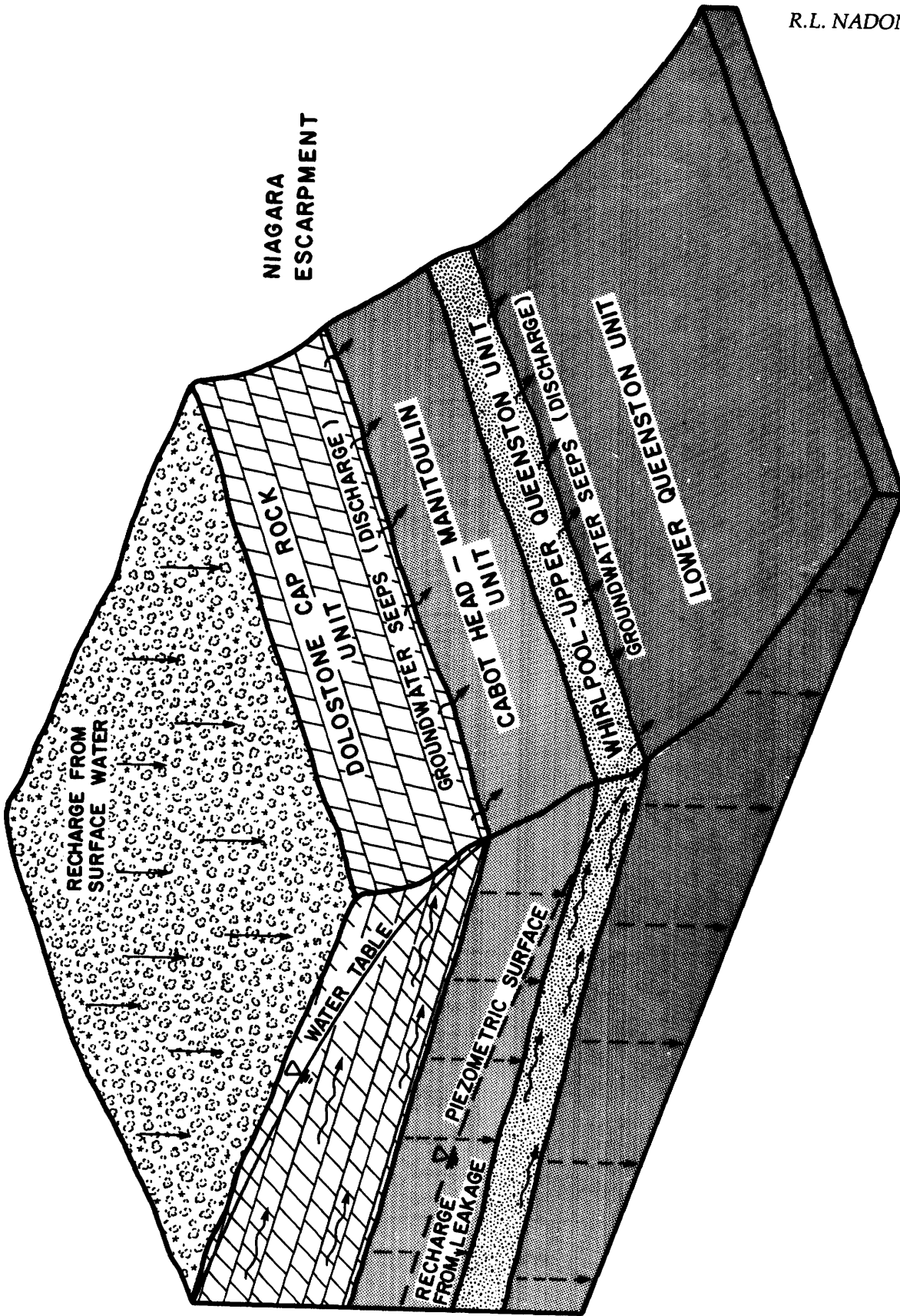


Figure 12—Idealized groundwater flow system at the Dufferin quarry site.

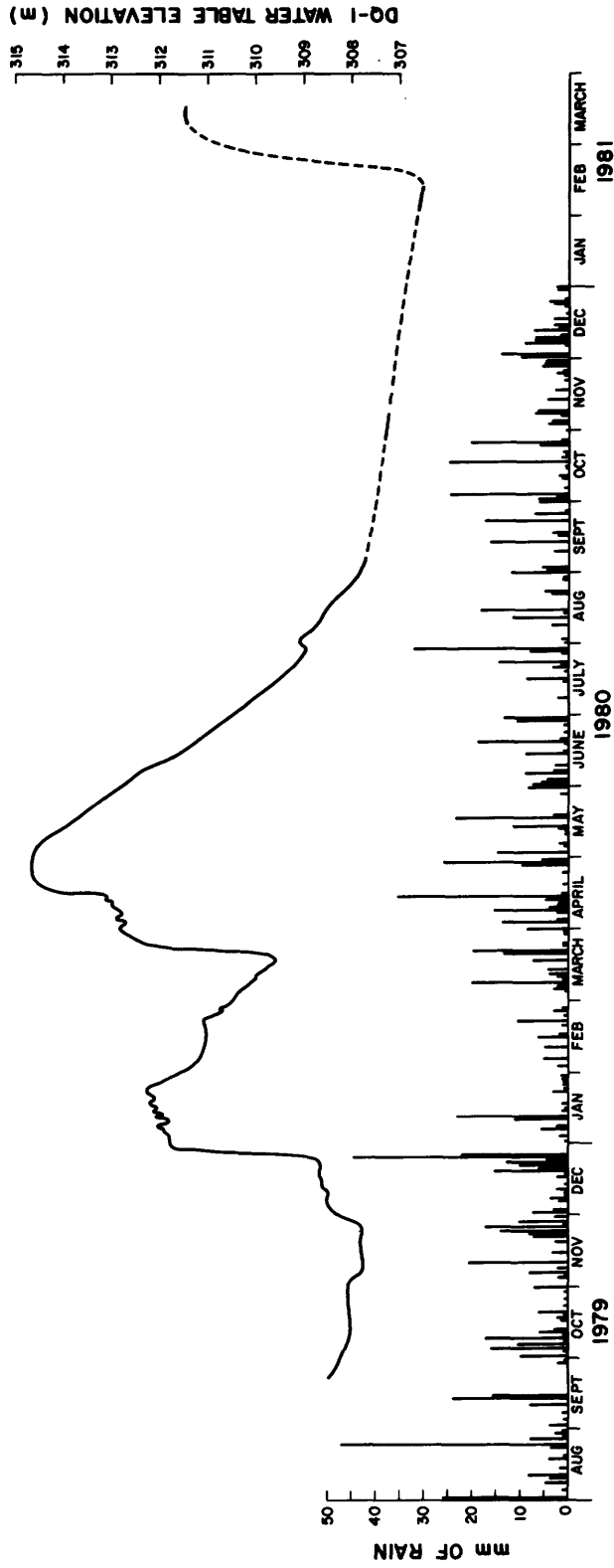


Figure 13—Hydrograph for borehole DQ-1 and daily precipitation distribution.

tion is necessary, however, if any attempt is to be made at quantifying the flow system, as must be done to predict the hydrogeological consequences of mining within these bedrock units.

Above the escarpment, much of the water from precipitation is trapped in surface depressions forming bogs and swamps. There is no well developed surface drainage pattern which suggests that water must evaporate, or be absorbed by the vegetation, or infiltrate the dolostone bedrock. In areas where overburden is very thin, infiltration of water into the dolostone cap rock unit occurs rapidly. Evidence of this is shown in Figure 13 which is the hydrography for well DQ-1 plotted together with the daily precipitation measurements taken at a nearby station during the period August 1979 to December 1980. Major rain events in December, 1979, and April, 1980, show a same-day sudden rise in water levels demonstrating that recharge occurs without a long time lag.

The low permeability of the Cabot Head – Manitoulin unit forces groundwater moving in the overlying saturated portion of the fractured dolostone unit to flow horizontally. Constant hydraulic heads with depth in this unit (see Figure 10a), as measured during borehole injection tests, support this conclusion. From the elevation of the water table in the study area, it is apparent that flow is generally easterly towards the escarpment face where discharge points in the form of seeps are found in several locations near the contact of the dolostone and shale.

The Whirlpool sandstone and the top few metres of the Queenston shale are the only other rocks at the Dufferin quarry site in which significant groundwater flow occurs. These formations are confined above by the Cabot Head – Manitoulin unit and below by the lower part of the Queenston shale. The only source of recharge is downward leakage of groundwater from the dolostone cap rock through the Cabot Head and Manitoulin Formations. Unusually high vertical downward gradients exist across these two formations. At the Dufferin quarry site, hydraulic heads in the Whirlpool sandstone are about 28 m below those in the dolostone cap rock (see Figure 10a) creating a hydraulic gradient of about 1.3. This very high gradient combined with the fact that the permeability of the cap rock unit is greater than that of the Whirlpool – Upper Queenston unit, is proof that the Cabot Head – Manitoulin unit forms an effective barrier to vertical groundwater movement. Hydraulic head measurements in the Whirlpool – Upper Queenston unit (see Figure 10) indicate that groundwater flow is horizontal. From the limited data available it appears that the direction of flow is also easterly towards the discharge points at outcrops of the Whirlpool and Queenston Formations along the base of the Niagara Escarpment.

MODELLING OF GROUNDWATER SYSTEM

An assessment of inflows and extent of dewatering for a hypothetical underground mine excavated in the Amabel Formation and in the Whirlpool-Manitoulin Formations is in progress. The groundwater flow system for each of these two cases is being modelled using a two-dimen-

sional transient finite element program developed by Frind (1976). Results of this work will be presented in the final report.

REFERENCES

- Acres
1974: Underground Space Utilization, Acres Research and Development program; unpublished report, Acres Consulting Services Limited.
1976: Underground Aggregate Mining Preliminary Feasibility Study; prepared for the Ontario Ministry of Treasury, Economics and Intergovernmental Affairs, and the Niagara Escarpment Commission by Acres Consulting Services Limited.
- Bolton, T.E.
1957: Silurian stratigraphy and paleontology of the Niagara Escarpment in Ontario; Geological Survey of Canada, Memoir 289, 145p.
1964: Pre-Guelph Silurian formations of the Niagara Peninsula; American Association of Petroleum Geologists Guidebook, Geology of Central Ontario, p.55-80.
- Caley, J.E.
1940: Paleozoic Geology of the Toronto-Hamilton area, Ontario; Geological Survey of Canada, Memoir 224, 284p.
- Frind, E.O.
1976: Transient Two-dimensional Confined-unconfined Aquifer Model; unpublished Short User's Guide, Department of Earth Sciences, University of Waterloo.
- Legget, R.
1978: Energy, Geology and the Underground; Geoscience Canada, Vol.5 No. 3 p.119-123.
- McCreath, D.R., and Mitchell, D.E.
1978: Build underground and conserve energy: Fact or Fiction; Engineering Journal, April 1978, p.14-16.
- Neuman, S.P.
1975: Analysis of Pumping test data from Anisotropic Unconfined Aquifers Considering Delayed Gravity Response; Water Resources Research, Vol.2, No.2 p.329-342.
- Ontario Mineral Aggregate Working Party
1976: A Policy for Mineral Aggregate Resource Management in Ontario; Ministry of Natural Resources.
- Proctor and Redfern
1974: Towards the Year 2000 — A study of mineral aggregate in Central Ontario; prepared for Ontario Ministry of Natural Resources by Proctor and Redfern Limited.
- Sanford, B.V.
1969: Geology, Toronto-Windsor Area; Geological Survey of Canada, Map 1263A, scale 1:250,000.
- Stauffer, Sr., T.
1975: Kansas City: A model of underground development; unpublished paper presented at "The New Industrial Space", Queen's Park, Toronto, Ontario.
- Telford, P.G.
1978: Silurian Stratigraphy of the Niagara Escarpment, Niagara Falls to the Bruce Peninsula; in Geological Association of Canada, Field Trips Guidebook, Toronto '78.
1976: Paleozoic Geology of Southern Ontario; Ontario Division of Mines, Maps 2336 to 2343, scale 1:50,000.

Grant 78 Terrain Characteristics and Physical Processes in Small Lagoon Complexes

J.E. Otto¹ and R.W. Dalrymple²

¹Department of Geological Sciences, Brock University

²Department of Geological Sciences, Queen's University

ABSTRACT

Sixteen Mile Creek is located on the southwest shore of Lake Ontario, 5 km west of St. Catharines. Detailed examination of cores from the lagoon reveals five stratigraphic units. They are (from the base up): 1) Pink Clay, average grain size 6.7 ϕ and organic content 2-9 percent; 2) "Bottom" Sand, average grain size 4.9 ϕ ; 3) Gittja, mean grain sizes 7.2-9.2 ϕ and organic content 5-35 percent; 4) Brown Clay, average grain size 9.2 ϕ and organic content 9 percent; and 5) Gray Clay, grain size 6.5-9.5 ϕ and average organic content 6 percent. Radiocarbon dating indicates that flooding of the lagoon began approximately 5250 years ago initiating deposition of the Gittja; after 3725 years B.P. Brown Clay accumulated contemporaneously in the deeper parts of the lagoon. Deposition kept pace with rising lake levels until approximately 1500 years B.P. when capture of Sixteen Mile Creek by Twenty Mile Creek reduced sediment input and allowed inundation of the marsh and deposition of the Gray Clay. Chemical analysis of the recent sediments reveals that concentrations of copper and phosphorous are highest in the delta area. Zinc concentrations reach maxima at both the upper and lower ends of the lagoon. Zinc, copper and phosphorous commonly increase in abundance upwards through the Gray Clay.

INTRODUCTION

During the last several thousand years, water levels in the lower Great Lakes have slowly risen as a result of isostatic rebound of their outlets. In the process, the lower reaches of streams which had become incised during the preceding low-level stage were flooded creating small lagoons. These lagoons now act as traps for river-borne (polluted?) sediments, and are often the sites of intense recreational and other cultural activities, yet little is known about past or present sedimentation patterns in them. Consequently the Sixteen Mile Creek lagoon, located 5 km west of St. Catharines (Figure 1), was selected for detailed sedimentological and geochemical investigation. This lagoon is representative of the many such embayments which exist around all of the lower Great Lakes,

and was chosen because it is easily accessible but little frequented or developed, and because it is intermediate in size and stage of evolution (infilling) between such local extremes as the smaller, almost completely infilled, Fifteen Mile Creek lagoon, and the much larger and deeper Twenty Mile Creek lagoon (Jordan Harbour). The study has four objectives: 1) the detailed description (physical, chemical and biological) of the Recent and modern sediments filling the lagoon; 2) documentation or reconstruction of the processes and depositional environments responsible for the sediments; 3) reconstruction of the history of lagoon infilling, including the influence of lake-level changes and changing conditions in the drainage basin of the Sixteen Mile Creek on sedimentation patterns and rates; and 4) examination of trace-element variation (temporal and spatial) in the sediments with the aim of assessing the role of such lagoons as natural pollution traps. This report is a preliminary summary of our observations and tentative conclusions pertaining particularly to the first three objectives.

GENERAL SETTING

The Sixteen Mile Creek has its headwaters above the Niagara Escarpment and flows over till-mantled Lockport Dolomite before descending the escarpment through a deeply incised gorge 5.2 km above the head of the lagoon. The drainage basin of the Sixteen Mile Creek presently occupies 16 km², however J.J. Flint (Brock University, personal communication, 1980) has discovered that the upper reaches of the Sixteen Mile Creek were captured by the Twenty Mile Creek approximately 1500 years B.P., reducing the area draining into the Sixteen Mile Creek lagoon by about one-half.

The lagoon is situated on the flat to gently rolling plain at the base of the Niagara Escarpment. The underlying bedrock is Queenston shale but this is not exposed in the vicinity of the study area. Surrounding surficial sediments consist of clay tills, overlain by lacustrine sands and silts (Wickland and Mathews 1963) deposited in glacial Lake Iroquois which existed approximately 13 000-11 000 years B.P. at an elevation about 35m above the present level (75 m above sea level) of Lake Ontario (Karrow *et al.* 1961).

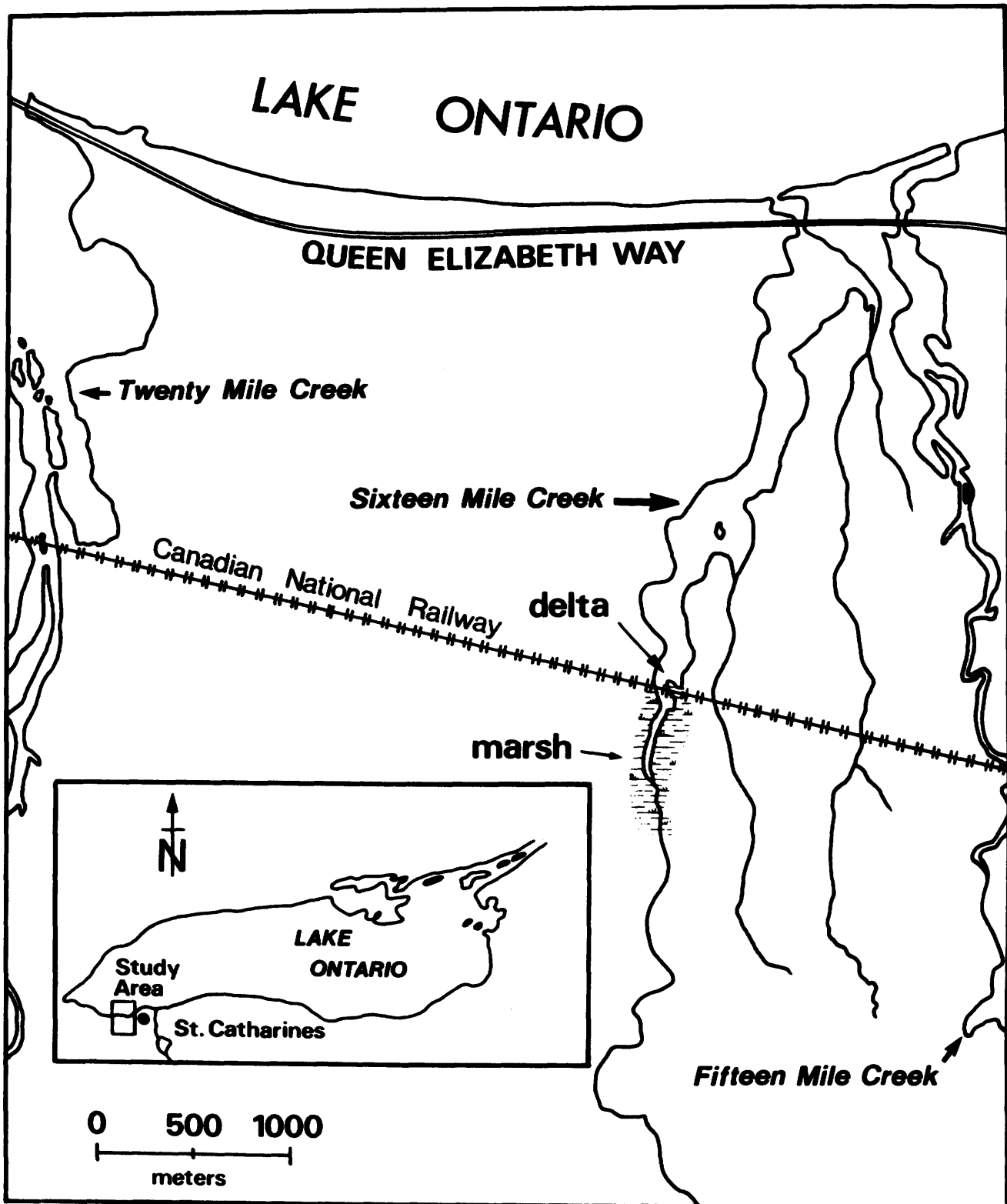


Figure 1— Location map of the study area and surrounding region.

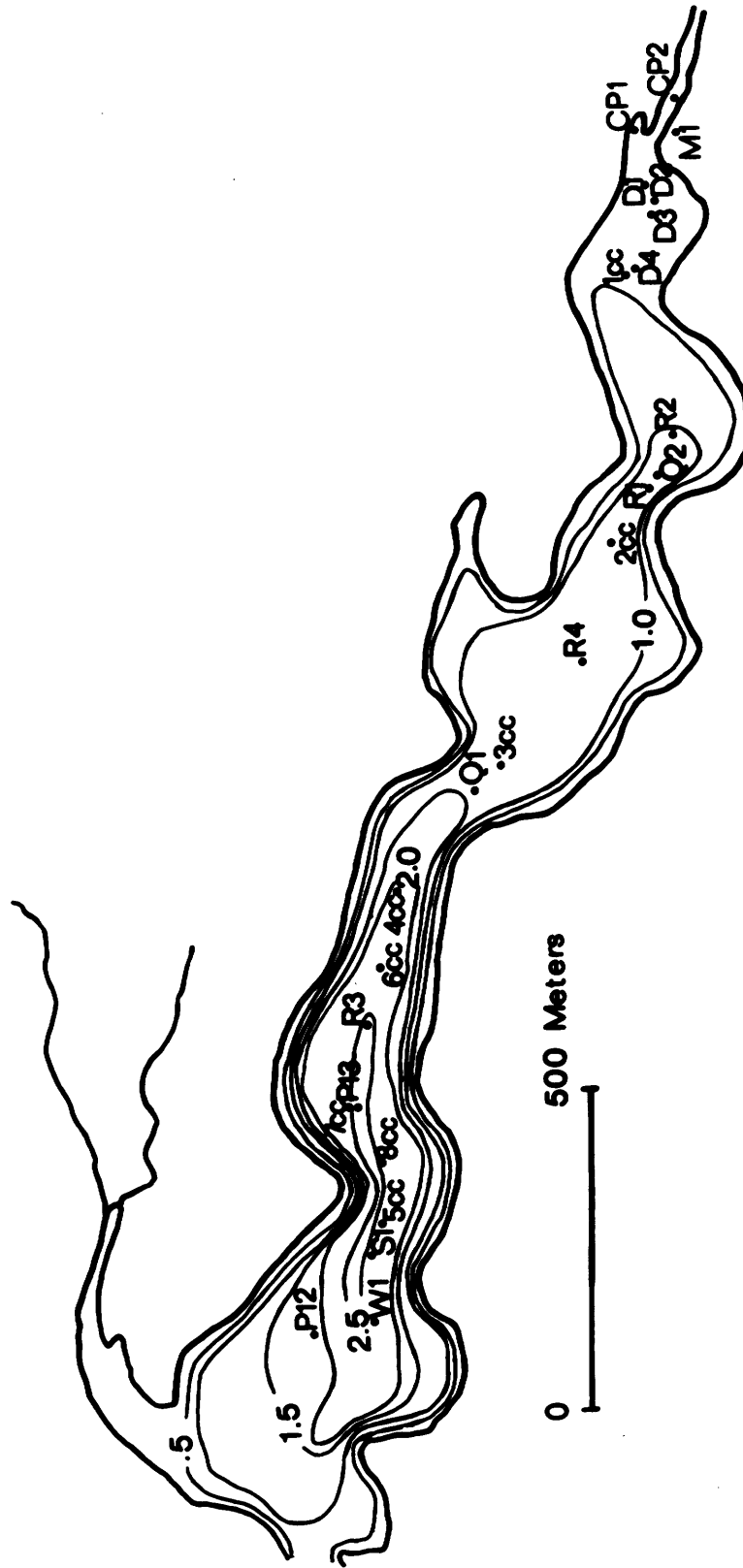


Figure 2—Bathymetry of the Sixteen Mile Creek lagoon (contour interval 0.5 m) as measured in late Fall, 1979. Core identities and locations are indicated by numbered dots.

Since 1938, the lagoon has been bounded at its northern (downstream) end by a weir situated beneath the Queen Elizabeth Highway (QEW), which maintains the lagoon at a level higher than Lake Ontario. Previously, the lagoon extended directly to the shoreline where it was separated from the lake by a sandy barrier spit. From the QEW, the lagoon stretches 2.6 km inland, to a point just upstream of the Canadian National Railway, and has an average width slightly less than 200 m giving a surface area of approximately 500 000 m². An additional 25 000 m² of flat, low lying marsh occurs at its headward end. Water depths in the lagoon average approximately 1.0 m but are 2.5 m or more just upstream of the weir (Figure 2). The lagoon is bordered by steep valley walls which rise up to 23 m above water level and have slopes commonly exceeding 30 degrees.

Prior to 1775, the entire Niagara Peninsula was heavily wooded. Settlement and clearing of the land for agriculture purposes advanced rapidly after this date, but was not complete until 50 or 60 years later (Wickland and Mathews 1963). Urban development in the valley of Sixteen Mile Creek is minor.

METHODOLOGY

An initial characterization of lagoon morphology was obtained using a Ratheon Explorer II recording fathometer. The bathymetric map shown in Figure 2 has been prepared from these records using an arbitrary high-water-level datum (late Fall). Surficial sediment samples were collected throughout the lagoon using an Echman grab sampler, and 13 shallow (1.5 m long) cores were obtained along the length of the lagoon. Sixteen deep cores, up to 6 m long, were collected along the axis of the lagoon (Figure 2) using a Livingston piston corer. Core spacing was generally 150-200 m but decreased to about 50 m in the "delta" region immediately downstream from the creek mouth. For comparative purposes, three short cores were obtained from the Fifteen Mile Creek lagoon, and one long and five short cores were collected from Jordan Harbour. All short cores were extruded and described in the field, and samples were retained at 10 cm intervals for grain size and chemical analyses. The long cores were wrapped in plastic and returned to the laboratory for more detailed examination.

Hydraulic and suspended sediment data were collected during the spring of 1980 from the lower reaches of the Sixteen Mile Creek, near the headward end of the marsh. Due to weather conditions, these data only cover low (0.27 m³/s) to intermediate (0.66 m³/s) discharge events. These data have not yet been analyzed and are not discussed here.

In the laboratory, five representative deep cores were X-rayed using a Faxitron X-ray unit to reveal structures not otherwise visible in extruded cores (see Figure 7). Eleven of the long cores were sampled at approximately 10 cm intervals, for grain size, organic content and mineralogic and chemical analyses. Two additional cores were sampled for moisture-content determinations,

and a pollen analysis is underway on one core (40 samples). Samples were also obtained at suitable locations for ¹⁴C age determinations and submitted to the ¹⁴C dating laboratory at Brock University.

Grain size analyses (104 samples) were performed using standard sieve and pipette techniques (Carver 1974; Folk 1974). Representative cumulative curves are shown in Figure 5. Graphical summary statistics and size frequency distributions were calculated for all samples. Major element (6 samples) and trace element (P,Ca,Zn,Cu,Ni)(150 samples) abundances of the sediments were determined using X-ray fluorescence. Organic material was first removed by heating the sample to 550°C, and the organic content determined by noting the weight loss.

GENERAL STRATIGRAPHY

Upon examination of the deep cores, the valley fill was subdivided into five stratigraphic units on the basis of grain size, organic and water content, and colour (Figures 3 and 4). From the base up these units are informally called 1) Pink Clay, 2) "Bottom" Sand, 3) Gittja, 4) Brown Clay, and 5) Gray Clay.

PINK CLAY

The lowest unit penetrated consists of a uniform, massive-looking clayey silt (all textural classifications follow Shepard 1954) which averages 15 percent sand, 54 percent silt, and 31 percent clay (Figure 5). Average mean grain sizes (Figure 6) range from 5.1 to 7.4 ϕ and do not show any consistent trend down the axis of the lagoon. In fresh cores, this unit has a greyish colour with a noticeable pink tinge. The organic content varies from 2 to 9 percent (see Figure 4), and the water content averages 26 percent. This unit is very compact and difficult to penetrate and was not reached in every core (see Figure 3). It appears to be present throughout the length of the lagoon however, but its thickness is unknown. It upper surface slopes markedly downstream; it was encountered at 158 cm in the delta region (core D1), and at 800 cm near the weir (core P12). The upper contact of the Pink Clay is generally abrupt and is marked either by a sharp increase in organic and water content and a noticeable colour change (Pink Clay to Gittja), or by an increase in sand and organic content (Pink Clay to "Bottom" Sand).

The depositional environment of the Pink Clay and its stratigraphic relationship to the other units are not clear at this time. Its very poorly sorted nature (see Figure 5), pink colour (Queenston shale admixture?) and massive appearance suggest that it may represent either till or (post-glacial) lacustrine sediment with a significant ice-rafted component. The appreciable organic content is incompatible with the first interpretation however, and the absence of lamination with the latter. Further coring to define its areal extent better, and the results of the pollen analysis, should help to resolve this problem.

GRANT 78 SEDIMENTATION IN SMALL LAGOON COMPLEXES

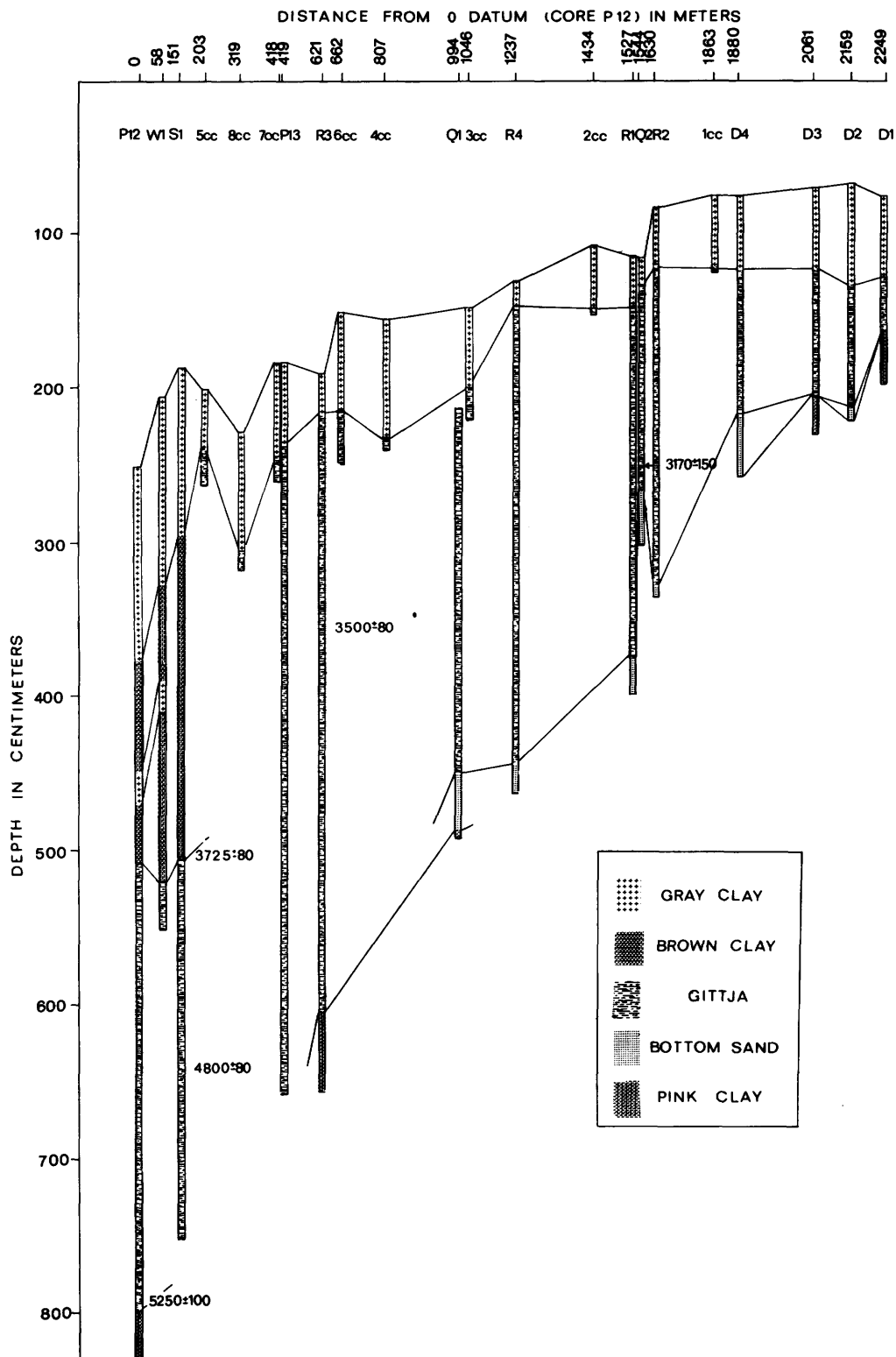


Figure 3—Generalized stratigraphy of the Sixteen Mile Creek lagoon and stratigraphic position of all ¹⁴C dates. The zero vertical datum is the water surface; the tops of the cores are located at the sediment-water interface. Horizontal distances are listed in metres upstream from core P12.

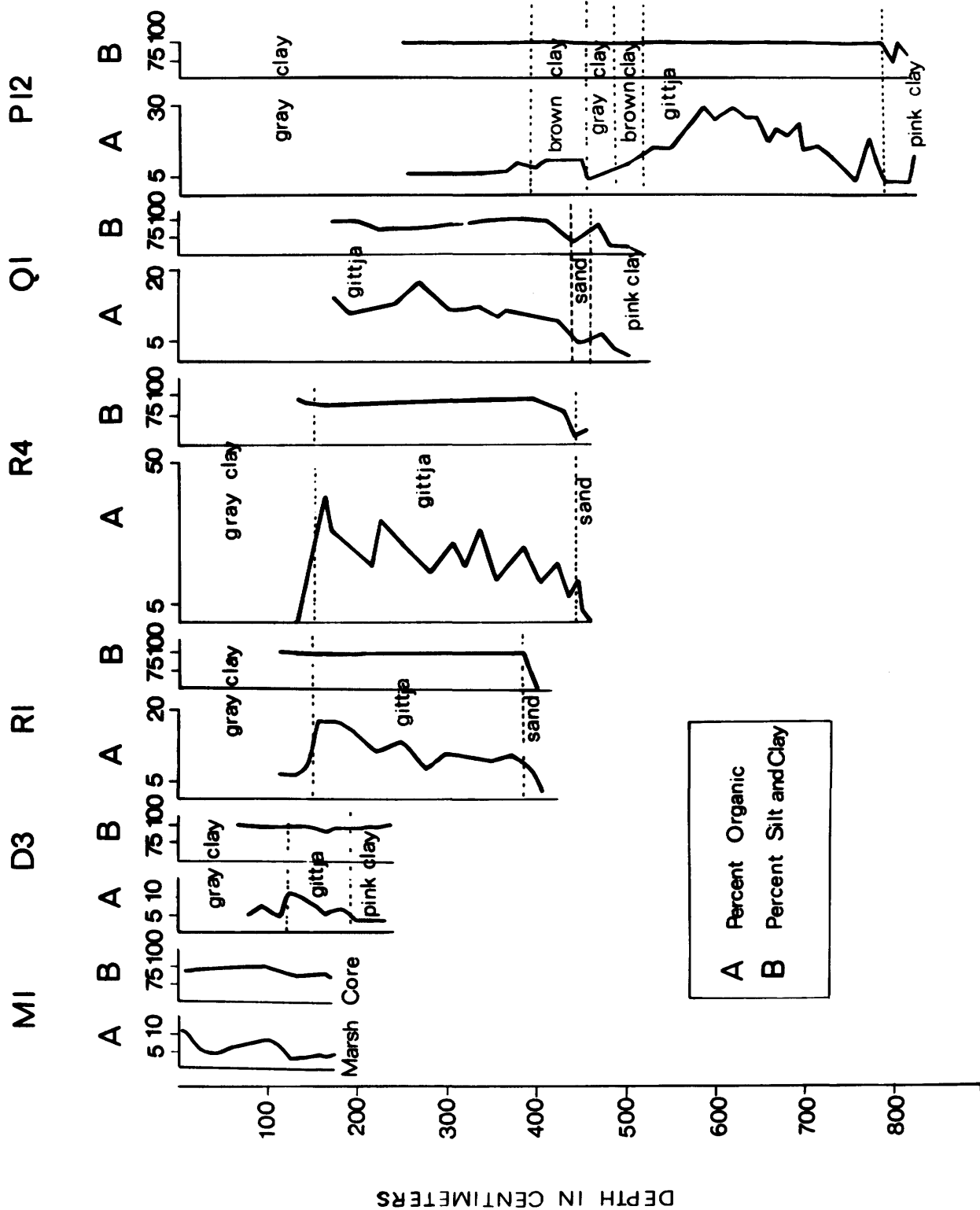


Figure 4— Vertical variation in (A) organic content, and (B) silt and clay content in six representative cores. For locations refer to Figure 2. The zero datum for depth, as in Figure 3, is the water surface. The uppermost sample in each core was obtained from within 5 cm of the sediment surface.

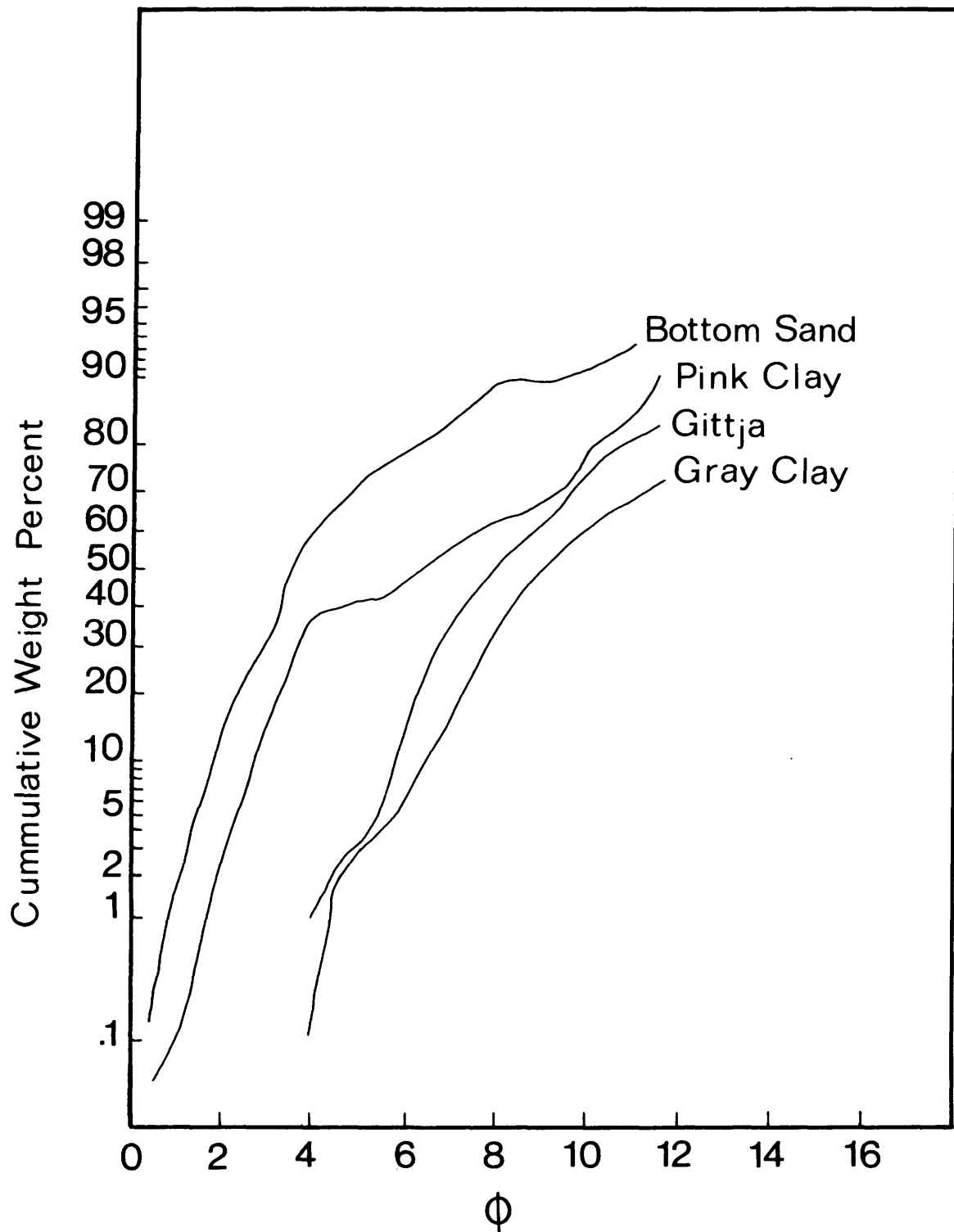


Figure 5— Representative cumulative curves illustrating the grain-size distributions in the Pink Clay, "Bottom" Sand, Gittja and Gray Clay. Sand 0-4 φ; silt 4-8 φ; clay >8 φ.

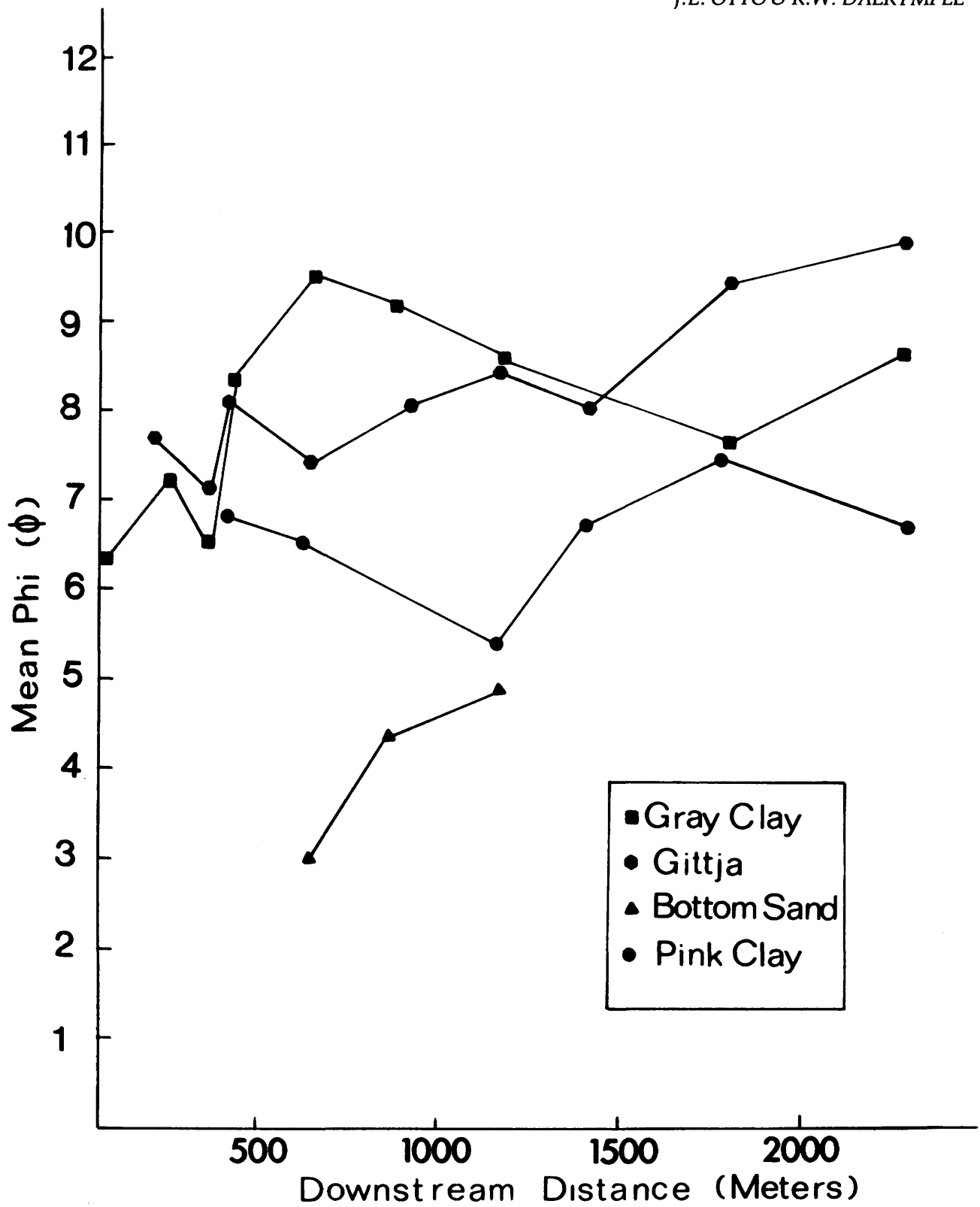


Figure 6— Plot of average mean grain size (the average of all mean sizes obtained in each core) against distance downstream from the head of the lagoon for the Pink Clay, "Bottom" Sand, Gittja and Gray Clay.

"BOTTOM" SAND

A unit of sand-silt-clay averaging 38 percent sand, 30 percent silt, and 32 percent clay (see Figure 5), overlies the Pink Clay throughout much of the lagoon; it is absent consistently only at the downstream end. Average mean grain sizes in this unit fall between 3.0 and 4.9 ϕ (See Figure 6), and suggest that a downstream-fining trend exists. The contact between the sand and the overlying Gittja is gradational: some sand occurs in the lower gittja, and some organic material, including fragments of wood, occurs in the sand (see Figure 4). This contact occurs at a depth of 200 cm in the delta region and descends to 450 cm in core Q1. The maximum thickness of sand recovered is 40 cm in core D4 (see Figure 3). Sedimentary structures have not been observed.

The sandy nature of this unit, combined with the possible downstream fining, strongly suggests that it was deposited in a stream channel and/or lagoonal-deltaic environment. The coarser grain size of the sand relative to sediments in the present delta region (see below) indicates that stream discharges at the time of deposition were higher than today. This is what would be expected if deposition predated the capture of the upper reaches of the Sixteen Mile Creek.

GITTJA

This unit comprises the largest proportion of the valley fill cored. Its thickness increases from 45 cm at the head to a maximum in excess of 400 cm in core P13 (see Figure 3), and then decreases further downstream to 286 cm in the core P12. The inorganic component of the Gittja consists of a silty clay averaging 2 percent sand, 45 percent silt and 53 percent clay (see Figure 5), but average mean grain sizes decrease downstream from 7.2 to 9.6 ϕ (see Figure 6). Water content is generally high and averages 47 percent, whereas the percentage of organic material varies markedly between clay-rich and organic-rich layers (Figures 4 and 7) with a range from 5 percent to 35 percent. A progressive upward increase in organic content is evident in all cores however, despite the variability (see Figure 4). Bioturbation is usually absent in the lower parts of the unit, but is present in minor amounts towards the top (Figures 7c and 7d). The contact of the Gittja with the overlying Gray Clay is abrupt, and is marked by a distinct colour change associated with a sudden decrease in organic content (see Figure 4, cores D3, R1, and R4). The vertical transition into the Brown Clay in the lower reaches of the lagoon is more gradual (see Figure 4, core P12). The upper surface of the Gittja slopes gently toward Lake Ontario from a depth of 125 cm in the delta region to 240 cm in core P13. From this point it descends rapidly to approximately 500 cm in cores P12 and S1 (see Figure 3).

The character of this unit indicates that it was deposited in a marshy to very shallow lagoonal environment with periodic input of silt and clay, possibly during floods. Gittja is presently forming in an environment such as this in the very shallow peripheral regions of the Fifteen Mile

Creek Lagoon (see Figure 1). The radiocarbon dates obtained show that the Gittja is transgressive. Deposition commenced at the downstream end of the lagoon (core P12) 5250 \pm 100 years B.P. and progressed steadily headward as lake levels rose, reaching the location of core Q2 sometime shortly before 3170 \pm 150 years B.P. (see Figure 3). The date at which Gittja deposition started corresponds closely with the age of the "Dune" lake stage as defined by Sutton *et al.* (1972), but the extent to which this stillstand influenced sedimentation is not clear. Organic matter deposition in the downstream area (core S1) had ceased by 3725 \pm 80 years B.P.; however, the age of the upper contact of the Gittja elsewhere in the lagoon remains to be determined.

BROWN CLAY

A brown silty clay averaging 40 percent silt and 60 percent clay occurs above the Gittja in the distal portion of the lagoon. Its mean grain size averages approximately 9.2 ϕ , and it has average organic and moisture contents of about 9 percent and 54 percent respectively. This clay is weakly laminated, and exhibits little bioturbation. In cores P12 and W1 a 20 cm thick bed of gray clay occurs in the middle of the Brown Clay. The contacts are abrupt and show a marked colour change and a decrease in organic content from brown to gray clay (see Figure 4). The upper surface of the Brown Clay is encountered at a depth of 300 cm in core S1, and descends regularly to 375 cm in core P12. The maximum thickness of Brown Clay is 215 cm.

A ^{14}C date obtained at the base of the Brown Clay in core S1 indicates that clay deposition commenced 3725 \pm 80 years B.P. (see Figure 3). After this, deposition of the Brown Clay and Gittja continued simultaneously, with Brown Clay restricted to the deeper portion of the lagoon. A similar facies relationship exists today in the Fifteen Mile Creek Lagoon. During deposition of the two units, the facies boundary between them remained remarkably stationary between cores S1 and P13, indicating that sedimentation kept pace with rising lake levels.

GRAY CLAY

The uppermost unit in all cores is a highly bioturbated (see Figure 7), gray silt clay (average composition 3 percent sand, 43 percent silt and 54 percent clay) in which compaction increases rapidly with depth. The variation of average mean grain size with distance down the lagoon shows an inverted "V"-shaped pattern (see Figure 6), decreasing rapidly downstream at first from 6.3 ϕ in the stream channel to 9.5 ϕ in core R2, and then slowly increasing to 7.0 ϕ in core R3. By core P12 the clay is again slightly finer (8.6 ϕ). Organic and water contents in this unit average 6 percent and 39 percent respectively.

The distribution of the Gray Clay and its low organic content suggests deposition in a lagoon with greater water depths than those which prevailed during formation of the Gittja and Brown Clay; in fact the pronounced coar-

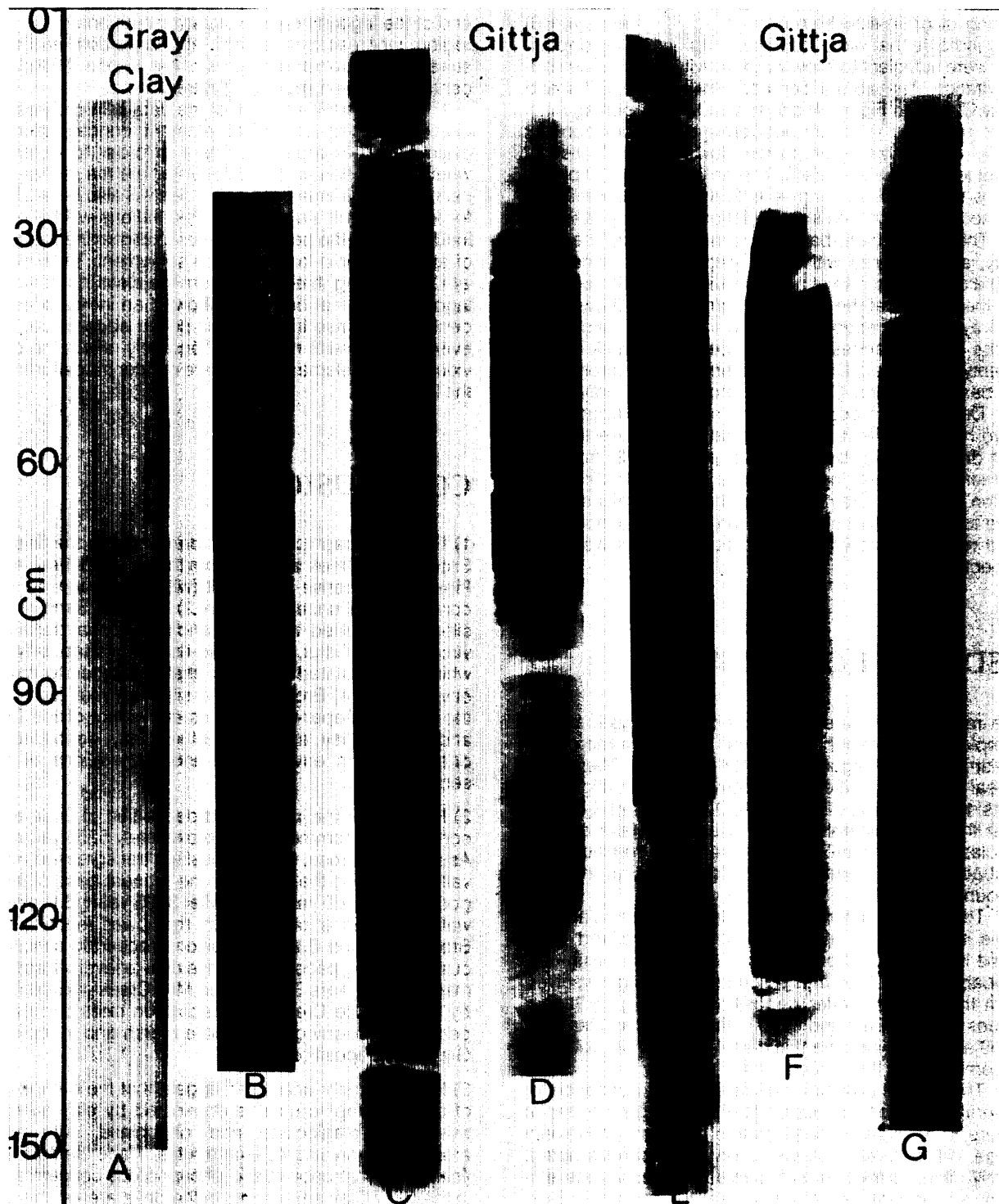


Figure 7— Representative X-radiographs for Gray Clay (A and B) and Gittja (C-G) from core P12. The blotchy appearance in A, B, and parts of C and D are indicative of bioturbation. The well defined lamination in the Gittja is produced by alternating clay-rich (dark) and organic-rich (light) layers. The extremely light-coloured bands are composed of leaves.

sening of grain size from core R2 to R3 (see Figure 6) may indicate that water depths during Gray Clay deposition were sufficient to allow wave activity to influence sedimentation. The abrupt contact between the Gittja and Gray Clay (see Figure 4) shows that the deepening must have occurred relatively suddenly, a phenomenon not easily attributable solely to the slow, steady (?) rise of water levels in Lake Ontario. The only alternative explanation is that the deepening reflects a sudden decrease in the sedimentation rate in association with rising lake levels. The intense bioturbation present throughout the Gray Clay, as compared with underlying units, is consistent with a decreased rate of accumulation, and it is suggested, therefore, that the transition from Gittja or Brown Clay to Gray Clay corresponds closely in time with the capture of the upper reaches of the Sixteen Mile Creek by the Twenty Mile Creek. Dating to confirm the synchronism of the base of the Gray Clay will be undertaken shortly.

Deforestation accompanying settlement appears to have had little effect on sedimentation because the limited data obtained by Terasmae *et al.* (1972) from the Sixteen Mile Creek lagoon places the rise in *Ambrosia* pollen within the Gray Clay, and there is no evidence to date to suggest that sedimentation rates have increased as a result of deforestation and cultivation as would be expected.

SEDIMENT CHEMISTRY

The results of major-element chemical analyses on six samples, three from the head and three from the downstream end of the lagoon, are listed in Table 1. The values reveal no striking differences between the stratigraphic units; the high values for SiO_2 , Al_2O_3 , Na_2O and K_2O suggest that clay minerals, quartz, Na-plagioclase and orthoclase predominate in all samples. Iron sulphides are probably also abundant, and rutile may occur in minor amounts.

The low values for CaO and MgO are particularly notable in light of the abundance of limestone and dolostone in the tills and bedrock of the drainage basin. It is probable that calcite and dolomite are being dissolved from the sediment after deposition. The slightly higher values for both CaO and MgO in the Gray Clay (samples W1/9 and D3/1) indicate that dissolution has not yet gone to completion in this surficial unit.

The vertical variation in trace element abundance for several cores from various parts of the lagoon is shown in Figure 8. Analysis of these data is in a very preliminary stage, but several tentative observations can be noted. Firstly, little correlation is observed between trace element abundance and the stratigraphy below the Gray Clay. Concentrations of zinc, and to a lesser extent copper and phosphorous, do tend to increase in the upper portion of the Gray Clay (see particularly cores D1 and W1), while nickel generally shows no systematic pattern. Secondly, within the Gray Clay, the highest concentrations of phosphorous and copper occur at the headward

end of the lagoon near the stream mouth and in the delta region, whereas zinc is most abundant both at the upstream and downstream ends of the lagoon. Nickel concentrations again show no apparent trend.

More detailed analysis of the data is in progress, including attempts to relate element concentrations to grain size and organic content in order to determine which component(s) of the sediment are the primary carriers for each element. The samples will also be analysed for lead, and all elemental concentrations will be examined in light of the pollen analyses to determine the extent of anthropogenic loading since settlement. Terasmae *et al.* (1972) using three cores from the distal portion of the lagoon found that only lead showed an increase coincident with the rise in *Ambrosia* pollen abundance; however, these results may not adequately reflect the behaviour of those elements which are concentrated further up the lagoon.

CONCLUSIONS

1) Five stratigraphic units are identifiable in the fill of the Sixteen Mile Creek lagoon. From the base up these are 1) Pink Clay, a dense clayey silt (with a pronounced sand component) of uncertain origin; 2) "Bottom" Sand, a sand silt-clay deposited in a fluvial and/or lagoonal-deltaic environment; 3) Gittja, an organic-rich, laminated, silty clay which accumulated in a very shallow lagoon to marshy environment; 4) Brown Clay, a silty clay that represents the slightly deeper-water facies equivalent of the Gittja; and 5) Gray Clay, a bioturbated silty clay, deposited in a deeper lagoon environment under conditions of slow sedimentation.

2) Flooding of the lagoon and deposition of Gittja at the northern end commenced approximately 5250 years B.P. As lake levels rose, Gittja deposition transgressed up the valley, reaching the vicinity of the present head of the lagoon about 3000 years B.P. After 3725 years B.P. deeper water conditions prevailed in the lower reaches, and Brown Clay and Gittja deposition proceeded simultaneously, keeping pace with the rise of lake level. At approximately 1500 years B.P. Sixteen Mile Creek was captured by Twenty Mile Creek and deposition rates decreased, permitting drowning of the Gittja marsh and inception of Gray Clay deposition.

3) Major element analyses suggest that the composition of all stratigraphic units is dominated by clay minerals, quartz, Na-plagioclase and orthoclase, with lesser amounts of iron sulphides and rutile. Trace element analyses show that copper and phosphorous concentrations in the Gray Clay are highest in the delta area at the head of the lagoon and that zinc is most abundant at both upstream and downstream ends of the lagoon. Zinc, copper and phosphorous show varying degrees of concentration in the upper sediment layer, presumably as a result of human input (pollution). More detailed examination of the geochemical data is in progress.

Table 1—Summary of major element analyses for six samples from the Sixteen Mile Creek Lagoon.

	D3/1	D3/10	D3/15	W1/9	W1/25	P12/7s3
SiO ₂	69.20	71.20	71.50	62.58	66.72	69.28
Al ₂ O ₃	13.59	13.89	13.18	17.13	15.08	13.47
MgO	1.53	0.98	0.95	1.92	1.04	1.23
Fe ₂ O ₃	5.52	4.74	4.96	7.32	6.03	5.15
CaO	1.65	0.96	0.93	2.23	1.01	1.27
Na ₂ O	3.09	3.34	3.28	1.46	2.83	3.33
K ₂ O	2.78	2.73	2.69	3.55	3.26	2.82
TiO ₂	0.93	0.91	0.89	1.02	1.01	0.87
MnO	0.07	0.07	0.00	0.04	0.07	0.07
P ₂ O ₅	0.36	0.33	0.30	0.36	0.38	0.32
	98.72	99.15	98.68	97.61	97.43	97.81

* total iron expressed as Fe₂O₃

The first part of all sample numbers gives the core number: D3 comes from the head of the lagoon, and W1 and P12 from the downstream end. The stratigraphic units from which each sample was taken are as follows: D3/1 - Gray Clay; D3/10 - Gitty; D3/15 - Pink Clay; W1/9 - Gray Clay; W1/25 - Brown Clay; P12/7s3 - Gitty.

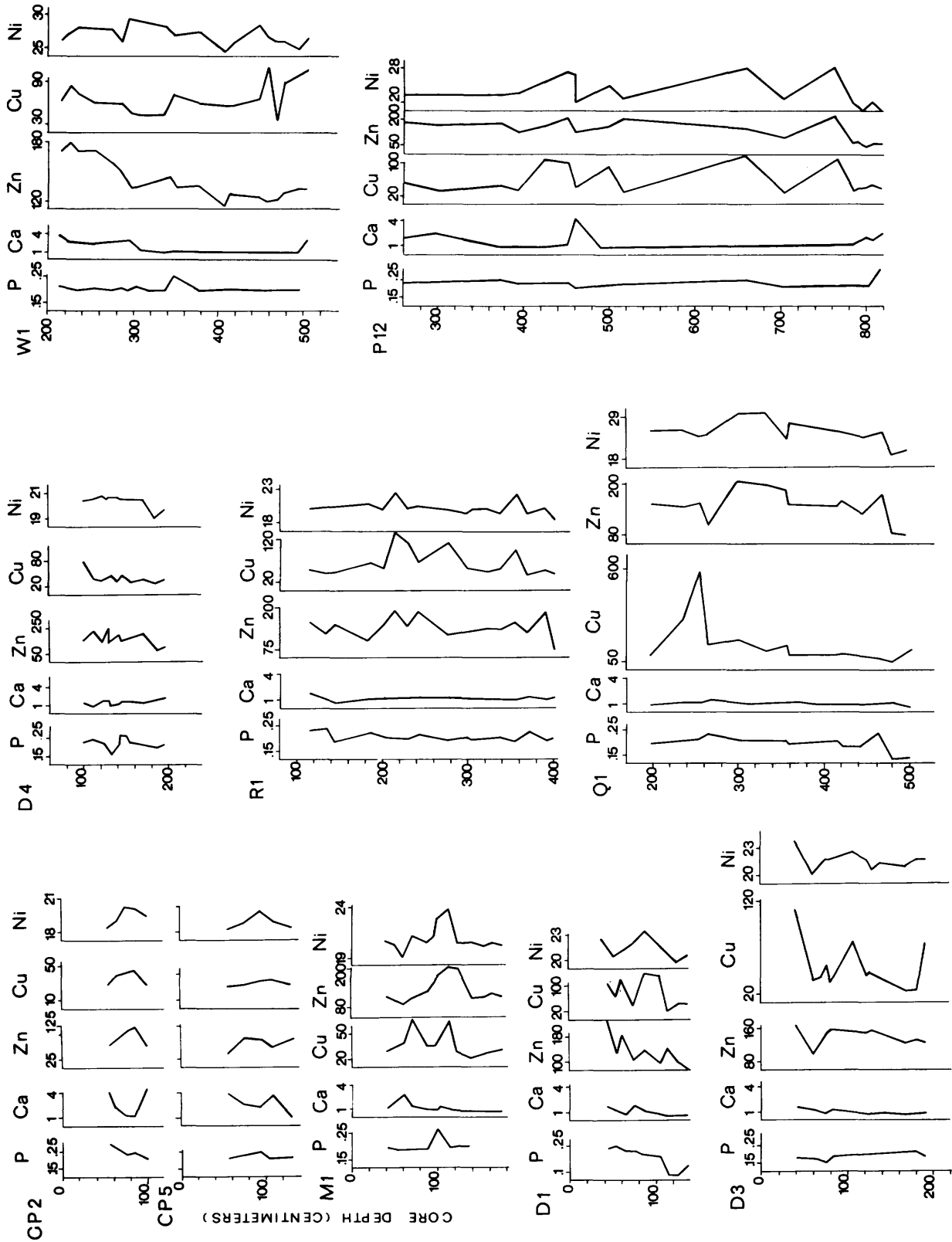


Figure 8— Vertical variation of trace-element abundances in 10 cores from the Sixteen Mile Creek lagoon. For core locations see Figure 2. All depths are measured from the water surface with the first sample collected within the top 5 cm of the sediment. Concentrations of phosphorous and calcium are expressed as weight percentages. Zinc, copper and nickel abundances are given in parts per million.

ACKNOWLEDGMENTS

The authors gratefully acknowledge J.J. Flint, Brock University, for his critical review and suggestions, J. Terasmae, Brock University, for the use of field equipment, Howard Melville of the Brock University ¹⁴C dating laboratory for providing the dates, and P.J. Barnett, Ontario Geological Survey, for his support of this project.

REFERENCES

Carver, R.E.
1974: Procedures in Sedimentary Petrology; Wiley-Interscience, Toronto, 653p.
Folk, R.L.
1974: Petrology of Sedimentary Rocks; Hemphill Publishing Company, Austin, 170p.

Karrow, P.F., Clark, J.R., and Terasmae, J.
1961: The Age of Lake Iroquois and Lake Ontario; Journal of Geology, vol.69, p.659-667.
Shepard, F.P.
1954: Nomenclature Based on Sand-Silt-Clay Ratios; Journal of Sedimentary Petrology, vol.24, p.151-158.
Sutton, R.G., Lewis, T.L., and Woodrow, D.L.
1972: Post-Iroquois Lake Stages and Shoreline Sedimentation in Eastern Ontario Basin; Journal of Geology, vol.80, p.346-356.
Terasmae, J., Fortescue, J.A.C., Flint, J.J., Gawron, E.F., Winn, R.F. and Winn, C.E.
1972: Palynology and Chemistry of Lake Sediment Cores from Southern Ontario, Related to Man's Activities on the Environment; Brock University Department of Geological Sciences, Research Report Series No. 10.
Wickland, R.E., and Mathews, B.C.
1963: The Soil Survey of Lincoln County; Report No.34 of the Ontario Soil Survey, Canada Dept. of Agriculture and the Ontario Agricultural College, 48 p.

Grant 19 Palynostratigraphic Working Standard for Intra-Basinal Correlation of Albian Lignitic Strata, Moose River Basin, Ontario

Mary Lynn Richardson and Geoffrey Norris

Department of Geology, University of Toronto

ABSTRACT

Detailed palynologic analysis of 60 Cretaceous samples from one drillhole (OGS78-01) in the Adam Creek area has provided a working standard for future palynostratigraphic correlations in the southern portion of the Moose River Basin. The present work follows preliminary analyses by Norris and Dobell, which provided tentative correlations of lignitic strata in eight drillholes and one outcrop in this area. Three palynofloral assemblage zones (Zones I - III), erected by Norris for the central and eastern portions of the Moose River Basin, were used as the basis for these correlations.

The present study confirms that three palynofloral zones can be recognized in drillhole OGS78-01, but demonstrates that a number of species thought to be diagnostic of Zones I, II, or III are not restricted to these zones, and provides a revision of the boundary between the two oldest zones in this drillhole. In view of the discrepancies found in using previous zonation, an alternative nomenclature is used to identify zones within the working standard established here.

Three Opper zones, Zones A - C are recognized; Zone B is tentatively divided into two subzones. Lignite in drillhole OGS78-01 is restricted to Zone A and Subzone B1. Zone A lignite is represented by six 2-4 foot beds of woody lignite contained within a thick sequence of black, carbonaceous clay. Lignite beds in Subzone B1 attain a maximum thickness of 3 feet and are interbedded with dominantly non-carbonaceous strata in which several fining upwards sequences can be recognized.

INTRODUCTION

Drilling programmes by the Ontario Division of Mines (now the Ontario Geological Survey) have improved understanding of the lignitic Cretaceous strata in the Moose River Basin. Palynostratigraphic studies were initiated on the Mesozoic basin fill as penetrated by several drillholes (Figure 1) and a preliminary zonation was established by Norris (1979; in press) for the northern and northeastern part of the basin and extended to the southern margin of the basin by Norris and Dobell (1980).

The present study focuses on a single drillhole near the southern margin of the basin (Telford and Verma 1978) which was included by Norris and Dobell (1980) in their preliminary study to establish a three-fold zonation of Albian strata. The purpose of this study is to report on precise palynostratigraphic relationships, to improve resolution of the zones, and thereby to provide a palynostratigraphic working standard for the Mattagami Formation of the Moose River Basin.

The subject drillhole (OGS78-01) is located in Kipling Township on the west side of Adam Creek (see Figure 1) about 1 km north of the basin margin (Latitude 50°10' 45''N, Longitude 82° 05' 45''W). It penetrated the Mattagami Formation between 158 feet and 522 feet and intersected several lignite seams as indicated in Figure 2 with an aggregate thickness of approximately 15 feet. The cored section of Mattagami Formation was sampled for palynologic study and 66 horizons were studied in detail. Most samples were palyniferous as indicated in Figure 2.

Miospores were identified by reference to preliminary work by Norris (in press) and to other pertinent literature listed therein. Species were determined in one of three categories: abundant (more than 25 percent relative abundance); common (5-25 percent relative abundance); and present (less than 5 percent relative abundance).

RESULTS, ZONATION AND DISCUSSION OF ZONES

Species distributions and abundances are indicated in Figure 2. Three Opper zones are recognized as follows with boundaries drawn on prominent range tops:

- Zone C 158-170 feet
- Zone B 174-344 feet
 - Subzone B2 174-202 feet
 - Subzone B1 205-344 feet
- Zone A 345-522 feet

These zones span Middle and Late Albian as discussed by Norris (in press) and Norris and Dobell (1980).

Miospore assemblages in each zone are tabulated below and long-ranging species are separated from spe-

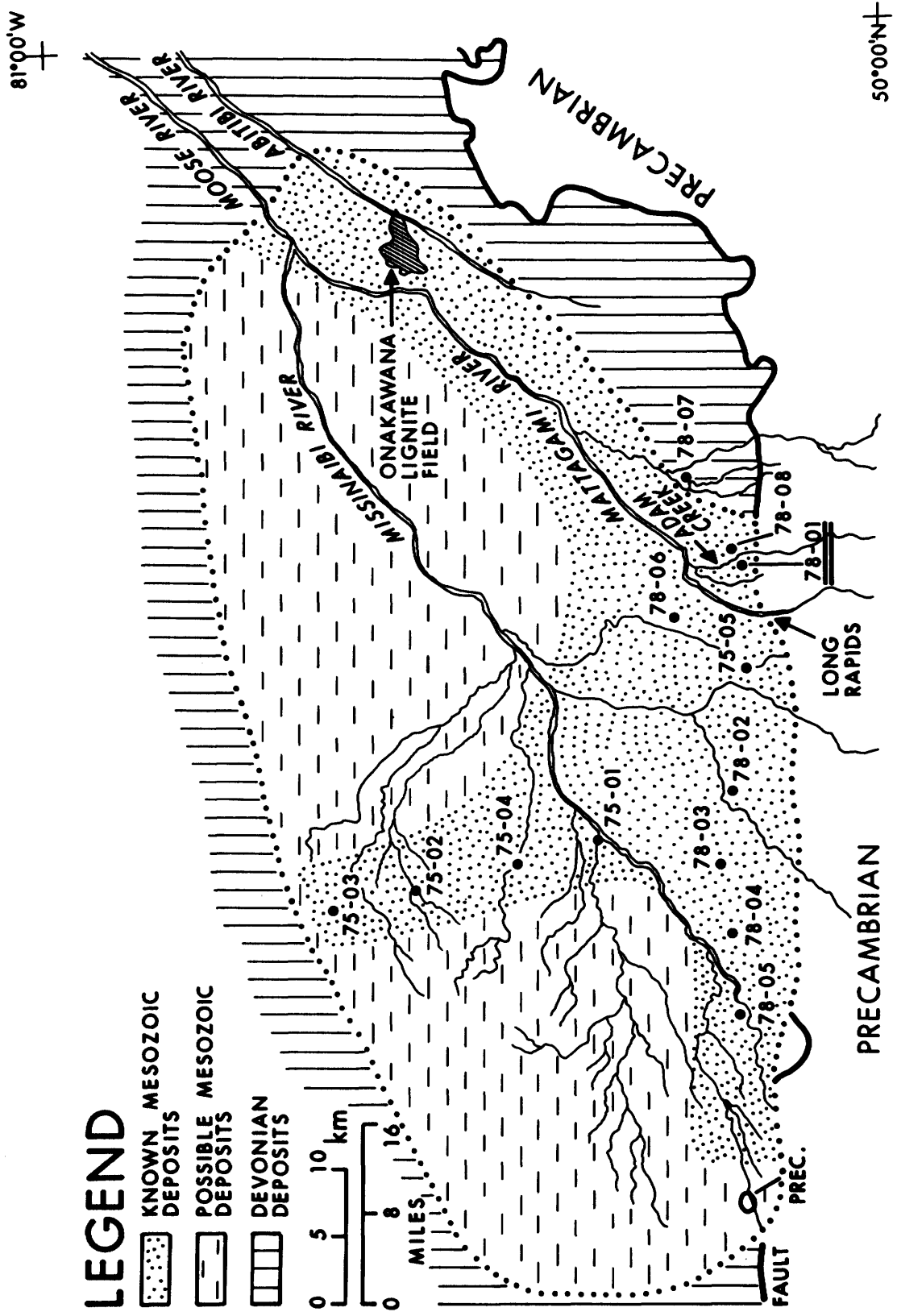


Figure 1—Map of Moose River Basin showing location of drillholes; drillhole OGS78-01 is the basis for the present report.

cies with range tops in the zone and those restricted to the zone (or sub-zone).

ZONE A (522-345 feet)

LONG-RANGING SPECIES

Alisporites bilateralis Rouse
Baculatisporites sp. 483 (Norris, in press)
Cicatricosisporites hallei Delcourt and Sprumont
Cicatricosisporites sp. cf. *C. potomacensis* Brenner
Cerebropollenites mesozoicus (Couper) Nilsson
Cyathidites minor Couper
Gleicheniidites senonicus Ross
Gleicheniidites sp. 496 (Norris, in press)
Inaperturopollenites dubius (Potonié and Kremp)
 Thomson and Pflug
Microreticulatisporites uniformis Singh
Osmundacidites wellmanii Couper
Perinopollenites elatoides Couper
Polycingulatisporites reductus (Bolkhovitina)
 Playford and Dettmann
Stereisporites antiquasporites (Wilson and Webster)
 Dettmann
Taurocusporites segmentatus Stover
Vitreisporites pallidus (Reisinger) Nilsson
Vitreisporites sp. (of Singh 1971)
Verrucosisporites sp. cf. *V. rotundus* Singh

SPECIES FOUND ONLY IN ZONE A

Cicatricosisporites sp. cf. *C. potomacensis* Brenner
Cicatricosisporites sp. cf. *C. ludbrookii* Dettmann
 (of Norris 1979)
Cicatricosisporites auritus Singh
Cingulatisporites sp.
Classopollis sp. cf. *C. classoides* Pflug
Coronatispora sp.
Cycadopites sp. cf. *C. scabratus* Stanley
Impardecispora marylandensis (Brenner) Srivastava
Impardecispora purverulenta (Verbitskaya)
 Venkatachala et al.
Klukisporites areolatus Singh
Lycopodiumsporites crassimacerius Hedlund
Phyllocladites ellipticus Cookson
Polycingulatisporites radiatus Singh
Polycingulatisporites reductus (Bolkhovitina)
 Playford and Dettmann
Pristinusporites sp. 428 (Norris, in press)
Pteruchipollenites sp. 474 (Norris, in press)
Reticulatasporites sp. 499 (Norris, in press)
Rugubivesiculites rugosus Pierce
Trilobosporites humilis Delcourt and Sprumont
Undulatisporites undulapolus Brenner
Lycospora sp.

DISCUSSION. Zone A in drillhole OGS78-01 is associated with a thick sequence of carbonaceous clays containing several 2-4 foot lignite beds and underlain by orange to red, stratified clayey silts which are virtually barren of palynomorphs. Below these red beds, the oldest sample prepared for palynologic study is a carbonaceous

clay which contains many spore and pollen species found to be common throughout the Cretaceous strata of the drillhole section.

The oldest lignite bed sampled for palynomorphs (390-392 feet) contains a fairly rich palynoflora including two species, *Trilobosporites humilis* (diagnostic of Zone II of Norris 1979) and *Undulatisporites undulapolus*, found only in Zone A during this study.

The sample retrieved from immediately below this lignite bed (398-402 feet) yielded the widest diversity of palynomorphs in the drillhole section, including the only specimens seen during this study of *Impardecispora marylandensis* and *I. purverulenta* which have been thought to be restricted to, and diagnostic of, Zone III of Norris (1979). Associated with this flora are relatively common specimens of *Taurocusporites segmentatus* and two species of the genus *Polycingulatisporites*.

Reticulatasporites sp. 499, one of the diagnostic species of Zone I of Norris (1979) was found in most samples included in Zone A here. It was not found higher in the section than 345 feet, and appears to also provide one of the most diagnostic species of Zone A as identified in the present study (cf. Norris and Dobell 1980).

In addition to the species listed above, Zone A contains a number of diverse, long-ranging, bisaccate pollen species which were not found to be particularly common in any of the samples included in this zone, but which are better represented in samples higher in the section.

The most abundant species seen in slides from Zone A samples was *Gleicheniidites senonicus*, which was found to be consistently less common than *Inaperturopollenites dubius* in Zones B and C.

ZONE B (344 feet - 174 feet 2 inches)

SUBZONE B1 (344-205 feet)

LONG-RANGING SPECIES

Alisporites bilateralis Rouse
Alisporites grandis (Cookson) Dettmann
Appendicisporites bilateralis Singh
Appendicisporites potomacensis Brenner
Cerebropollenites mesozoicus (Couper) Nilsson
Cyathidites australis Couper
Deltoidospora diaphana Wilson and Webster
Deltoidospora hallii Miner
Gleicheniidites senonicus Ross
Gleicheniidites sp. 496 (Norris, in press)
Inaperturopollenites dubius (Potonié and Kremp)
 Thomson and Pflug
Microreticulatisporites uniformis Singh
Osmundacidites wellmanii Couper
Vitreisporites pallidus (Reisinger) Nilsson

SPECIES WITH RANGE TOPS IN SUBZONE B1 (# denotes restriction to this subzone)

Appendicisporites unicus (Markova) Singh
 # *Araucariacites* sp.
 # *Baculatisporites* sp. 477 (Norris, in press)
 # *Cicatricosisporites imbricatus* (Markova) Singh

Cicatricosisporites sp. cf. *Anemia exiloides*
(Maljavkina) Bolkhovitina (of Norris 1979)
Cicatricosisporites sp. cf. *C. dorogensis* (Potonié
and Gelletich)
Cicatricosisporites sp. cf. *C. ludbrookii* Dettmann
(of Norris 1979)
Converrucosisporites sp. cf. *P. platyverrucosus*
Brenner
Cyathidites australis Couper
Gleicheniidites apilobatus Brenner
Inaperturopollenites sp. 438 (Norris, in press)
Lycopodiumsporites austroclavatifidites (Cookson)
Potonié
Microreticulatisporites uniformis Singh
Ornamentifera baculata Singh
Podocarpidites herbstii Burger
Pristinuspollenites sp. 450 (Norris, in press)
Rouseias sp. 446 (Norris, in press)
Todisporites major Couper

SUBZONE B2 (202 feet 6 inches - 174 feet 2 inches)**LONG-RANGING SPECIES**

Alisporites bilateralis Rouse
Alisporites grandis (Cookson) Dettmann
Appendicisporites bilateralis Singh
Appendicisporites potomacensis Brenner
Cedripites canadensis Pocock
Cerebropollenites mesozoicus Couper
Eucommiidites minor Groot and Penny
Gleicheniidites senonicus Ross
Inaperturopollenites dubius (Potonié and Kremp)
Thomson and Pflug
Osmundacidites wellmanii Couper
Parvisaccites radiatus Couper
Perinopollenites elatoides Couper
Podocarpidites granulatus Singh
Podocarpidites naumovai (Naumova) Singh
Podocarpidites radiatus Brenner
Taxodiaceapollenites hiatus (Potonié) Kremp

SPECIES WITH RANGE TOPS IN SUBZONE B2 (# denotes restriction to this subzone)

Abiespollenites sp.
Appendicisporites bifurcatus Singh
Appendicisporites bilateralis Singh
Appendicisporites erdtmanii Pocock
Appendicisporites potomacensis Brenner
Appendicisporites problematicus (Burger)
Brenner
Appendicisporites spinosus Pocock
Callialasporites dampieri (Balme) Dev
Cicatricosisporites australiensis (Cookson) Potonié
Cicatricosisporites hallei Delcourt and Sprumont
Cicatricosisporites hughesi Dettmann
Cicatricosisporites venustus Deak
Cicatricosisporites sp. 441 (Norris, in press)
Concavissimisporites punctatus (Delcourt
and Sprumont) Brenner
Concavissimisporites variverrucatus (Couper)
Brenner
Cupuliferoidaepollenites sp. 447 (Norris, in press)

Deltoidospora diaphana Wilson and Webster
Distaltriangulisporites irregularis Singh
Distaltriangulisporites irregularis (Singh) Singh
Eucommiidites minor Groot and Penny
Foraminisporites sp. 487 (Norris, in press)
Gleicheniidites sp. 496 (Norris, in press)
Laevigatosporites ovatus Wilson and Webster
Lycopodiumsporites reticulumsporites (Rouse)
Dettmann
Marattisporites sp. 455 (Norris, in press)
Matonisporites crassiangulatus (Balme) Dettmann
Perotriletes sp. 476 (Norris, in press)
Phyllocladites inchoatus (Pierce) Norris
Pityosporites alatisporites (Rouse) Singh
Podocarpidites canadensis Pocock
Podocarpidites minisculus Singh
Podocarpidites naumovai (Naumova) Singh
Pteruchipollenites sp. 492 (Norris, in press)
Stereisporites antiquasporites (Wilson and Webster)
Dettmann
Vitreisporites pallidus (Reisinger) Nilsson
Verrucosisporites sp. cf. *V. rotundus* Singh
Undulatisporites sp.

DISCUSSION OF ZONE B. Zone B in drillhole OGS78-01 coincides with a thick interval of successively fining-upwards strata which culminate in thin lignite beds. Scattered samples throughout this interval contain very few, if any, palynomorphs, but no direct correlation between these barren samples and the dominant sample lithology is readily apparent. Most of the lignite found in drillhole OGS78-01 is contained within Subzone B1, which occupies 139 feet of the section described for this hole. No distinct horizon of range tops is found in this interval until the Subzone B2 boundary (205 feet). Higher than 205 feet, a steady succession of range tops is found in closely-spaced samples containing very abundant palynomorphs.

Most of the specimens identified in Subzone B1 first appeared in Zone A. *Microreticulatisporites uniformis*, *Osmundacidites wellmanii*, and *Cyathidites australis*, which have been considered to define Zone I of Norris (1979), are all found in Zone B, and *O. wellmanii* appears in the youngest Cretaceous sample which is here considered to represent Zone C. *Todisporites major*, considered to be restricted to Zone III of Norris (1979), was found in two samples near the base of the Zone B interval, and was not among the abundant specimens of the youngest samples. The only angiospermous pollen identified in this study, *Cupuliferoidaepollenites* sp. 447, first appeared at the top of Subzone B1.

Subzones B1 and B2 share a large number of diverse species of which six species are listed as common for both subzones. *Inaperturopollenites dubius* was found to be the dominant species throughout Zone B, in contrast with its relatively limited abundance, compared with *Gleicheniidites senonicus*, in Zone A.

Subzone B2 is characterized by the apparently restricted appearance of diverse schizacean spores and several new species of gymnosperms. The former are primarily associated with carbonaceous clay samples which

may be coeval with lignite facies elsewhere in the southern portion of the Moose River Basin. The diversification of gymnospermous species in the subzone is associated with a mottled silty clay facies which was particularly rich in palynomorphs.

ZONE C (158-170 feet)

LONG-RANGING SPECIES

Alisporites grandis (Cookson) Dettmann
Biretisporites potoniei Delcourt and Sprumont
Cerebropollenites mesozocus (Couper)
Perinopollenites elatoides Couper
Baculatisporites comaumensis (Cookson) Potonié
Inaperturopollenites dubius (Potonié and Kremp)
 Thomson and Pflug

SPECIES FOUND ONLY IN ZONE C

Acanthotriletes varispinosus Pocock
Cicatricosisporites mohroides Delcourt and Sprumont
Cicatricosporites phaseolus (Delcourt and Sprumont) Krutsch
Foraminisporis asymmetricus (Cookson and Dettmann) Dettmann

DISCUSSION OF ZONE C. Zone C is found only in the youngest Cretaceous sample for which palynomorphs are present in drillhole OGS78-01. The stratum from which the sample was retrieved is overlain by Cretaceous gravelly sands unsuitable for palynomorph preservation, and by Pleistocene tills. It is assumed that Zone C was truncated at this interval, and species listed last in this sample do not represent range tops.

CONCLUSIONS

Detailed palynologic analyses in a cored section of the Mattagami Formation allows the recognition and refinement of three spore-pollen zones. These zones (Middle to Late Albian) are based on the distribution of 106 miospores species. Lignites accumulated in the lowest two zones. The refined zonation includes new information on spore-pollen species ranges and will be useful for precise correlation of lignitic strata in the Moose River Basin.

REFERENCES

- Norris, G.
 1979: Palynostratigraphy of lignite-bearing Mesozoic sediments, Moose River Basin James Bay Lowland; Ontario Geological Survey Miscellaneous Paper 87, p.67-68.
 in press: Mesozoic palynology of the Moose River Basin, Ontario; in *Aspects of the Mesozoic Geology of the Moose River Basin, James Bay Lowland*, Telford, P.G. and Verma, H.M., editors, Ontario Geological Survey Geoscience Study.
 Norris, G. and Dobell, P.
 1980: Palynostratigraphic correlation of Cretaceous lignitic strata, southern Moose River Basin, Ontario; Ontario Geological Survey Miscellaneous Paper 93, p.179-184.
 Singh, C.
 1971: Lower Cretaceous microfloras of the Peace River Area, northwestern Alberta; Research Council of Alberta, Bulletin 28, 542 p.
 Telford, P.G. and Verma, H.
 1978: Cretaceous stratigraphy and lignite occurrences in the Smoky Falls area, James Bay Lowland, preliminary lithological logs from the 1978 drilling program; Ontario Geological Survey Open Report 5255, 57p.

Grant 32 Volcanic-Tectonic Setting of Gold Deposits in the Timmins District — Carbonate-Bearing Rocks at Dome Mine

R.G. Roberts and D.J. Reading

Department of Earth Sciences, University of Waterloo

ABSTRACT

The carbonatized rocks of the Dome Mine comprise 1) basaltic flows on the south limb of the Porcupine Syncline which host gold-bearing, ferroan dolomitic sedimentary rocks and associated quartz veins, 2) "carbonate rock" and "highly altered" units which host the fuchsite-quartz vein and the tourmaline-quartz vein respectively, and 3) mafic volcanic rocks of the South Greenstones exposed in the mine. The "carbonate rock", "highly altered" unit, South Greenstones of the mine, and South Greenstones exposed at surface constitute a volcanic sequence that progresses from ultramafic komatiite, through mafic komatiite, to mafic rocks of magnesium-rich tholeiite composition. The field evidence suggests that the Timiskaming metasediments and the South Greenstones constitute a continuous sequence.

During hydrothermal alteration, magnesium, silicon, aluminum, titanium and iron were immobile. Calcium and potassium were added to the rocks and sodium depleted.

INTRODUCTION

This report describes the carbonate-bearing volcanic rocks at the Dome Mine, Timmins, and is part of a study of the volcanic and tectonic setting of the gold deposits of the Timmins district.

The carbonate-bearing rocks discussed here are: 1) altered basaltic flow rocks of the south limb of the Porcupine Syncline which host the interflow, ferroan dolomite sedimentary rocks and associated quartz veins; 2) a zone of carbonate-rich rocks which host the fuchsite-quartz vein and the tourmaline-quartz vein; and 3) altered volcanic rocks of the South Greenstones (Figure 1).

An understanding of the alteration process is important since it is now realized that carbonate alteration is characteristic of many Archean gold camps. The geology of the zone of carbonate-rich rocks is important, also, because it occurs at a critical stratigraphic position.

LITHOLOGY

BASALT FLOWS (PORCUPINE SYNCLINE)

The flows are pillowed, variolitic, and massive. The asso-

ciated tuffs consist predominantly of altered glass fragments. The mineral assemblage is plagioclase (albite), quartz, chlorite, epidote, and ferroan dolomite. There is no systematic relationship between carbonate content and position within the flow.

ZONE OF CARBONATE-RICH ROCKS

The zone of carbonate-rich rocks includes talc schist and two carbonate-rich units. The carbonate-rich units are the predominant lithologies and are referred to in the mine as "carbonate rock" and "highly altered". Both rock types are composed of ferroan dolomite, minor amounts of magnesite, quartz, chlorite and green mica (fuchsite), but the "highly altered" unit is characterized by larger amounts of chlorite and fuchsite which give the unit a green cast and allow it to be distinguished from the pale brown "carbonate rock". The "highly altered" unit is at least in part fragmental, in which clasts up to 4 cm across were recognized.

SOUTH GREENSTONES

In the mine, the South Greenstones are uniform, foliated, dark green rocks, composed of chlorite, quartz, ferroan dolomite, epidote and stilpnomelane. The overlying units, exposed at surface, are grey, pillowed and massive mafic flows composed of altered plagioclase, chlorite, actinolite, with minor amounts of quartz and carbonate.

STRATIGRAPHY

The zone of carbonate-rich rocks lies between the south-facing South Greenstones and south-facing turbidite sedimentary rocks (Timiskaming metasediments) of the Porcupine Syncline (see Figure 1). The age and tectonic relationships of these rocks are controversial. Davies (1977) suggested that a fault occurs at about the position of the carbonate-rich zone, and that the South Greenstone unit is the faulted equivalent of volcanic rocks to the west. The volcanic rocks to the west underlie the Porcupine Syncline and the basalt flows that host the gold-bearing carbonate sedimentary rocks in the Dome Mine. Further evidence for the correlation of the South Green-

stones with the structurally underlying volcanic rocks is provided by their comparable trace element content (Davies and Whitehead 1980). In contrast to this interpretation, the author has suggested (Roberts 1980) that volcanic activity involved the development of basins and intervening dome structures, which now constitute the major structural features of the district. According to this interpretation the volcanic rocks of the South Greenstones were emplaced in a basin that formed after the basin that now forms the Porcupine Syncline. Consequently, it is suggested that the Timiskaming metasediments and the flows of the South Greenstones constitute an essentially conformable, south-facing sequence. Although faults parallel to the contacts of the units occur within the carbonate-rich zone, and at the contact of the "carbonate

rock" and the Timiskaming metasediments, the evidence of observations of underground exposures is that the metasediments and the altered rocks are a continuous sequence. This evidence is primarily the fact that conformable, lenticular units of "carbonate rock" occur within the metasediments. The lens of carbonate observed by the senior author is approximately 2 m thick and occurs approximately 10 m north of the "carbonate rock" — metasediment contact on the 20th level of the mine. An interfingering relationship between "carbonate rock" and metasediments on a scale such that they can be traced in an underground drift, occurs on the 10th level of the mine. It may be noted also that shales occur at the contact between the "carbonate rock" and the "South Greenstones" of the mine, on the 12th level.

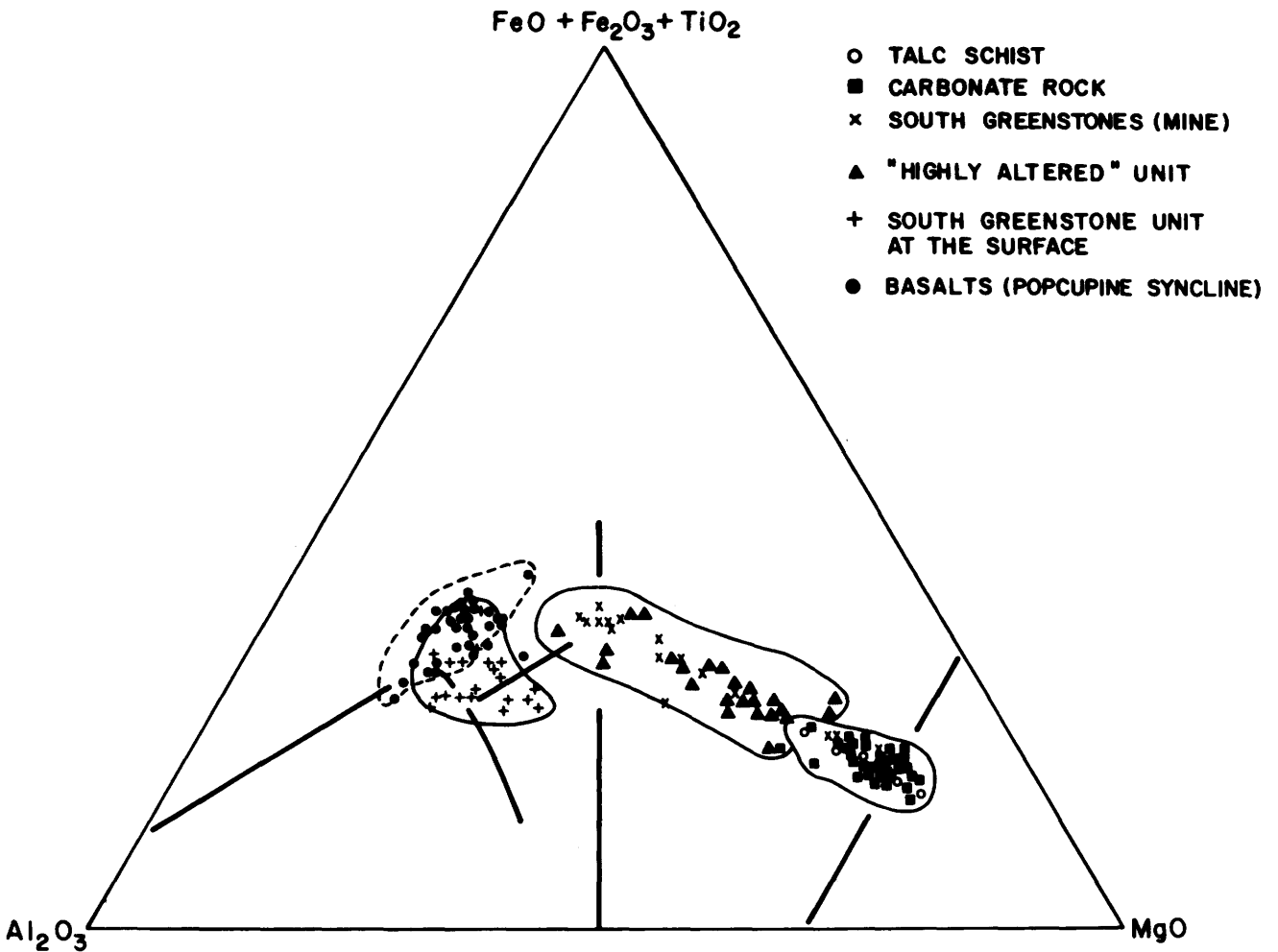


Figure 2—Classification of volcanic rock units discussed in the text, using Jensen (1976) cation plot.

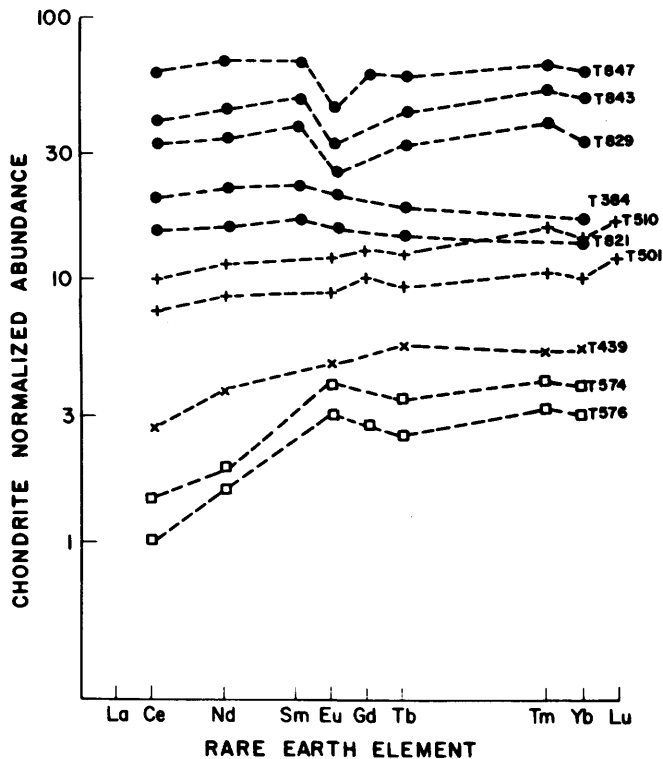


Figure 3—Rare earth element patterns for "carbonate rock" (squares), South Greenstones of mine (x), South Greenstones at surface (+), and basaltic rocks of the Porcupine Syncline (*).

GEOCHEMICAL CLASSIFICATION

The various altered rocks fall into well defined groups (Figure 2) on the cation plot (Jensen 1976). The "carbonate rock" and the talc schist plot in the komatiitic field at the mafic-ultramafic boundary. The South Greenstones of the mine and the "highly altered" unit occupy the same position in the mafic komatiite field. The mafic flows of the South Greenstones at surface plot in the magnesium-rich tholeiite field, and the mafic rocks of the south limb of the Porcupine Syncline plot in the iron-rich tholeiite field.

The REE patterns (Figure 3) confirm the classification given by the cation plot. The REE pattern for the "carbonate rock" and the South Greenstones of the mine have the low absolute value and light rare earth depletion typical of komatiitic rocks. The REE patterns of the magnesium-rich tholeiites of the South Greenstones at surface and the iron-rich tholeiites of the Porcupine Syncline basalts, compared to that of the "carbonate rock" indicate more highly fractionated rocks with typical basaltic abundances.

GEOCHEMISTRY OF ALTERATION

The variation of the major elements between and within the altered units is illustrated in Figure 4a-h. The most obvious manifestation of alteration is the presence of carbonate in the rocks, and a direct relationship is assumed between degree of alteration and the amount of carbonate. Figure 4a demonstrates that "loss on ignition" (L.O.I.) may also be used as an indicator of alteration, and also that the degree of alteration increases with the mafic character of the rocks. Thus the most altered rocks (highest carbonate content) are the ultramafic komatiitic rocks ("carbonate rock"). This relationship between rock type and degree of alteration is further illustrated in Figures 4b, d and e. Thus magnesium, iron, silicon and aluminum are relatively immobile during alteration or at least the degree of transfer of these elements is such that it does not disguise the classification of the original rock. The plot of MgO versus Ni (Figure 4c) further demonstrates that the magmatic relationship between magnesium and nickel is retained through the alteration process.

Calcium is apparently mobile in the alteration process. There is no linear relationship between carbonate and calcium content (Figure 4f). This is confirmed by the molecular proportional ratio plots (Figures 4g, h), where the mobility of calcium may be contrasted with the relatively immobile nature of Fe and Si when Mg is held constant.

MASS TRANSFER

The basaltic rocks of the Porcupine Syncline have a greater variation of carbonate content (and hence a wider range of alteration) than the other altered units. Figures 5a and 5b illustrate the mass transfer of elements for a single flow, calculated at constant volume (Figure 5a), and constant aluminum (Figure 5b). The two diagrams provide essentially the same result. There is very little variation in magnesium, silicon and total iron. Aluminum is constant at constant volume, and is followed by titanium. Calcium increases regularly with alteration, and there is a more irregular increase of potassium. There is a net loss of sodium.

CONCLUSIONS

- 1) The carbonate-rich zone, the South Greenstones of the Dome Mine, and the mafic South Greenstones exposed at surface constitute a volcanic sequence that progresses from ultramafic komatiite at the base, through mafic komatiite, to magnesium-rich tholeiite at the top.
- 2) The degree of alteration (carbonatization) was dependent on the original rock composition.
- 3) Magnesium, iron, silicon, aluminum, and titanium were relatively immobile during alteration. Calcium and potassium were added, and sodium depleted during alteration.

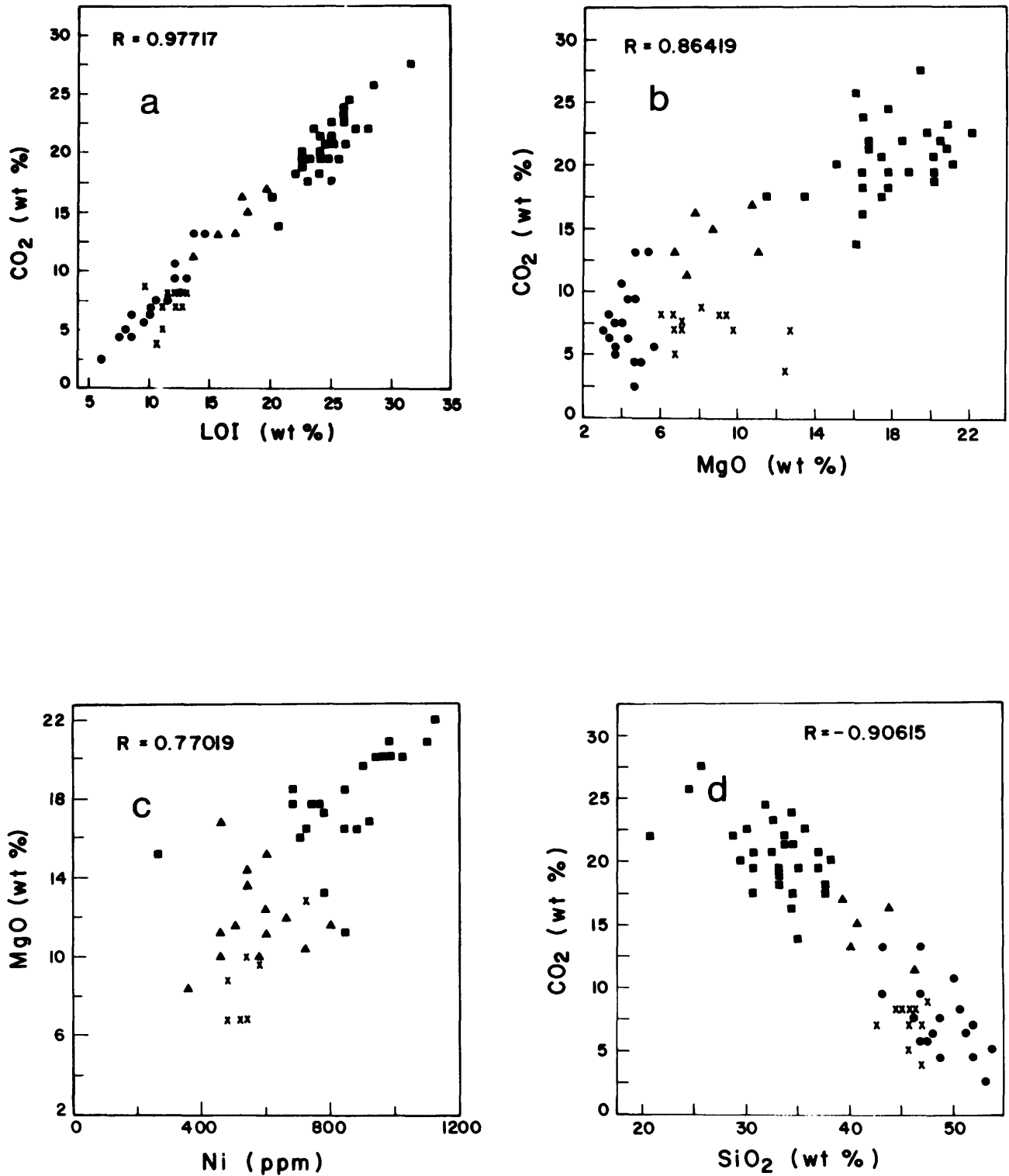
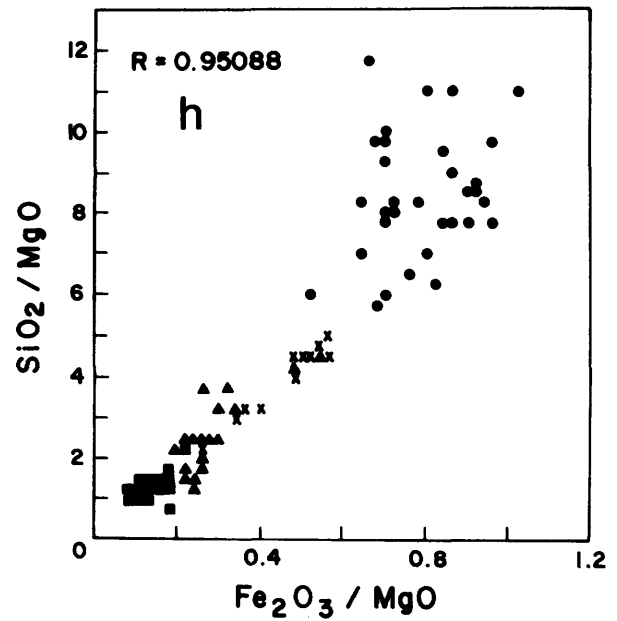
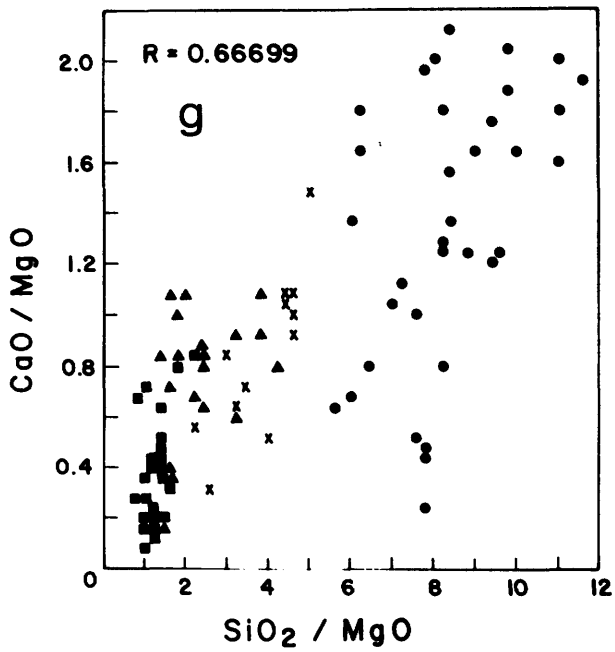
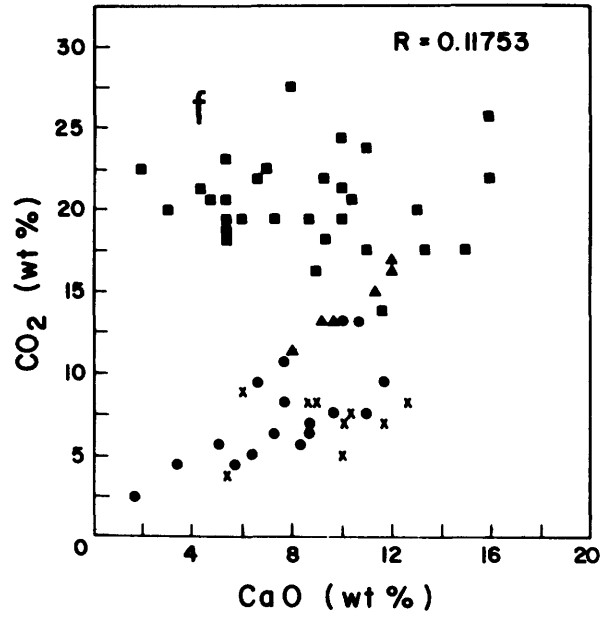
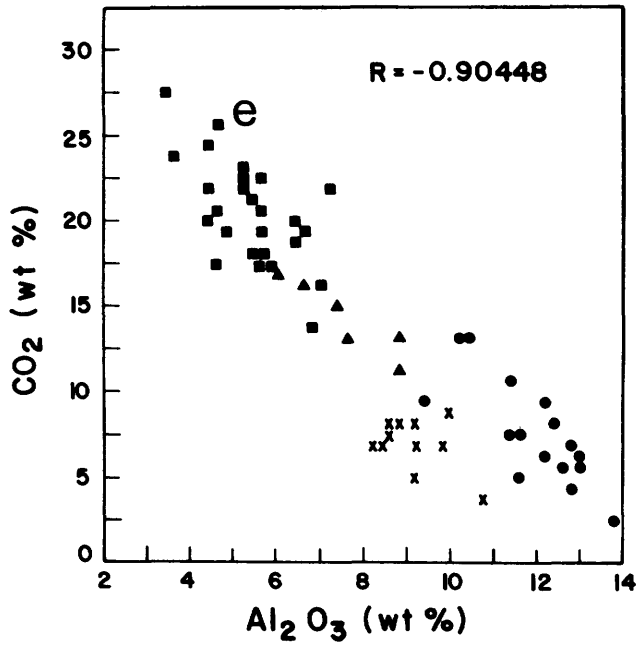


Figure 4—Variation diagrams for the altered units. R is correlation coefficient. Symbols as in Figure 2.



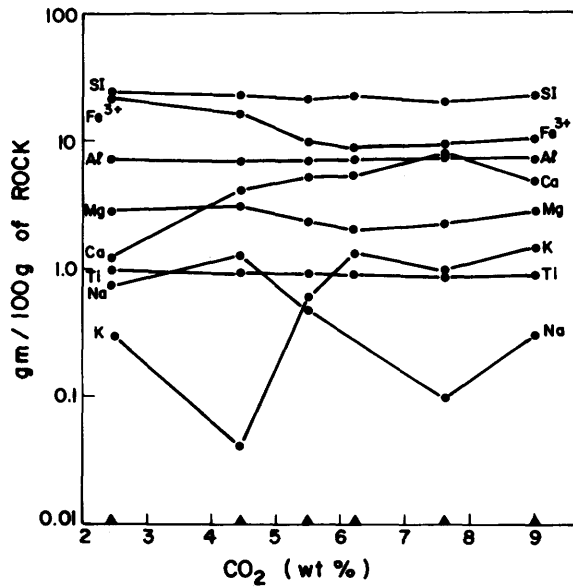


Figure 5a—Metasomatic variation diagram for a basaltic flow from the Porcupine Syncline illustrating mass transfer at constant volume.

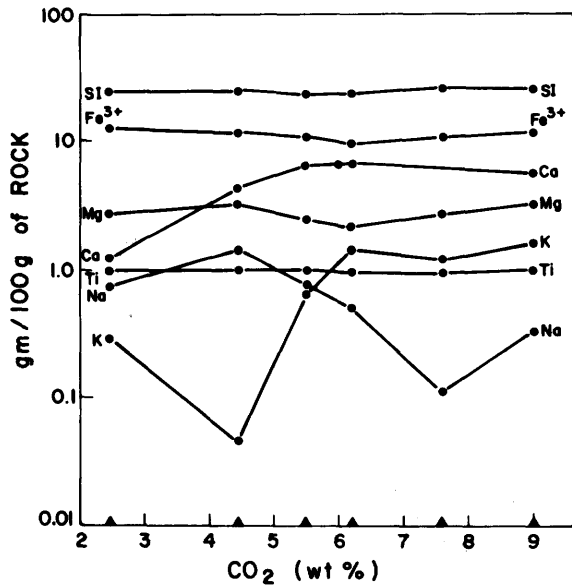


Figure 5b—Metasomatic variation diagram for a basaltic flow from the Porcupine Syncline illustrating mass transfer at a constant aluminum.

REFERENCES

- Davies, J.F.
1977: Structural interpretation of the Timmins mining area, Ontario; Canadian Journal of Earth Sciences, vol.14, p.1040-1053.
- Davies, J.F. and Whitehead, R.E.S.
1980: Further immobile element data from altered volcanic rocks, Timmins mining area, Ontario; Canadian Journal of Earth Science, Vol.17, p.419-423.
- Jensen, L.S.
1976: A new cation plot for classifying subalkalic volcanic rocks; Ontario Division of Mines, Miscellaneous Paper 66, 22p.
- Roberts, R.G.
1980: The volcanic-tectonic setting of gold deposits in the Timmins district; Grant 32, p. 185-194, in Geoscience Research Grant Program, Summary of Research 1979-80, Edited by E.G. Pye, Ontario Geological Survey, Miscellaneous Paper 63, 262p.

Grant 87 Stability of Compressed Shales in Ontario

J-C. Roegiers and R.H. Mills

Department of Civil Engineering, University of Toronto

ABSTRACT

The research was directed towards better understanding of cohesion in compacted shales and the variation of strength caused by water-solid interaction. The effect of water in porous solids is known to be a function of the quantity of water retained by the solid at various relative humidities and is related to the internal surface area of the solid. Internal surface area was estimated by the Brunauer, Emmett and Teller (BET) theory, after bringing the rock samples to equilibrium at various values of relative humidity.

Sorption isotherms on a sample of Queenston shale from the Burlington area gave an internal surface area of 39 000 m²/kg or about 104 000 m²/m³. Concurrent Brazilian splitting tests showed a relationship between strength and the number of water monolayers contained in the pores of specimens. Gain or loss of moisture is associated with large volume changes but when such volume changes were restrained, the corresponding pressures were not measurable. Attempts to stabilize the shale with plastic coating material were not successful.

INTRODUCTION

Rehbinder *et al.* (1944) published the first systematic study of the weakening effect of adsorbed surface films in rocks. At about the same time Orowan (1944) showed that the work of creating new surfaces in propagating cracks in a solid was reduced by changes in surface energy caused by sorption of vapour and gases from the atmosphere. Derjaguin and Abrikosova (1958; Derjaguin 1960) described direct measurements of molecular attraction of separate pieces of quartz glass. Schöning (1959) measured the modulus of rupture of glass in controlled atmospheres of varying relative humidity θ . He found that sorption of water vapour from the dry state caused a reduction of strength in the range $0 < \theta < 10$ percent followed by an increase to a maximum at $\theta \cong 20$ percent followed by further reduction to a constant minimum extending over the range 30 percent $< \theta < 100$ percent.

Derjaguin and Nerpin (1965) first described the wedging action of water in areas of restricted adsorption as "disjoining pressure." Mills (1960) discussed the influence of free water on the strength of concrete and, later (1966) described the influence of changes in surface energy due to water sorption on volume change and strength of concrete.

The present investigation was based on the assumption

that shale derives its strength from molecular bonds, mainly van der Waal's forces, and that the attenuation of these bonds by water sorption is responsible for the readily observable weakening of shale exposed to the atmosphere.

Queenston shale from this source was chosen because a considerable body of test data exists (Horvath 1980) and because it probably represents a lower bound of performance with respect to durability and loss of strength due to moisture change. Furthermore cores from the site were available in large quantities.

Specimens from these cores were cut dry with a bandsaw and brought to mass equilibrium at various values of relative humidity. Splitting tensile strength tests were carried out and the moisture content was determined by oven-drying at 110°C.

DESCRIPTION OF SHALE

The following description was abstracted from Horvath (1980). The shale tested in this study was obtained from the National Sewer Pipe Limited quarry located on the east side of King Road less than 1 km north of Highway 403 in Burlington, Ontario. The rock was predominantly a brick red shale with layers of harder, grey, calcareous material. The red shale, comprising 80-95 percent of the rock mass, consisted of clay minerals, quartz and calcite in proportions 60:26:14. The rock unit from which the cores were taken is about 180 m thick and of relatively uniform quality; the average strength anisotropy, determined as the ratio of point-load strength perpendicular to the bedding plane to that parallel to the bedding plane, ranged from 0.91 to 1.68 with an average of 1.18. The rock was also subjected to the slake durability test in which about 500 g of oven-dried lumps are rotated in water in a drum made with 2 mm opening wire mesh. The mass percentage of material retained after 10 minutes at 20 revolutions per minute is taken as the first cycle slake durability ID1. If the test is repeated for the same sample, this is called the second cycle slake durability ID2. The sample tested gave ID1 ranging from 70-76 percent and ID2 ranging from 30-56 percent. The shale is therefore classified as having poor to fair weathering characteristics.

PHYSICAL PROPERTIES

Data obtained in a companion program (Horvath 1980) are summarized in Tables 1 and 2.

Table 1—Physical properties of Queenston shale. From Horvath (1980).

	<u>Range</u>	<u>Average</u>
σ_C (MPa)	2.8 - 14.2	8.0
τ_{max} (MPa)		1.06
τ_R (MPa)		0.30
ϕ° (PEAK)		55.0
ϕ° (RESID)		30.0
SECANT E (GPa)	0.41 - 1.18	0.74
POISSON'S RATIO	0.19 - 0.35	0.30
POINT LOAD STRENGTH (MPa)	0.57 - 0.66	0.60

RESULTS OF THE PRESENT PROGRAM

The average saturated surface dry bulk density of the shale was determined to be 2.56, and the specific gravity of the solid phase to be 2.82 giving a pore volume of 14.4 percent. The moisture content of the sealed cores was 4.6 percent and the saturated surface-dry moisture content was 5.9 mass percent of the solid equilibrated at 100°C.

Table 2—Mineral composition of Queenston shale. From Horvath (1980).

	<u>Mass %</u>
Clay Materials	60
Quartz	26
Calcite	11
Dolomite	3

CONDITIONING OF SAMPLES

Discs 12 mm thick were cut from 54 mm diameter cores recovered from the site. These were placed in batches of 10 in vacuum dessicators over saturated salt solutions giving various values of ambient vapour pressure p relative to the saturation vapour pressure p_s . A nominally dry atmosphere $p = 10^{-4}$ Torr was provided by an Edwards vacuum coating unit. The various atmospheres were as follows:

- 1) Dry at $p = 10^{-4}$ Torr;
- 2) $p/p_s = 0.07$ over saturated solution of NaOH;
- 3) $p/p_s = 0.32$ over saturated solution of CaCl_2 ;
- 4) $p/p_s = 0.74$ over saturated solution of NaCl.

Table 3—Sorption data for Queenston shale samples.

p/p_s	0.105	0.200	0.320	0.460	0.660	0.750	1.0
$\Delta W \times 10^3$	5.0	8.0	11.6	15.5	17.5	20.0	59.0
S	0.5	1.1	2.6	1.8	1.5	3.9	3.6

S = standard deviation
 ΔW = change in water mass per unit mass of dry solid

The salt solutions were placed in the bottom of vacuum dessicator vessels and the specimens were placed on a rack above together with two weighing bottles, one containing H_2SO_4 solution, and the other concentrated H_2SO_4 . The H_2SO_4 solution was at a concentration corresponding to p/p_s greater than that of the intended atmosphere. The specimens and acid bottles were weighed at regular time intervals until the acid concentrations matched the nominal p/p_s and there was no significant change in the weight of the specimens. All of the specimens lost weight. The second driest atmosphere, nominally $p/p_s = 0.07$, in fact stabilized at $p/p_s = 0.105$.

During the conditioning process many specimens suffered damage due to spalling and were not tested. The casualties were

- 20 percent at $p/p_s = 0.105$;
- 42 percent at $p/p_s = 0.32$; and
- 60 percent at $p/p_s = 0.74$.

Sound specimens which were tested in the various environments gave the results tabulated in Table 4.

For individual specimens, the splitting strength σ_T could be expressed as a linear function of V_m :

$$\sigma_T = 8.34 - 0.4 V_m; \text{ with a correlation coefficient } r^2 = 0.73.$$

SORPTION DATA

Assuming that moisture in the specimens was in mass equilibrium with that in the acid bottles, the water mass per unit mass of oven dried solid and the corresponding values of p/p_s are given in Table 3.

The corresponding BET constants (Brunauers *et al.* 1938) were:

$$\begin{aligned} \text{monolayer capacity } V_m &= 9.8 \times 10^{-3} \text{ g/g} \\ \text{surface area } S &= 35.09 \times 10^3 \text{ m}^2/\text{kg} \\ &= 104 \times 10^6 \text{ m}^2/\text{m}^3 \end{aligned}$$

IMMERSION IN WATER

The time taken to develop maximum expansion and damage due to cracking was about 30 minutes. Expansion microstrain ϵ_s was a linear function of the logarithm of time t (seconds):

$$\begin{aligned} \epsilon_s &= 25\,000 \log t - 36\,900 \mu\text{m}, \\ r^2 &= 0.98. \end{aligned}$$

Table 4—Variation of splitting strength σ_T with relative vapour pressure p/p_s and moisture content ΔW .

p/p_s	0	0.105	0.32	0.75	1.00
$\Delta W (10^3)$	0	5.0	11.6	20.0	59.0
σ_T (MPa)	9.3	6.9	3.8	3.1	0
S	0.8	0.4	1.2	0.4	-

S = Standard deviation for strength values

OTHER MECHANICAL TESTS

Cylinders which were tested in uniaxial compression yielded compressive strength $\sigma_c = 11.1$ MPa; elastic modulus $E = 0.87$ GPa; Poisson's ratio = 0.28, and ultrasonic pulse velocity = 3300 m/s.

STABILIZATION WITH PLASTIC SEALANT

A water soluble plastic M175 developed by Dowell Research and Development for this project was applied as a coating. This material was designed to polymerize in situ. It was anticipated that this treatment would inhibit gain or loss of moisture and hence stabilize the shale. A strong but flexible skin was formed on the specimens but this did not prevent their disintegration when exposed to water.

TESTS ON DEBRIS

The debris from various tests was pulverized and dried and subjected to various soil tests with results as follows.

- Liquid limit = 22.3.
- Plastic limit = 15.6.
- Plasticity index = 6.7.
- Volumetric shrinkage = 14.6 percent.
- Shrinkage limit = 12.5 percent.
- Linear shrinkage = 2.7 percent.

DISCUSSION

The results thus far obtained for a particular shale show that the rock is highly sensitive to energy changes accompanying gain or loss of moisture and that this is a function of pore size distribution.

FUTURE PLANS AND CONCLUSIONS

The program is proceeding with sorption-length change and strength tests on 150 mm lengths of core and on 12 mm thick discs. The ultra-sonic pulse velocity measuring instrument originally built in the Department of Civil Engineering is being re-designed and modified with the help of Professor V.M. Ristic of the Department of Electrical

Engineering at the University of Toronto. In its modified form the instrument will be used to monitor the influence of moisture content on both shear and compression wave pulse velocity. A pressure cell capable of producing a cylindrical specimen 25 mm diameter by 50 mm length under a pressure of 500 MPa and temperature of 200°C has been made. Work is proceeding on re-constituted shale made by hot pressing powdered material. At present this work is not funded and is therefore proceeding slowly.

ACKNOWLEDGMENTS

The authors wish to thank Professor G.N. Kuang, Mr. S. Nesbitt, and Mr. Peter Seto of the Department of Civil Engineering, University of Toronto, for their valuable assistance.

REFERENCES

- Brunauers, S., Emmett, P.H., and Teller, E.
1938: J. American Chem. Soc. Vol. 60, p.309.
- Derjaguin, B.V.
1960: The force between molecules; Scientific American Vol. 203-1.
- Derjaguin, B.V. and Abrikosova, I.I.
1958: Direct measurements of molecular attraction of solids; J. Phys. Chem. Solids, Vol. 5, p.1-10.
- Derjaguin, B.V. and Nerpin, S.
1965: Role of capillary and surface forces in moisture transfer in porous bodies; RILEM Bulletin No. 27, p.55-57.
- Horvath, R.G.
1980: Research Project Report on Load Transfer System for Rock Socketed Drilled Pier Foundations; DSS File Number 10SX.31155-9-4420.
- Mills, R.H.
1960: Strength-maturity relationship for concrete which is allowed to dry; RILEM Symposium on Concrete and Reinforced Concrete in Hot Countries, Haifa, 1960.
- 1966: Effects of sorbed water on dimension, compressive strength and swelling pressure of hardened cement paste; Highway Research Board Special Report 90, Washington.
- Orowan, E.
1944: Nature Vol. 154, p.341.
- Rehbinder, P.A., Schreiner, L.A. and Zhigach, K.F.
1944: Hardness Reducers in Drilling; (English Translation 1948), CSIRO Melbourne.
- Schoning, F.R.L.
1959: Fracture of glass at various vapour pressures; Unpublished Ph.D. Thesis, University of the Witwaterstand, Johannesburg.

Grant 96 Mineralization in the Whitewater Group, Sudbury Basin

D.H. Rousell

Department of Geology, Laurentian University

ABSTRACT

Rocks of the Whitewater Group, of Aphebian (Middle Precambrian) age, constitute the fill of the Sudbury Basin and comprise three formations which are, from oldest to youngest: the Onaping, a massive heterogeneous breccia; the Onwatin, argillite and siltstone; and the Chelmsford, mainly greywacke.

Mineralization in the group is as follows. 1) Disseminated sulphide fragments in the Onaping Formation. The fragments occur throughout the formation and consist largely of pyrrhotite with minor chalcopyrite, sphalerite, galena, marcasite, and pyrite. The Ni content and that of other trace elements is low. 2) Zn, Cu, Pb, Au and Ag in a local carbonate-chert unit at the base of the Onwatin Formation (Vermilion and Errington Mines). The unit may have formed by hot-spring activity or may have been produced by chemical or biochemical precipitation. 3) Pyrite and base metals in the Onwatin Formation. Abundant carbonaceous material in the Onwatin Formation, probably of organic origin, gave rise to reducing conditions which led to the formation of pyrite as disseminated grains and lenses. Relatively high values of Cu, Zn and Ni occur locally in the formation. 4) Quartz veins in the South Range at the Nickel Irruptive-Onaping contact. Metals present at these properties are Zn and Pb (Foisey); Cu, Au and Co (Papineau); and Pb, Zn and Ag (Moore Lake). The veins were probably emplaced during the time of basin deformation. Analyses of vein material from two former gold "mines" (Creighton and Gordon Lake) yielded no Au values. 5) Mineralized quartz-carbonate veins in a mafic sill at the Onwatin-Chelmsford contact. Cu, Zn, and Au values are locally relatively high. 6) Anthraxolite veins (95 percent C) formed in the Onwatin Formation by remobilization of carbonaceous material during metamorphism.

GEOLOGICAL SETTING

The Sudbury Basin is situated near the junction of three structural provinces of the Canadian Shield: it lies within the Southern Province, with the Superior Province to the northwest and the Grenville Province to the southeast (Figure 1). The basin is elliptical in plan view, 58 km long and 26 km wide, with the long axis trending N65°E. The outer segments may be divided into three ranges: East, North, and South.

Rocks of the Whitewater Group, of Aphebian (Middle Precambrian) age, comprise the fill of the basin and there are no known equivalent rocks outside the basin. The group consists of three formations which are, from oldest to youngest, the Onaping, Onwatin and Chelmsford Formations. Contacts between the formations are gradational and conformable. The Onaping Formation is a massive breccia which grades from very coarse at the base to fine grained at the top. Fragments consist of quartzite, granitic rocks, and a variety of devitrified glasses. A distinctive breccia, consisting mainly of quartzite fragments as much as 100 m in length, occurs at the base of the formation. Igneous rocks underlie, penetrate, and locally form the matrix of the basal breccia. These igneous rocks may be related to the micropegmatite phase of the Nickel Irruptive (Stevenson 1963), the oxide-rich phase of the Nickel Irruptive (Peredery and Naldrett 1975), or may represent melt rocks formed by meteorite impact (Peredery 1972). The Onwatin Formation is composed of argillite and siltstone. A local carbonate-chert unit (Vermilion member) occurs at the base of the formation. The Chelmsford Formation consists largely of greywacke with minor argillite and siltstone and represents a proximal turbidite sequence (Rousell 1972). The rocks of the Whitewater Group contain abundant carbonaceous material and this imparts a dark colour to the rocks. The Nickel Irruptive was emplaced between the Onaping Formation and the footwall rocks, outcrops in the form of an elliptical ring, and outlines the basin perimeter. The basin was formed approximately 1.9 Ga ago (Gibbins and McNutt 1975a) and its origin is controversial. It was long regarded as being of volcanic origin, and is still regarded as such by some, until Dietz (1962) proposed that the basin was excavated by meteorite impact.

The Sudbury Basin was deformed by an orogenic event 1.6-1.8 Ga ago (Gibbins and McNutt 1975b). The basin, once less elliptical than its present form in plan view, was flattened by a 'push' directed toward the northwest. A penetrative tectonic foliation and lineation were developed in the Onaping Formation and locally in the Nickel Irruptive of the South and East Ranges (Brocum and Dalziel 1974, Rousell 1975). Further to the northwest, the deformation intensity decreased and the rocks of the Onwatin and Chelmsford Formations developed a cleavage and yielded by folding. Still further to the northwest the deformation was slight as only a local and weak foliation is present in the Onaping rocks of the North Range. Later episodes of brittle deformation produced joints. (Rousell and Everitt, in press).

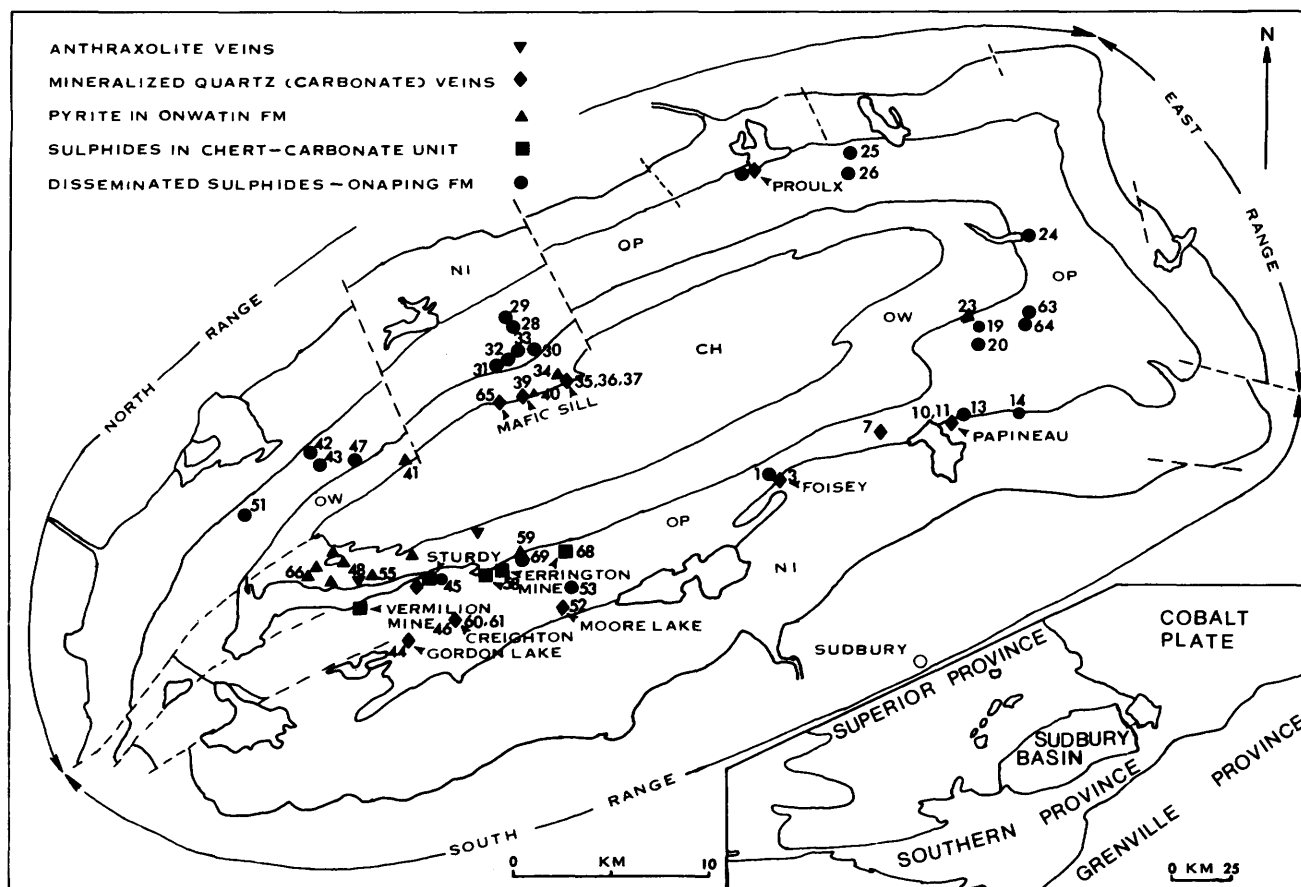


Figure 1—Geological map of the Sudbury Basin showing the location of mineral occurrences in the Whitewater Group. Numbers correspond to specimen numbers in the tables (prefixed by W in tables). NI, Nickel Irruptive; OP, Onaping Formation; OW, Onwatin Formation; and CH, Chelmsford Formation. Inset map indicates the regional setting of the basin.

The prominent nickel-copper ores of the Sudbury basin are within a distinctive inclusion-bearing facies known as the sublayer (Souch *et al.* 1969, Pattison 1979). The sublayer occurs between the Nickel Irruptive and the footwall and in radiating dikes known as offsets. The major sulphide minerals are pyrrhotite, pentlandite, and chalcopyrite.

The rocks within the basin contain a variety of mineral occurrences including two former base metal mines and two gold properties defunct before the turn of the century. Little new data on the mineralization has appeared in over 20 years and many of the occurrences are poorly known. The purpose of this investigation is to provide a comprehensive account of the mineralization within the Whitewater Group.

MINERAL OCCURRENCES

All mineral occurrences within the Whitewater Group that are known to the writer are shown in Figure 1. The data is derived from the literature, files of the Ontario Geological Survey, and personal observations. For the purposes of this report the mineralization may be grouped as follows: 1) disseminated sulphides in the Onaping Formation; 2) sulphides in a local carbonate-chert unit; 3) pyrite in the Onwatin Formation; 4) mineralized quartz (carbonate) veins; and 5) anthraxolite veins. The mineralization is diagrammatically represented in the columnar section of Figure 2.

DISSEMINATED SULPHIDES IN THE ONAPING FORMATION

One type of mineral occurrence in the Onaping Formation consists of disseminated sulphide fragments. There are a number of occurrences of this type recorded in the literature and several of them are exposed in trenches and pits. The sulphide content of these is variable, and some appear to have been reported mainly because of their accessibility. Disseminated sulphides are also present in the igneous rocks which occur below and locally form the matrix of the basal quartzite breccia. The sulphide fragments are tectonically elongated in the South and East Ranges. The present study indicates the disseminated sulphides occur throughout the entire Onaping Formation. The sulphide fragments seldom exceed 0.5 cm in length and the volume percent of sulphide fragments is generally less than 10 percent. Polished section examination indicates that pyrrhotite is the major sulphide mineral with individual grains approximately 0.5 mm or less in diameter. Chalcopyrite is common but, in general, comprises less than 1 percent by volume of the total sulphide material. Other sulphide minerals that occur in minor amounts include sphalerite, galena, marcasite, and pyrite.

Desborough and Larson (1970) identified the following sulphide minerals in specimens of the Onaping Formation from the South Range and the Onaping Falls locality in the North Range: pyrrhotite, nickel marcasite, "pure" pyrite, nickel pyrite, sphalerite, and chalcopyrite. Pyrrhotite is the most abundant sulphide mineral and it is locally replaced by nickel pyrite and nickel marcasite. The nickel and cobalt contents of grains of pyrrhotite, pyrite and marcasite were determined by means of electron microprobe analysis. The nickel content of pyrrhotite is of particular interest. The range for eight grains is 0.1 to 0.35 weight percent and the average is 0.28 weight percent nickel. According to Hawley (1962) the nickel content of pyrrhotite from several nickel-copper mines of the basin ranges from 0.76 to 2.65 weight percent with an average value for all mines of 1.62 weight percent. Thus the nickel content of pyrrhotite from the Onaping Formation is appreciably less than the nickel content of pyrrhotite in the nickel-copper mines.

Table 1 sets out chemical data for 24 specimens of the Onaping Formation and 2 specimens of the igneous matrix of the basal breccia. Trace element data from the Onaping Formation contained in Sadler (1958) and Arengi (1977) are given in Table 4 in terms of average values. Compared to Table 1, Sadler's (1958) data indicates higher Cu and Ni values and Arengi's (1977) data show higher Zn, Ni, and Cr values but lower Pb values.

The average abundance of certain elements in the earth's crust and three common rock types (Krauskopf 1979) are given in Table 4 for comparative purposes. It is difficult to compare the Onaping Formation with standard rock types because of the heterogeneous nature of the unit (Peredery 1972). The average values of Cu, Zn, Co and Pb in the Onaping Formation (Table 1) are somewhat greater than the average value of these elements in the crust (see Table 4). The average Onaping Zn, Co, and Pb

values exceed those of the average basalt (see Table 4) while Ni values in the Onaping are, surprisingly, relatively low.

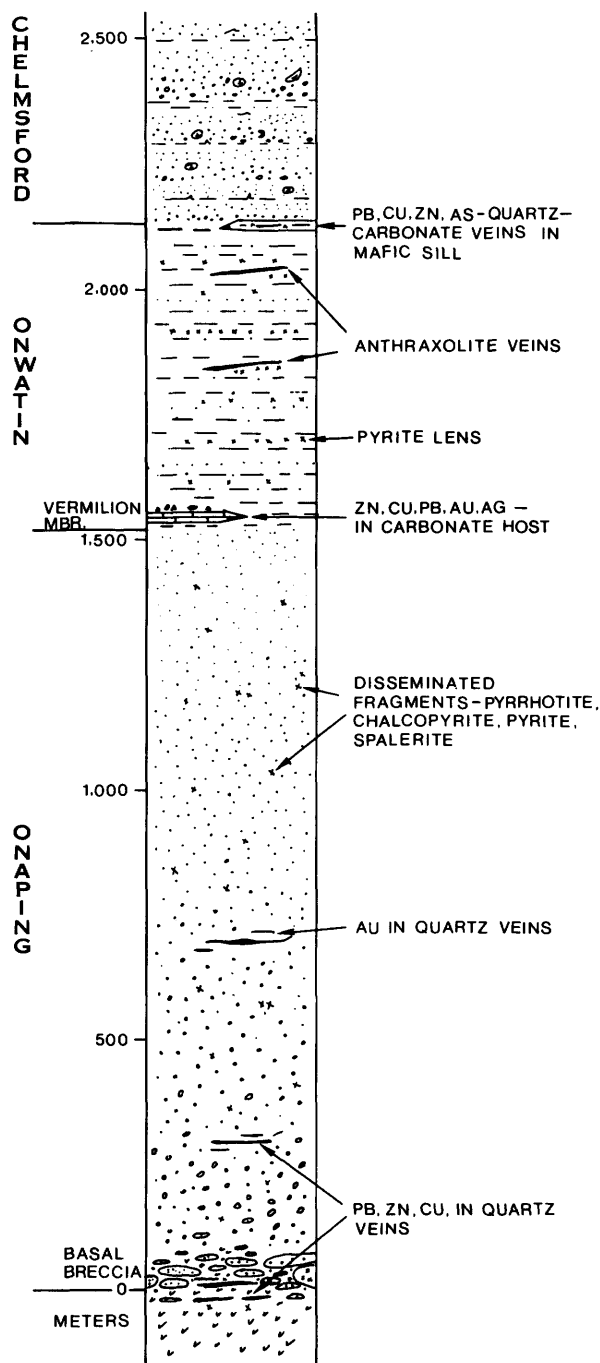


Figure 2—Diagrammatic representation of mineralization in the Whitewater Group.

Table 1—Chemical analyses of specimens from the Onaping Formation.

Spec. No.	PPM								PPB	%
	Cu	Zn	Ni	Co	Pb	Ba	Cr	Ag	Au	Fe ₂ O ₃
W1	60	650	65	50	960	614	105	0.8	ND	8
W13	15	130	ND	130	ND	41	36	ND	ND	1.8
W14	50	25	11	45	ND	569	41	ND	10	3.0
W19	30	110	60	30	5	652	92	ND	10	1.1
W20	15	100	13	20	ND	470	88	ND	30	10.0
W24	20	50	13	20	2	254	76	ND	ND	9.0
W25	160	35	55	55	ND	158	95	ND	ND	7.2
W26A	245	55	80	60	3	175	127	ND	ND	12.8
W28	55	200	60	65	25	813	99	ND	70	7.7
W29	270	370	65	55	15	141	102	0.3	ND	9.3
W30	17	50	60	30	5	749	87	ND	ND	7.3
W31	20	65	55	52	10	586	83	ND	ND	7.5
W32	45	35	70	37	8	764	102	ND	ND	7.7
W33	35	125	60	25	25	466	91	0.2	ND	10.0
W42	75	35	70	30	13	622	110	0.5	ND	9.2
W43	35	10	70	65	10	446	98	ND	ND	8.0
W45	ND	ND	11	200	ND	679	93	ND	ND	0.1
W47	85	80	58	60	7	496	96	ND	ND	8.3
W51-1	30	10	62	50	ND	674	102	ND	ND	7.2
W51-2	265	180	12	121	217	1474	9	0.7	ND	4.3
W53	80	65	60	85	17	215	113	0.3	ND	5.7
W58	85	95	58	45	25	440	92	ND	ND	3.3
W63	45	87	55	30	3	725	103	ND	ND	6.9
W64	65	155	72	32	15	1040	133	ND	ND	8.3
W68	1300	30,000	28	14	525	45	26	4.1	30	4.0
W69	325	23,250	147	100	6250	2839	146	4.1	ND	4.9
Mean	79	116	54	55	62	575	95	-	-	7.2

- Notes:
1. Total Fe as Fe₂O₃.
 2. ND - not detected.
 3. W13 and W14 - igneous matrix of the basal quartzite breccia; and W68 - from dump of Errington No.3 shaft.
 4. W13, W14, W68 and W69 - omitted from mean calculation.
 5. Location of specimens shown on Figure 1 (W omitted for brevity).

In summary, the sulphide fragments in the Onaping Formation resemble the nickel-copper ores of the basin in that pyrrhotite is the major sulphide mineral but differ in the absence of pentlandite in the fragments. This lack of pentlandite, together with the low Ni content of pyrrhotite in the sulphide fragments, may account for the comparatively low Ni content of the Onaping Formation.

SULPHIDES IN A CARBONATE-CHERT UNIT

The Vermilion Mine, the Sturdy property, and the three shafts of the Errington Mine are located in the southwestern corner of the basin (see Figure 1). These Zn-Cu-Pb-Au-Ag deposits occur at the contact between the Onaping and Onwatin Formations, are within a shear zone, and are on the site of a magnetic high (GSC 1960). The shear zone and magnetic high extend to the northeast and beyond the mines. These mines have been shut down for a

number of years and the reason for this was not a lack of metal but rather problems of recovery because of the fine-grained nature of the ore. Giant Yellowknife Mines Limited completed a drilling program in 1979 at the Vermilion Mine in order to obtain fresh material for recovery tests. The geology of the mines has been described by Burrows and Rickaby (1930), Thomson (1956) and Martin (1957). In brief, the ore occurs in a local and distinct carbonate-chert unit, the Vermilion member, and consists of pyrite, sphalerite, chalcopyrite, galena, marcasite, and pyrrhotite. The ore bodies were intensely folded and faulted and the structure is complex. The folds are overturned to the northwest and are doubly plunging and, in this regard, resemble folds in the Chelmsford Formation. The folds are asymmetrical such that the southeastern limbs are long and attenuated whereas the northwestern limbs are shorter. The orebodies are offset by steep southeasterly dipping reverse faults.

Table 2—Chemical analyses of specimens from the Onwatin Formation.

Spec. No.	PPM								PPB	%
	Cu	Zn	Ni	Co	Pb	Ba	Cr	Ag	Au	Fe ₂ O ₃
W23	12	50	45	45	6	2619	87	0.3	ND	8.3
W34	ND	20	30	ND	7	383	102	0.6	ND	2.3
W40	30	40	65	45	15	543	128	ND	ND	4.5
W41-2	4	10	50	20	17	337	110	0.6	ND	3.4
W48-1	90	75	155	68	8	287	77	0.3	ND	4.6
W55-1	50	60	26	51	ND	471	121	0.3	ND	3.1
W59	55	1250 ³	100	85	35	4828 ³	120	ND	10	9.4
W66	90	25	43	21	5	756	84	0.5	ND	2.9
Mean	41	40	64	42	12	770	104	-	-	4.5

- Notes: 1. Total Fe as Fe₂O₃.
 2. ND - not detected.
 3. Omitted from mean calculation.
 4. Location of specimens shown on Figure 1 (W omitted for brevity).

A specimen from an exposure of the Onaping Formation, located between the Errington No. 2 and No. 3 shafts contains high values of Zn and Pb (W69, Table 1). This suggests that the upper part of the Onaping Formation (below the Vermilion member) is also mineralized.

Rocks on the dump of the Vermilion Mine (see Table 4, line 3) and the Errington No. 2 shaft contain abundant sulphides whereas those on the dump of the Errington No. 3 shaft, the most northeasterly shaft, appear to contain little mineralization. A chemical analysis of a specimen from the Errington No. 3 shaft dump (W68, Table 1) indicates a high value of Zn and more modest values of Cu and Pb. The mineralization of the Sturdy property is supposedly related to the carbonate-chert horizon (Thomson 1956) but none of this material is present on the surface in outcrop or in a dump. However, sulphide-bearing quartz veins are exposed on the property.

The Vermilion member is poorly exposed, so the lateral extent of the unit can only be traced by drilling. According to Arengi (1977), a drillhole located northeast of the Errington No. 3 shaft (between localities 1 and 7, Figure 1) penetrated 50 m of the member. Other drill holes, located between the drillhole noted above and Errington No. 3, intersected only 2 m of the member. Average metal values of four specimens from these drillholes are given in Table 4 and, apart from modest Zn values, are relatively low in metal content.

ONWATIN FORMATION

The Onwatin Formation is rich in pyrite. This pyrite occurs as abundant silt-size grains arranged parallel to the bedding and as massive stratiform lenses. These lenses are 1 to 3 cm in thickness but locally lenses are as thick as 20 cm. The presence of pyrite along cleavage planes indi-

cates remobilization. Pyrite cubes, as much as 2 cm in diameter, occur as local masses and are the result of re-crystallization. This type of occurrence is common north of Vermilion Lake and many are exposed in trenches and pits.

Table 2 sets out chemical data for eight specimens of the Onwatin Formation. All specimens, except W23, are from the western portion of the basin; the formation is poorly exposed in the northeastern part of the basin. The average values of Cu, Zn, Ni and Pb tend to be less than those of the average shale (see Table 4); the Cr content is approximately the same and the Co content is twice that of the average shale. Specimen W59, collected from an exposure between Errington No. 2 and No. 3 shafts, and near the base of the unit, contains relatively high values of Zn and Ba.

Average metal values of chemical analyses of specimens of the Onwatin Formation from Arengi (1977) and the Onwatin Formation and the Onaping-Onwatin transition zone from Sadler (1958) are given in Table 4. All metal values are appreciably higher than those in the average shale (see Table 4). For the Onwatin Formation, the data of Arengi (1977) indicates particularly high values of Zn, Ag and Cu; and that of Sadler (1958) high Zn values. The transition zone is notably high in Cu and Ag compared with the average shale.

The specimens of the Onwatin Formation chemically analyzed by Sadler (1958) and Arengi (1977) yielded considerably higher metal values than those analyzed by the writer. Much of the material of these investigators came from drill holes which apparently intersected relatively mineral-rich zones.

QUARTZ (CARBONATE) VEINS

In the South Range sulphide-bearing quartz veins occur

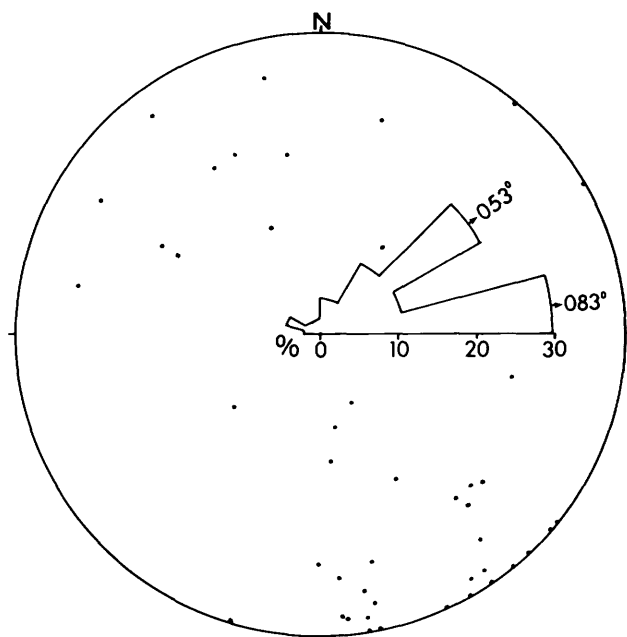


Figure 3—Lower hemisphere, equal-area plot of poles to 47 quartz veins in the Whitewater Group. Rose diagram indicates preferred orientations of the strikes of the veins.

at the Nickel Irruptive-Onaping Formation contact (Foisey and Papineau properties) and in the lower part of the Onaping Formation (Moore Lake occurrence). Gold-bearing quartz veins are also present in the lower part of the Onaping Formation. In the North Range a mafic sill, located at the Onwatin-Chelmsford Formations contact, is the locus for mineralized quartz-carbonate veins (see Figure 2). Quartz veins are prominent in the South Range but relatively scarce in the North Range. Mineralized quartz veins have not been reported in the East Range.

Figure 3 is a stereographic plot of poles to 47 quartz veins all but four of which are from the South Range. In general, the veins dip steeply and the rose diagram of the strikes indicates two dominant trends, N53°E and N83°E. In the southwestern portion of the South Range the lithologic contacts and the foliation strike approximately N53°E; in the eastern part of the South Range the strike of the contacts and foliation turn (at Foisey property, Figure 1) and strike approximately N83°E. In the former locality quartz veins strike at N53°E and in the latter locality at N83°E. Accordingly, quartz veins in the South Range strike parallel to lithologic contacts and the foliation.

SULPHIDE-BEARING QUARTZ VEINS

The Foisey property is located in Lot 2 Concession III, Rayside Township. There are a number of quartz veins in the vicinity of the property. The most mineralized vein is approximately 1 m in thickness and is within the igneous

rock which forms the matrix of the basal quartzite breccia of the Onaping Formation. Black sphalerite, together with some galena and chalcopyrite, form local blebs as much as 3 cm across. Polished section examination indicates that sphalerite, galena and chalcopyrite comprise approximately 90 percent, 9 percent, and 1 percent of the total sulphides, respectively. Sphalerite occurs as masses over 1 cm across, galena occurs as tiny (0.01 mm) inclusions in the sphalerite and as individual grains 1 mm in diameter, and chalcopyrite occurs as grains 0.01 mm in diameter with the sphalerite. Chemical analysis of a specimen of the vein (W3-1A, Table 3) indicates high values of Zn and Pb and the presence of minor amounts of Ag and Au. The Co content is also high compared to the average Co content of common rock types (see Table 4). An analysis of the igneous country rock (W3-2, Table 3) indicates the metal content of this rock is low.

The geological setting of the Papineau property (located in Lot 3, Concession V, Blezard Township) is somewhat similar to that of the Foisey property but the sulphide mineralogy is different. Quartz veins and blebs, as much as 5 m in thickness are very numerous in this locality and they are within an igneous rock (micropegmatite ?) that is below the basal breccia of the Onaping Formation. At the Papineau shaft a 2.5 m wide quartz vein contains massive arsenopyrite and some pyrite. Mauve-coloured carbonate material contains chalcopyrite, malachite and azurite. Polished section examination reveals that over 90 percent of the sulphides consist of arsenopyrite and less than 10 percent is chalcopyrite. Chemical analyses of two specimens from the vein (W10-A and W10-B, Table 3) indicate relatively high Cu values, moderately high Au and Co values and traces of silver. Specimen W10-B gave the highest Au value of any specimen analyzed in the present study. A few tens of metres north of the shaft is a trench 65 m long and 3 m wide. Broken vein material contains arsenopyrite and a chemical analysis of this material (W11, Table 3) indicates relatively high Au, Co and Ba values.

The Moore Lake occurrence (Lot 4, Concession V, Creighton Township) consists of several quartz veins, approximately 10 cm in width, within the basal breccia of the Onaping Formation. Galena occurs in masses as much as 5 cm in width together with black sphalerite, pyrite, and minor chalcopyrite. The presence of these minerals was confirmed by polished section examination. A chemical analysis of a specimen from the vein (W52-2, Table 3) shows high Pb and Zn values and the highest Ag value of any chemically analyzed specimen in the study. The country rock contains considerable pyrite but a chemical analysis (W52-1, Table 3) indicates low metal values.

The Proulx property is located in the North Range (Lot 3, Concession I, Howell Township) and on the south shore of Nelson Lake (formerly Trout Lake). Burrows and Rickaby (1930) briefly described the occurrence. A shaft was sunk to a depth of at least 20 m and two quartz veins 1.5 and 2.4 m in thickness contain appreciable amounts of sphalerite, galena, and chalcopyrite. The country rock is the basal quartzite breccia of the Onaping Formation. At present there is no trace on the surface of the shaft or of quartz veins.

Table 3—Chemical analyses of specimens from quartz veins and host rocks.

Spec. No.	PPM								PPB	%
	Cu	Zn	Ni	Co	Pb	Ba	Cr	Ag	Au	Fe ₂ O ₃
W3-1A	160	85000	22	200	6750	464	59	7.6	60	4.6
W3-2	10	130	25	80	45	637	34	ND	ND	2.7
W7-1	15	85	27	30	10	1628	91	0.2	ND	4.9
W10-A	5000	0.5	6	160	25	77	18	1.7	860	2.5
W10-B	3000	0.8	40	580	80	125	29	3.4	2400	17.9
W11	150	ND	10	305	3	1477	4	0.4	820	3.8
W35-1	55	165	22	70	115	440	25	1.4	ND	8.9
W36-1	60	10	40	230	ND	46	31	7.3	1610	35.8
W37	10,000	2500	40	280	420	1	17	1.5	ND	0.9
W39-1	3	5	10	165	ND	6	16	ND	10	3.2
W39-2	2	55	50	37	5	341	22	0.6	30	5.9
W44-1	ND	25	15	87	310	221	17	0.7	ND	0.06
W44-2	ND	ND	32	155	ND	21	12	ND	ND	0.9
W44-3	2	5	55	45	2	739	131	ND	ND	6.1
W46	30	75	31	40	ND	395	66	ND	ND	2.1
W52-1	45	50	25	200	15	83	52	ND	ND	2.7
W52-2	50	19250	56	160	27250	70	37	264	ND	6.3
W60	20	150	132	120	10	1546	492	ND	ND	1.9
W61-1	160	10	36	62	15	213	96	ND	ND	7.7
W61-2	5	3	22	215	ND	59	15	ND	ND	0.01
W61-3	40	7	38	133	11	662	18	ND	ND	3.3
W61-4	40	95	54	68	15	19	9	ND	ND	9.3
W65	135	50	25	40	ND	62	10	0.7	ND	6.4

- Notes:
1. Total Fe as Fe₂O₃.
 2. ND - not detected.
 3. W3-2 - igneous rock; W35-1, W39-2, W46, W61-1, and W65 - mafic sill; and W52-1 Onaping Fm
 4. Location of specimens shown on Figure 1 (W omitted for brevity).

GOLD-BEARING QUARTZ VEINS

The Gordon Lake and Creighton "gold mines", apparently abandoned around the turn of the century, occur in the southwestern portion of the basin (Figure 1). Both are briefly described by Blue (1893).

The Gordon Lake Mine is located in Lot 2, Concession IV, Fairbank Township; a prominent outcrop of quartz-rich rock on the west side of the Gordon Lake Road is presumably the site of the "mine". The quartz-rich rock is penetrated by a 10 m long adit and there is a 22 m long trench. The rock is pale pink, medium grained, and contains numerous quartz veins and blebs as much as 30 cm wide. The quartz-rich unit is approximately 12 m in thickness, dips steeply to the southeast, and is internally folded. In thin section the pink quartz rock consists of strained quartz grains, together with some plagioclase grains, in a fine grained mosaic of recrystallized quartz. Locally the quartz is highly fractured. Pyrite and limonite are abundant. A light green rock consisting of carbonate, quartz, and chlorite occurs beneath the quartz-rich unit. The writer tentatively interprets the quartz rock as a quartzite fragment from the basal breccia of the Onaping Formation that has been emplaced in its present position in the Onaping Formation by faulting. Chemical analyses of

three specimens from the property (W44-1, W44-2, W44-3, Table 3) indicate no Au nor significant amounts of any other metal.

The Creighton Mine is located in Lot 11, Concession V, Creighton Township. During the time of operation gold values* were apparently between \$4 and \$20 per ton of ore (Blue 1893). An abandoned shaft (surface dimensions 5.5 m by 3 m) is located on the property and there is a large dump. Quartz vein material extends over a width of 12 m with as much as 4 m of continuous exposure. The vein was traced for 100 m along strike until it disappears into a swamp. The country rock, the Onaping breccia, contains some disseminated sulphides and the quartz vein contains some pyrite and limonite. Table 3 gives a chemical analysis of the country rock (W61-1) and analyses of three specimens of the quartz veins (W61-2, W61-3, and W61-4). No Au was detected and the values of the other metals are low. Similar results were obtained from a specimen from a quartz vein near the Creighton Mine (W60).

*In 1893 the price of gold was \$20 per ounce.

Table 4—Published trace element analyses of the Whitewater Group and of "average" rocks.

	PPM								PPB
	Cu	Zn	Ni	Co	Pb	Ba	Cr	Ag	Au
Onaping ¹	58	376	106	60	16	—	447	10	—
Onwatin ²	230	1917	133	49	53	778	225	17	—
Vermilion ³	10313	34590	62	193	14259	215	68	71	—
Vermilion ⁴	34	390	62	30	111	248	70	11	—
Onaping ⁵	154	97	118	33	60	—	76	7	—
Transition ⁶	394	163	223	70	70	—	134	4	—
Onwatin ⁷	168	1320	144	55	62	—	129	2	—
Crust ⁸	50	70	75	22	12.5	500	100	.07	30
Granite ⁸	12	50	0.8	3	20	700	20	.04	20
Basalt ⁸	100	100	150	48	3.5	300	200	0.1	40
Shale ⁸	50	90	80	20	20	600	100	0.6	30

Notes:

1. Average of 7 samples from two DDH's located in the central portion of the South Range (Arengi 1977).
2. Average of 6 samples from three DDH's - two located as in note 1 and one from the North Range - immediately east of locality 35, Figure 1 (from Arengi 1977).
3. Average of 4 samples from Vermilion mine dump (Arengi 1977).
4. Average of 4 samples from two DDH's as in note 1 (Arengi 1977).
5. Average of 7 samples from four DDH's and three outcrops - 6 samples from the northeastern portion of the South Range and one from the East Range (Sadler 1958).
6. Onaping-Onwatin transition zone. Average of 5 samples from three DDH's in northeastern part of the South Range (Sadler 1958).
7. Average of 11 samples from several DDH's and outcrops - North and South Range (Sadler 1958).
8. Average abundance of trace elements (Krauskopf 1979).

SULPHIDE-BEARING QUARTZ-CARBONATE VEINS IN A MAFIC SILL

A mafic sill as much as 30 m in thickness, and exposed at three localities over a length of 4 km, occurs at the Onwatin-Chelmsford Formations contact. The sill is located in Balfour Township in the North Range. The rocks are strongly altered but primary pyroxene is locally preserved. The sill is the locus of mineralized quartz-carbonate veins and these have been explored by numerous pits and trenches. The veins are as thick as 1.7 m and are irregular, and vein material is commonly intimately mixed with the mafic rocks. The carbonate is buff-coloured, weathers to a chocolate brown, and is probably ankerite or siderite. Pyrite, commonly in the form of cubes, locally weathers to limonite and hematite. Arsenopyrite is a prominent mineral, occurs in local masses a few centimetres across, and as narrow veinlets in quartz and in the mafic rock. Chalcopyrite is locally present and weathers to malachite.

Table 3 sets out chemical analyses of three specimens of the mafic rock and three specimens of the quartz-carbonate veins. The specimens of the mafic rock (W35-1, W39-2, and W65) all contain disseminated pyrite

but none have appreciable metal values; W39-2 contains traces of Au. Specimen W36-1 is from a vein with massive arsenopyrite and contains appreciable Au, a high Fe₂O₃ content, and some Co and Ag. Specimen W37 is from a vein with visible chalcopyrite and displays high Cu and Zn values and a modest Pb content. Specimen W39-1 apparently represents a barren vein.

ANTHRAXOLITE VEINS

An anthraxolite vein occurs in the Onwatin Formation in Lot 10, Concession I, Balfour Township. The anthraxolite is a black, dense, platy material and contains considerable pyrite and some quartz. The anthraxolite consists of approximately 95 percent carbon (Burrows and Rickaby 1930). The vein was explored by an inclined shaft 30 m in length and two smaller inclined shafts. The deposit generated considerable local interest before the turn of the century as it was thought the material could be used as a fuel. However, it proved unsuitable due to the high ash content. Another similar anthraxolite vein, not located on any published map nor reported in the literature, occurs in Lot 5, Concession VI, Fairbank Township (see Figure 1, Locality 48).

ORIGIN OF MINERALIZATION

Theories as to the origin of the mineralization of the White-water Group are limited to brief suggestions regarding the Vermilion-Errington deposits. The mineralization must be considered in terms of the origin of the Sudbury Basin.

The disseminated sulphides in the Onaping Formation resemble the Ni-Cu ores at Sudbury in that pyrrhotite is the dominant sulphide mineral but differ in the lack of pentlandite. Consequently the relationship between the disseminated sulphides and these ores is uncertain. If the basin is of volcanic origin, then sulphide-rich rocks must have been present prior to their incorporation into the Onaping Formation. If the basin was formed by meteorite impact then sulphide-rock pods presumably occurred at depth (Pattison 1979). These sulphides were brecciated and became part of the fall-back breccia.

Martin (1957) suggested that the Vermilion-Errington deposits might be the result of hot-spring activity during a late phase of Onaping volcanism. Card and Hutchinson (1972) elaborated on this concept and considered the deposits in terms of regional volcanic-tectonic cycles. The Onaping Formation is regarded as a product of explosive volcanism during a second cycle. During the later phases of this cycle two metal- and sulphur-rich phases supposedly formed: a melt which differentiated at depth to form the Nickel Irruptive and the Ni-Cu ores outside the basin, and a volatile phase which escaped to the surface to form the Vermilion-Errington deposits inside the basin. The writer suggests that the host rocks of the Vermilion-Errington deposits may represent local carbonate banks that were produced by chemical or biochemical precipitation. The ore minerals may have been precipitated at the same time as the host rocks or they may be due to diagenetic processes.

The Onwatin Formation is rich in carbonaceous material that is probably of organic origin. Metamorphism has locally remobilized and concentrated this material in the form of anthraxolite veins. Arengi (1977) examined this material under the scanning electron microscope and found elongate, segmented structures which resemble modern and fossil algal filaments. The formation may have been deposited in a deep basin with bottom waters that were stagnant and anoxygenic, with a benthonic population of anaerobic bacteria, and with a floating algal mat. It is suggested that the pyrite grains and lenses formed under these conditions.

The Onaping-Onwatin transition zone and the basal argillite unit of the Onwatin Formation may represent a metal-rich horizon possibly similar to such ore-bearing shales as the Kupferschiefer (Jung and Knitzschke 1976), those of the Zambian (Fleischer *et al.* 1976) and White Pine (Brown 1971) copper deposits, and the shale-hosted lead-zinc deposits of the Rocky Mountain belt (Blusson 1976). Exposures of this horizon, however, are limited to a few scattered outcrops in a zone extending from the Errington No. 3 shaft southwesterly to Vermilion Lake (see maps in Thomson 1956 and Burrows and Rickaby 1930).

The Onaping rocks of the South Range are charac-

terized by a tectonic foliation and numerous quartz veins whereas those of the North Range are undeformed and quartz veins are scarce. The strike of the quartz veins in the South Range is parallel to the strike of the tectonic foliation and the veins are not geometrically related to a prominent northwesterly trending joint set (Rousell and Everitt, in press). Accordingly, the veins were likely emplaced during the major deformation of the basin (~ 1.7 Ga) rather than during a later episode of brittle deformation.

The exact time of emplacement of the mineralized mafic sill and the enclosed quartz-carbonate veins is not known. A similar mafic sill occurs in the Onwatin Formation south of the Chelmsford outcrop belt (Burrows and Rickaby 1930). Cleavage in the Onwatin Formation passes into sill rocks suggesting this sill was emplaced before or during basin deformation.

ACKNOWLEDGMENTS

D.G. Innes, consulting geologist, drew my attention to several of the mineral occurrences. Field and laboratory assistance was provided by L. Dupuis, O. Kehinde-Phillips, E. Ludwig and V. Smith of Laurentian University. Susan Cunningham typed the manuscript.

REFERENCES

- Arengi, J.T.
1977: Sedimentary evolution of the Sudbury Basin; unpublished M.Sc. thesis, University of Toronto, 141p.
- Blue, A.
1893: The Creighton gold mine; Third Annual Report of the Ontario Bureau of Mines, p.45-47.
- Blusson, S.L.
1976: Selwyn Basin, Yukon and Districts of Mackenzie; Geological Survey of Canada, Paper 76-1A, Report of Activities Part A, p.131-132.
- Brocum, S.J. and Dalziel, I.W.D.
1974: The Sudbury Basin, the Southern Province, and the Penokean Orogeny; Geological Society of America, Bulletin, Vol.85, p.1571-1580.
- Brown, A.C.
1971: Zoning in the White Pine copper deposit, Ontonagon County, Michigan; Economic Geology, Vol.66, p.543-573.
- Burrows, A.G. and Rickaby, H.C.
1930: Sudbury Basin area; Ontario Department of Mines, Vol.38, Part 3, 55p.
- Card, K.D. and Hutchinson, R.W.
1972: The Sudbury structure: its regional geological setting; p.67-78 in *New Developments in Sudbury Geology*, J.V. Guy-Bray, editor, Geological Association of Canada, Special Paper 10.
- Desborough, G.A. and Larson, R.R.
1970: Nickel-bearing iron sulphides in the Onaping Formation, Sudbury Basin, Ontario; Economic Geology, Vol.65, p.728-730.
- Dietz, R.S.
1962: Sudbury structure as an astrobleme; Abstract, Transactions of the American Geophysical Union, Vol.42, p.445-446.

GRANT 96 MINERALIZATION IN THE WHITEWATER GROUP

- Fleischer, V.D., Garlick, W.G. and Haldane, R.
1976: Geology of the Zambian Copper Belt; p.223-350 in Handbook of Stratabound and Stratiform Ore Deposits. Vol. 6, K.H Wolf, editor, Elsevier.
- Gibbins, W.A. and McNutt, R.H.
1975a: The age of the Sudbury Nickel Irruptive and the Murray Granite; Canadian Journal of Earth Science, Vol.12, p.1970-1989.
1975b: Rubidium-strontium mineral ages and polymetamorphism at Sudbury, Ontario; Canadian Journal of Earth Sciences, Vol.12, p.1990-2003.
- GSC
1960: Aeromagnetic Map 706G; Geological Survey of Canada.
Hawley, J.E.
1962: The Sudbury ores: their mineralogy and origin; The Canadian Mineralogist, Vol.7, part 1, 207p.
- Jung, W. and Knitzschke, G.
1976: Kupferschiefer in the German Democratic Republic (GDR) with special reference to the Kupferschiefer deposit in the southeastern Harz foreland; p.353-402 in Handbook of Stratabound and Stratiform Ore Deposits, Vol. 6, K.H. Wolf, editor. Elsevier.
- Krauskopf, K.B.
1979: Introduction to Geochemistry; McGraw-Hill, 617p.
- Martin, W.G.
1957: Errington and Vermilion Lake Mines; p.363-376 in Structural Geology of Canadian Ore Deposits, Vol. 2., 6th Commonwealth Mining and Metallurgical Congress.
- Pattison, E.F.
1979: The Sudbury Sublayer; Canadian Mineralogist, Vol.17, p.257-274.
- Peredery, W.V.
1972: Chemistry of fluidal glasses and melt bodies in the Onaping Formation; p. 49-59 in New Developments in Sudbury Geology, J.V. Guy-Bray, editor, Geological Association of Canada, Special Paper 10.
Peredery, W.V. and Naldrett, A.J.
1975: Petrology of the upper irruptive rocks, Sudbury, Ontario; Economic Geology, Vol.70, p.164-175.
- Rousell, D.H.
1972: The Chelmsford Formation of the Sudbury Basin — a Precambrian turbidite: p. 79-91 in New Developments in Sudbury Geology, J.V. Guy-Bray, editor, Geological Association of Canada, Special Paper 10.
1975: The origin of foliation and lineation in the Onaping Formation and the deformation of the Sudbury Basin; Canadian Journal of Earth Sciences, Vol.12, p.1379-1395.
- Rousell, D.H. and Everitt, R.A.
In press: Jointing in the Sudbury Basin, Ontario; in Proceedings of the Third International Conference on Basement Tectonics, D.W. O'Leary, editor.
- Sadler, J.F.
1958: A detailed study of the Onwatin Formation; unpublished M.Sc. thesis, Queen's University, Kingston, 184p.
- Souch, B.E., Podolsky, T. and Geological Staff.
1969: The sulphide ores of Sudbury: their particular relationship to a distinctive inclusion-bearing facies of the Nickel Irruptive; p. 252-261 in Magmatic Ore Deposits, H.D.B. Wilson, editor, Economic Geology Monograph 4.
- Stevenson, J.S.
1963: The upper contact phase of the Sudbury micropegmatite; Canadian Mineralogist, Vol.7, p.413-419.
- Thomson, J.E.
1956: Geology of the Sudbury Basin; Ontario Department of Mines, Vol.65, Part 3, p.1-56.

Grant 88 Metallogeny and Economic Potential of the Western Lake St. Joseph Metavolcanic-Metasedimentary Belt

R.J. Shegelski

Department of Geology, Lakehead University

ABSTRACT

The western Lake St. Joseph metavolcanic-metasedimentary belt contains three lithostratigraphic formations which are defined by transitions from mafic volcanism to felsic volcanic-epiclastic deposition. The formations in ascending order are the Blackstone Formation, the Western Lake St. Joseph Formation, and the Carling Formation, and they collectively form the Lake St. Joseph Group. The Carling Formation is the most diverse and is subdivided into a mafic-felsic volcanic member and an epiclastic member. Sulphide mineralization is locally concentrated at the contact between mafic and felsic rocks of the volcanic member. The felsic fragmental rock acts as host and here silicified clasts are set in a matrix of chlorite, garnet, and iron sulphides. Geochemical analyses on the mineralized samples and the surrounding rocks revealed no anomalous patterns of major element or trace element concentrations. The internal organization of the felsic fragmental host rocks suggests that they are distal flank or reworked deposits. The sulphide mineralization is therefore not likely to be related to hydrothermal fumaroles but instead may represent epigenetic deposition from laterally migrating fluids along a permeable horizon. The epiclastic member of the Carling Formation is an upward-fining classical turbidite sequence, which is capped by an Algoma-type laminated iron formation. This sequence is overlain by massive to crossbedded arkosic greywacke and graded-stratified rudite which are interpreted as facies of a prograding submarine fan. The laminated iron formation has been metamorphosed to quartz-hematite-magnetite schist, and has been sufficiently concentrated by syngenetic deposition and tectonic thickening to form a potentially economic oxide facies iron deposit.

INTRODUCTION

The Lake St. Joseph metavolcanic-metasedimentary belt occurs along the southern margin of the Uchi Subprovince in the Canadian Shield. Recent lithostratigraphic subdivision of this belt (Berger 1981) is based on cyclic volcanism in which mafic volcanic bases and felsic volcanic-epiclastic tops define formations. The lower Blackstone Formation and the overlying Western Lake St. Joseph Formation do not appear to contain significant

concentrations of sulphide or oxide mineralization. The overlying Carling Formation is diverse and contains a volcanic member and an epiclastic member. The volcanic member consists of tholeiitic basalts overlain by felsic volcanoclastic rocks which locally host iron sulphide mineralization. The epiclastic member contains sedimentary rocks of submarine fan and turbidite association which host oxide facies laminated iron formation (LIF).

The objective of the research project was to describe and attempt to explain the processes by which mineralization took place. In the case of the sulphide mineralization, a geochemical programme was initiated to determine whether the sulphide showings might be related to processes which form volcanogenic Cu-Zn massive sulphide deposits. The diverse Carling Formation was considered most favourable for massive sulphide deposits because, in comparison to the threefold stratigraphic subdivision of the Uchi-Confederation Lakes metavolcanic-metasedimentary belt (Nunes and Thurston 1980), this formation is the most likely stratigraphic equivalent to the mineralized cycle III quartz-feldspar porphyry dome of the Uchi-Confederation belt.

The association of LIF deposits with submarine fans and turbidites has been documented in other metavolcanic-metasedimentary belts (Dunbar and McCall 1971; Shegelski 1978) and those at Lake St. Joseph have recently been described by Meyn and Palonen (1980). The present study has utilized detailed mapping in the vicinity of Eagle Island (Figure 1) to refine interpretation of stratigraphic succession and depositional environment.

The sulphide showings are located on the northeast shore of western Lake St. Joseph (Figure 1) at the contact between pillow basalts and overlying felsic volcanoclastic rocks. A layered mafic sill has intruded the footwall basalts close to the contact. A small area (Figures 1,2) was sampled in detail in order to detect any footwall alteration to the sulphide showings. Whole rock and trace element analyses were used to scrutinize for depletion of Na₂O or CaO or enrichment in MgO, FeO or SiO₂. Trace element abundances of base metals were examined for anomalous patterns and immobile elements were determined in order to discriminate rock types.

GEOLOGICAL BACKGROUND

The Lake St. Joseph area has previously been mapped

by Bruce (1923) and Clifford (1969). The stratigraphy and geochemistry of the volcanic rocks in the area were discussed by Clifford and McNutt (1970), and regional studies by Breaks and Bond (1976) and Thurston and Breaks (1978) covered this area. At the time of the present study, a detailed stratigraphic investigation of the western end of Eagle Island was completed and results were in press (Meyn and Palonen 1980). A M.Sc. thesis on the stratigraphy of western Lake St. Joseph (Berger 1981) has recently been completed and provides the framework for the present study.

RESULTS

SEDIMENTARY MEMBER, EAGLE ISLAND

Detailed mapping on Eagle Island indicates that the sedimentary member of the Carling Formation accumulated in a deep submarine basin as basin plain turbidites which

were overlain by submarine fan facies. The basin plain turbidites form a series of thinning-upward, fining-upward cycles which are defined by an upward gradation from classical turbidite sequences through interlayered pelagic mudrock (pelagite) and LIF (Figure 3) into solely chemical LIF deposits. The uppermost fining-upward cycle is capped by an abnormally thick layer of LIF which has been further thickened tectonically in fold closures on Eagle Island and forms a potentially economic iron oxide deposit. This deposit is overlain by a sequence of classical turbidites which coarsen upwards. The turbidites are overlain by massive to crossbedded arkosic greywacke followed by graded-stratified pebbly sandstone and conglomerate typical of submarine fans (Walker 1979). The sedimentary member is therefore interpreted to have formed on the edge of a submarine basin near to a volcanic flank. Accumulation of turbidites and chemical sediments ceased when this area was covered by a prograding submarine fan.

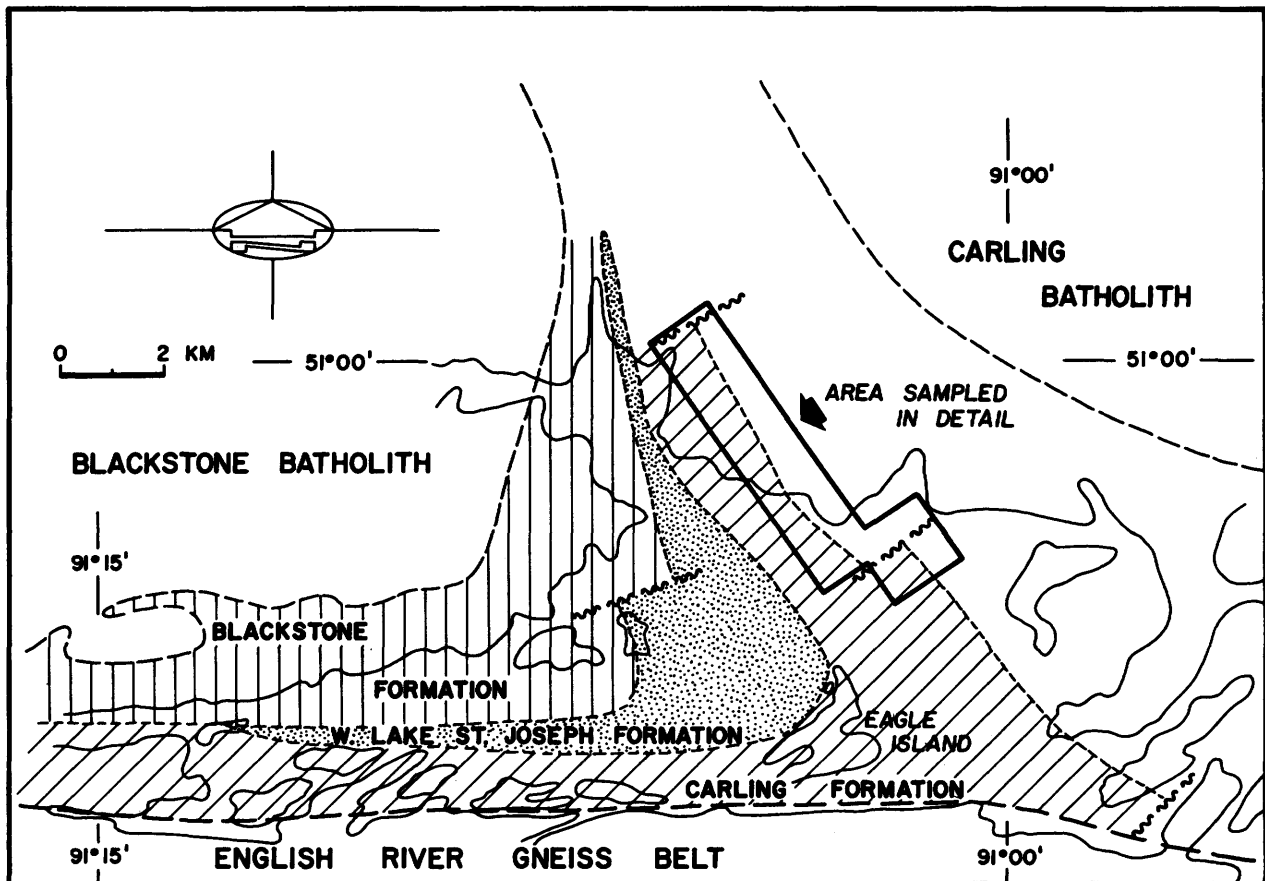


Figure 1—Stratigraphic subdivision (after Berger 1981) of western Lake St. Joseph area. Areas studied in detail include Eagle Island (Carling sedimentary member) and the northeast shore (Carling volcanic member).

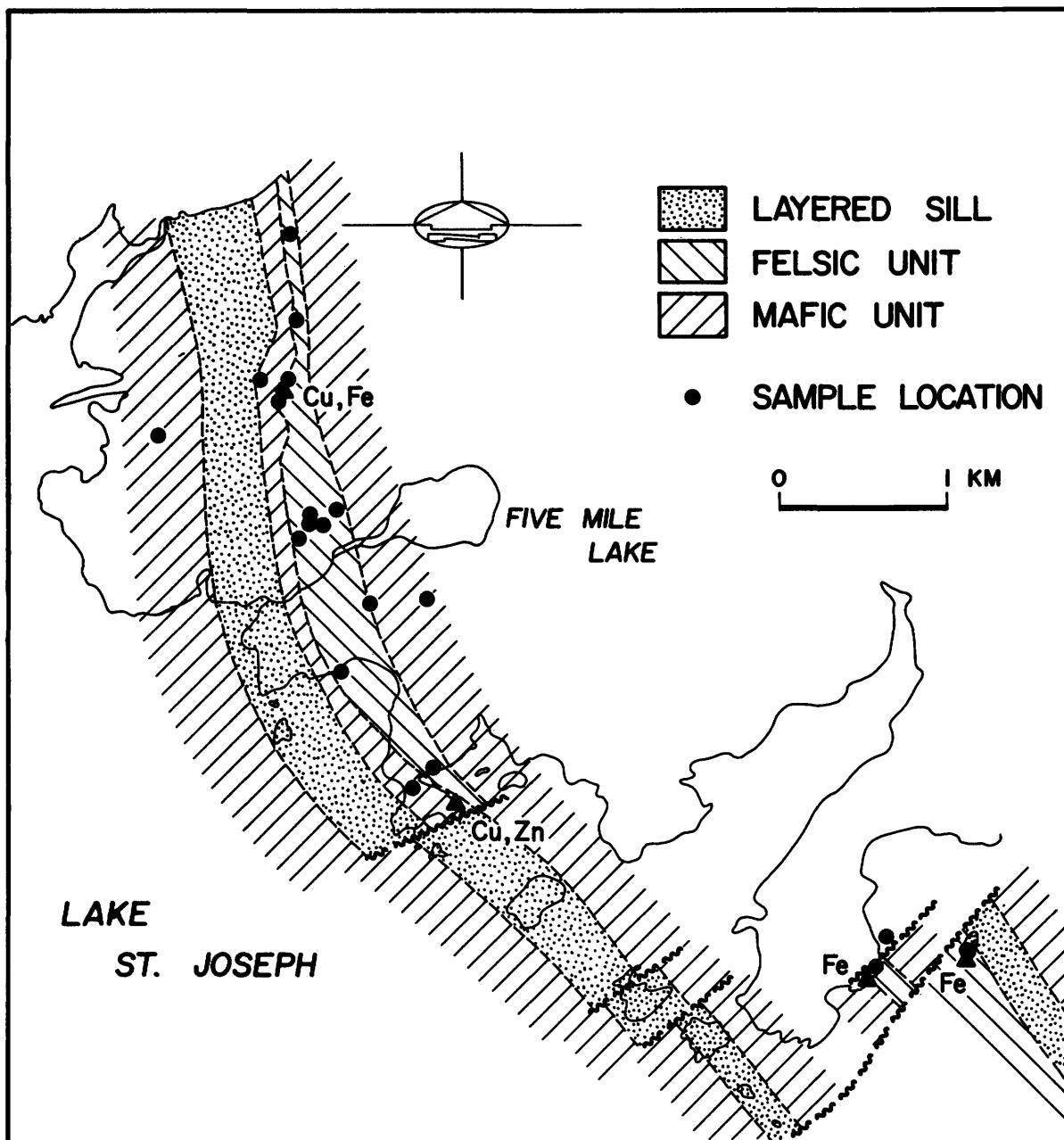


Figure 2—Geology of the Carling volcanic member, northeast shore, with locations of sulphide showings (triangles) and areas of detailed sampling.

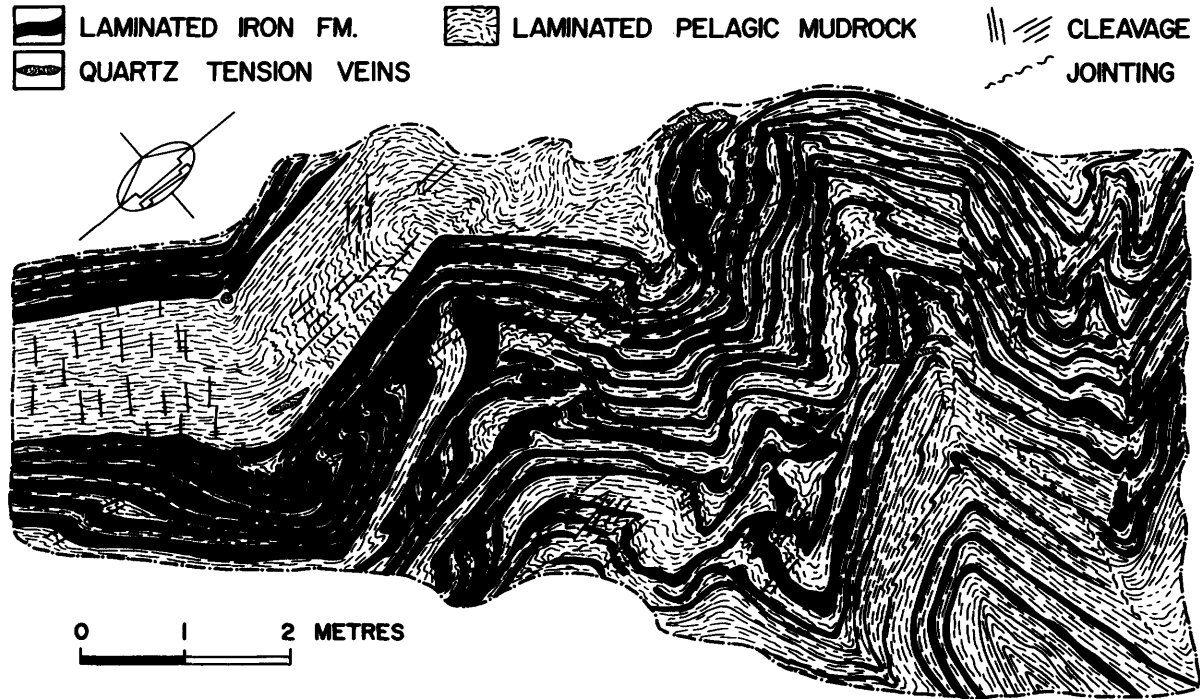


Figure 3—Detailed map of interlayered pelagic mudrock and laminated iron formation from Eagle Island.

VOLCANIC MEMBER, NORTHEAST SHORE

Detailed sampling and geochemical analyses of the volcanic member of the Carling Formation on the northeast shore of western Lake St. Joseph have outlined six separate lithologic populations including: basalt, polymict pyroclastic-epiclastic rocks, felsic tuff, felsic volcanic clastic or flow rocks, an enigmatic felsic feldspar porphyry, and sulphide-rich samples.

The basalts are similar in composition to enriched Archean tholeiites (Condie 1976) and fall within the tholeiitic field on the AFM plot (Figure 4). They discriminate into the low-K field on a Ti-Y-Zr plot (Figure 5) and generally fall into the high-Fe tholeiite field on the Jensen cation plot.

Polymict volcanoclastic rocks and polymict matrices to breccias have variable compositions which are intermediate between the basalts and the felsic volcanic flows, clasts and tuffs (Table 1). The intermediate compositions could have formed by mechanical mixing of basaltic and felsic fragments during reworking and resedimentation of volcanic debris from the volcanic flanks. The intermediate position of epiclastic rocks on the AFM plot (see Figure 4) is compatible with a process of mechanical mixing. The intermediate compositions reported by Clifford and McNutt (1970) might also be products of this same process because field relationships suggest that the majority of fragmental rocks in the Lake St. Joseph

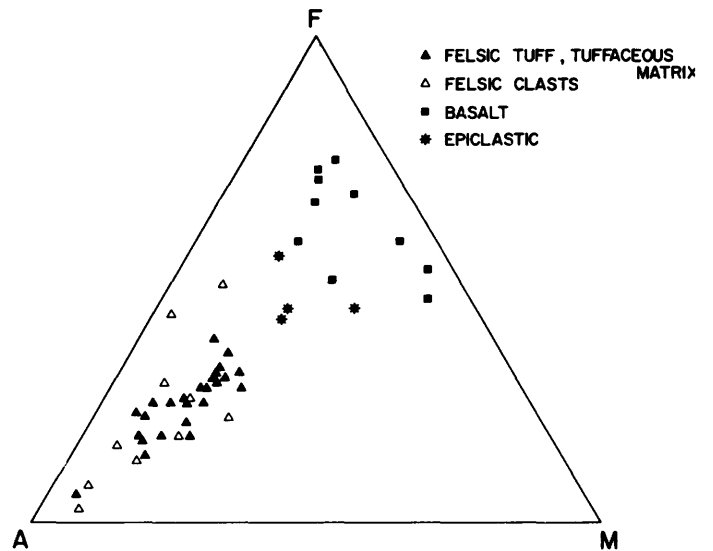


Figure 4—AFM plot of volcanic and epiclastic rocks from the Carling Formation. A = $Na_2 + K_2O$; F = $FeO + Fe_2O_3 + 0.9 TiO_2$; M = MgO (all weight percent).

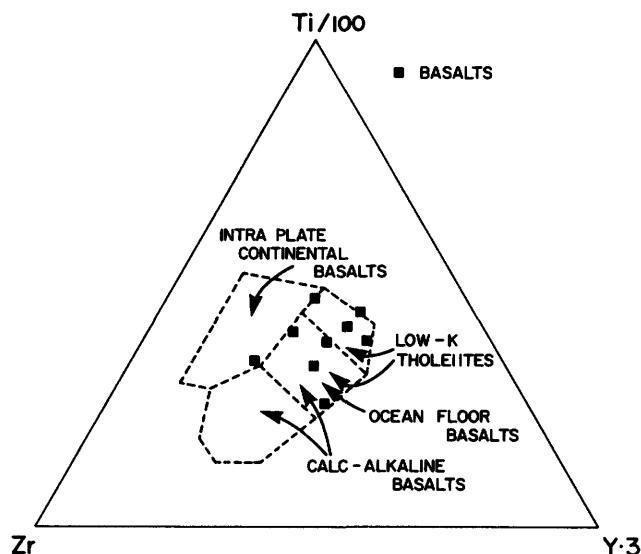


Figure 5—Ti-Zr-Y plot of basalts from the Carling Formation.

area have been resedimented. In addition, analyses from the present study and analyses from the three formations at western Lake St. Joseph (Berger 1981) show a distinct compositional bimodal distribution for the volcanic rocks.

The presence of size gradation over a 30 m thickness and local planar lamination and compositional layering (not bedding) in the felsic fragmental rocks of the Carling Formation suggests that these rocks are subaqueous pyroclastic flow deposits (Lajoie 1979) and/or resedimented pyroclastic debris. The felsic volcanic flows, clasts and tuffs (Table 1) are compositionally similar to Archean rhyodacites and are comparable to the depleted siliceous volcanic rocks of Condie (1976). The absence of unsorted vent-facies breccias, the paucity of flows and the apparent absence of quartz-feldspar porphyry domes indicate that these rhyodacites are distal from their source. Therefore there is less chance of finding localized heat sources and highly porous host rocks in which Cu-Zn massive sulphide deposits could have been generated.

Histograms of trace element analyses for Ni, Co, Cu, Zn and Mn in basalts, felsic tuffs, felsic clasts and sulphide rich samples are presented in Figures 6 to 10. Other elements (Ag, Pb, As) were analysed for but were found to occur only in very low concentrations. Both major element and trace element analyses do not indicate any abnormal compositions in these samples, such as might be expected if alteration zones were present. Even those samples which contained iron sulphides did not show abnormally high contents of Cu or Zn, and the chalcopyrite and sphalerite which occur with iron sulphides in veins in footwall pillow basalts are considered to be highly localized.

Five samples of felsic feldspar porphyry come from two separate areas which are near the contact of the lay-

ered sill (see Figure 2). Although the total alkali content is similar to that of the felsic volcanic rocks, these feldspar porphyries are depleted in K_2O , depleted to a lesser extent in CaO and markedly enriched in Na_2O in comparison. The porphyritic to fragmental textures of these samples resemble those of the felsic volcanic rocks. Furthermore, only the alkalis and trace elements Rb and Sr differ from those of the felsic volcanic rocks, thereby suggesting that albitization of feldspars in the felsic volcanic rocks has occurred near to the layered sill. This abnormal chemistry is therefore more likely associated with metasomatism in the thermal aureole of the layered sill rather than being a result of hydrothermal alteration.

DISCUSSION

SEDIMENTARY MEMBER, EAGLE ISLAND

The laminated oxide iron formations (LIF) at western Lake St. Joseph are typical of Algoma-type, turbidite-hosted deposits. They are formed by background chemical precipitation in a deep turbidite basin (Shegelski 1978) and are normally uneconomic in the natural state because clastic influx of turbidites causes dilution and lowers the iron content. In the case of the Eagle Island deposit, there was a sufficient lull in clastic sedimentation to allow the deposition of several tens of metres of chemical sediment. Subsequent isoclinal folding and local tectonic thickening at fold closures has produced thicknesses of LIF up to 600-700 m. The present attitude of bedding and lineation is subvertical suggesting that these thicknesses of LIF persist to depth. If an open pit operation becomes feasible on Eagle Island, tonnage limitation would be controlled in large part by the depth to which the iron formation could be mined.

VOLCANIC MEMBER, NORTHEAST SHORE

Iron sulphides in the volcanic member of the Carling Formation occur as isolated stringers in the footwall pillow basalts and as more substantial concentrations up to 30 m thick but averaging 3 m thick at the contact between pillow basalts and overlying felsic volcanic rocks. The sulphides are pyrrhotite, pyrite and minor sphalerite and chalcopyrite and, in showings at the mafic-felsic contact, they occur along with the chlorite and garnet as a matrix to silicified felsic clasts. These sulphide showings differ from volcanogenic massive sulphide deposits in several respects: they are stratabound rather than stratiform, they were likely deposited below rather than at the seawater-host rock interface, they may have formed by fluids which were migrating laterally (rather than vertically) along the contact between relatively impermeable pillow basalts and highly porous felsic fragmentals and therefore accumulated at the base of the felsic sequence rather than at the top, and finally, absence of any compositional layering or stratification in the mineralization suggests that the sulphides formed by an epigenetic cementation process which is perhaps related to the intrusion of the layered sill.

Table 1—Major and trace element abundances in whole-rock samples from the Carling Formation.

(Wt.%)	BASALTS (N=7)	(EAT)* ENRICHED ARCHEAN THOLEIITE	MAFIC MATRIX OF A BRECCIA	MAFIC CRYSTAL TUFF	POLYMICT LAPILLI TUFF	FELSIC TUFFS (N=24)	FELSIC CLASTS, FLOWS (N=10)	(DSV)* DEPLETED SILICEOUS VOLCANICS	FELSIC FELDSPAR PORPHYRY (N=5)
SiO ₂	45.2	49.7	51.6	54.0	57.4	67.6	69.9	66.2	68.3
Al ₂ O ₃	15.1	14.9	14.2	14.4	21.4	16.1	15.8	16.5	16.3
TiO ₂	0.9	1.0	0.4	0.4	0.4	0.3	0.3	0.3	0.5
FeO	12.4	8.8	10.2	9.9	3.3	1.8	1.3	1.0	1.4
Fe ₂ O ₃	3.7	2.6	4.9	0.8	1.2	0.8	0.8	0.9	0.3
MgO	5.7	6.3	2.8	3.2	2.3	1.4	0.9	1.6	1.4
MnO	0.6		0.2	0.3	0.1	0.05	0.05		0.05
CaO	9.4	9.4	3.9	5.4	5.9	3.8	3.1	3.9	2.6
Na ₂ O	1.8	2.1	2.4	4.0	5.3	4.3	4.1	5.2	7.6
K ₂ O	0.6	0.3	0.3	0.3	2.0	1.8	1.4	2.0	0.1
P ₂ O ₅	0.2		0.1	0.3	0.1	0.1	0.1		0.1
CO ₂	4.0		8.1	3.1	0.1	1.6	1.6		0.4
H ₂ O				3.0	0.6				0.4
Total	99.6		99.5	99.8	100.5	99.6	99.3		99.4
(ppm)									
Cu	28	110	17	13	115	44	38		48
Zn	122	100	107	67	94	70	46		41
Ni	158	100	86	36	88	55	42	25	50
Co	138	50	130	134	156	111	101	8	130
Ti	9370		4600	4600	4900	4230	3600		5500
Mn	1930		990	950	490	234	143		250
Rb	23	10	11	32	42	55	34	33	B.D.
Sr	124	165	247	395	277	269	395	600	69
Y	26	15	23	7	14	19	21	2	28
Zr	72	100	66	90	181	160	108	50	160
Nb	13		16	15	34	22	15		14

B.D. - below limit of detection.

* Condie (1976)

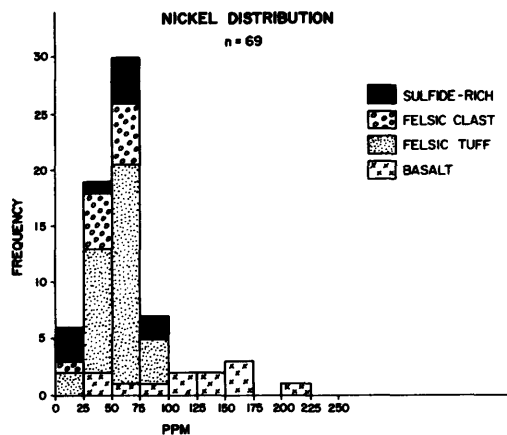


Figure 6—Histogram of nickel (ppm) in rocks from the Carling Formation, NE shore. Note: "Sulphide-Rich" samples are from mineralized felsic fragmental rocks near NE shore of western Lake St. Joseph; "Felsic Clast" samples are fragments from felsic volcanic clastic or flow rocks.

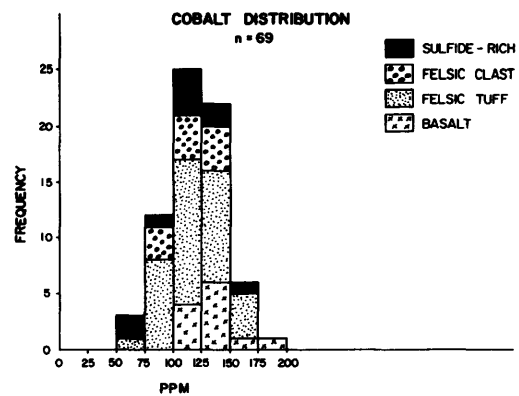


Figure 7—Histogram of cobalt (ppm) in rocks from the Carling Formation, northeast shore.

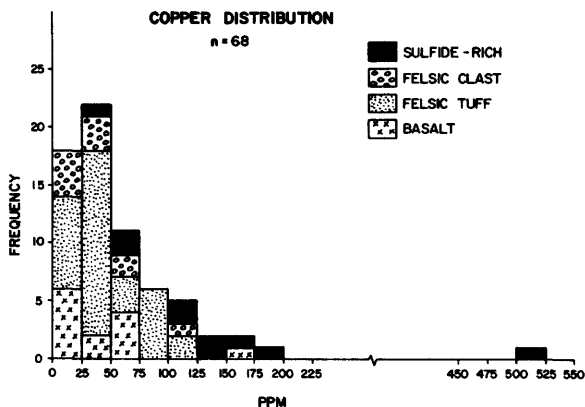


Figure 8—Histogram of copper (ppm) in rocks from the Carling Formation, northeast shore.

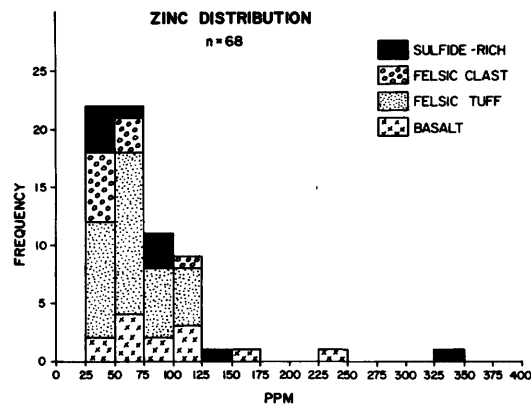


Figure 9—Histogram of zinc (ppm) in rocks from the Carling Formation, northeast shore.

CONCLUSIONS

Laminated oxide facies iron formations (LIF) at western Lake St. Joseph are interlayered with turbidite and submarine fan deposits. The LIF formed syngenetically from aqueous iron and silica species which continuously precipitated as a pelagic chemical sediment. Deposits of LIF are normally uneconomic in their natural state because they are diluted by turbidites. However, there was a sufficiently long period of increased chemical precipitation and/or an absence of clastic influx in the Lake St. Joseph area to accumulate an abnormally thick LIF deposit. This deposit has been subsequently upgraded by tectonic

thickening to form a potentially economic iron deposit on Eagle Island.

The sulphide showings on the northeast shore of western Lake St. Joseph occur in a potentially favourable stratigraphic horizon but they do not appear to be related to the types of hydrothermal systems which form volcanogenic massive sulphide deposits. Instead, they are localized, epigenetic, stratabound occurrences. These sulphides possibly formed by lateral migration of mineralizing solutions along the boundary between impermeable footwall pillow basalts and porous hanging wall felsic volcanic rocks. The source of the mineralizing solutions is unknown but may be related to the intrusion of a layered sill which underlies the mineralization.

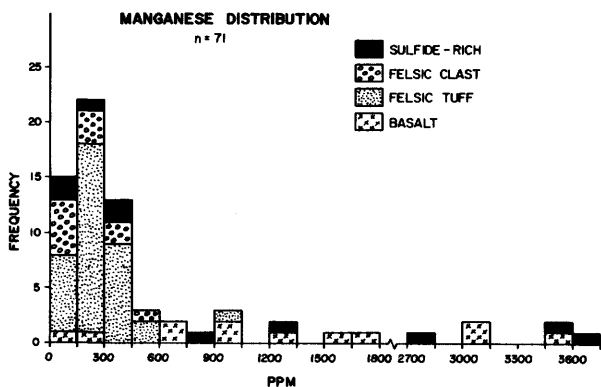


Figure 10—Histogram of manganese (ppm) in rocks from the Carling Formation, northeast shore.

ACKNOWLEDGMENTS

The author would like to thank B. Berger for his excellent field and laboratory assistance throughout this study. Special thanks is extended to J.V. Huddart of Algoma Steel Corporation, Limited for use of their facilities on Eagle Island. The technical assistance of support staff at Lakehead University is greatly appreciated.

This research was partially supported by National Research Council Grant A6108.

REFERENCES

- Berger, B.R.
1981: Stratigraphy of the Western Lake St. Joseph Greenstone Terrain, Northwestern Ontario; unpublished M.Sc. thesis, Lakehead University, 117p.

GRANT 88 METALLOGENY WESTERN LAKE ST. JOSEPH AREA

- Breaks, F.W. and Bond, W.D.
1976: Preliminary geological synthesis of the English River Subprovince, Northwestern Ontario and its bearing upon mineral exploration; Ontario Geological Survey Miscellaneous Paper, 72, 55p.
- Bruce, E.L.
1923: Iron formations of Lake St. Joseph; Ontario Department of Mines, Vol.31, p.1-32.
- Clifford, P.M.
1969: Geology of the Western Lake St. Joseph Area; Ontario Department of Mines, Geological Report 70, 61p.
- Clifford, P.M. and McNutt, R.H.
1970: Evolution of Mt. St. Joseph — an Archean Volcano; Canadian Journal Earth Sciences, Vol.8, p.150-161.
- Condie, K.C.
1976: Trace-element geochemistry of Archean greenstone belts; Earth-Science Reviews Vol.12, p.393-417.
- Dunbar, G.J. and McCall, G.J.H.
1971: Archean turbidites and banded ironstones of the Mt. Belches area (Western Australia); Sedimentary Geology, Vol.5, p.93-133.
- Lajoie, J.
1979: Facies Models 15, Volcaniclastic Rocks; Geoscience Canada. Vol.6, p.129-139.
- Meyn, H.D. and Palonen, P.A.
1980: Stratigraphy of an Archean Submarine Fan; Precambrian Research. Vol. 12, p.257-285.
- Nunes, P.D. and Thurston, P.C.
1980: Two hundred and twenty million years of Archean evolution: a zircon U-Pb age stratigraphic study of The Uchi-Confederation Lakes greenstone belt, northwestern Ontario; Canadian Journal of Earth Sciences. Vol.17, p.711-721.
- Shegelski, R.J.
1978: Stratigraphy and geochemistry of Archean iron formations in the Sturgeon Lake-Savant Lake greenstone terrain, Northwestern Ontario; unpublished Ph.D. thesis. University of Toronto, 251p.
- Thurston, P.C. and Breaks, F.W.
1978: Metamorphic and tectonic evolution of the Uchi-English River Subprovince; Geological Survey of Canada, Paper 78-10, p.49-62.
- Walker, R.G.
1979: Facies Models 8: Turbidites and associated coarse clastic deposits; p. 91-103, in Facies Models, R.G. Walker, Editor, Geoscience Canada Reprints, Series 1.

Grant 20 Magnetism and Stratigraphy in Volcanic and Sedimentary Rocks of the Abitibi Belt

D. W. Strangway, J. W. Geissman, J. Bambrick, S. Letros, and A. Tasillo

Departments of Physics and Geology, University of Toronto

ABSTRACT

Iron-rich and magnesium-rich tholeiitic basalts of the late Archean Kinojevis Group, central Abitibi Belt, Ontario, contain a natural remanent magnetization that is generally multivectorial. The magnetization components in all basalt units reside in pure magnetite, not the originally precipitated magnetic phases. Any original thermoremanent magnetism was lost by chemical reconstitution of the magnetic oxides in response to primary deuteric conditions, long-term burial regional metamorphism under prehnite-pumpellyite facies conditions, and possibly intrusion by Matachewan dikes. "Contact" tests on samples taken near the contacts with Matachewan dikes indicate that the flow units are indeed capable of retaining a very latest Archean or earliest Proterozoic field (e.g. $D = 194.9^\circ$, $I = -14.3^\circ$, $k = 8.1$, $\alpha_{95} = 7.9^\circ$; $n = 45$ vectors, 38 samples). Most high coercivity, high blocking temperature directions from samples from other flows, corrected for nearly penecontemporaneous downwarping, are in reasonable agreement with those of Matachewan dikes, allowing the conclusion that these components reflect a general late Archean or early Proterozoic field for the Superior Province.

Paleomagnetic studies (97 samples, 28 sites) on the calc-alkaline volcanic rocks of the Blake River Group, dated at 2703 ± 2 Ma, show both stable single- and multivectorial components of magnetization; however, there was found to be poor consistency of in situ magnetization directions linearly decaying to the origin in vector analysis. A test on the Chaput Hughes conglomerate member of the Timiskaming Group suggested the retention of a predepositional remanence. Cobbles derived from alkaline volcanic rocks of the Timiskaming Group and volcanic rocks of the Kinojevis and Blake River Groups have dispersed directions of magnetization. In situ magnetization directions of the matrix of the conglomerate are well grouped, and upon correction for tectonic deformation yield an antipodal pre-Matachewan dike direction. Paleomagnetic data for alkaline volcanic rocks of the Timiskaming Group and a Matachewan diabase dike from a down-faulted block suggest the fault block has been rotated clockwise and subsequently tilted to the west.

On the basis of their remanence properties, samples from the late Archean Ghost Range Complex (dated at 2710-2703 Ma), an east-trending, layered, mafic to ultramafic extrusive sequence in the central Abitibi Belt, can be divided into three groups. Group 1 samples contain a

high coercivity, high blocking temperature (greater than 520°C) magnetite-dominated remanence ($D = 260^\circ$, $I = -4^\circ$, $k = 8.9$, $\alpha_{95} = 6.0^\circ$, virtual geomagnetic pole = 1°E , 5°S), in good agreement with the albeit few previous results bearing on the late Archean apparent polar wander path for North America. Group 2 samples contain a low coercivity, low blocking temperature (less than 310°C), scattered remanence residing in pyrrhotite. Often, both remanences coexist in a single lithology at a given site. Group 3 samples contain distributed coercivity and blocking temperature remanences, again residing in magnetite, that are more scattered but statistically identical to the mean Group 1 direction. The Group 1 direction confirms that the Ghost Range Complex has remained essentially stable since emplacement.

High resolution aeromagnetic data from the Larder Lake-Kirkland Lake region have been analyzed to develop maps for geologic interpretation. Apparent susceptibility has been used to produce a map which shows clearly the major lithologies in a major synclinorium in the Abitibi "greenstone" belt. Calc-alkaline volcanic rocks of the Blake River Group are weakly magnetic, but show ring-like anomalies associated with intrusions where magnetite has been formed in the country rock. Alternating units of Mg-rich and Fe-rich tholeiitic basalts of the Kinojevis Group show a strong magnetization associated with the Fe-rich phases. Gabbroic intrusions underlain by serpentinite and peridotite give strong levels of magnetization. These various units have been sampled and it is shown that the susceptibility is not high enough to account for the anomalies. Rather, the anomalies are associated with the mean natural remanent magnetization in the formations sampled. These studies have led to a revised geological map of this region. Similar maps of the Timmins area have now been completed and will be available in a coloured version (J. Bambrick, Ph.D. thesis in prep., University of Toronto).

INTRODUCTION

Efforts to investigate the Archean geomagnetic field of the North American craton have largely concentrated on intrusive igneous bodies, e.g. dikes (Irving and Naldrett 1977; Ernst and Halls 1980; Schutts, 1980; Fahrig *et al.* 1965; Strangway 1964), stocks and batholiths (Dunlop and Buchan 1975, 1976; Dunlop 1980; Irving and Naldrett 1977) and sills and laccoliths (Bergh 1970; Ueno and Irving 1976; Irving and Naldrett 1977). These units

are relatively well dated and either have not been deformed subsequent to emplacement or have relatively simple tectonic histories, although it is difficult to prove this for batholiths (Beck 1980). In addition, properties of the natural remanent magnetization (NRM) of these lithologies suggest the presence of an initial thermoremanent magnetization (TRM). Compilation of apparent polar wander (APW) paths from these data for the Archean (e.g. Irving 1969) is therefore straightforward. While extrusive rocks comprise a significant portion of Archean terrains, they have been studied paleomagnetically only infrequently and those few studies that have been done have been largely unsuccessful in deciphering any totally consistent record (Halls 1975; Pesonen 1973; Schwarz 1966, 1977; D.J. Dunlop, Department of Physics, University of Toronto, personal communication).

Metavolcanics are of great interest because they contain critical information on the structural and metamorphic histories of Archean terrains, because they may shed light on paleo-ocean floor alteration and hydrothermal convection processes (Humphris and Thompson 1978; Seyfried and Bishoff 1973; Andrews 1979; Dimroth and Lichtblau 1979), and because they are genetically related to massive sulphide mineralization. Emplacement in the subaqueous environment and the related deuteri-

alteration may have resulted in a complex NRM in these units, even prior to effects associated with regional metamorphism or prolonged burial. We describe here the NRM and magnetic properties of metavolcanics and metasediments in the central Abitibi "greenstone" belt between Kirkland Lake and Lake Abitibi (Figure 1a). The low degree of deuteri alteration and dynamothermal metamorphism (Dimroth and Lichtblau 1979) and the near absence of later intrusive activity all, in theory, imply the retention of at least the high blocking temperature portion of a TRM. In turn, the relatively simple structural history of some of the stratigraphic units allows application of a TRM to define APW paths. In some instances, these units reliably record the geomagnetic field during emplacement.

GENERAL GEOLOGY

The study area (Figure 1a,b) is part of Goodwin and Ridler's (1970) "Noranda-Benoit volcanic complex", in the central Abitibi Belt. Briefly, the Ontario portion of the complex is composed of rocks representing at least three subalkaline volcanic cycles, each of which was assoc-

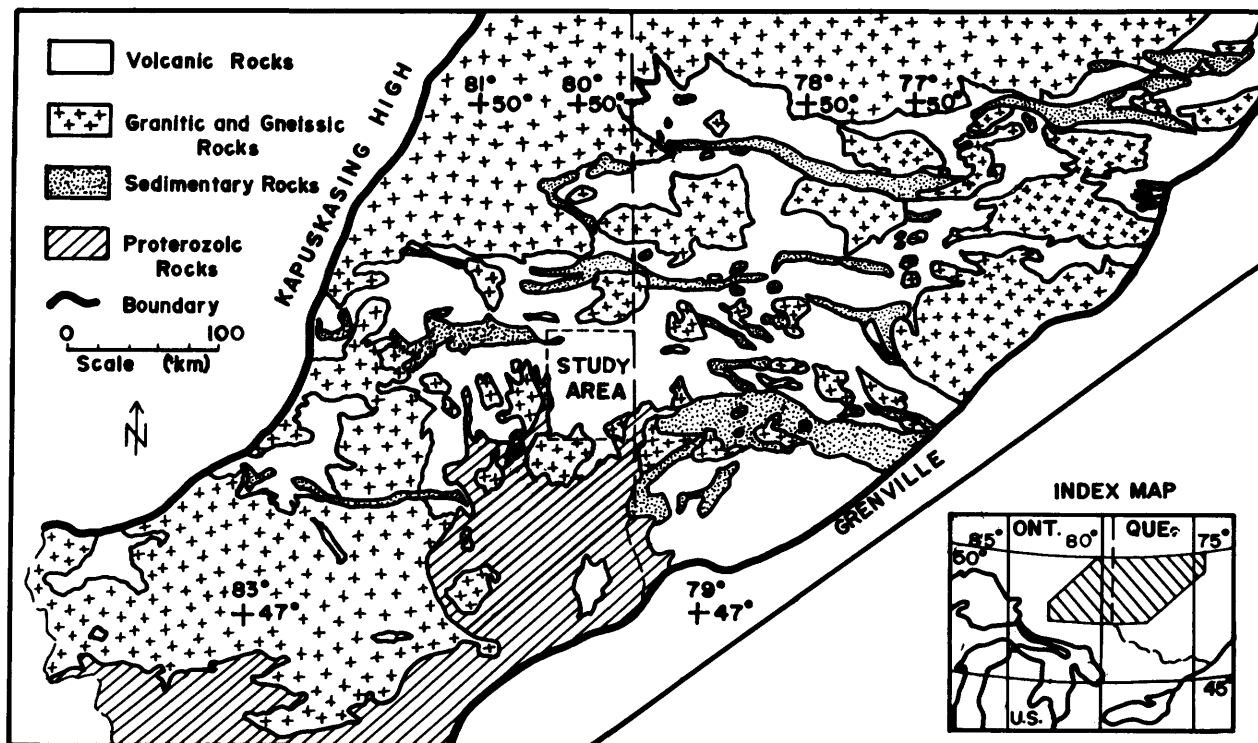


Figure 1a —Generalized geologic map of the central part of the Abitibi Belt.

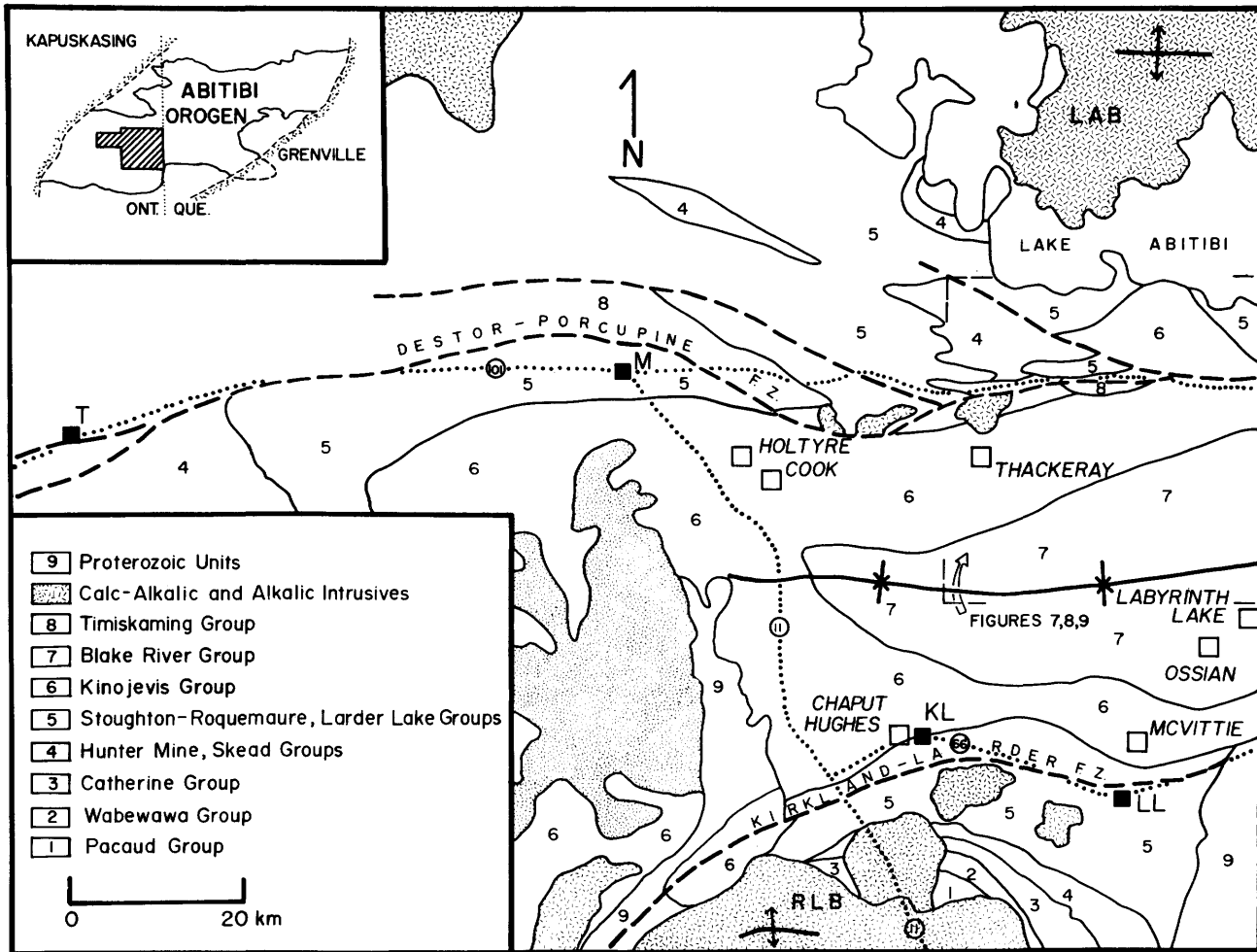


Figure 1b.—Areal distribution of stratigraphic units in the study area. Modified from Jensen (1979). LAB, Lake Abitibi Batholith; RLB, Round Lake Batholith; KL, Kirkland Lake; LL, Larder Lake; T, Timmins; M, Matheson.

iated with sedimentation and intrusion of comagmatic units (Jensen 1978a, 1981). The stratigraphic sequence is illustrated in Figure 2.

Remnants of the oldest volcanic cycle are preserved south of Kirkland Lake, where they were intruded by the Round Lake Batholith (RLB), and near Lake Abitibi.

At the base of the uppermost volcanic cycle, flows of ultramafic and basaltic komatiite are interlayered with calc-alkaline tuff and tuff-breccia, conglomerate, greywacke, argillite, chert and iron formation associated with the waning stages of the earlier volcanic cycle. The ultramafic and mafic members of this sequence, collectively termed the Stoughton-Roquemaure Group in the north and the Larder Lake Group in the south (Jensen 1979), become predominant upwards in the section. The petrology and geochemistry of these volcanic rocks and intrusive equivalents have been well described, particularly in Munro Township, their type locality (Pyke *et al.* 1973;

Arndt 1977). The Stoughton-Roquemaure Group is approximately 10 km in thickness and is conformably overlain by the Kinojevis Group which consists of a 10 km thick succession of alternating Mg- and Fe-rich tholeiitic basalts, with minor andesite, dacite and rhyolite. Tabular flows average about 65 m in thickness and are often traceable for several kilometres. Each flow typically consists of a basal zone of flattened glass shards (hyaloclastite) and spherulites, a central zone of coarse cumulate material overlain by granular basalt, and a flow top which is often highly vesiculated and shard-rich (Jensen 1978b; Jackson 1980). Glomeroporphyritic horizons rich in plagioclase phenocrysts are common at the top of Mg-rich Kinojevis flows. Individual flows either alternate between Fe- and Mg-rich compositions or occur in groups of several Fe- or Mg-rich units. Pearce and Birckett (1974) suggest, on petrologic and geochemical grounds, that each flow has experienced some degree of in situ differentia-

tion. Units of pillowed lava and pillowed breccia form the remaining 40 percent of the rocks. Both the Stoughton-Roquemaure Group and the Kinojevis Group are considered to represent melts derived from the mantle (Jensen 1981).

Stratigraphically above the Kinojevis lavas is the Blake River Group, consisting of 12 km of calc-alkaline volcanic rocks which occupy the centre of the regional Noranda-Benoit synclinorium (Figure 1b). The Blake River Group is believed to have been formed by the partial melting of ultramafic and mafic volcanic rocks belonging to the lower komatiitic and tholeiitic groups (Jensen 1981).

An alkaline volcanic cycle is preserved on both the south limb of the synclinorium, along the Kirkland Lake-Larder Lake Fault Zone and on the north limb, along the Destor-Porcupine Fault Zone (Figure 1b). In the south, approximately 3 km of fluvial sedimentary rocks and turbidites, trachytes and syenite stocks, collectively forming the Timiskaming Group, either are in fault contact with or unconformably overlie volcanic rocks of the uppermost subalkaline cycle.

North-trending Matachewan diabase dikes cut all units representing the volcanic cycles. However, the dikes, usually recognized by their aeromagnetic anomaly

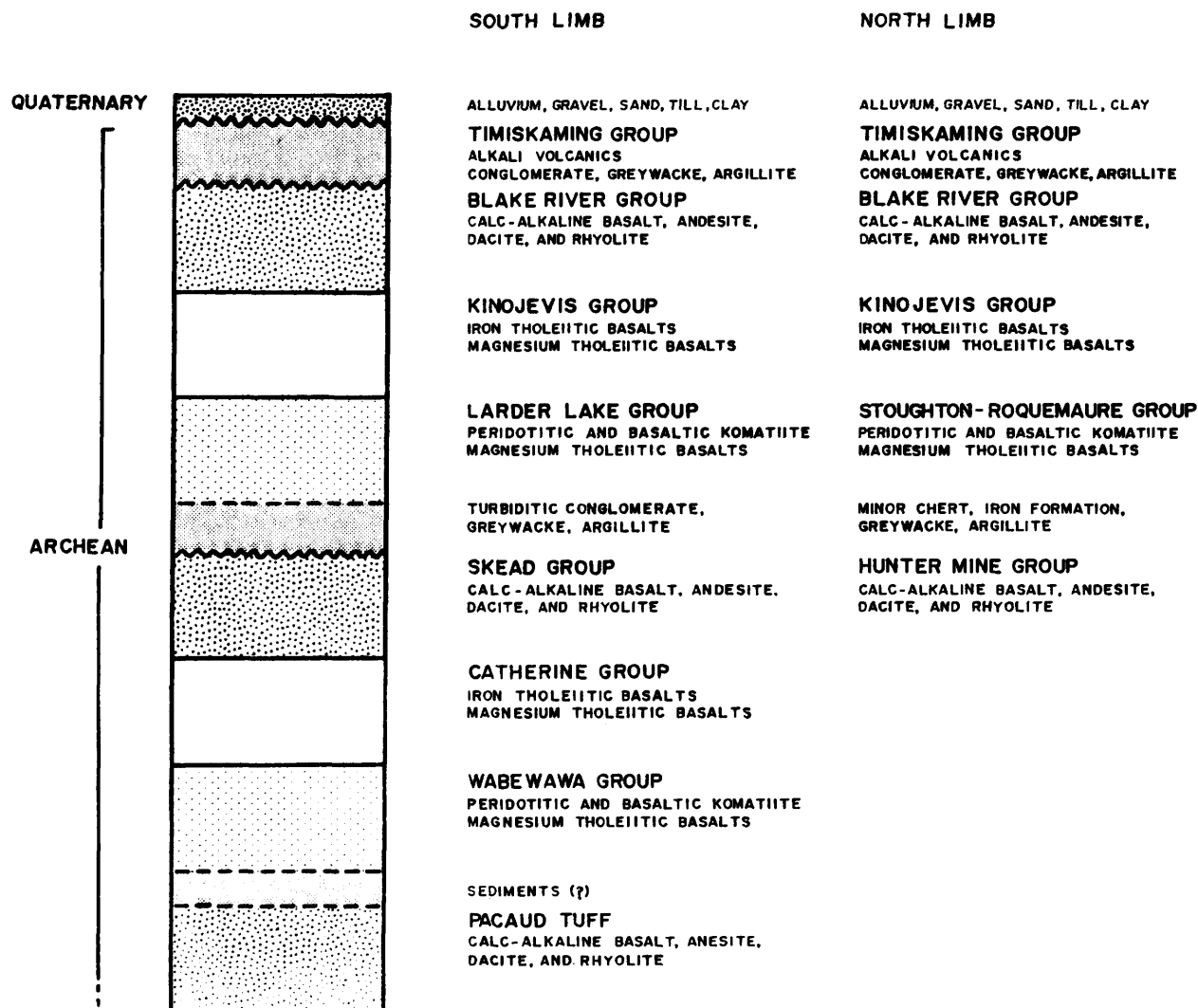


Figure 2—Stratigraphic column of the north and south limb of the Noranda-Benoit synclinorium. On the south limb, the Pacaud Tuffs represent the top of the lowermost subalkaline volcanic cycle; the Wabewawa, Catherine, and Skead Groups represent the second cycle; and the Larder Lake, Kinojevis, and Blake River Groups represent the third cycle. On the north limb, the uppermost subalkaline cycle is represented by the Stoughton-Roquemare, Kinojevis, and Blake River Groups, and is underlain by an older cycle represented by the Hunter Mine Group (Jensen 1979).

lies, are rare or non-existent in the central part of the Noranda-Benoit synclinorium (Map 2393, Lumbers and Milne 1979; Map 2205, Pyke, Ayres and Innes 1973). Their abundance increases westward from a point approximately 10 km east of Highway 11, reaching a maximum density (approximately 2 dikes/km) west of Timmins.

PALEOMAGNETISM IN THE ABITIBI BELT

PRESERVATION OF PRIMARY MAGNETISM

Thermoremanent magnetism (TRM) may be preserved in some units of the Noranda-Benoit volcanic complex; there are several reasons to believe it can be detected.

1) The prehnite-pumpellyite to subgreenschist facies (Jolly 1974) of regional and/or burial metamorphism of the terrain led Irving and Naldrett (1977) to suggest that the TRM might be preserved if most of it originally formed with discrete, high, blocking temperatures. Metamorphism, in more detail, is complex in the area (Dimroth and Lichtblau 1979). Nevertheless, apart from local contact aureoles around intrusions, the prograde metamorphic mineral assemblages (Jolly 1974; Pearce and Birckett 1974) indicate that temperatures never exceeded 400°C in any metamorphic event and were probably much less. Volcanic textures, much of the original igneous mineral assemblages, and original intraflow chemical variations are still preserved, especially in Kinojevis flows (Pearce and Birckett 1974; Jensen 1978a; Dimroth and Lichtblau 1979). Moreover, in some parts of Kinojevis flows, the original magnetic mineralogy is still preserved.

2) Units of the second and third volcanic cycles (see Figure 2) were emplaced within a well bracketed, short time-period. Dacites underlying the Stoughton-Roquemaure Group east of Munro Township give a U-Pb zircon age of 2710 ± 2 Ma, while volcanic and subvolcanic units forming the top of the Blake River pile give an age of 2703 ± 2 Ma (Nunes and Jensen 1980). These values, however, are systematically younger than the Sm-Nd age of 2765 ± 47 Ma of komatiites and related intrusive rocks of the Stoughton-Roquemaure Group, Munro Township, reported by Zindler *et al.* (1978). The Rb-Sr age of Matachewan dikes is 2690 ± 93 Ma (Gates and Hurley 1973), in agreement with field relations. Such a small difference in age, if real, between the volcanic and sedimentary rocks of the second and third volcanic cycles of the Noranda-Benoit volcanic complex and the Matachewan dikes suggests that the TRM (or depositional remanent magnetization) directions in these various units should be similar. Any post-depositional tectonism of the volcanic and sedimentary rocks, prior to intrusion of Matachewan dikes, would have dispersed the directions. In turn, the preservation of a TRM in the volcanic and sedimentary rocks might be implied if, after correction for pre-Matachewan tectonism, the magnetization directions are identical.

3) In conjunction with the prior point, the structural history of the second and third volcanic cycle units appears to

be relatively straightforward. Development of the major east-trending synclinorium occurred during the deposition of the Kinojevis and Blake River Groups (Jensen 1981). In situ magnetization data from Kinojevis and older units may thus be reliably corrected for structure because they represent lava successions tilted into monoclines.

Further evidence supporting preservation of primary magnetization has been found in the Timiskaming Group, which stratigraphically directly overlies the Blake River Group. The Chaput Hughes conglomerate of the Timiskaming Group contains cobbles retaining a predepositional remanence.

KINOJEVIS GROUP

Interpretation of the paleomagnetic data (Table 1) from the Kinojevis tholeiites involves three important features. First, individual samples usually contain at least one magnetization component of intermediate to high blocking temperatures and coercivities. Such components generally display linear decays during demagnetization and therefore represent a relatively discrete period of geologic time. Second, "contact" tests (this study; Pesonen 1973) indicate the ability of at least some units to retain a statistically well-grouped secondary TRM imparted by Matachewan dikes. Additional magnetization components, some perhaps chemical in origin, have been superimposed upon the overprinted TRM. Third, original titanomagnetites of all flows have been in part converted to essentially pure magnetites (Table 2) in a probably complex series of changes, beginning with deuteric oxidation and exsolution, and possibly continuing in metamorphism, somewhat analogous to the magnetization history of modern ophiolite complexes.

As noted previously, the thermal history of this area is complex, but critical information bearing on the magnetization features listed above is available. Maximum regional metamorphic temperatures, as determined by prehnite phase equilibria, were about 400°C. Metamorphic temperatures could have been much less; the upper stability limit of prehnite-chlorite-quartz assemblages (very common in Kinojevis Group units) is approximately 200°C at pressure of 3 kb, and decreases at higher pressures (Nitsch 1971). Schwarz and Buchan (1980) and Schutts, Ph.D. candidate, University of Toronto, (personal communication) suggested that the ambient temperature of presently exposed country rock at Munro Township during Abitibi dike intrusion (dated at approximately 2150 Ma) was $250 \pm 25^\circ\text{C}$, implying a prolonged deep burial for this area. Assuming a maximum "burial" temperature of 350°C and a (conservative) minimum duration of heating of 1.0 Ga, an original remanence residing in essentially pure magnetite capable of surviving heating must theoretically have blocking temperatures in excess of 500°C (Pullaiah *et al.* 1975). If high blocking-temperature remanence is well grouped initially, it will remain well grouped after burial and uplift. The maximum ambient temperature estimate may in fact be too high and consequently lower blocking temperature re-

Table 1—Typical rock magnetic and remanence properties, Kinojevis Group tholeiites. †

Sample	Rock Type, Township	H _c	H _{cR}	J _s [*]	J _r /J _s [*]	T _C	X _i	X _p	NRM	H _½ [‡]	T _B
26A	high Fe-tholeiite flow base, Cook	—	—	—	—	—	0.86x10 ⁻⁵	—	0.035	50.0	380-540
27F	high Fe-tholeiite flow center, Cook	3.5	—	65900.0	0.04	568	4.05x10 ⁻³	3.83x10 ⁻⁷	0.86	5.5	—
28A	high Fe-tholeiite flow base, Cook	7.0	29.0	61.6	0.15	560	1.11x10 ⁻⁴	2.10x10 ⁻⁶	0.096	14.0	—
29A	high Mg-tholeiite glomeroporphyritic top, Cook	—	—	3.4	—	230.570	4.29x10 ⁻⁵	1.90x10 ⁻⁶	0.0067	47.0	—
40D	high Mg-tholeiite flow top, Cook	5.0	—	14.0	0.21	—	3.43x10 ⁻⁵	2.30x10 ⁻⁶	0.0061	48.0	350-540
40J	high Mg-tholeiite flow center, Cook	—	—	—	—	—	9.43x10 ⁻⁵	—	0.049	60.0	480-580
40T	high Mg-tholeiite flow center, Cook	11.0	21.0	5334.0	0.11	560	9.43x10 ⁻⁵	2.5x10 ⁻⁶	8.2	7.0	—
40BB	high Mg-tholeiite flow base, Cook	—	—	—	—	560	8.57x10 ⁻⁵	—	0.120	9.0	410-580
41B	high Mg-tholeiite glomeroporphyritic top, Cook	16.0	160.0	126.0	0.02	—	2.20x10 ⁻⁵	3.00x10 ⁻⁶	0.0098	36.0	300-580
124B	high Mg-tholeiite glomeroporphyritic top, McVittie	3.7	—	5180.0	0.02	583	1.21x10 ⁻³	6.90x10 ⁻⁷	0.52	8.0	NRM-400
124C	high Mg-tholeiite flow top, McVittie	8.1	—	80780.0	0.06	575	1.44x10 ⁻³	6.67x10 ⁻⁶	10.30	7.5	NRM-580
124E	high Mg-tholeiite flow top, McVittie	7.0	—	14420.0	0.08	572	6.98x10 ⁻³	1.83x10 ⁻⁶	11.40	7.6	—
124K	high Mg-tholeiite flow center, McVittie	6.1	—	2576.0	0.06	576	4.43x10 ⁻³	9.00x10 ⁻⁷	30.1	4.0	NRM-580
124BB	high Mg-tholeiite flow base, McVittie	2.6	8.0	14600.0	0.03	578	1.19x10 ⁻²	6.71x10 ⁻⁶	60.3	11.0	—
124II	high Mg-tholeiite flow base, McVittie	8.0	100.0	117.6	0.04	—	5.14x10 ⁻⁵	8.30x10 ⁻⁷	0.0055	15.0	NRM-550
125A	high Fe-tholeiite flow center, Thackeray	—	—	14.1	0.06	578	5.14x10 ⁻⁵	8.10x10 ⁻⁶	0.031	18.0	NRM-580
125B	high Fe-tholeiite flow center, Thackeray	4.5	25.0	742.0	0.08	577	3.00x10 ⁻⁴	2.00x10 ⁻⁶	0.291	7.0	—
125K	high Fe-tholeiite flow center, Thackeray	9.5	—	182.0	0.26	555	8.57x10 ⁻⁵	1.60x10 ⁻⁶	0.40	14.5	280-590
125M	high Fe-tholeiite flow center, Thackeray	1.0	—	8208.0	0.10	575	9.43x10 ⁻⁵	3.5x10 ⁻⁶	9.80	5.5	300-580
125N	high Fe-tholeiite flow center, Thackeray	7.3	—	10659.0	0.11	575	1.41x10 ⁻³	2.5x10 ⁻⁶	12.1	6.5	180-580
125O	high Fe-tholeiite flow center, Thackeray	4.1	—	342.0	0.17	578	2.49x10 ⁻⁴	4.71x10 ⁻⁶	4.2	7.0	—
125P	high Fe-tholeiite flow center, Thackeray	6.6	78.0	98.0	0.064	569	2.50x10 ⁻⁴	6.31x10 ⁻⁶	3.20	7.0	200-580
125T	high Fe-tholeiite hyaloclastite base, Thackeray	6.1	48.0	28.0	0.24	580	1.89x10 ⁻⁴	4.51x10 ⁻⁶	0.43	13.0	180-580
131F	high Fe-tholeiite flow top, Thackeray	2.1	—	168.0	0.06	576	—	6.00x10 ⁻⁶	0.0060	30.0	450-580
131I	high Fe-tholeiite flow center, Thackeray	5.5	—	8.8	0.13	560	—	1.61x10 ⁻⁶	0.21	12.0	—
131K	high Fe-tholeiite flow center, Thackeray	16.8	44.0	2058.0	0.20	574	—	9.01x10 ⁻⁶	4.10	11.0	200-575
128B	high Mg-tholeiite flow base, Thackeray	6.1	—	203.0	0.08	573	2.57x10 ⁻⁴	2.31x10 ⁻⁶	0.065	4.0	200-580
129B	high Mg-tholeiite flow center, Thackeray	3.8	—	6160.0	0.03	575	1.11x10 ⁻²	5.53x10 ⁻⁶	3.81	8.0	400-580
129F	high Mg-tholeiite flow top, Thackeray	3.0	18.0	490.0	0.09	—	4.63x10 ⁻⁴	2.41x10 ⁻⁶	0.376	15.0	300-480
300B	Matachewan Dike Cook	—	—	—	—	—	—	—	0.223	19.0	350-580
300C	high Fe-tholeiite adjacent to dike, Cook	—	—	—	—	—	—	—	0.087	63.0	400-580
300D	high Fe-tholeiite adjacent to dike, Cook	—	—	—	—	—	—	—	7.6	12.0	—

NOTES: H_c = coercivity; H_{cR} = coercivity of remanence; J_s = saturation magnetization; J_r/J_s = ratio of saturation remanence to saturation magnetization; T_C = Curie temperature, X_i = initial susceptibility; X_p = paramagnetic susceptibility; NRM = intensity of the natural remanent magnetization; H_½ = median destructive field; T_B = blocking temperature range of the remanence decaying to the origin in thermal demagnetization.

*J_s and J_r/J_s values were often difficult to determine accurately because of the high (10⁻⁶ or greater) values of paramagnetic susceptibility in conjunction with low saturation magnetization values for many samples.

†Units are as follows: H, mT; J, Am⁻¹; T, °C.

Table 2—Magnetite and ilmenite compositions from selected Kinojevis Group units.

	Sample 129B (1)	(2)	(3)	Sample 124A (4)	Sample 125N (5)	Sample 124E (6)	(7)	(8)	(9)
TiO ₂	0.27	49.50	47.83	0.35	6.63	24.58	28.41	26.06	0.66
Al ₂ O ₃	0.32	0.00	0.00	0.17	0.27	0.00	0.16	0.00	0.39
FeO*	93.28	42.61	42.96	89.45	84.70	70.85	67.20	69.58	89.23
FeO	25.21	37.43	37.88	31.31	39.02	54.31	57.27	54.65	35.54
Fe ₂ O ₃ **	68.06	5.72	5.58	63.92	50.21	18.16	10.91	16.41	59.03
MnO	0.00	6.34	5.65	0.00	0.58	0.00	0.00	0.00	0.00
MgO	0.00	0.00	0.00	0.00	0.00	0.00	0.00	0.00	0.00
V ₂ O ₅	—	—	—	0.00	—	0.66	0.77	0.70	0.25
SiO ₂	—	0.40	0.62	0.86	0.81	0.60	0.77	0.54	2.45
SUM***	100.03	99.40	97.56	96.61	97.52	98.32	98.29	98.36	98.32
Formulae normalized about 3(spinel) or 2(rhombohedral) cations:									
Fe ⁺⁺	1.01	0.80	0.83	1.04	1.27	1.73	1.81	1.74	1.15
Fe ⁺⁺⁺	1.97	0.11	0.11	1.91	1.47	0.52	0.31	0.47	1.72
Ti	0.01	0.96	0.94	0.01	0.19	0.70	0.81	0.75	0.02
Mn	0.00	0.14	0.13	0.00	0.02	0.00	0.00	0.00	0.00
Mg	0.00	0.00	0.00	0.00	0.00	0.00	0.00	0.00	0.00
Al	0.01	0.00	0.00	0.01	0.01	0.00	0.01	0.00	0.02
V	—	—	—	0.00	—	0.02	0.02	0.02	0.01
Si	—	0.01	0.02	0.03	0.03	0.02	0.03	0.02	0.10
Mol % Ulvospinel(spinel) or Hematite(rhombohedral):									
	1.10	6.3	6.4	1.0	19.7	72.9	83.9	76.1	2.3

*Total FeO as determined by electron microprobe.

**The amount of Fe₂O₃ is calculated from stoichiometry.

***The sum of the oxides is calculated using the calculated weight percent Fe₂O₃.

The method of calculating end member percentages along the spinel and rhombohedral solid solution joins from the number of moles of an element per formula unit is essentially that of Bohlen and Essene (1977).

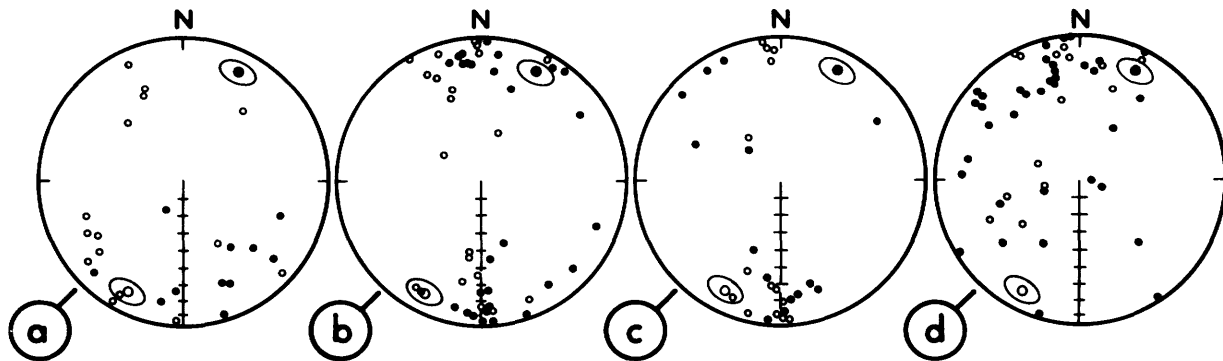


Figure 3—Ultimate directions of magnetization, corrected for regional tilt, of the Kinojevis Group flows. Solid circles represent projections on the horizontal plane; open circles represent projections on the north-south vertical plane. In each projection, the normal and reverse polarity Matachewan directions are shown with their associated cones of 95 percent confidence (Irving and Naldrett 1977). **a.** High iron flow at Lavaflow Mountain, Cook Township; **b.** high iron flow in Thackeray Township; **c.** Low iron flow in Thackeray Township; **d.** Low iron flow in McVittie Township.

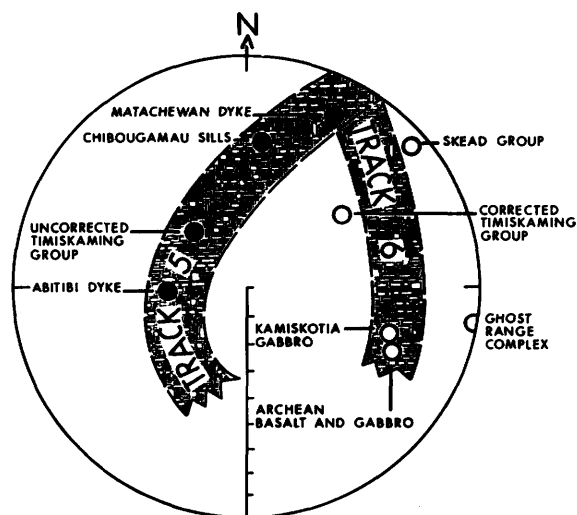


Figure 4—Paleomagnetic field directions in Abitibi coordinates for Timiskaming Group, Track 5 (1800 to 2600 Ma, Irving and McGlynn 1975), and Track 6 (2600 to 2800 Ma, Irving and Naldrett 1977).

manences might be preserved. For example, the Matachewan dike remanence present in "wallrock" Kinojevis tholeiites is isolated in thermal demagnetization between approximately 350°C and 580°C. In this case, then, if the Matachewan remanence was a complete TRM due to reheating, then Pullaiah *et al.*'s (1975) curves would indicate a maximum ambient temperature of about 150°C for unblocking TRM of up to 350°C.

In most Kinojevis Group units examined, both high and low blocking-temperature magnetization components are reasonably scattered and must have been acquired over a significant period of time. It therefore appears that the formation of low-titanium magnetites (see Table 2) in the Kinojevis tholeiites continued during burial and metamorphism. On the basis of electron microprobe analyses of oxides in Kinojevis units and Matachewan dikes in Pesonen's (1973) study area, Hanes (1973) suggested that most titanium loss and hence formation of low-titanium magnetites from originally high-ulvospinel titanomagnetites took place prior to Matachewan dike emplacement. This observation supports Jensen's (1981) belief that downwarping and burial of the major Noranda-Benoit synclinorium occurred concurrently with the deposition of the upper Kinojevis Group and the Blake River Group. Deformation was essentially complete by the time of Matachewan dike activity. There is a characteristic magnetization component from Timiskaming sedimentary rocks near Kirkland Lake which, when corrected for structure, yields a pre-Matachewan dike paleopole (See Figure 4). This observation lends further credence to this argument. On this premise, we have corrected the high blocking-temperature, high coercivity magnetization

components in samples from Cook, Thackeray, and McVittie Townships for post-emplacement synclinorium deformation (Figure 3). The data have been corrected assuming simple tilt about a horizontal east-striking axis (assuming a 0° plunge of the synclinorium). Additional structural corrections (e.g. to account for an apparent shallow eastward plunge of the synclinorium) as employed by Pesonen (1973) who assumed a simple, but significant post-folding eastward tilting of the synclinorium, were not used. The eastward plunge of the synclinorium in the sampling area was probably assumed during downwarping of the region, not at a later time, and conventional corrections for this feature may not accurately reflect the true deformation of the units (Jensen 1981).

BLAKE RIVER GROUP

The Blake River Group, a calc-alkaline volcanic pile in the core of the Abitibi Belt, was included in our paleomagnetic studies because it was also suggested that the Blake River rocks could retain a (primary) thermoremanent magnetization (TRM) component. Because the geology of the area has been relatively well established (Jensen 1972, 1975a, 1975b, 1978a), and the ages of the units are relatively well bracketed (2710 ± 2 to 2703 ± 2 Ma) by U-Pb zircon dating (Nunes and Jensen 1980),

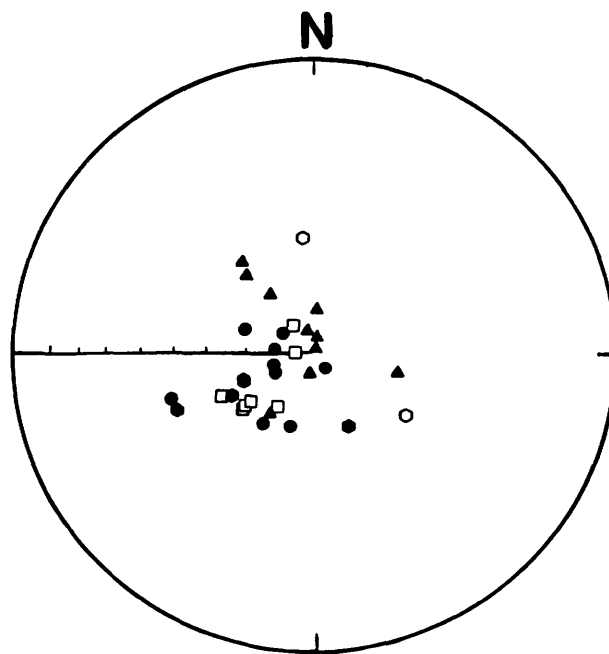


Figure 5—Ultimate directions for Holtyre Fault Block. Hexagons, magnesium-rich tholeiite; triangles, conglomerate; circles, Matchewan dike; squares, trachyte flows. Closed symbols represent downward inclination and open symbols upward inclination.

magnetization components can be referred back to the horizontal and, in theory, compared to components in undefined units of comparable age (e.g. early Proterozoic Matachewan dikes).

NRM directions within the Blake River Group were found to be dispersed on the sampling-site, formation, and regional levels. Thirty four percent of the 153 specimens demagnetized revealed a single component of magnetization, while the remaining specimens revealed multivectorial magnetization. Generally, secondary components within a site display uniform coercivities and blocking temperatures. Their directions are random, such that thermal overprinting cannot be assigned to a specific geologic event.

The scattered magnetization components in the Blake River samples indicate a more complex thermal history than was expected. Although the high coercivity, high blocking-temperature components should record the Earth's field at time of formation, it is possible that magnetite formed over a long time period during deuteric alteration, burial and subsequent uplift, leading to directional scatter of the eventually blocked magnetization components. Large scale structures are not considered responsible for the randomization of remanence since it was found on a sub-sample scale.

TIMISKAMING GROUP

Uranium-lead isotopic dating brackets rocks of the Blake River Group between 2710 ± 2 Ma and 2703 ± 2 Ma (Nunes and Jensen 1980), and the Timiskaming Group is believed to have been deposited immediately after volcanism ceased (Hyde 1978, 1980; Jensen 1981). This age suggests that syngenetic magnetization components should have directions essentially in agreement with the Matachewan event, dated at 2690 ± 3 Ma (Gates and Hurley 1973), and that no post-magnetization deformation has taken place.

The test of the Chaput-Hughes conglomerate has proved to be the most conclusive in documenting pre-tectonic, syndepositional primary magnetization. In the conglomerate, most directions within individual cobbles are consistent with the exception of "greenstone" cobbles of weak intensities believed to have been derived from the Blake River Group. Some pre-Timiskaming lithologies have evidently preserved an earlier remanence. Directions of magnetization of individual cobbles are random in relation to directions of the interbedded sandstones. The sandstone lenses possess well-grouped magnetization directions suggesting that randomization of remanence in the Blake River volcanic rocks took place prior to deposition of the conglomerate.

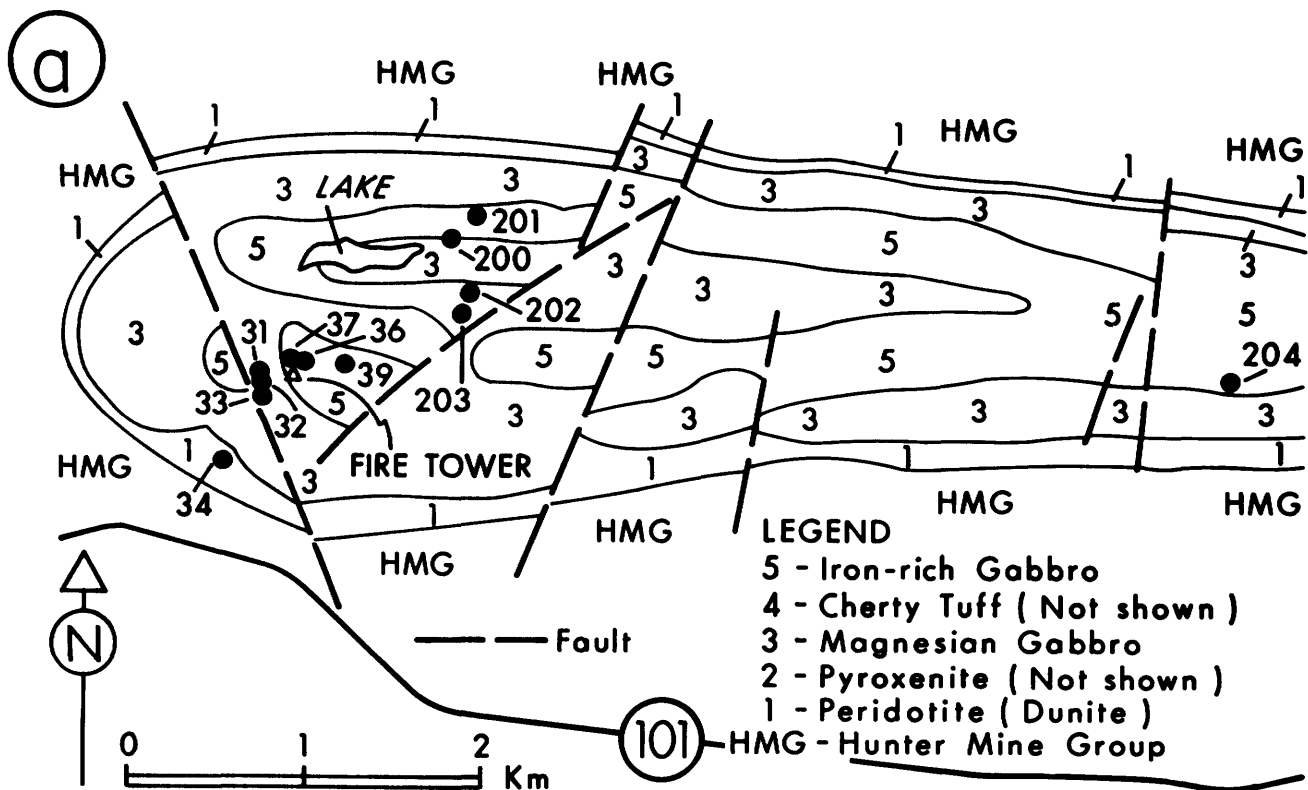


Figure 6—Generalized geologic map of the Ghost Range Complex showing locations of sampling sites (circles). Modified after Jensen (1981).

Two interpretations of the magnetization direction of the sandstone beds can be made. The in situ direction lies between that of the Abitibi dikes, dated by Hanes (1979) using $^{40}\text{Ar}/^{39}\text{Ar}$ method at 2104 ± 40 Ma, and that of the Chibougamau sills, which have a suggested age of 2600 Ma (Ueno and Irving 1976). The in situ direction thus implies an age of approximately 2300 Ma. This age could not reflect primary magnetization carried by low titanium magnetite, being in conflict with observed geology (i.e. the Timiskaming Group conformably overlies the dated Blake River Group in Quebec, and it is cut by Matachewan dikes in Ontario). Structurally correcting the mean magnetic direction of the sandstone yields a direction $D = 232.7$, $I = 47.8$, whose antipole give a pre-Matachewan, post-Skead result (Figure 4). This implied age is in general agreement with the observed geology and the rock magnetic properties.

HOLTYRE FAULT BLOCK

The undeformed Timiskaming trachyte flows and Matachewan diabase dike of the Holtyre Fault Block display well grouped mean ultimate directions (Figure 5). Low-titanium magnetite is the magnetic carrier in the Matachewan dike, and low-titanium magnetite and hematite in the trachyte flows are believed to have had their magnetizations blocked concurrently since the ultimate

component in specimens is isolated between 300° and 620°C .

Interpreting these directions suggests a model in which a Matachewan dike intruded flat lying sedimentary rocks and alkaline volcanic rocks. The fault block was subsequently rotated 80° clockwise, accounting for the northerly trend of the conglomerate and trachyte flows, and the easterly trend of the dike. The block was later tilted 60° to 90° to the west. This model is supported by the data from the trachyte flows; we infer that they acquired a TRM that was an antipodal Matachewan dike direction. A clockwise rotation of 80° and later tilting of the flows to the west would result in the ultimate in situ directions, and would also produce the observed geology.

GHOST RANGE COMPLEX

The Ghost Range Complex (Figure 6) is one of a series of east-trending layered ultramafic complexes situated just north of the Destor-Porcupine Fault (see Figure 1b). The complexes are related to the Stoughton-Roquemaure Group, and the Ghost Range Complex unconformably overlies the Hunter Mine Group. The age of the complex is bracketed between 2710 ± 2 Ma (U-Pb age on samples from Hunter Mine Group, Nunes and Jensen 1980) and

Table 3—Typical rock magnetic and remanence properties, Ghost Range Complex rock types.

Sample	Rock Type	H_c (mT)	H_{cr} (mT)	J_s (Am $^{-1}$)	J_r/J_s	T_c	X_i	NRM(Am $^{-1}$)	$H_{1/2}$ (mT)	T_B
37A	Fe-gabbro, pyrrhotite-free (G-1)	6.8	78.0	—	0.10	575	6.0×10^{-5}	0.0047	26.0	510-580
37G	Fe-gabbro, pyrrhotite-free (G-1)	8.0	90.0	110	0.036	—	8.6×10^{-5}	0.016	45.0	300-585
37J	Fe-gabbro, pyrrhotite-free (G-3)	—	—	—	—	580	3.0×10^{-4}	0.61	7.0	150-560
36C	Fe-gabbro, pyrrhotite-free (G-1)	—	—	—	—	573	6.2×10^{-5}	0.0032	59.0	100-530
34A	Serpentinite (G-3)	6.1	30.0	920	0.069	574	4.2×10^{-3}	0.25	7.0	50-540
200E	Mg-gabbro, pyrrhotite-bearing (G-2)	—	—	—	—	305,564	6.1×10^{-5}	0.14	18.0	100-310
201E	Fe-gabbro, pyrrhotite-bearing (G-2)	—	—	—	—	280,560	4.7×10^{-5}	0.0093	3.0	25-570
201F	Fe-gabbro, pyrrhotite-bearing (G-2)	15.0	27.0	—	0.068	310,550	4.4×10^{-4}	0.190	—	—
202G	Fe-gabbro, pyrrhotite-free (G-1)	8.0	—	—	—	—	3.0×10^{-5}	0.0029	44.0	200-570
202J	Fe-gabbro, pyrrhotite-bearing (G-2)	—	—	—	—	265	9.0×10^{-5}	0.500	—	130-310
202L	Fe-gabbro, pyrrhotite-bearing (G-2)	2.2	—	—	—	300	8.1×10^{-5}	0.360	3.0	80-310
203B	Fe-gabbro, pyrrhotite-free (G-1)	6.8	27.0	—	0.16	575	4.8×10^{-5}	0.031	9.0	200-560
204F	Fe-gabbro, pyrrhotite-bearing (G-2)	9.3	17.0	—	0.28	280,550	5.2×10^{-5}	0.019	14.0	80-310

NOTES: H_c = coercivity; H_{cr} = coercivity of remanence; J_s = saturation magnetization; J_r/J_s = ratio of saturation remanence to saturation magnetization; T_c = Curie temperature; X_i = initial susceptibility; NRM = intensity of the natural remanent magnetization; $H_{1/2}$ = median destructive field; T_B = blocking temperature range of the remanence decaying to the origin in thermal demagnetization.

* J_s and J_r/J_s values were often difficult to determine accurately because of the high (5×10^{-5} or greater) paramagnetic susceptibility of many samples.

Table 4—Summary of Ghost Range Complex paleomagnetic directions and poles.

Group	n/N	in situ			k	VGP	corrected		
		Decl.(°)	Incl.(°)	α_{95} (°)			Decl.(°)	Incl.(°)	VGP
1	70/33	260	-4	6.0	8.9	1E, 5S (antipode)	279	-7	1E, 3S
2	23/15	75	66	37.9	1.6	19W, 42N	61	63	7W, 49N
3	42/24	274	13	18.1	2.5	12E, 8S (antipode)	276	12	10E, 9S

NOTES: n/N = the number of vectors per number of independently oriented samples used to calculate mean direction; α_{95} = radius of circle of 95% confidence; k = estimate of precision parameter; VGP = Virtual Geomagnetic Pole Position.

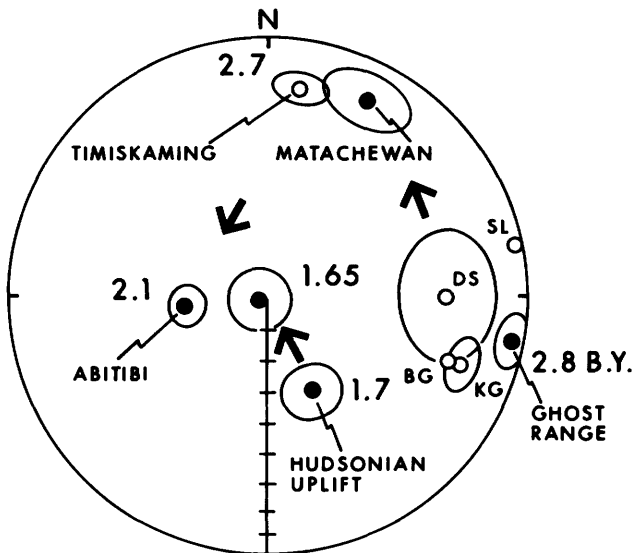


Figure 7—Paleomagnetic field directions in Abitibi coordinates for the Ghost Range Complex and other data from late Archean/early Proterozoic time, North American craton. KG = Kamiskotia Gabbro (Irving and Naldrett 1977), DS = Dundonald Sill (Irving and Naldrett 1977), SL = Shelly Lake Granite, A component (Dunlop and Buchan 1976), BG = Abitibi basalts and gabbros, without α_{95} provided (Schutts 1980), Timiskaming = Timiskaming non-marine facies sedimentary rocks (this paper).

2765±47 Ma (Sm-Nd age on samples from Stoughton-Roquemaure Group, Zindler *et al.* 1978).

The Ghost Range magnetic data (Table 3) provide additional evidence for the existence of an equatorial paleopole (Table 4, Figure 7) for the North American craton prior to Matachewan DiKE activity. If the characteristic remanence of the Ghost Range Complex is a TRM, as we propose, then the pre-Matachewan data in Figure 7 indicate a rapid rate of apparent polar wander (from 52°/100 Ma to 52°/200 Ma) for the Superior Province prior to Matachewan dike intrusion. The interpretation for a rapid migration is dependant on the Rb-Sr age given by Gates and Hurley (1973) for the Matachewan dikes. It would be useful to redate these dikes using the U-Pb zircon method or the samarium-neodymium method to better define their age and this interpretation of the Archean APW path for North America.

AEROMAGNETIC INTERPRETATION OF THE ABITIBI BELT

During July 1972, the Geological Survey of Canada carried out a high-resolution aeromagnetic survey of the Kirkland Lake area using a Beechcraft B80 Queenair aircraft equipped with a digital recording rubidium-vapour magnetometer system. The magnetometer is capable of recording the total magnetic field to a resolution of 0.02 γ (1 γ = 1 nT = 10⁻⁵ gauss). About 12,800 line-kilometres were flown using a line spacing of 463 m at a flight elevation of 305 m. The main survey lines were oriented in a north-south direction, and double control lines, spaced 2.3 km apart, were flown in an east-west direction roughly paralleling the geological trend of the area. The data were then compiled, levelled, and interpolated on a square grid by computer. The survey data are on magnetic tape both in flight line form and as gridded values. The entire Kirkland Lake aeromagnetic survey encompasses an area 84 km by 56 km (4704 km²) between Latitudes 48° and 48°45'N and Longitudes 79°30'W and 80°15'W. The block studied by us is approximately located between Latitudes 48°15'N and 48°37'N and Lon-

gitudes 79°30'W and 80°00'W comprising about 1200 km².

The principal goal of the work reported here was to improve the geological mapping of the Kirkland Lake-Larder Lake area using high-resolution aeromagnetic data and geophysical processing techniques to enhance the presentation of results. Control on the magnetic properties of the units was provided by a ground sampling program (Geissman *et al.* in preparation; Tasillo *et al.* in preparation). Magnetic property studies provided information on sample susceptibilities, natural remanent magnetization (NRM) intensities and direction of magnetization of surface lithologies critical for interpretation of the aeromagnetic data.

All geophysical data processing was performed at the University of Toronto Computer Center. Most of the processing was done using Fortran programming on an IBM 3033 computer, and extensive use was made of the Gould and Calcomp flatbed plotters. The Applicon colour plotter of Dataplotting Services Incorporated, Toronto, was used for the production of colour contour maps (Letros *et al.* in preparation).

SUSCEPTIBILITY AND REMANENT MAGNETIZATION

Rock samples collected for measurement consisted of oriented blocks or in situ drill cores. Susceptibility was measured by a bridge method, and remanent magnetiza-

tion by a Develco cryogenic magnetometer, PAR spinner magnetometer, or a portable Schonstedt magnetometer. Over 400 specimens were obtained in the Kirkland Lake-Larder Lake area for paleomagnetic study, and these were averaged to give 90 samples for processing analysis. The results of these measurements for the five major rock types in the area as well as the Koenigsberger ratio Q (NRM/induced magnetization) and apparent susceptibility are given in Table 5.

The data in Table 5 indicate that susceptibility values for calc-alkaline volcanic rocks and magnesium-rich tholeiitic basalt are much lower than those for granite, gabbro, and iron-rich tholeiitic basalt. Iron-rich tholeiites have the largest susceptibilities and remanent magnetizations. Anomalously high values of remanent magnetization were considered to represent lightning-struck samples, and were excluded from the averages given in Table 5. The higher NRM intensities (e.g. 10^{-3} emu/cm³ in Blake River Group units) may correlate with retention of primary magnetite in some lithologies. For example, although magnetic minerals of the calc-alkaline rocks often are too fine-grained to be defined petrographically, units at several sites have magnetite grains with exsolved ilmenite lamellae altered to leucoxene and rutile (Geissman *et al.* in preparation; Tasillo *et al.* in press).

Usually, high Q values indicate that the majority of the samples display substantial remanence, especially in mafic and ultramafic units. The total-field map (Letros

Table 5—Magnetic property summary of rock samples from Kirkland Lake-Larder Lake area.

Rock Type	Number of Samples	Intensity of Remanent Mag. (cgsx10 ⁶)			Intensity of Induced Mag. (cgsx10 ⁶) (avg.)	Q Ratio (avg.)	Apparent Susceptibility (cgsx10 ⁶) (avg.)
		Min.	Max.	Avg.			
Calc-Alkaline Volcanic Rocks (less-doubtful samples)	46	0.05	28.7	2.8	0.62	5.6	5.5
Magnesium-Rich Tholeiites	9	1.2	10.9	4.4	0.82	5.5	8.0
Iron-Rich Tholeiites (less-doubtful samples)	15	1.2	10000.	1227.	33.4	50.5	2100.
Iron-Rich Tholeiites (with doubtful samples)	17	1.2	13600.	2370.	31.1	600.	4000.
Gabbros	11	7.3	890.	185.	29.5	37.	310.
Granites	8	7.4	245.	78.	20.0	3.5	140.
All Samples	89	0.05	10000.	238.	11.4	9.6	408

Samples Further To South And West Where Metamorphic Grade Is Higher

Calc-Alkaline Volcanic Rocks	63			61.5	14.5	7.8	122.
Magnesium-Rich Tholeiites	20			22.8	17.7	3.1	47.4

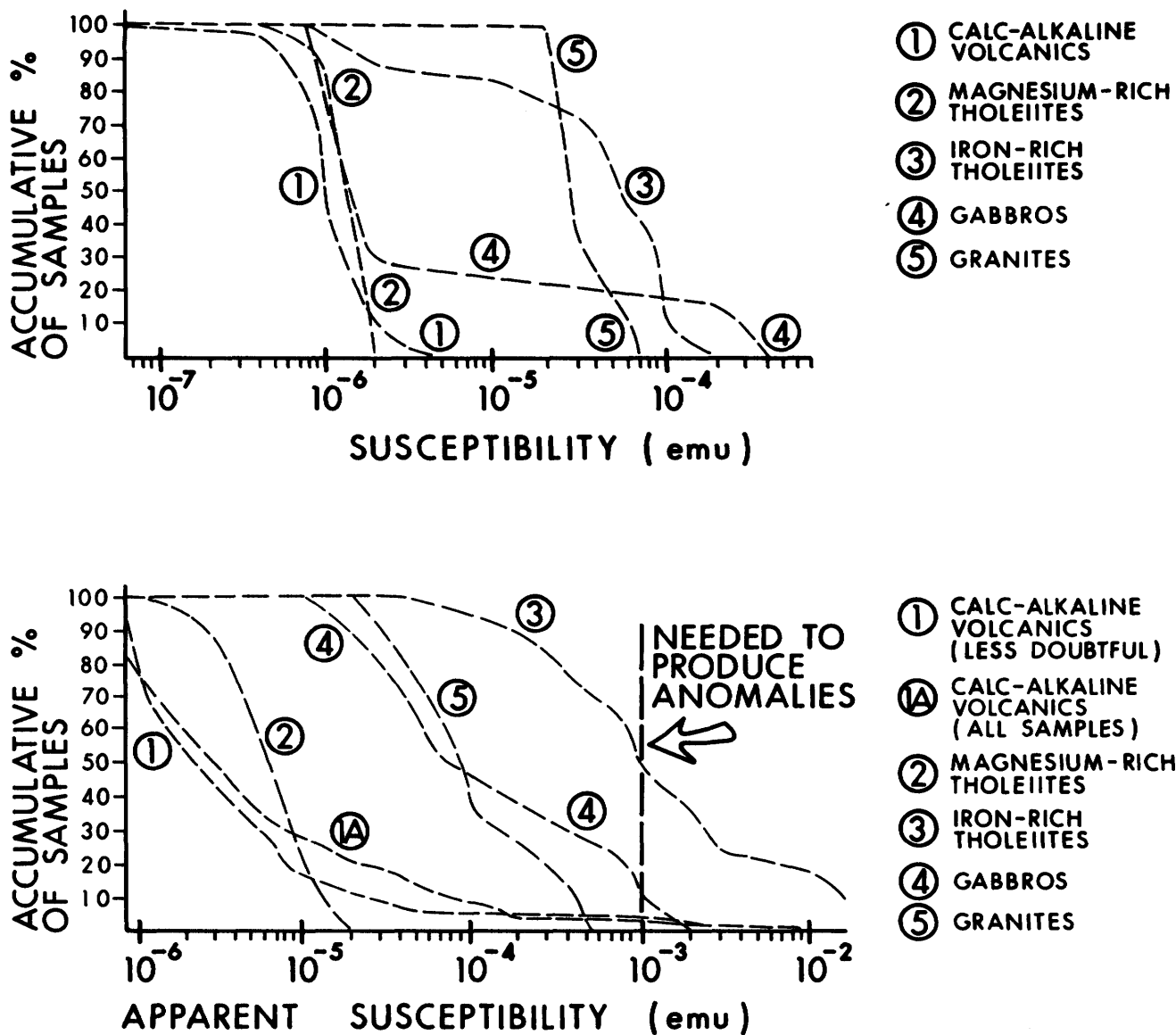


Figure 8—Graph of cumulative percentage of samples versus measured susceptibility (upper diagram), and cumulative percentage of samples versus measured natural remanent magnetization (shown as apparent susceptibility) (lower diagram).

et al. in press) indicates that the anomaly patterns are reasonably well balanced, with only a few negative anomalies, indicating that from flight height the anomalous magnetic field is caused by a magnetization in the direction of the Earth's field. This suggests that the large remanences displayed are either in the direction of the total field or randomly distributed in direction such that the remanent field contribution tends to zero, or that the strongly magnetized samples are only a part of a dominantly inductively magnetized mass.

Remanence directions, while nearly randomly distributed, do cluster around the total field direction ($D = 349.7^\circ$, $I = 75.9^\circ$), with the mean declination and inclination of the remanence vector being $D = 225^\circ$, $I = 82.6^\circ$. The remanence direction is similar to the results of Kornik *et al.* 1975) in the Timmins area. Data scatter will tend to reduce the mean overall effect of remanence on the anomalies.

Figure 8 shows graphs of the cumulative percent of the number of sample measurements versus a) susceptibility, and b) natural remanence calculated as an apparent susceptibility. A vertical line marking the minimum susceptibility required to produce an anomaly, is shown in Figure 8. None of the rock types in the study area have sufficiently high susceptibilities to produce the anomalous patterns, making the consideration of remanent magnetization essential.

Figure 8 indicates that about 45 percent of the iron-rich tholeiites have apparent susceptibilities equal to or greater than that required to produce the anomalous patterns. The remanence carried by iron-rich tholeiites is considered to be the primary source of the magnetic anomalies in the Kirkland Lake area. Also, upper gabbroic intrusions and basal, poorly sampled peridotite and serpentinite, have adequate natural remanences (apparent susceptibilities) to explain the anomalies in the Ghost Range Complex.

Samples of calc-alkaline units and magnesium-rich tholeiites were examined in the southern part of the study area where the metamorphic grade is higher. These data, presented in Table 5, indicate that the NRM intensities, induced magnetization, and apparent susceptibilities have increased by over an order of magnitude and are similar in both units, but the Q values have remained relatively unchanged.

GEOLOGIC INTERPRETATION

By using the method outlined in this study, the geology of an area such as the Kirkland Lake-Larder Lake area with very limited (10-20 percent) bedrock exposure may be interpreted. The magnetic study has:

- 1) clearly outlined formation contacts between magnesium- and iron-rich tholeiites and the boundary between the Kinojevis Group and the Blake River Group;
- 2) delineated the lithologies north of the Ghost Range Complex where limited mapping has previously been done, and outlined a fault-block structure (triangular syncline) in Frecheville Township and the extent of the Ghost Range Complex;

- 3) outlined the formation contacts between felsic intrusions and the surrounding volcanic rocks more clearly, particularly the granitic intrusion in Harker Township;
- 4) delineated areas of syenitic intrusions throughout the study area where magnetite developed during contact metamorphism.
- 5) extended into Elliot Township the trace of a thin olivine diabase dike cutting the Clifford Stock; and
- 6) provided an overall lithologic framework for an area having limited rock exposure.

ACKNOWLEDGMENTS

We express our sincere appreciation to the Ontario Geoscience Research Fund for the financial assistance that made this project possible. We especially appreciate the opportunity to work with L. S. Jensen who assisted us in many ways. We are pleased to report that four manuscripts have been submitted to the Canadian Journal of Earth Sciences and four more are in various stages of preparation. In addition, S. Letros and A.M. Tasillo completed M.Sc. theses and Bambrick will submit his Ph.D. thesis in September.

REFERENCES

- Andrews, A.J.
1979: On the effect of low-temperature seawater-basalt interaction on the distribution of sulfur in oceanic crust, layer 2; *Earth and Planetary Science Letters*, Vol. 46, p.68-80.
- Arndt, N.T.
1977: Thick layered peridotite-gabbro flows in Munro Township, Ontario; *Canadian Journal of Earth Sciences*, Vol. 14, p.2620-2637.
- Beck, M.E., Jr.
1980: Paleomagnetic record of plate-margin tectonic processes along the western edge of North America; *Journal of Geophysical Research*, Vol. 85, p. 7115-7131.
- Bergh, H.W.
1970: Paleomagnetism of the Stillwater Complex, Montana; p.143-158 in *Paleogeophysics*, Runcorn, editor, Acad. Press.
- Dimroth, E. and Lichtblau, A.P.
1979: Metamorphic evolution of Archean hyaloclastites, Noranda Area Quebec, Canada; Part I: Comparison of Archean and Cenozoic sea floor metamorphism, *Canadian Journal of Earth Sciences*, Vol. 16, p.1315-1340.
- Dunlop, D.J.
1980: Paleomagnetism of the Archean Poohbah Lake Alkaline Complex, Northwestern Ontario; abstract, *EOS Transactions of the American Geophysical Union*, Vol. 61, p.214.
- Dunlop, D.J. and Buchan, K.L.
1975: Paleomagnetism of the Shelley Lake Granite; *Proc. 1975 Geotraverse Conference*, Department of Geology, University of Toronto, p.94-95.
- 1976: Paleomagnetism of the Shelley Lake Granite; *Proceedings of the 1976 Geotraverse Conference*, University of Toronto, p.94-95.
- Ernst, R. and Halls, H.C.
1980: Extension of the Matachewan and Abitibi Diabase Dike Swarms West of the Kapuskasing Structural Zone, Northern Ontario; *Transactions of the American Geophysical Union*, Vol. 61, p. 215.

- Fahrig, W.F., Gaucher, E.J. and Larochelle, A.
1965: Paleomagnetism of diabase dikes of the Canadian Shield; *Canadian Journal of Earth Sciences*, Vol. 2, p.278-298.
- Gates, T.M. and Hurlley, P.M.
1973: Evaluation of Rb-Sr dating methods applied to Matachewan, Abitibi, Makenzie and Sudbury dikes swarms in Canada; *Canadian Journal of Earth Sciences*, Vol. 20, p.900-919.
- Geissman, J.W., Strangway, D.W., Tasillo, A.M., and Jensen, L.S.
in prep: Paleomagnetism and structural history of the Ghost Range Igneous Complex, Central Abitibi Belt, Ontario: Further evidence for the later Archean geomagnetic field of North America; submitted to *Canadian Journal of Earth Sciences*.
- Geissman, J.W., Strangway, D.W., Tasillo, A.M. and Jensen, L.S.
in prep: Paleomagnetism of Late Archean Metavolcanics and Metasediments, Abitibi Orogen, Canada I. Tholeiites of the Kinojevis Group; submitted to *Canadian Journal of Earth Sciences*.
- Goodwin, A.M. and Ridler, R.H.
1970: The Abitibi Orogenic Belt; in *Symposium on Basins and Geosynclines of the Canadian Shield*, ed. A.J. Baer, Geological Survey of Canada, Paper 28.
- Halls, H.C.
1975: Paleomagnetism of Archean greenstones from Frenchville Township, Ontario; *Proceedings of the 1975 Geotraverse Conference, University of Toronto*, paper 26.
- Hanes, J.A.
1973: Petrographic and thermomagnetic study of Blake River Group mafic volcanics; Unpublished MSc thesis, University of Toronto, Toronto, 192p.
- 1979: An ^{40}Ar - ^{39}Ar geochronological study of Pre-Cambrian diabase dikes; Unpublished Ph.D. Thesis, University of Toronto, 240p.
- Humphris, S.E. and Thompson, G.
1978: Hydrothermal alteration of oceanic basalts by seawater; *Geochimica et Cosmochimica Acta*, Vol. 42, p.107-125.
- Hyde, R.S.
1978: Sedimentology, volcanology, stratigraphy, and tectonic setting of the Archean Timiskaming Group, Abitibi Greenstone Belt, Northeastern Ontario, Canada; Unpublished Ph.D. Thesis, McMaster University, Hamilton, Ontario, 422p.
- 1980: Sedimentary facies in the Archean Timiskaming Group, and their tectonic implications, Abitibi greenstone belt, Northeastern Ontario, Canada; *Precambrian Res.*, Vol. 12, p.161-195.
- Irving, E.
1969: Paleopoles and paleolatitudes of North America and Speculation about Displaced Terrains; *Canadian Journal of Earth Science*, Vol. 16, p. 669-694.
- Irving, E. and McGlynn, J.C.
1976: Proterozoic magnetostratigraphy and the tectonic evolution of Laurentia; *Phil. Trans. Royal Society*, Vol. A280, p.433-468.
- Irving, E. and Naldrett, A.J.
1977: Paleomagnetism in Abitibi Greenstone Belt, and Abitibi and Matachewan Diabase Dikes: Evidence of the Archean geomagnetic field; *Journal of Geology*, Vol. 85, p.157-176.
- Jackson, M.C.
1980: Geology and Petrology of Archean basalt and associated rocks at Lava Flow Maintain, NE Ontario; Unpublished MSc thesis, University of Toronto, 260p.
- Jensen, L.S.
1972: Geology of Melba and Bisley Townships, District of Timiskaming; Ontario Div. Mines, Geol. Report 103, 27p.
- 1975a: Geology of Clifford and Ben Nevis Townships, District of Cochrane; Ontario Div. Mines, Geol. Report 132, 55p.
- 1975b: Geology of Pontiac and Ossian Townships, District of Timiskaming; Ontario Div. Mines, Geol. Report 125, 40p.
- 1978a: Geology of Thackeray, Elliot, Tannahill, and Dokis Townships; Ontario Geological Survey, Report 165, 71p.
- 1978b: Archean komatiitic, tholeiitic, calc-alkalic and alkalic volcanic sequence in the Kirkland Lake Area; *Geological Society of America, Annual Meeting Guidebook, Toronto*, p.237-259.
- 1979: Larder Lake synoptic mapping project; p.64-69 in *Summary of Field Work*, by the Ontario Geological Survey, ed. by V.G. Milne, O.L. White, R.B. Barlow, and C.R. Kustra, Ontario Geological Survey, Miscellaneous Paper 90.
- 1981: Petrogenic model for the Archean Abitibi Belt in the Kirkland Lake area, Ontario; Unpublished Ph.D. Dissertation, University of Saskatchewan, Saskatoon, 550p.
- Jolly, W.T.
1974: Regional Metamorphic Zonation as an aid in study of Archean Terranes: Abitibi region, Ontario; *Canadian Mineralogist*, Vol. 12, p.499-508.
- Kornik, L.J., McGrath, P.H., Holrody, M.T. and Hood, P.J.
1975: Evaluation of High-Resolution Aeromagnetic Survey Data over a Test Range in the Timmins Area, Ontario; p.23-38 in *Report of Activities, part B. Geol. Surv. Canada, Paper 75-1B*.
- Larochelle, A.
1966: Paleomagnetism of the Abitibi dike swarm; *Canadian Journal of Earth Sci.*, Vol. 3, p.671-683.
- Letros, S., Strangway, D.W., Tasillo, A.M., Geissman, J.W., and Jensen, L.S.
in prep: Aeromagnetic interpretation of the Kirkland-Larder Lake region, central Abitibi Greenstone Belt, Ontario; submitted to *Canadian Journal of Earth Sciences*.
- Lumbers, S.B. and Milne, V.G.
1979: Ontario Geological Map, East-Central Sheet; Ontario Geological Survey, Map 2393, Scale 1: 1013 760.
- McGlynn, J.C., Hanson, G.N., Irving, E., and Park, J.K.
1974: Paleomagnetism and age of Nonacho Group sandstones and associated Sparrow dikes, District of Mackenzie; *Canadian Jour. Earth Sci.*, Vol. 11, p.30-42.
- Nitsch, K.H.
1971: Stabilitätsbeziehungen von prehnit- and pumpellyit haltigen paragenesen; *Contributions to Mineralogy and Petrology*, Vol. 30, p. 240-260.
- Nunes, P.D., and Jensen, L.S.
1980: Geochronology of the Abitibi Metavolcanic belt, Kirkland Lake Area, Ontario — *Progress Report*; Ontario Geological Survey, Miscellaneous Paper 92, p.40-45.
- Park, J.K.
1975: Paleomagnetism of the Flin Flon — Snow Lake Greenstone Belt, Manitoba and Saskatchewan; *Canadian Journal of Earth Sciences*, Vol. 12, p.1272-1290.
- Pearce, T.H. and Birckett, T.C.
1974: Archean metavolcanic rocks from Thackeray Township, Ontario; *Canadian Mineralogist*, Vol. 12, p.509-519.
- Pesonen, L.J.
1973: The magnetic properties and paleomagnetism of some Archean volcanic rocks from the Kirkland Lake area; Unpublished M.Sc. thesis, University of Toronto, Toronto, 134p.
- Pulliaiah, G., and Irving, E.
1975: Paleomagnetism of the contact aureole and late dikes of the Otto Stock, Ontario, and its application to Early Proterozoic apparent polar wander; *Canadian Jour. Earth Sci.*, Vol. 12, p.1609-1618.
- Pulliaiah, G., Irving, E., Buchan, K.L., and Dunlop, D.J.
1975: Magnetization changes caused by burial and uplift; *Earth and Planetary Science Letters*, Vol. 28, p.133-143.

GRANT 20 MAGNETISM AND STRATIGRAPHY OF THE ABITIBI BELT

- Pyke, D.R., Ayres, L.D. and Innes, D.G.
1973: Timmins-Kirkland Lake, Districts of Cochrane, Sudbury and Timiskaming; Ontario Geological Survey, Map 2205, Geological Compilation Series, Scale 1 inch to 4 miles.
- Pyke, D., Naldrett, A.J. and Eckstrand, O.R.
1973: Archean Ultramafic flows in Munro Township, Ontario; Geological Society of America, Bulletin, Vol. 84, p.955-978.
- Ridler, R.H. and Foster, J.H.
1975: Archean paleomagnetic stratigraphy of the Skead Group, Kirkland Lake Area; Proceedings of the 1975 Geotraverse Conference, University of Toronto, Paper 28.
- Schutts, L.D.
1980: Precambrian multicomponent NRM in rocks from the Canadian Shield, Abitibi Supergroup; EOS, American Geophysical Union Trans., Vol. 61, p. 213-214.
- Schwarz, E.J.
1966: Magnetization of Precambrian sulfide deposits and wall rocks from the Noranda district, Canada; Geophysics, Vol. 31, p.797-802.
1977: Remanent magnetism of an ultramafic flow from Munro Township, Ontario; Geological Survey of Canada, Paper 77-1B, p.197-198.
- Schwarz, E.J. and Buchan, K.L.
1980: Reset magnetization in dyke contacts and implications for vertical motion in the Southern and Superior Provinces; abstract, EOS, American Geophysical Union, Trans., Vol. 66, p.214.
- Seyfried, W.E. and Bishoff, J.L.
1973: Hydrothermal transport of heavy metals by seawater; the role of seawater/basalt ratios; Earth and Planetary Science Letters, Vol. 19, p. 177
- Strangway, D.W.
1964: Rock magnetism and dike classification; Journal of Geology, Vol. 72, p.648-663.
- Tasillo, A.M., Geissman, J.W., Strangway, D.W. and Jensen, L.S. in prep: Paleomagnetism of Late Archean Metavolcanics and Metasediments, Abitibi Orogen, Canada II. Blake River and Timiskaming Groups; submitted to Canadian Journal of Earth Sciences.
- Ueno, H. and Irving, E.
1976: Paleomagnetism of the Chibougamou greenstone belt, Quebec, and the effects of Grenvillian post-orogenic uplift; Precambrian Research, Vol. 3, p.305-315.
- Zindler, A., Brooks, C., Arndt, N.T. and Hart, S.
1978: Nd and Sm isotope data from komatiitic tholeiitic rocks of Munro Township, Ontario; United States Geological Survey, Open File Report 78-701, 476p.

Grant 56 Part B Geochemistry and Field Relations of Lode Gold Deposits in Felsic Igneous Intrusions — The Gutcher Lake Stock

P. A. Studemeister, R. Kerrich, and W. S. Fyfe

Department of Geology, University of Western Ontario

ABSTRACT

The Gutcher Lake stock consists of trondjemite and is partly enveloped by a biotite-epidote-hornblende contact aureole. The stock intrudes a greenschist-facies, volcano-sedimentary rock succession near Wawa, Ontario. Native gold and chalcopyrite coexist in crosscutting veins of quartz-carbonate within or adjacent to the stock, and in concordant stringers or lenses in ferruginous chemical metasedimentary units near the stock's contact. The wallrock of pyrite-chlorite-white mica-quartz-ankerite veins was altered by a reducing, low chlorinity CO₂-H₂O fluid that induced addition of Si, Fe, K, S, and Rb and leaching of Na. Features that distinguish gold-bearing from barren veins include 1) a spatial association with sulphidic metasedimentary units, 2) concentrations of sulphide minerals, and 3) low chlorine content.

Mass balance calculations suggest that contact metamorphism induced addition of Fe, Mn, K, S, Cl, and Rb in an environment which was shallow, oxidizing, and chlorine-laden compared to the subsequent regional metamorphic environment. A greenschist facies mineral assemblage partly replaced the precursor quartzofeldspathic and epidote-hornblende mineralogies of the stock and its contact aureole respectively, and the transformation resembles vein wallrock alteration.

A concentration of Cu-Au-bearing iron formation and mudstone adjacent to the stock's upper (north) contact suggests exhalative volcanic activity during stock intrusion. The distribution of gold-bearing veins in the area is partly due to the susceptibility of the anhydrous mineralogies of the stock and its contact aureole to hydration and CO₂-fixating reactions during regional metamorphism.

INTRODUCTION

Native gold and chalcopyrite coexist with pyrite, pyrrhotite, white mica, chlorite, ankerite, and quartz in fractures transecting margins and contact wallrocks of the Gutcher Lake stock. The stock (Figure 1) intrudes a greenschist facies volcano-sedimentary succession of the Early Precambrian Michipicoten "greenstone" belt, 25 km north-east of Wawa, Ontario. In addition, similar metal concentrations occur as concordant stringers and lenses in sulphidic metasedimentary units near the stock's contact. Ego Mines Limited reported 390,000 t (tonnes) averaging 1.60 percent copper and 3.77 g/t gold for Cu-Au deposits

adjacent to the stock's north contact (The Northern Miner 1979). The only past producer in the Gutcher Lake area is the Amherst gold mine which yielded 75.5 kg of gold prior to suspension of mining activity in 1938 (Bruce 1940).

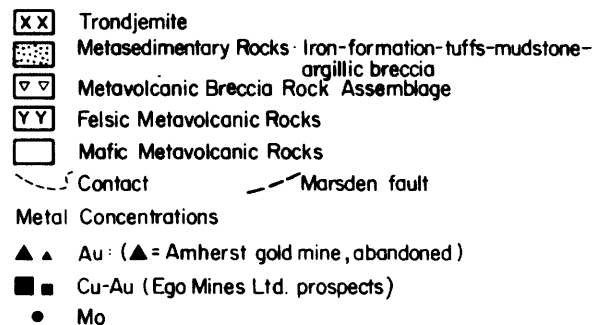
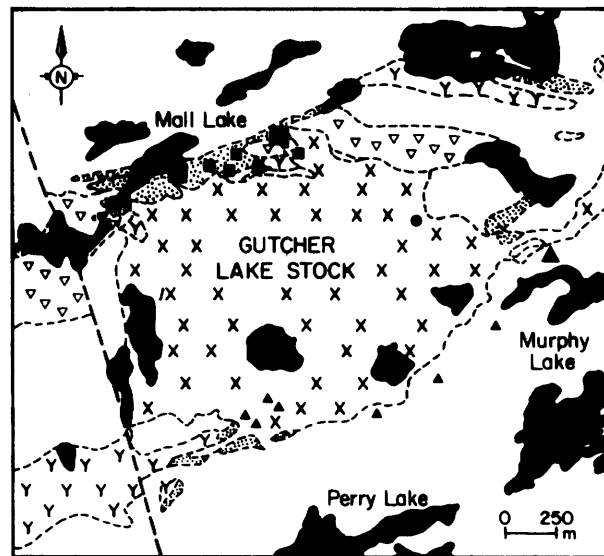


Figure 1—Geology of the Gutcher Lake stock, Abotossaway Township, Algoma District, Ontario.

GUTCHER LAKE STOCK

The Gutcher Lake stock is an oval-shaped trondhjemite body, approximately 4 km² in surface area (see Figure 1). A transition is observed from massive, granitoid-textured, medium-grained rocks with a dominant chlorite-quartz-feldspar mineral assemblage in the central portion to a narrow, fissile, finer grained border zone with a dominant albite-chlorite-calcite-white mica-quartz mineral assemblage. The mineral assemblage of the border zone suggests transformation under conditions of the greenschist facies grade of regional metamorphism.

An assessment of chemical changes, which accompanied hydration and carbonate replacement alteration during regional metamorphism of the Gutcher Lake stock's border zone, was obtained by using a mass balance equation including compensation for inherent rock heterogeneity (Appendix 1). Results of calculations indicate that the transformation of granitoid-textured quartzofeldspathic parent rocks to finer grained daughter rocks rich in chlorite, white mica, calcite, and quartz involved significant additions of Si, Fe, Mn, K, volatiles (CO₂ + H₂O), Rb, and S, with concomitant loss of Na, Ca, Sr, and Cl (Figure 2; Tables 1a and 1b). Stock alteration involved a reducing fluid as attested by $(Fe^{+2}/Fe_t)_{rock} \cong 0.81$ and $\cong 0.66$ for rock suites of the border zone and core of the stock, respectively (Figure 3).

REGIONAL AND CONTACT METAMORPHISM

Two metamorphic episodes are recorded in Early Precambrian rocks of the Gutcher Lake area: initial contact metamorphism accompanying intrusion of the Gutcher Lake stock that culminated in a narrow epidote-hornblende hornfels aureole, and subsequent regional metamorphism that superimposed a greenschist facies mineral assemblage on the entire rock succession (Table 2). The regional greenschist-facies mineral assemblage in mafic volcanic rocks is white mica-albite-quartz-ankerite-calcite-epidote-actinolite-chlorite, corresponding to an equilibration temperature and pressure of approximately 300° to 500°C and 2 to 9 Kbar, respectively (Turner 1981). In rocks remote from the aureole, iron-aluminum-rich chlorite is ubiquitous, the amphibole mineral is actinolite (<3 percent Al₂O₃), and the epidote mineral species is pistacite (Table 3).

The contact aureole partly enveloping the Gutcher Lake stock consists of metavolcanic hornfels composed of calcite, chlorite, actinolite, biotite, epidote, and hornblende (see Table 2). The assemblage corresponds to epidote-hornblende hornfels facies partly retrograded to lower greenschist facies. The following observations suggest retrograde metamorphism of the contact metamorphic facies: 1) amphiboles are zoned with horn-

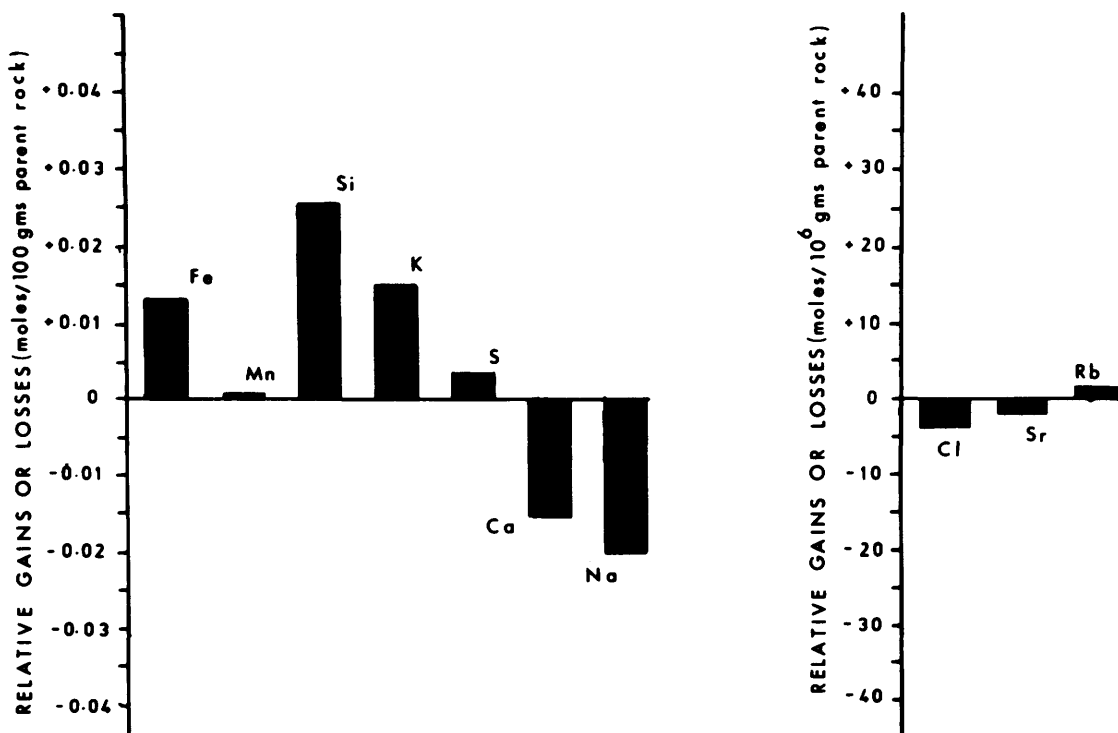


Figure 2—Significant chemical changes during alteration of the Gutcher Lake stock.

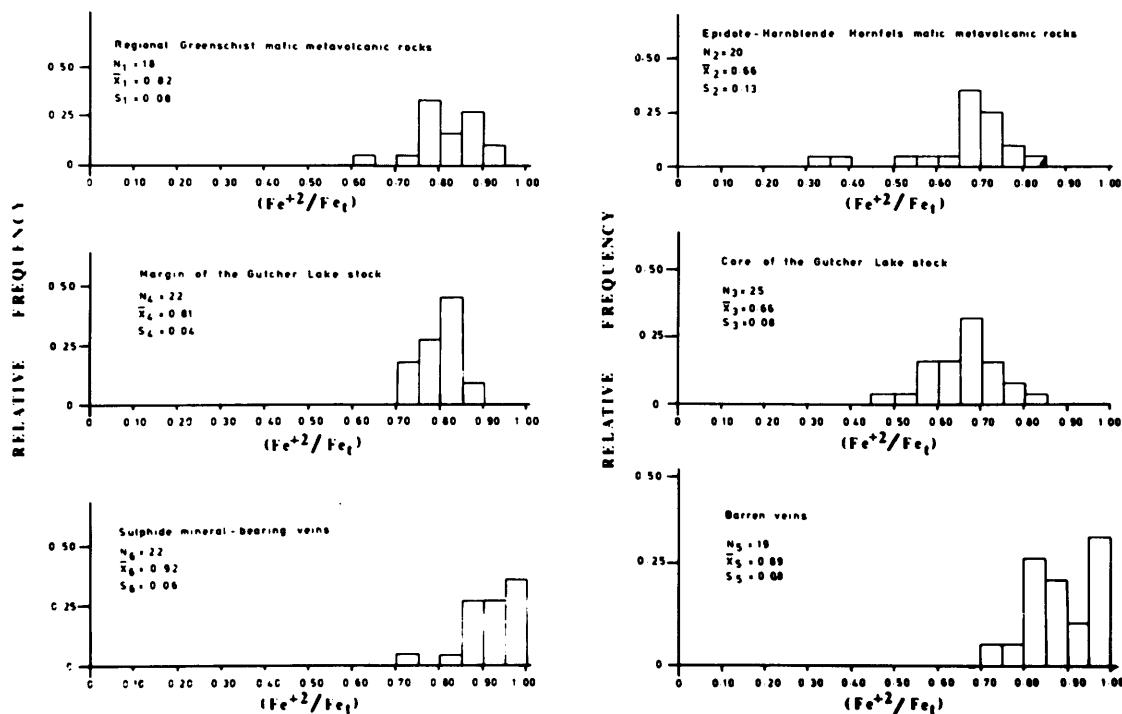


Figure 3—Histograms of Fe^{+2}/Fe_t for various rock suites from the Gutchur Lake area. N = number of samples, \bar{X} = mean, S = standard deviation.

blende cores and actinolitic rims; 2) hornblende grains have embayed fringes of fissile, finer grained quartz-actinolite-calcite-chlorite mineral aggregates; and 3) quartz-calcite-chlorite-ankerite microveinlets and major veins criss-cross the aureole. Mineral microprobe analyses of a rock collected near Murphy Lake within the stock's aureole are presented in Table 3.

In comparison to actinolite, hornblende has lower SiO_2 , higher Al_2O_3 and TiO_2 , and excess FeO_t over MgO content (Figure 4, Table 3). Actinolites coexisting with hornblende near the stock's contact have slightly higher TiO_2 , Al_2O_3 , and FeO_t (total Fe expressed as FeO) contents relative to their counterparts outside the aureole (Figure 4), as might be expected if the former set are in reaction with hornblendes. Most epidotes within the aureole have higher iron and lower aluminium content than epidotes in regionally metamorphosed rocks (Figure 4). Chlorites replacing, or lining microveinlets transecting epidote-hornblende mineral assemblages are optically similar to chlorites in rocks away from the aureole, but differ in having a higher iron and lower magnesium content (Figure 4).

The chemical composition of a set of mafic metavolcanics with a dominant biotite-epidote-hornblende mineral assemblage (hornfels facies) was compared with that of a set with an actinolite-epidote-calcite-chlorite assemblage (greenschist facies) (Table 4). A modified version of Gresens' (1967) mass balance equation (Appendix 2) was used to assess possible chemical changes in volcanic rocks during contact metamorphism. Results of calculations indicate that contact metamorphism involved fixation of greater amounts of Fe, Mn, K, Rb, S, and Cl but lower amounts of Mg and volatiles ($CO_2 + H_2O$) compared to regional metamorphism of equivalent rocks (Figure 5; Table 5).

The redox state of iron, $(Fe^{+2}/Fe_t)_{rocks}$, is significantly lower in epidote-hornblende hornfels metamorphic rocks compared to similar rocks with a regional greenschist-facies mineral assemblage (Figure 3; Table 6). Furthermore, aureole rocks that have experienced moderate or intense retrograde metamorphism to the lower grade greenschist facies have higher $(Fe^{+2}/Fe_t)_{rock}$ than relatively unaltered rocks, approximately the same as regionally metamorphosed rocks.

GRANT 56 PART B GUTCHER LAKE STOCK

Table 1a—Average chemical composition of the Gutcher Lake stock.

Component (wt%)	Rock Sample Set			
	Relatively unaltered core		Altered margin	
	\bar{X}_1	S_1	\bar{X}_2	S_2
	$N_1=20$		$N_2=20$	
SiO ₂	67.09	1.315	66.09	2.831
TiO ₂	0.44	0.055	0.43	0.074
Al ₂ O ₃	15.73	0.542	15.12	0.899
Fe ₂ O ₃	4.08	0.778	4.93	2.255
MnO	0.04	0.011	0.07	0.045
MgO	1.46	0.241	1.46	0.545
CaO	3.02	0.692	2.08	1.378
K ₂ O	0.63	0.338	1.29	0.630
P ₂ O ₅	0.06	0.024	0.06	0.052
Na ₂ O	5.31	0.542	4.51	1.583
L.O.I.	2.32	0.557	3.91	1.542
Total:	100.18		99.95	
S	0.04	0.043	0.14	0.249
(ppm)				
Cr	27	21.9	14	9.6
Ba	192	83.3	267	162.4
Nb	20	7.5	27	11.9
Zr	112	7.9	108	6.3
Y	9	1.9	11	3.9
Sr	368	77.6	191	79.1
Rb	14	7.0	28	11.4
Pb	9	4.1	9	3.8
Co	33	17.2	28	12.2
Zn	26	12.0	37	33.9
	$N_1=17$		$N_2=16$	
Cl	196	75.1	80	67.8
S.G.	2.760	0.054	2.732	0.034
(Al ₂ O ₃ /TiO ₂)	35.75		35.16	

L.O.I. : Loss on ignition at 1000°C.

S.G. : Specific gravity.

Total iron reported as Fe₂O₃.

\bar{X}_i : Mean S_i : Standard deviation N_i : Number of samples

Table 1b—Average chemical changes during alteration of the Gutcher Lake stock.

Component	$X_{2-1} = (F_{\bar{v}} \bar{\beta}_2 \bar{X}_2 / \bar{\beta}_1) - \bar{X}_1$ (gms/100 gms of parent rock)	t-test statistic	
		Calculated value $(t_i)_{0.90}$	Critical value $(t_c)_{0.90}$
SiO ₂	+1.52	+1.90	+1.33
TiO ₂	0.00	+0.04	+ 1.33
Al ₂ O ₃	-0.03	-0.12	+1.33
Fe ₂ O ₃	+1.04	+1.88	+1.33
MnO	+0.03	+2.55	+1.33
MgO	+0.05	+0.35	+1.33
CaO	-0.86	-2.41	+1.33
K ₂ O	+0.71	+4.30	+1.33
P ₂ O ₅	+0.01	+0.60	+1.33
Na ₂ O	-0.62	+1.60	+1.33
L.O.I.	+1.73	+4.57	+1.33
S	+0.11	+1.80	+1.33
	(gms/10 ⁶ gms of parent rock)	$(t_i)_{0.995}$	$(t_c)_{0.995}$
Cr	- 12	-2.31	+2.86
Ba	+ 85	+2.03	+2.86
Nb	+ 8	+2.55	+2.86
Zr	0	+0.02	+2.86
Y	+ 2	+1.66	+2.86
Sr	-170	-6.73	+2.86
Rb	+ 15	+4.88	+2.86
Pb	0	-0.06	+2.86
Co	- 3	-0.65	+2.86
Zn	+ 12	+1.46	+2.86
Cl	-113	-4.52	+2.92

The calculated and critical values for the t-test statistic have confidence coefficients 0.90 and 0.995 for major and trace elements, respectively.

Table 2—Metamorphic mineral assemblages of mafic volcanic rocks in the Gutcher Lake area.

Minerals	Metamorphic Zones			
	Hornblende-epidote Hornfels Facies			Regional Greenschist Facies
Major Minerals:				
Chlorite	—	—	—	—
Actinolite	—	—	—	—
Epidote	—			—
Hornblende	—			
Biotite	—			
Quartz	—	—	—	—
Carbonate minerals (calcite + ankerite)	—	—	—	—
Albite	—	—	—	—
Accessory Minerals:				
Sphene	—	—	—	—
Magnetite	—	—	—	—
Sulphide minerals (pyrrhotite+pyrite+ chalcopyrite)	—	—	—	—
<hr/>				
Relative content:	Abundant	-	—	
	Subordinate	-	—	
	Rare or Absent	-		

GRANT 56 PART B GUTCHER LAKE STOCK

Table 4—Average chemical composition of mafic metavolcanics from the Gutcher Lake area.

Component (wt%)	Regional Greenschist Facies		Hornblende-Epidote Hornfels Facies	
	\bar{X}_1	S_1	\bar{X}_2	S_2
	$N_1=19$		$N_2=19$	
SiO ₂	47.23	2.887	50.64	5.311
TiO ₂	0.97	0.239	1.02	0.187
Al ₂ O ₃	13.57	1.152	13.79	1.342
Fe ₂ O ₃	12.62	1.711	15.41	5.042
MnO	0.20	0.063	0.28	0.132
MgO	5.93	1.171	4.90	1.222
CaO	8.92	2.284	9.48	2.618
K ₂ O	0.04	0.090	0.35	0.490
P ₂ O ₅	0.04	0.029	0.10	0.079
Na ₂ O	1.52	0.673	1.79	1.327
L.O.I.	8.63	2.477	2.20	0.736
Total:	99.67		99.96	
S (ppm)	0.10	0.047	0.44	0.601
Cr	205	107.0	134	99.3
Ba	29	72.3	67	100.6
Nb	15	10.8	21	7.9
Zr	84	12.3	104	25.4
Y	24	6.6	30	7.5
Sr	140	59.8	184	99.7
Rb	5	7.4	16	20.0
Cl	75	77.0	1420	1385.7
	$N_1=14$		$N_2=16$	
Au (ppb)	<10	<10	16	13.9
Ag	<0.4	<0.4	<0.4	<0.4
Cu	87	33.5	150	237.3
Zn	89	21.6	89	61.3
Pb	<2	<2	<2	<2
Co	42	11.9	53	29.3
Mo	4	1.3	4	1.2
Ni	69	35.4	66	41.8
	$N_1=9$		$N_2=11$	
As	7	4.7	14	17.6
Sb	0.8	0.5	1.8	1.3
W	4	2.8	4	3.7
Hg (ppb)	8	5.6	10	10.0
S.G.	2.873	0.077	3.080	0.120
(Al ₂ O ₃ /TiO ₂)	13.99		13.52	

L.O.I.: Loss on ignition at 1000°C.

S.G. : Specific gravity.

Total iron reported as Fe₂O₃. \bar{X}_1 : Mean S_1 : Standard deviation N_1 : Number of samples

Table 5—Average chemical changes during contact metamorphism, relative to regional metamorphism, of mafic volcanic rocks (Gutcher Lake area).

Component (gms/100 gms of parent rock)	$\Delta\bar{X} = \Delta\bar{x}_2 - \Delta\bar{x}_1$	t-test statistic	
		Calculated value $(t_i)_{0.90}$	Critical value $(t_c)_{0.90}$
SiO ₂	+2.41	+0.64	<u>+1.33</u>
TiO ₂	+0.02	+0.18	<u>+1.33</u>
Al ₂ O ₃	-0.28	-0.27	<u>+1.33</u>
Fe ₂ O ₃	+3.06	+1.67	<u>+1.33</u>
MnO	+0.10	+2.09	<u>+1.33</u>
MgO	-1.57	-2.51	<u>+1.33</u>
CaO	+0.34	+0.28	<u>+1.33</u>
K ₂ O	+0.39	+2.67	<u>+1.33</u>
P ₂ O ₅	+0.08	+3.03	<u>+1.33</u>
Na ₂ O	+0.28	+0.62	<u>+1.33</u>
L.O.I.	-8.60	-9.65	<u>+1.33</u>
S	+0.43	+2.42	<u>+1.33</u>
(gms/10 ⁶ gms of parent rock)		$(t_i)_{0.995}$	$(t_c)_{0.995}$
Cr	-101	-2.23	<u>+2.88</u>
Ba	+ 48	+1.30	<u>+2.88</u>
Nb	+ 7	+1.62	<u>+2.88</u>
Zr	+ 22	+2.08	<u>+2.88</u>
Y	+ 7	+2.01	<u>+2.88</u>
Sr	+ 50	+1.37	<u>+2.88</u>
Rb	+ 14	+2.22	<u>+2.88</u>
Cl	+1723	+4.57	<u>+2.88</u>
Cu	+ 88	+1.13	<u>+2.95</u>
Co	+ 18	+1.69	<u>+2.96</u>
Ni	+ 2	+0.10	<u>+2.98</u>
As	+ 10	+1.37	<u>+2.95</u>

The calculated and critical values for the t-test statistic have confidence coefficients 0.90 and 0.995 for major and trace elements, respectively.

Table 6—The oxidation state of iron for selected rock suites from the Gutcher Lake area.

Sample Set Description	Sample Number (Fe ⁺² /Fe _t)	Statistical Function	Sample Set Description	Sample Number (Fe ⁺² /Fe _t)	Statistical Function
I) Mafic metavolcanics in the regional greenschist facies (quartz-albite-epidote-actinolite-calcite-chlorite)	1a	0.76	IV) Fine grained, fissile rocks from the border zone of the Gutcher Lake stock (chlorite-calcite-albite-white mica-quartz ± pyrite)	3v	0.59
	1b	0.76		3w	0.66
	1c	0.83		3x	0.66
	1d	0.78		3y	0.57
	1e	0.61		4a	0.78
	1f	0.73		4b	0.80
	1g	0.76		4c	0.73
	1h	0.90		4d	0.84
	1i	0.89		4e	0.84
	1j	0.87		4f	0.89
	1k	0.84		4g	0.82
	1l	0.82		4h	0.84
	1m	0.76		4i	0.87
	1n	0.91		4j	0.84
	1o	0.87		4k	0.79
	1p	0.92		4l	0.83
	1q	0.78		4m	0.82
	1r	0.89		4n	0.75
II) Mafic metavolcanics in the epidote-hornblende hornfels facies (magnetite-biotite-epidote-hornblende ± pyrrhotite with incipient calcite-actinolite-chlorite)	2a	0.32	4o	0.75	
	2b	0.69	4p	0.85	
	2c	0.69	4q	0.82	
	2d	0.68	4r	0.79	
	2e	0.73	4s	0.80	
	2f	0.75	4t	0.78	
	2g	0.67	4u	0.85	
	2h	0.75	4v	0.74	
	2i	0.51	V) Wallrocks and core of sulphide-mineral-bearing quartz-carbonate veins (chalcopyrite-pyrrhotite-pyrite-calcite-albite-white mica-chlorite-quartz-ankerite)	5a	1.00
	2j	0.37		5b	0.90
	2k	0.76		5c	0.74
	2l	0.80		5d	0.96
	2m	0.83		5e	0.95
	2n	0.71		5f	0.87
	2o	0.74		5g	0.81
	2p	0.66		5h	0.90
	2q	0.64		5i	1.00
	2r	0.59		5j	0.86
	2s	0.70		5k	0.95
	2t	0.69		5l	0.95
2xa	0.90	5m		0.97	
2xb	0.81	5n		0.93	
2xc	0.91	5o		0.94	
2xd	0.67	5p		0.90	
2xe	0.89	5q		0.87	
2xf	0.71	5r		0.98	
2xg	0.76	5a		0.99	
III) Granitoid-textured rocks from the core of the Gutcher Lake stock (chlorite-quartz-feldspar with accessory epidote, white mica, and calcite)	3a	0.65		5t	0.93
	3b	0.72	5u	0.96	
	3c	0.68	5v	0.97	
	3d	0.61	VI) Wallrocks and core of barren quartz-carbonate veins (albite-chlorite-white mica-quartz-ankerite)	6a	0.81
	3e	0.83		6b	0.74
	3f	0.74		6c	0.78
	3g	0.60		6d	0.83
	3h	0.66		6e	0.83
	3i	0.77		6f	0.84
	3j	0.72		6g	0.84
	3k	0.66		6h	0.86
	3l	0.57		6i	0.86
	3m	0.73		6j	0.87
	3n	0.70		6k	0.88
	3o	0.68		6l	0.90
3p	0.76	6m		0.91	
3q	0.63	6n		0.96	
3r	0.66	6o		0.97	
3s	0.49	6p	0.98		
3t	0.52	6q	0.99		
3u	0.61	6r	0.99		
			6s	1.00	

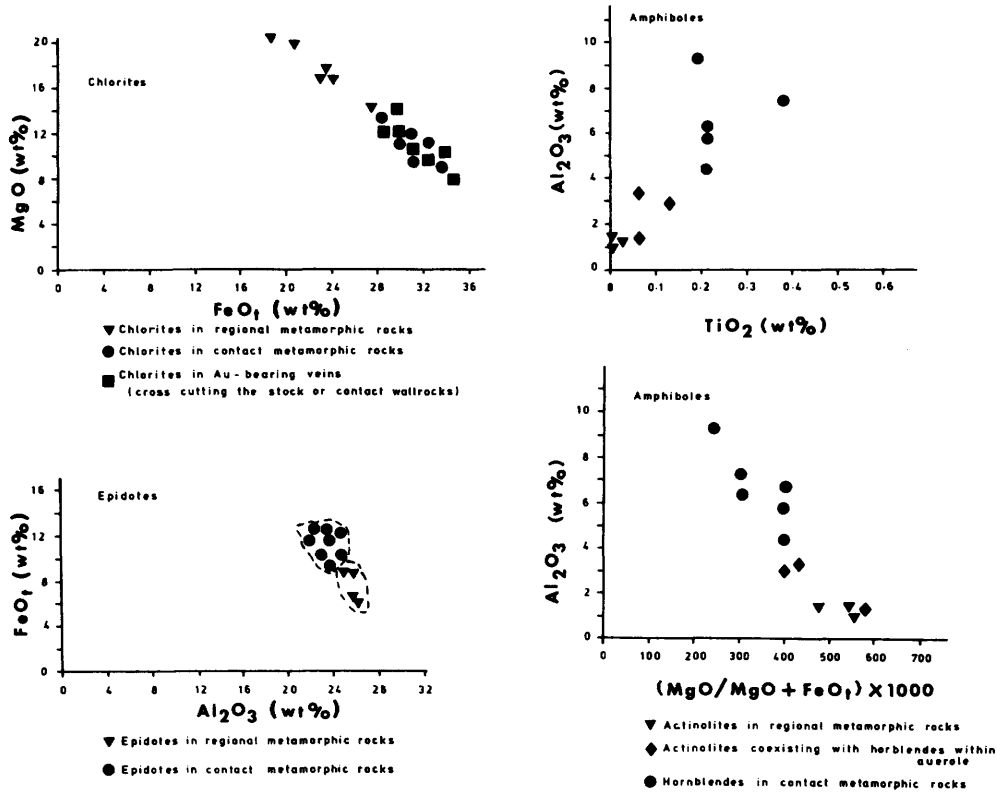


Figure 4—Compositional variation diagrams of metamorphic minerals from the Gutcher Lake area. Each recording represents an average of 5 to 20 spot microprobe analyses.

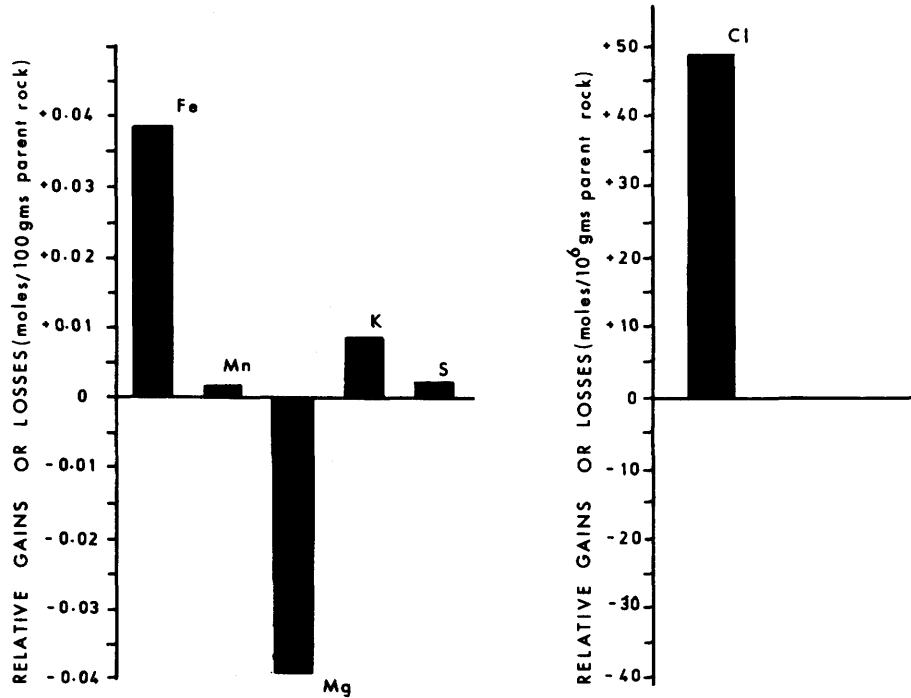


Figure 5—Significant chemical changes during contact metamorphism, relative to regional metamorphism, of mafic volcanic rocks (Gutcher Lake area).

METALLIFEROUS METASEDIMENT UNITS

Sequences of mafic metavolcanic flow in the Gutcher Lake area locally contain interflow units consisting of banded iron formation and sulphidic mudstone interbedded with clastic metasediments and felsic metavolcanic tuffs (see Figure 1). Iron formations are banded concentrations of chert, magnetite, pyrite, and rare chalcopyrite, commonly with interbedded mudstone and tuff beds. Sulphidic mudstones are fine grained magnetite-actinolite-quartz-calcite-biotite-chlorite-epidote rocks which locally display crude bedding and clastic debris, and contain up to 30 percent pyrite, pyrrhotite, and chalcopyrite. Near Mall Lake, mudstones are host to small auriferous massive sulphide pods and lenses. Chemical analyses of sulphidic units near Mall Lake revealed that concentrations of Cu, Ag, Co, and Au (Table 7, "North Contact Zone") accompany Fe, Si, and S.

Sulphidic iron formation bands and mudstones are also intercalated within metavolcanics adjacent to the Gutcher Lake stock's east and south contacts, near gold-bearing quartz-carbonate veins. Chemical analyses revealed major concentrations of sulphur but generally lower contents of base and precious metals compared to sulphidic horizons near the stock's north contact (Table 7). A genetic relationship between sulphide-mineral-bearing metasediments and gold-bearing quartz-carbonate veins is suggested by spatial association, similar sulphide mineralogy, recognition of metasedimentary inclusions within some vein sections, and a common substantial organic carbon content (Figure 6).

QUARTZ-CARBONATE VEINS

Quartz-carbonate veins spatially associated with the Gutcher Lake stock occupy shear zones, and consist of a calcite-white mica-chlorite-quartz-ankerite mineral assemblage supporting nil to 60 percent admixed pyrite, pyrrhotite, chalcopyrite, sphalerite, arsenopyrite, and native gold. The vein gangue minerals replace a precursor quartzofeldspathic or a biotite-epidote-hornblende mineral assemblage where the wallrocks are respectively trondhjemite or mafic metavolcanics. The composition of chlorites in gold-bearing veins is higher in FeO, and lower in MgO than chlorites in regionally metamorphosed rocks outside the aureole, and similar to retrograde chlorites in epidote-hornblende bearing rocks (Figure 4).

Most Au or Cu-Au-bearing veins transect peripheral parts of the Gutcher Lake Stock, or metavolcanics and metasediments adjacent to the stock, and are near sulphidic metasediments. Most barren quartz-carbonate veins transect internal parts of the stock remote from exposed contacts and syngenetic sulphide mineral concentrations. Barren and metal-bearing veins have similar attitudes and gangue mineralogies suggesting that both entities were coeval.

Mass balance calculations were performed on eight suites of wallrock samples collected perpendicular to

vein trends to compare chemical changes accompanying barren and gold-bearing vein formation (Tables 8-12). Consistent chemical changes with increasing white mica-chlorite-quartz-ankerite alteration towards the cores of barren and metal-bearing veins include net addition of Si, Fe, K, volatiles ($\text{CO}_2 + \text{H}_2\text{O}$), and Rb with concomitant leaching of Na. Wallrocks of gold-bearing veins experienced major additions of sulphur and leaching or redistribution of chlorine, whereas barren vein wallrocks experienced trivial gains in sulphur yet addition of chlorine (e.g. Figures 7 and 8).

Sections of sulphide-mineral bearing and barren quartz-carbonate veins were analyzed for Au, Ag, Cu, Zn, Pb, Co, Mo, Ni, As, S, and Cl (Tables 13 and 14), and results suggest that the former differ from the latter in:

1) major concentrations of gold with or without copper, cobalt, and silver (see Tables 13 and 14);

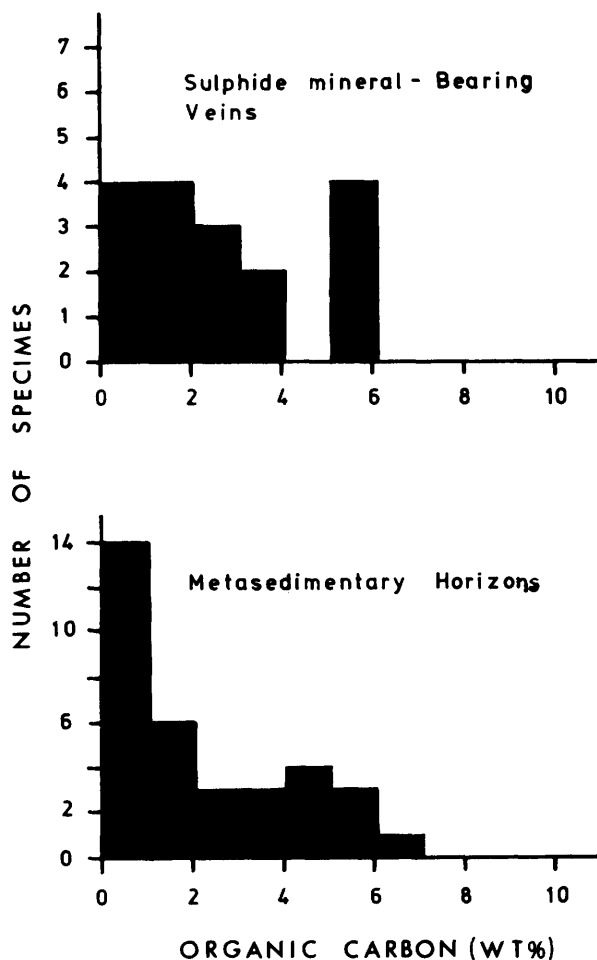


Figure 6—Histogram of organic carbon content for sulphide-mineral-bearing quartz-carbonate veins and metasediments (Gutcher Lake area).

Table 7—Chemical analyses of selected metalliferous metasediments from the Gutcher Lake area.

Rock Sample	Au (ppb)	Ag (ppm)	Cu (ppm)	Zn (ppm)	Pb (ppm)	Co (ppm)	Mo (ppm)	Ni (ppm)	Hg (ppb)	As (ppm)	S (wt%)	C _{org.} (wt%)
(A) North Contact Zone												
1: Cpy-Py-Qtz Ironstone	720	120	6.50%	5000	<2	680	16	270	839	650	25.0	
2: Cpy-Po-Py bearing mudstone	530	176	18.00%	1100	<2	480	28	135	1800	8	32.7	6.89
3: Cpy-Po-Py bearing mudstone	550	16	6.65%	3500	<2	455	8	825	1220	55	32.5	4.50
4: Py-Po-Qtz bearing mudstone	540	<0.4	650	62	<1	210	12	330	18		2.3	1.33
5: Sulphidic mudstone	490	3	4400	134	10	134	6	164	106		2.4	0.96
6: Cpy-Py bearing chert	1933	140	9.48%	870	<10	70	10	94		30	10.0	
7: Py bearing chert	310	14	6800	60	<10	560	<5	45		208	18.1	
8: Py-Mgt-Qtz ironstone	3500	<3	290	510	<10	238	<5	5		46	11.0	
9: Mgt ironstone	20	<0.4	12	26	<2	52	6	20			0.1	
10: Py-Qtz-Mgt ironstone	1130	<3	101	22	<10	5	6	<5		70	17.7	5.39
11: Cpy-Py-Mgt- Qtz ironstone	1065	25	2.99%	290	<10	270	<5	278		20	15.3	3.22
12: Mgt ironstone	50	<0.4	32	46	<2	46	2	18			0.1	0.02
13: Cpy-Po bearing mudstone	30	3	9600	118	24	466	4	11400	71		24.3	2.32
14: Cpy-Po bearing mudstone	20	6	1.39%	146	56	500	4	17200	18		26.5	5.05
15: Cpy-Py bearing mudstone	200	1	1540	89	<1	44	4	61	62		0.3	0.58
16: Sulphidic chert	3050	12	1.05%	30	<2	3.85%	1830	1750			23.5	3.71
17: Cpy-Py bearing mudstone	8400	20	5.09%	210	<10	257	7	496	405	21	9.4	2.03
18: Cpy-Py-Po bearing mudstone	2400	106	16.4%	5700	<10	680	77	920		210	23.6	

continued

GRANT 56 PART B GUTCHER LAKE STOCK

Table 7 continued

Rock Sample	Au (ppb)	Ag (ppm)	Cu (ppm)	Zn (ppm)	Pb (ppm)	Co (ppm)	Mo (ppm)	Ni (ppm)	Hg (ppb)	As (ppm)	S (wt%)	C _{org.} (wt%)
<u>(B) South Contact Zone</u>												
1: Mgt-Py-Qtz bearing mudstone	90	<3	1230	30	<10	30	<5	22		2	3.3	
2: Cpy-Py-Po bearing mudstone	5767	63	17.0%	1020	<10	230	<5	62		68	21.7	
3: Py bearing chert	90	<3	240	139	<10	44	8	27		68	7.4	
4: Py bearing chert	30	2	1150	492	<2	6	4	12		5	3.2	3.44
5: Py bearing tuffaceous chert	90	2	155	48	144	115	6	91			9.4	
6: Py bearing chert	370	<0.4	725	29	<2	42	6	93			6.7	3.58
7: Py bearing tuffaceous chert	20	<0.4	190	40	<2	48	10	175			0.5	1.20
8: Py bearing chert	180	<3	111	14	<10	178	16	156		450	17.7	
<u>(C) East Contact Zone</u>												
1: Py bearing chert	30	<3	76	72	<10	26	5	17		232	31.2	
2: Sulphidic mudstone	80	1	645	97	<2	56	4	50			8.5	0.17
3: Po bearing cherty mudstone	10	<0.4	345	38	<2	27	8	29			0.7	0.06
4: Sulphidic mudstone	30	1	235	342	<2	30	8	13			6.8	0.10
5: Po bearing mudstone	30	1	205	352	<2	32	8	19			0.8	0.60
6: Po bearing mudstone	20	1	695	89	<2	44	6	29			4.3	3.36
7: Py-Qtz ironstone	10	1	30	8	<2	35	2	34			9.7	

Table 8—Major and trace element composition of wallrocks to a barren quartz-carbonate vein at increasing alteration states (Gutcher Lake area).

Component (wt%)	Rock Sample						
	05	6F	6E	6D	6C	6B	6A
SiO ₂	66.69	67.23	66.87	62.91	74.09	5.55	22.46
TiO ₂	0.45	0.46	0.45	0.50	0.30	0.03	0.01
Al ₂ O ₃	15.07	15.83	15.89	15.23	13.42	1.11	0.45
Fe ₂ O ₃	4.06	4.32	3.86	3.52	0.80	7.48	5.98
MnO	0.03	0.02	0.03	0.05	0.03	0.52	0.42
MgO	1.76	1.66	1.78	1.80	1.07	14.61	12.02
CaO	2.43	1.12	1.81	4.74	1.51	27.28	23.03
Na ₂ O	4.73	4.87	2.35	1.06	0.75	0.00	0.00
K ₂ O	1.13	1.20	2.53	2.07	3.28	0.16	0.01
P ₂ O ₅	0.04	0.05	0.05	0.06	0.01	0.00	0.00
L.O.I.	3.11	2.75	3.74	5.98	4.79	42.20	34.97
Total	99.50	99.51	99.36	97.92	100.05	98.94	99.35
S (ppm)	0.03	0.04	0.03	0.05	0.02	0.03	0.03
Y	11	14	12	9	5	15	10
Zr	101	104	108	87	88	44	38
Nb	38	48	35	45	27	25	23
Cr	9	0	37	17	8	0	0
Ba	306	396	408	444	305	25	2
Ni	91	90	83	86	73	72	78
Sr	246	202	147	102	152	143	117
Rb	25	29	47	58	53	7	3
Co	33	44	28	32	23	6	14
Zn	13	14	10	0	0	8	3
Cl	50	150	50	50	50	<50	50
S.G.	2.73	2.71	2.81	2.74	2.75	2.92	2.87
Al ₂ O ₃ /TiO ₂	33.49	34.41	35.31	30.46	44.73	37.00	45.00

L.O.I. : Loss on ignition at 1000°C.

S.G. : Specific gravity.

Total iron reported as Fe₂O₃.

GRANT 56 PART B GUTCHER LAKE STOCK

Table 9—Volume factors, F_v , corresponding to isochemical behavior of individual major and trace elements at increasing alteration states (Gutcher Lake area).

Component	Rock Pairs					
	5+6F	6F+6E	6E+6D	6D+6C F_v	6C+6B	6B+6A
SiO ₂	1.00	0.97	1.09	0.85	12.57	0.25
TiO ₂	0.99	0.99	0.92	1.66	9.42	3.05
Al ₂ O ₃	0.96	0.96	1.07	1.13	11.39	2.51
Fe ₂ O ₃	0.95	1.08	1.12	4.38	0.10	1.27
MnO	1.51	0.64	0.62	1.66	0.05	1.26
MgO	1.07	0.90	1.01	1.68	0.07	1.24
CaO	2.19	0.60	0.39	3.13	0.05	1.21
Na ₂ O	0.98	2.00	2.27	1.41	∅	∅
K ₂ O	0.95	0.46	1.25	0.63	19.31	16.28
P ₂ O ₅	0.81	0.96	0.85	5.98	∅	∅
L.O.I.	1.14	0.71	0.64	1.24	0.11	1.23
S	0.76	1.29	0.62	2.49	0.63	1.02
Y	0.79	1.13	1.37	1.79	0.31	1.53
Zr	0.98	0.93	1.27	0.99	1.88	1.18
Nb	0.80	1.32	0.80	1.66	1.02	1.11
	128+5E	5E+5D	5D+5C	5C+5B	5B+5A	5A+154
SiO ₂	1.05	0.99	1.01	1.07	0.76	1.05
TiO ₂	0.89	0.94	1.06	0.69	1.60	2.54
Al ₂ O ₃	1.00	0.99	1.07	0.71	2.20	2.17
Fe ₂ O ₃	0.91	0.89	1.41	0.43	2.81	0.23
MnO	0.42	1.15	1.06	1.98	∅	∅
MgO	0.85	1.09	4.09	6.74	1.69	0.41
CaO	0.81	1.09	0.84	∅	∅	∅
Na ₂ O	0.96	1.21	0.81	1.39	2.09	2.50
K ₂ O	0.72	0.57	2.44	0.34	1.65	3.21
P ₂ O ₅	1.47	0.98	1.06	0.79	∅	∅
L.O.I.	0.60	1.21	1.06	1.17	1.50	0.32
S	2.95	0.02	4.68	6.92	0.02	0.27
Y	0.57	1.47	0.85	0.62	4.06	0.77
Zr	1.15	0.97	1.06	0.75	1.45	1.49
Nb	0.91	0.85	1.38	0.76	0.95	1.47

Table 10—Chemical changes in wallrocks to a barren quartz-carbonate vein at increasing alteration states (Gutcher Lake area).

Component	5+6F	6F+6E	6E+6D	6D+6C	6C+6B	6B+6A
	(gms/100 gms of parent rock)					
$(F_v)_{w}^{Al, Ti}$	0.97	0.97	1.02	1.31	10.72	2.69
SiO ₂	-1.95	+0.03	-4.30	+34.50	-10.92	+53.83
TiO ₂	-0.01	-0.01	+0.05	- 0.11	+ 0.04	0.00
Al ₂ O ₃	+0.17	+0.15	-0.74	+ 2.41	- 0.79	+ 0.08
Fe ₂ O ₃	+0.10	-0.44	-0.36	- 2.47	+84.34	+ 8.33
MnO	-0.01	+0.01	+0.02	- 0.01	+ 5.89	+ 0.59
MgO	-0.16	+0.13	+0.01	- 0.39	+165.2	+17.17
CaO	-1.35	+0.70	+2.90	- 2.75	+309.0	+33.61
Na ₂ O	-0.04	-2.51	-1.30	- 0.07	- 0.75	0.00
K ₂ O	+0.03	+1.34	-0.47	+ 2.24	- 1.46	- 0.13
P ₂ O ₅	+0.01	0.00	+0.01	- 0.05	- 0.01	0.00
L.O.I.	-0.46	+1.01	+2.21	+ 0.32	+475.6	+50.26
S	+0.01	-0.01	+0.02	- 0.02	+ 0.32	+ 0.05
	(gms/10 ⁶ gms of parent rock)					
Y	+ 3	- 2	- 3	- 2	+ 166	+ 11
Zr	- 1	+ 5	- 22	+ 29	+ 413	+ 57
Nb	+ 8	- 13	+ 10	- 10	+ 258	+ 36
Cr	- 9	+ 37	- 20	- 7	- 8	0
Ba	+ 77	+ 14	+ 34	- 43	- 20	- 20
Ni	- 4	- 7	+ 3	+ 10	+ 247	+ 134
Sr	- 36	- 98	- 46	+ 98	+ 1476	+ 166
Rb	+ 3	+ 18	+ 11	+ 12	+ 27	+ 1
Co	+ 10	- 16	+ 4	- 2	+ 45	+ 31
Zn	+ 1	- 4	- 10	0	+ 91	0
Cl	+ 95	- 100	0	+ 16	+ ~235	+ ~132

$(F_v)_{w}^{Al, Ti}$: volume factor used in calculations is the weighted average of $(F_v)^{Al}$ and $(F_v)^{Ti}$.

GRANT 56 PART B GUTCHER LAKE STOCK

Table 11—Major and trace element composition of wallrocks to a gold-bearing quartz-carbonate vein at increasing alteration states (Gutcher Lake area).

Component (wt%)	Rock Samples						
	128	5E	5D	5C	5B	5A	154
SiO ₂	67.02	62.86	62.29	65.17	60.35	80.42	74.29
TiO ₂	0.40	0.44	0.46	0.46	0.66	0.42	0.16
Al ₂ O ₃	15.32	15.05	14.86	14.61	20.36	9.39	4.19
Fe ₂ O ₃	3.94	4.25	4.68	3.51	8.10	2.93	12.12
MnO	0.03	0.07	0.06	0.06	0.03	0.00	0.00
MgO	1.15	1.33	1.20	0.31	0.05	0.03	0.07
CaO	2.96	3.59	3.23	4.06	0.00	0.00	0.00
Na ₂ O	4.61	4.73	3.84	5.09	3.62	1.76	0.68
K ₂ O	0.76	1.04	1.78	0.77	2.21	1.36	0.41
P ₂ O ₅	0.06	0.04	0.04	0.04	0.05	0.00	0.00
L.O.I.	3.76	6.11	4.94	4.94	4.16	2.81	8.45
Total:	100.01	99.51	97.38	99.02	99.59	99.12	100.37
S (ppm)	0.09	0.03	1.24	0.28	0.04	2.17	7.65
Y	7	12	8	10	16	4	5
Zr	117	100	101	101	134	94	61
Nb	24	26	30	23	30	32	21
Cr	31	0	0	21	38	14	0
Ba	212	280	279	157	387	207	60
Ni	11	93	85	86	92	92	29
Sr	330	301	281	298	499	201	21
Rb	22	24	39	21	48	28	81
Co	33	29	30	37	32	116	9
Zn	42	29	5	5	11	0	317
Cl	150	<50	150	100	<50	<50	130
S.G.	2.71	2.76	2.81	2.66	2.69	2.65	2.74
Al ₂ O ₃ /TiO ₂	38.30	34.21	32.30	31.76	30.85	22.36	26.19

L.O.I. : Loss on ignition at 1000°C.

S.G. : Specific gravity.

Total iron reported as Fe₂O₃.

Table 12—Chemical changes in wallrocks to a gold-bearing quartz-carbonate vein at increasing alteration states (Gutcher Lake area).

Component	128+5E	5E+5D	5D+5C	5C+5B	5B+5A	5A+154
	(gms/100 gms of parent rock)					
$(F_v)_w^{Al,Ti}$	0.96	0.97	1.07	0.70	2.00	2.30
SiO ₂	- 5.56	- 1.34	+ 3.72	-22.45	+98.10	+96.25
TiO ₂	+ 0.03	+ 0.01	+ 0.01	+ 0.01	+ 0.17	- 0.04
Al ₂ O ₃	- 0.61	- 0.37	- 0.06	- 0.20	- 1.86	+ 0.57
Fe ₂ O ₃	+ 0.22	+ 0.37	- 1.12	+ 2.22	- 2.33	+25.89
MnO	+ 0.04	- 0.01	0.00	- 0.04	- 0.03	0.00
MgO	+ 0.15	- 0.14	- 0.89	- 0.31	+ 0.01	+ 0.14
CaO	+ 0.55	- 0.40	+ 0.88	- 4.06	0.00	0.00
Na ₂ O	+ 0.01	- 0.94	+ 1.27	- 2.53	- 0.15	- 0.14
K ₂ O	+ 0.26	+ 0.72	- 1.00	+ 0.79	+ 0.47	- 0.38
P ₂ O ₅	- 0.02	0.00	0.00	0.00	+ 0.05	0.00
L.O.I.	+ 2.21	- 1.23	+ 0.06	- 2.00	+ 1.38	+17.29
S	- 0.06	+ 1.19	- 0.96	- 0.25	+ 4.24	+16.02
	(gms/10 ⁶ gms of parent rock)					
Y	+ 5	- 4	+ 2	+ 1	- 8	+ 8
Zr	- 19	0	+ 1	- 6	+ 51	+ 51
Nb	+ 1	+ 4	- 7	- 2	+ 33	+ 18
Cr	- 31	0	+ 21	+ 6	- 10	- 14
Ba	+ 62	- 5	- 120	+ 117	+ 21	- 64
Ni	+ 80	- 9	+ 2	- 21	+ 89	- 23
Sr	- 36	- 24	+ 21	+ 55	- 103	+ 18
Rb	+ 2	+ 15	- 18	+ 13	+ 7	- 8
Co	- 5	+ 1	+ 8	- 14	+ 197	+ 21
Zn	- 14	- 24	0	+ 3	- 11	+ 638
Cl	- ~126	+ ~123	- 49	- 82	+ ~49	+ ~237

$(F_v)_w^{Al,Ti}$: volume factor used in calculations is the weighted average of $(F_v)^{Al}$ and $(F_v)^{Ti}$.

GRANT 56 PART B GUTCHER LAKE STOCK

Table 13—Chemical analyses of sulphide-bearing quartz-carbonate veins from the Gutcher Lake area.

Rock Sample	Au (ppb)	Ag (ppm)	Cu (wt%)	Zn (ppm)	Pb (ppm)	Co (ppm)	Mo (ppm)	Ni (ppm)	Hg (ppb)	As (ppm)	W (ppm)	S (wt%)	C _{Org.} (wt%)
(A) North Contact Zone													
E-49-5	1100	28	3.00	220	<2	1550	6	82	1080	7000	1700	17.4	3.25
E-49-8	2400	70	11.70	950	<10	900	33	1700	2620	71	14	27.0	5.71
E-49-6D	7200	54	8.28	410	<10	1940	5	300	791	1775	470	37.4	5.45
E-49-15B	34700	76	2.40	230	10	1360	5	383	1130	224		33.7	
E-49-14B	73000	84	7.44	380	13	780	6	400		270		31.3	5.83
E-24-3D	1100	22	2.62	89	<10	49	36	17	42	37	<1	3.8	0.73
E-27-7A	30900	113	20.10	540	<10	960	37	406	486	6900	60	23.2	1.66
E-27-7B	0.29%	74	9.36	170	<10	1280	22	700		3800	76	12.4	
E-31-15A	303	160	9.64	1860	10	291	24	720		<1		28.2	
E-31-10	1130	138	7.76	890	<10	500	71	800		10		26.6	
E-A	1250	17	8.55	1250	<2	645	26	525	3060	810	<1	36.3	5.90
E-49-7	4650	43	6.56	640	<10	1600	18	212	357	1740	650	17.0	1.98
E-51-3	7500	240	16.40	2540	<10	920	161	800		760		25.7	
E-51-9	1400	89	5.16	520	<10	2120	6	1000		730		40.0	
E-51-6	1900	152	12.60	1540	<10	860	29	460		325		24.2	
E-2-15	60	3	0.31	18	<2	46	4	5				0.37	
(B) East Contact Zone													
(ppm)													
E-50-2	19600	462	4.80%	4.42%	1540	332	5	55	838	36	2	13.7	3.67
E-64-2	810	20	1.65%	1250	<2	45	2	76				4.8	2.25
E-68-10	6250	20	2.05%	1250	6	56	8	20				6.5	1.67
E-68-1D	19500	21	2.45%	2050	36	44	4	17				5.8	
E-41-8C	1400	4	1200	46	13	17	2.74%	11		2		2.4	
E-64-1	170	4	1400	392	<2	64	6	135				3.6	
E-72-4	350	2	1450	2620	<2	55	4	36				1.0	
(C) South Contact Zone													
E-69-8	11500	3	160	14	6	21	8	16				4.0	0.48
E-69-13A	1350	3	425	162	6	13	8	18				6.5	0.21
E-69-9A	3850	3	1350	12	2	40	4	23				3.4	
E-69-15B	59500	6	2650	90	<2	52	4	29				3.4	
E-69-15E	5450	6	74	40	20	80	8	125				13.8	
E-75-5A	8950	2	125	7	<2	165	8	15				2.2	
E-36-6A	3100	<3	650	10	<10	19	19	7		30		8.0	0.56
E-36-6B	3250	<3	136	12	<2	200	8	44	13	190	2	2.0	
E-15-5	30300	<3	380	12	<10	39	9	32	13	22	25	5.3	1.70
E-15-4	2150	<3	34	8	<10	216	19	14	13	160	9	6.2	2.34
E-36-11	3400	<3	155	90	<10	30	<5	42	33	1430	120	11.6	2.22

Rock samples have a carbonate-sulphide-quartz laden mineral assemblage and were collected from the core of veins.

Table 14—Trace element analyses of barren quartz-carbonate veins crosscutting the Gutcher Lake stock or the intruded rock sequence.

Rock Sample	Au (ppb)	Ag (ppm)	Cu (ppm)	Zn (ppm)	Pb (ppm)	Co (ppm)	Mo (ppm)	Ni (ppm)	Hg (ppb)	As (ppm)	W (ppm)	S (wt%)
E-41-9A	<10	<0.4	6	34	<2	26	6	18	8	5	5	0.11
E-12-4B	20	<0.4	20	68	<2	24	4	20	8	7	4	0.13
E-69-3A	10	0.4	12	69	<2	8	10	6				0.09
EW-36-1	<10	<0.4	17	48	<1	10	4	10	<8	20	12	0.00
E-3-10	<10	<0.4	900	22	<1	45	6	4	9	8	<1	0.00
E-72-4	<10	<0.4	5	30	<2	27	8	23				0.04
E-66-4	<10	0.8	6	7	<2	1	10	7				0.03
E-50-3	10	<0.4	42	40	<2	26	6	28				0.30
E-48-6	20	<0.4	20	38	<2	20	8	20				0.16
E-69-6	10	<0.4	12	4	<2	1	8	3				0.03
E-10-8A	10	<0.4	20	16	<2	105	6	8	8	3	2	0.17
E-2-2	<10	<0.4	3	4	<1	38	2	1	9	13	4	0.14
E-31-9	30	<0.4	300	52	<2	54	8	22		7	<1	0.00
E-66-11	<10	<0.4	7	8	<2	1	8	6				0.03
E-29-7	60	<0.4	176	340	<2	24	4	18	13	19	<1	0.46

Rock samples are quartz-carbonate mineral laden assemblages collected from the core of veins.

2) sulphur content exceeding 1 percent (Figure 9); and
 3) chlorine content of less than 300 ppm, barren veins average between 500 and 600 ppm Cl (Figure 10).

The redox state of iron, $(Fe^{+2}/Fe_t)_{rock}$, for suites of wallrock plus vein samples of barren and sulphide-bearing veins averages between 0.9 and 1.0 (see Figure 3 and Table 6) with no apparent differences between the two. The reduced state of iron suggests wallrock alteration involved large volumes of a reducing fluid.

EXPLORATION STRATEGIES FOR GOLD DEPOSITS

1) Exploration should be directed towards Early Precambrian volcano-sedimentary successions metamorphosed under regional greenschist facies conditions. Regional amphibolite-grade metamorphic terrains are unlikely to have a high gold potential *except* where there is intense retrograde metamorphism to greenschist-facies mineral assemblages.

2) Within greenschist-facies terrains, exploration should be concentrated along the border zones and within the contact wallrocks of granodioritic-trondhjemitic plutons having the following characteristics:

- a) a regional greenschist-facies mineral assemblage has been superimposed on the precursor quartzofeldspathic assemblage;
- b) they are transected by quartz-carbonate veins and veinlets; and
- c) they have contact aureoles of substantial dimensions and metamorphic grade above regional facies, partly retrograded to a lower grade greenschist facies.

3) The most likely sites of precious metal orebodies are in fractures transecting contact aureoles and border zones of plutons, and particularly near or within syngenetic sulphide-bearing metasedimentary units. Internal parts of a pluton and rocks remote from its thermal aureole are less likely to hold major gold deposits.

4) Regional geochemical surveys may suggest a high gold potential where:

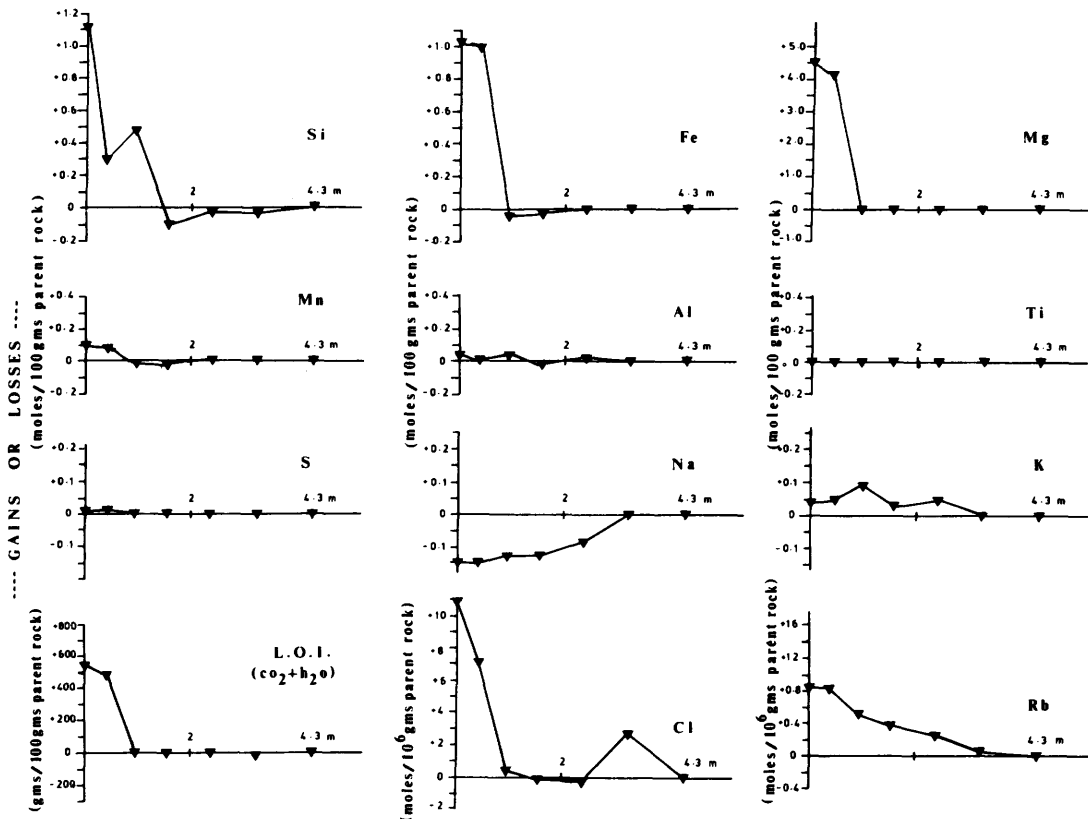


Figure 7—Compositional variations due to progressive hydrothermal alteration in wallrocks of a barren quartz-carbonate vein (Gutcher Lake area).

- a) anomalies in the redox state of iron and in chlorine content occur in rocks hosting gold-bearing veins;
- b) anomalous content of gold occurs in the associated pluton and accompanying aureole;
- c) substantial concentrations of sulphide minerals, and chlorine contents of less than 300 ppm occur in quartz-carbonate veins; and
- d) rocks hosting veins are enriched in Fe, Mn, Si, and K.

5) Iron enrichment (e.g. disseminated magnetite) in the contact aureole around a pluton may be detectable as a weak magnetic anomaly in regional geophysical surveys, and this anomaly may delineate favorable host rocks for gold-bearing veins.

CONCLUSIONS

1) Mafic volcanic rocks adjacent to the Gutcher Lake stock acquired an iron-potassium-rich biotite-epidote-hornblende mineral assemblage during contact

metamorphism. This transformation involved gains in Fe, Mn, K, S, Rb, and Cl, losses in Mg, and occurred in a relatively shallower, more oxidizing regime compared to the regional metamorphic environment.

2) Regional metamorphism transformed mafic volcanic rocks outside the stock's aureole into rocks with a quartz-albite-epidote-actinolite-calcite-chlorite mineral assemblage and with a redox state of iron, $(Fe^{+2}/Fe_t)_{rock}$, of ~ 0.82 . Metamorphism involved a CO_2-H_2O fluid and was coeval with retrograde metamorphism of the stock's aureole, alteration of the stock, and formation of gold-bearing quartz-carbonate veins.

3) Retrograde metamorphism of the stock's aureole superimposed a lower grade, greenschist-facies mineral assemblage on hornfelsic rocks and involved addition of volatiles ($CO_2 + H_2O$), loss of Cl, and change in the redox state of iron, $(Fe^{+2}/Fe_t)_{rock}$, from ~ 0.66 to ~ 0.81 .

4) Chlorite-white mica-calcite-quartz alteration of the Gutcher Lake stock during regional metamorphism involved addition of Si, Fe, Mn, K, volatiles ($CO_2 + H_2O$), S, and Rb, leaching of Na, Ca, Cl, and Sr, and changes in the redox state of iron from ~ 0.66 to ~ 0.81 .

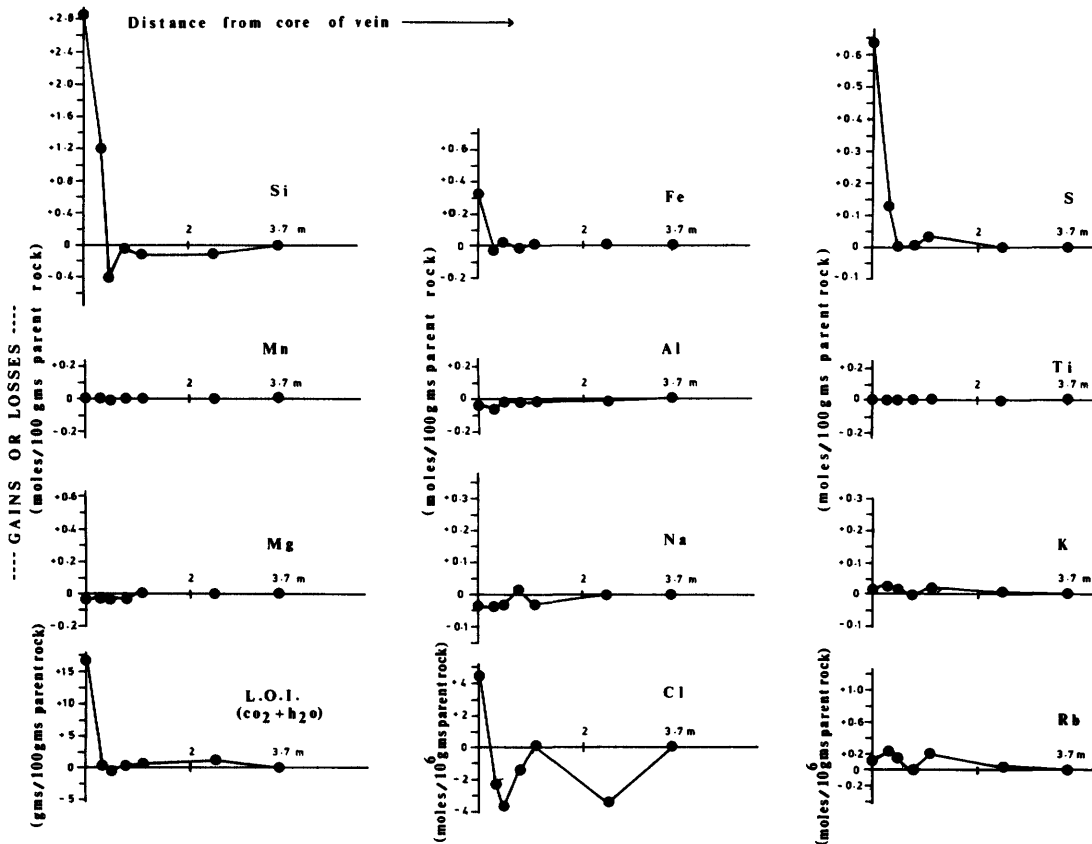


Figure 8—Compositional variations due to progressive hydrothermal alteration in wallrocks of a gold-bearing quartz-carbonate vein (Gutcher Lake area).

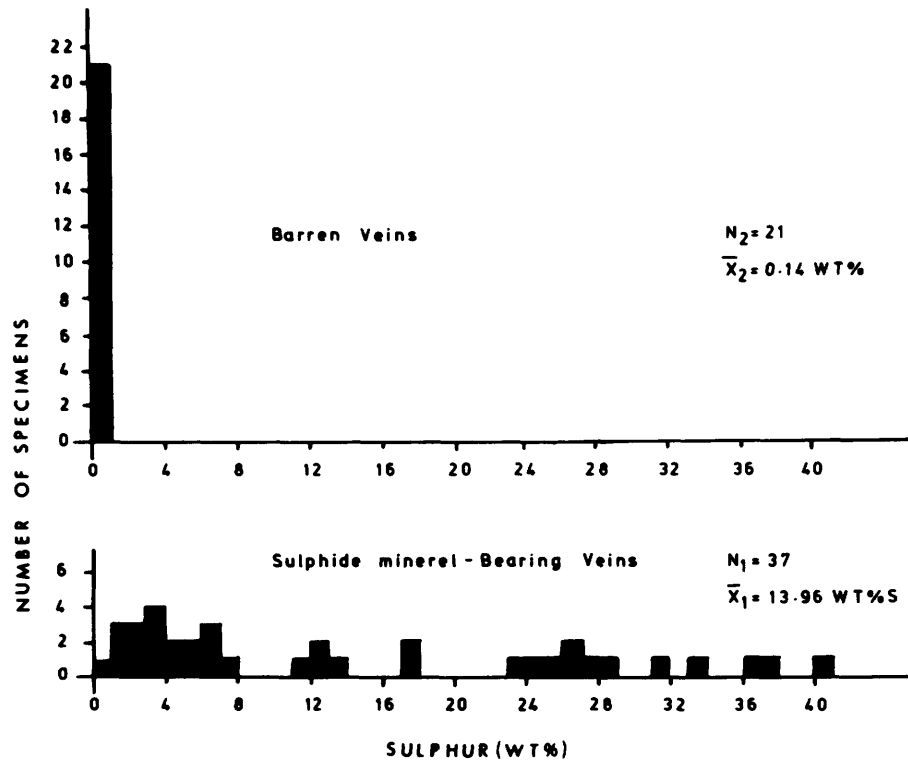


Figure 9—Histogram of sulphur content for quartz-carbonate veins in the Gutcher Lake area.

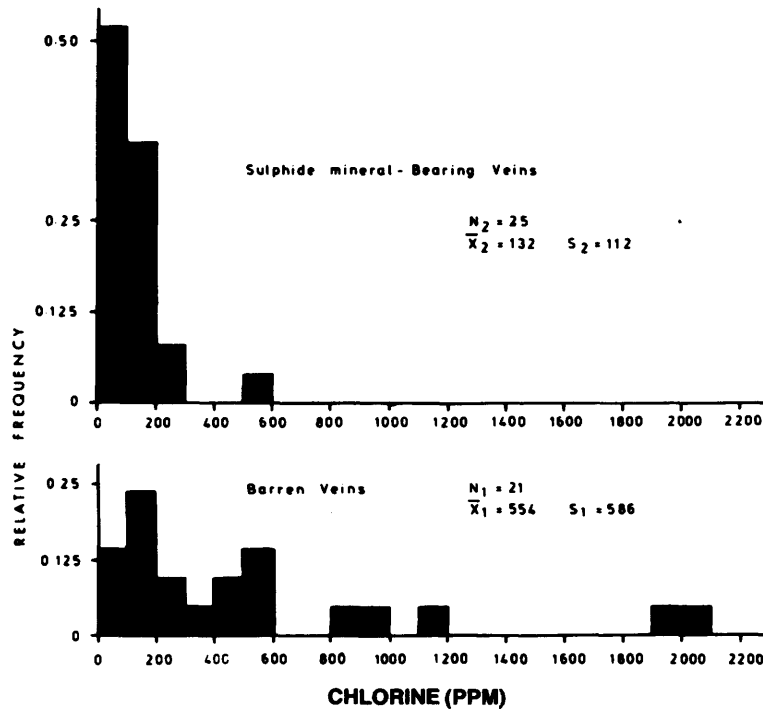


Figure 10—Histogram of chlorine content for quartz-carbonate veins (Gutcher Lake area).

5) White mica-chlorite-quartz-ankerite alteration of wall-rocks of barren and gold-bearing quartz-carbonate veins, occupying fractures transecting marginal parts and contact wallrocks of the Gutcher Lake stock, involved large additions of Si, Fe, K, volatiles (CO₂ + H₂O), and Rb, leaching of Na, and intense reduction of the redox state of iron to ~0.90.

6) Gold-bearing veins differ from more common and coexisting barren veins in that the former set have major concentrations of sulphide minerals and chlorine contents of less than 300 ppm. Wallrock alteration associated with the gold-bearing veins involved major addition of sulphur with trivial or no gain in chlorine.

7) Field and geochemical evidence suggests a genetic link between sulphide-mineral-bearing metasedimentary units and later metal-bearing veins around the Gutcher Lake stock.

8) Two stages of metal concentration around the Gutcher Lake stock are recognized. Initial syngenetic deposition of Cu-Au-bearing, ferruginous sediments was broadly coeval with stock intrusion and contact metamorphism; subsequent remobilization of pre-existing sulphide mineral concentrations was concomitant with native gold precipitation along fractures during regional metamorphism.

APPENDIX 1

Mass Balance Equation for Alteration of the Gutcher Lake Stock

Gresens (1967) derived a general equation expressing the chemical change accompanying the transformation of a given parent to its complement daughter rock, and incorporating whole rock analyses, specific gravity, and volume changes accompanying alteration. Simple inspection of parent-daughter pairs of rock analyses is not satisfactory for deducing chemical changes because comparisons should take into account the rocks' specific gravity and possible volume changes accompanying transformation particularly if alteration induced changes in volatile content.

Gresens' mass balance equation can be modified to express the most probable value for the chemical change, taking into account inherent parent and daughter rock heterogeneity, by assigning mean values to the equation's variables. The variance of the chemical change was expressed in terms of the variances of the equation's variables, and an unbiased measure of significance was assigned employing the null hypothesis test explained in Ostle (1963) and Bevington (1969). Variability in the physical and chemical traits of rocks becomes significant when large rock volumes are considered in the alteration process, and probably exceeds in magnitude variability due to analytical uncertainty.

Gresens' mass balance equation, modified to incorporate rock heterogeneity, can be expressed as follows:

$$\begin{aligned} \Delta X_i &= f(\bar{\beta}^d \bar{\beta}^p, \bar{x}_i^d, \bar{x}_i^p, F_v) \\ \Delta X_i &= a[F_v \bar{x}_i^d (\bar{\beta}^d / \bar{\beta}^p) - \bar{x}_i^p] \end{aligned} \quad (1)$$

where,

ΔX_i average chemical change in component i,
 a initial quantity of parent rock,
 F_v average volume factor,
 $\bar{x}_i^{d,p}$ average weight fraction of component i in daughter and parent rock suites, respectively,
 $\bar{\beta}^{d,p}$ average specific gravity of the daughter and parent rock suites, respectively.

The parent and daughter rock suites are described respectively by the parameters (N_p, $\bar{\beta}^p$, S^p, $\bar{x}_1^p, \dots, \bar{x}_n^p, S_1^p, \dots, S_n^p$) and (N_d, $\bar{\beta}^d$, S^d, $\bar{x}_1^d, \dots, \bar{x}_n^d, S_1^d, \dots, S_n^d$) where N is the number of rock samples in the suite, $\bar{\beta}$ is the average specific gravity, S is the standard deviation in $\bar{\beta}$, \bar{x}_i is the average weight fraction of component i, and S_i is the standard deviation in \bar{x}_i .

Equation (1) was employed to assess the net chemical changes accompanying the transformation of precursor medium-grained, granitoid-textured, quartzofeldspathic rocks to their complement finer-grained, fissile, chlorite-white mica-calcite-rich rocks along margins of the Gutcher Lake stock (see Tables 1a and 1b). A parent rock suite consisting of 20 rock specimens was collected from the core of the stock to represent rocks with minimal alteration. A daughter rock suite consisting of 20 specimens was collected from the stock's margins and included only rocks with intense alteration.

APPENDIX 2

Mass Balance Equation for Contact Metamorphism Around Gutcher Lake Stock

The absence of unmetamorphosed volcanic rocks in the Gutcher Lake area precludes quantifying the absolute chemical changes accompanying contact or regional metamorphism of mafic volcanic rocks with equation (1). Nevertheless, chemical changes during contact metamorphism of mafic volcanic rocks around the Gutcher Lake stock may be quantified relative to possible chemical changes accompanying regional metamorphism of similar rocks removed from the intrusive contact, if one assumes a common precursor parent volcanic rock for both rock populations.

Two sample suites each with 19 specimens of pillowed and massive mafic metavolcanics with contrasting metamorphic mineral assemblages were collected and analyzed (see Table 4). The first suite consists of mafic metavolcanics in the regional greenschist facies, and the second suite consists of equivalent rocks in the epidote-hornblende hornfels facies with minimal retrograde metamorphism to the regional facies.

The net chemical change in component i during regional metamorphism of mafic volcanic rocks is given by equation (1):

$$\Delta X_i^r = a[F_v^r \bar{x}_i^r (\bar{\beta}^r / \bar{\beta}^p) - \bar{x}_i^p] \quad (2a)$$

The net chemical change in component i during contact metamorphism of equivalent rocks is similarly:

$$\Delta X_i^c = a[F_v^c \bar{x}_i^c (\bar{\beta}^c / \bar{\beta}^p) - \bar{x}_i^p] \quad (2b)$$

where $\bar{\beta}^p$ and \bar{x}_i^p refer respectively to the average specific gravity and composition of the parent tholeiitic basalt.

The relative chemical change during metamorphism becomes:

$$\begin{aligned} \Delta X_i &= \Delta X_i^c - \Delta X_i^r \\ \Delta X_i &= a[F_v^c \bar{x}_i^c (\bar{\beta}^c / \bar{\beta}^p) - F_v^r \bar{x}_i^r (\bar{\beta}^r / \bar{\beta}^p)] \end{aligned} \quad (3)$$

The volume factor F_v^c can be expressed in terms of F_v^i if one or more immobile components are identified; similar (Al_2O_3/TiO_2) values for both metamorphic rock suites suggests that aluminium and titanium remained relatively immobile during metamorphism.

Rearranging equation (3), the volume factor F_v^c becomes:

$$F_v^c = F_v^i (\bar{x}_{Al,Ti}^i \beta^i / \bar{x}_{Al,Ti}^c \beta^c) = F_v^i C_o \quad (4a)$$

An expression for the volume factor F_v^i may be obtained by solving equation (2a) on the assumption that aluminium and titanium remained immobile during regional metamorphism of parent tholeiitic basalts. Rearranging equation (2a):

$$F_v^i / \beta^i = (\bar{x}_{Al,Ti}^i / \bar{x}_{Al,Ti}^c \beta^c) = C_i \quad (4b)$$

The average aluminium and titanium contents of a parent tholeiitic basalt are taken from Table 2 in Cann (1971).

Substituting variables C_o and C_i into equation (3), the net chemical change in component i becomes an expression with seven variables, each with respective means and standard deviations;

$$\Delta X_i = f(\bar{x}_i^i, \bar{x}_i^c, \beta^i, \beta^c, C_o, C_i), \quad (5)$$

$$\Delta X_i = a[(C_o C_i \beta^c \bar{x}_i^i) - (C_i \beta^i \bar{x}_i^c)].$$

APPENDIX 3

Evaluation of Variance for Mass Balance Equations (Gutcher Lake Area)

Given a function $x = f(u, v, w, \dots)$, the variance for x can be expressed in terms of the variances $\alpha^2 u, \alpha^2 v, \alpha^2 w, \dots$ for the variables u, v, w, \dots as follows (Bevington 1969):

$$\alpha_x^2 \cong \alpha_u^2 (\partial x / \partial u)^2 + \alpha_v^2 (\partial x / \partial v)^2 + 2\alpha_{uv} (\partial x / \partial u) (\partial x / \partial v) + \dots \quad (6a)$$

where the first two terms are averages of squares of deviations and usually dominate in the expression. The third term will vanish if fluctuations in u and v are uncorrelated.

If fluctuations in the values of u and v are uncorrelated, equation (6a) reduces to:

$$\alpha_x^2 \cong \alpha_u^2 (\partial x / \partial u)^2 + \alpha_v^2 (\partial x / \partial v)^2 + \dots \quad (6b)$$

(with additional similar terms corresponding to additional variables).

From the general equation (6b), a specific formula for the variance in ΔX_i for equation (1) is:

$$S_{\Delta X_i}^2 = a^2 S_1^2 + a^2 S_2^2$$

where,

$$S_1^2 = [S_{F_v^i}^2 / (F_v^i)^2 + (S_{\bar{x}_i^i}^2) / (\bar{x}_i^i)^2 + (S_{\beta^i}^2) / (\beta^i)^2 + (S_{\beta^c}^2) / (\beta^c)^2] (F_v^i \bar{x}_i^i \beta^i / \beta^c)^2$$

$$S_2^2 = (S_{\beta^i}^2)^2$$

APPENDIX 4

Statistical Inference Concerning Results of Mass Balance Calculations (Gutcher Lake Area)

Given two normal populations with means μ_1 and μ_2 with variances α_1^2 and α_2^2 respectively, inference concerning the difference between μ_1 and μ_2 can be tested with the Null Hypothesis Test. The following is a brief outline of the test and its parameters as described in detail in Ostle (1963):

Null Hypothesis $H_o: \mu_1 - \mu_2 = 0$

Alternative Hypothesis $H_a: \mu_1 - \mu_2 \neq 0$ hence, $\mu_1 \neq \mu_2$

The calculated t-test statistic:

$$t = (\bar{X}_1 - \bar{X}_2) / (S_1^2 / N_1 + S_2^2 / N_2)^{1/2}$$

where,

$$\bar{X}_1 \cong \mu_1$$

$$\bar{X}_2 \cong \mu_2$$

$$S_1^2 \cong \alpha_1^2$$

$$S_2^2 \cong \alpha_2^2$$

The Null Hypothesis is rejected if:

$$t_c \geq + (w_1 t_1 + w_2 t_2) / (w_1 + w_2) \text{ or,}$$

$$t_c \leq - (w_1 t_1 + w_2 t_2) / (w_1 + w_2)$$

where,

t_c = critical value of the t-test statistic

$$w_1 = S_1^2 / N_1$$

$$t_1 :: (1 - \gamma/2)(N_1 - 1)$$

$$w_2 = S_2^2 / N_2$$

$$t_2 :: (1 - \gamma/2)(N_2 - 1)$$

γ = coefficient of confidence.

REFERENCES

- Bevington, P. R.
1969: Data reduction and error analysis for the physical sciences; McGraw-Hill Book Company, New York, 336p.
- Bruce, E. L.
1940: Geology of the Goudreau-Lochalsh area; Ontario Dept. Mines, Ann. Rept. Vol. 49, Pt. 3, 50p.
- Cann, J.R.
1971: Major element variations in ocean-floor basalts; Phil. Trans. Soc. London A. Vol. 268, p.495-505.
- Gresens, R. L.
1967: Composition-volume relationships of metasomatism; Chemical Geology, Vol. 2, p.47-65.
- The Northern Miner
1979: Ego is re-evaluating property; Northern Miner Press, Oct. 18, 1979, Vol. 65, No. 32, p.B29.
- Ostle, B.
1963: Statistics in research; The Iowa State University Press, 585p.
- Turner, F. J.
1981: Metamorphic petrology: mineralogical, field, and tectonic aspects; 2nd edition, McGraw-Hill Book Company, New York, 524p.

Grant 5 Magnetic and Paleomagnetic Characteristics of the Archean Iron Formation and Host Rocks at the Adams Mine, Ontario

D.T.A. Symons, A. W. Quick, and M. Stupavsky

Department of Geology, University of Windsor

ABSTRACT

The magnetic and paleomagnetic characteristics were examined for the Algomian-type iron formation (IF) deposits and Archean volcanic host rocks (HR) of the Adams Mine using 1476 oriented specimens. The iron formation specimens have specific gravities (SG) ranging from ~ 2.7 to ~ 5.0 gm cm $^{-3}$. The low-field susceptibility perpendicular to bedding (k_{\perp}) for the iron formation has a lognormal mean of 4.52×10^{-2} cgs cm $^{-3}$ giving $k_{\perp IF} \cong 192 k_{\perp HR}$. The correlation coefficient for $k_{\perp IF} = 0.0698$ SG -0.179 is $+0.73$ so that average ore has a $k_{\perp IF} \cong 0.0645$. The anisotropy of magnetic susceptibility (AMS) ratio of $k_{\parallel IF}/k_{\perp IF} = 1.62$ where $k_{\parallel IF}$ is the susceptibility parallel to bedding. The natural remanent magnetizations (NRM) of the host rock and iron formation have means of 5.97×10^{-6} and 1.21×10^{-2} emu cm $^{-3}$ giving Koenigsberger ratios of 0.013 and 0.67. In the anomaly calculations, the host rock NRM and k_{\perp} can be omitted. The iron formation NRM has a directionally dependent augmenting factor of $+17$ percent for the deposits. Shock and storage tests indicate that the iron formation NRM is relatively stable. Using the AMS ratio, a demagnetizing factor of 2π and the NRM augmenting factor in addition to the usual input parameters gives fits of computed to measured airborne magnetic anomalies of 3, 7, 8, and 17 percent. Alternating field, thermal, and chemical demagnetization plus fold and contact tests isolates 1) a pre-folding, primary depositional A component in the iron formation of ~ 2700 Ma; 2) postfolding, secondary Kenoran orogenic metamorphic B component in the host rock of ~ 2500 Ma; and 3) postfolding, secondary metamorphic C components in the host rock and in the baked contact zone of the iron formation against an Abitibi dike, and a primary C component in the dike itself which are related to intrusion of the dikes at ~ 2200 Ma.

INTRODUCTION

In this project the magnetization of four Archean Algomian-type banded iron formation (IF) ore deposits and their host rocks (HR) are being studied. The purposes are 1) to provide average values for their magnetic properties so that their magnetic anomalies may be correctly interpreted; and 2) to analyze their paleomagnetic properties

so that their ore genesis may be better understood. Results have been reported for the Sherman Mine (Symons and Stupavsky 1979, 1980) and the Moose Mountain Mine (Symons *et al.* 1980). This paper reports on the Adams Mine. Data analysis is being completed on the Griffiths Mine.

The Adams Mine is located near Kirkland Lake in Boston Township (79.90°W, 48.01°N) (Figure 1). After discovery in 1902 (Ratcliffe 1957), an airborne magnetometer survey was run in 1948. Jones and Laughlin Steel Corporation brought the property into production in 1964 at a rate of 10^6 tons of magnetite pellet concentrate per year.

GEOLOGY

Boston Township is in the Abitibi Belt of the Superior Province of the Canadian Shield. The oldest Archean strata are Keewatin-type metavolcanics giving a U/Pb age of 2703 ± 2 Ma (Nunes and Jensen 1980); associated metasediments include the iron formation (IF) (Lawton 1957; Dubuc 1965). The metavolcanics are mafic to intermediate flows with some fragmental, felsic flow and tuff units which contain minor pyrrhotite and pyrite. The IF occurs in several horizons along a 10 km by 1 km iron range. Its magnetite-oxide facies has thin (< 2 cm) alternating bands of black magnetite and grey-red chert with trace amounts of hematite, chlorite, tremolite, and pyrite. Its siliceous facies contains massive cherty quartzite with < 5 percent disseminated magnetite and trace amounts of graphite. These strata have been intruded by diorite. Unconformably overlying are Timiskaming-type conglomerate and greywacke which give an updated Rb-Sr age of 2368 ± 48 Ma (Fairbairn *et al.* 1966). During the subsequent Kenoran orogeny, Haileyburian-type mafic intrusions were emplaced. Next, Algomian-type granite-syenite stocks and lamprophyre dikes were emplaced, including the Lebel syenite stock. The adjacent and similar Otto stock gives ages by several methods ranging from 1730 ± 50 to 2500 ± 100 Ma as discussed below. The Archean strata were folded into a tight isoclinal syncline (Figure 2) with a plunge of $\sim 60^\circ$ SW and limbs dipping at $50-90^\circ$ SE. Pillows indicate that the south limb is overturned and the north limb eroded. Regional metamorphism reached mid-greenschist facies conditions. The Lebel stock has a garnet amphibolite contact aureole. All of the Archean rocks were cut by northeast-trending vertical Proterozoic dikes (Abitibi-type?).

SAMPLING

At each of the 45 sample sites of mafic metavolcanics (Figure 2), five cores were drilled, and oriented to within $\sim 2^\circ$ using a solar compass. Two or more 2.5 cm right cylindrical specimens were sliced from each core. A total of 171 hand samples of iron formation were collected from the four Adams Mine pits (Figure 3). They were oriented to within $\sim 3^\circ$ using bench maps and an inclinometer. Four or more 1 cm right cylindrical specimens were cored from each sample. Overall, 1476 specimens were used in this study. Additional details on the sampling, methods, and results of this study can be found in Quick (1981).

SPECIFIC GRAVITY

The specific gravity (SG) of 547 IF specimens was measured to $\pm 0.001 \text{ g cm}^{-3}$ using a pycnometer method. The values range from ~ 2.70 for barren chert to ~ 5.00 for pure magnetite (Figure 4a) with a mean of 3.24 ± 0.51 (standard deviation). This is lower than the 3.49 average for Adams Mine ore which contains 22 percent magnetic Fe content, because of a sampling bias towards lean IF from the pit walls.

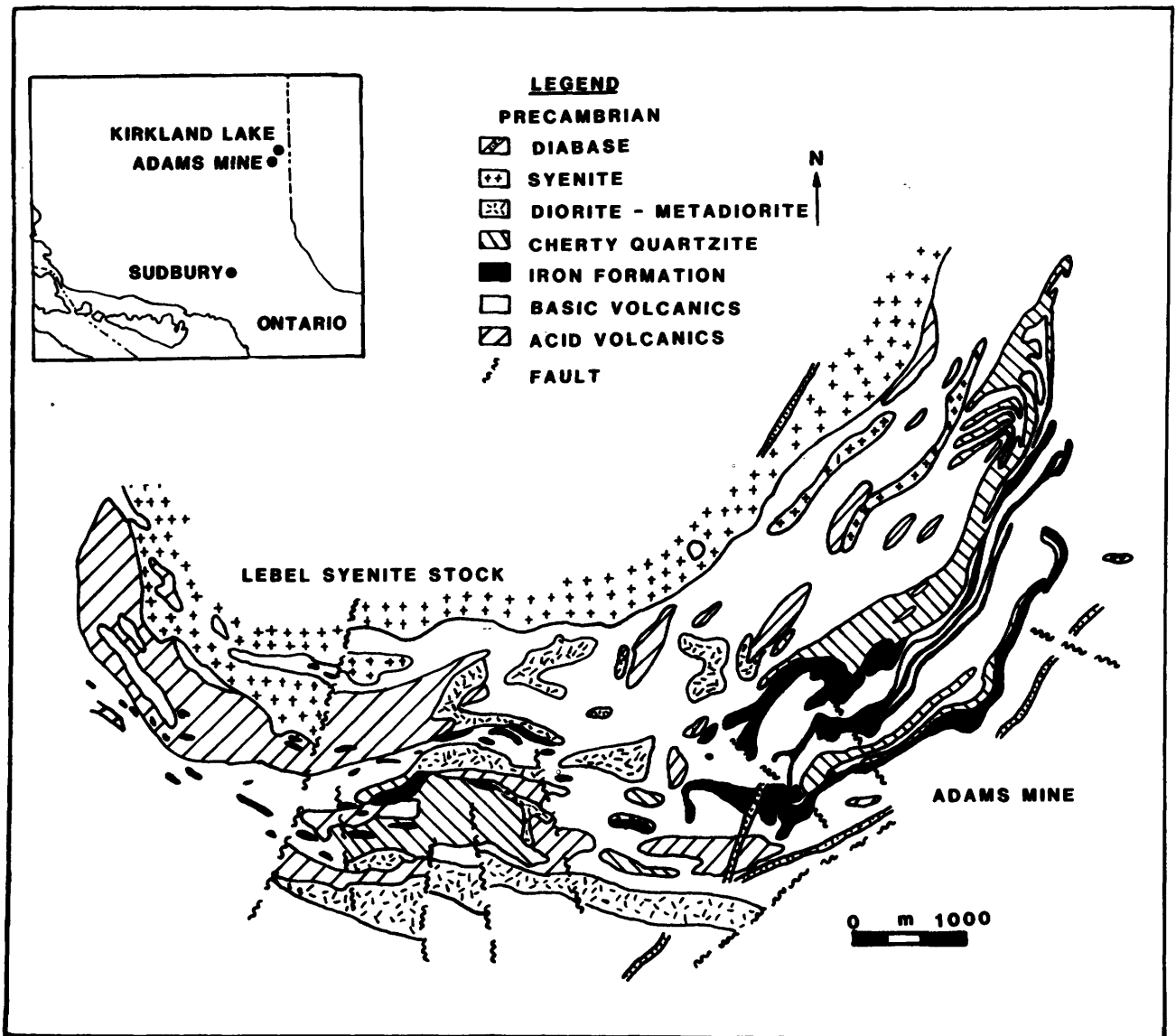


Figure 1—Location and geology of the Boston Township iron range.

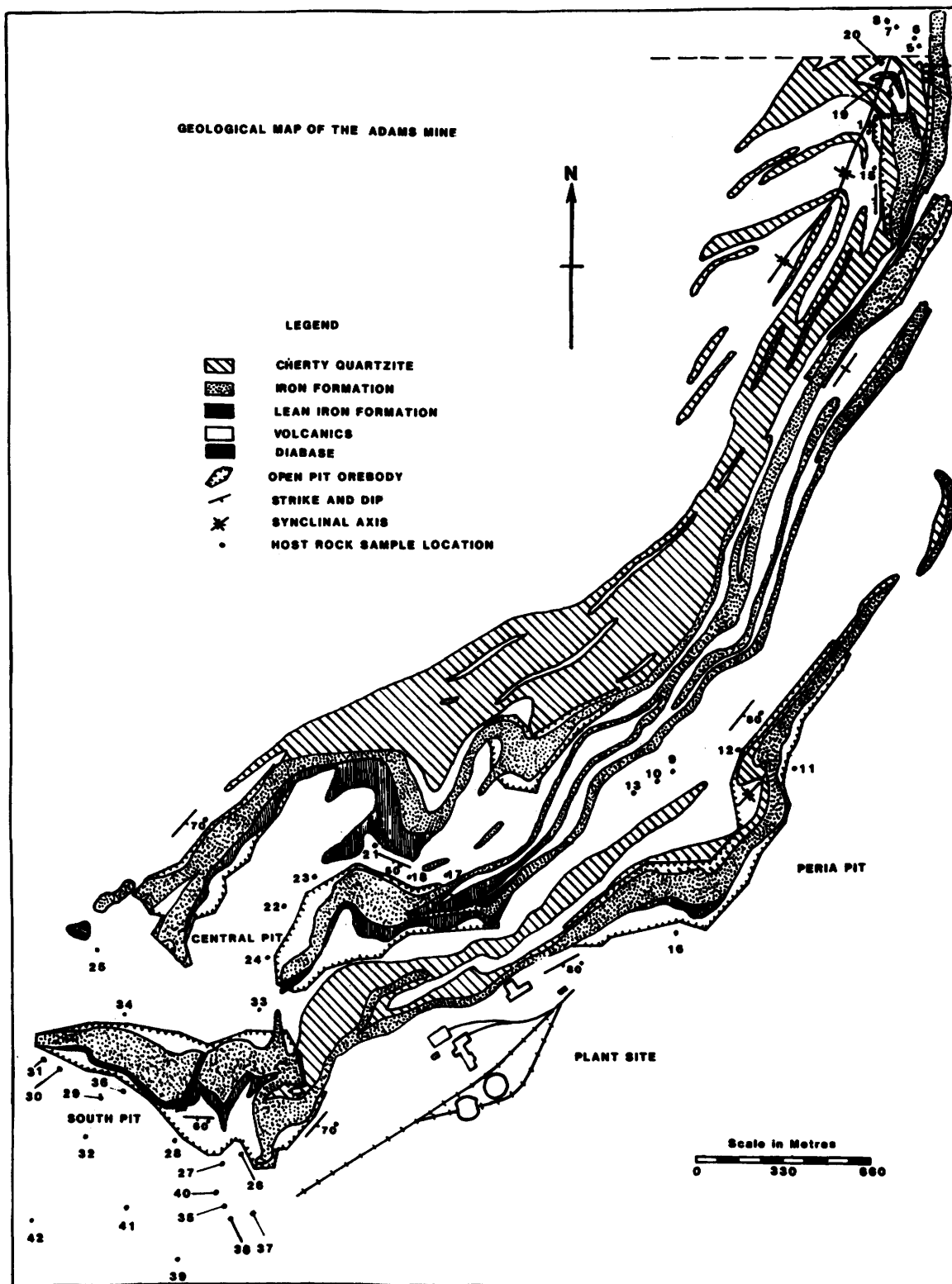


Figure 2—Geology of the Adams Mine and host rock sample locations.

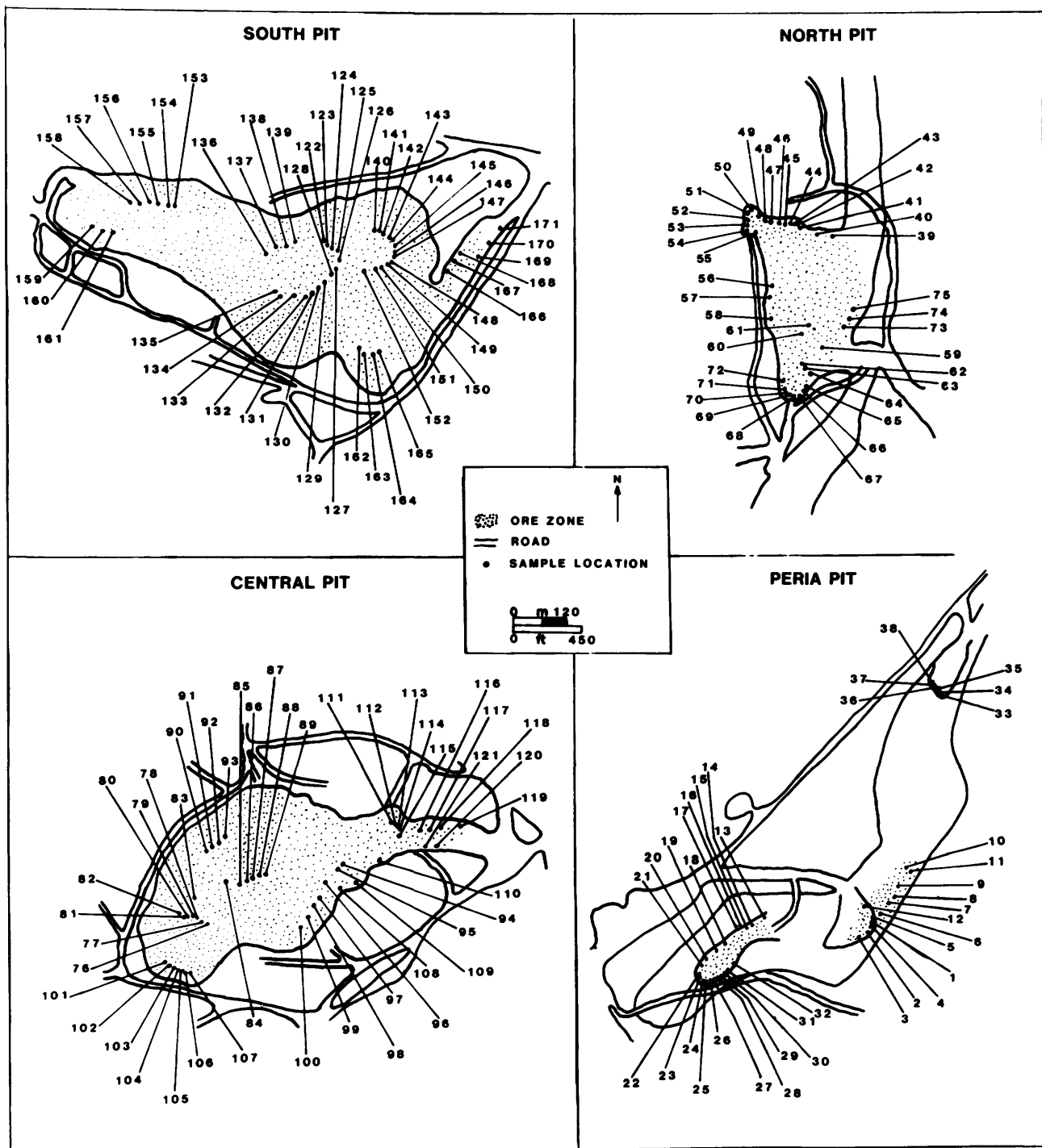


Figure 3—Iron formation sample locations.

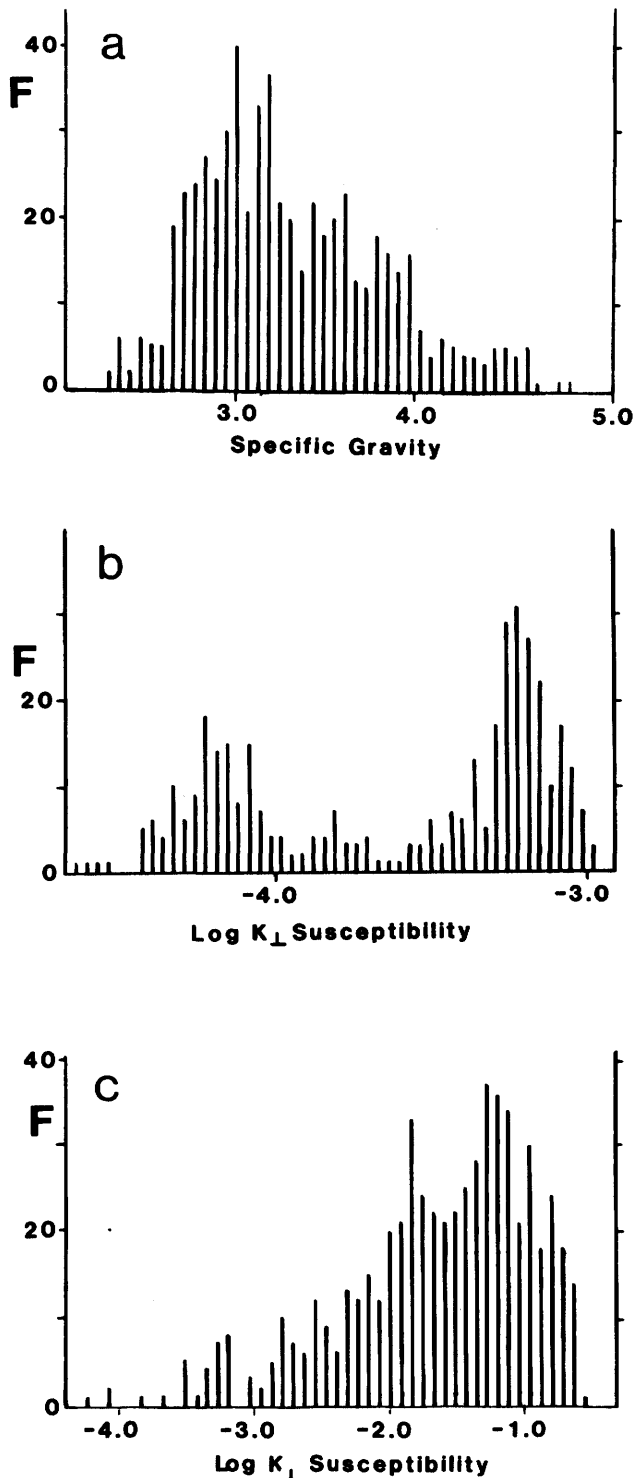


Figure 4—Histograms of the frequency (F) of **a.** specific gravity of iron formation in values $gm\ cm^{-3}$; **b.** hostrock k_{\perp} susceptibility values in $cgs\ cm^{-3}$; and **c.** iron formation k_{\perp} susceptibility values in $cgs\ cm^{-3}$.

MAGNETIC SUSCEPTIBILITY

A toroid bridge (Christie and Symons 1969) was used to measure the low-field magnetic susceptibility perpendicular to bedding (k_{\perp}) of 524 HR and 592 IF specimens. The $k_{\perp HR}$ values have a bimodal lognormal distribution reflecting felsic and mafic HR populations (Figure 4b) with an overall lognormal mean of 2.35×10^{-4} $cgs\ cm^{-3}$. The $k_{\perp IF}$ values have a lognormal distribution (Figure 4c) with a lognormal mean of 4.52×10^{-2} $cgs\ cm^{-3}$. Because $k_{\perp IF} \cong 192\ k_{\perp HR}$, it is valid to ignore $k_{\perp HR}$ for the background in calculating the magnetic anomaly. The regression fit between $k_{\perp IF}$ and SG gives the relationship $k_{\perp IF} = 0.0698\ SG - 0.179$ with a high correlation coefficient of +0.73 (Figure 5). Thus average Adams Mine ore has a $k_{\perp IF}$ of $0.0645\ cgs\ cm^{-3}$.

ANISOTROPY OF MAGNETIC SUSCEPTIBILITY

The low-field anisotropy of magnetic susceptibility ellipsoid was determined from nine measurements on each of 592 IF cores. The axial magnitude ratios have mean values for k_{int}/k_{min} of 1.47 and for k_{max}/k_{min} of 1.63 (Figure 6e,f). Within 95 percent confidence limits, k_{min} is perpendicular to bedding (i.e., $k_{min} \cong k_{\perp}$) and k_{int} and k_{max} are in the bedding plane. Thus the mean bedding plane susceptibility, $k_{\parallel} = (k_{int} + k_{max})/2 = 1.55\ k_{\perp}$. The small IF cores are often confined to one band and hence may appear more isotropic than reality. Therefore, 15 large 2.5 cm cores were measured which give $k_{\parallel} = 1.69\ k_{\perp}$. This effect is likely partially offset by sampling bias because well banded IF is easier to sample than massive cherty IF. Thus the accepted ratio is a compromise of $k_{\parallel} = 1.62\ k_{\perp}$.

NATURAL REMANENCE

HOST ROCK

A Schonstedt SSM-1A spinner was used to measure the natural remanent magnetization (NRM) of 524 HR specimens. Their NRM intensities ($J_{r HR}$) have a lognormal distribution (Figure 6a) and mean of 5.97×10^{-6} $emu\ cm^{-3}$. Similarly, their Koenigsberger ratios (Q_{HR}) of remanent to induced magnetization have a lognormal distribution (Figure 6b) with a mean of 1.3×10^{-2} . With the induced magnetization of the IF being $\sim 4300\ J_{r HR}$, the latter can obviously be omitted from the anomaly calculation. A storage test run on 16 HR specimens by placing their NRM vector antiparallel to the Earth's magnetic field (EMF) for a five-week period yielded a 6.8 percent change in $J_{r HR}$ with a $6.2^{\circ} \pm 4.4^{\circ}$ change in NRM direction. This test indicates that the HR NRM is relatively stable with small viscous remanence (VRM) components.

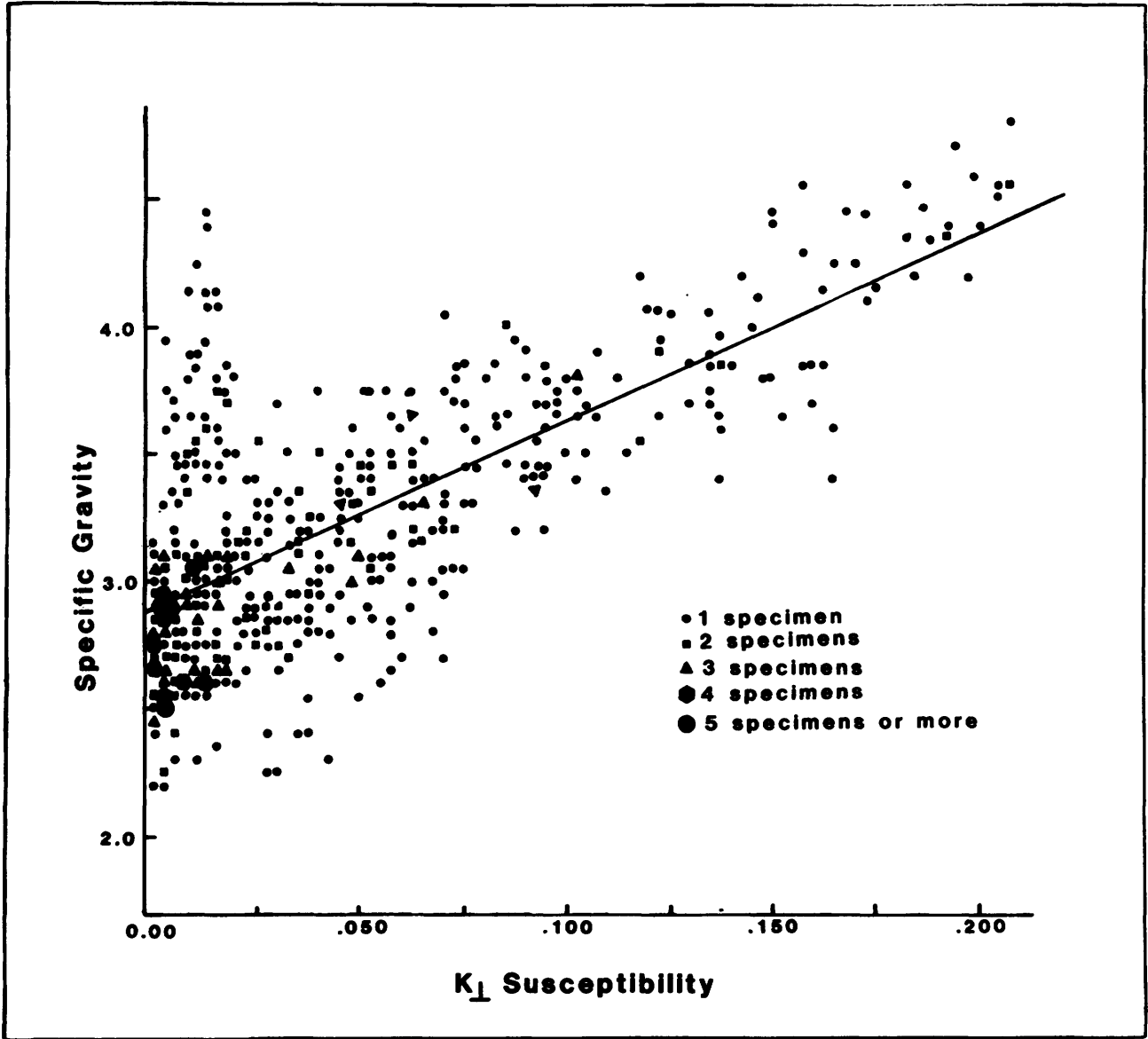


Figure 5—Regression fit between the IF specific gravity values in gm cm⁻³ and the k_⊥ susceptibility values in cgs cm⁻³.

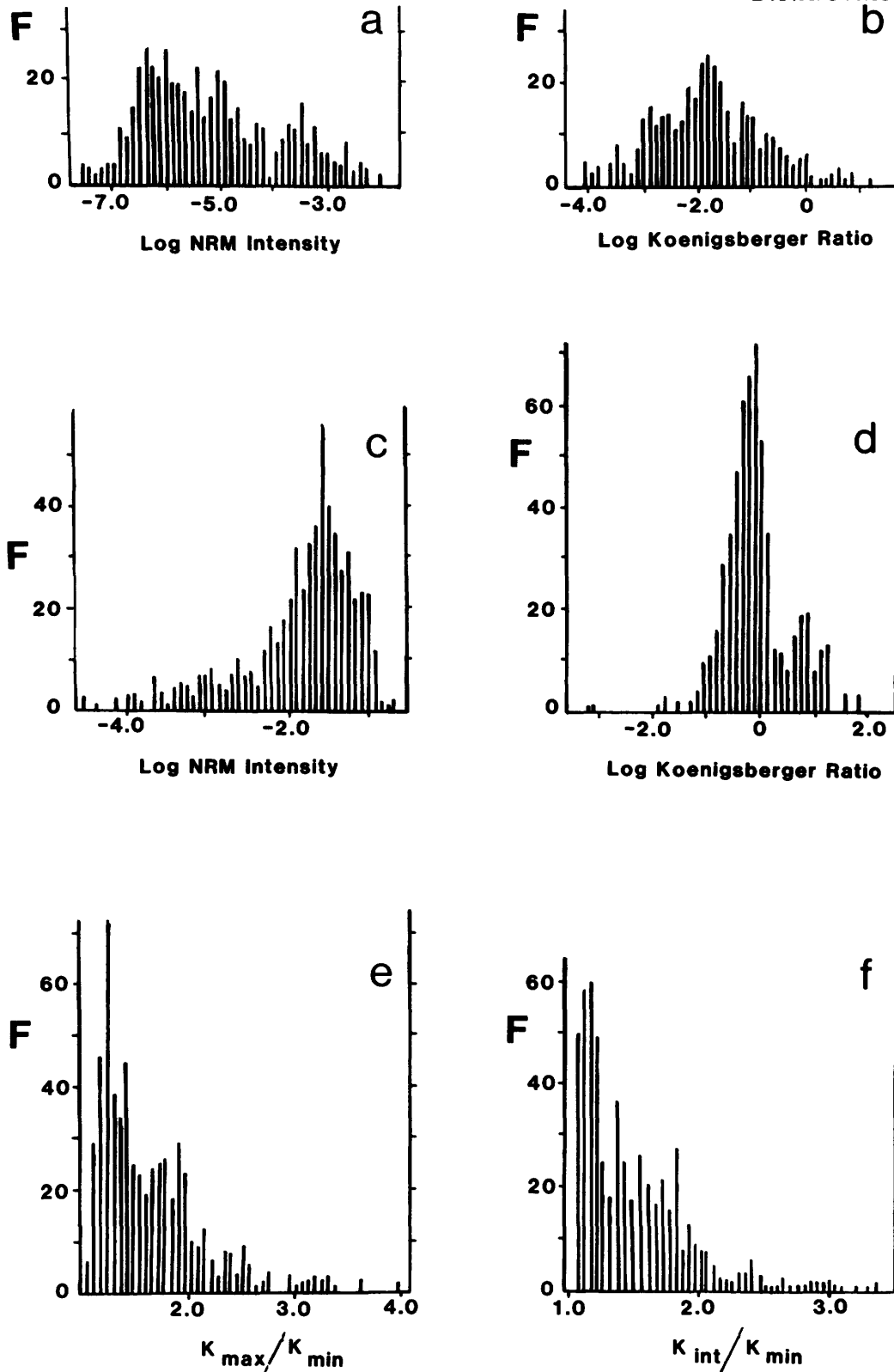


Figure 6—Histograms of the frequency (F) of values for **a.** HR NRM intensities in emu cm^{-3} ; **b.** HR Koenigsberger ratios; **c.** IF NRM intensities in emu cm^{-3} ; **d.** IF Koenigsberger ratios; **e.** IF k_{max}/k_{min} ratios; and **f.** IF k_{int}/k_{min} ratios.

IRON FORMATION

The 592 IF specimens also show a lognormal distribution of $J_{r, IF}$ values with a mean of 1.21×10^{-2} emu cm^{-3} (Figure 6c), and of Q_{IF} values with a mean of 0.67 (Figure 6d). The linear relationship $J_{r, IF} = 0.215 K_{\perp} + 0.016$ has a good correlation coefficient of +0.55. The mean NRM direction, averaging all vectors regardless of polarity, is 92.8° , 52.3° (7.4°), i.e., declination, inclination (radius of 95 percent confidence or α_{95} , Fisher 1953). This direction deviates from the Earth's magnetic field direction of 352° , 76° by an angle (θ) of 42.6° . The ratio of the vector resultant (R) to the number of specimen directions (N) gives an effective Koenigsberger ratio, $Q_e = Q(R/N)$. Thus the NRM increases the induced magnetic intensity (J_i) by Q_e ($\cos \theta$) J_i to give an augmenting factor of 0.17 J_i . A five-week storage test on 18 representative IF specimens gives a 3.6 percent change in $J_{r, IF}$ with a $4.8^{\circ} \pm 3.0^{\circ}$ change in NRM direction which indicates that the IF NRM is stable with a small VRM component. A shock test was run on 26 IF specimens to assess the possibility of dynamite induced effects. The specimens were struck 20 times on an aluminum plate with their NRM vector parallel to the EMF and measured, and the process repeated antiparallel to the EMF. This test gives a 40 percent mean reduction in $J_{r, IF}$ with a $20^{\circ} \pm 18^{\circ}$ directional change, thereby indicating the potential for blast induced effects which would effectively decrease the computed augmenting factor by ~ 40 percent of 0.17 J_i or 0.07 J_i (i.e., 7 percent of total peak anomaly). Shapiro and Ivanov (1966) and Cisowski and Fuller (1978) have shown that such shock-induced components are readily removed in the initial alternating field (AF) and thermal demagnetization steps.

MAGNETIC MODEL

The computer model for the theoretical magnetic anomaly calculation uses the equations for a thick sheet model of infinite strike and dip extent. Using the South Pit ore zone as an example, it incorporates 1) the EMF intensity of 59,760 γ and direction of 352° , 76° (CDM 1965); 2) the strike of 93° (587°E), dip of 60°S , and thickness of 165 m; 3) the $k_{\perp, IF}$ of 0.067 cgs cm^{-3} ; 4) the anisotropy ratio of $k_{\parallel} = 1.57 k_{\perp}$; 5) the demagnetizing factor of 2π (Gay 1963); 6) the NRM augmenting factor of 0.17 J_i or a 17 percent directionally dependent increase (Strangway 1965); and 7) a terrain clearance of 308 m (1000 feet) for comparison to the measured airborne anomaly. The theoretical magnetic anomaly for the South Pit computes to 10,000 γ . This agrees within 8 percent of the measured peak anomaly of 10,750 γ (i.e., peak of 72,250 γ less a background of 59,500 γ , GSC 1975). The Perria, North, and Central Pits peak anomalies agree within 3, 17, and 7 percent respectively. Conventional interpretation, excluding the anisotropy, demagnetizing, and NRM factors leads to differences of >40 percent in all cases. Type curves for the airborne magnetic anomaly over an orebody of the South Pit dimensions and characteristics are given for varying attitudes (Figure 7). These curves (Fig-

ure 7a) show that the deposit would give an anomaly of only $\sim 3200 \gamma$ in its original flat-lying position, or of $\sim -2600 \gamma$ if it were completely overturned in the syncline. The curves also show the virtual absence of dip-induced skew to the anomaly shape. Thus conventional interpretation would predict approximately vertical dips from any IF anomaly regardless of its real dip. Further the strike direction of the IF has little effect on the anomaly magnitude or shape (Figure 7b).

AF CLEANING

Alternating field (AF) step demagnetization was done on pilot specimens using a Schonstedt GSD-1 AF demagnetizer at steps of 5, 10, 15, 20, 30, 40, 50, 60, 70, 80, 90, and 100 mT peak intensities. The optimum AF cleaning fields for the remaining specimens were chosen using the paleomagnetic stability index (PSI) criteria of Symons and Stupavsky (1974). Fold tests were run including plunge and bedding tilt corrections.

HOST ROCK

The 45 HR pilot specimens, one per site, show a wide range of AF cleaning behaviours which is consistent with their wide lithologic range. Most show a rapid decay of NRM intensity (Figure 8a) and a rapid swing of NRM direction at $>80 \text{ deg T}^{-1}$ away from the EMF direction (Figure 8b) up to ~ 20 mT as VRM components are removed. They typically retain only ~ 30 percent and ~ 10 percent of their NRM intensity by 40 and 100 mT respectively, and give PSI minima of $\sim 30 \text{ deg T}^{-1}$ between 15 and 40 mT. Above ~ 40 mT large anhysteretic remanence (ARM) components are induced in the specimens. A further nine specimens per site were cleaned at 20 to 40 mT. Conventional tiered statistics after screening by rejecting 1) core means for which the two specimen directions diverged by $>20^{\circ}$; 2) site means with only one valid core mean; and 3) core means diverging by $>40^{\circ}$ from the remaining specimen site mean, left only four sites with an $\alpha_{95} < 20^{\circ}$. Plotting all the specimen directions on a Schmidt net and then contouring using as 1 percent smoothing circle yielded two clear anomalies, B and C, of 95 percent confidence as defined by the $E + 2\sigma$ level criteria of Kamb (1959) (Figure 8c). Using only specimens within the $E + 2\sigma$ contour level, a fold test shows that both B and C are postfolding at >95 percent confidence. The mean direction of B is 305.0° , 79.1° (4.2°) and of C is 189.9° , 53.9° (3.7°).

IRON FORMATION

The 70 representative IF pilot specimens show a fairly consistent AF cleaning behaviour. Most show a rapid decay to ~ 10 percent of their NRM intensity by ~ 40 mT, and then flatten out to leave ~ 5 percent by 100 mT (Figure 8d). Only five specimens show a much slower decay rate. The directional change is $>50 \text{ deg T}^{-1}$ up to 10 mT

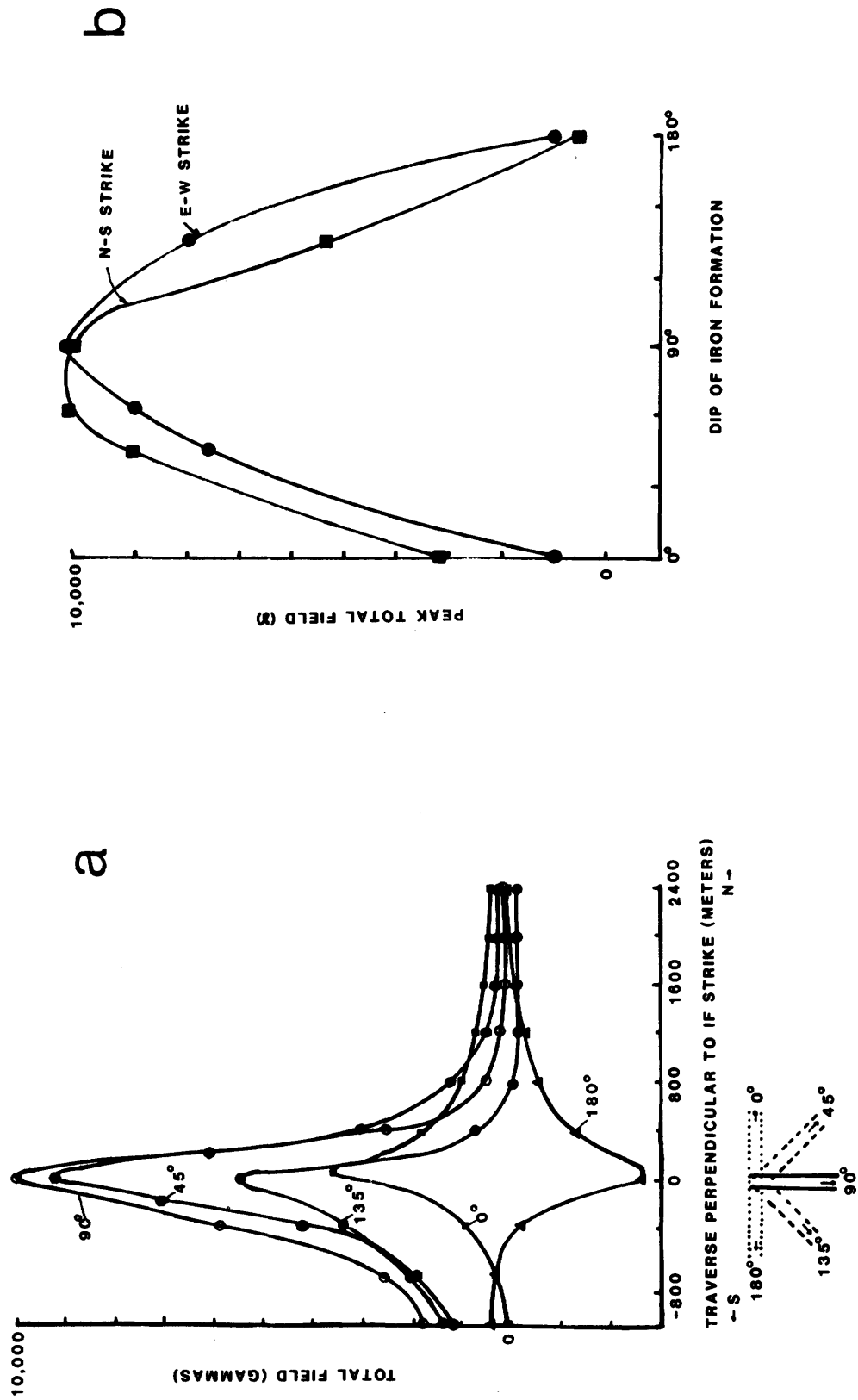


Figure 7—Computed magnetic anomaly type curves for the South Pit ore zone at a terrain clearance of 308 m giving **a.** the profiles of the total field for various angles of dip with the strike perpendicular to the EMF direction; and **b.** the peak total field anomaly for various dips for a north-south and an east-west oriented IF.

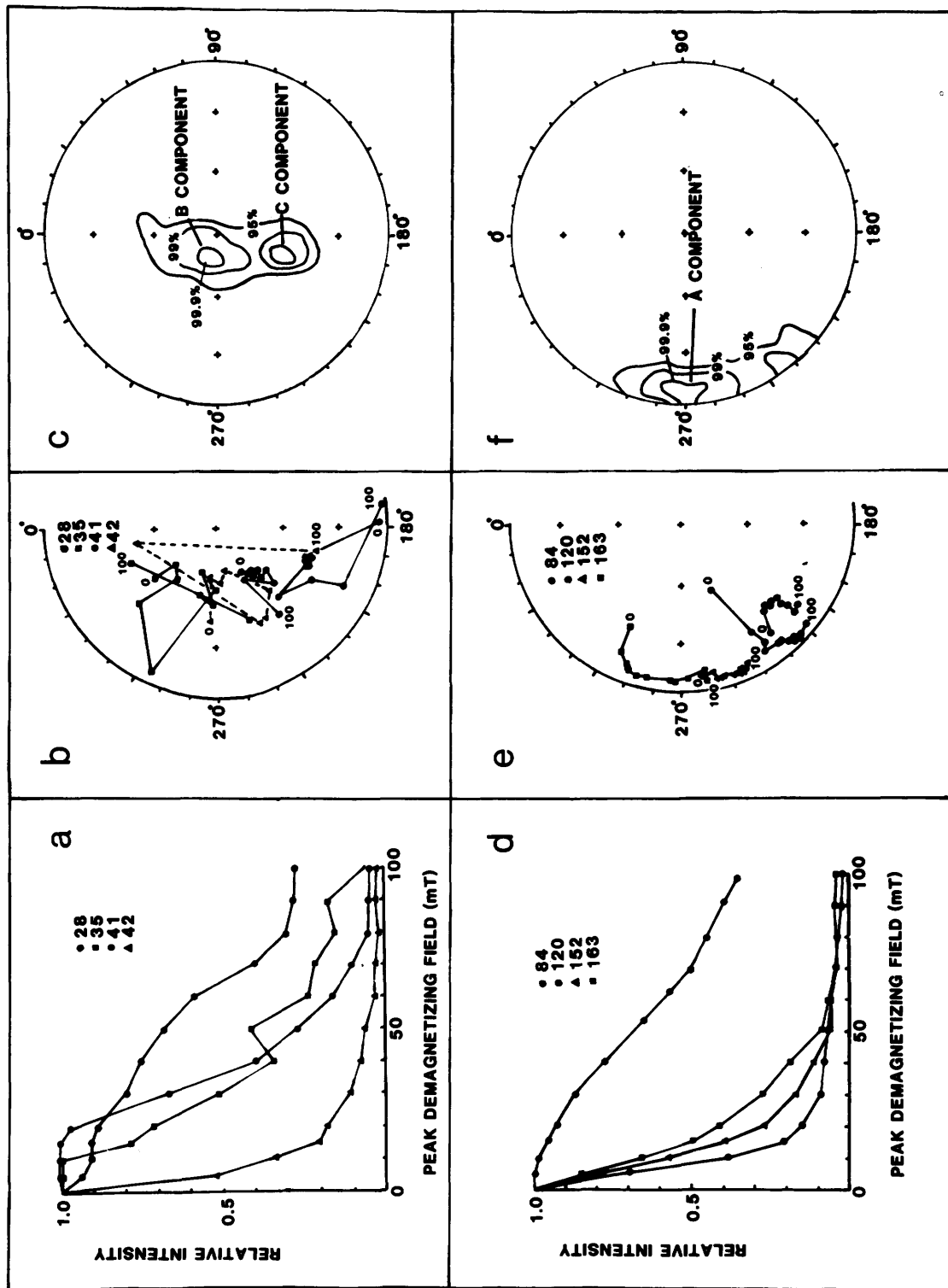


Figure 8—AF demagnetization data for HR: **a.** relative intensity decay curves for four examples against peak field in mT on step demagnetization; **b.** directional movement for four examples on AF step demagnetization from 0 to 100 mT on a Schmidt net (solid symbols “down”, open symbols “up”); **c.** stereocontour plot of all AF demagnetized specimen directions on a Schmidt net with confidence levels; and for **d.** relative intensity decay plots for four examples; **e.** directional movement plots for four examples after tectonic correction; and **f.** stereocontour plot of all AF demagnetized specimen directions after tectonic correction.

and then flattens out to ~ 30 deg T^{-1} up to 100 mT as stable end-points are isolated (Figure 8e). A further three to five specimens per block sample were AF cleaned at PSI minimum fields of 40 to 70 mT. Conventional tiered statistics isolated 32 blocks with an α_{95} of $< 20^\circ$. A fold test indicates that they have a prefolding A remanence component at 262.2° , 7.2° (6.5°) with > 95 percent confidence. Plotting all the specimen directions on a Schmidt contour plot also defines a prefolding A component at 256.2° , 7.4° (3.3°) (Figure 8f).

THERMAL CLEANING

Thermal cleaning using steps of 100, 200, 300, 400, 500, 550, 600, and 650°C was done using a non-inductive shielded oven. The 24 representative HR specimens showed three types of behaviour: 1) three specimens did not change from B and C component directions throughout the cleaning, indicating hematite components; 2) 14 specimens proved stable up to $\sim 300^\circ\text{C}$ with B and C component directions and then scattered, indicating low coercivity magnetite components; and 3) seven specimens showed scattered directions throughout the entire cleaning procedure, indicating unstable remanence components. The 22 representative IF specimens typically show a rapid drop to ~ 30 percent of their NRM in-

tensity by $\sim 400^\circ\text{C}$ indicating a significant "soft" remanence component in coarse-grained magnetite. Thereafter they form a "knee" with the bulk of the remaining magnetization being removed between 500 and 600°C with an A component end-point mean direction of 258.2° , 0.4° (17.3°) (Figure 9a).

CHEMICAL CLEANING

Chemical cleaning was done on 19 representative IF pilot specimens using a $12N$ HCl bath in nested mu metal shielding cans. The specimens were measured after immersion periods of 21, 87, 180, 271, 385, 525, 668, 830, 1017, 1161, and 1641 hours. Of these, 13 remained intact throughout the process. They show a rapid intensity drop in the first 100 hours as coarse-grained magnetite in the magnetite bands was preferentially leached (Figure 9b). The directions swing and define A component end-point directions as the component residing in finer grained magnetite in the chert bands is isolated (Figure 9c).

BAKED CONTACT TEST

A vertical 50 m wide "Abitibi" diabase dike cuts the South Pit iron formation from which were taken 15 dike speci-

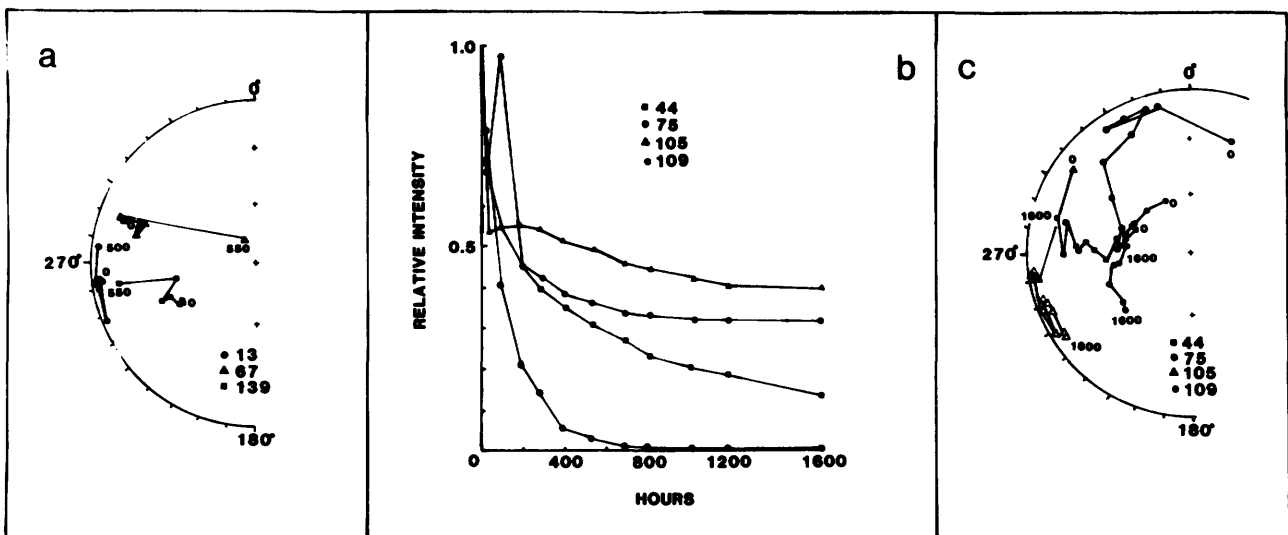


Figure 9—Example IF specimen results showing **a.** directional movement on thermal step demagnetization from NRM (0) to the end point (500, 550) in $^\circ\text{C}$ after tectonic correction; **b.** relative intensity decay curves on chemical step demagnetization; and **c.** directional movement on chemical step demagnetization from NRM (0) to end point at 1600 hours.

Table 1—Pole positions derived from magnetic components.

Group			Number of Vectors	Pole Positions			
Unit	Component	Correction		Long. °W	Lat. °N	dp °	dm °
IF	A	prefolding	151	37.9	6.4	1.7	3.3
HR	B	postfolding	46	112.0	56.3	7.6	8.0
HR	C	postfolding	30	88.1	-7.1	3.7	5.3
Dike	C	postfolding	14	75.6	-23.9	3.4	5.9
Contact	C	postfolding	12	70.1	-32.7	17.5	33.91

Note: dp and dm are the radii of the oval of 95% confidence.

mens and 19 IF samples. The IF samples were spaced at about equal intervals along a 45 m profile extending into the IF perpendicular to the dike contact. After AF and thermal cleaning of pilot specimens, the dike specimens were cleaned at 30 mT to give a C component direction of 175.8°, 33.0° (5.2°). After AF and thermal cleaning of 10 and 17 IF specimens respectively, the vector removed data was examined in the ~40 mT and ~500°C range. For the eight samples closest to the dike, the 13 available vectors give a mean C component direction of 171.6°, 16.9° (32.8°) whereas the 12 available vectors from the more remote IF samples give a mean direction of 291.3°, -5.5° (24.6°) which after correction is the A component direction of 255°, -11°.

PALEOMAGNETIC DISCUSSION

The pole positions for the various components are listed in Table 1. The A component is found only in the IF. The baked contact test indicates that it predates intrusion of the "Abitibi" dikes. The fold test shows that it is a prefolding component and hence predates the ~2500 Ma Kenoran orogeny. Thermal tests show that it resides primarily in magnetite with blocking temperatures of 525 ± 25°C, and chemical tests show that it resides preferentially in fine-grained magnetite disseminated throughout the chert bands. Therefore, it is thought to be a primary depositional remanence. Its pole position indicates an age of ~2700 Ma on the apparent polar wander (APW) curve of Irving (1979) (Figure 10a) which agrees with the 2703 Ma age found for Keewatin-type volcanics of the Abitibi Belt (Nunes and Jensen 1980). The pole also agrees closely with primary poles determined for the Sherman and Moose Mountain iron formations which have radically dif-

ferent tectonic corrections (Symons and Stupavsky 1980; Symons *et al.* 1980).

The B component isolated in the HR is post folding in origin. It resides in magnetite having an AF coercivity of <40 mT and a thermal coercivity of <300°C except for the occasional hematitic specimen. The pole position for the HR B component falls close to the poles for the metamorphic overprint (HD, Figure 10a) found in the Keewatin-type metavolcanics, Timiskaming-type metasediments, and Haileyburian-type diorite near Noranda to the northwest in the Abitibi Belt, as well as, for the Algoman-type granite (AL, Figure 10a) that intrude them (Londry and Symons 1976). In the Noranda area, the terminal Kenoran orogenic thermal event that reset the K-Ar ages occurred at 2525 ± 25 Ma (Dallmeyer *et al.* 1975), and it would also reset these low coercivity components (Pullaiah *et al.* 1975). The pole is also close to the pole of the Otto stock (Pullaiah and Irving 1975; Cavanaugh and Seyfert 1977). The Otto syenite is a few kilometres to the west and petrologically similar to the Lebel stock. It gives K-Ar ages of 1830 ± 70 and 2520 Ma, Rb/Sr ages of 1730 ± 50, 2160 ± 80, and 2470 Ma, and a U/Pb zircon age of 2500 ± 100 Ma (Aldrich and Weatherill 1960; Purdy and York 1968; Bell and Blenkinsop 1976; and T. Krogh, Jack Satterly Geochronology Laboratory, personal communication, in Cavanaugh and Seyfert 1977). This suggests that the best age for these poles is 2500 ± 100 Ma. Other relevant poles for the terminal Kenoran orogeny include the Matachewan dikes (MD, Figure 10a) (Irving and Naldrett 1977) which have been dated by Gates and Hurley (1973) at 2690 ± 93 Ma; the Chibougamau sills (CS, Figure 10a) (Ueno and Irving 1976) which are thought to be somewhat younger than the Rb/Sr age of 2563 ± 79 Ma reported by Jones *et al.* (1974); the Munro lavas (MN, Figure 10a) (Irving and Naldrett 1977) that have been meta-

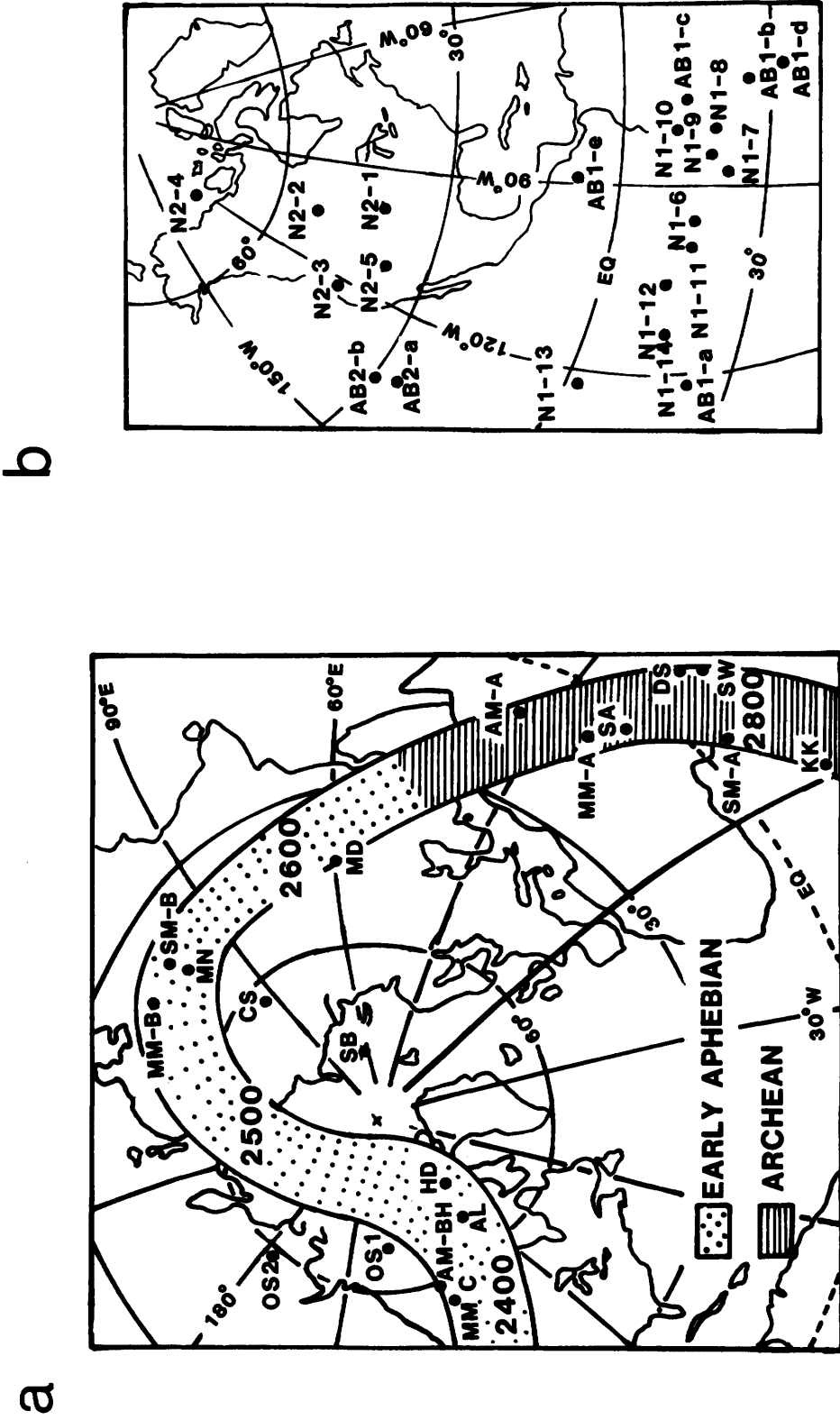


Figure 10—a. Apparent polar wander curve for 16 North American Precambrian samples, showing the Archean curve modified from Irving (1979) with poles from the Sherman Mine (SM-A, SM-B) (Symons and Stupavsky 1980), Moose Mountain Mine (MM-A, B, C) (Symons et al. 1980) and the Adams Mine (AM-A, AM-BH) (this paper), MN from the Munro lavas (Irving and Naldrett 1977) and OS2 from the Otto Stock (Cavanaugh and Seyfert 1977); **b.** poles from the Abitibi dikes of Larochele (1966) (Ab1-a, Ab1-b, Ab2-a), Irving and Naldrett (1977) (Ab2-b), and this study (Ab1-c plus the baked contact Ab1-d and HR C component Ab1-e), and from the Nipissing Diabase after compilation by Morris (in press) showing N1-6 to N1-14 and N2-1 to N2-5 poles.

morphosed by the Kenoran orogeny in the Abitibi Belt; and the Shelley Lake granite overprint B pole (SB, Figure 10a) (Dunlop 1978) which is a Kenoran metamorphic overprint acquired at ~2500 Ma based on $^{40}\text{Ar}/^{39}\text{Ar}$ dating (Berger *et al.* 1978).

The HR C component is a postfolding, low AF coercivity (<30 mT), low thermal coercivity (<300°C) component residing in relatively unstable magnetite domains. This component was also isolated in the NNE-trending "Abitibi" diabase dike and its baked IF contact where it resides in magnetite with AF coercivities of >500 mT and thermal coercivities of >550°C. Therefore, the HR C component is attributed to thermal metamorphic overprinting accompanying dike emplacement. Larochelle (1966) obtained two poles from Abitibi dikes: Ab1 was found in one NNE-trending dike with a pole of 122°W, -21°N and in two ENE-trending dikes with a pole of 73°W, -24°N, and Ab2 was found in 10 ENE-trending dikes with a pole of 134°W, 27°N. Irving and Naldrett (1977) found an Ab2 pole in two ENE-trending dikes with a pole of 135°W, 30°N. From contact test thermal analysis, they concluded that their Ab2 pole was primary, and therefore, that the Ab1 poles were secondary Hudsonian overprints. The contact test thermal evidence of this study indicates that the Ab1 poles are also primary. Therefore, Larochelle (1966) was correct in suggesting two ages of Abitibi dike emplacement. Gates and Hurley (1973) ran Rb-Sr dates on the same Abitibi dikes that Larochelle (1966) studied. They found an age of 2102 ± 67 Ma using the more recent ^{87}Rb λ decay constant of $1.42 \times 10^{-11} \text{ yr}^{-1}$ (Steiger and Jager 1977) for the Ab2 dikes, and rerunning their data, an age of 2206 ± 132 Ma for the Ab1 dikes. The striking aspect of this split is the coincidence of the N1 and N2 poles for the Nipissing Diabase with the Ab1 and Ab2 poles respectively for the Abitibi dikes (Figure 10b) with the obvious implication that the dikes were feeders for two episodes of Nipissing sills. The analysis also supports the analyses of Morris (1979, in press) and of Stupavsky and Symons (in preparation) that the APW path for post-Huronian time tracks from south to north with decreasing age rather than the converse as Irving (1979) has drawn it.

ACKNOWLEDGMENTS

We wish to thank Mr. R. A. Rouleau of DOFASCO for permission to work in the Adams Mine; Mr. K. Oliver, the Mine Geologist for geological advice and collecting help; Messrs. J. Huschilt, D. Dunsmore, and D. D. Symons for their efforts in sample collecting and preparation; Mrs. C. Chinnick and Miss A. Stanta for technical help; and Dr. A. Turek for recalculating the radiometric data.

REFERENCES

Aldrich, L.T. and Weatherill, G.W.
1960: Rb-Sr and K-Ar ages of rocks in Ontario and northern Michigan; *Journal of Geophysical Research*, Vol. 65, p. 337-340.

Bell, K., and Blenkinsop, J.
1976: A Rb-Sr whole rock isochron from the Otto stock, Ontario; *Canadian Journal of Earth Science*, Vol.13, p.998.

Berger, G. W., York, D., and Dunlop, D. J.
1978: $^{40}\text{Ar}/^{39}\text{Ar}$ dating of multicomponent magnetizations from the Shelley Lake granite of northwestern Ontario; *Geological Association of Canada, Abstract*, Vol.3, p.365.

CDM
1965: Isoclinic, isogonic and isodynamic charts, Canada; Canadian Department of Mines, Technical Surveys.

Cavanaugh, M. D., and Seyfert, C. N.
1977: Apparent polar wander paths and the joining of the Superior and Slave Provinces during early Proterozoic time; *Geology*, Vol.5, p.207-211.

Christie, K. W., and Symons, D.T.A.
1969: Apparatus for measuring magnetic susceptibility and its anisotropy; *Geological Survey of Canada, Paper 69-41*, 10p.

Cisowski, S. M., and Fuller, M.
1978: The effect of shock on the magnetism of terrestrial rocks; *Journal of Geophysical Research*, Vol.83, p.3441.

Dallmeyer, R. D., Maybin, A. H., and Durocher, M. E.
1975: Timing of Kenoran metamorphism in the eastern Abitibi greenstone belt, Quebec: evidence from $^{40}\text{Ar}/^{39}\text{Ar}$ ages of hornblende and biotite from post-kinematic plutons; *Canadian Journal of Earth Science*, Vol.12, p.1864-1873.

Dubuc, F.
1965: *Geology of the Adams Mine*; *Canadian Mining and Metallurgical Bulletin, Transactions*, Vol.69, p.176.

Dunlop, D. J.
1978: A regional paleomagnetic study of rocks from the 'Superior Geotraverse' area, northwestern Ontario; *Geological Association of Canada, Abstract*, Vol.3, p.393.

Fairbairn, H. W., Hurley, P. M., and Card, K. D.
1966: Age relations of volcanics at Kirkland Lake, Ontario, with the Round Lake pluton; *Massachusetts Inst. Tech., 14th Annual Report*, p.141.

Fisher, R. A.
1953: *Dispersion on a sphere*; *Proceedings of Royal Society of London, Series A*, 217, p.295-305.

Gates, T. M., and Hurley, P. M.
1973: Evaluation of Rb-Sr dating methods applied to Matachewan, Abitibi, Mackenzie, and Sudbury dike swarms in Canada; *Canadian Journal of Earth Science*, Vol.10, p.900-919.

Gay, S. P.
1963: Standard curves for interpretation of magnetic anomalies over long tabular bodies; *Geophysics*, Vol.28, p.161-200.

GSC
1975: Kirkland Lake, Ontario; *Geological Survey of Canada, Aeromagnetic Series Map 20, 137G*, scale 1:25,000.

Irving, E.
1979: Paleopoles and paleolatitudes of North America and speculations about displaced terrains; *Canadian Journal of Earth Science*, Vol.16, p.669-694.

Irving, E., and Naldrett, A. J.
1977: Paleomagnetism in the Abitibi greenstone belt and Abitibi and Matachewan diabase dikes: evidence of the Archean geomagnetic field; *Journal of Geology*, Vol.85, p.157-176.

Jones, L. M., Walker, R. L., and Allard, G. D.
1974: The rubidium-strontium whole-rock age of major units of the Chibougamau greenstone belt, Quebec; *Canadian Journal of Earth Science*, Vol.11, p.1550-1561.

Kamb, W. B.
1959: Ice petrographic observations from the Blue Glacier, Washington, in Relation to Theory and Experiment; *Journal of Geophysical Research*, Vol.64, p.1891.

- Laroche, A.
1966: Paleomagnetism of the Abitibi dyke swarm; Canadian Journal of Earth Science, Vol.3, p.671-683.
- Lawton, K. D.
1957: Geology of the Boston Township and part of the Pacaud Township; Ontario Department of Mines, Vol. 66, Part 5.
- Londry, J. W., and Symons, D.T.A.
1976: Paleomagnetism of Archean rock units and mineralization of the Noranda area, Quebec; Bulletin of Canadian Association of Physicists, Vol.32, Number 3, p.36.
- Morris, W. A.
1979: A positive contact test between Nipissing diabase and Gowganda argillites; Canadian Journal of Earth Science, Vol.16, p.607-611.
- in press: Fault block rotations in the Southern Province as defined by paleomagnetism of the Nipissing diabase; Canadian Journal of Earth Science.
- Nunes, P. D., and Jensen, L. S.
1980: Geochronology of the Abitibi Metavolcanic Belt, Kirkland Lake area—Progress report; Ontario Geological Survey, Miscellaneous Paper 92, p.40-45.
- Pullaiah, G., and Irving, E.
1975: Paleomagnetism of the contact aureole and late dikes of the Otto stock, Ontario, and its application to early Proterozoic apparent polar wandering; Canadian Journal of Earth Sciences, Vol.12, p.1609-1618.
- Pullaiah, G., Irving E., Buchan, K. L., and Dunlop, D. J.
1975: Magnetization changes caused by burial and uplift; Earth and Planetary Science Letters, Vol.28, p.133-142.
- Purdy, J. W., and York, D.
1968: Rb-Sr whole-rock and K-Ar mineral ages of rocks from the Superior Province near Kirkland Lake, northern Ontario, Canada; Canadian Journal of Earth Sciences, Vol.5, p.699-705.
- Quick, A. W.
1981: Component magnetization of the iron formation and deposits at the Adams Mine, Kirkland Lake, Ontario; M.A.Sc. thesis, University of Windsor, 112p.
- Ratcliffe, J. H.
1957: The Boston Township iron range; p.195-210 in Method and Case Histories in Mining Geophysics, Sixth Commonwealth Mining and Metallurgical Congress.
- Shapiro, V.A., and Ivanov, N.A.
1966: Dynamic remanence and the effect of shock on remanence on strongly magnetic rocks; Doklady Akademii Nauk SSSR, Vol.173, p.6-8.
- Steiger, R. H., and Jager, E.
1977: Subcommission geochronology: convention of the use of decay constants in geo- and cosmochronology; Earth and Planetary Science Letters, Vol.36, p.359-362.
- Strangway, D. W.
1965: Interpretation of the magnetic anomalies over some Precambrian dikes; Geophysics, Vol.30, p.783-796.
- Stupavsky, M., and Symons, D.T.A.
in preparation: Incursion of Grenvillian remanence overprint into rocks of the Southern Province, Canadian Journal of Earth Science.
- Symons, D.T.A., and Stupavsky, M.
1974: A rational paleomagnetic stability index; Journal of Geophysical Research, Vol.79, p.1718-1720.
- 1979: Magnetic Characteristics of the Iron Formation near Temagami, Ontario; Ontario Geological Survey, Miscellaneous Paper 87, p.133-147.
- 1980: Magnetic anomaly type curves and paleomagnetism of Algoman-type iron formation near Temagami, Ontario; Ontario Geological Survey, Miscellaneous Paper 93, p.215-219.
- Symons, D.T.A., Walley, D. S., and Stupavsky, M.
1980: Component magnetization of the Algoman iron formation and host rock, Moose Mountain mine, Ontario; Ontario Geological Survey, Miscellaneous Paper 93, p.198-214.
- Ueno, H., and Irving, E.
1976: Paleomagnetism of the Chibougamau greenstone belt, Quebec, and effects of Grenvillian post-orogenic uplift; Precambrian Research, Vol.3, p.303-315.

Grant 8 Interpretational Support for EM Prospecting

G. F. West

Geophysics Laboratory, Department of Physics, University of Toronto

ABSTRACT

Analogue and numerical modelling methods have been developed and employed to study various interpretation problems that arise in EM prospecting. The problems studied include the anomalies generated by irregular conductive overburden, the influence of overburden and host-rock conductivity on the response of bedrock conductors, the interpretation of drillhole EM surveys, uses of electric field measurements in EM surveys, and how to model and take account of the interaction between multiple conductors. Test surveys have been carried out and the results compiled with pre-existing survey data of various types for sites in Cavendish and Thomas Townships.

INTRODUCTION

The purpose of this three-year research program, now just completed, was to use computer and analogue scale modelling to improve the capabilities of electromagnetic prospecting methods. Specifically, the aim was to make it possible to search more deeply and to discriminate more effectively between prospective targets and geological noise. The program consisted of a number of related projects which fall into one of three categories:

- 1) creating modelling facilities;
- 2) using the modelling facilities to study various EM interpretation problems; and
- 3) studying typical field cases in detail to verify the proposed interpretation methods.

The individual studies are described in detail as they are completed in the report series "Research in Applied Geophysics" available from the Geophysics Laboratory, Department of Physics, University of Toronto, Toronto, M5S 1A7, attention Ms. C. Sheward (416-978-5175).

The research studies have been carried out by graduate students A. Dyck, T. Eadie, J.S. Holladay, J. Macnae, A. Tejero-A., M. Vallee, C. Villegas-G., and P. Walker of the University of Toronto and J. Hanneson of the University of Manitoba, assisted by computer scientist M. Bloore and electronics engineer A. Wieckowski, and supervised by the author.

MODELLING FACILITIES

As reported in the 1978-1979 and 1979-1980 Summary of Research, we have constructed a versatile, analogue

scale modelling facility for time and frequency domain studies in the 100 Hz - 500 kHz band and are now using it for interpretation studies (Villegas-G. 1979). Also, a set of computer programs for interactive computation of the response of various common EM prospecting systems to plate-like and spherical conductors where the host medium is very resistive have been created (Dyck *et al.* 1980) and made available to outside users both on the Department of Physics VAX computer and other facilities. Utility programs for computing the frequency response of a layered earth (Eadie 1979) and for converting frequency-domain EM responses to time-domain response (Holladay 1981) have also been created for routine modelling studies.

STUDIES OF INTERPRETATION PROBLEMS

IRREGULAR OVERBURDEN

A common problem of EM surveys in areas such as the Abitibi Clay Belt is how to distinguish anomalies due to prospective conductors in the bedrock from those due to the irregular conductive overburden. Villegas-G. (1979) has made an analogue model study of horizontal-loop EM (HLEM) response to overburden valleys, ridges, and steps. Valleys in particular produce anomaly profiles that look much like those over a typical steeply dipping, dike-like, bedrock conductor. Luckily, overburden-generated anomalies do have some identifying features that can be seen in multiseparation and/or multifrequency survey data. Since irregularities in the overburden cause profile anomalies by redistribution of the normal eddy currents induced in the overburden rather than by local induction at the site of the irregularity, it is particularly helpful if one can estimate the average overburden conductance from the data. The phase of anomalies due to irregularities can be predicted from this estimate and thus the anomalies can be identified. Eadie (1979) has provided some nomograms for interpreting HLEM regional overburden response.

EFFECT OF CONDUCTIVE OVERBURDEN OR HOST ROCK ON A BURIED TARGET

J. Hanneson (1981) has constructed a numerical modelling program to compute HLEM response to a vertical, rectangular plate-like conductor situated in a conductive

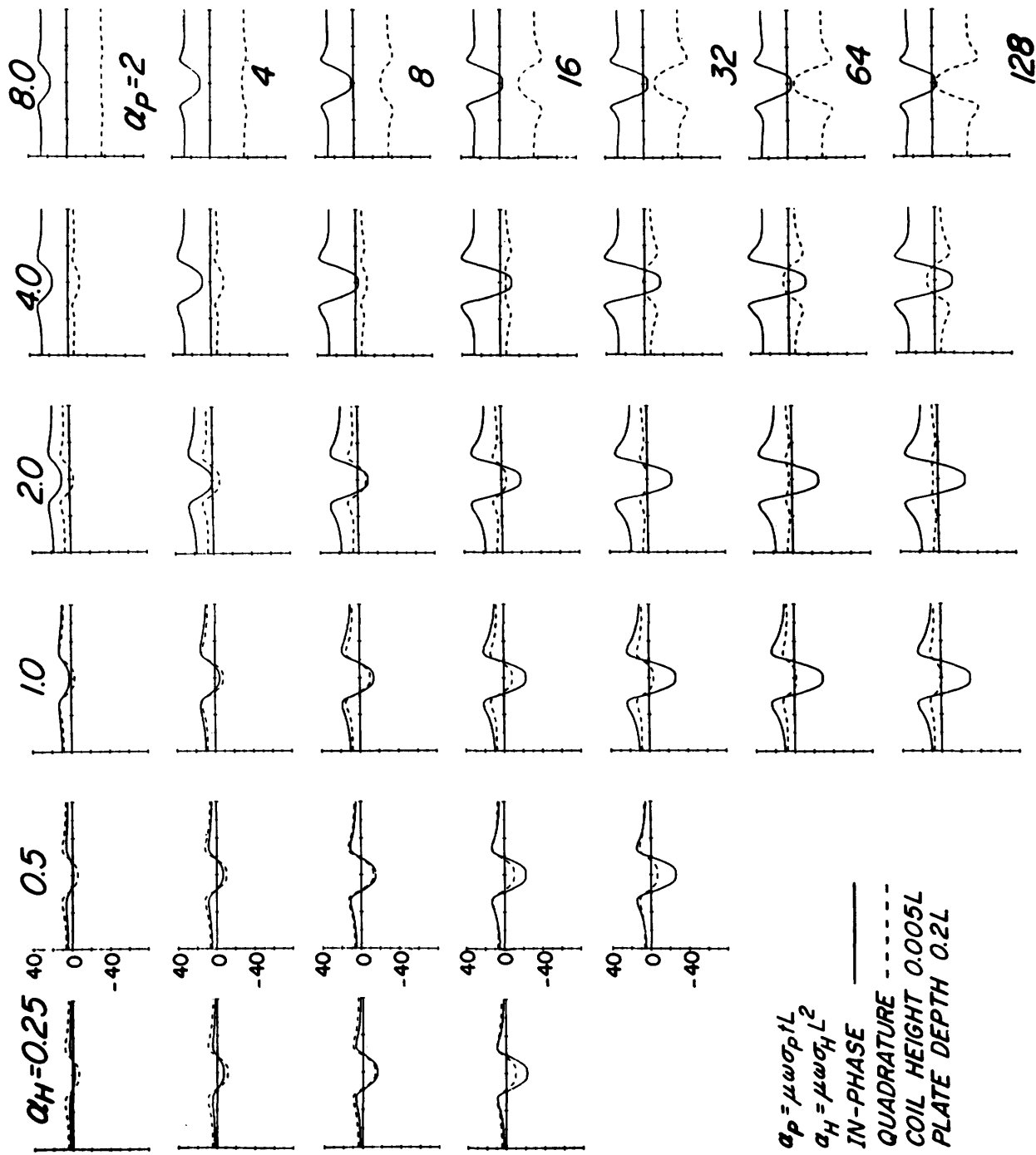


Figure 1—Horizontal loop EM (HLEM) profiles over a vertical thin plate conductor (strike extent $3L$, depth extent $1.5L$, where l is coil separation) in a homogeneous conductive half space, shown for varying response parameter of the plate (α_P) and of the half space (α_H). The anomaly profiles all have the same general form although the anomaly amplitudes and base levels change markedly.

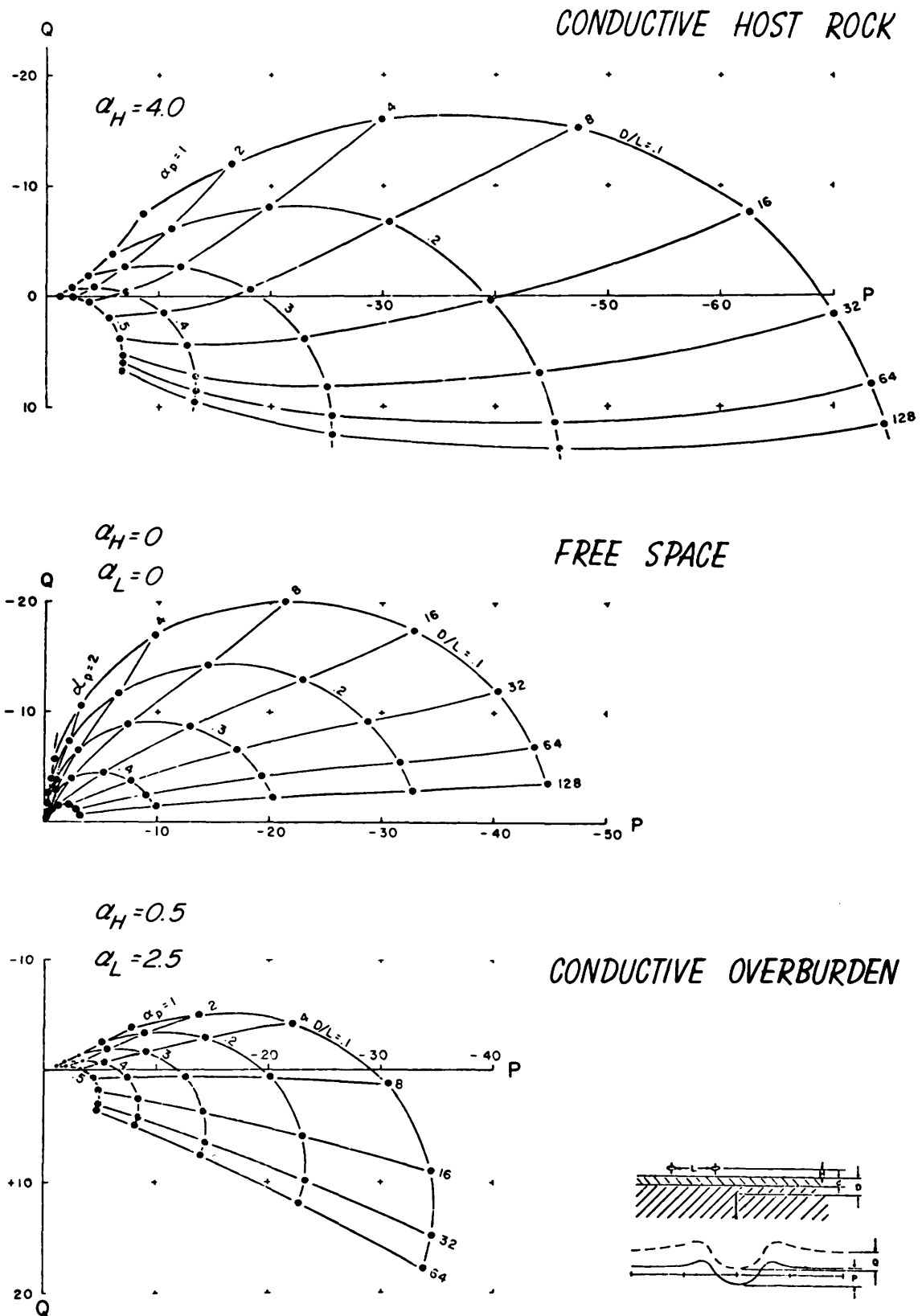
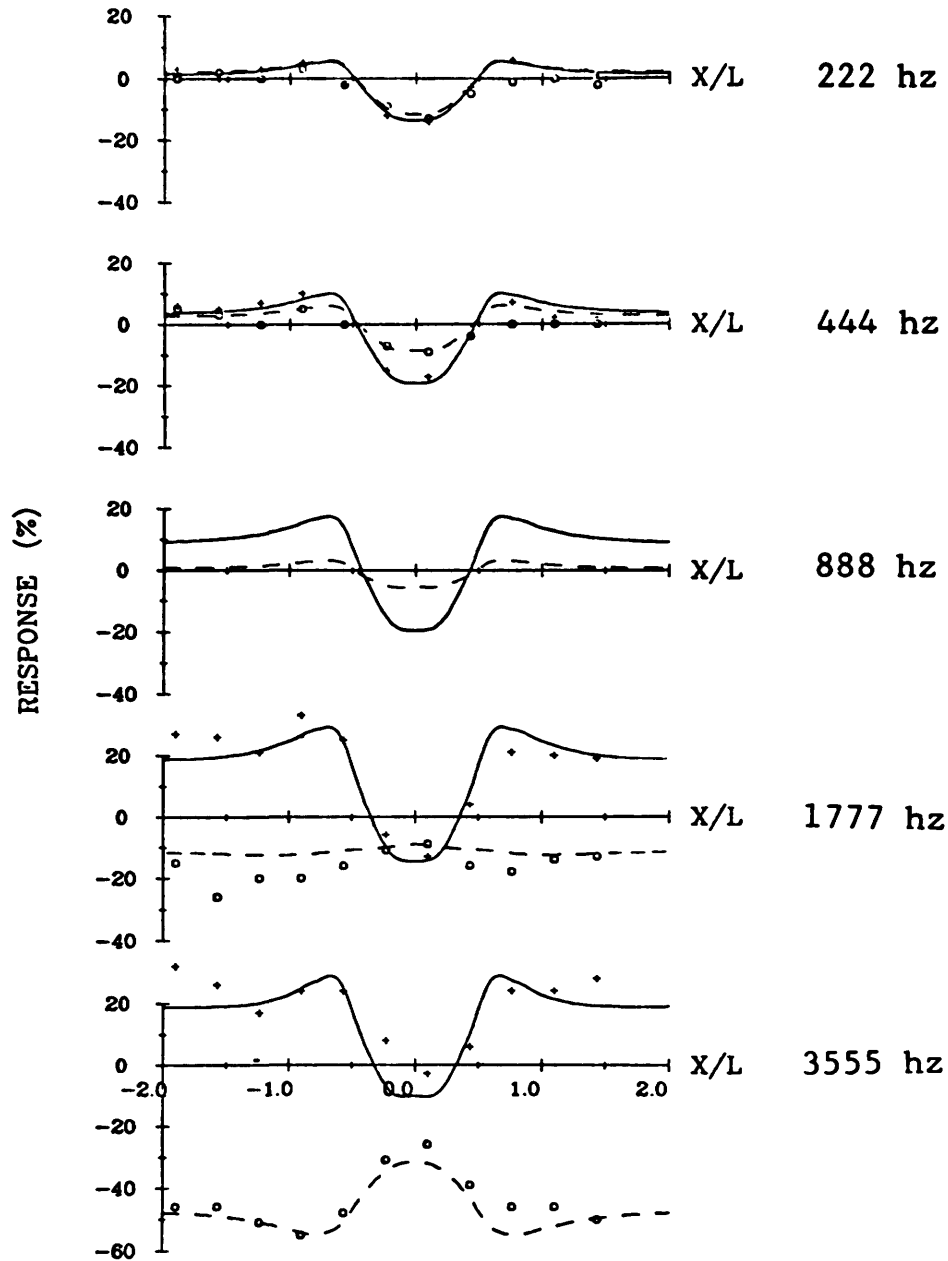


Figure 2—Phasor diagrams of HLEM anomaly amplitude for the same plate conductor as in Figure 1, shown as a function of α_p and D/L . Results for three different host media are shown: a uniformly conductive host ($\alpha_H = 4$), an insulating host medium, and a conductive overburden ($\alpha_L = 2.5$, $D/L = 0.05$) over a poorly conductive host medium ($\alpha_H = 0.5$). Taking the free space case as a reference, the conductive host causes a strong enhancement of the anomaly along with prominent phase rotation, whereas the conductive overburden causes a phase rotation with modest attenuation.



	COMPUTED	OBSERVED	
IN PHASE	—————	+ + + + +	
QUADRATURE	-----	
PLATE CONDUCTIVITY	= 41 S/M	COIL SEPARATION	= 150 M
LAYER CONDUCTIVITY	= .068 S/M	COIL HEIGHT	= 0.75 M
HOST CONDUCTIVITY	= .0096 S/M	LAYER THICKNESS	= 7.5 M
FREQUENCY = VARIABLE		PLATE DEPTH	= 30 M
PLATE SIZE (LENGTH x WIDTH x THICKNESS)	= 450 M x 225 M x .75 M		

Figure 3—A field example of multifrequency HLEM from the Abitibi area of Ontario with fitted model response. Note the sign reversal of the quadrature anomaly at 3555 Hz.

half-space with a conductive overburden layer. The solution is obtained by an integral equation method where the current induced in the plate is represented by global basis functions of polynomial type, and the kernel function of the integral equation is the Green's dyadic for a conductive half-space, or layer over a half-space, as required.

Hannesson has used his program to compute responses for a great variety of host rock and overburden conditions. A set of typical HLEM profiles is shown in Figure 1. The profile shape of the plate anomaly is not greatly affected by host rock and overburden conductivity. However, the amplitude and phase of the anomaly may be strongly altered. Phasor diagrams of anomaly amplitude have been constructed for many cases. Three examples are shown in Figure 2 which indicate the effect of increasing overburden and host rock conductivity.

If the host rock is resistive, a conductive overburden rotates the phase of the target anomaly, and attenuates it. When the bedrock is conductive, the target anomaly is enhanced by gathering of current induced in the host rock into the target body. The enhancement is significant if the response parameter of the host medium $\alpha_H = \sigma\mu\omega L^2$ (σ conductivity, μ permeability of space, ω angular frequency, L coil separation of HLEM system) exceeds about 0.25 and is totally dominant at $\alpha_H = 8$. For a 150 m HLEM system operating at 880 Hz, these values correspond to host rock resistivities of 640 and 20 ohm metres. Since most Precambrian rocks have resistivities that are well above 1000 ohm metres, HLEM surveys on the Canadian Shield are unlikely to be affected by current gathering from the host rock, although anomaly phase rotation due to conductive overburden is quite common. Figure 3 shows an example of such field data fitted by model data.

ELECTRIC FIELD MEASUREMENT

J. Macnae (1981) has explored the uses of electric field measurements that could be made during an EM survey in addition to the more usual magnetic field measurements. The study was done using the UTEM system which is a time-domain EM that utilizes a large, fixed loop transmitter and has a square wave system function. Macnae has shown that the late time E field response has considerable interpretational value in delineating lateral contrasts in ground resistivity irrespective of the general magnitude of the resistivity values. An example of late time electric field mapping at the Thomas Township test site is shown in Figure 4. Another example over a barren site with a gradually changing overburden thickness is shown in Figure 5.

Macnae has carried out several surveys, a variety of numerical and analogue scale model studies, and a theoretical analysis of several aspects of the data. In addition to late time E field mapping, the electric field transients can assist in H field interpretation, and in some cases induced polarization response of the ground can be observed.

DRILLHOLE EXPLORATION

In the past few years, new equipment has become available for making EM surveys from deep boreholes, using a large, surface transmitter loop. The Crone PEM system is the most widely used apparatus. A. Dyck has investigated some of the tricky interpretation problems that arise from such surveys. There is much more possibility for ambiguity in the interpretation of drillhole data than surface surveys, as the target may lie in any direction from the survey line and the line is usually an isolated profile rather than part of a suite of profiles covering a large surface.

Key aids for drillhole interpretation are the PLATE and SPHERE numerical models mentioned above (Dyck *et al.* 1980). These programs make specific provision for drill hole geometries. Figure 6 shows a set of field data from the Sudbury Basin and shows how three alternative interpretations are tested.

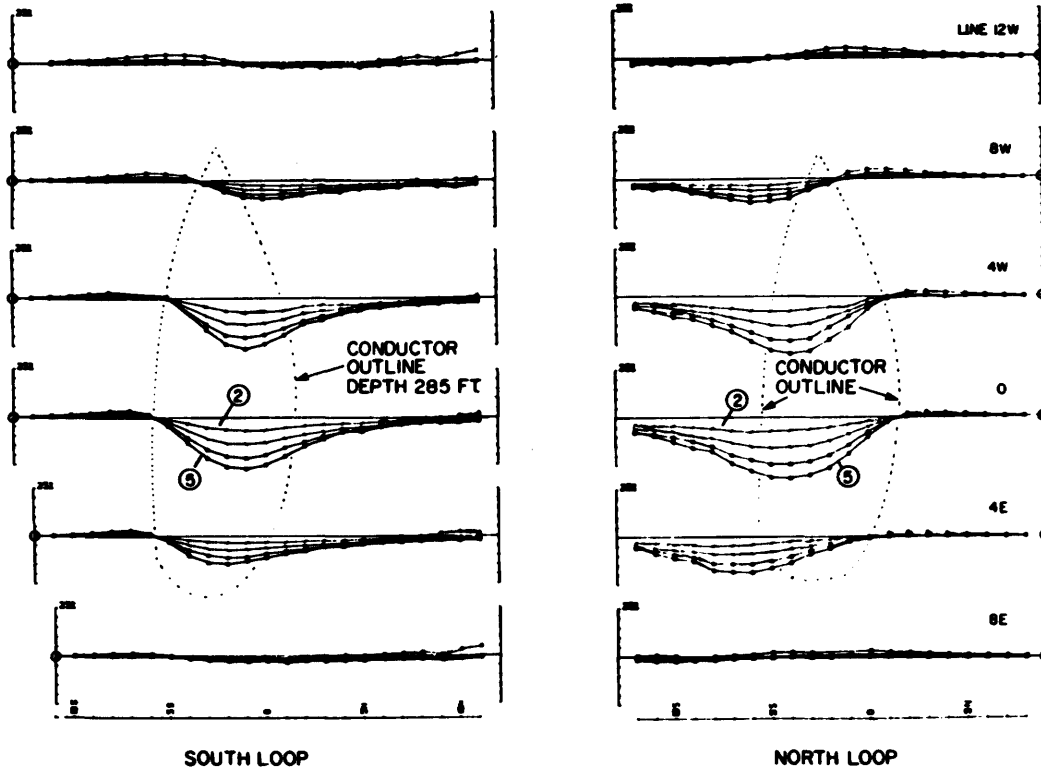
When only a simple axial solenoid is available as receiver, it is generally necessary to use several transmitter locations to resolve ambiguities in target position. Even so, ambiguities may remain. Dyck has studied how the migration of the eddy currents with time (or frequency) can help resolve the problems. A report on this work should be available by Fall, 1981. A useful atlas of charts showing the precise configuration of primary fields has been provided by Macnae (1980b).

MULTIPLE CONDUCTOR PROBLEMS

Many exploration situations involve several nearby targets, and especially as we employ geophysical methods with greater penetrating power, we tend to see two or more conductors simultaneously influencing the measurements. M. Vallée has examined a problem noted in exploring the deeper parts of the Athabaska Basin for basement graphitic zones with the Turam or UTEM method. Conductors are found, but classical interpretation techniques mislocate the targets somewhat. An example is shown in Figure 7. A mislocation by 15 percent of the depth may not be important when the target is at 50 m, but is very significant when the target is at 300 m depth. Vallée has shown that the effect is due to nearby graphitic zones located outside the survey area, but within the area of influence of the transmitter loop, and has shown how an allowance can be made for the effect if the presence of the zones is known.

The multiple conductor problem is much more acute when the conductors are closer and the induced currents interact strongly. The effects are very often seen in surface surveys of banded, conductive formations and in drillhole surveys. To allow modelling of such effects, P. Walker is expanding the basic theoretical framework of the PLATE model from the form developed by Annan (1975) for a single target conductor in free space to the more general problem of several conductors which may lie under a conductive overburden. The basic formulation is complete and programs to implement the formulation are being written and tested. We hope that the programs will be in a basic but fully usable form by Fall, 1981. Re-

UTEM VERTICAL MAGNETIC FIELD SURVEYS



UTEM LATE TIME ELECTRIC FIELD

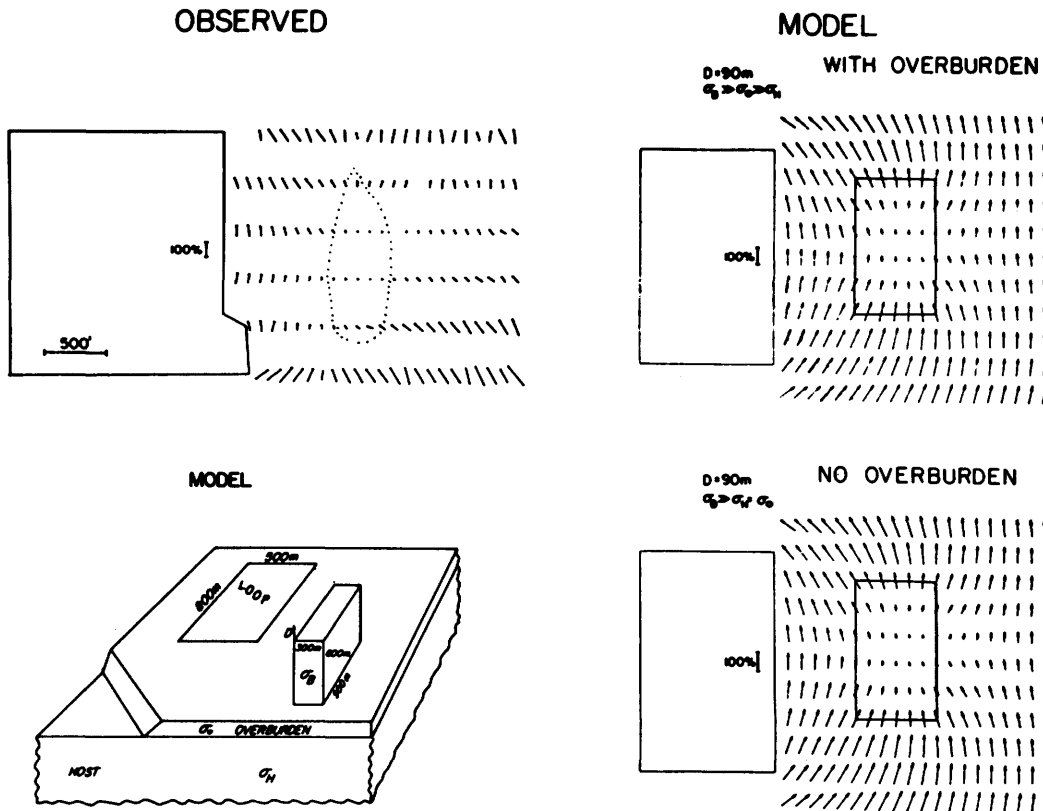


Figure 4—A UTEM survey at the Thomas Township test site showing profile results for the secondary vertical magnetic field (later time channels 5 - 2 only) and a vector map of the late time electric field. The effect of the bedrock conductor at 285 feet depth is evident. A model calculation for the E field data is included.

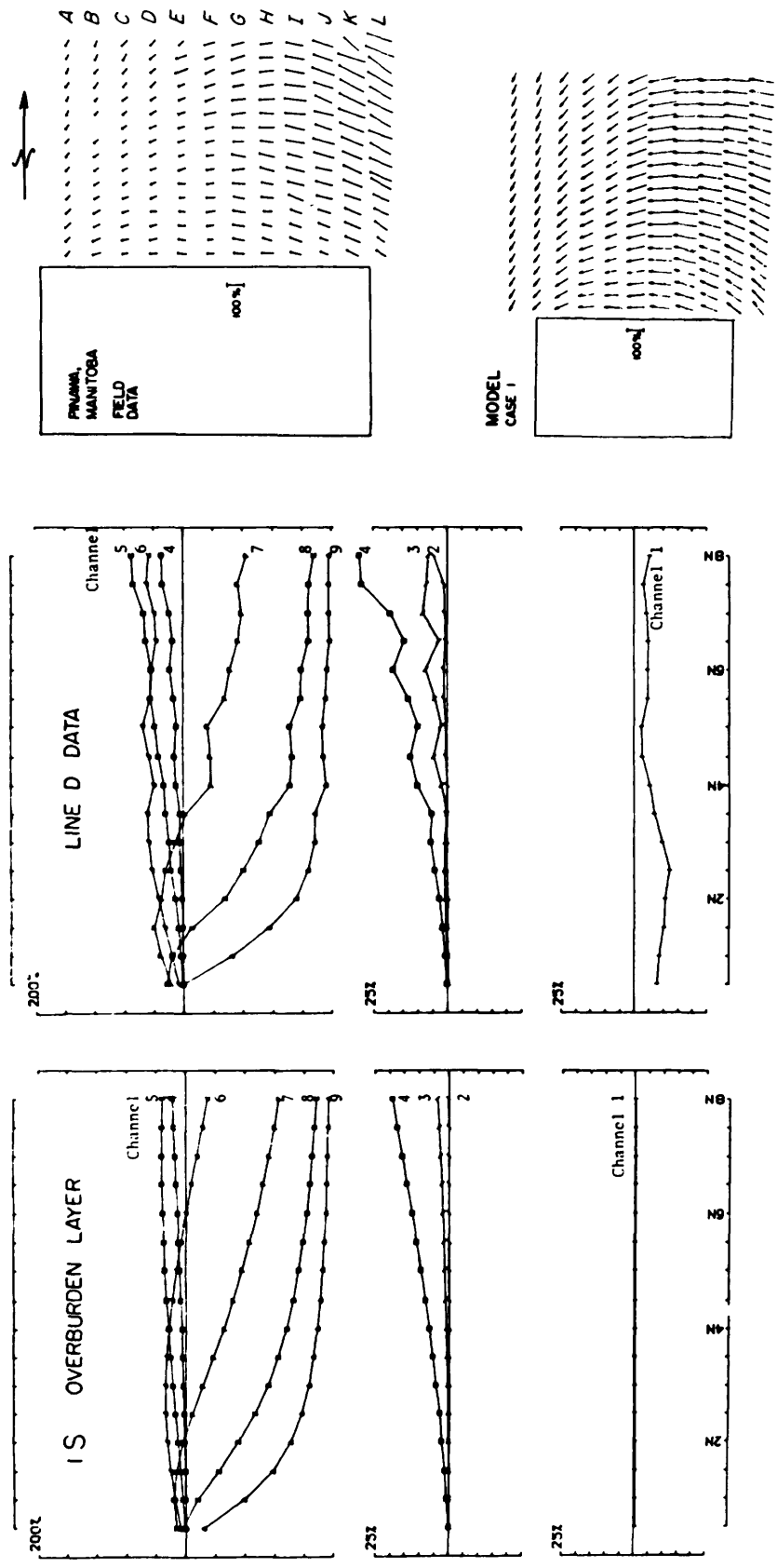


Figure 5—Excerpts of a UTEM survey over a laterally varying conductive overburden at Pinawa, Manitoba. The bedrock is quite highly resistive with no known conductive features in it. Note how the late time E field vectors are attracted to the more conductive or thicker overburden (line A end of grid) but the amplitudes of the vectors are reduced.

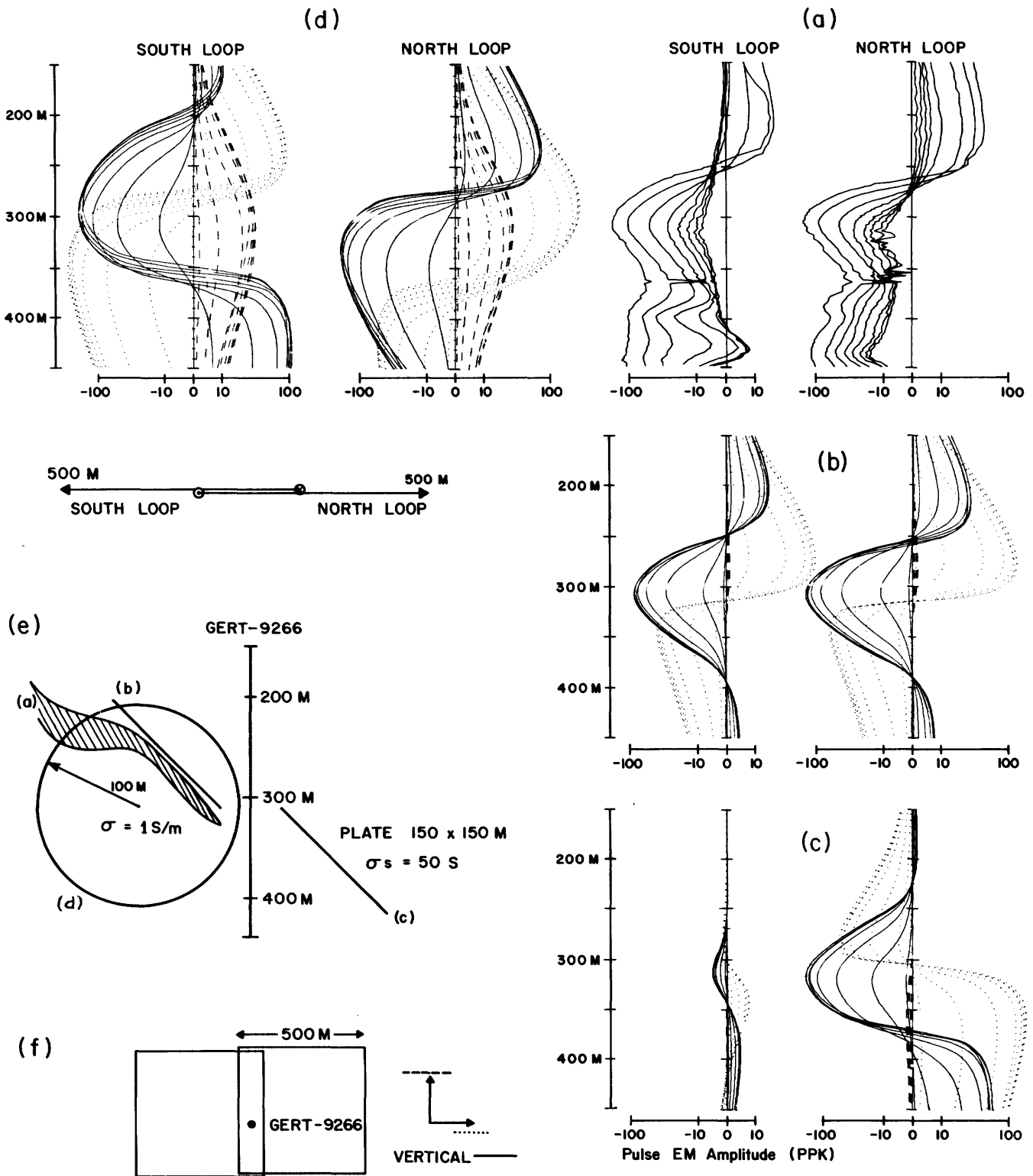


Figure 6—Example of a drillhole PEM survey on the Gertrude sulphide zone at Sudbury, Ontario. The target zone is easily detected by the survey profile (a). Model studies are shown for comparison (b,c,d) which help define the position and shape of the target. Locations of the actual and model conductors are shown in (e). The transmitter loop positions are shown in (f) (reduced scale).

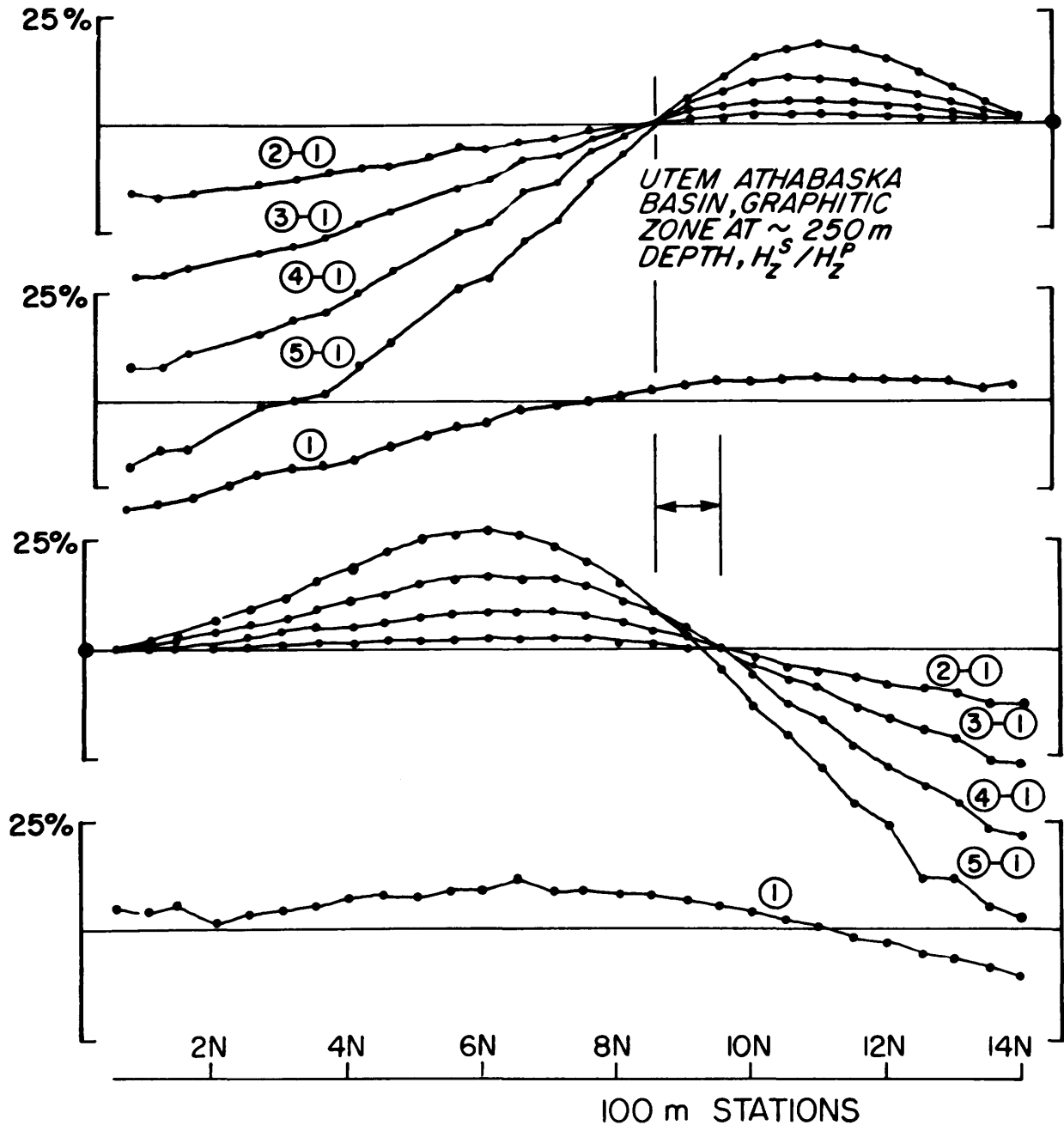


Figure 7—UTEM vertical secondary field profiles from two different loops over a conductive graphitic zone in the basement of the Athabaska Basin. Estimated depth-to-top is 285 m. The zone is clearly revealed by the crossovers of the profiles, but interpretations based on single conductor models disagree on the exact position of the conductor ($\pm 50\text{m}$). The apparent anomaly offsets are due to the presence of similar graphitic zones on the back sides of the transmitter loops which distort the base levels of the profiles in a highly systematic manner.

ports on Walker's and Vallée's work should be available at that time.

SURVEYS AND SURVEY COMPILATIONS

A compilation of new data on the Cavendish Township geophysical test site including detailed UTEM, HLEM, magnetic and other surveys has been produced by Macnae (1980a). A UTEM survey was carried out and compiled with existing HLEM and Crone PEM surveys for a test site in Thomas Township in northern Ontario near Timmins. The conductor is a strongly conductive graphitic pod situated beneath 285 feet of overburden. The site is an interesting contrast with the shallow conductors at Cavendish Township. A compilation report will be available by Fall, 1981.

REFERENCES

- Annan, A. P.
1975: The Equivalent Source Method for Electromagnetic Scattering Analyses and Its Geophysical Application; unpublished Ph.D. thesis, Memorial University of Newfoundland, 242p.
- Dyck, A.V., Bloore, M. and Vallee, M.A.
1980: Operating Manual and Documentation for Interactive EM Modelling Programs PLATE and SPHERE; unpublished project report, Research in Applied Geophysics, No. 14, Geophysics Laboratory, Department of Physics, University of Toronto.
- Eadie, T.
1979: Stratified Earth Interpretation using Standard Horizontal Loop Electromagnetic Data; unpublished project report, Research in Applied Geophysics, No. 9, Geophysics Laboratory, Department of Physics, University of Toronto.
- Hanneson, J.E.
1981: The Horizontal Loop EM Response of a Thin Vertical Conductor in a Conducting Half-Space; unpublished project report, Research in Applied Geophysics, No. 19, Geophysics Laboratory, Department of Physics, University of Toronto.
- Holladay, J.S.
1981: YVESFT and CHANNEL: A Subroutine Package for Stable Transformation of Sparse Frequency Domain EM Data to the Time Domain; unpublished project report, Research in Applied Geophysics, No. 17, Geophysics Laboratory, Department of Physics, University of Toronto.
- Macnae, J.C.
1980a: The Cavendish Test Site: A UTEM Survey Plus Compilation of Other Ground Geophysical Data; unpublished project report, Research in Applied Geophysics, No. 12, Geophysics Laboratory, Department of Physics, University of Toronto.
- 1980b: An Atlas of Primary Fields Due to Fixed Transmitter Loop EM Sources; unpublished project report, Research in Applied Geophysics, No. 13, Geophysics Laboratory, Department of Physics, University of Toronto.
- 1981: Geophysical Prospecting with Electric Fields from an Inductive EM Source; unpublished project report, Research in Applied Geophysics, No. 18, Geophysics Laboratory, Department of Physics, University of Toronto.
- Villegas-G., C.J.
1979: On the Electromagnetic Response of Non-Uniform Overburden Layers: Scale Model Experiments; unpublished project report, Research in Applied Geophysics, No. 10, Geophysics Laboratory, Department of Physics, University of Toronto.

Grant 30 Carbonate, Alkali and Arsenic Anomalies Associated with Gold Mineralization, Timmins Area

R.E.S. Whitehead, J.F. Davies, R.A. Cameron, and D. Duff

Department of Geology, Laurentian University

ABSTRACT

CO₂ content indicates the quantity of carbonate in altered basaltic rocks but it is not a reliable measure of the intensity of carbonate alteration. The CO₂/CaO molar ratio, which correlates with the relative proportions of individual carbonate species, is a superior index of the intensity of carbonatization. The Timmins gold-bearing district is characterized by pervasive carbonatization, with large areas yielding CO₂/CaO ratios greater than 1, representing CO₂ supersaturation relative to CaO. The mean CO₂/CaO ratio in the Timmins area is 0.67 compared to 0.13 in two unmineralized control areas. Regional arsenic levels in the gold-bearing area average 4 ppm compared to about 0.35 ppm for the non-mineralized areas. The average K₂O and Rb levels are similar in both mineralized and non-mineralized areas (about 0.30 percent K₂O and 7 ppm Rb). Although there appears to have been no wholesale addition of K₂O or Rb to the mineralized area from external sources these alkalis have been redistributed internally, resulting in patterns of local enrichments and depletions which are characteristic of the mineralized region.

Local target area anomalies associated with known mineralization consist of CO₂/CaO > 1.5, As > 10 ppm and/or K₂O > 0.75 percent. Not all three values are required to be above these thresholds in order to identify local target areas. Combinations such as CO₂/CaO > 1.5 and As < 10 ppm, CO₂/CaO 1-1.5 and K₂O < 0.75 percent, or K₂O < 0.75 percent and As > 10 ppm are also equally indicative of proximity to mineralization. Gold mineralization and associated anomalies occur throughout the entire volcanic succession and are not restricted to any particular stratigraphic units. The levels and patterns of alteration and gold mineralization appear to be structurally controlled.

INTRODUCTION

Although carbonatization, alkali alteration and arsenic enrichment are characteristic of wall rocks surrounding many gold-bearing quartz veins in mafic volcanic rocks (Boyle 1979), few data are available on the distribution, intensity or patterns of alteration beyond the wall rocks immediately adjacent to the veins. The purpose of this study is to:

1) compare regional levels of CO₂, alkalis and As in a

mineralized area with those in lithologically comparable but unmineralized areas;

2) determine local variations in intensity and extent of alteration and their relationship to areas of gold mineralization; and

3) define regional and local (target area) anomalies that might be useful in gold exploration.

CO₂, CaO, K₂O, Na₂O, Rb and As were determined for approximately 400 surface samples and 120 mine samples from the test area which includes at least 15 gold mines in Tisdale Township and parts of the adjacent townships of the Timmins district. Similar determinations were made for about 100 samples from "unmineralized" control areas without known, substantial gold deposits (Zavitz, Semple, Hutt and Douglas Townships south of Timmins, and Holloway, Thackeray and Elliot Townships east of Timmins). Immobile trace element contents (TiO₂, Y, Zr) were used to establish that the samples from the mineralized area were originally chemically equivalent, within limits, to those from the unmineralized control areas.

This study was essentially regional, with detail only down to target-area dimensions (within 500 feet of known mineralization). No attempt has been made to correlate anomalies with the gold content of the wall-rocks immediately adjacent to veins. Detectable gold anomalies, in the ppb range, rarely extend more than a few tens of feet from veins and are, therefore, much smaller than the large carbonate, alkali and As anomalies outlining general target areas. Gold analysis would be useful in identifying individual drill targets within the target area encompassed by the carbonate, alkali and As anomalies.

Figure 1 outlines the geology and structure of the test area; sample sites and the locations of both past and present gold producers are shown on Figure 2. The lithostratigraphic volcanic units (sub-groups) of the Tisdale Group are those established for the mines of the area (see Ferguson *et al.* 1968). The surface distribution and configuration of the four sub-groups displayed in Figure 1 have been confirmed from TiO₂, Cr, Zr and Y plots (Davies *et al.* 1979; Davies and Whitehead 1980). The mafic volcanic rocks of the Northern sub-group are magnesian basalts; the Central sub-group is tholeiitic; the Vipond and Gold Centre sub-groups are tholeiitic but approaching calc-alkaline.

The structure of the test area (Figure 1) is essentially that presented by Davies (1977) and is consistent with the volcanic stratigraphy which in turn is supported by the immobile trace element data. Arguments for the exist-

ence of the Dome Fault (DF), disputed by Roberts (1980), the Central Tisdale Anticline (CTA), questioned by Karvinen (1978), and the Gillies Lake Fault (GLF) have been presented elsewhere (Davies and Whitehead 1980).

CARBONATE SPECIES, CO₂/CAO MOLAR RATIOS, AND INTENSITY OF CARBONATIZATION

The degree of carbonate alteration is commonly expressed in terms of CO₂ content of altered rocks. A more rigid interpretation is that CO₂ content measures the

quantity of carbonate present but reveals little or nothing about the intensity of the carbonatization process. On the other hand, variations in carbonate mineral compositions and species zoning, for example from ankerite or dolomite to calcite outward from veins, result from changes in f_{CO₂} and intensity of CO₂ metasomatism.

Carbonatization is not only dependent on the availability of Ca, Mg and Fe in silicates but is also a function of T and f_{CO₂}. Studies by Billings and White (1950) and Harte and Graham (1975) clearly indicate that in rocks of basaltic composition containing actinolite, chlorite and epidote, calcite forms before dolomite or ankerite and at lower mole fraction, X_{CO₂}, than that required to form the latter species. Harte and Graham (1975) discuss reactions of the types listed below (equations 1-4).

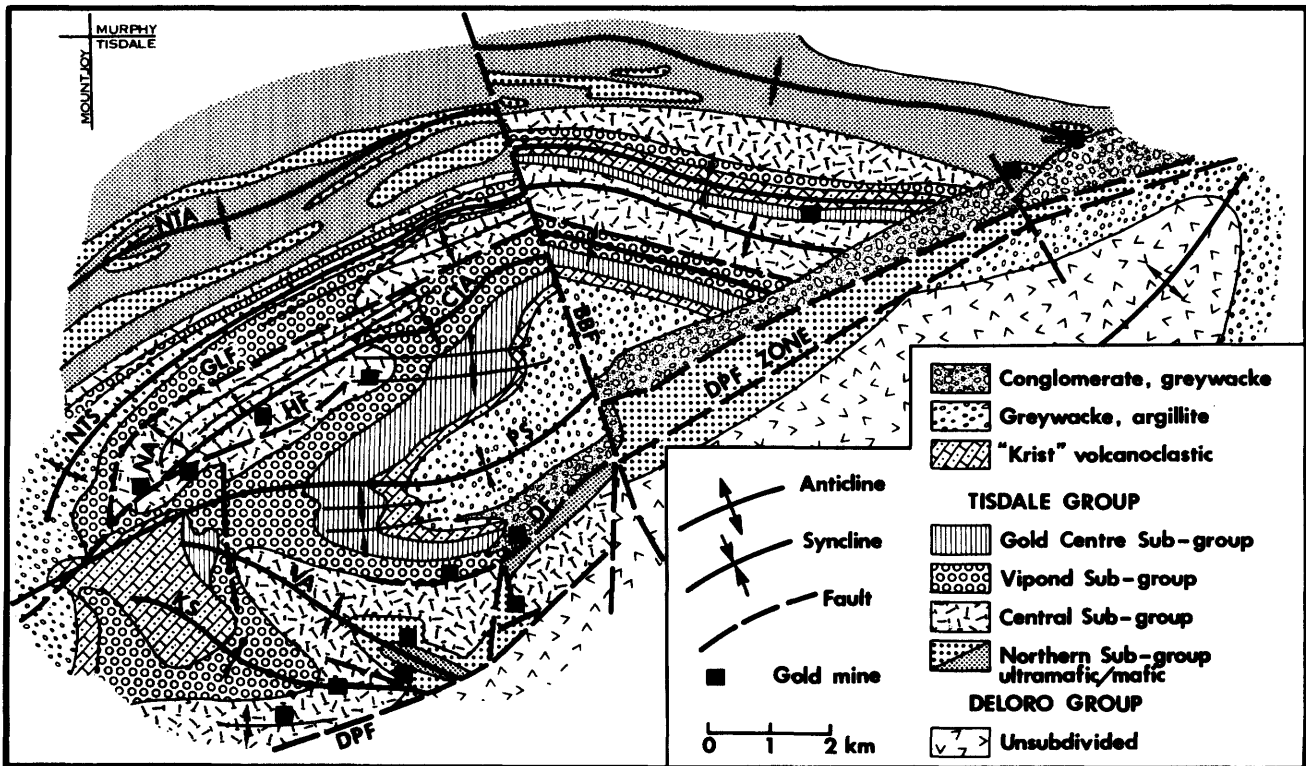
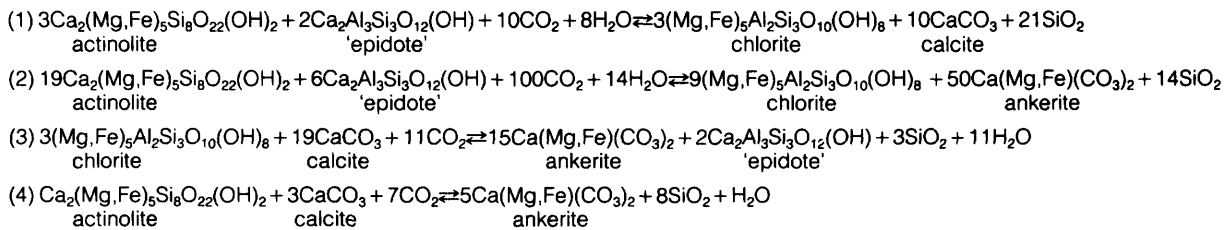


Figure 1—Geology and structure of the Timmins area. (NTA North Tisdale Syncline; CTA Central Tisdale Anticline; PS Porcupine Syncline; VA Vipond Anticline; KS Kayorum Syncline; GLF Gillies Lake Fault; HF Hollinger Fault; DF Dome Fault; DPF Destor-Porcupine Fault; BBF Burrows-Benedict Fault.)

The data of Skippen (1971) suggest a similar relationship between calcite-dolomite and f_{CO_2}/f_{H_2O} for rocks of ultramafic composition. However, since ultramafites contain different silicates (e.g. serpentine, talc, tremolite) than metabasalts (e.g. actinolite, chlorite, epidote) the $T-X_{CO_2}$ conditions necessary to form a particular carbonate species will differ for the two rock types.

It is difficult to determine directly the proportions of individual carbonate species in fine-grained rocks, particularly where hundreds of samples are involved. A reliable, rapid method of estimating relative intensity of carbonate alteration utilizes the CO_2/CaO molar ratios of carbonatized metabasalts. The molar ratio CO_2/CaO of pure calcite is 1, whereas that for dolomite and ankerite is 2. The relative proportions of calcite and dolomite (or ankerite) were determined in several dozen samples of basalt by X-ray diffraction and the results compared with the CO_2/CaO molar ratios of the same samples. Samples with $CO_2/CaO < 1$ contained only calcite as the carbonate species; since the ratio for pure calcite is 1, some of the CaO in these samples must remain in silicate form. In samples where ratios equal 1, all or most of the CaO exists as calcite; little dolomite or ankerite was detected in these samples. A CO_2/CaO ratio of 1 represents CO_2 saturation relative to CaO. Ratios between 1 and 2 contained mixtures of calcite and ankerite or dolomite. At ratios equal to 2 only dolomite (and/or ankerite) was present.

Several samples yielded ratios in excess of 2. Mixtures of dolomite or ankerite with magnesite or siderite would produce these high ratios. Alternatively, ferroan ankerite in which Fe^{+2} substitutes for Ca^{+2} can produce ratios greater than 2. Deer *et al.* (1962, p.296) reported an analysis of ferroan ankerite from which a calculated ratio of 3.9 is obtained. Samples of basalt from the test area with ratios greater than 2 yielded no magnesite or siderite, but only ankerite (dolomite), peaks. It was concluded that ferroan ankerite probably was the dominant carbonate species in these samples.

The X-ray diffraction data confirm that CO_2/CaO molar ratios serve as a measure of the proportions of calcite and dolomite or ankerite in carbonatized metabasalts and therefore also as a measure of the intensity of carbonate alteration.

Figure 3 illustrates the relationship between CO_2 content and the CO_2/CaO molar ratios. The slopes of lines through the origin represent CaO contents. The amount of CO_2 taken up by the rock is controlled by both the CaO content and f_{CO_2} , which determines whether calcite or dolomite (and/or ankerite) forms. At any particular CO_2/CaO ratio the CO_2 content can vary widely depending on the CaO content of the rock. On the other hand, at any specific percentage CO_2 the CO_2/CaO ratio can also vary greatly depending on the proportions of calcite to dolomite or ankerite in the rock. This results from the pro-

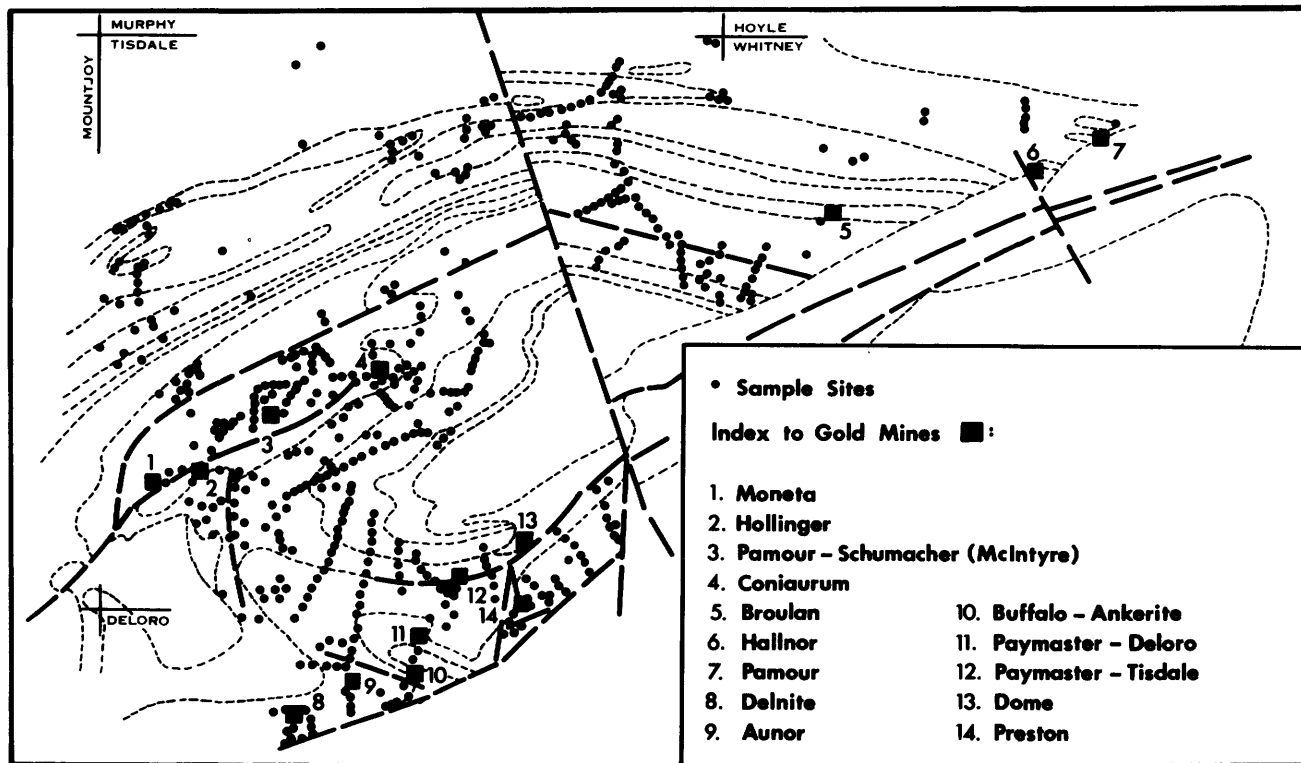


Figure 2—Sample locations and gold mines.

gressive alteration first to calcite and subsequently, at higher f_{CO_2} , to dolomite (or ankerite). The path of alteration of a rock with a given CaO content will follow the sloping line, from the origin, representing that percentage CaO (e.g. A→B, Figure 3). Addition of CaO or its removal at any stage in the alteration process will only affect the quantity of carbonate formed but not the CO_2/CaO ratio, provided f_{CO_2} remains relatively constant. The path will change in a vertical to near vertical direction (e.g. B→C) and continued alteration will then follow the sloping line representing the changed CaO content of the rock (e.g. C→D).

On Figure 3 "mineralized" surface samples (solid circles) and "mineralized" underground samples (solid triangles) are distinguished from "unmineralized" (open circles). The proportion of "mineralized" to "unmineralized" increases as the CO_2/CaO molar ratio increases. "Mineralized" samples are those situated not more than 500 feet from known gold mineralization.

REGIONAL CARBONATE, ALKALI AND AS LEVELS

Contoured values of CO_2 , CO_2/CaO , As, K_2O and Rb, for the Timmins area are presented in Figures 4 to 8. CO_2 ,

CO_2/CaO , As, K_2O and Rb levels are distinctly higher in the region where major gold mines are located than in the northern unmineralized parts of the test area. Contours of weight percent CO_2 (Figure 4) and CO_2/CaO (Figure 5) appear to be equally effective in distinguishing the central mineralized part from northern unmineralized part of the Timmins area. However, within the mineralized portion the CO_2/CaO ratios more clearly define local target areas of intense carbonatization.

Comparison of frequency plots (Figure 9), means and standard deviations (Table 1) of data from the unmineralized control areas and the entire test area reveal significant differences in intensity of carbonate alteration (CO_2/CaO ratios) and As levels. Large parts of the Timmins area have experienced an overall enrichment in CO_2 and As (indicated by CO_2/CaO ratios greater than about 0.75 and As levels greater than 1 ppm). Most of this enrichment has occurred in the mineralized part of the Timmins area, between the Destor-Porcupine and Gillies Lake Faults.

There are no significant differences in the average K_2O and Rb levels of the test area and control areas (Table 1). This suggests that there was no wholesale addition of these alkalis from external sources into the rocks of the Timmins area which, consequently, cannot be regarded as anomalous in K_2O and Rb relative to the un-

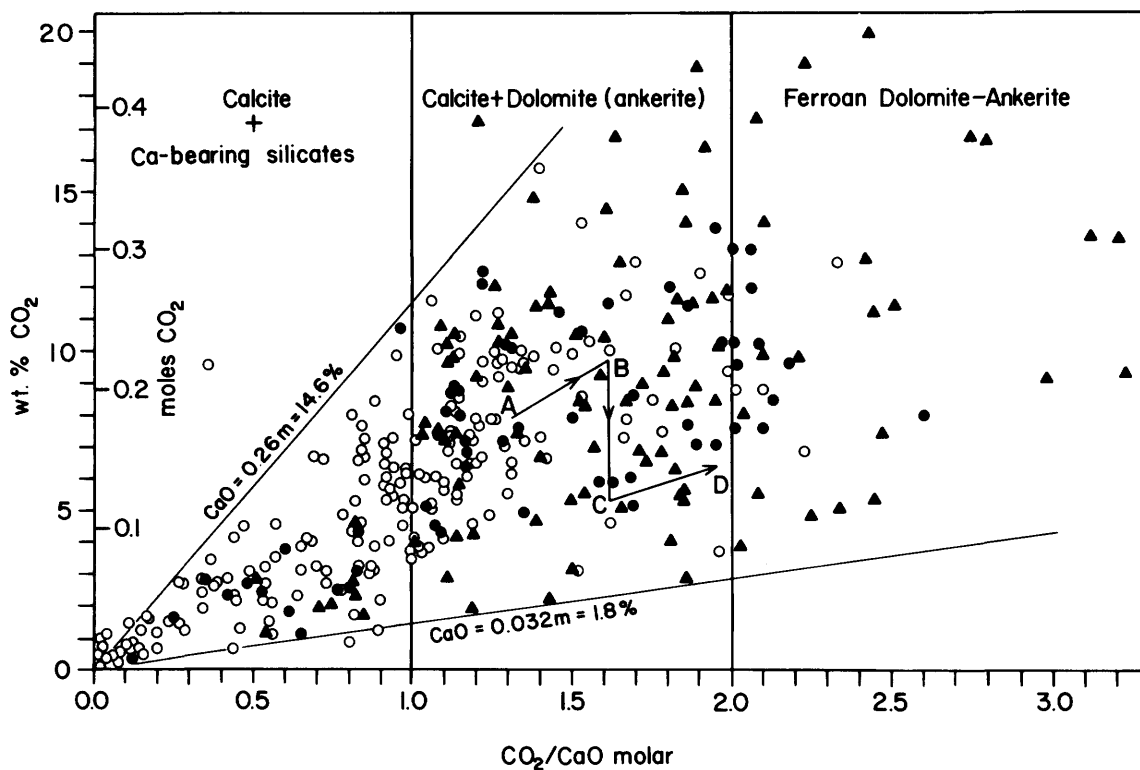


Figure 3—Plot of weight percent CO_2 against CO_2/CaO molar ratio; samples of altered basalt, Timmins area. Solid circles and triangles are "mineralized" samples and open circles are "unmineralized" samples. See text for further explanation.

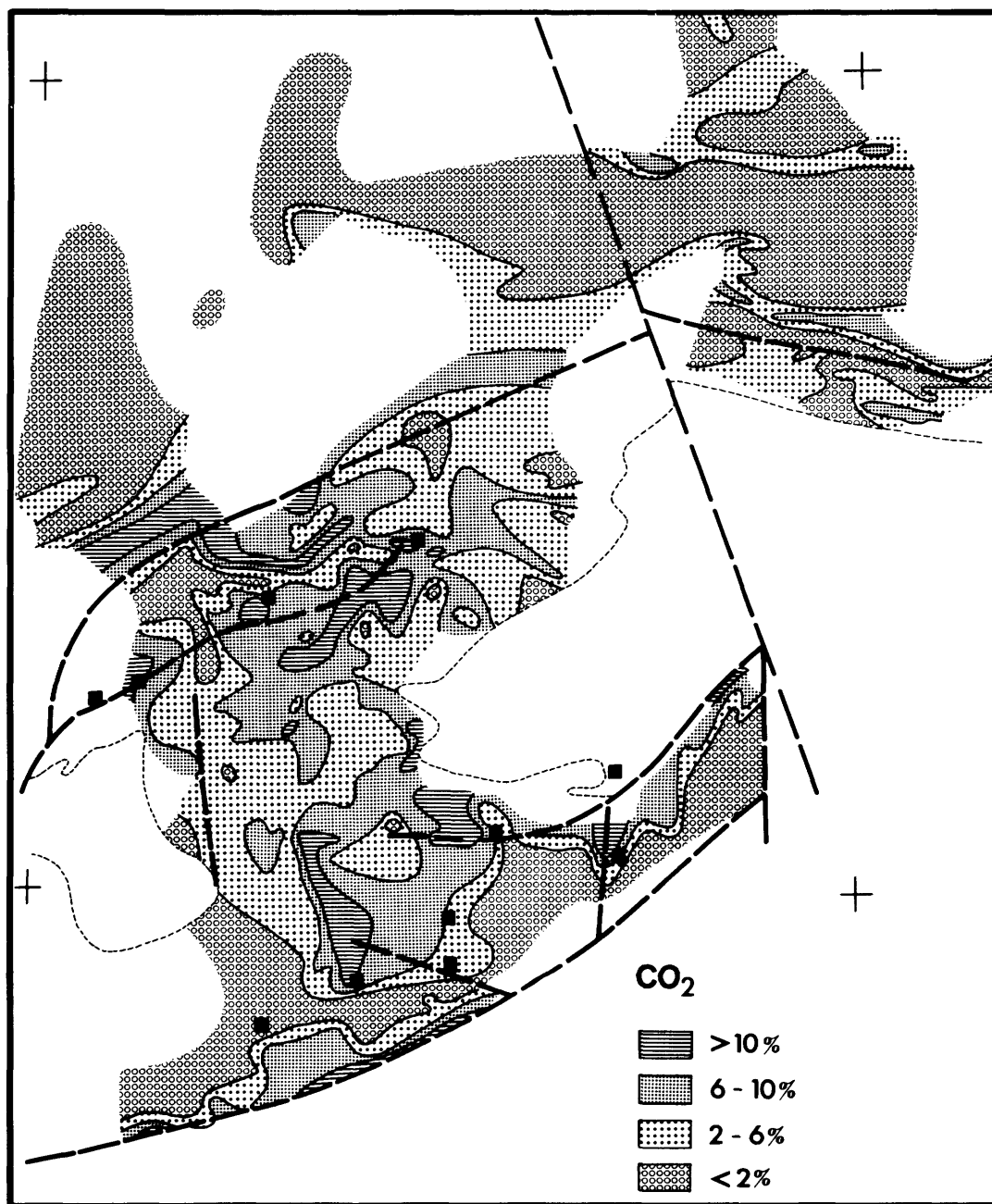


Figure 4—Contours of weight percent CO₂, Timmins area.

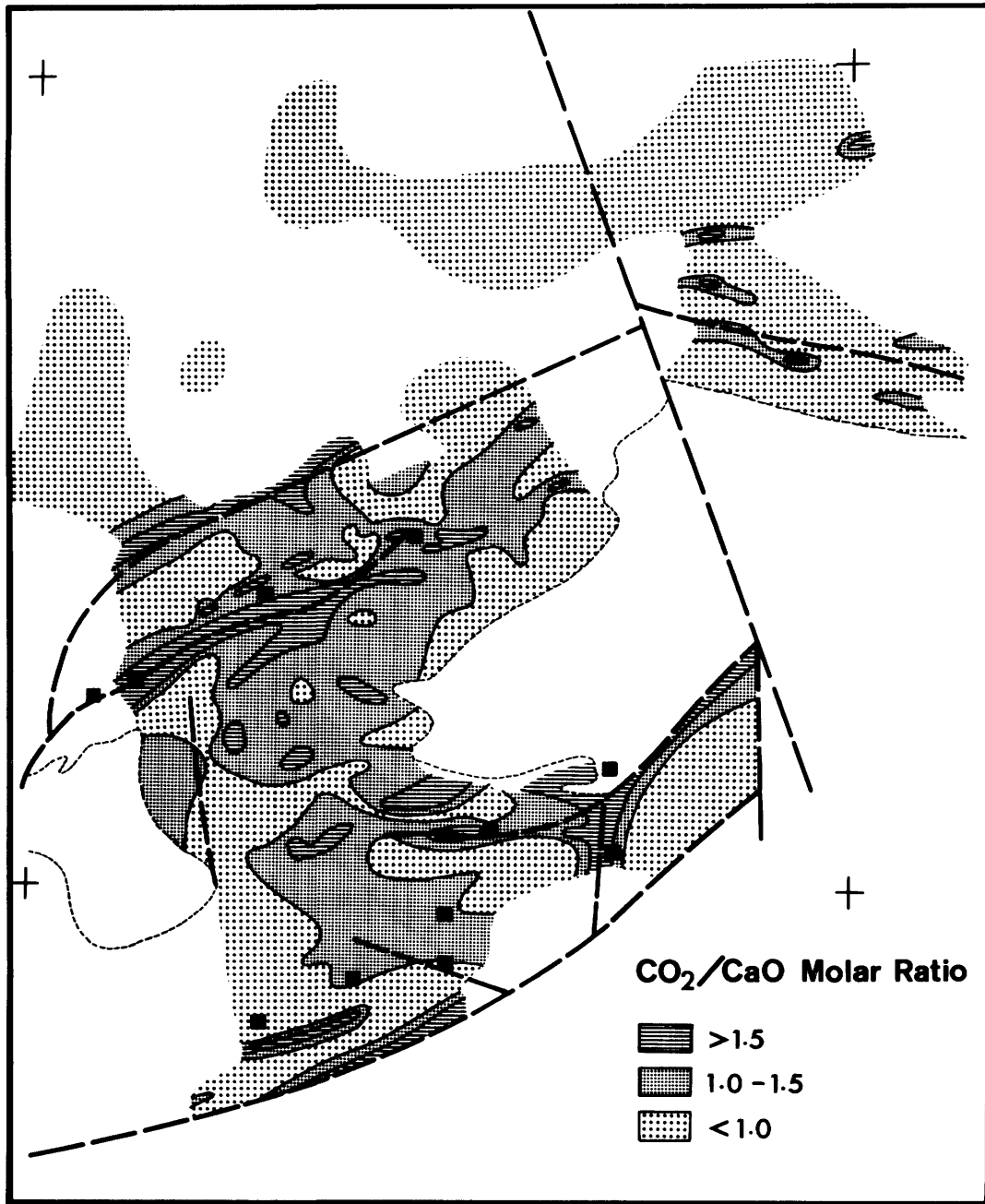


Figure 5—Contours of CO₂/CaO molar ratios, Timmins area.

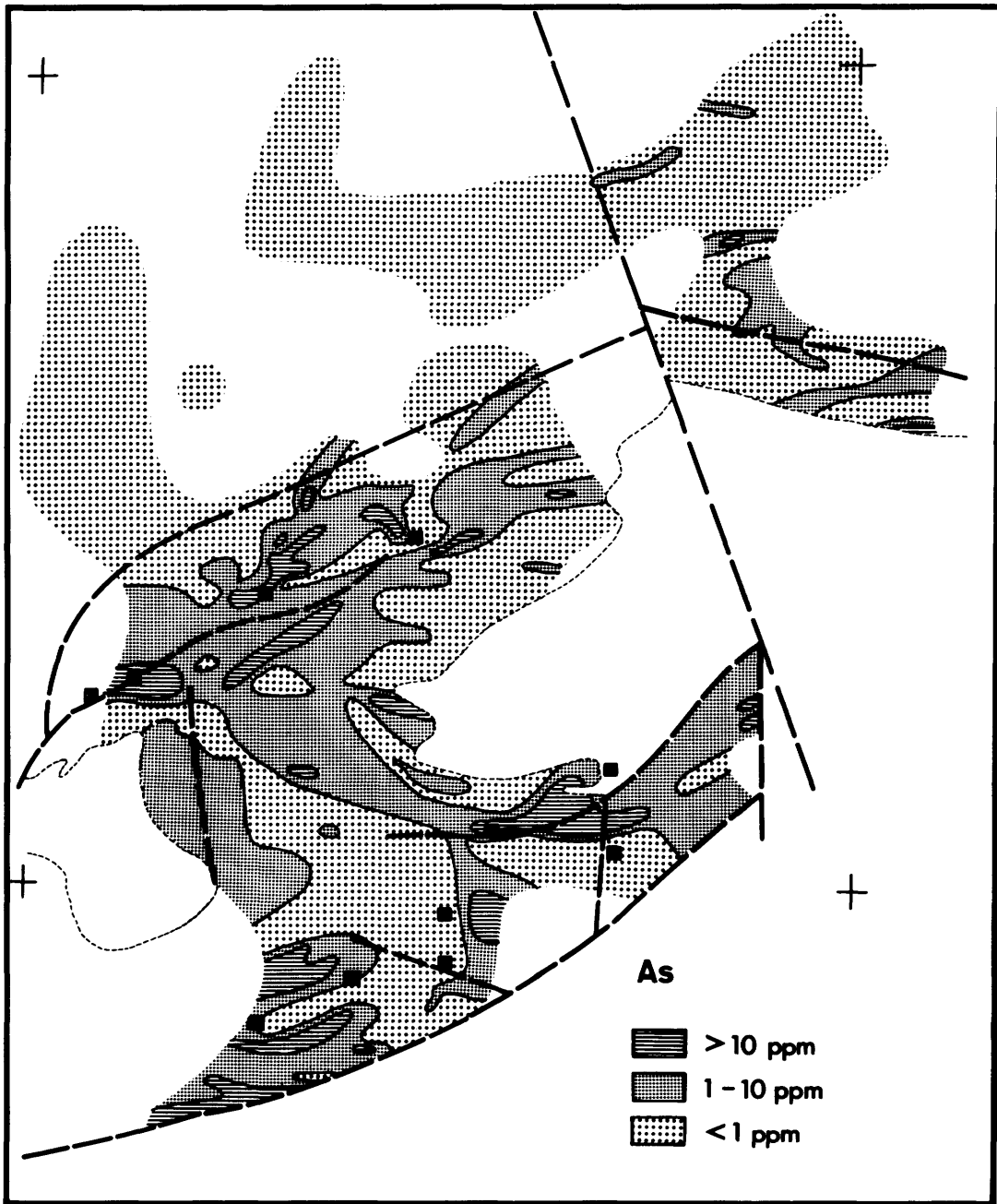


Figure 6—Contours of parts per million As, Timmins area.

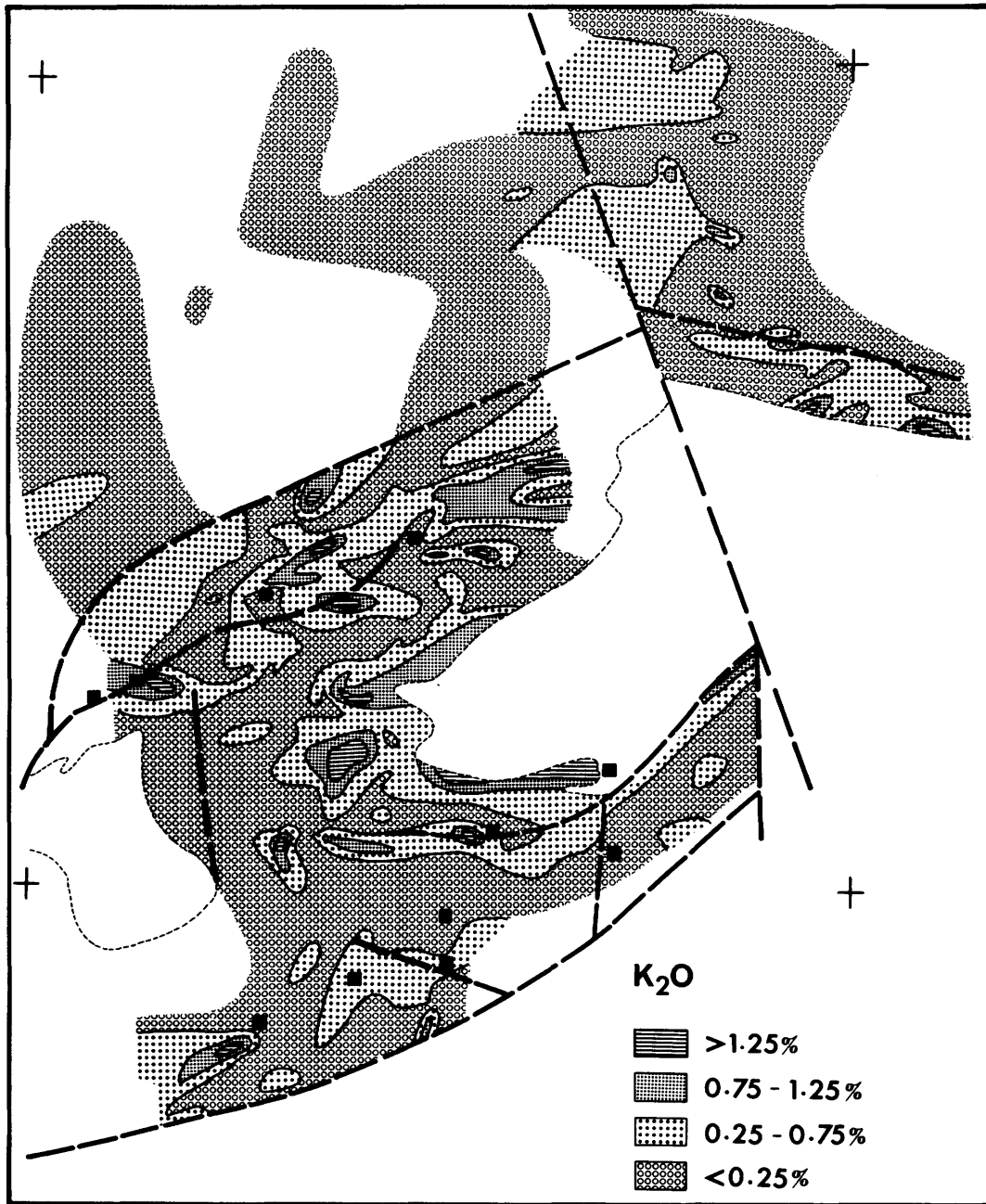


Figure 7—Contours of weight percent K₂O, Timmins area.

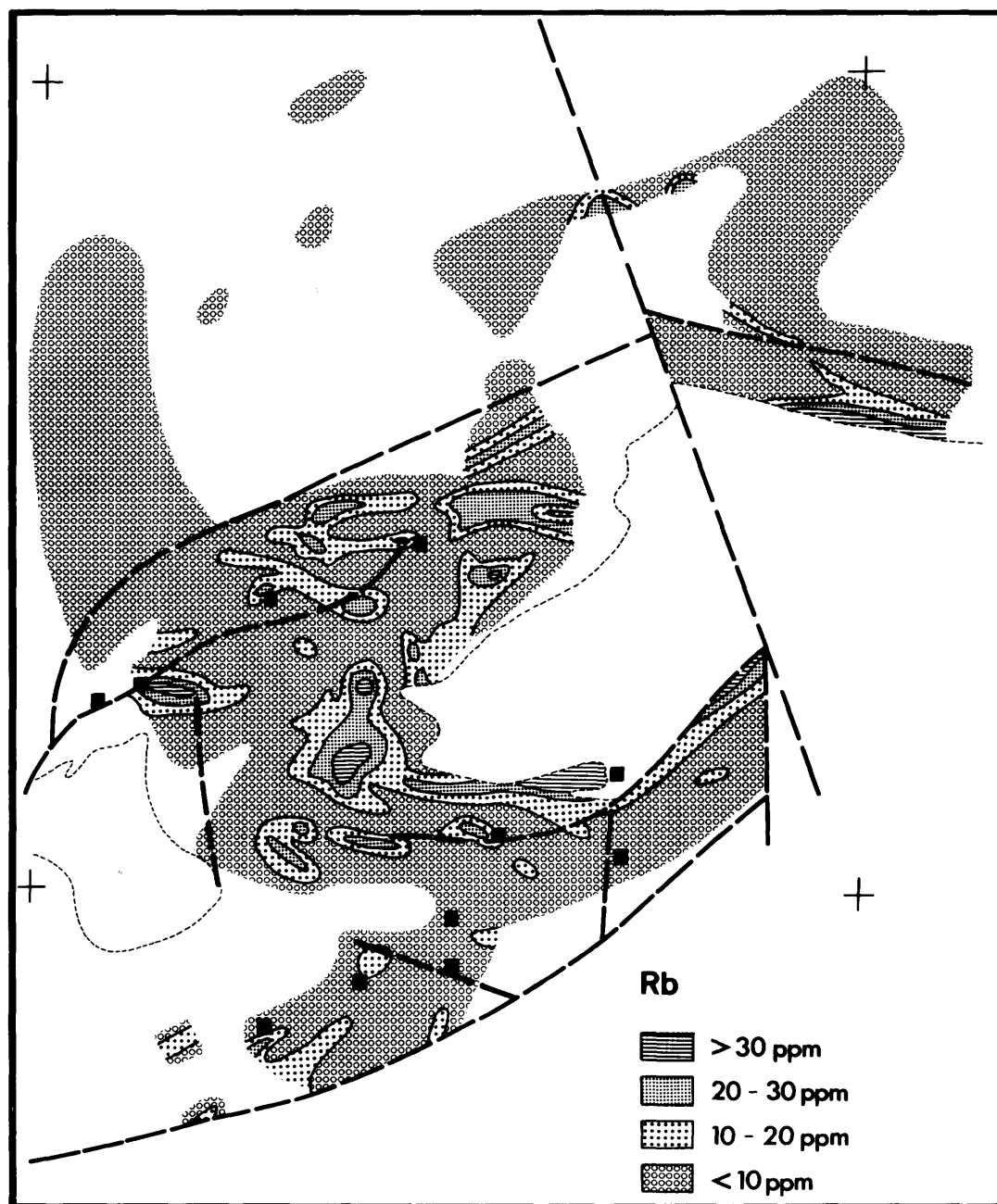


Figure 8—Contours of parts per million Rb, Timmins area.

Table 1—Means and standard deviation, background and Timmins areas.

	Background (Control) Areas			Timmins Area		
	n	mean	S.D.	n	mean	S.D.
CO ₂ /CaO *	99	0.133	0.266	372	0.67	0.67
As ppm	113	0.33	0.31	386	4.02	10.64
K ₂ O %	101	0.28	0.20	425	0.33	0.47
Rb ppm	101	6.53	6.96	453	8.20	11.4

* Excludes ultramafites

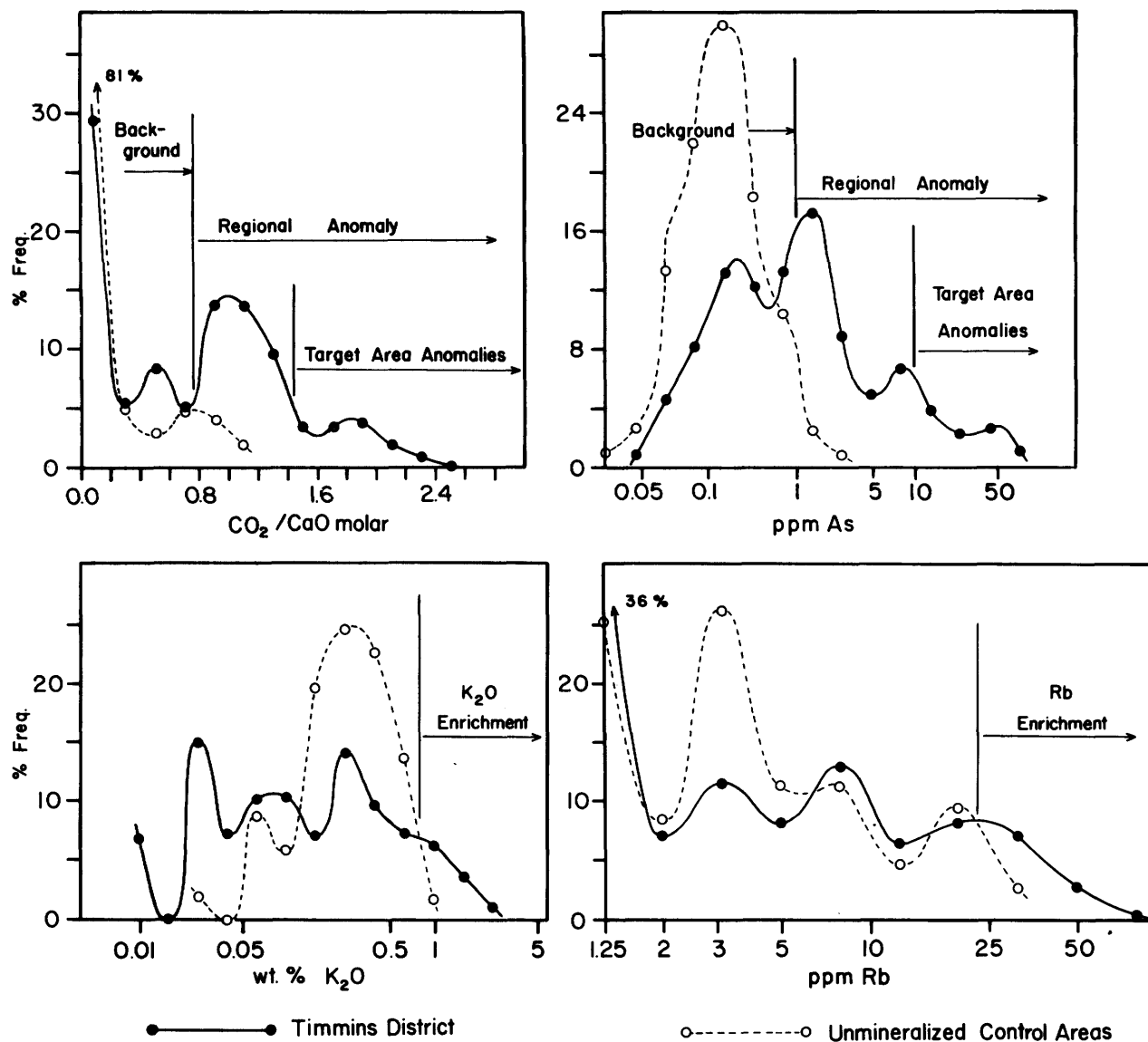


Figure 9—Frequency distribution plots of CO₂/CaO, As, K₂O and Rb from the mineralized Timmins area and unmineralized control areas. The CO₂/CaO ratios are arithmetic; K₂O, As and Rb abundances are logarithmic.

mineralized control areas. The nature of the frequency distributions (Figure 9), indicates remobilization of K_2O and Rb, with areas of enrichment and depletion throughout the Timmins area. The most extensive remobilization of K_2O and Rb (Figures 7,8) appears to have occurred in association with intense CO_2 alteration (Figure 4). It should be noted that Rb has experienced considerable remobilization even under conditions of low-grade regional metamorphism in the control areas.

TARGET-AREA ANOMALIES

Estimated threshold values defining target area anomalies are $CO_2/CaO = 1.5$ and $As = 10$ ppm (Figure 9). These values and the regional thresholds values of 0.75 CO_2/CaO and 1 ppm As correspond to the contoured intervals on Figures 5 and 6 with one exception. The exception is that on Figure 5 the more conservative contour value $CO_2/CaO = 1$, marking CO_2 saturation relative to calcite, is used in place of $CO_2/CaO = 0.75$. The selected local threshold values of 0.75 percent K_2O and 20 ppm Rb may require some modification for particular lithologies within the Tisdale Group as discussed below.

Table 2 presents data for less altered ($CO_2/CaO < 0.75$) and more altered ($CO_2/CaO > 0.75$) samples of each sub-group of the Tisdale Group. The K_2O and Rb contents of less altered samples from the magnesian basalts of the Northern sub-group are lower than those in the other three sub-groups which all have similar mean K_2O and Rb values. The proposed threshold values of 0.75 percent K_2O and 20 ppm Rb are conservative for the tholeiitic Central, Vipond and Gold Centre sub-groups but are too high for rocks of the Northern sub-group. Consequently some target area anomalies in this sub-group may not be detected using K_2O and/or Rb alone.

The mean K_2O and Rb contents in the majority of less altered rocks are comparable to the mean values obtained for the background control areas. The mean As

contents of the less altered samples of all sub-groups are 3 to 5 times higher than the mean for the background areas, confirming the presence of pervasive As enrichment throughout the entire mineralized area. The recommended target area threshold of 10 ppm As is conservative and levels between 1 and 10 ppm in association with $CO_2/CaO > 1.5$ are characteristic of some target areas. These As values are much lower than the threshold of 70 ppm recommended by Fyon and Crockett (1979) for some of the tholeiitic volcanic rocks of the Timmins area.

The more altered samples of basalts from all sub-groups are enriched in K_2O , Rb and As two- to five-fold relative to their less altered equivalents. This demonstrates a general correlation between K_2O , Rb and As enrichment and intensity of carbonate alteration.

A reasonably good spatial correlation exists between CO_2/CaO , As, K_2O and Rb anomalies as well as between them and such known mineralized areas as Hollinger, Pamour-Schumacher, Coniaurum, Dome and Paymaster-Tisdale Mines (see Figures 5 to 8). Even several small gold properties in the northeast quarter of Tisdale township can be detected. On the other hand, coincident anomalies of all four types are not associated with the Buffalo-Ankerite, Paymaster-Deloro or Aunor Mines. As implied above and demonstrated below, combinations of values, one or more of which may be below the designated threshold, are also significant indicators of gold mineralization.

Other groups of coincident anomalies such as those around the nose of the Porcupine Syncline, along the De-stor-Porcupine Fault, and along the Gillies Lake Fault are not known to be associated with important gold mineralization. However, these areas are worthy of further investigation. Two small As anomalies east of the Dome Mine lie in an area of low K_2O , Rb and CO_2/CaO ratios; these may be spurious and the result of surface contamination.

A test of confidence to be placed in the selected threshold values, and of the significance of anomalies in terms of gold mineralization, is afforded by considering a

Table 2— K_2O , Rb, As contents related to intensity of alteration in the sub-groups of the Tisdale Group.

	Less Altered ($CO_2/CaO < 0.75$)					More Altered ($CO_2/CaO > 0.75$)						
	% K_2O		ppm Rb		ppm As	% K_2O		ppm Rb		ppm As		
	n	mean (S.D.)	n	mean (S.D.)	n	mean (S.D.)	n	mean (S.D.)	n	mean (S.D.)		
Gold Centre	11	0.28(0.25)	11	7.5(6.6)	8	1.0(0.5)	32	0.62(0.53)	32	16.5(12.9)	31	4.9(14.6)
Vipond	28	0.15(0.19)	30	4.0(5.0)	26	1.5(2.6)	52	0.46(0.52)	51	11.7(14.5)	48	7.0(13.9)
Central	90	0.23(0.39)	91	5.1(8.6)	84	2.3(3.9)	104	0.38(0.44)	99	10.5(12.5)	97	6.4(12.9)
Northern	44	0.10(0.17)	44	2.1(2.5)	37	0.88(2.02)	10	0.63(0.51)	10	15.3(11.9)	9	20.2(27.7)
Mafic												
Northern	11	0.03(0.03)	11	2.0(1.5)	5	1.5(2.5)	5	0.01(0.01)	5	0.8(1.1)	2	13.7(18.8)
Ultramafic												

Table 3—Distribution of "mineralized" samples by categories representing increasing CO_2/CaO , As and K_2O . Total of 111 samples directly associated with gold-bearing veins at Dome and Pamour No. 1 Mines.

Category	Number	% of total
$\text{CO}_2/\text{CaO} < 1$	10	9%
$\text{CO}_2/\text{CaO} 1-1.5$	32	28.8
$\text{CO}_2/\text{CaO} > 1.5$	69	62.2
As < 1 ppm	6	5.4
As 1-10	45	40.5
As > 10	60	54.1
$\text{K}_2\text{O} < 0.75\%$	61	54.9
$\text{K}_2\text{O} > 0.75$	50	45.1

group of samples from wall-rocks surrounding veins in the Dome Mine and Pamour No. 1 Mine. The Dome samples are from a section traversing tholeiitic basalts of the Vipond and Gold Centre sub-groups. Those from the Pamour No. 1 are magnesian basalts of the Northern sub-groups. Table 3 summarizes the data by categories of increasing CO_2/CaO , As and K_2O . It is apparent that there is a progressive increase in the percentage of samples with higher CO_2/CaO and As. No such increase occurs in relation to K_2O , for this group of samples. The probable reason is that about half of the samples are from magnesian basalts of the Northern sub-group which had an initially lower K_2O content than the tholeiites of the Vipond and Gold Centre sub-groups (see Table 2). It is significant that not more than 60 percent of samples closely associated with gold mineralization can be expected to exceed the CO_2/CaO threshold of 1.5, nor about 50 percent to exceed the 10 ppm As and, perhaps, the 0.75 percent K_2O thresholds.

Table 4— CO_2/CaO , K_2O , As levels relative to gold mineralization, surface samples Timmins area.

Category	Total Samples	Mineralized Samples	Percent Mineralized
$\text{CO}_2/\text{CaO} < 1$	248	20	8.1
$\text{CO}_2/\text{CaO} 1-1.5$	98	24	24.5
$\text{CO}_2/\text{CaO} > 1.5$	52	26	50.0
As < 1 ppm	182	24	13.2
As 1-10	129	25	19.4
As > 10	41	17	41.5
$\text{K}_2\text{O} < 0.75\%$	361	50	13.8
$\text{K}_2\text{O} > 0.75$	58	19	32.8

Table 4 lists the surface samples according to the same categories as Table 3. "Mineralized" surface samples are defined as those situated not more than 500 feet from known gold mineralization. It is evident that the proportion of "mineralized" to "unmineralized" samples is much greater at higher CO_2/CaO , As and K_2O levels. It appears that the best single indicator of proximity to gold mineralization is the CO_2/CaO molar ratio. Arsenic by itself is less effective than the CO_2/CaO ratio, and K_2O alone is still less effective. However, K_2O and As in combination either with one another or with CO_2/CaO (Table 5) add a further degree of discrimination between "mineralized" and "unmineralized" samples. This is particularly significant in the category CO_2/CaO 1 to 1.5 where 24.5 percent of the samples are mineralized (see Table 4). Dividing these into sub-categories (Table 5) with K_2O greater and less than 0.75 percent reveals that 54.5 percent of the samples with $\text{K}_2\text{O} > 0.75$ percent and CO_2/CaO 1 to 1.5 are mineralized. Similarly 50 percent of the samples with As > 10 ppm and CO_2/CaO 1 to 1.5 are mineralized. A less marked increase in percentage of samples that are mineralized occurs when considering K_2O and As in the category $\text{CO}_2/\text{CaO} > 1.5$. The data of Table 5 also reveals that 67 percent of those samples containing more than 0.75 percent K_2O and 10 ppm As are mineralized, regardless of CO_2/CaO ratio. Not shown on Table 5 are combinations involving all three measurements: CO_2/CaO , As, and K_2O . Only nine samples contained coincident values above the thresholds for these three parameters; six (67 percent) of these samples were associated with known mineralization. In general, then, $\text{CO}_2/\text{CaO} > 1$, $\text{K}_2\text{O} > 0.75$ and As 10 ppm, in appropriate combinations, suggest a 50 to 67 percent probability of proximity to gold mineralization. That these expectations are realistic maxima is supported by the percentage distribution of CO_2/CaO , As and K_2O values from the mine samples (see Table 3), all of which are mineralized.

LOCALIZATION OF ALTERATION AND GOLD MINERALIZATION

Most of the recently proposed models of gold mineralization in the Timmins-Kirkland Lake-Larder Lake area recognize, as did the early workers in these camps, the importance of carbonate alteration. Most recent models invoke a two-stage process involving 1) initial concentration of gold and carbonate by synvolcanic or synsedimentary and pre-tectonic deposition, 2) subsequent syn-tectonic metamorphic remobilization and concentration to form "epigenetic" gold-bearing quartz veins. Differences in the various models relate mainly to the initial concentration of gold and carbonate, distribution of carbonate alteration and timing of the carbonatizing process.

Karvinen (1978,1980) regards stratigraphically distributed, exhalative carbonate horizons and associated felsic porphyries as initial sources of carbonate and gold

GRANT 30 GEOCHEMICAL ANOMALIES ASSOCIATED WITH GOLD MINERALIZATION

Table 5—Combinations of CO₂/CaO, K₂O, As (category and sub-category) relative to gold mineralization, surface samples, Timmins area.

	Category	Total Samples	Mineralized Samples	Percent Mineralized
CO ₂ /CaO < 1	K ₂ O < 0.75%	221	19	8.6
	K ₂ O > 0.75	18	1	5.6
CO ₂ /CaO 1.0-1.5	K ₂ O < 0.75	87	18	20.7
	K ₂ O > 0.75	11	6	54.5
CO ₂ /CaO > 1.5	K ₂ O < 0.75	30	13	43.3
	K ₂ O > 0.75	20	13	65.0
CO ₂ /CaO < 1	As < 1 ppm	132	7	5.3
	As 1-10	63	6	9.5
	As > 10	14	3	21.4
CO ₂ /CaO 1.0-1.5	As < 1	36	11	30.6
	As 1-10	46	9	19.6
	As > 10	8	4	50.0
CO ₂ /CaO > 1.5	As < 1	12	6	50.0
	As 1-10	15	9	60.0
	As > 10	18	10	55.6
K ₂ O < 0.75%	As < 1	147	17	11.6
	As 1-10	114	19	16.7
	As > 10	29	8	27.6
K ₂ O > 0.75%	As < 1	21	6	28.6
	As 1-10	15	4	26.7
	As > 10	12	8	66.7

in the Timmins area. Fyon and Crockett (1980) note that carbonatized rocks occur throughout the volcanic stratigraphy of those portions of the Tisdale Group studied by them. In some cases the alteration is described as stratabound and elsewhere as discordant; they present structural and textural arguments for a synvolcanic-pretectonic origin for the carbonatization.

Pyke (1976, 1980) emphasizes the role of major faults in localizing carbonate alteration. Komatiites which are very susceptible to alteration, and the location of which frequently coincides with that of major faults, are regarded as the probable sources of gold. He suggests that CO₂ from sedimentary sources was remobilized during folding and focussed along faults, altering the komatiites and releasing gold. Jensen (1980) also stresses the importance of major faults in localizing carbonatization and mineralization in the Kirkland Lake area. However, he regards basin-margin calcareous and carbonaceous sediments as the probable source of both CO₂ and Au. Downes (1980) supports the concept of postvolcanic or late syntectonic carbonatization. He reports unaltered ultramafic clasts in conglomerates overlying carbonatized volcanic rocks in the Kirkland Lake area. Downes also points out that the most commonly carbonatized lithology

in that area is ultramafic, resulting in the stratigraphic appearance of the carbonatized zone.

The results of the present study on carbonate distribution and the earlier studies of volcanic stratigraphy and immobile trace element data (Davies *et al.* 1979; Davies and Whitehead 1980) are difficult to reconcile with the concept of extensive, stratigraphically distributed and continuous carbonate units in the Timmins area. Both Karvinen (1980) and Fyon and Crockett (1980) recognize the locally transgressive nature of the carbonate. However, the degree of discordance of the "upper carbonate member" as mapped by Karvinen (1980) is extreme in some places. In the area of the Coniaurum and Pamour-Schumacher shafts (see Figures 1 and 2) this carbonate is shown by Karvinen (1980) as following the lower contact of the Vipond sub-group northeastward to just east of the Coniaurum shaft where it doubles back sharply through the shaft area and then extends southwest toward the Hollinger shaft. This path does coincide with a number of highly carbonatized locations (see Figure 5) but it transgresses from the bottom of the Vipond sub-group stratigraphically downward to rocks of the middle or lower part of the Central sub-group.

The same "upper carbonate member" is also shown

following along the contact between the Vipond and Central sub-groups, outlining the limbs of the Vipond Anticline (VA, Figure 1). However, the analytical data (see Figure 5) indicate that the highest intensity carbonatization occurs in the core of the anticline ($\text{CO}_2/\text{CaO} > 1.5$). A broad zone of slightly lower but still intense alteration (CO_2/CaO 1 to 1.5) blankets the entire area of Central and adjacent Vipond rocks, extending from the core of the fold to beyond both sides of the Vipond-Central contact. Consideration of carbonate alteration in terms of quantity (weight percentage CO_2 , Figure 4) rather than intensity (CO_2/CaO ratios) does not resolve these difficulties in reconciling the analytical data with the concept of stratigraphic carbonate units.

The patterns of alteration displayed in Figures 4 and 5 constitute strong evidence of large-scale regional pervasive carbonatization. Large areas with $\text{CO}_2 > 6$ percent and CO_2/CaO ratios greater than 1, representing CO_2 supersaturation relative to calcite, cut across the entire stratigraphic sequence of the Tisdale Group. Anomalies representing highest intensities of carbonatization ($\text{CO}_2/\text{CaO} > 1.5$) are distributed throughout all four sub-groups in the area between the Gillies Lake and Destor-Porcupine Faults. Most of them are not restricted to particular stratigraphic units. Some of the largest and most continuous anomalies do have a stratigraphic appearance but these occur mainly adjacent to faults and along zones of intense shearing which commonly are parallel or sub-parallel to flow contacts. Even parts of these are discordant. The one band of high CO_2/CaO not apparently related to shearing coincides with a Mg-rich flow south of the Aunor and Delnite shafts.

The spatial relationships between CO_2/CaO , As, K_2O and Rb anomalies and structures are revealed by comparing Figures 5 to 8 with Figure 1. Many of the anomalies that do not lie along fault zones coincide with fold axes and areas of strong schistosity. Perhaps more significant is the fact that the region of abundant anomalies is largely restricted to the area between the Gillies Lake and Destor-Porcupine Faults. This is an area of complex deformation caused by multiple folding, the last stage of which is represented by the Porcupine Syncline around which earlier folds have been re-oriented (Pyke 1976; Davies 1977).

Although there may be some synvolcanic, stratigraphically distributed carbonate in the area, the bulk of it cannot be identified as such. The present distribution and pattern of carbonatization and its relationship to volcanic stratigraphy and structure constitute strong evidence for syntectonic or late tectonic, post-depositional alteration. The patterns and distribution of extensive arsenic enrichment and remobilized K_2O and Rb, corresponding to the carbonate alteration at both the regional and local scales, support this conclusion.

APPLICATION TO GOLD EXPLORATION

The results of this study can be applied at various levels of detail in exploration for gold in basaltic rocks. At the reconnaissance level a sample density of about 25 sites per square mile, equivalent to 1000-foot spacing, should distinguish large regions with high potential for gold mineralization from those with low potential. Sampling at this density need not be undertaken indiscriminantly over large areas but should be based, in the first instance, on the presence of widespread megascopically visible carbonate alteration. Large areas (several square miles) with numerous CO_2/CaO ratios near 1 and As contents above 1 ppm can be considered favourable for more detailed exploration.

Preliminary indication of potential target areas (several thousand square feet in size) may be achieved with a sample spacing of 500 feet or less. Target areas can be identified by any of the following combinations of values:

CO_2/CaO 1-1.5 and > 1.5 , $\text{K}_2\text{O} > 0.75$ percent

CO_2/CaO 1-1.5, As > 10 ppm

$\text{CO}_2/\text{CaO} > 1.5$, As < 1 to > 10 ppm

$\text{K}_2\text{O} > 0.75$ percent, As > 10 ppm

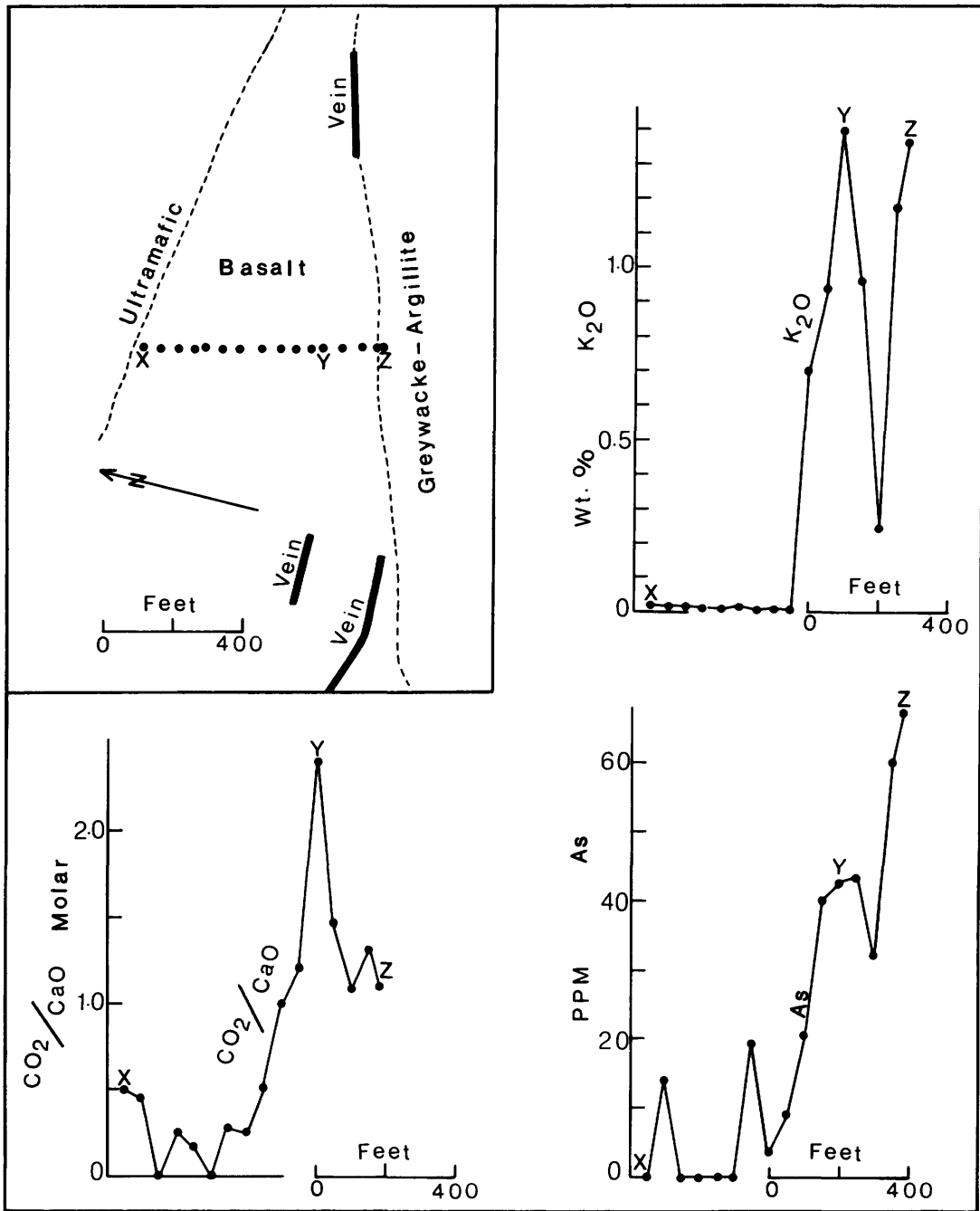
$\text{CO}_2/\text{CaO} > 1.5$, $\text{K}_2\text{O} > 0.75$ percent, As > 10 ppm

CO_2/CaO ratios, As and K_2O can also be used effectively in detailed underground exploration using either stope and drift samples or diamond drill core. An example is presented in Figure 10. The line of samples, taken at 50-foot intervals along a cross-cut on the 1400-foot level at Pamour No. 1 mine, is located about 500 feet from gold-bearing quartz veins that occur on both sides of the sampled section (XYZ). Plots of CO_2/CaO , K_2O and As clearly identify points Y and Z as anomalous. These points lie on the projections between the east vein and the two west veins and the anomalies clearly indicate the existence of gold mineralization along strike.

ACKNOWLEDGMENTS

Studies of the structure, stratigraphy and trace element analyses in the Timmins area have been supported by grants from the National Sciences and Engineering Research Council for Canada. Sample collection, CO_2 , alkali, and As analyses were funded by the Ontario Geological Survey Geoscience Research Grant Program. Analyses were conducted by M. Whitehead and M.L. Whitehead under the supervision of L. Dupuis, Senior Technologist, Department of Geology, Laurentian University.

We are grateful to the holders of mineral rights in the area for allowing access to their properties; the management and staffs of Pamour Porcupine Mines Limited and Dome Mines Limited were particularly helpful in arranging visits and in discussing geological problems.



REFERENCES

- Billings, M.P. and White, W.S.
1950: Metamorphosed Mafic Dikes of the Woodsville Quadrangle, Vermont and New Hampshire; *American Mineralogist*, Vol. 35, p.629-643.
- Boyle, R.W.
1979: The Geochemistry of Gold and its Deposits; *Geol. Surv. Canada, Bull.* 280.
- Davies, J.F.
1977: Structural Interpretation of the Timmins Mining Area, Ontario; *Canadian J. Earth Sci.*, Vol.14, p.1046-1053.
- Davies, J.F., Grant, R.W., and Whitehead, R.E.S.
1979: Immobile Trace Elements and Archean Volcanic Stratigraphy, Timmins Mining Area, Ontario; *Canadian J. Earth Sci.*, Vol.16, p.305-311.
- Davies, J.F., and Whitehead, R.E.S.
1980: Further Immobile Element Data from Altered Volcanic Rocks, Timmins Mining Area, Ontario; *Canadian J. Earth Sci.*, Vol.17, p.419-423.
- Deer, W.A., Howie, R.A., and Zussman, J.
1962: *Rock-Forming Minerals*, Vol. 5, Non-Silicates; Longmans, London.
- Downes, M.J.
1980: Structural and Stratigraphic Aspects of Gold Mineralization in the Larder Lake Area, Ontario; p.92-103 in *Genesis of Archean Volcanic-Hosted Gold Deposits*; Roberts, R.G., editor, Ontario Geol. Surv. Open File Report 5293.
- Ferguson, S.A. and associated geologists
1968: *Geology and Ore Deposits of Tisdale Township*; Ontario Dept. Mines, Geol. Rept. 58.
- Fyon, J.A., and Crockett, J.H.
1979: Geological and Geochemical Guide to Gold Mineralization in the Porcupine Camp; p.192-198 in *Summary of Field Work, 1979*, Milne, V.G., White, O.L., Barlow, R.B., and Kustra, C.R., editors, Ontario Geol. Surv., Misc. Paper 90.
- Fyon, J.A. and Crockett, J.H.
1980: Volcanic Environment of Carbonate Alteration and Strati-form Gold Mineralization, Timmins Area; p.44-65 in *Genesis of Archean Volcanic-Hosted Gold Deposits*, Roberts, R.G., editor, Ontario Geol. Surv. Open File Report 5293.
- Harte, B., and Graham, C.M.
1975: The Graphical Analysis of Greenschist to Amphibolite Facies Mineral Assemblages in Metabasites; *Jour. Petrol.*, Vol.16, Pt.2, p.347-370.
- Jensen, L.S.
1980: The Relationship between Volcanism and Gold Mineralization in the Kirkland Lake District; p.280-302 in *Genesis of Archean Volcanic-Hosted Gold Deposits*, Roberts, R.G., editor, Ontario Geol. Surv., Open File Report 5293.
- Karvinen, W.O.
1978: Structural Interpretation of the Timmins Mining Area: Discussion; *Canadian J. Earth Sci.*, Vol.15, p.854.
- 1980: Geology and Evolution of Gold Deposits, Timmins Area; p.1-43 in *Genesis of Archean Volcanic-Hosted Gold Deposits*, Roberts, R.G., editor, Ontario Geol. Surv., Open File Report 5293.
- Pyke, D.R.
1976: On the Relationship between Gold Mineralization and Ultramafic Volcanic Rocks in the Timmins Area, Northeastern Ontario; *Canadian Inst. Min. Met. Bull.*, Vol.69, No.773, p.79-87.
- 1980: Relationship of Gold Mineralization to Stratigraphy and Structure in Timmins and Surrounding Area; p.104-136 in *Genesis of Archean Volcanic-Hosted Gold Deposits*, Roberts, R.G., editor, Ontario Geol. Surv., Open File Report 5293.
- Roberts, R.G.
1980: The Volcanic-Hosted Gold Deposits, Tectonic Setting of Gold Deposits in the Timmins Area; p.359-387 in *Genesis of Archean Volcanic-Hosted Gold Deposits*, Roberts, R.G., editor, Ontario Geol. Surv., Open File Report 5293.
- Skippen, G.B.
1971: Experimental Data for Reactions in Siliceous Marbles; *Jour. Geol.*, Vol.79, p.457-481.

Grant 62 The Direct Dating of Ore Minerals

Derek York¹, A. Masliwec¹, C. M. Hall¹, P. Kuybida¹, W. J. Kenyon¹,
E. T. C. Spooner², and S. D. Scott²

¹Department of Physics, University of Toronto

²Department of Geology, University of Toronto

ABSTRACT

The preliminary results are presented of a study of the feasibility of the direct dating of sulphide ore minerals. Our studies of pyrites, galenas, chalcopyrites and sphalerites show that pyrite appears to be dateable with the ⁴⁰Ar/³⁹Ar variant of K-Ar dating. After an initial survey had shown that sulphides (particularly pyrite) contain sufficient potassium and argon for age analysis, detailed studies were carried out on pyrites from two different environments. Geco pyrites from the Manitouwadge area of northern Ontario were found to indicate an age of 2.5 ± 0.1 Ga on an isochron-type plot, in good agreement with ages of 2.62 ± 0.02 Ga obtained on mica found among the ore minerals. Pyrites from a Mississippi Valley type ore indicated an age on an isochron-type plot of 549 ± 20 Ma. Since the ore is found in upper Cambrian sedimentary rocks, this result strongly suggests that the ore was deposited very soon after deposition of the host sediments.

INTRODUCTION

The process of ore formation can only fully be understood if the chronology of the ore minerals is known. However, this parameter is often only poorly known because the low radioactivity content of sulphides makes them very difficult to date. The object of the present study was to take advantage of recent advances in the reliability of detection of very small amounts of radiogenic argon (Hall and York 1978) and to test the viability of the ⁴⁰Ar/³⁹Ar method of dating sulphides.

Preliminary studies have been made of pyrites, galenas, chalcopyrites and sphalerites to see if the method was feasible with all or any of these minerals types. When it was shown that pyrites were the most promising for ⁴⁰Ar/³⁹Ar analysis, attention was focussed on two quite different deposits to see in detail if indeed pyrites were dateable. Our results, presented below, appear to show that, in fact, pyrites can be dated.

EXPERIMENTATION

After a preliminary survey by flame photometry and atomic absorption had shown that pyrites and galenas generally had K-contents in the 10-100 ppm and 5-10 ppm ranges respectively, ⁴⁰Ar/³⁹Ar analyses were begun.

Irradiations of 150 megawatt-hours were chosen so that enough ³⁹Ar would be produced by neutron irradiation to be accurately measured with the mass spectrometer. The irradiations were done in the McMaster University uranium-enriched reactor. Because of the extremely low concentrations of potassium, it was necessary to irradiate samples of 1 to 2 g size. This resulted in fairly high levels of radioactivity being produced by the sulphides. To reduce this, later samples have been wrapped in cadmium foil for irradiation. The cadmium very effectively shields the samples from the thermal neutron component and thereby considerably lessens the induced radioactivity in the sulphides. The fast neutron flux needed to generate ³⁹Ar is, however, not seriously cut back, and so the use of cadmium foil is a significant step forward experimentally. However, to make the usual calcium and potassium associated corrections for interfering isotopes, it was necessary to irradiate pure calcium and potassium salts wrapped in cadmium foil so that new correction parameters could be determined.

Since ³⁸Ar is generated by neutron bombardment of chlorine, KCl samples were irradiated to calibrate the reactor so that chlorine concentrations in the sulphides could be measured. Thus from ³⁹Ar, ³⁷Ar and ³⁸Ar measurements, it was possible to calculate the K, Ca and Cl contents of the sulphides.

The neutron-irradiated samples were fused in an ultra-high vacuum system and the purified argon subsequently analyzed in an MS10 mass spectrometer. The "Zartman Hornblende 3 gr" was irradiated alongside the sulphides as an age standard, its age being taken as 1070 Ma (Alexander and Davis 1974; Hanes and York 1979).

Mineral separations were all performed with considerably greater care than for normal projects because of the extremely low potassium and argon concentrations dealt with here. All sulphide grains were hand-picked under binocular microscope to avoid contamination with silicates.

Table 1—K and Ar analytical data for pyrites, galenas and sphalerites.

<u>Sample</u>	<u>K(p.p.m.)</u>	$\frac{40}{\text{Ar}}$ ($\times 10^{-7}\text{cc/g}$)	$\frac{40}{\text{Ar}} / \frac{36}{\text{Ar}}$	<u>Run No.</u>
Geco:				
Pyrite	5.6	7.55	393	OGS10
"	8.8	8.49	444	OGS14
"	34.4	9.76	1219	OGS131
"	16.8	5.91	840	OGS132
"	4.8	5.40	631	OGS133
"	11.9	7.12	521	OGS134
Galena	<0.3	7.86	453	OGS 20
"	0.71	1.76	819	OGS 33
Sphalerite	0.3±0.3	3.41	615	OGS 6
"	0.3±0.3	1.67	436	OGS 11
Chalcopyrite	14.1	13.64	1197	OGS 38
Sturgeon Lake:				
Sphalerite		4.22	327	OGS 4
Renabie:				
Pyrite		40.16	1272	OGS 52
"	15.1	35.26	1169	OGS 15
MVT:				
Pyrite	78.10	8.07	509	OGS 17
"	23.62	5.99	437	OGS 19
"	19.70	5.42	382	OGS 45
"	102.30	9.64	567	OGS 46
"	113.00	9.45	576	OGS 92
"	71.60	14.04	428	OGS 93
"	114.10	3.96	542	OGS 96
"	431.20	14.11	713	OGS130
"	352.30	15.63	580	OGS135
"	45.50	5.90	485	OGS136
Galena	1.3	0.514	303	OGS 16
"	0.2	0.832	294	OGS 49
"	1.3	1.58	303	OGS 82
"	1.3	0.91	307	OGS 94
"	0.8	0.64	342	OGS 95
"	1.6	0.81	324	OGS129
Sudbury:				
Pyrite	1.6	8.85	308	OGS531
"	2.1	7.82	309	OGS537
Chalcopyrite	8.2	18.49	1622	OGS 32

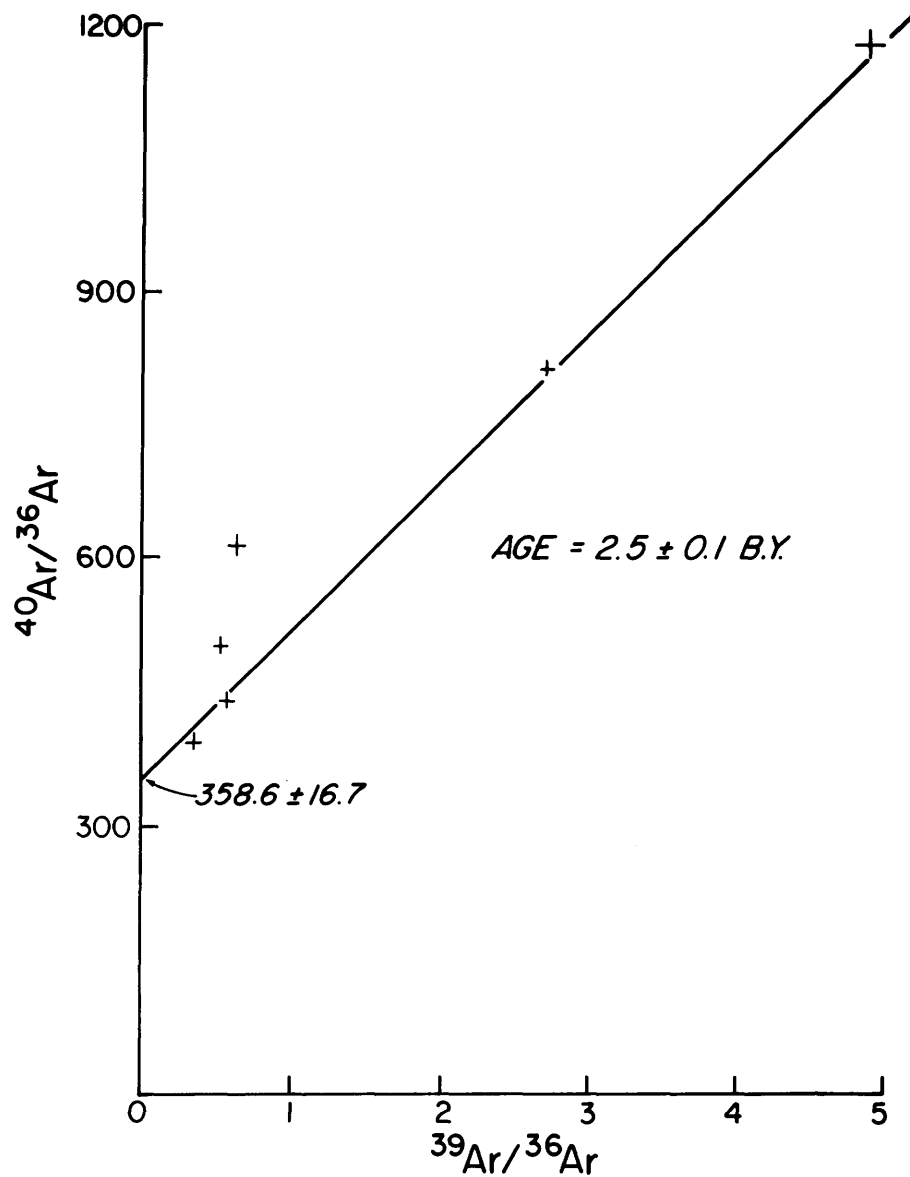


Figure 1—Argon correlation plot for Geco pyrites.

RESULTS

The sulphide data are shown in Table 1 and Figures 1 and 3. The Geco silicate data are presented in Figure 2.

GECO SULPHIDES

Some of the Geco ore samples examined were found to contain minute flakes of biotite. Several flakes were picked out from the ore from two different levels and

these were neutron-irradiated and step-heated so that a reliable reference age could be compared with the sulphide data. Both biotites gave excellent plateaus (Figure 2) in good agreement at about 2.62 Ga. The micas clearly cooled through a temperature of roughly 300°C about 2.62 Ga ago. Whether the ore had just formed then, or whether it had existed for quite a long time before finally cooling at 2.62 Ga ago, remains to be seen.

Six pyrites, one chalcopyrite, two galenas and one sphalerite were irradiated and their $^{40}\text{Ar}/^{36}\text{Ar}$ and $^{39}\text{Ar}/^{36}\text{Ar}$ ratios measured. These data are plotted in Figure 1

where it can be seen at once that five of the six pyrite points are highly linearly correlated. A best least-squares straight line was fitted to these data allowing carefully for error correlations (York 1969). While the data points are somewhat more scattered about the line than would be expected from experimental error alone, the age obtained from the slope of the best-fitting line is 2.5 ± 0.1 (1σ) Ga. This is a remarkable result, agreeing as it does within error with that on the associated biotites and represents the first ever successful dating of pyrite.

The fact that one of the six pyrite points falls well off the line, while the others exhibit more than experimental scatter, shows that not all the assumptions made in the age calculation are perfectly satisfied. The most likely explanation is that the $^{40}\text{Ar}/^{36}\text{Ar}$ ratio was not completely uniform at the time the pyrites became closed systems to argon diffusion. This comment is reinforced by the fact that the other sulphides at Geco (galenas, etc.) all seem characterized by their own different $^{40}\text{Ar}/^{36}\text{Ar}$ ratios. The average initial $^{40}\text{Ar}/^{36}\text{Ar}$ ratio indicated for the pyrites is

359 ± 17 (Figure 1). It would appear, however, that the Geco data show that Precambrian pyrites can be dated by the $^{40}\text{Ar}/^{39}\text{Ar}$ approach using the isochron plotting approach.

MISSISSIPPI VALLEY TYPE PYRITES AND GALENAS

The ten pyrite samples from one hand specimen of ore from the Mississippi Valley type (MVT) deposit in southeast Missouri show a strong linear correlation on the $^{40}\text{Ar}/^{36}\text{Ar}$ vs. $^{39}\text{Ar}/^{36}\text{Ar}$ plot (Figure 3). The scatter about a line is significantly greater than that expected solely from experimental error, showing that not all the assumptions usually made in age calculations are fully satisfied. However, the linear correlation is striking. When a least-squares line is fitted to the data, the best slope corresponds to an age of formation of 549 ± 20 Ma. This age agrees within experimental error with the assigned Upper Cam-

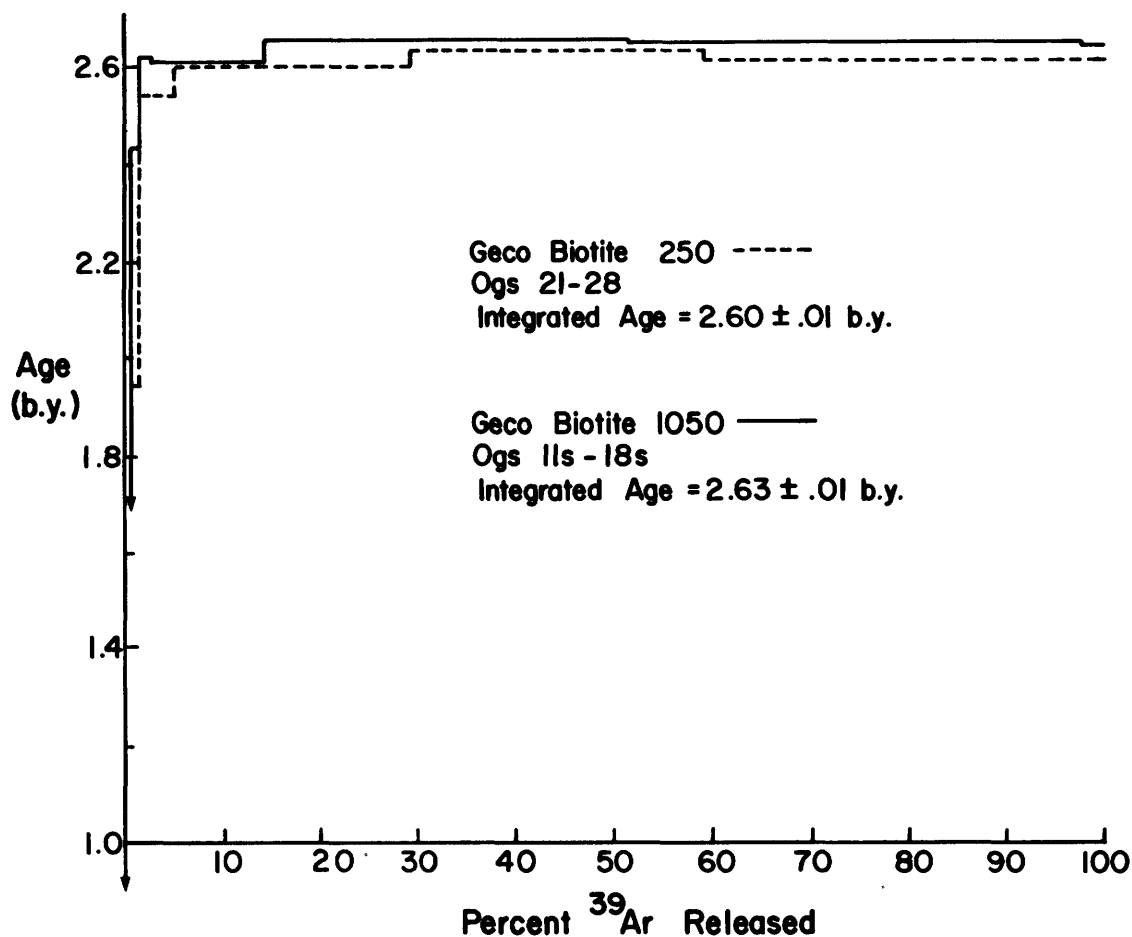


Figure 2— $^{40}\text{Ar}/^{39}\text{Ar}$ Age spectra for Geco biotites.

brian age of the sedimentary rocks enclosing the ore. If we are encouraged by the Geco result to interpret this indicated age as being reliable, then the simplest interpretation is clearly that the ore was deposited in this MVT deposit in southeast Missouri very soon after deposition of the sediments. If further work upholds this interpretation, then the enigma of the age of this famous deposit will have been solved.

The six galena data are more scattered still (see Table 1), almost certainly because of their extremely low potassium and radiogenic argon concentrations which make their analysis difficult. However, it is clear that the $^{40}\text{Ar}/^{36}\text{Ar}$ values present in the fluids from which the galenas formed were significantly different from those characterizing the pyrite-forming fluids. Thus while the galena data yet are too scattered to yield a meaningful age, the $^{40}\text{Ar}/^{36}\text{Ar}$ measurements seem to show very clearly that the pyrites and galenas formed at significantly different times, so that in the interval between formations, the ore-forming fluid had changed significantly in composition.

SUMMARY

Our research so far has shown the following.

- 1) It is possible to date pyrites with the $^{40}\text{Ar}/^{39}\text{Ar}$ method if isochron plotting is used.
- 2) Pyrites from the Geco Mine indicate an age of 2.5 ± 0.1 Ga for the ore. This agrees within error with the age of about 2.62 Ga obtained by step-heating biotites extracted from the ore.
- 3) Pyrites from the St. Jo Mine in southeast Missouri indicate an age for the deposit of 549 ± 20 m.y. This strongly suggests that the ore was emplaced shortly after deposition of the surrounding sediments.
- 4) The $^{40}\text{Ar}/^{36}\text{Ar}$ ratios indicate that the pyrites and galenas in the MVT specimen formed at quite different times.
- 5) The $^{40}\text{Ar}/^{36}\text{Ar}$ measurements at Geco show big differences among these ratios in pyrite, galena, chalcopyrite and sphalerite. This, along with point (4) above, strongly indicates that the different mineral types from a deposit cannot be expected to fall on a single isochron. Any isochrons found will probably be mineral-specific.

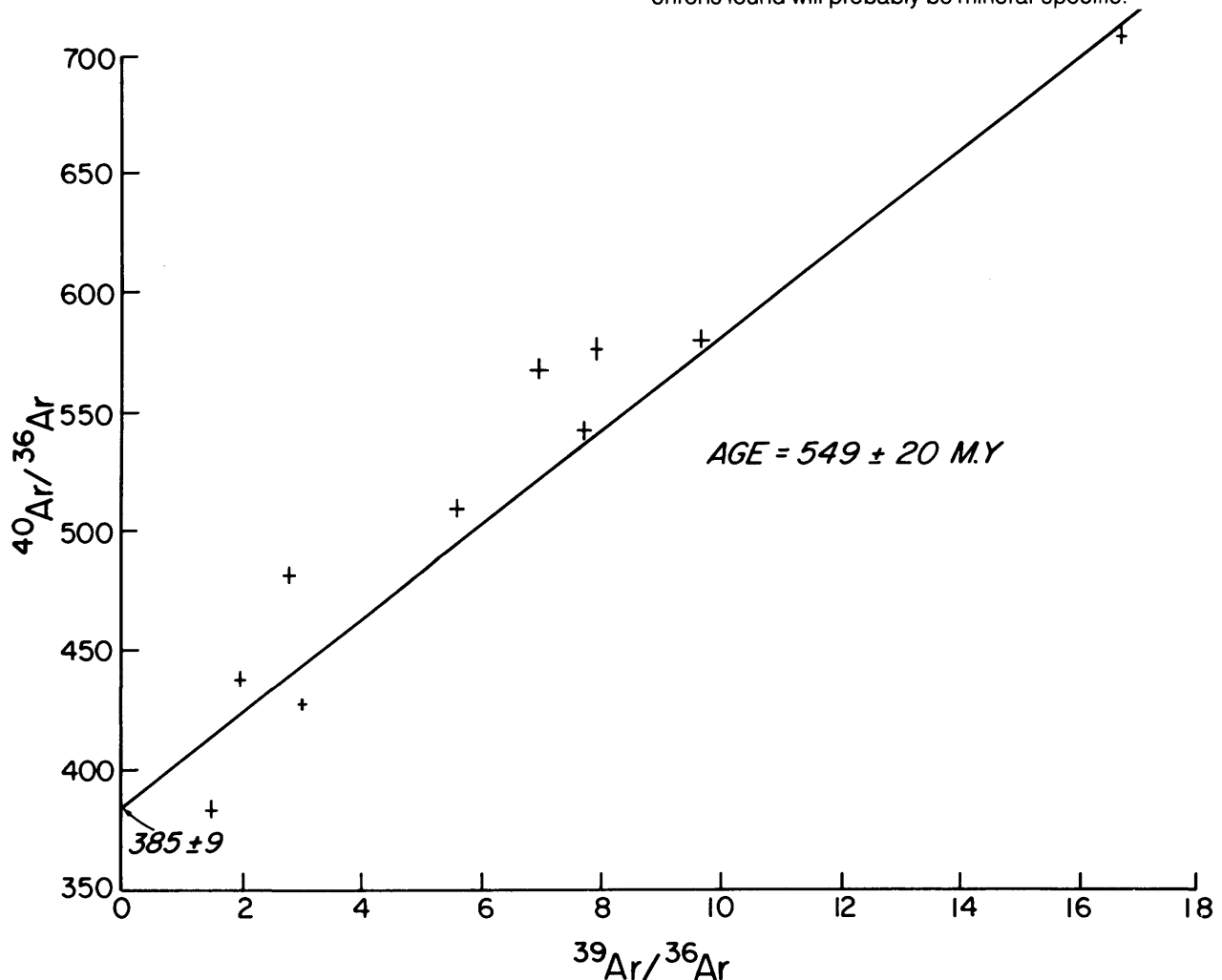
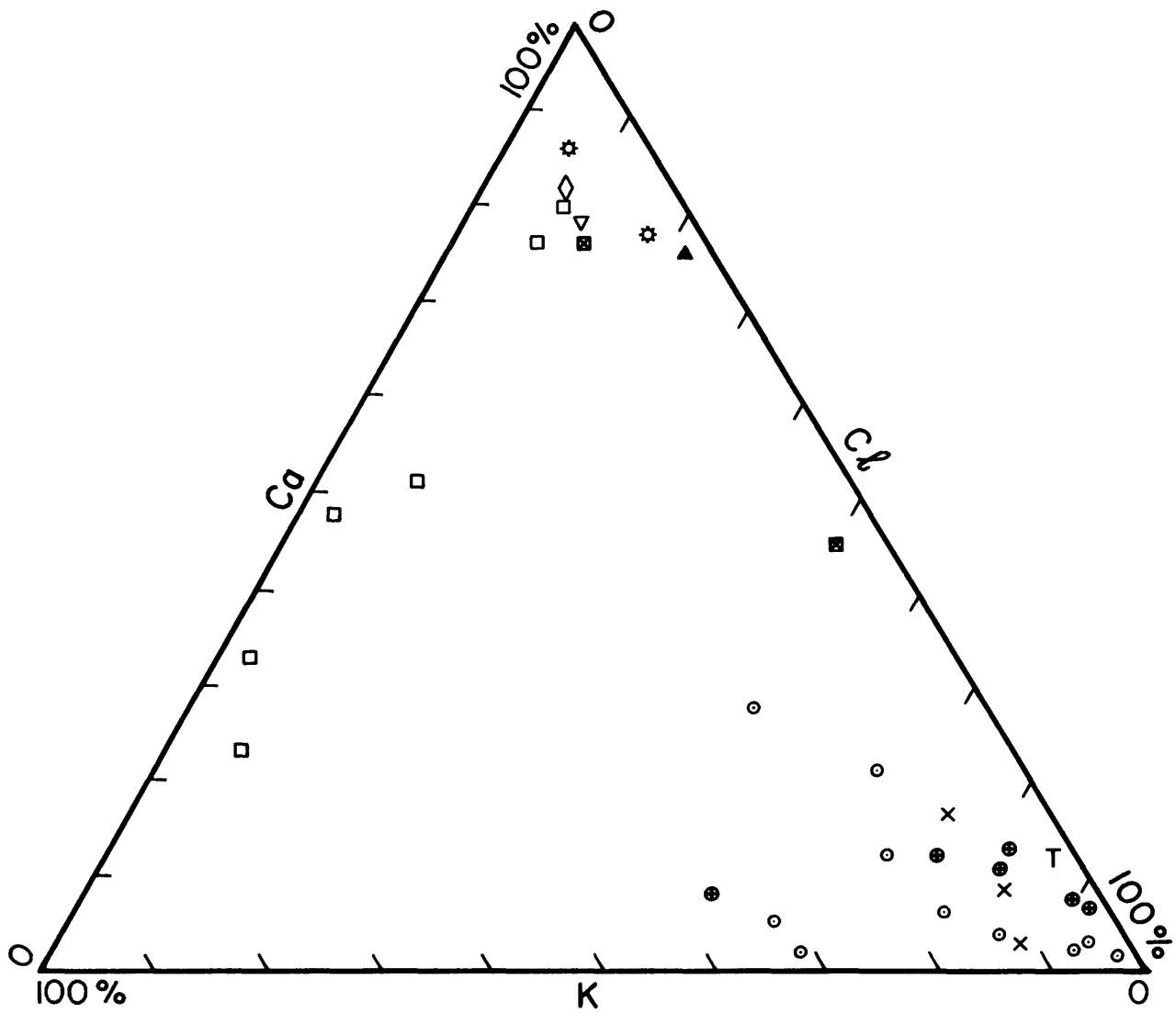


Figure 3—Argon correlation plot for Mississippi Valley type pyrites.



LEGEND

- | | |
|-------------------------|-----------------------|
| ○ MVT PYRITES | × BROKEN HILL GALENAS |
| ● MVT GALENAS | ☆ GECO GALENAS |
| ■ SUDBURY PYRITES | ▽ GECO SPHALERITES |
| ▲ SUDBURY CHALCOPYRITES | ◇ GECO CHALCOPYRITES |
| | □ GECO PYRITES |
- T K-Ca-Cl COMPOSITION OF A TYPICAL FLUID INCLUSION (ROEDDER, 1976)

Figure 4—K-Ca-Cl concentrations plot for Geco and other sulphides.

6) Whereas the ^{36}Ar in MVT pyrites is fairly uniformly distributed, the potassium varies by a factor of twenty among the samples from one hand specimen. This is a potentially good situation for obtaining isochrons and also suggests that the potassium may exist in small regions of high potassium concentration. From the K/Cl/Ca measurements (Figure 4), it seems clear that these hypothesized concentrations are in fluid inclusions.

We conclude that pyrites can be dated by the $^{40}\text{Ar}/^{39}\text{Ar}$ method and that the application of this technique to sulphides generally has considerable geochronological and geochemical potential. This investigation opens up a new field of research in economic geology.

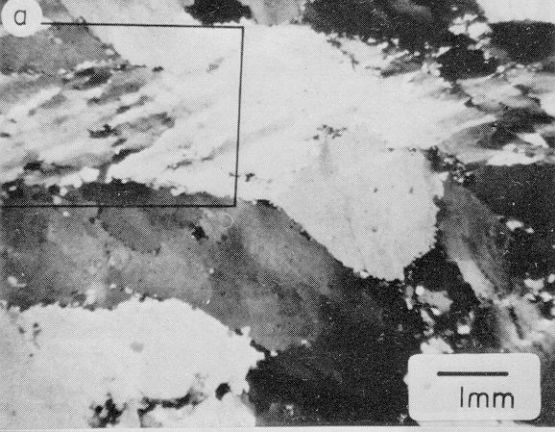
ACKNOWLEDGMENTS

This project is funded principally by the Ontario Geoscience Research Grant Program, but is also significantly supported by N.S.E.R.C. grants. We are indebted to Professor F. W. Beales, University of Toronto, for providing the southeast Missouri samples. The McMaster University

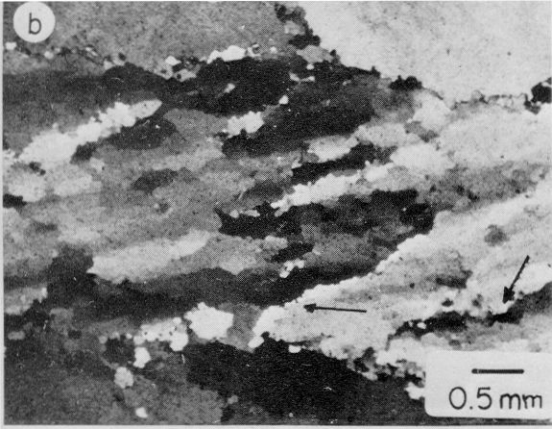
reactor personnel were extremely cooperative and helpful with all the irradiations.

REFERENCES

- Alexander, E.C., and Davis, P.K.
1974: ^{40}Ar - ^{39}Ar Ages and Trace Element Contents of Apollo 14 Breccias, an Interlaboratory Cross-Calibration of ^{40}Ar - ^{39}Ar Standards; *Geochimica et Cosmochimica Acta*, Vol. 38, p.911-928.
- Hall, C.M., and York, D.
1978: K-Ar and $^{40}\text{Ar}/^{39}\text{Ar}$ Age of the Laschamp Geomagnetic Polarity Reversal; *Nature*, Vol. 274, p.462-464.
- Hanes, J.A., and York, D.
1979: A Detailed $^{40}\text{Ar}/^{39}\text{Ar}$ Age Study of an Abitibi Dike from the Canadian Superior Province; *Canadian Journal of Earth Sciences*, Vol. 16, p.1060-1070.
- Roedder, E.
1976: Fluid Inclusion Evidence on the Genesis of Ores in Sedimentary and Volcanic Rocks; Chapter 4 in *Handbook of Stratabound and Stratiform Ore Deposits*, edited by K.H. Wolf, Elsevier, Amsterdam.
- York, D.
1969: Least Squares Fitting of a Straight Line with Correlated Errors; *Earth and Planetary Science Letters*, Vol. 5, p.320-324.



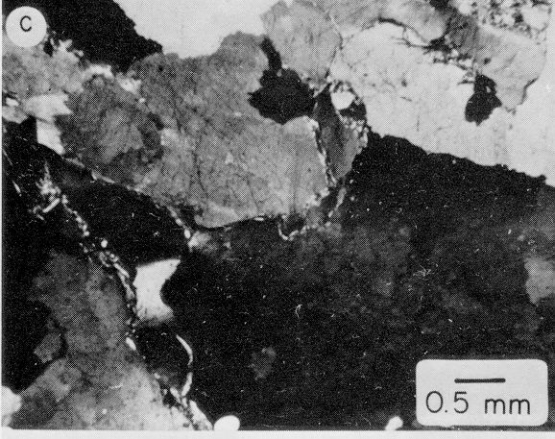
b



0.5 mm

C

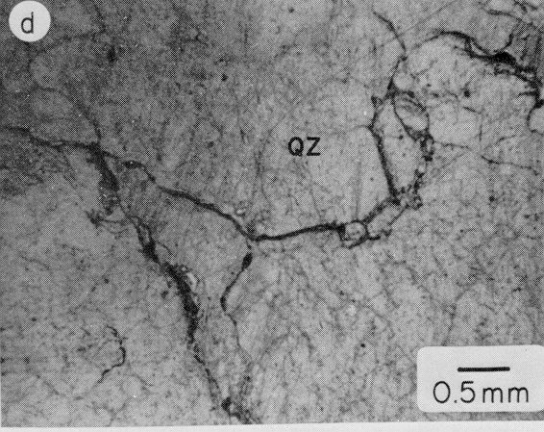
—
0.5 mm



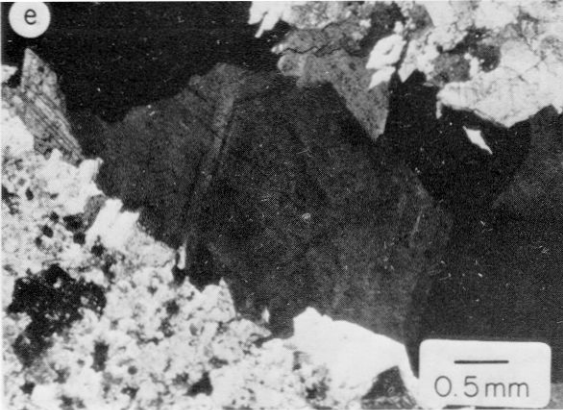
d

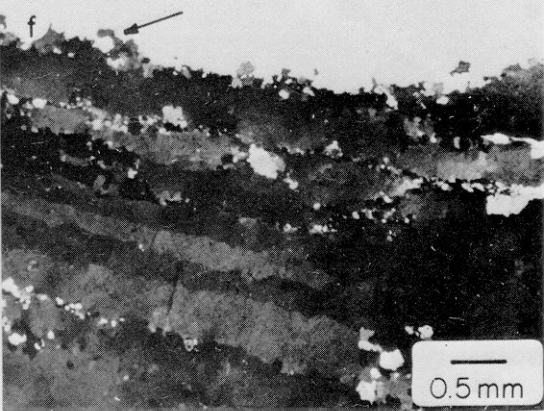
QZ

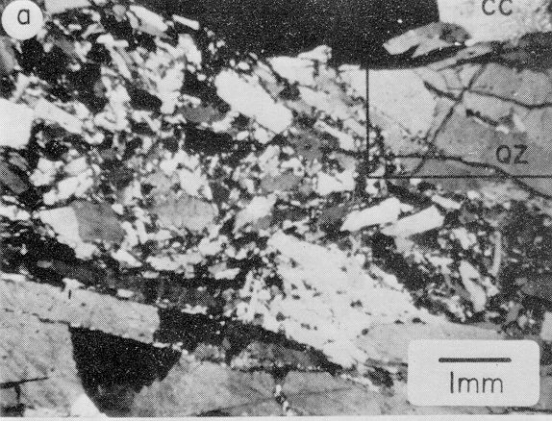
—
0.5mm



e







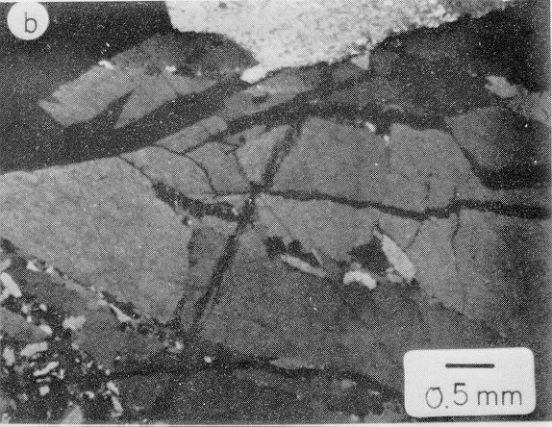
a

CC

QZ

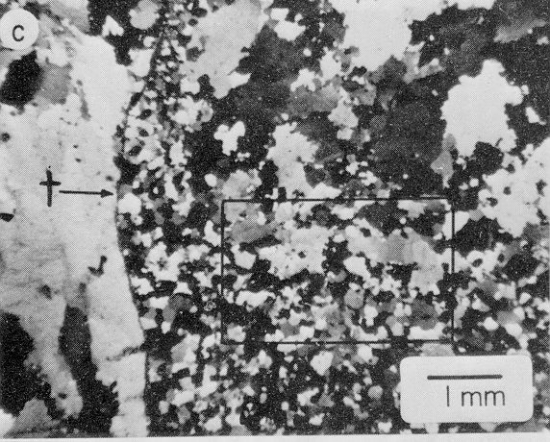
1mm

b

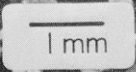
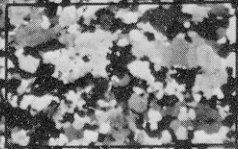


0.5 mm

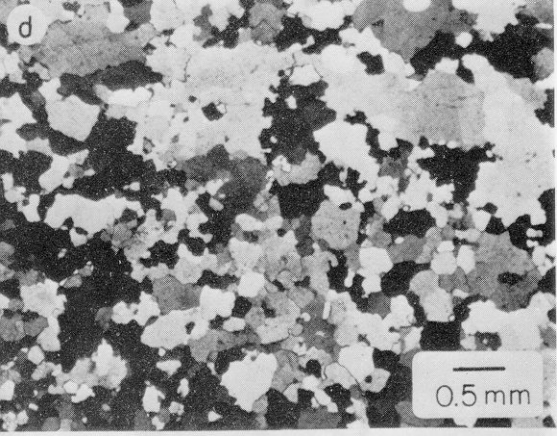
A black and white micrograph showing a fractured material. The material is dark and exhibits a network of cracks forming irregular polygonal shapes. The cracks are dark and prominent against the lighter background of the material. In the top left corner, there is a small white circle containing the letter 'b'. In the bottom right corner, there is a white rectangular box containing a horizontal scale bar and the text '0.5 mm'.



c

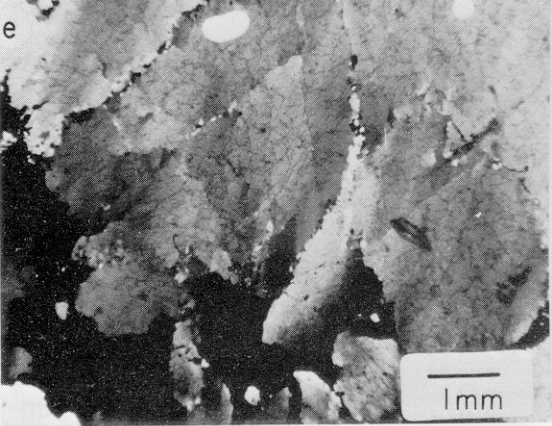


d

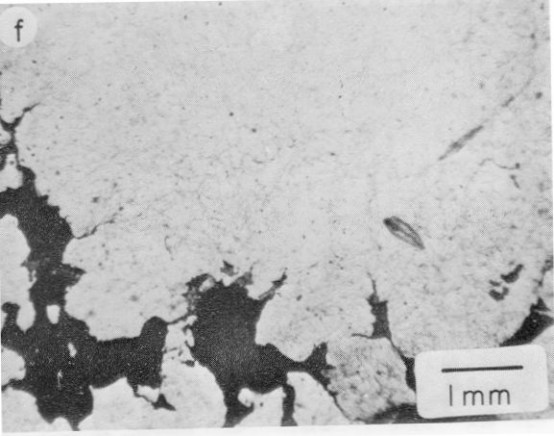


0.5 mm

A black and white micrograph showing a complex, speckled pattern of light and dark regions. The pattern consists of irregular, interconnected shapes of varying sizes, creating a porous or cellular appearance. In the top-left corner, there is a small white circle containing the letter 'd'. In the bottom-right corner, there is a white rectangular box containing a horizontal scale bar and the text '0.5 mm'.

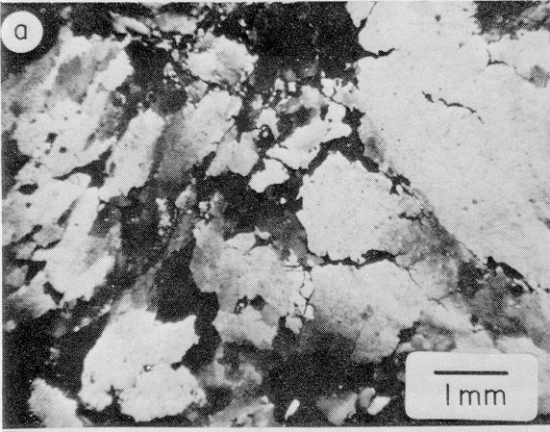


f



A black and white micrograph showing a biological specimen with a porous, irregular structure. The specimen is light-colored with dark, branching, and somewhat crystalline regions. A scale bar in the bottom right corner indicates a length of 1 mm. A small circular marker with the letter 'f' is in the top left corner. Two elongated, dark, spindle-shaped structures are visible in the upper right quadrant.

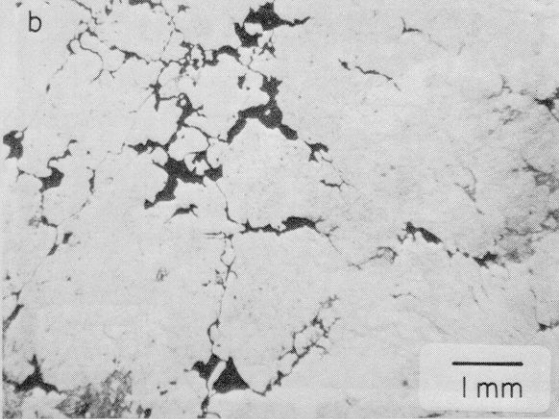
1mm



a

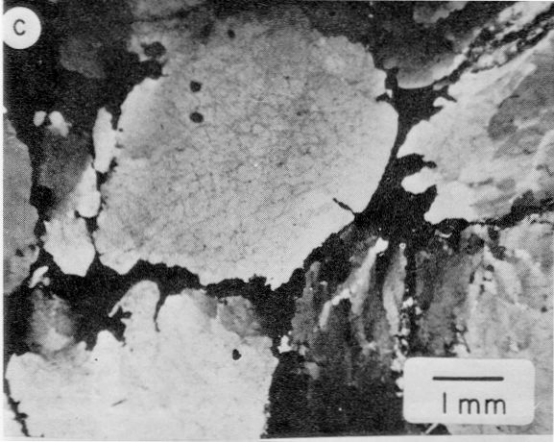
1 mm

b



1 mm

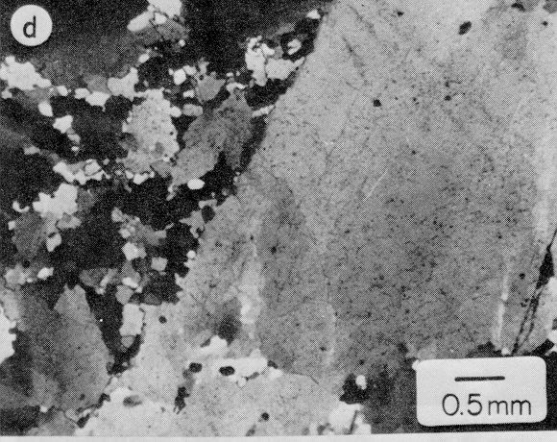
C

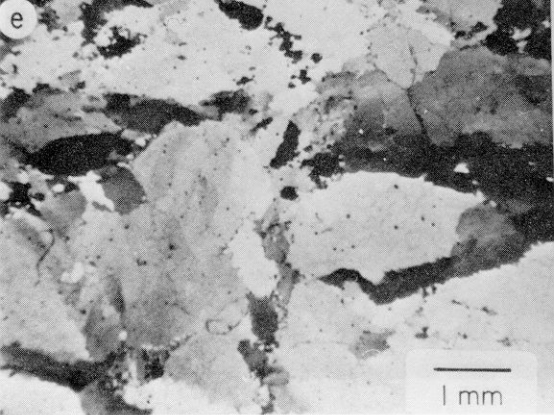


1 mm

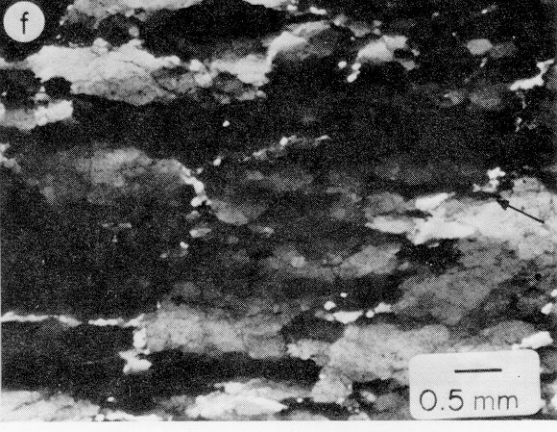
d

—
0.5 mm



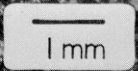
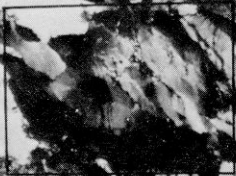


f

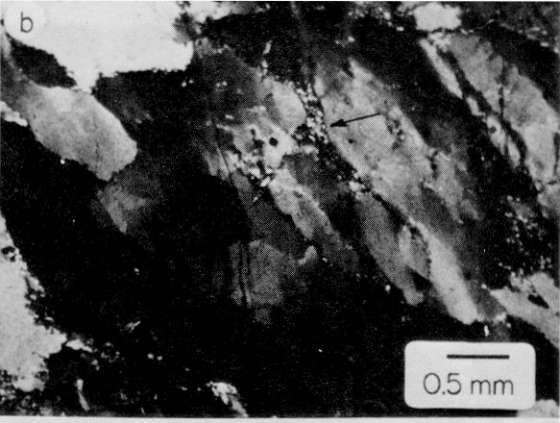


—
0.5 mm

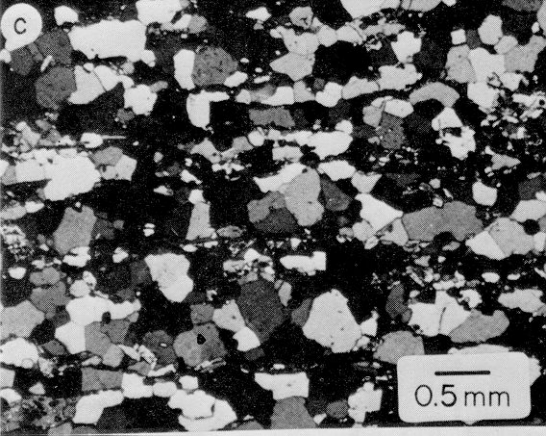
1



b



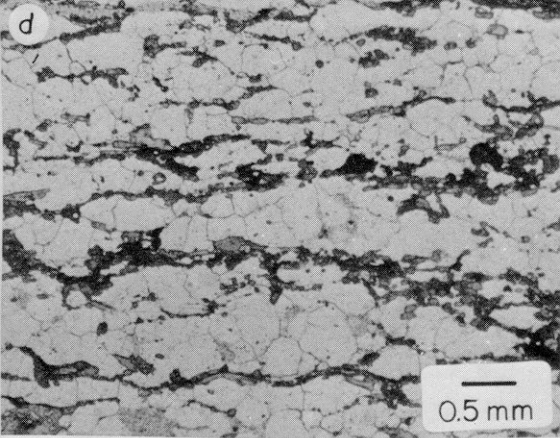
0.5 mm



C

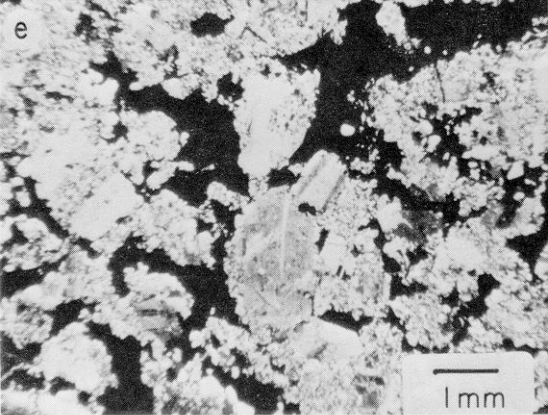
0.5 mm

d



—
0.5 mm

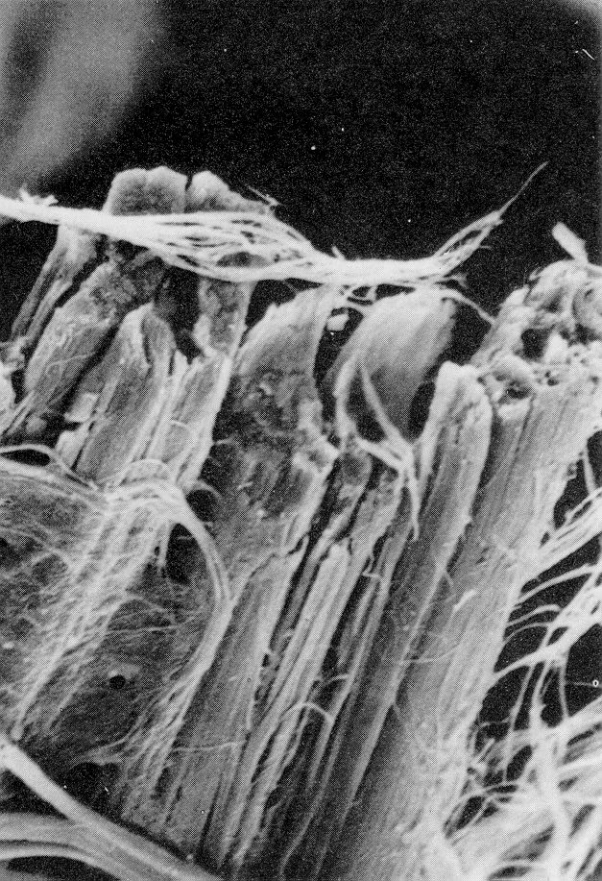
e

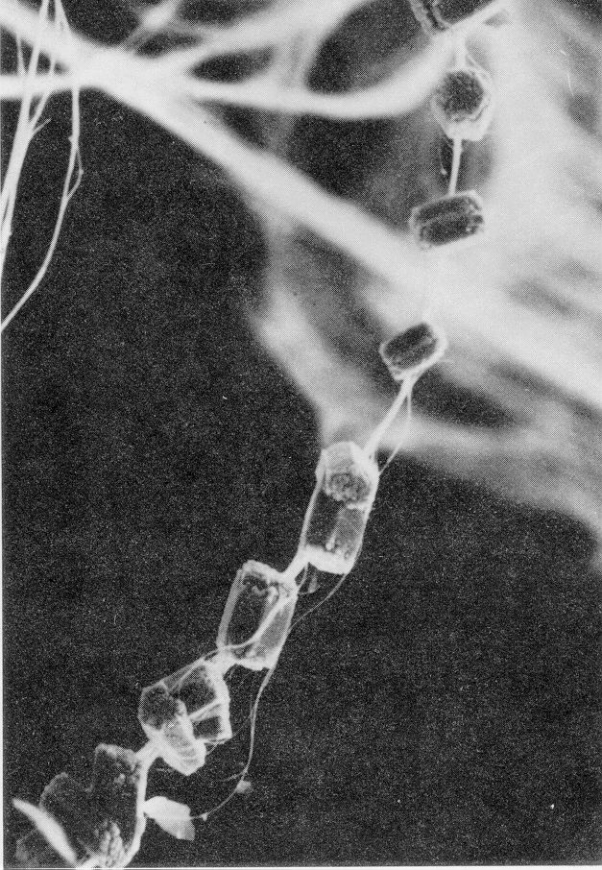


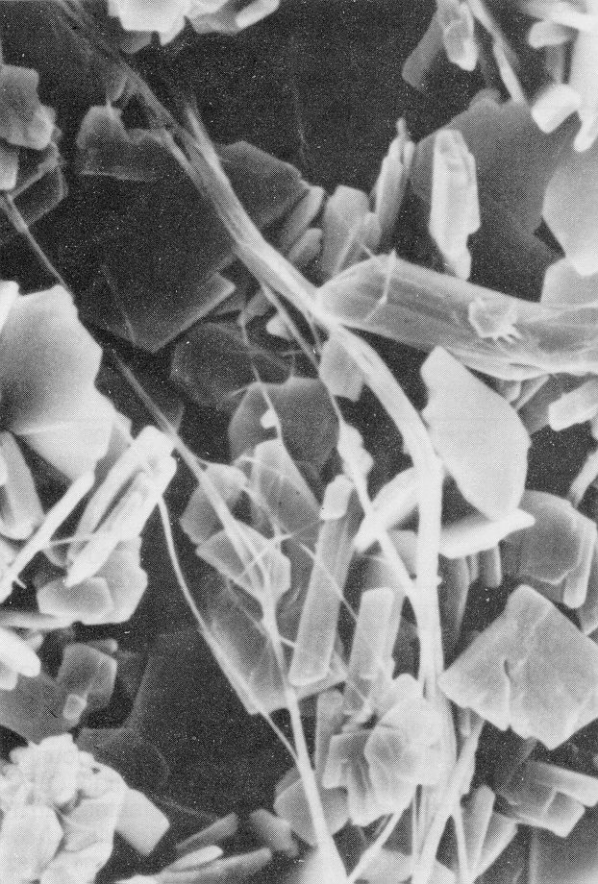
f

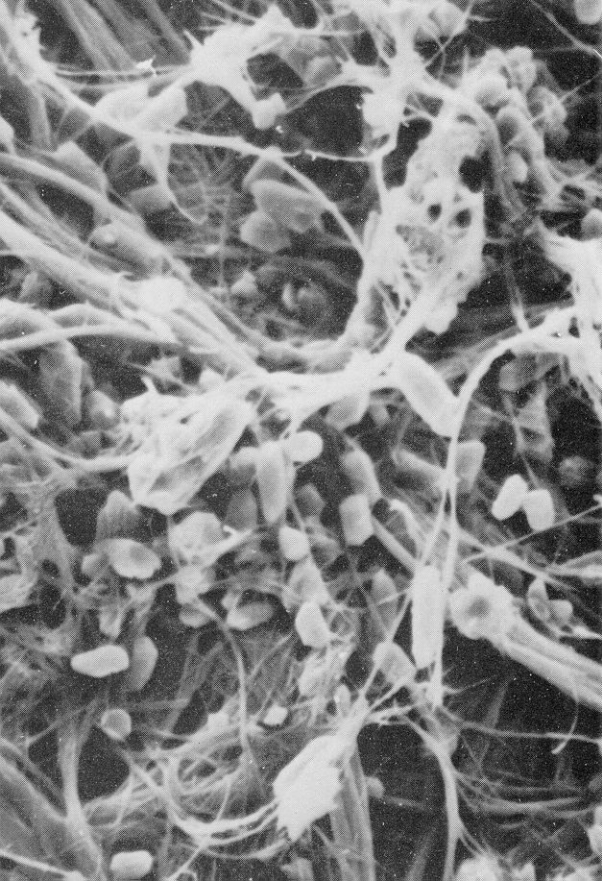
AB

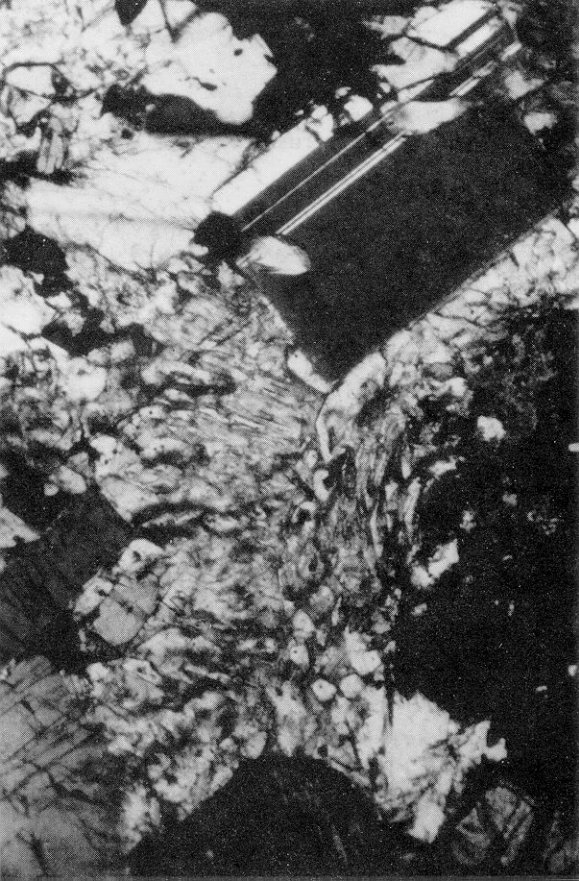
1mm



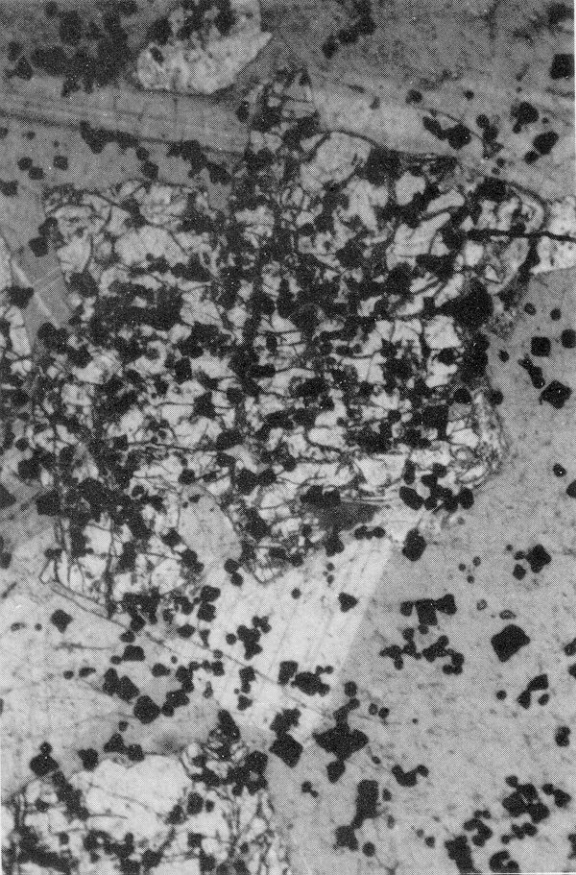




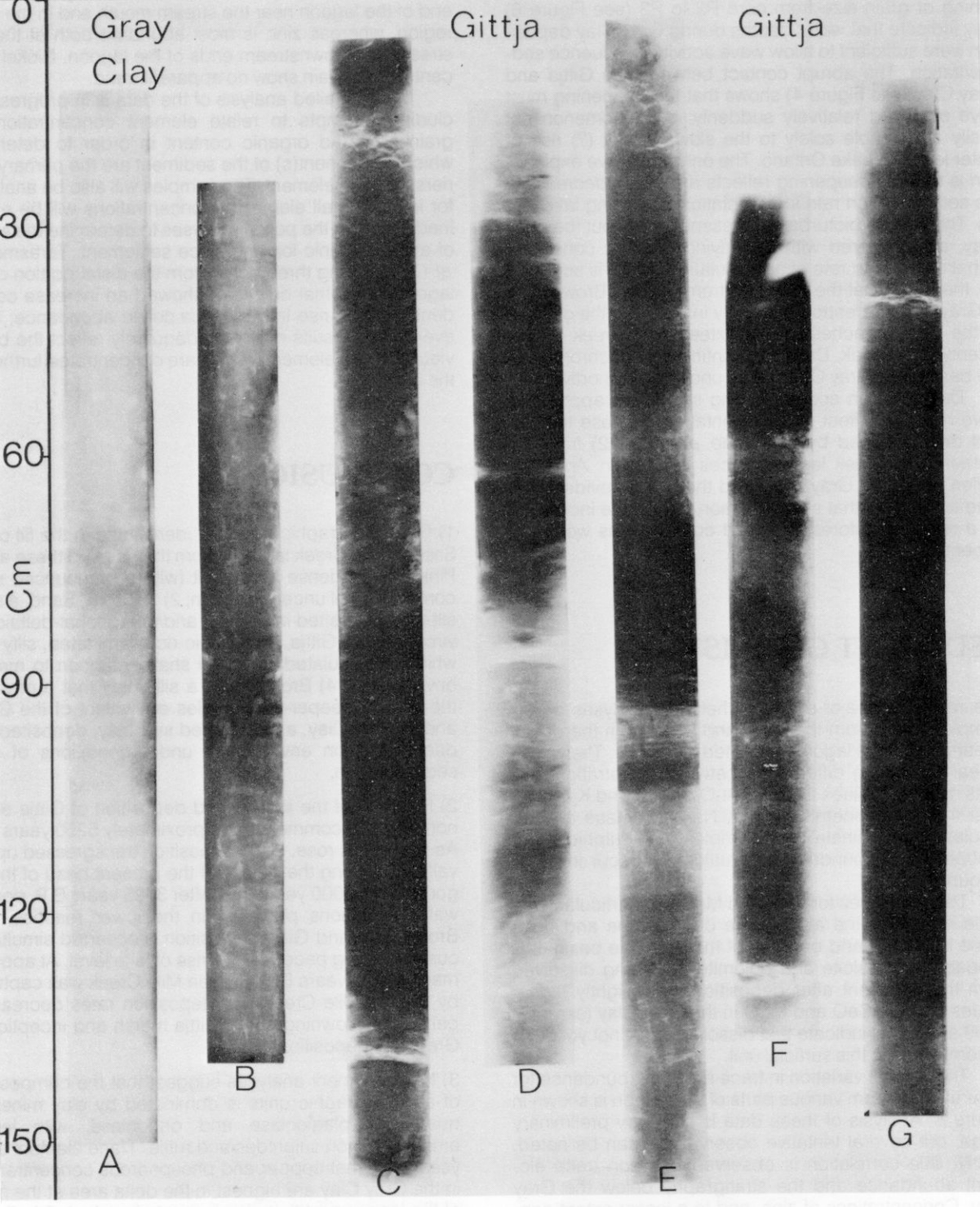




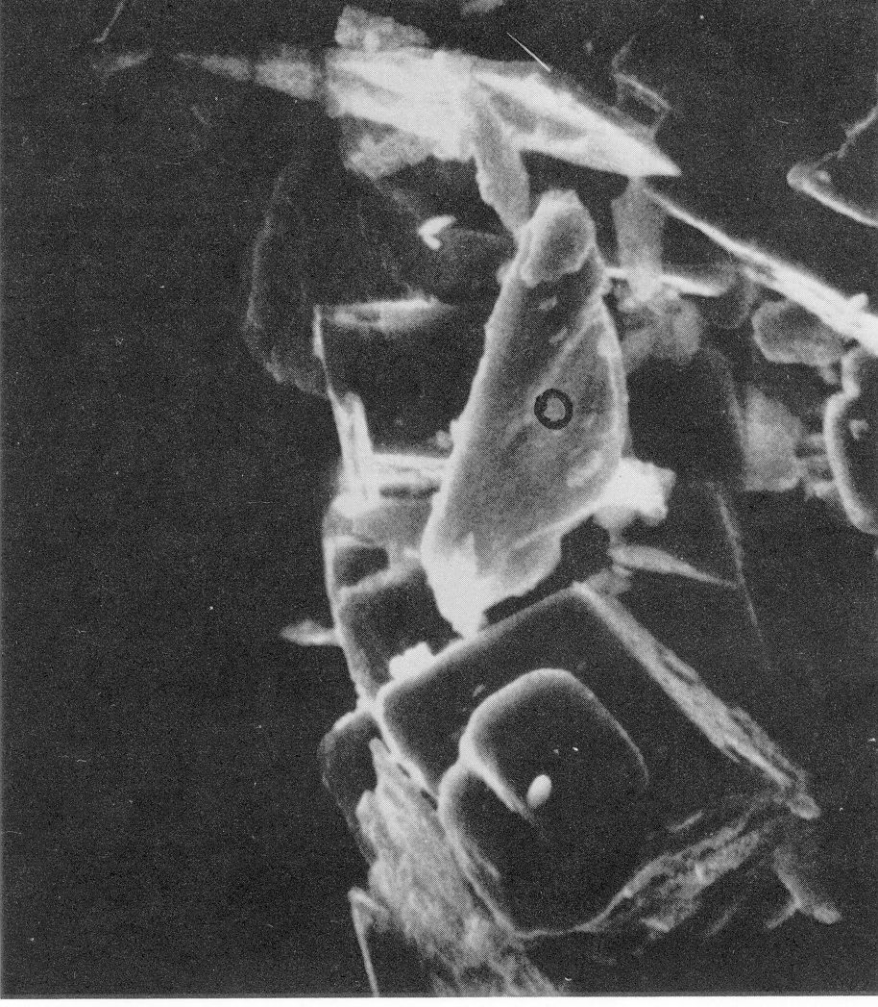








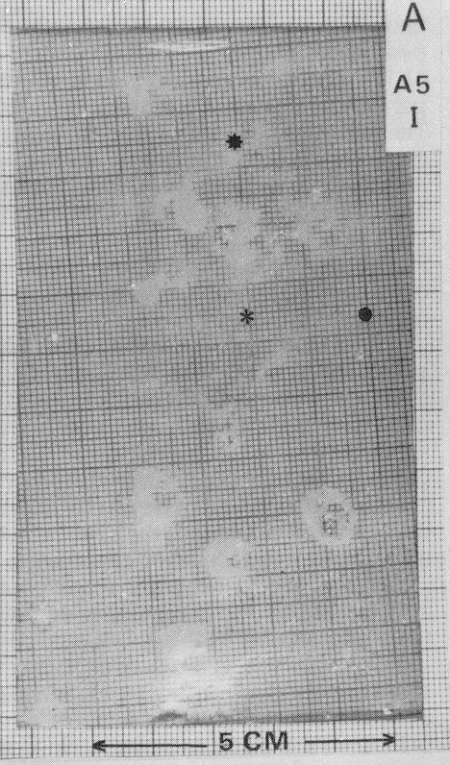




A

A5

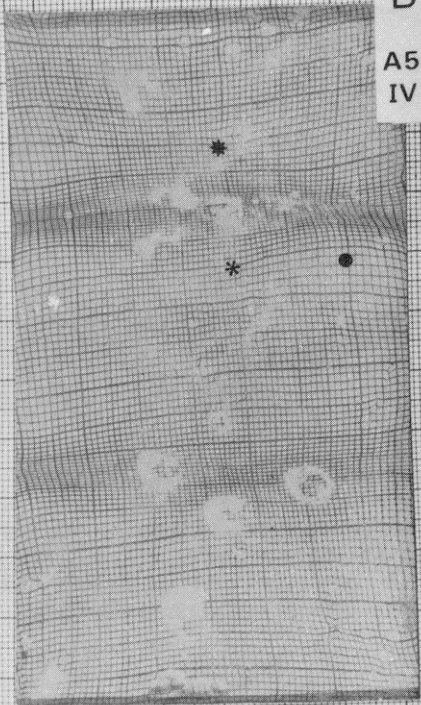
I



5 CM

B

A5
IV



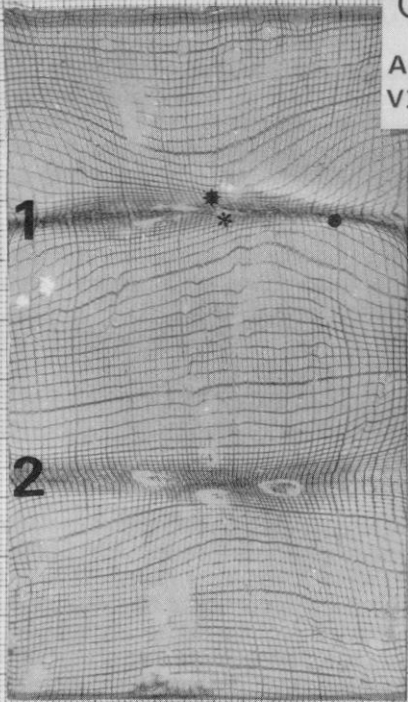
C

A5

VII

1

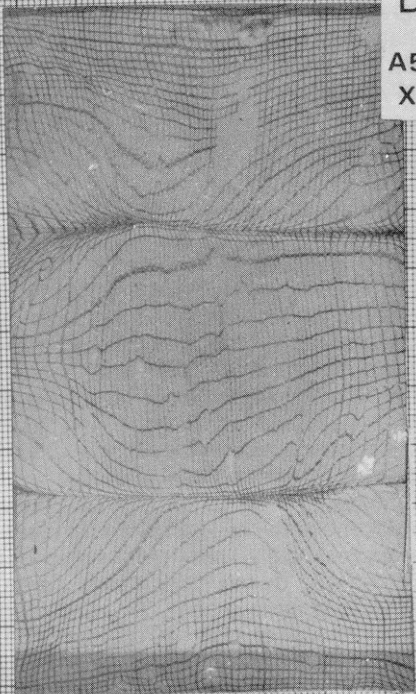
2

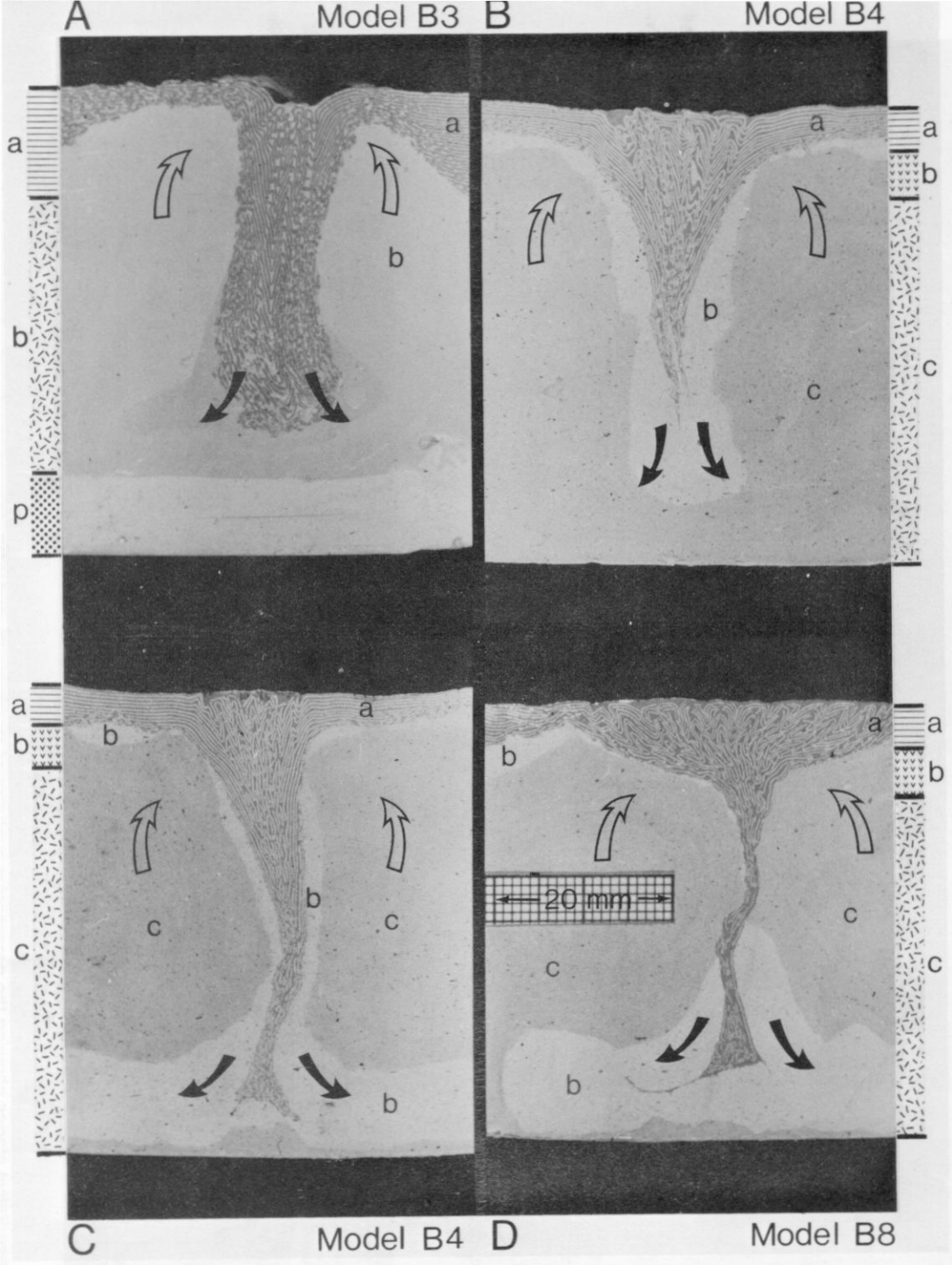


D

A5

X



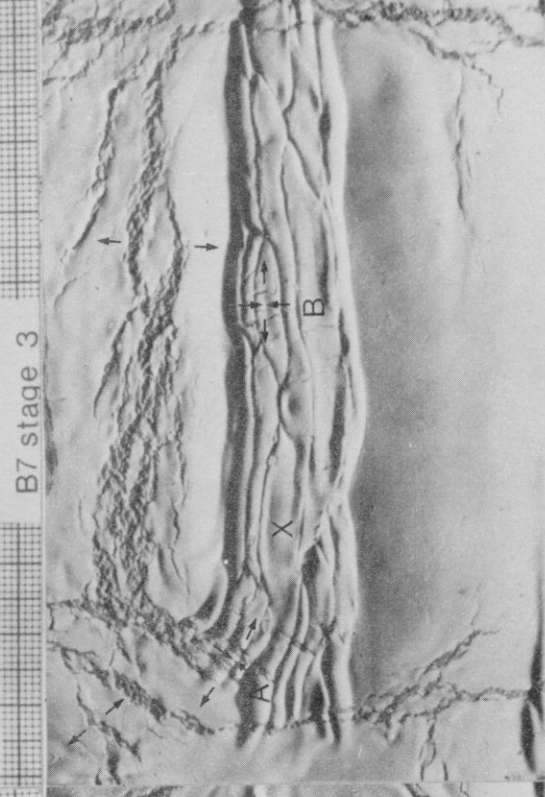




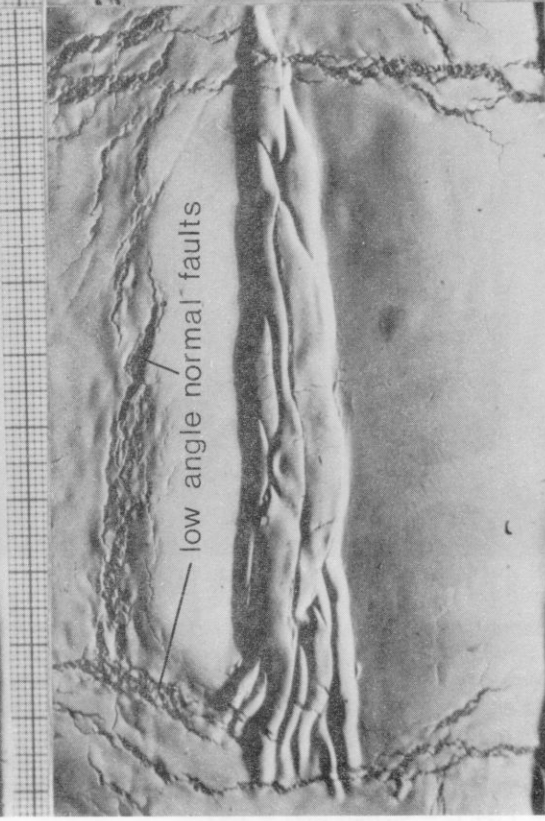
B7 stage 2



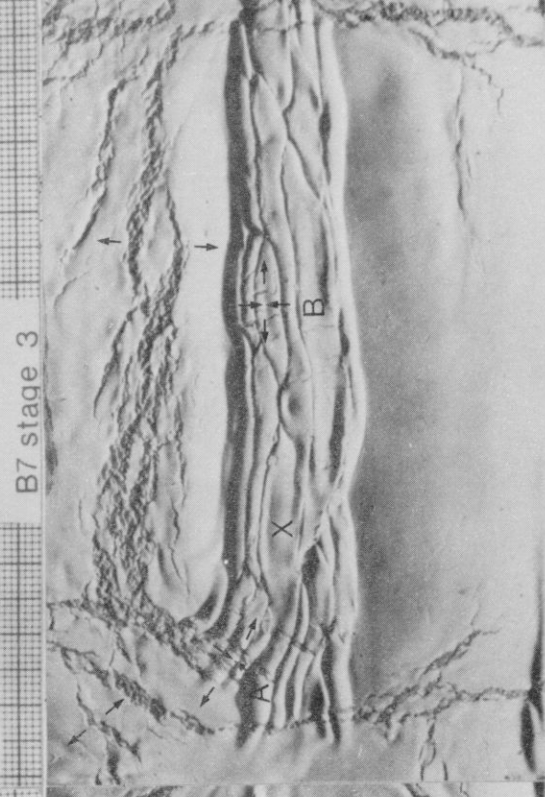
tight syncline
broad anticline



low angle normal faults



B7 stage 4



B7 stage 5

30 mm











0 1 2 3 4 5 cm

